

INDIAN JOURNAL OF PHYSICS

VOL. 29

AND

PROCEEDINGS

OF THE

Indian Association for the Cultivation of Science, Vol. 38

(Published in Collaboration with the Indian Physical Society)

(With Sixteen Plates)

Printed by Kalipada Mukherjee, Eka Press, 2041. B. T. Road, Calcutta
and published by the Registrar, Indian Association for the Cultivation
of Science, Jadavpur, Calcutta 32

1955

Price Rs. 20 or £ 2

INDIAN JOURNAL OF PHYSICS, 1955

CONTENTS

No. 1. January

1. The Visible Emission Spectrum of Se_2 —By V. Leelavathi and P. Tiruvenganna Rao 1
2. Diffusion Coefficients and law of Molecular Interaction—By M. P. Madan 11
3. The Band Spectra of Thallium Iodide and Fluoride—By J. V. Ramana Rao and P. Tiruvenganna Rao 20
4. Magneto-Elasticity of Polycrystalline Iron and Nickel—By V. Narasimhan 27
5. Spectroscopic Constants of Molecules. III. Regularities in Vibration Frequencies in a Molecular Group—By Y. P. Varshni and K. Majumdar 38

No. 2. February

6. Calculation of the Dipole Moments of Tri-substituted Benzenes—By D. V. G. L. Narasimha Rao 49
7. Scattering of Light by Colloidal Particles and the Determination of their Size—By Y. G. Naik and D. K. Sohoni 55
8. Intrinsic Viscosity-Molecular Weight Relationship of High Polymers. A New Equation—By Santi R. Palit 65
9. Beta Energetics and Nuclear Shell Structure—By S. N. Ghoshal and A. N. Saxena 81
10. Analysis of G-M Counter Impulses by the method of Delayed Coincidences—By Satya Pal Puri and P. S. Gill 95

No. 3. March

1. Vibrational Analysis of the Tantalum Oxide Bands—By D. Premaswarup 109

12.	A Study of Transistors connected in Parallel—By Anadi Nath Daw	121
13.	Thermal Diffusion of Gas Mixtures and Determination of Force Constants—By S. C. Saxena	131
14.	A Study of A. C. Resistivity of Calcutta Soil—By S. P. Bhattacharyya	141
15.	Force Constants for Substituted Germanes. Part I. GeH_3Cl and GeD_3Cl .—By S. L. N. G. Krishnamachari	147
16.	A Wide-band Frequency Modulated System with Asymmetrical 3-phase Oscillator—By P. Kundu	151

No. 4. April

17.	Absorption of Microwaves and U. H. F. Radiowaves in Phenol, Cyclohexanol and I-Bromo 2-Chloroethane—By D. K. Ghosh ..	161
18.	Analysis of Sky-wave Field Intensity. Part I—By S. N. Mitra and R. B. L. Srivastava	167
19.	Raman Spectra of Ortho and Meta Dichlorobenzene in different States and at different Temperatures—By D. C. Biswas ..	179
20.	On the Quantitative Relation between Isotopic Beta Radiation and its Photographic Response—By R. K. Poddar ..	189
21.	Fermi's Statistical Theory of Multiple Pion Production—By K. K. Singh	199

No. 5. May

22.	The Emission Spectrum of Bromine—By P. B. V. Haranath and P. Tiruvenganna Rao	205
23.	Analysis of Sky-wave Field Intensity. Part II—By S. N. Mitra and R. B. L. Srivastava	227
24.	Baryon Meson System in Pais Formalism : The Scattering Matrix—By S. P. Misra	243

LETTER TO THE EDITOR

1.	Raman Spectrum of <i>o</i> -Chloroethylbenzene—By S. L. N. G. Krishnamachari and V. Ramakrishna Rao	254
----	---	-----

No. 6. June

25. Raman Spectra and Fluorescence of a few Substituted Toluenes in the Solid State at Different Low Temperatures—By D. C. Biswas	257
26. Spin-Echo Modulation due to Magnetic Dipole Interaction between a Closely Interacting Pair of Nuclei in Crystals—By T. P. Das and S. K. Ghosh Roy	272
27. Electronic Collisional Frequency in the F-Region over Calcutta—By S. Datta	279
28. Spectroscopic Constants of Molecules. IV. Similarities in Ground State Vibration Frequencies of Isoelectronic Diatoms —By Y. P. Varshni and K. Majumdar	285
29. Analysis of some Indian Ores and Minerals by Bent Mica Crystal Spectrograph—By Probhat Kumar Bhattacharyya	292
30. The Effect of Fluid Motion on Heat Transmission. Part III. By D. G. Kapadnis	296

No. 7. July

31. Fredholm Theory and Hankel Transform of the Schrödinger Equation—By S. N. Biswas	309
32. On the Deviation of Magnetic Moments of $S_{\frac{1}{2}}$ Nuclei from the Schmidt Limits - By M. L. Chaudhury	319
33. On the Energy Response and Resolution of a Scintillation Counter—By Sobhana Dhar	329
34. Ultrasonic Absorption in Solutions—By Bibhuti Bhusan Deo	352
35. An X-ray Study on Bivalent Silver and Copper Nicotinate Compounds —By D. M. Chakraborty and B. Banerjee	357

No. 8. August

36. On the Raman Spectra of Ethylene Chlorhydrine and <i>n</i> -Propyl Chloride in the Vapour State—By M. Mazumder	361
37. Pulse Techniques for Acoustical Measurements in Broadcast Studios—By R. K. Vepa and N. K. Trivedi	369

38. On the Variation of p-p Scattering Cross section with Energy —By C. C. Banerjee	380
39. Force Constants for Substituted Germanes—By S. L. N. Krishnamachari	384
0. Mass Asymmetry Effect in Hutchisson's Theory of Vibrational Transition Probabilities—By N. R. Tawde and P. V. Chandra-treya	388
41. On Two-directional focussing Magnetic Analysers—By S. B. Karmohapatro	393
42. Dipole moment of Indene—By D. V. G. L. Narasimha Rao ..	398

No. 9. September

43. Flexure of thin Elastic Plates under Specified Edge Traction—By V. Cadambe, R. K. Kaul and S. G. Tewari	403
44. Source-Straggling of α -Particles from a Polonium Source—By N. K. Saha and K. L. Kaila	417
45. An Improved Method of Measuring the Absolute Susceptibilities of Single Crystals over wide Ranges of Temperatures —By S. K. Dutta Roy	429
46. An Approximate Method of Calculating the Vibration Frequencies, of 1, 1, 1—Trichloroethene Molecule—By D. C. Biswas ..	442

LETTER TO THE EDITOR

2. New Evidence for the Preponderance of the cis form in ortho-Chlorophenol Molecule—By Dilip Kumar Ghosh	450
---	-----

No. 10. October

47. Higher Approximations to Diffusion Coefficients and Determination of Force Constants—By S. C. Sexana	453
48. Shrinkage effect of close Components in Spectroscopic Instruments—By Mahendra Singh Sodha	461
49. The Isograph—an Electronic Root Finder—By A. K. Choudhury..	468
50. Raman Spectra of Frozen Solutions of Carbon Disulphide in Aliphatic Solvents—By G. S. Kastha	474

51. Ionisation loss of α -Particles at Low Energies below 4 Mev.—By K. L. Kaila	479
52. Muonic Interactions in Dense Material—By M. M. Biswas ..	490

LETTER TO THE EDITOR

3. Z_A Term in the Mass Formula · By A. N. Saxena	501
---	-----

No. 11. November

53. Raman Spectra of a Few Monosubstituted Benzene Compounds in the Solid State at Different Low Temperatures—By D. C. Biswas	503
54. A Method of Determining the Relative Amounts of D- and E- Region Absorptions of Medium and Short Radio Waves —By A. P. Mitra	518
55. A Null Method of Measuring Surface Tension with a Torsion Balance— By S. Venkataraman	522
56. The Dependence of the Composite Mean Life and Mu-Mesons on the Atomic Number of the Absorbers—By N. N. Biswas ..	527
57. Frequency of the Three-Phase R-C Coupled Oscillator—By H. Rakshit and M. C. Mallik	534
58. On Ultrasonic Wattage and Spectral Number Relationship—By K. Samal, K. M. Patanaik and A. K. Dutta ..	548

LETTER TO THE EDITOR

4. Raman Spectra of Solutions of <i>o</i> -Dichlorobenzene in Methyl- cyclohexane—By D. C. Biswas	553
--	-----

No. 12. December

59. Ultraviolet Absorption Spectra of Ortho- and Para-Tolunitrile in Vapour, Liquid and Solid States—By S. K. Sen ..	561
60. Effect of Hypo Concentration on the Clearing Time of Thick Emul- sions—By Yog Prakash	569
61. String under the Action of a Plane Rubber Wheel—By H. G. Mane	573

38.	On the Variation of p-p Scattering Cross section with Energy —By C. C. Banerjee	380
39.	Force Constants for Substituted Germanes—By S. L. N. Krishnamachari	384
40.	Mass Asymmetry Effect in Hutchisson's Theory of Vibrational Transition Probabilities —By N. R. Tawde and P. V. Chandrareya	388
41.	On Two-directional focussing Magnetic Analysers—By S. B. Karmohapatro	393
42.	Dipole moment of Indene —By D. V. G. L. Narasimha Rao ..	398

No. 9. September

43.	Flexure of thin Elastic Plates under Specified Edge Traction—By V. Cadambe, R. K. Kaul and S. G. Tewari	403
44.	Source-Straggling of α -Particles from a Polonium Source —By N. K. Saha and K. L. Kaila	417
45.	An Improved Method of Measuring the Absolute Susceptibilities of Single Crystals over wide Ranges of Temperatures —By S. K. Dutta Roy	429
46.	An Approximate Method of Calculating the Vibration Frequencies, of 1, 1, 1—Trichloroethene Molecule—By D. C. Biswas ..	442

LETTER TO THE EDITOR

2.	New Evidence for the Preponderance of the cis form in ortho-Chlorophenol Molecule —By Dilip Kumar Ghosh	450
----	---	-----

No. 10. October

47.	Higher Approximations to Diffusion Coefficients and Determination of Force Constants—By S. C. Sexana	453
48.	Shrinkage effect of close Components in Spectroscopic Instruments —By Mahendra Singh Sodha	461
49.	The Isograph—an Electronic Root Finder—By A. K. Choudhury ..	468
50.	Raman Spectra of Frozen Solutions of Carbon Disulphide in Aliphatic Solvents—By G. S. Kastha	474

- | | | |
|-----|---|-----|
| 51. | Ionisation loss of α -Particles at Low Energies below 4 Mev.—By
K. L. Kaila | 479 |
| 52. | Muonic Interactions in Dense Material—By M. M. Biswas .. | 490 |

LETTER TO THE EDITOR

- | | | |
|----|--|-----|
| 3. | Z_A Term in the Mass Formula—By A. N. Saxena | 501 |
|----|--|-----|

No. 11. November

- | | | |
|-----|---|-----|
| 53. | Raman Spectra of a Few Monosubstituted Benzene Compounds
in the Solid State at Different Low Temperatures —By D. C.
Biswas | 503 |
| 54. | A Method of Determining the Relative Amounts of D- and E-
Region Absorptions of Medium and Short Radio Waves By
A. P. Mitra | 518 |
| 55. | A Null Method of Measuring Surface Tension with a Torsion
Balance—By S. Venkataraman | 522 |
| 56. | The Dependence of the Composite Mean Life and Mu-Mesons on
the Atomic Number of the Absorbers By N. N. Biswas .. | 527 |
| 57. | Frequency of the Three-Phase R-C Coupled Oscillator—By H.
Rakshit and M. C. Mallik | 534 |
| 58. | On Ultrasonic Wattage and Spectral Number Relationship—By
K. Samal, K. M. Patanaik and A. K. Dutta .. | 548 |

LETTER TO THE EDITOR

- | | | |
|----|---|-----|
| 4. | Raman Spectra of Solutions of <i>o</i> -Dichlorobenzene in Methyl-
cyclohexane—By D. C. Biswas | 553 |
|----|---|-----|

No. 12. December

- | | | |
|-----|---|-----|
| 59. | Ultraviolet Absorption Spectra of Ortho- and Para-Tolunitrile
in Vapour, Liquid and Solid States—By S. K. Sen .. | 561 |
| 60. | Effect of Hypo Concentration on the Clearing Time of Thick Emul-
sions—By Yog Prakash | 569 |
| 61. | String under the Action of a Plane Rubber Wheel—By H. G. Mane | 573 |

62.	Ultrasonic Velocity in Zinc and Magnesium Sulphate Solutions at Different Concentrations and Temperatures—By B. S. Mohanty and B. B. Deo	577
63.	On the Absorption of 3.18 cm. Microwaves in some Substituted Phenols in the Liquid State—By Dilip Kumar Ghosh ..	581
64.	Thermal Conductivity and Force between Like Molecules—By S. C. Saxena	587

LETTER TO THE EDITOR

5.	The Ultraviolet Absorption Spectrum of <i>o</i> -Fluoro-Chloro-Benzene—By S. L. N. G. Krishnamachari	603
----	--	-----

AUTHOR INDEX

Author	Subject	Page
Banerjee, B. and Chakraburty, D. M.	An X-ray study on bivalent silver and copper nicotinate compounds	357
Banerjee, C. C.	On the variation of p-p scattering cross- -section with energy	380
Bhattacharyya, P. K.	Analysis of some Indian ores and minerals by bent mica crystal spectrograph	292
Bhattacharyya, S. P.	A study of A. C. resistivity of Calcutta soil	141
Biswas, D.C.	Raman spectra of ortho- and meta- dichlorobenzene in different states and at different tempera- tures	179
" "	Raman spectra and fluorescence of a few substituted toluenes in the solid state and at different low temperatures	257
" "	An approximate method of calculating the vibration frequencies of 1, 1, 1-trichloroethene molecule	442
" "	Raman spectra of a few monosubsti- tuted benzene compounds in the solid state and at different low temperatures.	503
" "	Raman spectra of solutions of <i>o</i> -dichloro- benzene in methylcyclohexane	558
Biswas, M. M.	Muonic interactions in dense materials	490
Biswas, N. N.	The dependence of the composite mean life of mu-mesons on the atomic number of the absorber	527
Biswas, S. N.	Fredholm theory and Hankel Trans- form of Schrödinger equation	309
Cadambe, V., Kaul, R. K. and Tewari, S. G.	Flexure of thin elastic plates under specified edge tractions	403
Chakraburty, D. M. and Banerjee B.	An X-ray study on bivalent silver and copper nicotinate compounds	357
Chandratreya, P. V. and Tawde, N. R.	Mass asymmetry effect in Hutchis- son's theory of vibrational transi- tion probabilities	388

Author	Subject	Page
Chaudhury, M. L.	On the deviation of magnetic moments of $S_{\frac{1}{2}}$ nuclei from the Schmidt limit	319
Choudhury, A. K.	The Isograph—an electronic root finder	468
Das, T. P. and Ghosh Roy, S. K.	Spin-echo modulation due to magnetic dipole interaction between a closely interacting pair of nuclei in crystals	272
Datta, S.	Electronic collisional frequency in the F-region over Calcutta	279
Daw, A. N.	A study of transistors connected in parallel	121
Deo, B. B.	Ultrasonic absorption in solutions	352
” ”	Ultrasonic velocity in zinc and magnesium sulphate solutions at different concentrations and temperatures	577
Dhar, S.	On the energy response and resolution of a scintillation counter	329
Dutta, A. K., Samal, K and Patanaik, K. M.	On ultrasonic wattage and spectral number relationship	548
Dutta Roy, S. K.	An improved method of measuring the absolute susceptibilities of single crystals over wide ranges of temperatures	429
Gill, P. S. and Puri, S. P.	Analysis of G-M. counter impulses by the method of delayed coincidences	95
Ghosh, D. K.	Absorption of microwaves and U.H.F. radio waves in phenol, cyclohexanol and 1-bromo 2-chloroethane	161
” ”	On the absorption of 3.18 microwaves in some substituted phenols in the liquid state.	581
” ”	New evidence for the preponderance of cis form in ortho-chlorophenol molecule	450
Ghoshal, S. N. and Saxena, A. N.	Beta energetics and nuclear shell structure	81
Ghosh Roy, S. K. and Das, T. P.	Spin-echo modulation due to magnetic dipole interaction between a closely interacting pair of nuclei in crystals	272

Author	Subject	Page
Haranath, P. B. V. and Rao, P. T.	The emission spectrum of bromine	205
Kaila, K. L. and Saha, N. K.	Source straggling of α -particles from a polonium source	417
Kaila, K. L.	Ionisation loss of α -particles at low energies below 4 Mev.	479
Kapadnis, D. G.	The effect of fluid motion on heat transmission	296
Karmohapatro, S. B.	On two-directional focussing magnetic analysers	393
Kastha, G. S.	Raman spectra of frozen solutions of carbon disulphide in aliphatic solvents	474
Kaul, R. K., Cadambe, V. and Tewari, S. G.	Flexure of thin elastic plates under specified edge traction	403
Krishnamachari, S. L. N. G.	Force-constants of substituted ger- manes. Part I, GeH_3Cl and GeD_3Cl	147
" "	Force-constants of substituted ger- manes. Part II. GeCl_3H and GeCl_4	384
" "	The ultraviolet absorption spectrum of <i>o</i> -fluorochlorobenzene	603
Krishnamachari, S. L. N. G. and Rao, V. R.	Raman spectra of <i>o</i> -chloroethylben- zene	254
Kundu, P.	A wide band frequency-modulated system with asymmetrical 3-phase oscillator	151
Leelavathi, V. and Rao, P. T.	The visible emission spectrum of Se_2 .	1
Madan, M. P.	Diffusion coefficients and law of mole- cular interaction	11
Mallik, M. C. and Rakshit, H. C.	Frequency of the three-phase R-C coupled oscillator	534
Majumdar, K. and Varshni, Y. P.	Spectroscopic constants of molecules. III. Regularities in vibration fre- quencies in a molecular group.	38
" "	Spectroscopic constants of molecules. IV, Similarities in ground state vibration frequencies of isoelectronic diatoms.	285
Mane, H. G.	String under the action of plane rubber wheel.	573

Author	Subject	Page
Mazumder, M.	On the Raman spectra of ethylene chlorhydrin and <i>n</i> -propyl chloride in the vapour state.	361
Misra, S. P.	Baryon meson system in pairs formalism. The scattering matrix—	243
Mitra, A. P.	A method of determining the relative amounts of D- and E- region absorptions of medium and short radio waves	518
Mitra, S. N. and Srivastava, R. B. L.	Analysis of sky-wave field intensity Part. I. 167	
” ”	Analysis of sky-wave field intensity. Part II.	227
Mohanty, B. S. and Deo, B. B.	Ultrasonic velocity in zinc and magnesium sulphate solutions at different concentrations and temperatures	577
Naik, Y. G. and Sohoni, D. K.	Scattering of light by colloidal particles and determination of their size	55
Narasimhan, V.	Magneto-elasticity of polycrystalline iron and nickel	27
Palit, S. R.	Intrinsic viscosity-molecular weight relationship of high polymers. A new equation	65
Patanaiik, K. M., Samal, K. and Dutta, A. K.	On ultrasonic wattage and spectral number relationship	548
Prakash, Yog.	Effect of hypo concentration on the clearing time of thick emulsions	569
Poddar, R. K.	On the quantitative relation between isotopic beta radiation and its photographic response	189
Premaswarup, D.	Vibrational analysis of the tantalum oxide bands	109
Puri, S. P. and Gill, P. S.	Analysis of G-M counter impulses by the method of delayed coincidence	95
Rakshit, H. and Mallik, M. C.	Frequency of three-phase R-C coupled oscillator	534
Rao, D. V. G. L. N.	Calculation of the dipole moments of tri-substituted benzenes	49
	Dipole moments of indene	398
Rao, J. V. R. and Rao, P. T.	The band spectra of thallium iodide and floride.	20

Author	Subject	Page
Rao, P. T. and Leelavati	The visible emission spectrum of Se_2	1
Rao, P. T. and Haranath, P. B. V.	The emission spectrum of bromine	205
Rao, V. R. and Krishnamachari, S. L. N. G.	Raman spectrum of <i>o</i> -chloroethyl benzene	254
Rao, P. T. and Rao, J. V. R.	The band spectra of thallium iodide and fluoride.	20
Saha, N. K. and Kaila, K. L.	Source-straggling of α -particles from a polonium source.	417
Samal, K., Patanaik, K.M. and Dutta A. K.	On ultrasonic wattage and spectral number relationship	548
Saxena, A. N. and Ghoshal, S. N.	Beta energetics and nuclear shell struc- ture	81
Saxena, A. N.	Z_4 term in the mass formula	501
	Higher approximation to diffusion coefficients and determination of force constants	453
Saxena, S. C.	Thermal diffusion of gas mixture and determination of force constants	131
” ”	Thermal conductivity and force bet- ween like molecules	587
Sen, S. K.	Ultraviolet absorption spectra of ortho and para tolunitrile in vapour, liquid and solid states	561
Singh, K. K.	Fermi's statistical theory of pion pro- duction	199
Sodha, M. S.	Shrinkage effect of the close components in spectroscopic instruments	461
Sohoni, D. K. and Naik, Y. G.	Scattering of light by colloidal particles and determination of their size	55
Srivastava, R. B. I. and Mitra, S. N.	Analysis of sky-wave field intensity Part I	167
” ”	” ” ” Part II	227
Tawde, N. R. and Chandratreya, P. V.	Mass asymmetry effect in Hutchisson's theory of vibrational transition probabilities	388
Tewari, S. G., Cadambe, V. and Kaul, R. K.	Flexure of thin elastic plates under specified edge traction	403
Trivedi, N. K. and Vepa, R. K.	Pulse techniques for acoustical measure- ments in broadcast studios.	369
Varshni, Y. P. and	Spectroscopic constants of molecules,	

Author	Subject	Page
Majumdar, K.	III. Regularities in vibration frequencies in a molecular group	38
” ”	Spectroscopic constants of molecules.	
	IV. Similarities in ground state vibration frequencies of isoelectronic diatoms	285
Vepa, R. K. and Trivedi, N. K.	Pulse techniques for acoustical measurements in broadcast studios	369
Venkataraman, S.	A null method of measuring surface tension with a torsion balance	522

SUBJECT INDEX

Subject	Author	Page
Absorption of 3.18 cm microwaves in some substituted phenols in the liquid state. On the	D. K. Ghosh	581
Absorption of microwaves and U.H.F. radio waves in phenol, cyclohexanol and 1-bromo2-chloroethane	D. K. Ghosh	161
Acoustical measurements in broadcast studios. Pulse techniques for	R. K. Vepa and N. K. Trivedi	369
Asymmetrical 3-phase oscillator. A wide-band frequency modulated system with	P. Kundu	151
Band spectrum of thallium iodide and fluoride. The	J. V. R. Rao and P. T. Rao	20
Baryon meson system in pais formalism. The scattering matrix—	S. P. Misra	243
Beta energetics and nuclear shell structure.	S. N. Ghoshal and A. N. Saxena	81
Cis form in the ortho-chlorophenol molecule. New evidence for the preponderance of the	D. K. Ghosh	450
Clearing time of thick emulsions. Effect of hypo concentration on the	Yog Prakash	569
Composite mean life of mu-mesons on the atomic number of the absorber. The dependence of the	N. N. Biswas	527
D- and E- region absorption of medium and short radiowaves. A method of determining the relative amounts of	A. P. Mitra	518
Diffusion co-efficients and law of molecular attraction.	M. P. Madan	11
Diffusion co-efficients and determination of force constants. Higher approximation to	S. C. Saxena	453
Dipole moments of tri-substituted benzenes. Calculation of the	D. V. G. L. N. Rao	49
Dipole moments of indene.	D. V. G. L. N. Rao	398
Electronic collisional frequency in the F-region over Calcutta.	S. Datta	279

Subject	Author	Page
Emission spectrum of bromine.	P. B. V. Haranath	205
Emission spectrum of Se_2 . The visible	V. Leelavati and P. T. Rao	1
Flexure of thin elastic plates under specified edge traction.	V. Cadambe, R. K. Kaul and S. G. Tewari	403
Force constants of substituted ger- manes. Part I. GeH_3Cl and GeD_3Cl	S. L. N. G. Krishnamachari	147
Force constants of substituted germanes. Part II. GeCl_3H and GeCl_4 .	" "	384
Fredholm theory and Hankel transform of the Schrödinger equation.	S. N. Biswas	309
G-M counter impulses by method of delayed coincidences. Analysis of	S. P. Puri and P. S. Gill	95
Heat transmission. The effect of fluid motion on . . Part III	D. G. Kapadnis	296
Hutchisson's theory of vibrational tran- sition probabilities. Mass asymme- try effect in	N. R. Tawde and P. V. Chandratreya	388
Indian ore and minerals by bent mica crys- tal spectrograph. Analysis of some	P. K. Bhattacharyya	292
Intrinsic viscosity-molecular weight relationship of high polymers. A new equation-	Santi R. Palit	65
Ionisation loss of α -particles at low energies below 4 Mev.	K. L. Kaila	479
Isograph—an electronic root finder. The	A. K. Choudhury	468
Isotopic beta radiation and its photo- graphic response. On the quanti- tative relation between	R. K. Poddar	189
Magnetic analyser. On two direc- tional focussing	S. B. Karmohapatro	393
Magnetic moments of S_8 nuclei from Schmidt limits. On the deviation of	M. L. Choudhury	319
Magneto-elasticity of polycrystalline iron and nickel.	V. Narasimhan	27
Multiple pion production. Fermi's sta- tistical theory of	K. K. Singh	199
Muonic interaction in dense materials.	M. M. Biswas	490
p-p Scattering cross-section with energy. On the variation of	C. C. Banerjee	380

Subject	Author	Page
Raman spectra of ethylene chlorhydrin and <i>n</i> -propyl chloride in the vapour state.	M. Mazumder	361
Raman spectra of a few monosubstituted benzene in the solid state at different low temperatures.	D. C. Biswas	503
Raman spectra of <i>o</i> -dichlorobenzene in methylcyclohexane.	D. C. Biswas	558
Raman spectra of frozen solution of carbon disulphide in aliphatic solvents.	G. S. Kastha	474
Raman spectra and fluorescence of a few substituted toluenes in the solid state at different low temperatures	D. C. Biswas	257
Raman spectrum of <i>o</i> -chlorobenzene.	S. L. N. G. Krishnamachari and V. R. Rao	254
Raman spectra of ortho- and meta- dichlorobenzene in different states and different temperatures.	D. C. Biswas	179
Resistivity of Calcutta soil. A study of A. C.	S. P. Bhattacharyya	141
Scattering of light by colloidal particles and determination of their size.	Y. G. Naik and D. K. Sohoni	55
Scintillation counter. Energy response and resolution of a . . . On the	S. Dhar	329
Source-straggling of α -particles from a polonium source.	N. K. Saha and K. L. Kaila	417
Sky-wave field intensity. Analysis of Part I	S. N. Mitra and R. B. L. Srivastava	167
" " " Part II	" "	227
Spectroscopic constants of molecules. III. Regularities in vibration frequencies in a molecular group	Y. P. Varshni and K. Majumdar	38
Spectroscopic constants of molecules. IV. Similarities in ground state vibration frequencies of isoelectronic diatoms.		285
Spectroscopic instruments. Shrinkage effect of close components in	M. S. Sodha	461

Subject	Author	Page
Spin-echo modulation due to dipole interaction between a closely interacting pair of nuclei in crystals.	T. P. Das and S. K. Ghosh Roy	272
String under the action of a plane rubber wheel.	H. G. Mane	573
Surface tension with a torsion balance.		
A null method of measuring	S. Venkataraman	522
Susceptibilities of single crystals over wide ranges of temperatures. An improved method of measuring the absolute	S. K. Dutta Roy	429
Tantalum oxide bands. Vibrational analysis of the	D. Premaswarup	109
Thermal conductivity and force between like molecules.	S. C. Saxena	587
Thermal diffusion of gas mixtures and determination of force constants.	S. C. Saxena	131
Three-phase R-C coupled oscillator. Frequency of the	H. Rakshit and M. C. Mallik	534
Transistors connected in parallel. A study of	A. N. Daw	121
Ultrasonic absorption in solutions.	B. B. Deo	352
Ultrasonic wattage and spectral number relationship.	K. Samal, K. M. Patanaik and A. K. Dutta	548
Ultrasonic velocity in zinc and magnesium sulphate solutions at different concentrations and temperatures.	B. S. Mohanty and B. B. Deo	577
Ultraviolet absorption spectrum of <i>o</i> -fluorochlorobenzene.	S. L. N. G. Krishnamachari	603
Ultraviolet absorption spectra of ortho and para tolunitrile in vapour, liquid and solid states.	S. K. Sen	561
Vibration frequencies of 1,1,1-trichloroethene molecule. An approximate method of calculating the	D. C. Biswas	442
X-ray study of bivalent silver and copper nicotinate compounds. An	D. M. Chakraborty and B. Banerjee	357
Z_4 term in mass formula	A. N. Saxena	501

THE VISIBLE EMISSION SPECTRUM OF Se_2

By V. LEELAVATHI AND P. TIRUVENGANNA RAO

PHYSICS DEPARTMENT, ANDHRA UNIVERSITY, WALT AIR

(Received for publication, August 15, 1954)

Plates I A-B

ABSTRACT. The emission spectrum of Se_2 as excited in a H F. discharge, was photographed on a three-prism glass Littrow spectrograph having a dispersion of 7Å/mm at λ 4000. A new system has been detected in the region $\lambda\lambda$ 5900–6500 in addition to the one reported by Rosen and Montfort in the region $\lambda\lambda$ 5900–5800. A vibrational analysis of the new system has shown that the approximate values of ω_1' and ω_1'' are 270 and 327 cm^{-1} . The system of Rosen and Montfort is also extended to include some more additional bands.

The electronic states in Se_2 are discussed in relation to those of O_2 , S_2 and Te_2 .

INTRODUCTION

The molecular spectrum of selenium has been the subject of numerous investigations in recent years. It was Messerschmitt (1907) who first obtained the spectrum in a discharge through selenium vapour and found that it consists of a large number of bands in the near ultraviolet and visible regions between $\lambda\lambda$ 3700–5900.

Later, Rosen (1927) studied the spectrum in absorption and was the first to propose a vibrational analysis attributing the bands to the diatomic molecule Se_2 . The following formula was deduced.

$$v = 27307 + (247.2 v' - 2.3 v'^2) - (397.5 v'' - 1.32 v''^2)$$

Nevin (1930) confirmed this analysis of Rosen but in addition arranged the emission bands at longer wavelengths into two more systems. The two systems obtained in emission were found by him to have a common final state which is the same as the ground state of the molecule as found in absorption by Rosen. According to Nevin (1930) the spectrum consists of 3 band systems, (1) the α main system observed both in emission and absorption, (2) the β diffuse and (3) the γ green-yellow systems observed in emission.

In a reinvestigation of the emission spectrum of selenium vapour, Rosen and Desirant (1935) and Rosen and Montfort (1936) arranged the bands observed by them into four more systems, three of which were found to have a common lower state, which is the ground state of the molecule and the fourth, an entirely new system, whose initial state is in common with the α -system but has a different final state. One of the systems, referred to as the system of fluctuations was the same as the γ -green yellow system of Nevin but with a different analysis.

A definite advance in our knowledge on the spectrum of Se_2 has been made by Asundi and Parti (1937), who interpreted all the bands except those found in absorption by Moraczewska (1930) and by Rosen and Montfort (loc. cit.) in emission as belonging to one extensive system which is analogous to the extensive main band system of sulphur. In their analysis the γ -bands of Nevin or the so called fluctuation bands of Rosen and Montfort belong to this main system. The new band system in the region $\lambda\lambda 6000-6800$ was represented by the formula

$$\nu = 16706 + 270 \nu' - 2.5 \nu'^2 - 325 \nu'' + \nu''^2.$$

An attempt has been made by Asundi and Parti to include these new bands of Rosen and Montfort in the main system. It was found that such an extension was not possible. Also this new system has not been observed by Asundi and Parti in a transformer discharge. Therefore, according to them the spectrum of Se_2 consists of two systems, 1 and 2 as shown in figure 1 both of which have a common initial level.

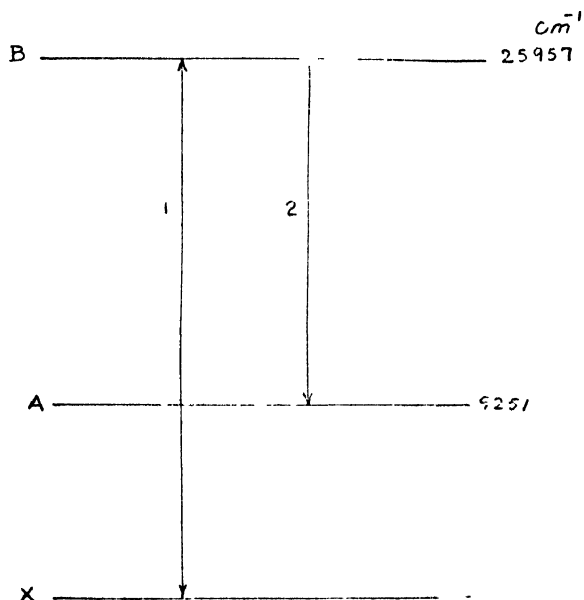


FIG. 1

1. Absorption and emission main band system
2. Bands of Rosen and Montfort in emission

Later, Rosen (1939) reinvestigated the spectrum of Se_2 in emission, absorption and fluorescence in the region $\lambda\lambda 5900-2800$ and gave the vibrational formula :

$$\nu = 25957 + 277.5 \nu' - 2.25 \nu'^2 - 391.5 \nu'' + 1.06 \nu''^2.$$

In this reinvestigation Rosen also found that the so called fluctuation bands interpreted earlier as belonging to a separate system by Rosen and Montfort, belong to bands of the series $\nu' = 7, 8, 9$ and 10 calculated for

the principal system for the isotopic molecules $\text{Se}_{80}\text{Se}_{80}$ and $\text{Se}_{80}\text{Se}_{78}$. They however, concluded that the unresolved patches associated with the fluctuation bands might belong to an independent system.

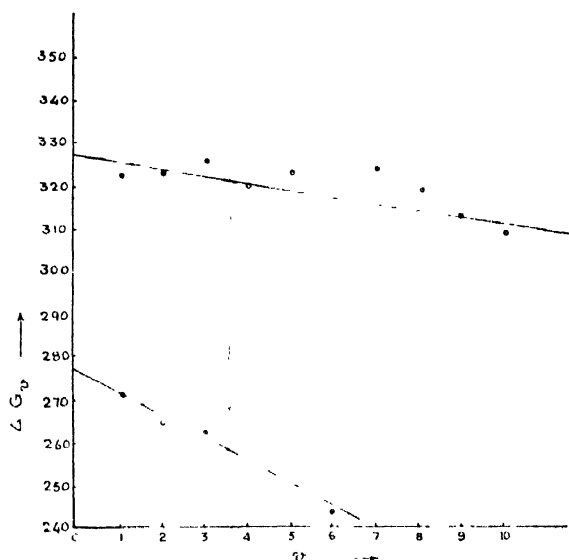


FIG. 2

ΔG_v : v curves for the system of Rosen and Montfort

In addition to the above systems attributed to Se_2 in the near ultraviolet and visible regions, two more systems were reported by Migeotte (1941, 42) in the region $\lambda\lambda$ 1038–1777 both of which have a common ground state.

The present paper describes the results of a reinvestigation by the authors of the emission spectrum of Se_2 in the red and the near infrared primarily with a view to studying the new system of Rosen and Montfort in greater detail. This study has led to the detection of yet another new system of Se_2 whose analysis is presented in the following pages.

EXPERIMENTAL

The method of excitation of the spectrum is by passing a H.F. discharge through low pressure selenium vapour. The experimental set up has been described fully by one of the authors (P. T. Rao, 1949). The spectrum which could also be easily excited in a discharge from a transformer was found to be quite similar to the one excited with the oscillator.

Using Ilford Special Rapid panchromatic plates, exposures varying from 20 to 45 minutes were found sufficient for a good reproduction of the bands on the glass Littrow instrument. With the Feuss spectrograph, an exposure of 3 to 15 minutes duration was found necessary. Bands above λ 6500 were faintly recorded on sensitized infrared plates and were not suitable for measurement.

DESCRIPTION OF THE PLATES

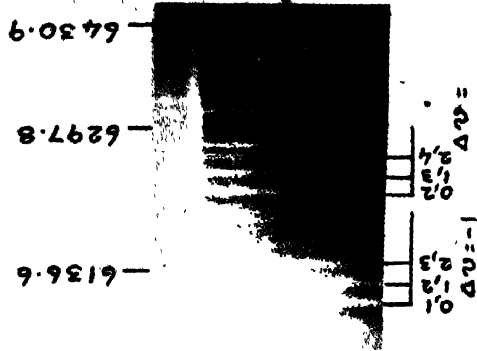
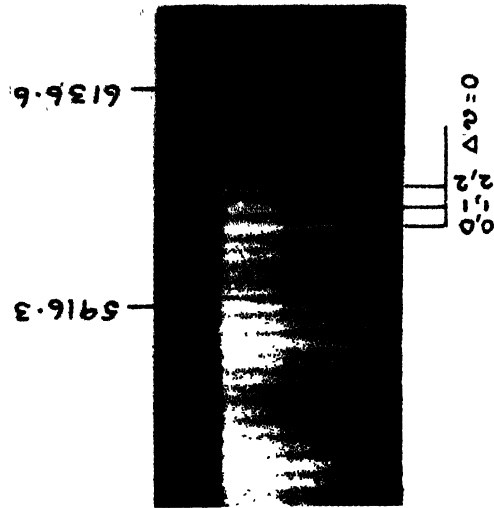
The main system of the spectrum of selenium extends from λ 3800 to λ 5973. The fall in intensity of the main system can be clearly seen from the bands between λ 5930 and λ 5973 which belong to this system. Above λ 5973 there is a general increase in intensity of the spectrum. The so called fluctuation bands of the main system can be seen to extend from λ 4700 to λ 5300. Above λ 5973 the bands appear in four marked distinct groups. These groups were attributed by Rosen and Montfort as belonging to $\Delta v=0, -1, -2$ and -3 sequences of this new system. Some of the bands assigned by them are shown in Plate I A which also clearly shows many more new bands in the $\Delta v=0, -1$ and -2 groups not reported by Rosen and Montfort.

Owing to the narrow spacings of the bands particularly in the $\Delta v=0$ and -1 sequences the spectrum was photographed on a higher dispersion of the three-prism glass Littrow instrument. A doubling was observed in the (0,0), (1,1), (0,1) and (1,2) bands in our plates taken on the glass Littrow spectrograph. A reproduction of the spectrum is shown in Plate I B. In the four groups $\Delta v=0, -1, -2$ and -3 as many as forty five bands could be measured while only twenty of these were assigned to this system by Rosen and Montfort.

VIBRATIONAL ANALYSIS

Table I gives the wavelength, wavenumber and intensity data of bands recorded in the region $\lambda\lambda$ 5970-6500. As these bands above λ 5970 including those of Rosen and Montfort were obtained in the present work under the same conditions of excitation as the main extensive system, the possibility of extending the main system to include the bands was at first considered. As has been remarked by Asundi and Parti it seemed at first possible to include a few bands as the frequency of 327 cm^{-1} might be regarded as the frequency of vibration of the ground state for high v'' values. But it was found that such an extension of their scheme for the main system was not possible. According to Rosen (1939) the well-resolved fluctuation groups belong to progressions with $v'=7, 8, 9$ and 10 calculated for the main system for the $\text{Se}_{80}\text{Se}_{80}$ and $\text{Se}_{80}\text{S}_{78}$. He also reports that bands of $\text{Se}_{80}\text{Se}_{78}$ of the series $v'=10$ coincide approximately with those of $\text{Se}_{80}\text{Se}_{80}$ of the series $v'=7$. A part of his scheme of the main system for the molecule $\text{Se}_{80}\text{Se}_{80}$ is shown in Table II. An extension of this scheme to include bands above λ 5973 was also not found possible. We are therefore of the opinion that the bands of Rosen and Montfort constitute a separate system. The characteristic sequence type of appearance of the system can be clearly seen by reference to Plate I A.

The last column of Table I gives the classification of bands belonging to the system of Rosen and Montfort. Of these, those that are marked



Emission spectrum of Se_2
tem of Rosen and Mount

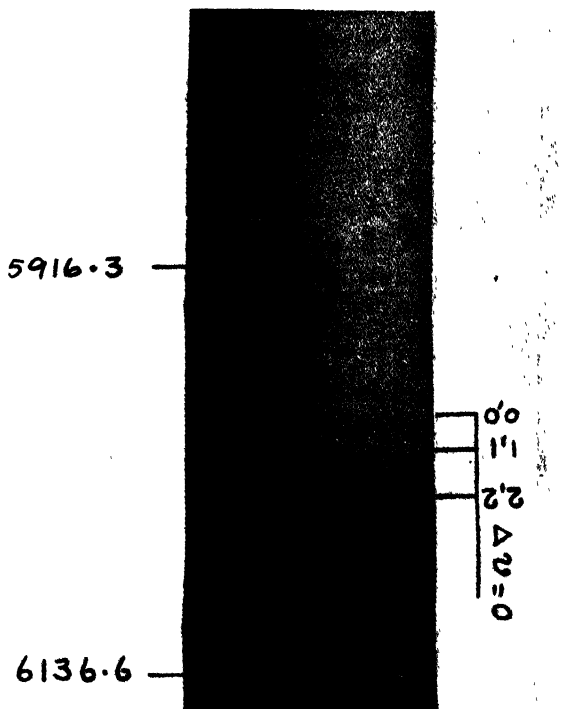


TABLE I

 Se_2 bands between $\lambda\lambda$ 5970–6500

Wavelength	Intensity	Wavenumber	Classification
6460.38	1	15473.7	5,8
6439.40	1	15525.1	4,7
6416.70	1	15580.0	3,6
6391.42	1	15641.7	2,5
6369.93	1	15694.4	1,4
6351.90	1	15738.8	0,3
6328.46	1	15797.3	5,7*
6314.12	1	15833.2	
6302.21	2	15863.1	
6289.76	2	15894.5	3,5
6267.67	3	15950.5	
6264.57	1	15958.4	2,4
6256.47	3	15979.0	
6245.58	4	16006.9	1,3
6233.16	3	16038.8	
6224.40	5	16061.4	0,2
6211.62	0	16091.8	
6203.20	1	16110.3	
6192.80	1	16143.3	
6183.66	0	16167.2	4,5 ^c
6176.49	1	16186.0	
6166.62	3	16211.9	3,4
6157.43	2	16236.1	
6147.81	4	16261.5	2,3
6138.44	2	16286.3	
6129.01	7	16311.3	
6123.07	7	16327.2	1,2
6116.32	1	16345.2	
6108.95	7	16361.9	
6101.88	8	16383.9	0,1
6089.58	3	16417.0	

TABLE I (contd.)

Wavelength	Intensity	Wavenumber	Classification
6078.21	3	16447.7	
6070.35	4	16469.0	
6059.72	3	16497.8	4.4*
6051.50	3	16520.3	
6042.29	5	16545.5	3.3*
6035.23	5	16564.8	
6024.03	6	16595.6	2.2
6014.51	4	16621.9	
6009.75	7	16635.1	
6003.88	8	16651.3	1.1
5991.22	9	16686.5	
5985.80	10	16706.2	0.0
5981.31	3	16714.1	

* These bands are newly assigned in the present work.

with an asterik are newly assigned in the present work. In view of the higher dispersion of the three-prism glass Littrow instrument employed by us, our data were considered more accurate. Using our data upto $\lambda 6500$ the vibrational constants of this system, whose vibrational array is shown in Table III, were calculated by drawing the $\Delta G_r : v$ curves. The estimated constants are

$$\omega_e' = 277, x_e' \omega_e' = 2.8, \omega_e'' = 327 \text{ and } x_e'' \omega_e'' = 0.75.$$

An approximate value of D'' the energy of dissociation of the lower state of the system is obtained as 4.4 eV by using the formula

$$\omega_e'^2 / 4x_e' \omega_e' = D.$$

The last column of Table I clearly shows that there are as many as twentyfive bands which are newly obtained in the present investigation and are not reported by Rosen and Montfort.

A doubling of the bands (0,0), (1,1), (0,1), and (1,2) of the system of Rosen and Montfort was clearly observed on our plates taken on the three-prism glass Littrow instrument. The separations do not seem to suggest a possible interpretation of these as the Q heads, the bands of Rosen and Montfort referred to above being the R heads.

A trial classification of the bands unassigned in the last column of Table I as forming part of the main system proved also futile. These bands might therefore belong to yet another new system, whose origin seems to

be near to that of the system of Rosen and Montfort. A vibrational array of these bands is displayed in Table IV. Only the groups $\Delta v=0, -1$ and -2 are observed in this system.

The classification of these bands is shown in the last column of Table V. It can be seen from Plate I B that members of this system occur in alternate places with those of Rosen and Montfort. The following approximate vibrational constants are suggested for this system.

$$\omega_e' = 270 \text{ and } \omega_e'' = 327$$

The electronic levels so far observed in Se_2 in comparison with those of the related molecule O_2 are discussed in the next section.

DISCUSSION OF ELECTRONIC STATES

The possible molecular terms arising from a combination of two unexcited atoms of selenium each in a 3P state are $^1\Sigma_g^+ (2)$, $^1\Sigma_u^-$, $^1\Pi_g$, $^1\Pi_u$, $^1\Delta_g$, $^3\Sigma_u^+ (2)$, $^3\Sigma_g^-$, $^3\Pi_g$, $^3\Pi_u$, $^3\Delta_u$, $^5\Sigma_g^+ (2)$, $^5\Sigma_u^-$, $^3\Pi_g$, $^3\Pi_u$ and $^5\Delta_g$. One of these terms should represent the ground state of the molecule Se_2 . For a proper understanding of the nature of the electronic states observed in Se_2 , a comparison of these with those of the related molecules O_2 , S_2 and Te_2 is desirable. A schematic diagram of the transitions so far observed in the visible and the near ultraviolet regions for these related molecules is shown in figure 3. The transition B to X represents the main system in each

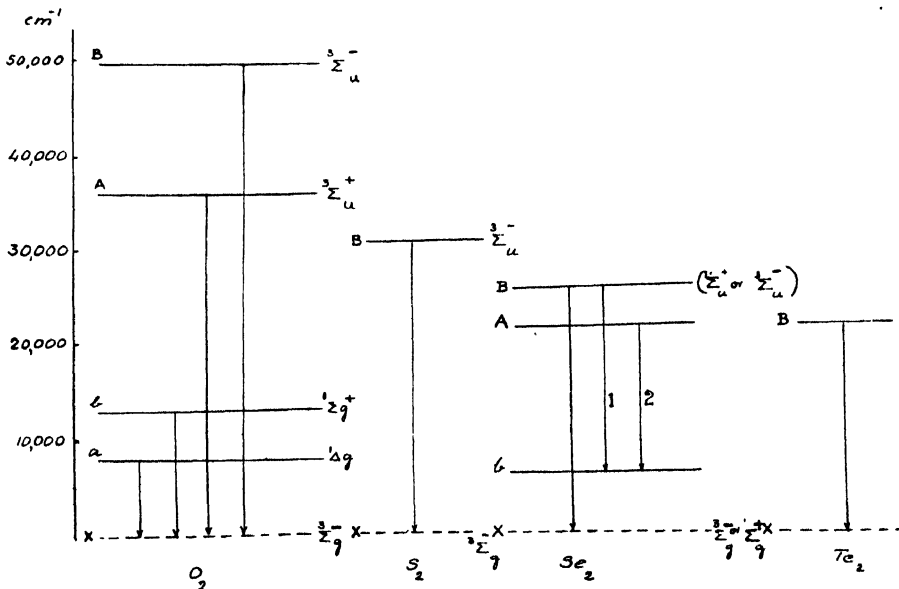


FIG. 3

Scheme of observed transitions in O_2 , S_2 , Se_2 and Te_2

1. System of Rosen and Montfort
2. New system

one of these molecules. While the ground state of the related molecules O_2 and S_2 is definitely known to be $^3\Sigma_g^-$, that of diatomic selenium vapour

may be either a $^3\Sigma_g^-$ or $^1\Sigma^+$. The evidence for considering the ground state of Se_2 as $^3\Sigma_g^-$ is that diatomic selenium vapour is found to be paramagnetic by Bhatnagar, Lessheim and Khanna (1937).

Further, Asundi and Parti (1937) showed that an accurate value of the energy of dissociation *viz.*, 2.7 ± 0.2 eV could be obtained only if the products of dissociation of the upper state *B* are an excited Se atom in a 1D state and an unexcited Se atom in a 3P state. This means that the level *B* must be a triplet level. The level *X* arises from a combination of $\text{Se } ^3P + \text{Se } ^3P$. On this basis the transition *B*–*X* in this molecule would be $^3\Sigma_u^- - ^3\Sigma_g^-$. But Olsson (1938) in his study of the rotational analysis of this system did not find any indication of triplet structure in the *B*–*X* system and attributed the transition *B*–*X* to $^1\Sigma_u^+ - ^1\Sigma_g^+$. Hence the ground state of the Se_2 molecule may be either a $^3\Sigma_g^-$ or $^1\Sigma_g^+$. However, a general comparison of the levels known in O_2 can be made with those of Se_2 .

The lowest electron configuration of the O_2 molecule can be written as $kk(\sigma_g 2s)^2(\sigma_u 2s)^2(\sigma_g 2p)^2(\pi_u 2p)^4(\pi_g 2p)^2$ giving rise to the molecular states $^1\Sigma_g^+$, $^3\Sigma_g^-$ and $^1\Delta_g$. All these three states have been observed for this molecule with $^3\Sigma_g^-$ as the ground state as shown in the figure. The $^1\Delta_g$ state is 0.98 eV, and the $^1\Sigma_g^+$ state is 1.63 eV, above the ground state. The first excited electron configuration of O_2 is $kk(\sigma_g 2s)^2(\sigma_u 2s)^2(\sigma_g 2p)^1(\pi_u 2p)^3(\pi_g 2p)^3$, which gives rise to the molecular states $^1\Sigma_u^+$, $^1\Sigma_u^-$, $^1\Delta_u$, $^3\Sigma_u^+$, $^3\Sigma_u^-$, $^3\Delta_u$. Of these only $^3\Sigma_u^+$ and $^3\Sigma_u^-$ have been identified.

The molecule Se_2 , which has similar electronic structure may be expected to give rise to the same molecular states. The level *b* in Se_2 is analogous to the level $^1\Sigma_g^+$ in O_2 . The system of Rosen and Montfort is due to the transition *B*–*b* since the initial state of their system is the same as the upper state of the main system. The new system reported in this work may have the lower state *b* in common with that of Rosen and Montfort, as the lower state frequency is of the order of 328 cm^{-1} . We may suggest tentatively that the upper state of the new system indicated by the level *A* may be analogous to the level *A* in O_2 .

TABLE II

Rosen's classification of the fluctuation bands due to the Se_{80} Se_{80} molecule

$\nu' \backslash \nu''$	26	27	28	29	30	31	32
7	18316	17980	17640	17306	16980		
8		18221	17889	17550	17215	16877	
9			18124	17785	17459	17123	16784
10				18029	17691	17358	17028

TABLE V
 Se_2 bands (new system)

Wavelength	Intensity	Wavenumber	Classification
6314.12	1	15833.2	4,6
6302.21	2	15863.1	3,5
6207.67	3	15950.5	
6256.47	3	15979.0	
6233.16	3	16038.8	0,2
6212.62	0	16091.8	5,6
6203.20	1	16116.3	
6192.80	1	16143.3	4,5
6176.49	1	16186.0	3,4
6157.43	2	16236.1	2,3
6138.44	2	16286.3	
6129.01	7	16311.3	1,2
6116.32	1	16345.2	
6108.95	7	16364.0	0,1
6089.58	3	16417.0	5,5
6078.21	3	16447.7	
6073.35	4	16469.0	4,1
6051.50	3	16520.3	3,3
6035.23	5	16564.8	2,2
6014.50	4	16621.0	
6009.75	7	16635.1	1,1
5991.22	9	16685.5	0,0

Note : Some of the unassigned bands may belong to the main system.

ACKNOWLEDGMENT

The authors take great pleasure in recording their thanks to Prof. K. R. Rao for his interest in the work.

REFERENCES

- Asundi, R. K. and Parti, Y. P., 1937, *Proc. Ind. Acad. Sci.*, **6A**, 207.
 Bhatnagar, S. S., Lessheim, H. and Khanna, M. L., 1937, *Nature.*, **140**, 152.
 Messerschmitt, J., 1907, *Zeit. Wiss. Phot.*, **8**, 249.
 Migotte, R., 1941, *Bull. Soc. Roy. Sci. Liege.*, **10**, 658-9.

- Migeotc, R., 1942, *Chem. Zentr.*, **1**, 2622.
 Moraczewska, M., 1930, *Zeit. fur. Phys.*, **62**, 270.
 Nevin, T. E., 1930, *Nature.*, **126**, 13.
 Olsson, E., (Stockholm, 1938) Dessertation.
 Rao, P. T. and Rao, K. R., 1949, *Ind. J. Phys.*, **23**, 186.
 Rosen, B., 1927, *Zeit. fur. Phy.*, **43**, 69.
 „ 1939, *Physica.*, **6**, 205.
 Rosen, B. and Desirant, M., 1935, *Bull. Acad. Roy. Belgium.*, 6th April p. 436.
 „ 1935, *Ibid.*, 6th July, p. 723.
 „ 1935, *Nature*, **136**, 913.
 „ 1935, *Bull. Soc. Roy. Liege.*, Nos. 6-7, p. 233.
 Rosen, B. and Montfort, F., 1936, *Physica.*, 3, 257.
 „ 1936, *Bull. Acad. Roy. Belgium*, 1st February p. 215.

DIFFUSION COEFFICIENTS AND LAW OF MOLECULAR INTERACTION

By M. P. MADAN

DEPARTMENT OF PHYSICS, UNIVERSITY OF LUCKNOW.

(Received for publication, September 27, 1954)

ABSTRACT. The experimental data on thermal diffusion and self-diffusion in conjunction with viscosity of various isotopic gases have been examined to study the law of molecular interaction on the basis of an exponential potential energy function, the collision integrals for which have been recently evaluated by Mason. The temperature dependence of thermal diffusion and viscosity has been used to obtain the intermolecular force constants. The results have been compared with those for a Lennard-Jones 12:6 potential and also with those given by Mason from virial, viscosity and crystal properties for an exp: six potential. The agreement is remarkably good. Utilizing the force constants obtained from thermal diffusion, coefficient of self-diffusion has been calculated and compared with the experimental results. From the considerations based on thermal diffusion data, a reason has been suggested for the unsuccessful behaviour of the exp:six potential for non-spherical molecules. The effect of second approximation to the thermal diffusion ratio on the intermolecular force constants has also been studied. It has been found that the conclusions are in accord with the author's statement made in an earlier paper.

1. INTRODUCTION

The best intermolecular potential which has been used to date for the study of the transport properties and their correlation with other properties of gases is of the Lennard-Jones form,* with a repulsion term varying as the inverse twelfth power of the distance of separation between the centre of two molecules and an attraction term varying as the inverse sixth power of separation distance. It is well known that the repulsion energy is more suitably described by an exponential form and therefore a potential energy function containing an exponential term will decidedly be a more realistic potential form than what has been used previously. Recently Mason (1954) has reported the transport property collision integrals for the gases whose molecules obey an exponential: six intermolecular potential of the form

$$E(r) = \frac{\epsilon}{1-6/\alpha} \left[\frac{\alpha}{r} e^{\alpha(1-r/r_m)} - (r_m/r)^6 \right] \quad (1)$$

where $E(r)$ is the potential energy of the molecules at separation distance r , r_m is the value of r for which $E(r)$ is minimum and α is the

* $E(r) = \epsilon \left[(r_m/r)^{12} - 2 \left(\frac{r_m}{r} \right)^6 \right]$, where r_m and ϵ are defined in connection with equation (1) and ϵ is the minimum potential energy.

additional parameter which may be considered a measure of the steepness of repulsion energy. Therefore assuming the validity of such an exponential function, more accurate and reliable information can be obtained about the law of molecular interaction.

Temperature variation of transport and other properties of gases provides a very effective means of evaluating the force constants α , ϵ , and r_m of equation (1). Mason and Rice (1954) have recently evaluated the potential parameters for a few gases using virial, viscosity and crystal properties of gases. As is well known, the coefficient of thermal diffusion is far more sensitive to the type of molecular interaction than the elementary gas coefficients, a determination of the law of molecular interaction from thermal diffusion will be much more accurate and useful than their determination from other properties.

Further, the theory of transport properties of gases as given by Chapman and Cowling (1939) gives only the first approximation expression for the thermal diffusion coefficient. The second approximation involves very complicated algebra and no expression for it has been given so far. Mason (1954) has, however, recently reported the second approximation expression for the thermal diffusion ratio kr .

Keeping the foregoing facts in view, we have, in the present paper, utilized the observed temperature dependence of thermal diffusion to correctly assess the law of force and investigate the effect of second approximation to the thermal diffusion ratio on the intermolecular force constants. However, for the sake of comparison the force constants ϵ and r_m have also been determined by a method, essentially different from that of Mason, using the temperature dependence of viscosity. The potential parameters thus obtained from thermal diffusion and viscosity have been compared with previous determinations by Mason for the exp: six model, including those obtained by Srivastava and Madan (1953a, 1953b) and Hirschfelder *et al* (1954) for the Lennard-Jones 12:6 model. To test the correctness of the force constants obtained, the coefficient of self-diffusion, which is quite sensitive to the force law, has been used to compare the experimental results with those obtained from theory. The results are also compared for the case of Lennard-Jones model using the force constants obtained from thermal diffusion (Srivastava and Madan, 1953 a and b) and from viscosity (Hirschfelder *et. al* (1954).

2. EVALUATION OF THE FORCE CONSTANTS

A. Thermal diffusion coefficient and the effect of second approximation on force constants

The only extensive data on thermal diffusion of gases at different temperatures are those of Stier (1942) for argon and neon. Unfortunately, the data on neon cannot be utilized due to the fact that the observed values

of thermal diffusion ratio for neon at high temperatures are much higher than those predicted by 12:6 model or the exp:six model. The data on thermal diffusion of other gases are much less extensive. However, methane, out of spherical molecules and oxygen and nitrogen out of non-spherical molecules were selected for investigation, the data for which have been reported by Davenport and Winter (1951).

The reduced thermal diffusion ratio k_T^* is given to a first approximation for the case of binary mixtures of heavy isotopes as (Mason, 1954)

$$[k_T^*]_1 = \frac{15}{2} \cdot \frac{(6C^* - 5)(2.1^* + 5)}{A^*(16A^* - 12B^* + 55)} \quad \dots (2)$$

and to a second approximation by

$$[k_T^*]_2 = (5/2) [X_1 X_2 Y_1 - X_3 Y_2] \quad \dots (3)$$

where A^*, B^*, C^* are ratios of the collision integrals given by $A^* = \Omega^{(2,2)*} / \Omega^{(1,1)*}$; $B^* = [5\Omega^{(1,2)*} - 4\Omega^{(1,3)*}] / \Omega^{(1,1)*}$ and $C^* = \Omega^{(1,2)*} / \Omega^{(1,1)*}$; and X_1, X_2, X_3, Y_1, Y_2 are complicated expressions in terms of the collision integrals. These expressions have been given by Mason.

The reduced thermal diffusion ratio $[k_T^*]$ is related to $[k_T]$, the thermal diffusion ratio as

$$[k_T] = [k_T^*] \frac{(M_1 - M_2)}{(M_1 + M_2)} x_1 x_2 \quad \dots (4)$$

where M_1, M_2 are the molecular weights of species 1 and 2 and x_1, x_2 are the mole fractions of the two components. The more frequently encountered R_T , the thermal separation ratio is given by

$$R_T = (118/105) k_T^* \quad \dots (5)$$

With the help of equations (2) and (5) values of R_T for the values of the parameter $\alpha=12$ to $\alpha=17$ were calculated for both first and second approximations (see Table I). Using the experimental data on argon plots were made for the experimental R_T vs. T and theoretical R_T vs. k_T/e , which indicated that the curve for $\alpha=12$ is not in the least in accord with the experimental data and so is the case for the curve $\alpha=13$ but the plot for the value of $\alpha=14$ showed a very good parallelism and agreement with the experimental results. Similar procedure was applied for the case of methane, oxygen and nitrogen, but due to their scanty data it was difficult to arrive at any definite conclusion; nevertheless, methane showed a clear tendency for $\alpha=14$ while the data on O_2 and N_2 showed a tendency for $\alpha>15<16$ and $\alpha>16$ respectively. These values are in excellent agreement with those found by Mason and Rice (1954).

It is interesting to note (see Table I) that the values of R_T for $\alpha>14$ do not show an inversion of sign at low temperatures, while there is sufficient theoretical and experimental evidence that R_T does change sign at low temperatures (Waldman, 1947; Troyer, van Itterbeek and Rietved, 1951; Srivastava and Madan, 1953a), and thus the validity of exp:six potential

for the values of parameter $\alpha > 14$ is open to question. This might be one of the important reasons that Mason and Rice (1954) find the exp: six potential unsuccessful in dealing with non-spherical molecules, which have a tendency for $z > 14$. Therefore, we restricted our detailed investigation only to argon and methane. An extensive data over long temperature range is desirable for a detailed investigation.

For the evaluation of the parameters ϵ and r_m the procedure adopted is analogous to that of Srivastva and Madan (1953a). Experimental thermal diffusion data of Stier (1942) for argon were reduced to obtain the values of R_T at different temperatures T by using the relations $R_T = A - B/T + C/T^2$ and $R_T = A + BT$ at very low temperatures. The two curves R_T vs T (experimental) and R_T vs kT/ϵ (theoretical) were plotted with arbitrarily different T and kT/ϵ scales. Drawing the abscissa for different R_T values we get the corresponding kT/ϵ and T values, from which ϵ is easily determined. These values of ϵ were then utilized in conjunction with the experimental viscosity data at different temperatures to obtain the value of r_m from equation (6). The values of ϵ and r_m were found using both $[R_T]_1$ and $[R_T]_2$, and are given in Table II. The same method was employed to get ϵ and r_m for the case of methane after reducing the data with the help of equation $R_T = R_\infty - B/T$ (Srivastava and Madan, 1953a) the values being given in Table III.

TABLE I

kT/ϵ	$[R_T]_1$			$[R_T]_2$			
	$\alpha = 14$	$\alpha = 15$	$\alpha = 16$	$\alpha = 12$	$\alpha = 13$	$\alpha = 14$	$\alpha = 15$
0.4				-0.0305	0.1765	0.0519	0.0817
0.5				-0.0932	-0.0437	-0.0042	0.0257
0.6	-0.0287	0.0021	0.0382	-0.1166	-0.0777	-0.0288	0.0023
0.7	-0.0302	0.0004	0.0360	-0.1158	-0.0720	-0.0304	0.0006
0.8	-0.0183	0.0117	0.0472	-0.1014	-0.0572	-0.0182	0.0118
0.9	-0.0026	0.0326	0.0674	-0.0775	-0.0356	0.0026	0.0323
1.0	0.0280	0.0568	0.0910	-0.0513	-0.0099	0.0274	0.0560
1.2	0.0836	0.1120	0.1461	0.0780	0.0471	0.0824	0.1103
1.4	0.1397	0.1665	0.2012	0.0652	0.1038	0.1378	0.1647
1.6	0.1909	0.2165	0.2505	0.1180	0.1558	0.1888	0.2117
1.8	0.2355	0.2607	0.2955	0.1659	0.2019	0.2341	0.2595
2.0	0.2746	0.2959	0.3360	0.2068	0.2429	0.2741	0.2995
2.5	0.3514	0.3775	0.4135	0.2888	0.3167	0.3535	0.3798
3.0	0.4054	0.4297	0.4686	0.3487	0.3825	0.4111	0.4371
3.5	0.4437	0.4686	0.5091	0.3898	0.4255	0.4534	0.4798
4.0	0.4720	0.4967	0.5371	0.4238	0.4562	0.4848	0.5107
5	0.5084	0.5347	0.5765	0.4619	0.4987	0.5258	0.5542
6	0.5314	0.5543	0.5968	0.4846	0.5218	0.5520	0.5769
7	0.5439	0.5682	0.6113	0.4961	0.5369	0.5667	0.5936
8	0.5520	0.5762	0.6181	0.5051	0.5459	0.5766	0.6020
9	0.5555	0.5820	0.6261	0.5093	0.5494	0.5822	0.6109
10	0.5589	0.5830	0.6294	0.5098	0.5520	0.5853	0.6120

TABLE II—Argon

[R _T] ₁			[R _T] ₂	
Temp (°K)	ε/k (°K)	r _m (Å)	ε/k (°K)	r _m (Å)
130	116.1	3.900	117.1	3.891
140	117.7	3.905	117.7	3.905
150	120.0	3.886	120.0	3.886
180	120.0	3.889	120.0	3.889
250	127.6	3.835	128.2	3.827
300	136.3	3.791	136.3	3.794
350	142.0	3.777	143.4	3.773
400	147.1	3.766	150.4	3.753
480	147.7	3.770	152.4	3.755
530	148.9	3.776	153.2	3.768

TABLE III—Methane

Temp. range °K	T	R _T	ε/k (°K)	r _m (Å)
195–135	281	0.25	153.5	4.241
295–708	443	0.41	147.7	4.204

Tables I and II show that the difference between [R_T]₁ and [R_T]₂ values is about 7%, which produces a difference of about 1% in the values of ε upto 400°K, while for slightly higher temperatures this difference is within 5%, taking also into account the most probable graphical and computational errors. Though this difference is more pronounced at higher temperatures, we cannot determine its magnitude as the theoretical values practically show no variation in this region; nevertheless it clearly indicates that the error involved in taking R_T = [R_T]₁, i.e., assuming the theoretical value of R_T to be given by [R_T]₁, is considerably less and lies well within the experimental errors in the measurement of R_T and its effect on the values of the intermolecular force constants is almost negligible. This is in agreement with our previous statement (Srivastava and Madan 1953a).

B. Viscosity

The coefficient of viscosity, η, for a single gas is given by

$$\eta \times 10^7 = 266.93(MT)^{1/2} r_m^{-2} [f_n / \Omega^{(2,2)*}], \quad \dots (6)$$

where M is the molecular weight, T is the absolute temperature r_m is the

separation distance for which $E(r)$ is minimum, $\Omega^{(2,2)*}$ is the reduced collision integral and is just the collision integral of Chapman and Cowling divided by its value for rigid spheres of diameter r_m . while f_n represents the infinite series and is a complicated function of the collision integral. This term is nearly unity and is a slowly varying function of kT/ϵ . Mason has tabulated the collision integrals in terms of $Z^{(l,n)}$ and for values of $\alpha=12$ to $\alpha=7$. $Z^{(l,n)}$ is related to $\Omega^{(l,n)*}$ as

$$Z^{(l,n)} = [kT/\epsilon(1-6/\alpha)]^{1/3} \Omega^{(l,n)*} \quad \dots (7)$$

Utilizing his tables $Z^{(l,n)}$ were first converted into $\Omega^{(l,n)*}$ and then the ratio $f_n/\Omega^{(2,2)*}$ which is used for a detailed analysis of viscosity data was calculated for various values of kT/ϵ .

For the evaluation of the force constants from the temperature dependence of viscosity, the method adopted has already been described in detail by Srivastava and Madan (1952a and b), for determining the force constants from self-diffusion and viscosity for the case of 12:6 model. The values of ϵ and r_m are given in Table IV for the gases investigated together with the temperature ranges for which they have been calculated, along with their average mean values.

3. COEFFICIENT OF SELF-DIFFUSION

Mason and Rice (1954) give for the diffusion coefficient the expression

$$D_{12} \times 10^4 = \frac{26.280(T^3(M_1 + M_2)/2M_1M_2)^{1/2}f_n}{Pr_m^2\Omega^{(1,1)*}} \quad \dots (8)$$

in which D_{12} is the coefficient of inter-diffusion in $\text{cm}^2 \cdot \text{sec}^{-1}$ and M_1, M_2 represent here the molecular weights and $\Omega^{(1,1)*}$ and f_n are slowly varying functions of kT/ϵ as already defined in section 2.

Except thermal diffusion coefficient, the coefficient of self-diffusion or inter-diffusion of a gas is much more sensitive to the law of molecular interaction than any other gas coefficient. Utilizing the self-diffusion data of Winn (1950), a comparison of the experimental values has been made with those obtained from theory, using the force constants derived from thermal diffusion both for the exp: six potential, as well as for the Lennard Jones 12:6 potential. Since the experimental data on self-diffusion usually refer to low temperatures values of ϵ and r_m have been selected for the temperature range 100° to 300°K . These values along with values of ϵ and r_m obtained by Srivastava and Madan (1953a and b), Hirschfelder et al (1954) for the 12:6 potential including those obtained by Mason and Rice (1954) for the exp: six potential are given in Tables V and VI.

The data of Winn (1950) give D_{11} which is calculated from the relation

$$D_{11} = [2M_2/(M_1 + M_2)]^{1/2} [D_{12}] \quad \dots (9)$$

but the quantity actually measured by him is the inter-diffusion of one

isotope into the other. So the value of D_{12} was calculated and converted to give D_{11} with the help of equations (8) and (9) and are given in Table VII. For the sake of comparison values obtained by Hirschfelder *et al* (1954) using the force constants obtained from viscosity data have also been listed in this table.

TABLE IV

Argon			Methane		
Temp. range (°K)	ϵ/k (°K)	r_m (Å)	Temp. range (°K)	ϵ/k (°K)	r_m (Å)
150-300	122.9	3.865	100-300	122.0	4.351
150-450	122.9	3.865	150-300	136.3	4.308
200-400	128.2	3.838	200-400	166.5	4.122
200-600	119.8	3.890	200-600	169.4	4.104
250-500	118.5	3.883	250-750	168.9	4.133
Mean	122.46	3.868	Mean	152.2	4.203

TABLE V

Exp. : six potential.

	From thermal diff. (present work)			From virial viscosity and crystal properties (Mason and Rice, 1954)			From the tempera- ture dependence of viscosity.	
	α	ϵ/k	r_m	α	ϵ/k	r_m	ϵ/h	r_m
Argon	14	122.9	3.868	14	123.2	3.866	122.45	3.868
Methane	14	150.5	4.222	14	152.8	4.206	152.20	4.203

TABLE VI

12:6 Potential

	From thermal diff. (Sri- vastava and Madan 1953a, b)		From viscosity (Hir- schfelder <i>et al</i> , 1954)		From self-diff. (Sri- vastava and Madan, 1952b)	
	ϵ/k	r_m	ϵ/k	r_m	ϵ/k	r_m
Argon	124.9	3.842	124	3.837	125.5	3.801
Methane	156.7	4.150	156.5	4.250	154.1	4.006

separation distance for which $E(r)$ is minimum, $\Omega^{(2,2)*}$ is the reduced collision integral and is just the collision integral of Chapman and Cowling divided by its value for rigid spheres of diameter r_m . while f_n represents the infinite series and is a complicated function of the collision integral. This term is nearly unity and is a slowly varying function of kT/ϵ . Mason has tabulated the collision integrals in terms of $Z^{(l,n)}$ and for values of $\alpha=12$ to $\alpha=7$. $Z^{(l,n)}$ is related to $\Omega^{(l,n)*}$ as

$$Z^{(l,n)} = [kT/\epsilon(1-6/\alpha)]^{1/3} \Omega^{(l,n)*} \quad \dots (7)$$

Utilizing his tables $Z^{(l,n)}$ were first converted into $\Omega_j^{(l,n)*}$ and then the ratio $f_n/\Omega^{(2,2)*}$ which is used for a detailed analysis of viscosity data was calculated for various values of kT/ϵ .

For the evaluation of the force constants from the temperature dependence of viscosity, the method adopted has already been described in detail by Srivastava and Madan (1952a and b), for determining the force constants from self-diffusion and viscosity for the case of 12:6 model. The values of ϵ and r_m are given in Table IV for the gases investigated together with the temperature ranges for which they have been calculated, along with their average mean values.

3. COEFFICIENT OF SELF-DIFFUSION

Mason and Rice (1954) give for the diffusion coefficient the expression

$$D_{11} \times 10^4 = \frac{26.280(T^3(M_1 + M_2)/2M_1M_2)^{1/2}f_n}{Pr_m^2\Omega^{(1,1)*}} \quad \dots (8)$$

in which D_{12} is the coefficient of inter-diffusion in $\text{cm}^2 \cdot \text{sec}^{-1}$ and M_1 , M_2 represent here the molecular weights and $\Omega^{(1,1)*}$ and f_n are slowly varying functions of kT/ϵ as already defined in section 2.

Except thermal diffusion coefficient, the coefficient of self-diffusion or inter-diffusion of a gas is much more sensitive to the law of molecular interaction than any other gas coefficient. Utilizing the self-diffusion data of Winn (1950), a comparison of the experimental values has been made with those obtained from theory, using the force constants derived from thermal diffusion both for the exp: six potential, as well as for the Lennard Jones 12:6 potential. Since the experimental data on self-diffusion usually refer to low temperatures values of ϵ and r_m have been selected for the temperature range 100° to 300°K . These values along with values of ϵ and r_m obtained by Srivastava and Madan (1953a and b), Hirschfelder et al (1954) for the 12:6 potential including those obtained by Mason and Rice (1954) for the exp: six potential are given in Tables V and VI.

The data of Winn (1950) give D_{11} which is calculated from the relation

$$D_{11} = [2M_2/(M_1 + M_2)]^{1/2} [D_{12}] \quad \dots (9)$$

but the quantity actually measured by him is the inter-diffusion of one

isotope into the other. So the value of D_{12} was calculated and converted to give D_{11} with the help of equations (8) and (9) and are given in Table VII. For the sake of comparison values obtained by Hirschfelder *et al* (1954) using the force constants obtained from viscosity data have also been listed in this table.

TABLE IV

Argon			Methane		
Temp. range (°K)	ϵ/k (°K)	r_m (Å)	Temp. range (°K)	ϵ/k (°K)	r_m (Å)
150-300	122.9	3.865	100-300	122.9	4.351
150-450	122.9	3.865	150-300	136.3	4.308
200-400	128.2	3.838	200-400	166.7	4.122
200-600	119.8	3.890	200-600	169.4	4.104
250-500	118.5	3.883	250-750	168.9	4.133
Mean	122.46	3.868	Mean	152.2	4.203

TABLE V

Exp.: six potential.

	From thermal diff. (present work)			From virial viscosity and crystal properties (Mason and Rice, 1954)			From the tempera- ture dependence of viscosity.	
	α	ϵ/k	r_m	α	ϵ/k	r_m	ϵ/h	r_m
Argon	11	122.9	3.868	11	123.2	3.866	122.45	3.868
Methane	14	150.6	4.222	14	152.8	4.206	152.30	4.203

TABLE VI

12:6 Potential

	From thermal diff. (Sri- vastava and Madan 1953a, b)		From viscosity (Hir- schfelder <i>et al</i> , 1954)		From self-diff. (Sri- vastava and Madan, 1952b)	
	ϵ/k	r_m	ϵ/k	r_m	ϵ/k	r_m
Argon	124.9	3.842	124	3.837	125.5	3.801
Methane	156.7	4.150	136.5	4.290	154.1	4.096

TABLE VII
 D_{11} in $\text{cm}^2 \cdot \text{sec}^{-1}$

	Temp °K	Exp. : six	12 : 6 (Present work)	12 : 6 (Hirschfelder et.al. 1954)	Exptl.
Argon	353.2	0.247	0.245	0.245	0.249
	295.2	0.178	0.177	—	0.178
	273.2	0.155	0.154	0.154	0.156
	194.7	0.0824	0.0815	—	0.0830
	90.2	0.0181	0.0178	—	0.0180
	77.7	0.0134	0.0132	0.0133	0.0134
Methane	353.2	0.308	0.309	0.293	0.318
	298.2	0.226	0.227	—	0.240
	273.2	0.192	0.192	0.183	0.206
	194.7	0.100	0.100	—	0.0992
	90.2	0.0216	0.0214	0.0187	0.0265

4. DISCUSSION OF RESULTS

A comparison of the force constants obtained by using different methods (see Table V) shows that the values of ϵ and r_m from thermal diffusion and viscosity by the present author are in excellent agreement with those reported by Mason and Rice (1954).

A comparison of the calculated and observed values of coefficient of self-diffusion (see Table VII) reflects that the agreement is very good for both argon and methane and is definitely somewhat better for the case of argon based on an exp:six potential though the experimental errors in the measurement of self-diffusion coefficient forbid arriving at a definite conclusion. Nevertheless there is a clear indication of the superiority of exp:six potential over the 12:6 potential. For the case of methane, lack of experimental data on thermal diffusion over a wide temperature range makes it impossible to establish the supremacy of one potential over the other. However, it may be remarked that Mason and Rice (1954) find a very poor agreement for the case of methane using the force constants from virial, viscosity and crystal properties. Even for the case of 12:6 potential, it is clear from Table VII that the values calculated by us are more in accord with the experimental data than those calculated by Hirschfelder et al (1954) using force constants from viscosity.

It is interesting to note from Table II, that ϵ and r_m show a slight variation with temperature. In the case of viscosity, as the calculations are made

for various small ranges, and further because the viscosity is not so sensitive to the force law as thermal diffusion, this variation is not so marked. Similar variation in the values of the force constants have been noted by Srivastava and Madan (1953a), Keyes (1951) and Whalley and Schneider (1952). Srivastava and Madan have also given reasons for this variation based on the Lennard-Jones 12:6 potential. No conclusions can be arrived at the present stage regarding the variation of these force constants with temperature. This requires a more thorough investigation by properly pooling together all the transport properties. Whether this variation in the values of ϵ and r_m mean that the force field is temperature dependent or is simply a reflection on the inadequacy of the potential form chosen, also, awaits a confirmation of Stier's thermal diffusion data along with an additional accurate and extensive experimental data over a wide temperature range for other gases.

ACKNOWLEDGMENTS

It is great pleasure to thank Prof. B. N. Srivastava, of the Indian Association for the Cultivation of Science Calcutta, for useful advice and encouragement and to Prof. P. N. Sharma (Lucknow) and Prof. J. O. Hirschfelder (Wisconsin) for much help and continued interest in the work presented here.

REFERENCES

- Chapman, S. and Cowling, T.G., 1939, 'The Mathematical theory of non-uniform gases' (Cambridge Univ. Press).
- Davenport, A.N., and Winter, E.R.S., 1951, *Trans. Farad. Soc.*, **47**, 1169.
- Hirschfelder, J.O., Curtiss, C.F., Bird, R., and Spatz, E.L., 1951, 'The Molecular theory of Gases and Liquids' (John Wiley and Sons, New York).
- Keyes, F.G., 1951, *Trans. Amer. Soc. Mech. Engrs.*, **73**, 589.
- Mason, E.A., 1954, *J. Chem. Phys.*, **22**, 169.
- Mason, E.A., and Rice, W.E., 1954, *J. Chem. Phys.*, **22**, 843.
- Srivastava, B.N., and Madan, M.P., 1952a, *Phil. Mag.*, **43**, 958.
- „ 1952b, *Proc. Nat. Acad. Sci.*, **21**, 254.
- „ 1953a, *J. Chem. Phys.*, **21**, 807.
- „ 1953b, *Proc. Phys. Soc. (London)*, **A 66**, 277.
- Stier, L., 1952, *Phys. Rev.*, **62**, 548.
- Troyer, A., van Itterbeek, A., and Rietveld A.O., 1951, *Physica*, **17**, 938.
- Waldman, Z., *Naturforsch. A*, 1947, **2**, 358.
- Whalley, E., and Schneider, W.G., 1952, *J. Chem. Phys.*, **21**, 657.
- Winn, E.B., 1950, *Phys. Rev.*, **80**, 1024.

THE BAND SPECTRA OF THALLIUM IODIDE AND FLUORIDE

By J. V. RAMANA RAO AND P. TIRUVENGANNA RAO

DEPARTMENT OF PHYSICS, ANDHRA UNIVERSITY, WALTAIR

(Received for publication, August 16, 1954)

Plates II A-B

ABSTRACT. The band spectra of TII and TIF are reinvestigated in emission in a high frequency discharge under higher dispersion than that employed previously. The analysis of the main system of TII proposed by P. T. Rao and K. R. Rao, has been confirmed. Using the more accurate data obtained in the present work, the following constants have been deduced.

$$\nu_e = 26362.4 \quad \omega_e' = 93.7 \quad x_e' \omega_e' = 0.107$$

$$\omega_e'' = 123.2 \quad x_e'' \omega_e'' = 0.088$$

In each one of these halides a new system has been detected. A vibrational analysis has also been proposed for each, which shows that the lower state is the ground state of the molecule.

The present work is a continuation of a series of investigations carried out by P. T. Rao and K. R. Rao (1949) and P. T. Rao (1950) on the halides of thallium. The characteristic band systems so far observed in each of these halides are briefly summarized in Table I.

EXPERIMENTAL

Recording of the spectrum of TII.

The experimental technique is the same as that employed by Rao and Rao (1949) in the previous investigation. But the low power oscillator (5 watts) used by them to excite the spectrum is replaced by a high power oscillator (100 watts) in the present work. A marked improvement in the structural appearance of the bands is noticed when this source is used. The spectrum is photographed on the following instruments: (1) 10ft. concave grating spectrograph—first order. (2) Three prism glass Littrow spectrograph, and (3) Fuess spectrograph. Exposures for about three to four hours on the grating spectrograph, half an hour on the glass Littrow spectrograph and about fifteen minutes on the Fuess spectrograph gave good pictures. The photographs taken on the above instruments are shown in Plates IIA and IIB.

Description of the Spectrum.

Plate IIB, figure 5 gives the general appearance of the spectrum from $\lambda 6300$ to $\lambda 3800$. The fall in the general intensity above $\lambda 4500$ and the increase in the intensity of the bands above $\lambda 5500$ clearly suggests the occurrence of a new system above $\lambda 5500$ which will be described later.

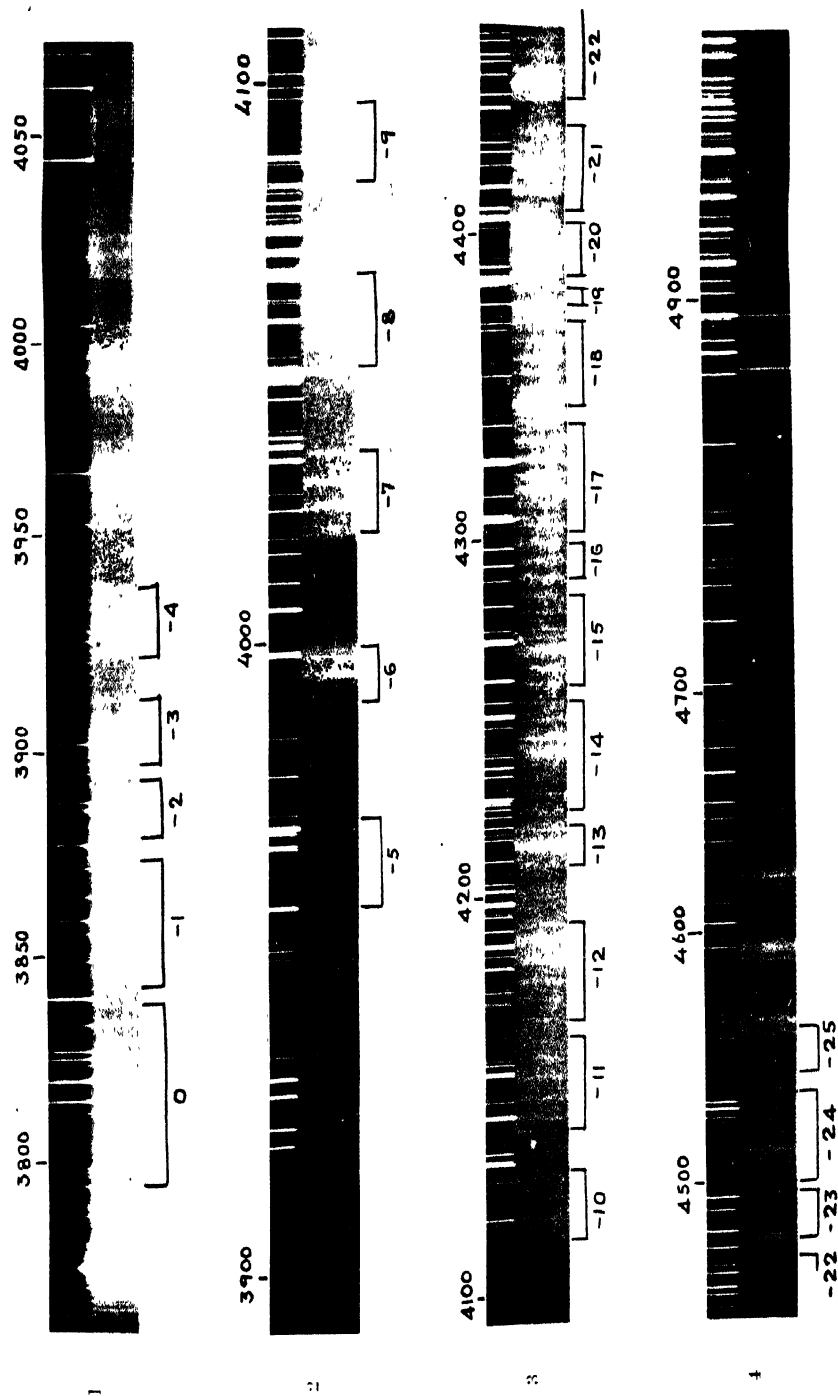


Fig. 1—Grating spectrogram. Figs. 2, 3, 4—Glass Littrow spectrograms



Fig. 5—Thallium iodide bands, system 31 — Σ — Fuess spectrograph (overall picture).
 Fig. 6—TlI bands (6338 Å — 5577 Å), Fuess spectrogram.
 Fig. 7—TlF bands (3500 Å — 3400 Å), (Quartz Littrow spectrogram).

TABLE I

Molecule	Author	Region	Transition
TlF	Butkow and Boizowa	$\lambda 2200$ (Absorption continuum)	
	Howell and Coulson	$\lambda 2350 - \lambda 2200$	$^1\Pi \rightarrow ^1\Sigma^+$
	"	$\lambda 2800 - \lambda 2600$	$^3(\pi)^+ \rightarrow ^1\Sigma^+$
	"	$\lambda 3100 - \lambda 2800$	$^3I \rightarrow ^3\Sigma^+$
TlCl	Butkow, Howell and Coulson	$\lambda 3400 - \lambda 3200$	$^3I \rightarrow ^1\Sigma^+$
	"	$\lambda 2545 - \lambda 2475$ (Absorption continuum)	
	"	$\lambda 3105$ (Absorption continuum)	
	Howell and Coulson	$\lambda 2890$ (Absorption continuum)	
	P. T. Rao	$\lambda 4150 - \lambda 3800$	
TlBr	"	$\lambda 4300 - \lambda 4150$	
	Butkow, Howell and Coulson	$\lambda 4500 - \lambda 0500$	$^3I \rightarrow ^1\Sigma^+$
	"	$\lambda 5330$ (Absorption continuum)	
	Howell and Coulson and P. T. R.	$\lambda 4000 - \lambda 3950$	
	"	$\lambda 4050 - \lambda 3800$	
TII	P. T. R. and K. R. R.	$\lambda 5300 - \lambda 3800$	$^3I \rightarrow ^1\Sigma^+$
	"	$\lambda 3700 - \lambda 3600$	$^3\Pi_0^+ \rightarrow ^1\Sigma^+$

Plate IIA, figure 1 is a grating spectrogram and figures 2, 3 and 4 are reproductions of photographs taken on the three prism glass Littrow instrument.

The main system attributed to the transition $^3I - ^1\Sigma^+$ extends from $\lambda 3800 - \lambda 5300$ consisting of about 200 bands. Further description of the spectrum is not necessary here as it is well described in Rao and Rao's paper (1949).

A brief system occurring in the region $\lambda 5500 - \lambda 6300$ shown in Plate IIB, figure 6, consisting of about 25 bands is also ascribed to the thallium iodide molecule.

Vibrational Constants.

From a study of the absorption spectrum of the molecule, Rao and Rao

were able to locate the $\Delta v=0$ sequence between $\lambda_{3795.4}$ and $\lambda_{3838.6}$. This necessitated a change in v' , v'' numbering of the bands which is adopted here.

The source of error involved in the determination of the vibrational constants arises from the absence of long progressions or sequences and the very low value of the anharmonicity constants. Most of the $\Delta G(v)$ values are obtained as differences from few band heads. The measurement of the individual band heads should, therefore, be very accurate in the determination of the vibrational constants. As such, a number of plates are taken on the grating spectrograph and for measurements in the region λ_{3800} to λ_{4000} these plates are used. Above λ_{4000} the bands are found unsuitable for measurement on the plates taken on the grating and, therefore, plates taken on the three-prism glass Littrow spectrograph are measured. Band head data upto λ_{4500} are only used in the calculation of the vibrational constants as the bands upto this limit can be accurately measured.

Adopting the same scheme of classification (Rao and Rao, 1949) a graphical method has been employed to estimate the constants for the upper and the lower states. The estimated constants are

$$\omega_e' = 93.7 \quad x_e' \omega_e' = 0.107$$

$$v_e = 26362.4$$

$$\omega_e'' = 123.2 \quad x_e'' \omega_e'' = 0.088$$

The system origin is calculated from the measurements of several bands in the entire range. There is a close agreement between the observed and calculated values of the wave numbers.

Determination of D' of TII.

The ground state of TII may be assumed to arise from a combination of two neutral atoms ($\text{Tl } ^2P + \text{I } ^2P$) and the upper state from a combination of (ex $\text{Tl } ^2S + \text{unex I } ^2P$). If this assumption is correct the energy of dissociation of the ground state (D'') can be deduced indirectly as follows. The value of D' is determined by Birge and Spomer's method. Using this value of D' , D'' is obtained from the following formula

$$v_0 + D' = D'' + v_{\text{atom}}.$$

The value of v_{atom} is the difference between the ground term $^2P_{1/2} = 49264.2$ and the first excited state $^2S = 22786.7$ of Tl, I.

$$v_{\text{atom}} = 26477.5 \text{ cm}^{-1}$$

$$D' = 20513.8$$

From the values of v_e , D' and v_{atom} , D'' is obtained as equal to 20398.2 cm^{-1} and in electron-volts it is equal to 2.53. This value is found to be in good agreement with the thermochemical and atomic fluorescence data.

DISCUSSION OF THE ANALYSIS

The main difficulty experienced by Rao and Rao in the vibrational analysis of the main system of TII is in respect of the magnitude of the

values of ω_e' and ω_e'' . Several alternatives of choice are available. The interval of about 30 cm^{-1} between the equispaced components in each sequence suggests the approximate value of the difference between ω_e' and ω_e'' . The individual values may be any one of the following sets.

ω_e'	ω_e''
90	120
120	150
150	180
180	210

Of these Rao and Rao preferred the set 90 and 120 from a comparison of the ground state constants of the halides of mercury, thallium, lead and bismuth and also from a comparison of the vibrational constants of thallium halides. Petrikaln and Hochberg (1933) have quoted a value 150 for ω_e'' . The agreement between the deduced value of the energy of dissociation and its value derived from other methods (thermochemical and atomic fluorescence methods) shows that the set of constants 90 and 120 is the most probable one. However, the value of D'' deduced directly from Birge and Sponer's method using the value of 123.2 for ω_e'' is somewhat high. In case a value for ω_e'' of the order of 150 is adopted, D'' would be still higher and deviate far from the true value. It is, therefore, believed that 120 is the right order of magnitude for ω_e'' .

New Observations in the Band Spectrum of Thallium Iodide.

As shown in Plate IIB, figure 5 the increase in the general intensity of the spectrum above $\lambda 5500$ suggests that the bands in the region $\lambda 5550 - \lambda 6340$ might belong to a new system arising in a new electronic transition. In obtaining these bands great care has been taken to suppress the emission bands of iodine which occur in the same region. These iodine bands are recorded on some of the plates when there is a slight leak in the vacuum system. Further optimum conditions of heating the discharge tube are found necessary for a good reproduction of the bands. These bands are shown in Plate IIB, figure 6.

There are about 25 bands, most of which are broad and diffuse, their direction of degradation being uncertain. A tentative vibrational scheme has been proposed for these bands as shown in Table II. A clue for the analysis has been afforded by the ground state progression with $v'=0$. The lower state of this system appears to be common to that of the main system. The approximate values for the vibrational constants are as follows.

$$\begin{aligned}\omega_e' &\sim 79 \\ \omega_e'' &\sim 126\end{aligned}$$

TABLE II

λ	0	1	2	3	4	5	6	7	8	9	10	11	ΔG°
0					16635 S 76.3	145.1	145.4	16376.3	16252.8	16134.0	16010.2	15891.6	15772.0
1		17070.7 75.8		16839.8	127.7								76.3
2	17279.5 80.7	17156.5											76.8
3	17360.2 72.1												80.7
4	17432.3 67.1												72.1
5	17499.4 74.8												67.1
6	17574.2												74.8
ΔG°	123.0		127.7	124.1	125.4	123.8	118.8	113.5	108.8	103.8	98.6	93.6	119.6

The wavelength and other data of the bands are shown in Table III.

The Band spectrum of Thallium fluoride.

The band spectrum of thallium fluoride was extensively studied both in emission and in absorption by Howell (1937) as a part of a series of investigations on the molecular spectra of heavy diatomic fluorides HgF, TlF, PbF and BiF. The band systems reported and analysed by him are briefly summarized in Table IV.

TABLE III

Wavelength	Int.	Wavenumber	Classification
6338.6	2	15772.0	0,11
6306.7	2	15851.8	
6290.9	2	15891.6	0,10
6244.3	2	16010.2	0,9
6196.4	2	16134.0	0,8
6151.1	2	16252.8	0,7
6134.1	2	16297.8	
6104.7	2	16376.3	0,6
6069.7	2	16470.7	
6058.3	3	16511.7	0,5
6013.1	5	16625.8	0,4
5985.6	5	16702.1	1,4
5962.0	5	16768.3	
5940.2	5	16829.8	1,3
5922.3	5	16880.7	
5871.8	3	17025.8	
5853.3	3	17079.7	1,1
5827.1	3	17156.5	2,1
5785.6	3	17279.5	2,0
5758.7	2	17360.2	3,0
5734.9	3	17432.3	4,0
5712.9	3	17499.4	5,0
5688.6	3	17574.2	6,0
5663.7	4	17651.4	
5577.0	2	17925.8	

TABLE IV

Level	ν_e	ω_e	$x_e \omega_e$
$^1\Pi$	455 ⁽¹⁰⁾	360	—
$^3(0)_+$	36869.5	360.65	12.25
3I	35180.7	439.87	8.60
$^1\Sigma$	0	475.00	1.89

No band systems corresponding to those observed in TlCl and TlBr by P. T. Rao (1950), Howell and Conlson, or to those reported for TlI in the present work are so far reported for this molecule. As a continuation of the work on TlI bands the authors photographed the spectrum of TlF in

the visible and near ultraviolet regions, under the same experimental conditions of excitation employed for photographing the TII spectrum.

Characteristic bands attributable to TIF were recorded in the region $\lambda_{3400}-\lambda_{3500}$, some of which have a similar appearance to those observed by Howell in the region $\lambda_{2800}-\lambda_{3200}$ analysed into two systems. These bands were also recorded on our plates. Plate IIB, figure 7 is a reproduction of the brief system obtained in the present investigation. There are about 7 bands. A peculiarity of the appearance of the bands observed by Howell is the occurrence of the so called "absorption lines" in the emission spectrum which were interpreted by him as the gaps produced by the missing lines around the band origins. The same peculiarity is noticed in the 0,0 and 0,1 bands of the present system for which a brief vibrational array is shown in Table V. The lower state of the system appears to be the ground state and the same as the lower state of the two ultraviolet systems. This system is then analogous to the new system reported for TII in the present work.

TABLE V

v'	v''	0		1		2	$\Delta G(v')$
0		29208.4	477.3	28731.1 191.3 28922.4	470.1		191.3
1						28452.0 185.2	185.2
2			477.3		470.4	28637.2	
$\Delta G(v'')$							

The following are the approximate values for ω_e' and ω_e''

$$\omega_e' \sim 194$$

$$\omega_e'' \sim 481$$

ACKNOWLEDGMENT

The authors take great pleasure in recording their thanks by Prof. K. R. Rao for his interest in the work.

REFERENCES

- Butkow, K., 1929, *Zeit. f. Physik.*, **58**, 232.
 Holst, W., 1934, *Zeit. F. Physik.*, **93**, 65.
 Howell, H. G., 1937, *Proc. Roy. Soc.*, **160**, 242.
 Howell, H. G., and Coulson, N., 1938, *Proc. Roy. Soc.*, **166**, 238.
 Howell, H. G., and Coulson, N., 1941, *Proc. Phys. Soc.* **53**, 706.
 Jennergren Carl Gustav, 1948, *Nature*, **161**, 315.
 Miescher, E., and Wehrli, M., 1934, *Helv. Phys. Acta.*, **73**, 293.
 Miescher, E., and Wehrli, M., 1935, *Helv. Phys. Acta.*, **8**, 279.
 Petrikaln, R., and Hochberg, J., 1923, *Zeit. f. Physik.*, **86**, 214.
 Ramasastry, C., 1947, *Ind. Jour. Phys.*, **21**, 272.
 Tiruvenganna Rao and K. R. Rao, 1948, *Curr. Sci.*, **17**, 121.
 Tiruvenganna Rao and K. R. Rao, 1948, *Curr. Sci.*, **17**, 182.
 Tiruvenganna Rao and K. R. Rao, 1949, *Ind. Jour. Phys.*, **23**, 185.
 Tiruvenganna Rao, 1950, *Ind. Jour. Phys.*, **24**, 432.

MAGNETO-ELASTICITY OF POLYCRYSTALLINE IRON AND NICKEL *

By V. NARASIMHAN†

PRESIDENCY COLLEGE, MADRAS

(Received for publication, September, 27, 1954)

ABSTRACT. Some of the experiments for the determination of changes in the elastic moduli of polycrystalline iron and nickel are described. The results are compared with those derived from Akulov's theory of the ΔE effect in ferromagnetics.

1. INTRODUCTION

It is well known that the elastic properties of ferromagnetic metals and their alloys undergo a systematic variation under the action of a magnetic field. Several interesting experiments have been described in the literature. Attention has been drawn particularly to the existence of the changes in the Young's modulus under the name of the ΔE effect. Many experiments have been conducted for the measurement of the changes in the Young's modulus of pure metals and their alloys of the ferromagnetic class. The methods fall under two categories viz., the statical type and the dynamical oscillatory type. In the former type, the work of Honda and Terada (1907) may be classed, while the experiments of Seigel and Quimby (1936), Cooke (1936) and Brown and Auwers (1935) belong to the latter method. The dynamical method consists in exciting the ferromagnetic specimen with a quartz oscillator, it becomes quite admirable for measurements on single crystals.

The development of the modern theory of ferromagnetism by Heisenberg (1928), Akulov (1933) and others, and the discovery of the existence of the 'domains' in ferromagnetic bodies have given further impetus to work on the behaviour of ferromagnetic materials under the action of stress and magnetic field. Akulov (log. cit.) has derived two formulae connecting the changes in the Young's modulus with the intensity of the applied magnetic field. Further deductions by Brown (1936) enable the changes in the modulus of rigidity of ferromagnetics due to the influence of a magnetic field to be estimated.

These formulae apply to the case of a polycrystalline quasi-isotropic ferromagnetic body in a strain-free state. Verification of these formulae have been attempted by several of the authors quoted above, by the dynamical

* Thesis approved by the University of Madras for the award of the M. Sc. Degree.

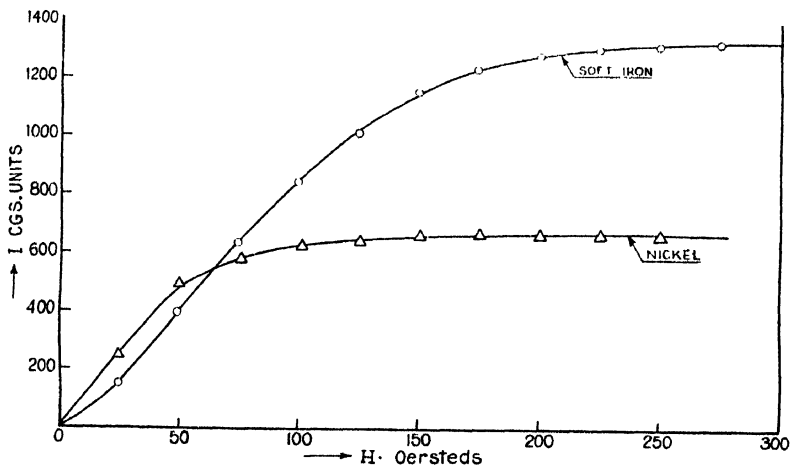
† At present working in the National Physical Laboratory of India, New Delhi-12.

method. While the dynamic method gives the adiabatic change in the elastic modulus the statical method yields the isothermal change. In the case of a solid, however, the difference between the isothermal and adiabatic changes is negligibly small. This paper deals with some of the experiments conducted by the author for the determination of the changes in the Young's modulus and rigidity modulus of soft iron and nickel by a statical method.

2. EXPERIMENTAL

The experiments may be subdivided into two sections one dealing with the changes in the rigidity modulus and the other dealing with the Young's modulus of the same ferromagnetic specimens.

The I - H curves of the specimens, figure 1, which were in the form of cylindrical rods, were first determined using a deflection magnetometer, the value of the horizontal component of the Earth's magnetic field being determined with a Kew magnetometer.



I - H CURVES OF IRON AND NICKEL

(a) The Rigidity Modulus

The experimental rods were 32 cms long and $\frac{1}{4}$ inch in diameter and carried two stout brass extensions at the ends in the form of rods 22 cms in length and $\frac{1}{2}$ inch in diameter. One end of this extension was clamped firmly at a suitable height by two brass blocks which had V grooves cut in them, the blocks and the rod being fixed to the top of a table by two long bolts and nuts. The free end of the extension piece had a hole $\frac{1}{4}$ inch in diameter and into this hole was engaged a hard steel bearing in the form of a cone. The cone formed part of a screw which was adjustable and clamped in position by a check nut. The cone assembly was mounted on a suitable upright made of brass. The free end also carried a thin wooden disc which facilitated the application of suitable twists to the free end of the rod by the usual method of double loading.

The solenoid to magnetise the rods under test was specially built. It was 45.5 cms long and was capable of accommodating the entire length of the experimental rods in the most uniform part of the field inside. The length of the solenoid over which the field was constant was determined by a separate experiment. The supports for the rod at each end were so adjusted that the axis of the experimental rod coincided with the axis of the solenoid.

The regulation of the current passing through the solenoid was accomplished by the use of the liquid rheostats suggested by Ewing. Two such rheostats, one with high resistance and the other with low resistance, enabled the current passing through the solenoid to be adjusted very critically. The magnetising current was measured by a calibrated Elliot ammeter. Provision was also made to demagnetise the experimental rod whenever required by an alternating current.

The method for the determination of small twists is an optical method using Newton's rings. The experimental rod carried at its free end a lever arm, (fixed to the extension), to the free end of which a lens was fixed. A glass plate placed just below the lens on an adjustable platform enables us to get a ring system by the usual method. It is possible to create a gap between the lens and the plate without affecting the ring pattern. A small variation of the rigidity of the rod under test produces a variation of the twist in the rod which is indicated by the formation or the collapse of the rings. The ring system, coupled to a lever of variable length, provided a very sensitive and accurate method of finding the minute variations of the modulus of rigidity.

In an actual experiment the rod was demagnetised and then brought to the mechanically cyclic state by continuous loading and unloading. The rod was then given a small initial twist by a small load. The loads used were immersed in a tub of water to prevent vibrations. A Newton's ring system was formed with the green line of the mercury arc (5461 Å. U.). By gradually lowering the lower plate a gap was formed between the lens and the plate. Watching through the microscope the current in the solenoid was increased till the first ring collapsed. The current value was noted. The process was continued for each collapsing ring till no more ring collapsed. From the known length of the lever and the value of current it is easy to find the change in the twist for a given value of magnetic field for a constant initial twist. The experiment was repeated for several different values of twist, for both the soft iron and the nickel rods. The variation of the angle of twist $\Delta\theta$ with field is given in figure 2.

(b) *Variation of Young's Modulus with Magnetic field*

To support the rod in such a way as to be in a completely uniform field, two identical solenoids were constructed. Analysis of the value of

the field, when they are a little separated, gave the following expression for the field in the gap :

$$H = 2\pi n I \left[\frac{\frac{3}{2} L + 2p}{\sqrt{\left(\frac{3}{2} L + 2p\right)^2 + R^2}} + \frac{L}{\sqrt{\left(\frac{L}{2}\right)^2 + R^2}} - \frac{L + 2p}{\sqrt{\left(\frac{L}{2} + 2p\right)^2 + R^2}} \right]$$

where $2p$ is the gap, L the length of one of the solenoids, R the radius of the core, n the number of turns per unit length. Preliminary experiments showed that the field in the gap diminished with increasing width of the gap. For a gap of 1 cm width the fall in the field was about 5 oersteds per ampere.

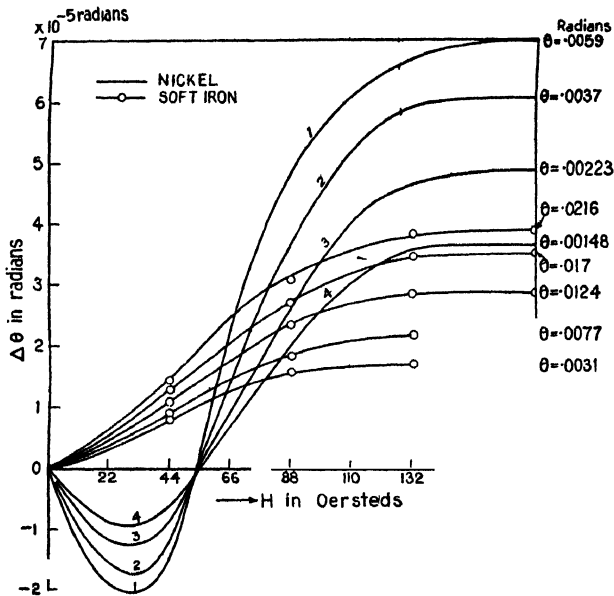


FIG. 2 Variation of the angle of twist, $\Delta\theta$, with field

For the measurement of the Young's modulus, the method of non-uniform bending was found suitable. The variation of the depression at the centre when the magnetic field was applied was found by the optical method using Newton's rings. To do this, a thin ebonite extension was fixed to the centre of the rod which was symmetrically supported between two knife edges placed inside the solenoids and loaded at the centre. The ebonite extension projected vertically above the solenoids and had a thin glass plate fixed to its top. A lens mounted on an adjustable table situated on an independent support enabled one to get a pattern of Newton's rings between the lens and the plate; the source of illumination being a sodium lamp. It was an easy matter to have a gap between the lens and the plate and still have a distinct ring system.

When the experimental rod has been thoroughly demagnetised and brought to a mechanically cyclic state, a small load was applied to the

centre of the rod and the steady ring system was observed through a microscope. When the rod is gradually magnetised the rings appear one after another showing that the rod tends to straighten itself. The value of the current for each new ring that formed was noted and the process continued till there were no more formation of rings. The experiment was repeated for several initial loads for both the iron and the nickel rods. The results are given in figure 3, 4 with H on the x -axis and the Δe (change in depression) on the y -axis for various constant initial loads.

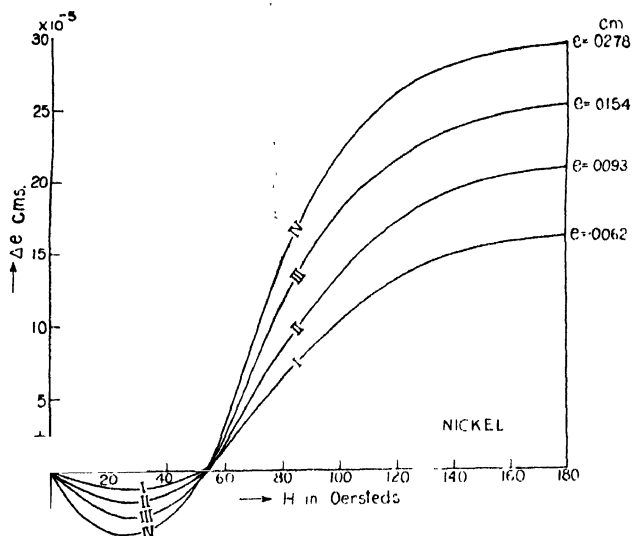


FIG. 3. Variation of depression of the rod with magnetic field (nickel).

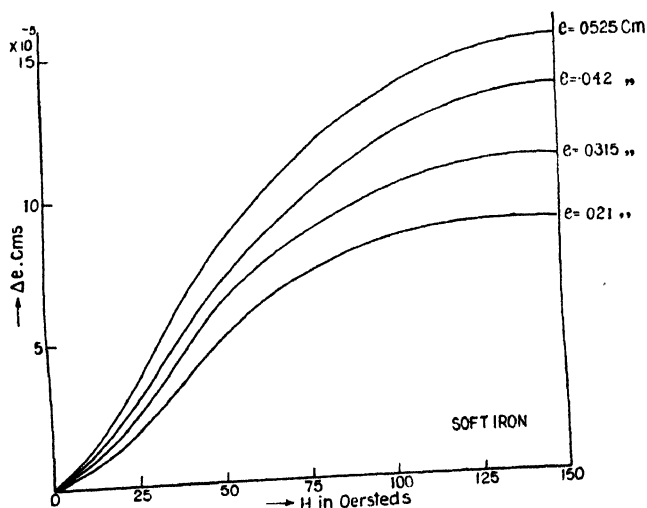


FIG. 4. Variation of depression of the rod with magnetic field (soft iron)

A glance at figures 1, 2, 3 and 4 shows a striking resemblance between the $\Delta\theta$ - H curves, Δe - H curves and I - H curves.

These experiments were repeated several times and on different days when the atmospheric temperature varied as much as 2 deg.C but the same results were obtained showing that small variations of atmospheric temperature did not appreciably affect the results. Lastly, the values of magnetic intensities were corrected for demagnetisation factors.

3. RESULTS

The specimens investigated were soft iron and nickel. They were certified by the suppliers to contain less than 0.1% impurities. They were 32 cms. in length and 0.25" in diameter.

Figure 1 gives the I - H curve and figure 2 gives the change in twist *i.e.* the change in rigidity of the specimen due to the action of the magnetic field. Likewise in figures 3 and 4, the change in the depression in the centre of the rod due to the action of the magnetic field is shown. In the case of both soft iron and nickel, it can readily be seen that the magnetic field increases the elastic coefficients. Nickel is peculiar in that for very low fields the elasticity decreases while for higher fields, the elasticity shows an increase. Also one does not fail to appreciate the striking similarity between these curves and I - H curve. The other notable feature is the saturation attained by these curves showing that the turning bodies inside the media are realities and the amount of turning i is a measure of the change in the magneto-elastic properties of the material.

An inspection of figures 2, 3 and 4 shows that the change in twist or depression produced by the magnetic field depends upon the initial value of the twist or depression given to the rod. This change decreases rapidly as the initial strain increases, in other words, it means that the elastic forces tend to oppose the magneto-elastic changes. It becomes clear therefore, that the changes in the elastic moduli must be greater in a strain-free rod than are indicated in actual experiments. It must be remembered that it is impossible to measure the changes in the elastic moduli of a rod except by straining it.

To determine the values of the changes in the elastic moduli in a strain-free state, the observed values have to be graphically extrapolated. These extrapolations are indicated in figures 5, 6, 7 and 8. When the percentage change in elasticity is plotted against initial strains and the curves so obtained are extrapolated for zero value of strain, we get the percentage change in elasticity in a strain-free rod.

Assuming the values of the constants, as given in Table I, we can calculate percentage change in elastic coefficients applying equations (1) and (2) in the case of the polycrystalline specimens between demagnetisation and saturation.

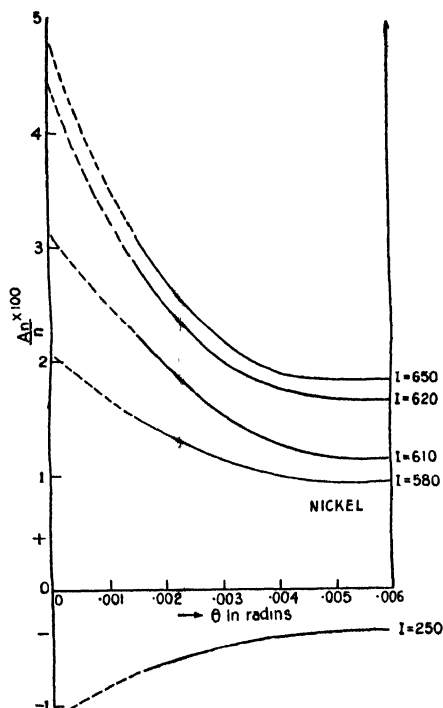


FIG. 5. Percentage change in rigidity modulus extrapolated to zero twist (nickel),

TABLE I

Constant	Iron	Nickel
Magnetostiction coefficient	19.5×10^{-6} (a)	27×10^{-6} (b)
Initial susceptibility	22.7 (c)	19.8 (d)
Young's modulus	19.6×10^{10} cgs units [†]	18.9×10^{10} cgs units [*]
Rigidity modulus	8.0×10^{10} Do. [*]	7.6×10^{10} Do. [*]
Saturation magnetic intensity	1300 Do. [*]	650 Do. [*]

(a) Webster (1925)
(b) Masiyama (1928)

(c) Cooke (1936)
(d) Becker & Kersten (1930)

(*) Author

It is seen that a saturating magnetic field produces an increase in the rigidity modulus of nickel by 4.64% and of iron 0.9%. Similarly, an increase of 0.64% in the case of iron and 3.70% in the case of nickel is shown in the values of the Young's modulus.

FIG. 6. Percentage in rigidity modulus extrapolated to zero twist (soft iron).

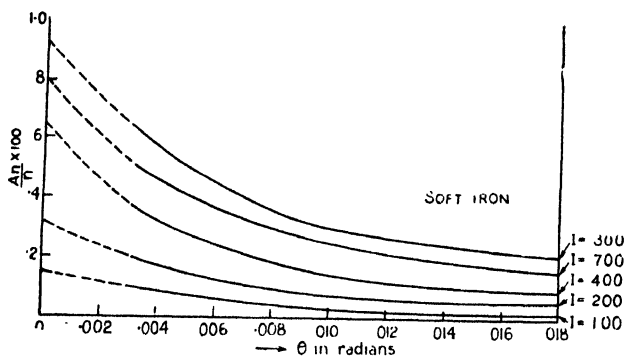


FIG. 7. Percentage change in Young's modulus extrapolated to zero depression (nickel).

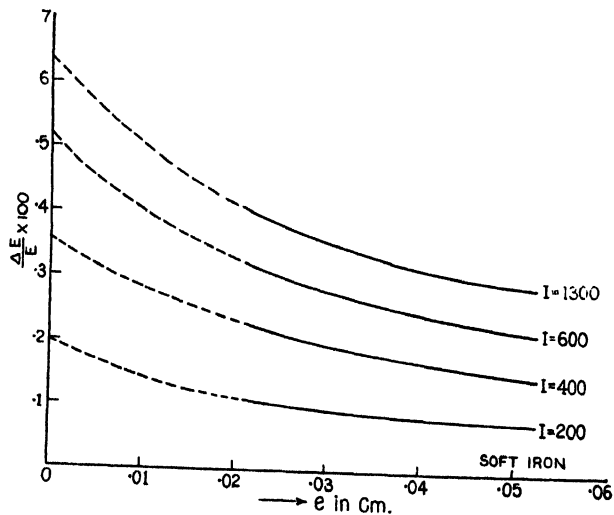
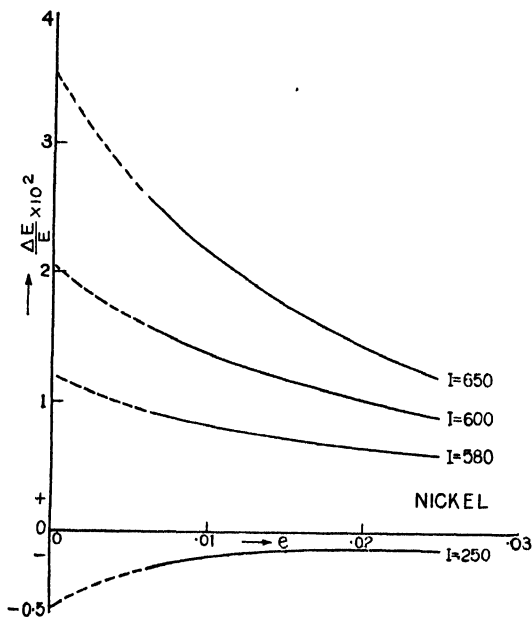


FIG. 8. Percentage change in Young's modulus extrapolated to zero depression (soft iron)

4. DISCUSSION

The modern theory of ferromagnetism is based on the discovery of the existence of minute microscopic regions inside the ferromagnetic body, called "domains," each domain being magnetised to saturation. The experiments of Barkhausen (1919), Vander Poll (1920), Bozorth and Dillinger (1930) have not only proved the existence of these domains but have led to an exact measurement of the size of these domains.

Inside a ferromagnetic body two kinds of forces are encountered with. One is the force of exchange between the uncompensated spins of the orbital electrons and the other the crystal structure forces. In a crystal these forces are distributed in a definite way so that some directions of magnetisation are more stable than the others. In the case of iron the direction of easy magnetisation is the 100 direction while in the case of nickel it is the 111 direction.

The application of a magnetic field initially turns the domains into alignment with the applied field while the field is small, but when the field becomes great the domains are rotated into alignment. In other words, it means that the effect of a magnetic field is to produce a slight deformation of the crystal as a whole.

It is well known that strain increases magnetisation. The effect of strain on a magnetised body is to align the directions of the micro-magnetisations of the domains into parallelism with the field so that the magnetisation increases. However, when the body is magnetised to saturation, strain does not increase the magnetisation.

While elastic deformation in the case of a magnetised body produces changes in magnetic intensity, the converse effect is the change in elastic properties by the application of a magnetic field. On the basis of the deformation produced in the crystalline structure by the application of a magnetic field Heisenberg (1931) has developed the theory of single crystal magnetostriction. Akulov (1933) extends this theory and derives an expression for the change in the elastic moduli of a polycrystalline specimen in which the distribution of the microcrystalline axes is random, in terms of the applied magnetic field, the saturation intensity of magnetisation, the initial susceptibility and the saturation magnetostriction coefficient along the direction of easy magnetisation.

Brown (1937) has shown from a theoretical study that the formulae of Akulov are essentially correct in giving the change of the Young's modulus between demagnetisation and saturation and explains some of the discrepancies between theory and experiment in the case of the experiments of Seigel and Quinby (1936) who employed a dynamical method for the determination of the changes in the Young's modulus.

The theoretical value of the change in the Young's modulus between demagnetisation and saturation in the case of a polycrystalline ferromagnetic specimen is given by Brown (1950) as

$$\frac{\Delta E}{E} = \frac{3}{5} \chi_0 \cdot \lambda^2 \cdot \frac{E}{I_\infty^2} \quad (1)$$

λ is the saturation magnetostriction coefficient along the direction of easy magnetisation of the crystal, χ_0 the corresponding initial susceptibility, I_∞ the saturation intensity of magnetisation and E the Young's modulus of the specimen in zero field.

An expression for the change in the rigidity modulus, n , of the specimen can be derived from the above formula on the assumption that the compressibility is independent of magnetisation since no magneto-mechanical process follows the application of uniform pressure and both in the demagnetised and saturated state the specimen is isotropic (Brown, *loc. cit.*). If the compressibility remains constant, the variation of n and E are obviously connected by the relation

$$\frac{\Delta n}{n} = \frac{3n}{E} \frac{\Delta E}{E} = \frac{9}{5} \chi_0 \cdot \lambda^2 \cdot \frac{n}{I_\infty^2} \quad (2)$$

The above equations are what we seek since they enable one to make a theoretical estimate of the changes in the elastic moduli of the ferromagnetic specimens.

In the case of soft iron and nickel the percentage change of elastic moduli from theory and experiment are gathered in Table II.

TABLE II

Material	Percentage change in Young's modulus		Percentage change in rigidity modulus	
	Expt.	Theory	Expt.	Thory
Soft iron	0.64	.736	.90	.567
Nickel	3.70	3.83	4.64	4.619

The agreement seems to be fair and within the limits of experimental errors ; it should be remembered that the theory is based on calculations made from averaging the properties of the constituent microcrystals inside the polycrystalline body. In Akulov's theory the strains are averaged assuming uniform stress in the microcrystals whereas it is possible to assume uniform strain and average the stresses. This would lead to a different value of the constants occurring in equations (1) and (2).

5. ACKNOWLEDGMENT

Thanks are due to the University of Madras for the grant of a scholarship, and the Presidency College, Madras, for providing all facilities for the conduct of this research.

REFERENCES

- Akulov, 1933, *Zeits f. Phys.* **85**, 661.
 Auwers, O. V., 1935, *Zeits f. Phys* **94**, 707.
 Barkhausen, H. 1919. *Phys Zeits* , **20**, 401.
 Berker, R. and Kersten. M , 1935, *Zeits f. Phys.*, **64**, 660
 Bozorth, R. M and Joy Dillinger, 1937, *Phys., Rev.*, **38**, 773
 Brown, W. F., 1936, *Phys., Rev* , **50**, 1159
 Brown, W. F, 1937, *Phys., Rev* , **52**, 323.
 Cooke, W. T., 1931, *Phys* , *Rev.*, **50**, 1156.
 Heisenberg, W., 1931, *Zeits. f. Phys* , **49**, 287.
 Honda, K. and Terada, T. 1907, *Phil. Mag.*, **13**, 36.
 Masiyama, Y. 1928, *Sci., Rep* , *Tohoku Imp , Univ* , **17**, 915.
 Siegel, S. and Quimby, S. L , 1936, *Phys* , *Rev.*, **49** 663.
 Vander Pol, B., 1923, *Proc , Amsterdam Acad.*, **23**, 637.
 Webster, W. L., 1925, *Proc , Roy , Soc., A.* **109**, 570.

SPECTROSCOPIC CONSTANTS OF MOLECULES

III. REGULARITIES IN VIBRATION FREQUENCIES IN A MOLECULAR GROUP

BY Y. P. VARSHNI AND K. MAJUMDAR

DEPARTMENT OF PHYSICS, ALLAHABAD UNIVERSITY, ALLAHABAD

(Received for publication, November 15, 1954)

ABSTRACT. Regular variation of vibration frequency ω , and force constants k , in a molecular group has been studied. It is shown that, in a molecular group, if the ω , of the series of molecules of a metallic element are plotted against the ω , of the corresponding molecules of another metallic element, straight lines are obtained. Unknown ω , have been predicted.

INTRODUCTION

With the gradual development of molecular spectrum studies, it became evident that some sort of classification was necessary.

Clark (1934 *a, b* ; 1935*a*) divided the diatoms into periods which were designated as KK, KL, KM etc., the letters indicating the closed electronic shells of the component atoms. Several workers have investigated diatoms on this basis and found fruitful regularities in diatoms belonging to the same period (Clark, 1934*a*, 1935*b*, 1936, 1938, 1941 ; Huggins, 1935, 1936 ; Wu and Chao, 1947 ; Allen and Longair, 1935 and others).

On the other hand regularities have also been traced in diatoms on basis of the Periodic Table. The diatoms can be classified depending on the type of linkage. Suppose a diatom consists of two atoms, one belonging to, say IV*b* group (C, Si, Ge, Sn, Pb) and the other to VII *b* group (F, Cl, Br, I, At) of the Periodic table. Examples of such diatoms will be CF, Si Cl, CCl, etc. Such diatoms have similar linkage. In the case cited they all have $^2\Pi$ ground state. Investigations on these lines have been made by Mecke (1927), Carrelli and Trautteur (1937), Lovera (1951) and others. Recent work of Pritchard and Skinner (1951) shows that excellent results are obtained for Badger's rule on group classification.

Sutherland (1940) found regularities on both classification, period as well as group.

In view of the fact that in Periodic Table regular variations of properties are found in groups as well as in periods, it is easy to see that regularities should exist in molecular 'periods' as well as in 'groups'. It would be appropriate to say that the properties of a diatom are determined both by the considerations of the 'period' and the 'group' to which it belongs.

In the present paper regularities in the ground state vibration frequencies of diatoms belonging to the same group have been studied. The groups will be denoted by the two subgroups of the Periodic Table to which the constituent atoms belong. Thus 4b-6b group denotes CO, CS,type of molecules. It is possible by these investigations to estimate unknown ω_e values ; they also point out anomalous values which may give a clue to the abnormalities existing in the electronic states.

If we arrange the vibration frequencies of molecules as shown in Table I, which shows 4b-6b group of molecules, certain regularities become apparent.

TABLE I

Vibration frequency (in cm^{-1})

	O	S	Se	Te
C	2170.2	1285.1	1036	~ 875
Si	1242	749.5	580	481.2
Ge	985.7	575.8	406.8	323.4
Sn	822.4	487.68	331.2	259.5
Pb	721.8	428.14	277.6	211.8

The vibration frequency is seen to decrease horizontally towards right hand side and vertically downwards. Very similar behaviour is found for the force constants as Table II shows.

TABLE II

Force constant k_e (in Des. = 10^5 dynes/cm)

	O	S	Se	Te
C	19.02	8.488	6.586	4.945
Si	9.246	4.938	4.094	3.130
Ge	7.526	4.358	3.743	2.776
Sn	5.615	5.536	3.566	2.439
Pb	4.556	2.992	2.595	2.086

An examination of the ω_e and k_e values of molecules of various groups showed that such regularities exist in all group for which data are available, except 1a-7b group. This group will be discussed later on.

If the vibration frequencies of the diatoms of a group having the same metallic atom are taken on abscissa and the vibration frequencies of other

diatoms of the same group having some other metallic atom are plotted against corresponding non-metallic elements, a straight line is obtained. For example, the vibration frequencies of SrF, SrCl, SrBr, SrI are linear with the vibration frequencies of CaF, CaCl, CaBr, CaI. This relationship has been examined for various groups for which data are available in figures 1-9. Deviations from a strictly linear relationship are without doubt real, however the discrepancies are of a minor nature. As the deviations seem to vary systematically in going down a group it is convenient to take the middle element in a group on the abscissa (thus Ga in IIIb group), but this is not very essential. It is best to choose that series as abscissa for which well established ω_e values are available. When only two points are available, the straight line has been drawn taking into consideration how the points on other lines are distributed. Thus the carbon line (figure 7) has been drawn, in analogy with other lines, such that the fluoride point is a little above and the chloride point a little below.

DATA

Excepting for the following molecules, for which more accurate values have been reported, the data have been taken from Herzberg (1950) and Rosen (1951).

TABLE III

Group	Molecules	Reference
1a-7b	KF, KCl, KBr, KI, RbF, RbCl, RbBr, RbI, CsF, CsCl, CsBr, CsI	Barrow and Caunt (1953)
1b-6b	AgO	Uhler (1953)
3b-7b	GaF, InF	Walti and Barrow (1952), Barrow, Jacquest and Thompson (1954)
5b-6b	AsS, SbS, BiS SbSe, SbTe, Bi Se, BiTe	Sur (1952) Sharma (1950, 1954)

DISCUSSION

It will be noticed that in general the linear relationship is well obeyed. As mentioned earlier, there are small and somewhat regular variations from the straight line. Usually the slope decreases as we go down a group.

Table IV lists the predicted values from the graphs for such molecules which have not been investigated or whose reported values of ω_e seem to be doubtful. The actual values can be expected to be within 5% of these estimated values. Individual groups are discussed below.

TABLE IV

Group	Abscissa	Molecule	Estimated ω_e	Remarks
1a-7b	K	NaI ²	465	Discrepancy
		CsI ²	350	
1b-7b	Cu	AgI ²	525	Discrepancy
2a-7b	Ca	RaI	160	
		BeBr	670	
		BeI	580	
2b-7b	Hg	ZnBr	280	
3b-7b	Ga	BI	570	
4b-7b	Pb	CBr	670	
		CI	570	
		SiI	340	
		GeI	230	
		SnI	190	
5b-6b	Bi	NSe	1000	
		NTe	880	
		AsSe	~700	
		AsTe	~660	
5b-7b	Bi	SbBr	225	
		SbI	175	

1a-7b Group.

CsI² does not fall on the straight line. However, there is considerable difference between the values reported by different workers for this molecule—385 (spectroscopic, Barrow and Caunt—1953), 270 ± 30 (radio frequency electric resonance spectrum—Trischka, 1948, 1949), 345 (theoretical value on a classical model—Rittner 1951). The graphical value 350 is very close to the value of Rittner. Barrow and Caunt also think that the spectroscopic value may be a little too high.

It is significant to note that the slope of sodium (Na) line is less than that of Rb, contrary to the behaviour of other molecules (only one more such example has been encountered—As).

A study of the ω_e and k_e values of this group reveals interesting irregularities.

TABLE V

Vibration frequency

	F	Cl	Br	I
Li				450
Na		380	315	286
K	400	305	230	200
Rb	390	270	180	145
Cs	385	240	168	120

TABLE VI

Force constant k_e (in Des. = 10^5 dynes/cm)

	F	Cl	Br	I
Li				.7845
Na		1.186	1.041	.9378
K	1.205	1.019	.818	.704
Rb	1.361	1.076	.788	.633
Cs	1.151	.95	.83	.551

While the ω_e values seem to be regular, such is not the case with the force constants. The k_e value for LiI is lower than that of NaI contrary to the expectation. It is interesting to note that the ω_e (LiI) = 616 or k_e (LiI) = 1.57 calculated by Rittner on a classical model of alkali-halides would give the correct trend to the force constants. On the other hand, considerations based on similarities in iso-electronic molecules do not support a value greater than 500 (to be discussed in Part IV). The trend of k_e values for bromides suggests that for CsBr a lower value near .76 is to be preferred to the reported value .83. Figure 1 also supports a lower value. The force constants of fluorides increase as we pass from K to Cs, instead of decreasing. As all the three values have been reported by the same workers (Barrow and Caunt) using the same methods, it cannot be said

which value is more reliable. The theoretical values of Rittner, $\text{KF} - 1.266$, $\text{RbF} - 1.166$, $\text{CsF} - 1.113$, have the correct trend. The anomaly of CsF has been discussed above also.

It would be obvious from these considerations that the situation of ω_e values of these diatoms is not very satisfactory. It should be remembered that the experimental investigation of these molecules is rather involved. The band systems arise from transitions from the stable ionic ground states to weakly bound upper states which dissociate into neutral atoms. These upper states are either purely repulsive, or have such shallow minima that their rotational and vibrational levels lie too close to be resolved. The bands are narrow and diffuse and it is very difficult to derive correct ω_e values (Barrow and Caunt, 1953).

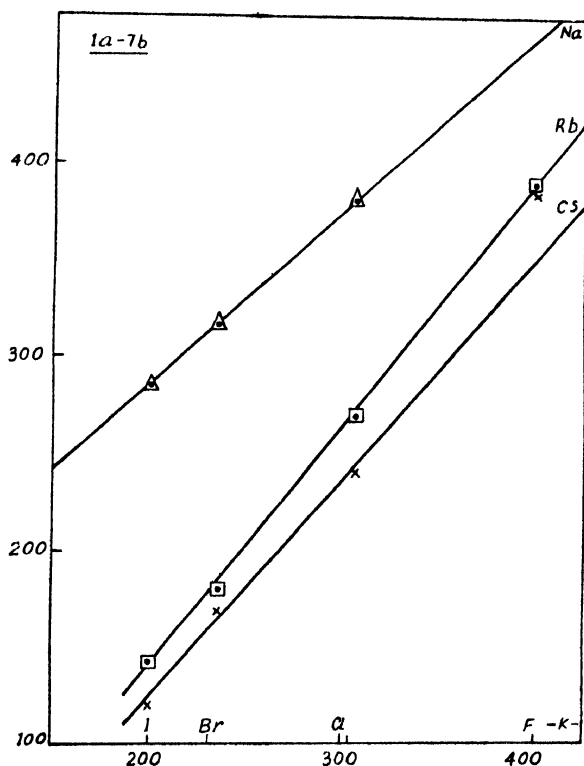


FIG. 1. 1a-7b Group

1b-7b Group (figure 2). Sufficient data for Au are not available. The straight line for Ag is satisfactory.

2a-7b Group (figure 3). The linearity is well obeyed.

2b-7b Group (figure 4). There is one discrepancy— ZnBr .

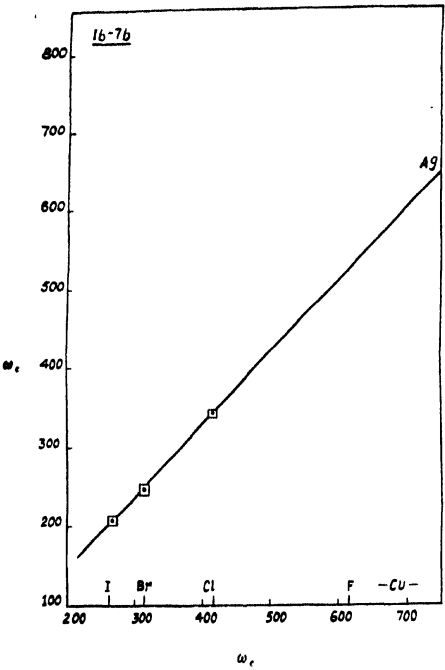


FIG. 2. 1b-7b Group

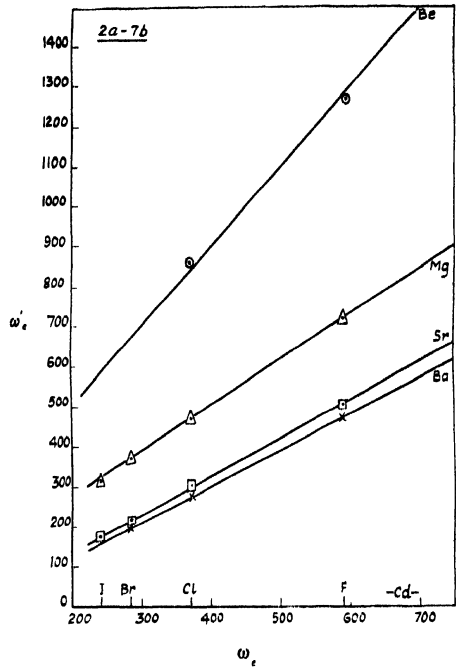


FIG. 3. 2a-7b Group

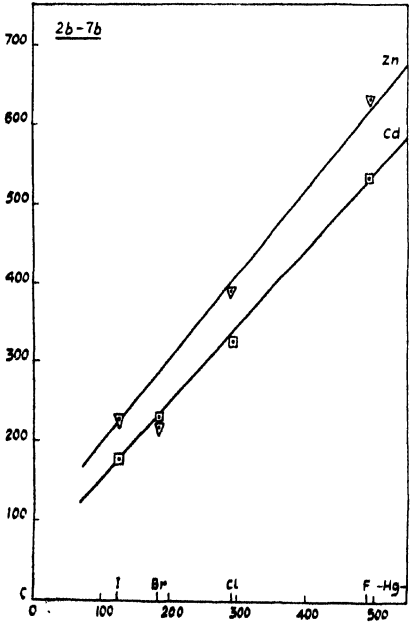


FIG. 4. 2b-7b Group

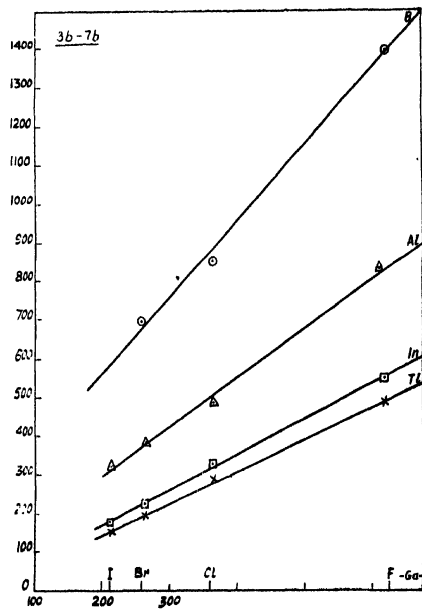


FIG. 5. 3b-7b Group

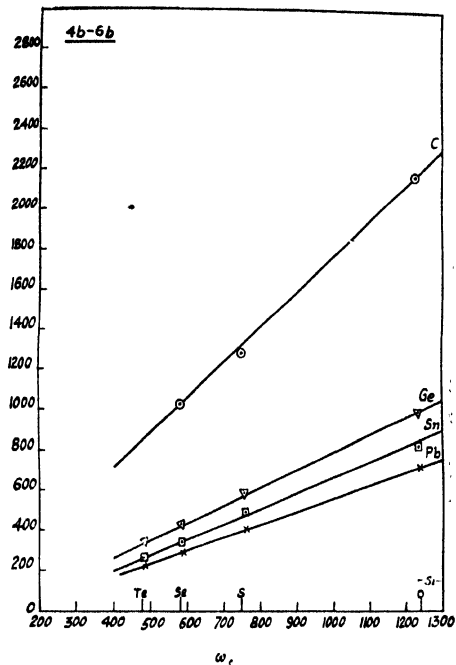


FIG. 6. 4b-6b Group

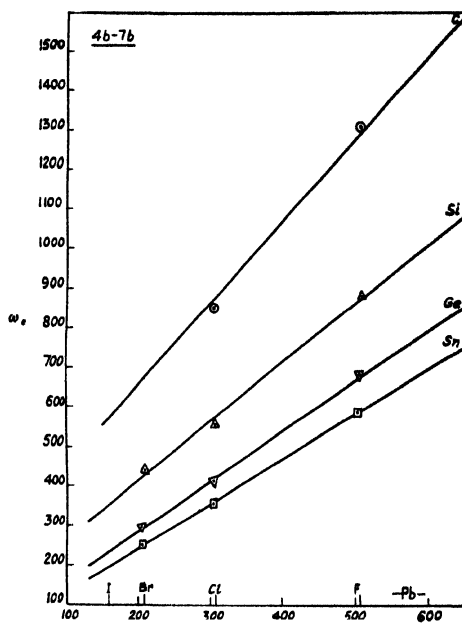


FIG. 7. 4b-7b Group

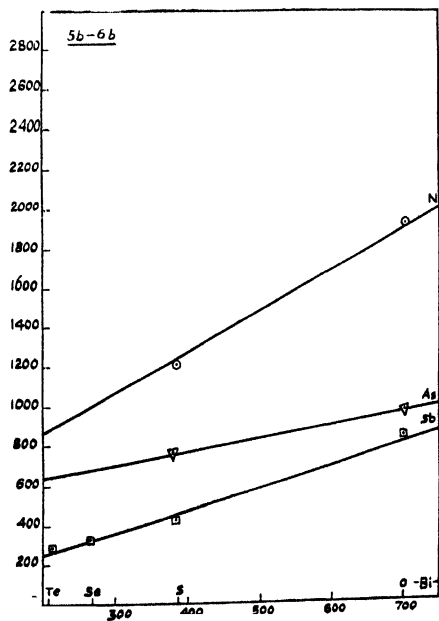


FIG. 8. 5b-6b Group

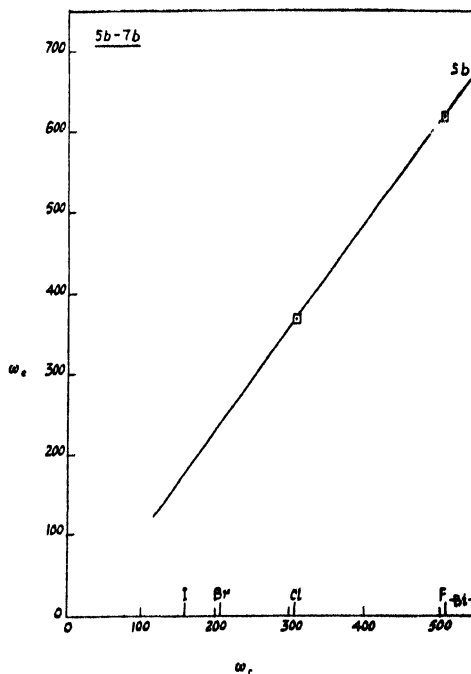


FIG. 9. 5b-7b Group

However, the experimental value of ω_2 of this diatom is not known correctly, even this is not certain whether the observed bands are due to ZnBr. An examination of the series ZnF-(630), ZnCl-(390.5), ZnBr-(220), ZnI-(223.4) shows that the experimental value is definitely in error.

3b-7b, 4b-6b, and 4b-7b Groups (figures 5, 6, 7). The straight lines are satisfactory.

5b-6b Group (figure 8). The slope of As line is lower than that of Sb line. As only two points are available for As, error in any of these is possible. If it is so, values for AsSe and AsTe will have to be modified accordingly. Further, $k_r(\text{AsS}) = 7.78$, comes out to be greater than $k_r(\text{AsO}) = 7.266$ which is again anomalous. We will return to this point in part IV.

5b-7b Group (figure 9). Only two points for Sb are available. The predicted values for SbBr and SbI are given in Table IV.

ACKNOWLEDGMENT

The authors are thankful to the Council of Scientific and Industrial Research for the financial assistance.

REFERENCES

- Allen, H. S., and Longair A. K., 1935, *Phil. Mag.*, **19**, 1052.
 Barrow, R. F., and Caunt, A. D., 1953, *Proc. Roy. Soc.*, **A219**, 120.
 Barrow, R. F., Jacquest, J. A. T., and Thompson, E. W., 1954, *Proc. Phys. Soc.*, **A67**, 528.
 Barrow, R. F. and Jevons, W., 1949, *Proc. Phys. Soc.*, **52**, 534.
 Barrow, R. F. and Jevons, W., 1944, *Proc. Phys. Soc.*, **56**, 204.
 Carrelli, A. and Trautteur, P., 1937, *Nuovo Cimento*, **14**, 301.
 Clark, C. H. D., 1934a, *Phys. Rev.*, **47**, 238.
 Clark, C. H. D., 1934b, *Proc. Leeds. Phil. Soc.*, **2**, 502.
 Clark, C. H. D., 1934c, *Phil. Mag.*, **18**, 452.
 Clark, C. H. D., 1935a, *Trans. Farad. Soc.*, **31**, 1017.
 Clark, C. H. D., 1935b, *Proc. Leeds. Phil. Soc.*, **3**, 26.
 Clark, C. H. D., 1936, *Phil. Mag.*, **22**, 1137.
 Clark, C. H. D. and Stoves, J. L., 1938, *Trans. Farad. Soc.*, **37**, 1324.
 Clark, C. H. D., and Webb, K. R., 1941, *Trans. Farad. Soc.*, **37**, 293.
 Herzberg, G., 1950, *Spectra of Diatomic Molecules* (D. Van Nostrand Co. Inc., New York).
 Huggins, M. L., 1935, *J. Chem. Phys.*, **3**, 473.
 Huggins, M. L., 1936, *J. Chem. Phys.*, **4**, 308.
 Ilovera, G., 1951, *Nuovo Cimento*, **8**, 1014.
 Mecke, R., 1927 *Z. Phys.*, **42**, 390.
 Pritchard, H. O., and Skinner, H. A., 1951, *J. Chem. Soc.*, 945.
 Rosen, B., 1951, *Donées Spectroscopiques Concernant les Molécules Diatomiques* (Hermann and Cie, Depositaires, Paris Ve).
 Sharma, C. B., 1950, *Curr. Sci.*, **19**, 114.
 Sharma, C. B., 1954, *Proc. Phys. Soc.*, **67**, 935.
 Sur, P. K., 1952, Thesis, Allahabad University.
 Sutherland, G. B. B. M., 1940, *J. Chem. Phys.*, **8**, 181.

- Trischka, J. W., 1948, *Phys. Rev.*, **74**, 718.
Trischka, J. W., 1949, *Phys. Rev.*, **76**, 1365.
Vago, R. F., and Barrow, R. F., 1947, Vol. Comm. Victor Henri.
Uhler, V., 1953, *Ark. Phys.*, **7**, 115.
Welti, D., and Barrow, R. F., 1952, *Proc. Phys. Soc.* **A65**, 629.
Wu, C. K. and Chao, S. C., 1947, *Phys. Rev.*, **71**, 118.

CALCULATION OF THE DIPOLE MOMENTS OF TRI-SUBSTITUTED BENZENES

By D. V. G. L. NARASIMHA RAO

PHYSICS DEPARTMENT, ANDHRA UNIVERSITY, WALTAIR

(Received for publication, September 26, 1951)

ABSTRACT. A general method is given for the calculation of dipole moments of 1, 2, 4 tri-substituted benzenes taking into account the induced effects, similar to the treatment of Smallwood and Herzfeld for the di-substituted compounds. The calculated values are given for five compounds for which the observed values are available and a comparison is made between the calculated and observed values.

INTRODUCTION

The dipole moments of poly-substituted benzenes calculated by the simple vectorial addition of the individual group moments reveal wide divergences between the calculated and the observed values in a majority of cases. Such divergences may arise from several causes, such as, the electrostatic attractions and repulsions, the induced effects or the occurrence of mesomerism etc. In the case of the di-substituted benzenes the induced effects are computed by Smallwood and Herzfeld (1930) adopting the plane hexagonal model for the benzene ring in the substituted compounds. This has provided a valuable correction. LeFevre and LeFevre (1936, 1937) applied the method for diphenyl, coumarin, and xanthone ring systems. Each atom or group is regarded as a sphere of uniform polarisability and the induced moments are calculated by assuming that this sphere is subjected to a field which is that produced at the centre of the sphere by the primary dipole. Smyth and McAlpine (1933) calculated the induction in each bond and obtained the bond polarisabilities in terms of the bond refractions. Groves and Sugden (1937) pointed out that when the atom or group is very near the primary dipole, allowance must be made for the variation of the field over the volume of the atom and this is done by means of the method of graphical integration suggested by Frank (1935).

THEORY

In this paper the method of calculation of Smallwood and Herzfeld is extended to the case of 1,2,4 tri-substituted benzenes. The resultant moment of a tri-substituted benzene compound is regarded as comprising of (1) the vector sum of the moments of primary dipoles, (2) the mutual induction of the three primary dipoles on one another and (3) the moments induced in the $-CH$ and $-C-C$ bonds of the hydrocarbon residue by the primary dipoles.

Figure 1 represents the case of a 1, 2, 4 substituted compound. The appropriate angles and distances may be understood from figure 2. The

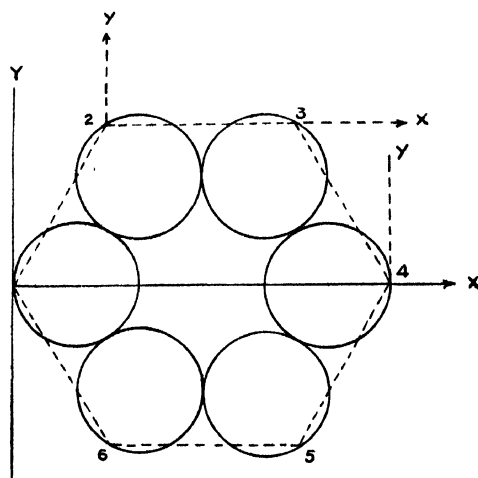


FIG. 1

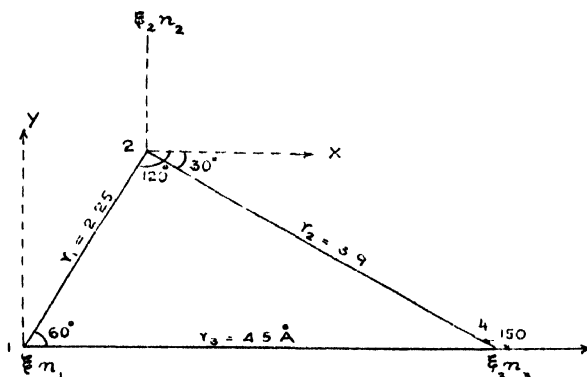


FIG. 2

notation used is the same as that of Smallwood and Herzfeld. ξ_1, ξ_2, ξ_3 represent the x-components and η_1, η_2, η_3 the y-components of m_{01}, m_{02} and m_{03} respectively. Using their equations and referring to figure 2, the interaction of the three dipoles on one another gives the following relations.

$$\left. \begin{aligned}
 & \xi_1^1 + (a_1/4)\xi_2^1 - 2a_3\xi_3^1 - (3\sqrt{3}/4)a_1\eta_2^1 = \xi_1 \\
 & (b_1/4)\xi_1^1 + \xi_2^1 - (5/4)b_2\xi_3^1 - (3\sqrt{3}/4)b_1\eta_1^1 + (3\sqrt{3}/4)b_2\eta_3^1 = \xi_2 \\
 & 2c_3\xi_1^1 + (5/4)c_2\xi_2^1 - \xi_3^1 - (3\sqrt{3}/4)c_2\eta_2^1 = -\xi_3 \\
 & -(3\sqrt{3}/4)a_1\xi_2^1 + \eta_1^1 - (5/4)a_1\eta_2^1 + a_3\eta_2^1 = \eta_1 \\
 & (3\sqrt{3}/4)b_1\xi_1^1 - (3\sqrt{3}/4)b_2\xi_3^1 + (5/4)b_1\eta_1^1 - \eta_2^1 - (b_2/4)\eta_3^1 = -\eta_2 \\
 & (3\sqrt{3}/4)c_2\xi_3^1 + c_3\eta_1^1 + (c_2/4)\eta_2^1 + \eta_3^1 = \eta_3
 \end{aligned} \right\} \quad (1)$$

Calculation of the Dipole Moments of Tri-Substituted Benzenes 51

where

$$\begin{aligned} x_1/r_1^3 &= a_1, & x_2/r_2^3 &= a_2, & x_3/r_3^3 &= a_3. \\ x_2/r_1^3 &= b_1, & x_2/r_2^3 &= b_2, & x_2/r_3^3 &= b_3. \\ x_3/r_1^3 &= c_1, & x_3/r_2^3 &= c_2, & x_3/r_3^3 &= c_3. \end{aligned}$$

x_1 , x_2 and x_3 represent the polarisabilities of the three substituent groups.

The fields of the induced moments are also considered in the above equations since we have written $\xi^1 = \xi + \xi_i$ and $\eta^1 = \eta + \eta_i$. Thus as a result of dipolar induction each ξ is modified to a certain ξ^1 and each η is modified to a certain η^1 . In order to obtain the numerical values for ξ^1 and η^1 the six equations (1) are solved by the method of post-multiplication giving the values for the six variables.

The induced moments in the remaining -CH groups at 3, 5 and 6 are calculated along similar lines. The values of the angles (v) and distances (r) are given in Table I. The data given in Table I are from Smallwood and Herzfeld, page 1921.

TABLE I.

Group		(3)	(5)	(6)
I	r v	3.0 30°	-3.0 -30°	2.25 -150° Å
II	r v	2.25 0°	1.5 -60°	3.0 -90°
III	r v	2.25 120°	-2.25 -120°	3.0 -150°

The total induced effect in the -CH groups at 3, 5 and 6 is given as

$$\left. \begin{aligned} \sum \xi_i &= 0.01320\xi_1^1 + 0.07456\eta_1^1 + 0.1021\xi_2^1 - 0.009324\eta_2^1 \\ &\quad - 0.01939\xi_3^1 + 0.01432\eta_3^1 \\ \sum \eta_i &= -0.07456\xi_1^1 + 0.06624\eta_1^1 - 0.009324\xi_2^1 - 0.02641\eta_2^1 \\ &\quad + 0.01432\xi_3^1 + 0.1406\eta_3^1 \end{aligned} \right\} \dots (2)$$

In evaluating the induced moments in the C-C bonds, the various angles and distances used are given in Table II. These values are derived using simple trigonometrical relations from the data in Table I, assuming plane hexagonal model for the benzene ring.

TABLE II.

Group		(1)	(2)	(3)	(4)	(5)	(6)
I	r v	1.3 30°	2.6 30°	3.433 11°	-3.138 -11°	2.6 -30°	1.3 -30° Å
II	r v	1.3 30°	2.6 -30°	3.438 $-49^\circ 6'$	-3.438 $-70^\circ 54'$	2.6 -90°	1.3 -90°
III	r v	1.3 -150°	2.6 -150°	-3.438 -160°	3.438 160°	2.6 150°	1.3 150°

The total induced moment in this case is obtained as

$$\left. \begin{aligned} \Sigma \xi_i^1 &= 1.3520 \xi_1^1 + 0.2150 \xi_2^1 - 0.7098 \eta_2^1 + 1.3520 \xi_3^1 \\ \Sigma \eta_i^1 &= -0.2952 \eta_1^1 - 0.7098 \xi_2^1 + 0.9399 \eta_2^1 - 0.2952 \eta_3^1 \end{aligned} \right\} \dots (3)$$

Combining eqns. (2) and (3) the result is

$$\left. \begin{aligned} \Sigma(\xi_i^1 + \xi_i^1) &= 1.3652 \xi_1^1 + 0.07456 \eta_1^1 + 0.3171 \xi_2^1 - 0.7191 \eta_2^1 \\ &\quad + 1.3326 \xi_3^1 + 0.01432 \eta_3^1 \\ \Sigma(\eta_i^1 + \eta_i^1) &= -0.07456 \xi_1^1 - 0.2290 \eta_1^1 - 0.7191 \xi_2^1 + 0.9135 \eta_2^1 \\ &\quad + 0.01432 \xi_3^1 - 0.1546 \eta_3^1 \end{aligned} \right\} \dots (4)$$

Finally the resultant moment M of the molecule is given as

$$M = \sqrt{M_x^2 + M_y^2} \dots (5)$$

where

$$\begin{aligned} M_x &= 2.3652 \xi_1^1 + 1.07456 \eta_1^1 + 1.3171 \xi_2^1 + 0.2809 \eta_2^1 + 2.3326 \xi_3^1 + 1.01432 \eta_3^1 \\ M_y &= 0.9254 \xi_1^1 + 0.7710 \eta_1^1 + 0.2809 \xi_2^1 + 1.9135 \eta_2^1 + 1.0143 \xi_3^1 + 0.8454 \eta_3^1. \end{aligned}$$

RESULTS

The final results for the five compounds considered, together with the observed values of Hassel and Naeshagen (1931) and Lutgert (1932) are tabulated in Table III.

TABLE III

Compound	M_{cal}	$M_{\text{eq}} (5)$	M'	M_{obs}	m_e value assumed
1, 2, 4 trichlorobenzene	1.64	1.24	1.40	1.25	$m_{e1} = 1.64$
2, 4 dinitrochlorobenzene	3.26	3.11	3.19	$3.0 \pm .1$ 3.29	$m_{e1} = 1.64$ $m_{e2} = 3.75$
2, 4 dinitrobromobenzene	3.26	3.72	3.51	$3.1 \pm .1$	$m_{e1} = 1.56$ $m_{e2} = 3.75$
2, 4 dinitroiodobenzene	3.31	4.92	4.29	$3.4 \pm .1$	$m_{e1} = 1.25$ $m_{e2} = 3.75$
2, 5 dichloronitrobenzene	3.75	3.31	3.48	3.45	$m_{e1} = 1.64$ $m_{e2} = 3.75$

The values under the column (M_{cal}) are obtained by the simple vectorial addition. The second column gives the values calculated using Eqn (5). It is very difficult to judge which value of m_e (the moment of the mono-substituted compound) is to be used in the calculation since, for the same mono-substituted compound various values have been reported in the literature. For uniformity the values of Hojendahl (1929) are assumed throughout. In the case of the iodo-compound, since his value is not available the value of Walden and Werner (1929) is used. It is unfortunate that there are no values available for the tri-substituted compounds by the same authors whose values are assumed for m_e . Thus, in view of the fact that the experimental values for the mono-and the tri-substituted compounds are determined by

different authors and since the values are liable to vary, the calculated and observed values may not be expected to agree closely. From Table III we note that a closer approximation to the observed values is obtained by using Eqn (5) than in the case of M_{vect} for three of the compounds studied (1, 2, 4 trichlorobenzene, 2, 4 dinitrochlorobenzene and 2, 5 dichloronitrobenzene). The polarisabilities of the groups increase as we go from chloro to bromo- to the iodo-compound and hence the induced effects also increase in the same direction. As we see from the table, the deviation between the calculated and the observed values also increases in the same direction.

In the above calculations, a correction for the dielectric constant of the internuclear space is also considered. LeFevre and LeFevre (1937) pointed out that the calculated induced moment must be reduced by the factor $(\epsilon + 2)/3\epsilon$ (ϵ being the dielectric constant of the internuclear space) in order to obtain the actual induced moment. The value of ϵ is obtained as 2.40 from measurements of the variation of the dielectric constant of benzene with pressure. Groves and Sugden also remarked that little error will be introduced by assuming $\epsilon = 2.40$ in the case of aromatic compounds. The reduction factor turns out to be $4.4/7.2$. The values obtained when this correction is applied are given under the column headed M' in Table III. The difference between $M_{\text{eq}}(5)$ and M_{vect} gives the induced moment. This difference multiplied by the factor $4.4/7.2$ gives the actual induced moment. This is added algebraically to M_{vect} to give the value under M' . By this process, the agreement with the observed value is improved for all the compounds studied except 1, 2, 4 trichlorobenzene where the induced contribution to the moment is considerably large.

The assumptions in the above method and other errors will have to be clearly stated. (1) The assumption that the dipoles are situated at the circumference of the carbon atoms to which the groups are attached, is an approximation. Smyth (1934) remarks that a consideration of the location of the centre of gravity of the charges assignable to the carbon halogen portion of the molecule in the halogenated compounds indicates the most probable location of the principal dipole to be approximately $7/8$ of the distance from the carbon nucleus to the halogen nucleus. But the first assumption is adopted, as otherwise the calculations become extremely complicated. (2) The distances between the various groups enter in the third power in the equations used for computing the induced moment, Hence a small error in the distance may cause a relatively large error in the final value of the moment. (3) The method has not taken into account the variation of the field of the dipole over the volume of the atom or group in which the moment is induced, since the distances under consideration are all greater than 1 A.U. The equation, assuming proportionality between the induced moment and the field of the primary dipole ($m_i = \alpha E$), breaks down at close distances. (4) Rotation round the bonds may also affect the

of the particle ($2\pi r$) and the wavelength of light (λ). There are marked changes in the intensity distribution of scattered light even for small changes in either the radius of the particle, the refractive index of the particle or the wave length of light used. It is possible to obtain the theoretical curves for the angular distribution of the intensity of scattered light by particles of different size parameters α and of different refractive indices. A comparison of the experimental curves of the intensity distribution of scattered light with the theoretical curves gives an estimate of the size of the particles.

DISSYMMETRY OF SCATTERED LIGHT

The second method is based on the dissymmetry of scattered light in the forward and the backward directions. Debye (1946) has worked out the theory of this method for particles of small refractive index. The details of theory and the experimental technique are described by Oster (1948), Mark (1947), and Zimm, Stein and Doty (1945). The Debye theory is not directly applicable to particles of large refractive indices. A study of the Mie scattering functions for particles of different sizes and of different refractive indices indicates, however, a possibility of the application of the dissymmetry method to particles of large refractive indices upto a certain limit of the sizes of the particles. A theoretical evaluation of the dissymmetry of the intensity of scattered light for particles of refractive index as large as 2, indicates that the dissymmetry, i.e., the ratio of the intensities of scattered light about two symmetrical angles in the forward and the backward directions, goes on systematically increasing with the radius of the particles upto a certain size parameter $\alpha (= 2\pi r/\lambda$, r being the radius of the particles and λ being the wavelength of light used). Beyond this value of α , the dissymmetry ratio begins to fluctuate with increasing α and has a number of maxima and minima. It is, therefore, possible to compare the experimental and theoretical dissymmetry values, and to estimate the size of the particles, provided the value of α lies below the given limit.

SCOPE OF THE PRESENT INVESTIGATION

The present investigation was, therefore, undertaken to determine the sizes of colloidal particles by using the above two mutually independent methods based on the scattering of light and also to see how far the two methods are in agreement with each other. Two sols, viz. Fe_2O_3 and As_2S_3 of refractive indices 2.40 and 2.67 respectively, are selected for this purpose. Their relative refractive indices with respect to water are 1.8 and 2 approximately. These sols were prepared according to the methods described by Trivedi and Pattani (1952). Double-distilled water and pyrex vessels were used in all stages of the experiment.

METHOD BASED ON THE ANGULAR DISTRIBUTION
OF SCATTERED LIGHT

By using the data from Lowan's Tables (1949), two sets of theoretical curves for the intensity distribution of scattered light by particles of refractive indices 1.8 and 2, and of different size parameters α ($\alpha < 2$) were obtained. The values of the scattering functions for refractive index 2 are directly available from the tables, but for refractive index 1.8, interpolation was used for obtaining these values. It was found that as the values of the scattering functions increase uniformly with α upto a value 6 for all refractive indices of the particles, this method of interpolation would be applicable in the present case and would not involve much error. Beyond $\alpha=6$, the scattering functions fluctuate rapidly with a large number of maxima and minima and hence interpolation would not be possible. While plotting these curves, the values of the intensity functions were normalized by taking the intensity of scattered light in a transverse direction (i.e. 90°) as unity for a given curve. These curves are shown by dotted lines in figures 2 and 3 for Fe_2O_3 and As_2S_3 respectively. The α value for each curve is indicated in the diagrams. In these curves, the direction of incidence (i.e. forward direction) is taken as zero degree.

Experimental.

In order to investigate the angular distribution of scattered light by the particles of the sol, a photo-cell was mounted on the telescope arm of a spectrometer. A monochromatic beam of light from a strong source was made to be incident through the collimator tube on a circular trough containing the colloidal solution. As the beam converged a little on entering the trough, the incident beam was focused by a lens on a small aperture in the collimating tube and a slightly divergent beam of light from this aperture entered the trough in such a way that the convergence due to the trough made the beam parallel on entering the trough. The experimental arrangement is shown in figure 1. Two suitable standardised

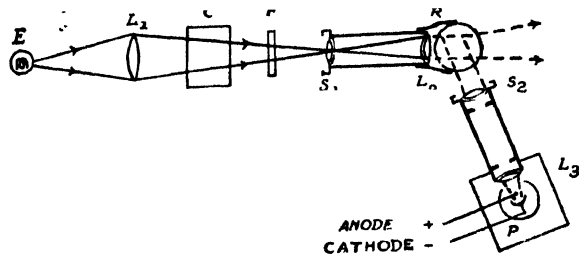


FIG. 1. Experimental arrangement

E—Source of light, L_1 , L_2 —collimators, C—water cell, F—light filter,
 S_1 , S_2 —slits, R—rubber guard ring, L_3 —converging lens, P—photocell

Kodak filters, having narrow transmission bands in the region of 5000 A.U. and 6550 A.U., were selected for getting monochromatic beam of light.

spherical size. Still however, the layout of the experimental curves does indicate a similarity with one or two adjoining theoretical curves. The values of the radii of the particles of the two sols are given in Table I.

TABLE I
Radius of particles from angular scattering of light

Sol	Refractive index	Wavelength in A.U.	α	Radius in μ	Mean radius in μ
Fe_2O_3	1.8	6550	0.5	0.039	0.037
		5000	0.6	0.035	
As_2S_3	2	6550	0.65	0.043	0.042
		5000	0.70	0.041	

METHOD BASED ON DISSYMMETRY OF
SCATTERED LIGHT

The theoretical values of the dissymmetry of scattered light for particles of different sizes and of relative refractive indices 1.8 and 2 were obtained by taking the ratio of the intensity functions I_{45} and I_{135} of scattered light at angles of 45° and 135° respectively (incident direction being taken as zero degree). These dissymmetry ratios are obtained from the data available in Lowan's tables of light scattering functions. These values of dissymmetry are shown graphically in figures 4 and 5 for two sols of refractive index 1.8 and 2 respectively. The dissymmetry ratio I_{45}/I_{135} is expressed by the symbol Z .

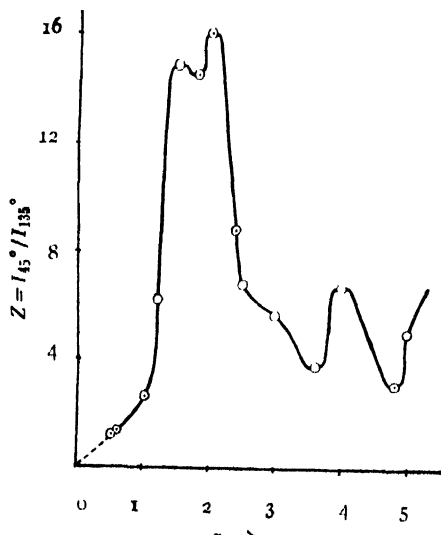


FIG. 4. Theoretical variation of dissymmetry with α for Fe_2O_3 refractive index = 1.8)

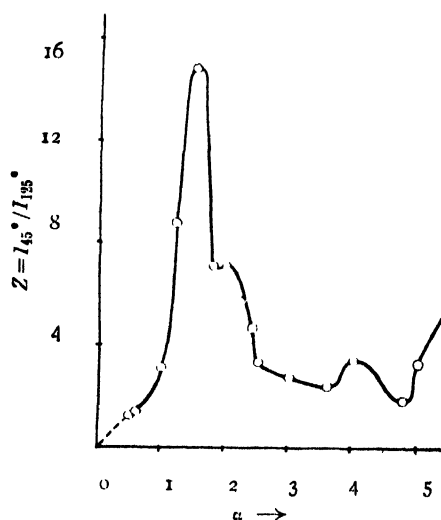


FIG. 5 Theoretical variation of dissymmetry with α for As_2S_3 (refractive index = 2)

The curves show that the dissymmetry function increases systematically with α upto a certain value, beyond which it begins to oscillate and gives rise to a number of maxima and minima. It can be seen that so long as the dissymmetry ratio lies below a value 3 for particles of refractive index 1.8, there is only one value of α for a given value of the dissymmetry ratio. Similarly so long as the dissymmetry ratio lies below a value 1.82 for particles of refractive index 2, there is only one value of α corresponding to a given value of the dissymmetry ratio.

If, therefore, the experimental dissymmetry values lie below 3 for Fe_2O_3 sol of relative refractive index 1.8, and below 1.82 for As_2S_3 sol of relative refractive index 2, it would be possible to estimate the size parameter α and hence the radius of the particles from an experimental determination of the dissymmetry ratios for the two sols. By using two wavelengths of light for the dissymmetry measurements, it becomes possible to obtain two independent α values for the same sol by this method. A mean value of the radius of the particles can then be obtained from these α values.

Experimental.

The experimental procedure consists in measuring the intensity I_{45} and I_{135} of scattered light of a given wavelength along 45° and 135° angles

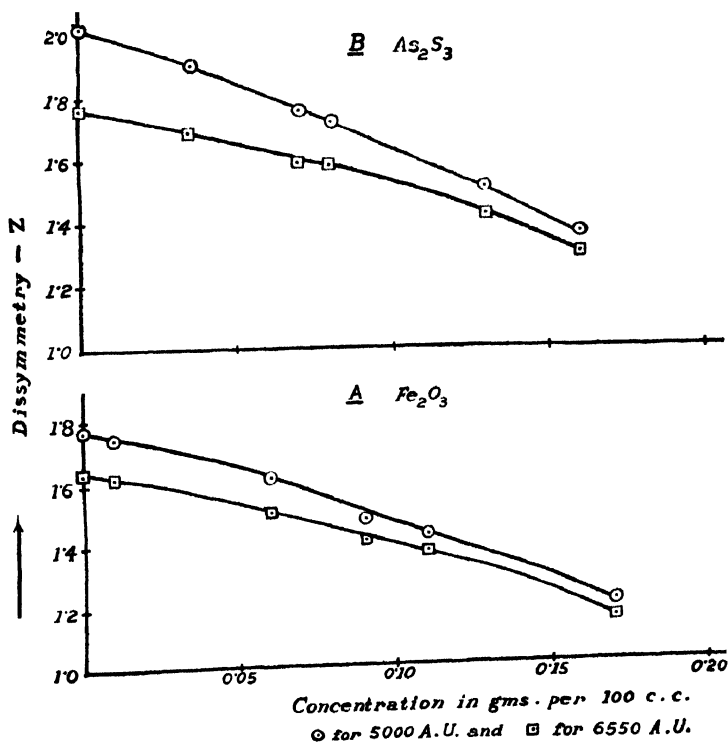


FIG. 6. Graph showing the variations of dissymmetry with concentration.
 B. For As_2S_3 sol. A. For Fe_2O_3 sol.

respectively. The same photoelectric photometer was used for this purpose. As the dissymmetry function is found to be dependent on the concentration to some extent, it is necessary to derive the value of the dissymmetry ratio at infinite dilutions for each wavelength of light used. The dissymmetry ratio $I_{4.5}/I_{13.5}$ was, therefore, determined for five different concentrations of a given sol for each wavelength of light used. The dissymmetry ratio at infinite dilution, which is also known as the intrinsic dissymmetry 'Z', is determined by extrapolation of the curve of dissymmetry ratio versus concentration in each case. These curves are given in figures 6A and 6B for Fe_2O_3 and As_2S_3 respectively. By using the values of the intrinsic dissymmetry, the values of α corresponding to each wavelength of light used was obtained from the theoretical dissymmetry ratio curves for the sol concerned. The radius of the particles r , can be calculated from the

relation $\alpha = \frac{2\pi r}{\lambda'}$, where λ' is the wavelength of light in water. The results

of these measurement are summarised in Table II. Again, in order to compare the values of the radii determined by the two optical methods, both the sets of results are summarised in Table III.

TABLE II

Radius of particles from dissymmetry

Sol	Relative refractive index	λ in A.U.	Experimental dissymmetry	α	Radius in μ	Mean radius in μ
Fe_2O_3	1.8	6550	1.62	0.66	0.052	0.048
		5000	1.77	0.73	0.044	
As_2S_3	2.0	6550	1.78	0.72	0.056	0.052
		5000	20.2	0.80	0.038	

TABLE III

Comparison of radii of particles from two optical methods

Sol	Radius of particles in μ		
	Angular scattering method	Dissymmetry method	Mean
Fe_2O_3	0.037	0.048	0.042
As_2S_3	0.042	0.052	0.047

The above results indicate that the values of the radii determined by the dissymmetry method are slightly higher than those determined by the angular scattering method. It is, however, likely that the dissymmetry method should be more reliable than the angular scattering method, because it involves intensity measurements at two specific angles and they can be done more accurately and quickly than a number of angular intensity measurements. If, therefore, intrinsic dissymmetry is determined accurately for any sol, it would give a reliable measure of the size of the particles of a sol if α is smaller than a given value for each sol. It will be necessary to construct a theoretical dissymmetry curve in each case.

As it is likely that the refractive index of the particles in the sol may not be exactly the same as that of the bulk material, dissymmetry values for different refractive indices varying from 1.33 to 2.0 were obtained from Lowan's Tables. It was, however, found that all the dissymmetry curves do not differ appreciably from each other upto $\alpha = 1.5$. The maximum difference in the values of dissymmetry for a given α , does not exceed by more than 15 per cent for variation of the values of refractive index from 1.33 to 2.0. Thus any small variation of the relative refractive index of the sol particles from the bulk material would not appreciably change the value of the radius of the particles determined by the present dissymmetry method.

CONCLUSIONS

The present investigation shows that it is possible to estimate the size of the particles by two independent methods based on Mie (1908) theory. The dissymmetry method due to Debye (1946) can also be applied to sol particles, of large refractive index but whose size parameter α does not exceed a certain value. The light scattering methods are more reliable than methods based on the transmission of light as the former is less likely to be affected by intrinsic absorption of light.

REFERENCES

- Debye, P., 1946, *J. App. Phys.*, **17**, 392.
 Guinpracht, R. C. and Sliepcevich, C. M., 1951, "Tables of Light Scattering Functions for Particles", Univ. of Michigan.
 La Mer, V. K. and Sinclair, D., 1943, Progress Report on the Verification of Mie's Theory, ORSD Report, 1857.
 La Mer, V. K. and Barnes, J. J. 1946, *J. Coll. Sci.*, **1**, 71, 79.
 La Mer, V. K. and Johnson, I., 1947, *J. Am. Chem. Soc.*, **69**, 1182.
 La Mer, V. K., Inn, C. Y. and Wilson, J. G. 1950, *J. Coll. Sci.*, **5**, 471.
 Lowan, N. A., 1949, Tables of Light Scattering Functions for Spherical Particles, Washington D. C.
 Mark, H., 1947, "Frontiers in Chemistry" Vol. V.
 Mie, G., 1908, *Ann. Physik*, **25**, 377.
 Oster, G. 1948, *Chem. Rev.*, **43**, 316.

Rayleigh, 1871, *Phil. Mag.*, **41**, 107 and 274.

Trivedi, A. M. and Pattani M. J., 1952, *J. Ind. Chem. Soc.*, **29**, 683.

Van der Hulst, H. C., 1946, "Optics of Spherical Particles", Dissertation, Utrecht, Holland.

Wyn-Williams, C. E., 1928, *Phil. Mag.*, **6**, 324.

Zimm, R. H. S ein, R S, and Doty, P., 1945, *Polymer Bull.*, **1**, 90.

INTRINSIC VISCOSITY-MOLECULAR WEIGHT RELATIONSHIP OF HIGH POLYMERS : A NEW EQUATION

BY SANTI R. PALIT

INDIAN ASSOCIATION FOR THE CULTIVATION OF SCIENCE, CALCUTTA-32.

(Received for publication, December, 22, 1954)

ABSTRACT—Based on Eyring's rate theory and the 'hole' theory of liquids the following equation, correlating the intrinsic viscosity, $[\eta]$ and molecular weight of polymers has been derived: $100\rho_0[\eta]=K_1M^{2/3}-\ln M+K_2$, where ρ_0 is the density of the polymer at infinite dilution and K_1 and K_2 are constants. All existing data have been found to be in agreement with this equation. The modified Staudinger equation, $[\eta]=KM^a$, which is in common use, is shown to be a special case of this equation and cases are cited where the latter equation is found to be invalid, whereas the new equation is found adequate.

Critical tests based on differential $[\eta]$ in two solvents for the same polymer have been devised and it is conclusively demonstrated that the modified Staudinger equation leads to inconsistent results and is untenable, whereas the new equation is in conformity with experimental facts.

INTRODUCTION

Great interest has been shown during the past few years in the relationship between the intrinsic viscosity and molecular weight of high polymers. The modified Staudinger equation, $[\eta]=KM^a$, the modification being variously ascribed to Mark, Kuhn or Houwink, is extensively used. Of late, attempts (Brinkman, 1947; Debye *et al*, 1948; Kirkwood *et al*, 1948; Flory, 1949) to derive this equation from theoretical considerations have been made, but so far with not quite satisfactory results. However, recent theoretical development in the field of liquid viscosity based on Eyring's rate theory can be extended to the high polymer field to obtain in a simple manner a satisfactory equation correlating $[\eta]$ and M of high polymers.

Derivation of the New Equation—Based on Eyring's rate theory (Glasstone *et al*, 1947) and the void structure of liquids, Telang (1949) has recently deduced the following equation [eqn. (1)] for the absolute value of the viscosity of any liquid. This equation has the unique feature of not containing any arbitrary constant and has been found to give correct values of molecular weight of many liquids where standard data for all the terms are available.

$$\eta = \frac{hNb}{V^{2/3}(V-b)^{1/3}} \exp\left(-\frac{1.091 \gamma V^{2/3}N^{1/3}}{RT}\right) \quad \dots (1)$$

where h is Planck's constant, N is Avogadro number, b is van der Waals constant, V is molar volume and γ is surface tension.

If we put $b_{sp}M$ and $v_{sp}M$ for b and V respectively, the equation, after taking logarithm becomes

$$\ln \eta = \frac{1.091 \gamma v_{sp}^{2/3} N^{1/3}}{RT} \cdot M^{2/3} - \ln M + \ln \frac{h N b_{sp}}{v_{sp}^{2/3} (v_{sp} - b_{sp})^{4/3}} \quad \dots (2)$$

$$\ln (\eta M) = k_1 \gamma (v_{sp} M)^{2/3} + k_2 \quad \dots (3)$$

In order to use equation (2) we have to evaluate log viscosity of the polymer from data on solution viscosity. Considering a dilute high polymer solution as a mixture of two liquids, the solvent of viscosity η_s and a hypothetical high polymer liquid of viscosity η_p and assuming that the mixture law on volume fraction basis holds good for log viscosity of dilute solutions of high polymers, we have

$$\ln \eta = (1 - \phi) \ln \eta_s + \phi \ln \eta_p \quad \dots (4)$$

where ϕ is the volume fraction of the polymer. If c is concentration in gms. per 100 cc and ρ_0 is the partial specific density of the polymer at infinite dilution, the above equation on proceeding to infinite dilution gives

$$\ln \eta_p = \left[\frac{1}{\phi} \ln \eta / \eta_s \right]_{\phi \rightarrow 0} + \ln \eta_s = 100 \rho_0 \left[\frac{1}{c} \ln \eta / \eta_s \right]_{c \rightarrow 0} + \ln \eta_s = 100 \rho_0 [\eta] + \ln \eta_s \quad \dots (5)$$

Substituting this value of log viscosity in equation (3), we obtain

$$100 \rho_0 [\eta] = k_1 \gamma (v_{sp} M)^{2/3} - \ln M + k_2 - \ln \eta_s \quad \dots (6)$$

Since the surface tension and specific volume of ordinary homologous liquids are found to attain a limiting value at quite a low molecular weight region, we can reasonably expect the same polymer irrespective of molecular weight to have nearly the same value of γ and v_{sp} and so we can put the foregoing equation in the following simple forms.

$$100 \rho_0 [\eta] + \ln M = K_1 [M]^{2/3} + K_2 \quad \dots (7)$$

$$[\eta] = 0.01 v_{sp} K_1 M^{2/3} - 0.023 v_{sp} \log M + K_2' \quad \dots (8)$$

If $[\eta]$ is expressed in cc per grain and is designated by Z_η in conformity with the very recent German practice our equations (7) and (8) become

$$\rho_0 Z_\eta = K_1 M^{2/3} - \ln M + K_2 \quad \dots (9)$$

$$Z_\eta = K_1 v_{sp} M^{2/3} - 2.303 v_{sp} \log M + K_2' \quad \dots (10)$$

Equations (7) and its other forms, viz. (8), (9) and (10) are our final equations.

It is realised that our assumption of mixture law for log viscosity for polymer solutions [equ (3)] is not beyond question, and no doubt, other types of mixture law (Partington, 1951) more in conformity with observations for mixtures, can be utilised and other equations similar in form to our equation

(7) can be deduced. We have, however, done this firstly in order to give our final equation a form containing $[\eta]$ on which extensive data are available and secondly, because it is known (Partington, 1951; Houwink, 1950) that a similar relationship holds good for mixtures of small molecules. It may also be pointed out that equation (3) demands that specific viscosity should be linear in ϕ at low dilutions and we know that this is theoretically justified by the equations of Sakurada (1934), Simha (1940), Kuhn (1933) and others (Guth, et al 1938) in dilute solutions and this has also been found to be experimentally true.

EXPERIMENTAL TEST OF THE PROPOSED EQUATION

We need now examine how far the new equation along with its logical consequences is in agreement with experimental facts, to what extent it is useful for computation of molecular weight from viscosity data and in what respect it differs from the existing equation; and further to devise some way of a critical assessment between the two.

Linear Relationship. A direct consequence of equation (7) is that a plot of $100 \rho_0 [\eta] + \ln M$ against $M^{2/3}$ should be linear. We have tested this relationship for a large number of polymers from available data and in all cases we have observed the plot to be linear. Some typical graphs are shown in figures 1 to 6 and the least square K_1 and K_2 values are collected in Table I. All references to the source of data used for these figures are given at the end of Table I.

In selecting our data we have taken molecular weight values up to about a million because we have felt that osmotic molecular weight for higher values of M are not very reliable owing to unavoidable experimental difficulties. It may also be pointed out that the value of ρ_0 need not be very accurate and hence if partial data are not available apparent data and even the density of the solid polymer would serve well for our equation, but the values of K_1 and K_2 necessarily depend on the chosen value of ρ_0 , and accepting a given value of ρ_0 at a certain temperature allowance has to be made if the same solvent-polymer system is studied at a somewhat different temperature by assuming that ρ_0 changes with temperature in the usual manner for liquids.

Curve A of figure 1 shows the required plot for polyisobutylene in diisobutylene with the very precise data of Flory (1943) covering a molecular weight range of about 10^3 to 10^6 , a more than hundred-fold increase in molecular weight. The plot is sensibly linear over the whole range. In the same graph is also shown a similar plot for the same polymer in cyclohexane (Krigbaum & Flory 1953) (curve B) and the plot is also found to be a good straight line.

TABLE I
 K_1 and K_2 values of polymers

Polymer	Solvent	Temp. °C	ρ_0	Range of M	$K_1 \times 10^3$	K_2	Ref.
Polyethylene	Decalin	70°	0.875	395–33,700	7.782	4.045	a
Polyisobutylene	Di-isobutylene	20°	0.930	$8.7 \times 10^3 - 1.3 \times 10^6$	2.402	11,744	b,c
"	Cyclohexane	30°	0.920	$38 \times 10^3 - 71 \times 10^4$	3.583	5.773	b
Polystyrene	Benzene	20°–40°	1.037– 1.055	$4 \times 10^3 - 1.4 \times 10^6$	2.862	7.397	d,e,f,g,h
"	Toluene	20°–30°	1.045– 1.055	$830 - 1.1 \times 10^6$	2.460	7.819	g,h,i,j,k,l
Polymethyl methacrylate	Acetone	20°	1.180	$25 \times 10^3 - 3.2 \times 10^6$	1.679	–5.460	m
"	Benzene	20°	1.180	$25 \times 10^3 - 3.2 \times 10^6$	2.634	–4.504	m
"	Chloroform	20°	1.180	$25 \times 10^3 - 6.1 \times 10^6$	3.316	3.344	m
"	Benzene	25°	1.180	$56 \times 10^3 - 4.1 \times 10^6$	2.852	4.998	n
Polymethyl acrylate	Benzene	35°	1.055	$46 \times 10^3 - 3.0 \times 10^6$	2.669	6.888	o
Cellulose acetate	Acetone	30°, 40°	1.335	$25 \times 10^3 - 1.3 \times 10^5$	ca. 32	ca. 10	p
"	"	26.5°	1.344	$31 \times 10^3 - 3.6 \times 10^5$	ca. 24	ca. –19	q
"	"	25°	1.345	$12 \times 10^3 - 1.2 \times 10^5$	ca. 40	ca. –48	r
Benzyl Cellulose	Chloroform	35°	1.185	$1 \times 10^4 - 2.4 \times 10^4$	ca. 15.5	ca. –1	s
Triphenylmethyl methyl ethyl cellulose	Dimethyl formamide	35°	1.195	$3 \times 10^4 - 6 \times 10^4$	ca. 11	ca. 9.0	t

- a. Ueberreiter, et al (1952) ; b. Flory (1943) ;
 c. Krigbaum and Flory (1953) ; d. Krigbaum, et al (1952) ;
 e. Kern and Rugenstein (1953) ; f. Bueche (1949) ;
 g. Bawn, et al (1950) ; h. Bawn, et al (1950) ;
 i. Goldberg et al (1947) ; j. Frank and Breitenbach, (1951) ;
 k. Alfrey, et al (1943) ; l. Marzolph and Schulz (1954) ;
 m. Schulz, et al (1953) ; n. Baxendale, et al (1946) ;
 o. Sen, Chatterjee and Palit (1952) ; p. Bartovics and Mark (1943) ,
 q. Badgley and Mark (1947) ; r. Phillip and Bjork (1951) ;
 s. Basu and Roy (1952) ; t. Roy Chowdhury (unpublished work from this laboratory).

In figure 2 are shown such plots for a few cellulose derivatives including a plot of cellulose acetate based on the data of Badgley and Mark (1947). It is of interest to note that though the conventional $\log[\eta]$ versus $\log M$ plot has been found by these authors to be curved in this case, our plot gives a very good straight line. We have, of course, omitted the two points for the two highest molecular weight fractions as the authors themselves have twice

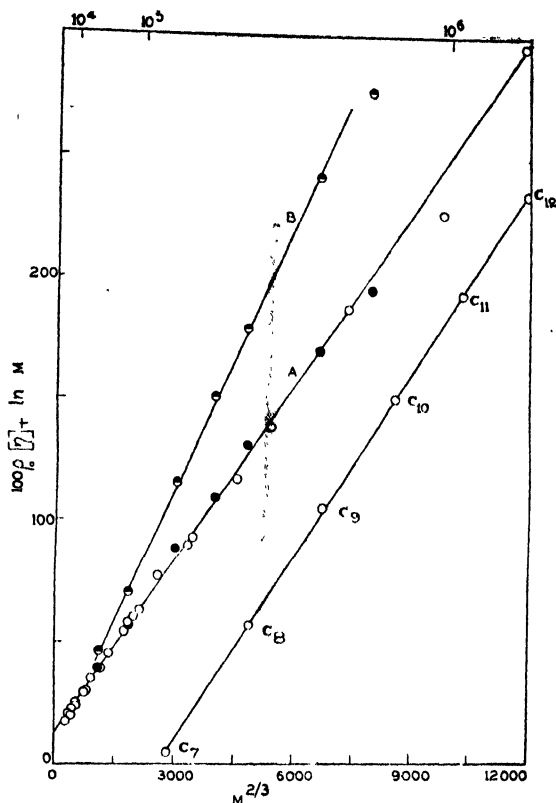


FIG. 1. Viscosity molecular weight plot for polyisobutylene. Curve A in di-isobutylene (open circles, ref: Flory, 1913; dark circles, ref: Krigbaum and Flory (1953). Curve B in cyclohexane, ref: *ibid*; $C\log(\eta M)$ Vs. $\gamma(Mv_r^{2/3})$ for straight chain alkanes in arbitrary units.

expressed uncertainty about them. This linearity, when the conventional $\log[\eta] - \log M$ plot fails, is not due to any insensitivity of our plot as compared to the conventional plot as would be discussed at length later on. In fact, our plot would be shown to be more sensitive than the conventional plot over a larger range of molecular weight. Similar plots have also been made in figure 2 for cellulose acetate based on other data, and a few other cellulose derivatives, e.g. triphenyl-methyl methyl ethyl cellulose in dimethyl formamide and benzyl cellulose in chloroform, etc., and all the curves are found to be linear in agreement with our equation.

We want to draw special attention to figure 3 wherein we have plotted the precise data of Ueberreiter, Orthmann and Sorge (1952) for polyethylene. They have not only determined M and $[\eta]$ values for four fractions but have also obtained data for a highly pure hydrocarbon, $C_{29}H_{58}$. They themselves find that their $\log[\eta] - \log M$ plot is wide off the point for the pure hydrocarbon. Their $\log[\eta] - \log M$ plot showing this departure has been also reproduced in figure 3. However, our plot passes through all the five points which conclusively proves that our equation is valid over

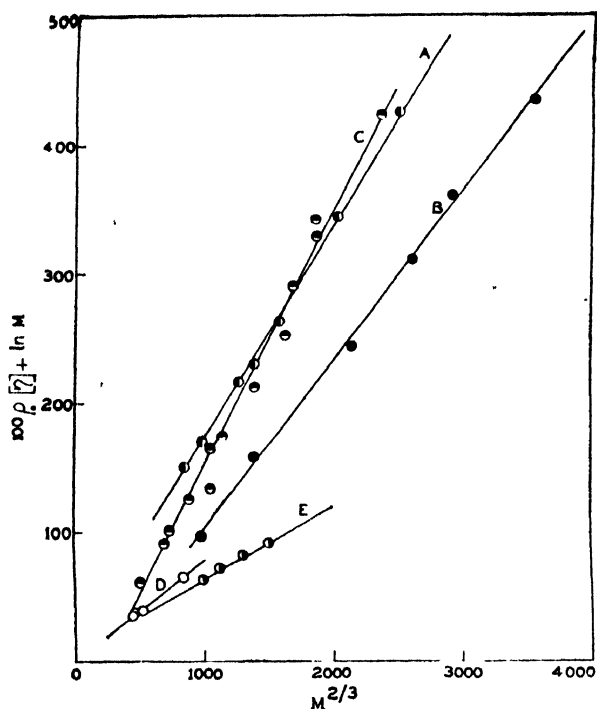


FIG. 2. Viscosity-molecular weight plot of cellulose derivatives. Curves A (Bartovics and Mark, 1943), B (Badgley and Mark, 1947) and C (Phillip and Bjork, 1951) are for cellulose acetate in acetone; D (Basu and Ray, 1952) for benzyl cellulose in chloroform and E (Roy Chowdhury) for triphenylmethyl-methyl-ethyl cellulose in dimethyl formamide.

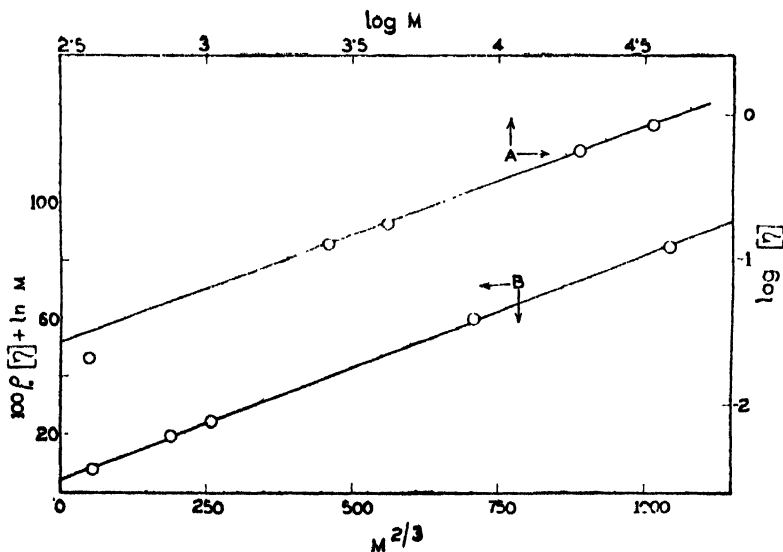


Fig. 3. Intrinsic viscosity-molecular weight relationship of polyethylene. Curve A is $\log[\eta]$ vs. $\log M$ plot. Curve B is according to the new equation $100\rho_0[\eta] + \ln M$ vs. $M^{2/3}$. Data taken from Ueberreiter, *et. al.* (1954).

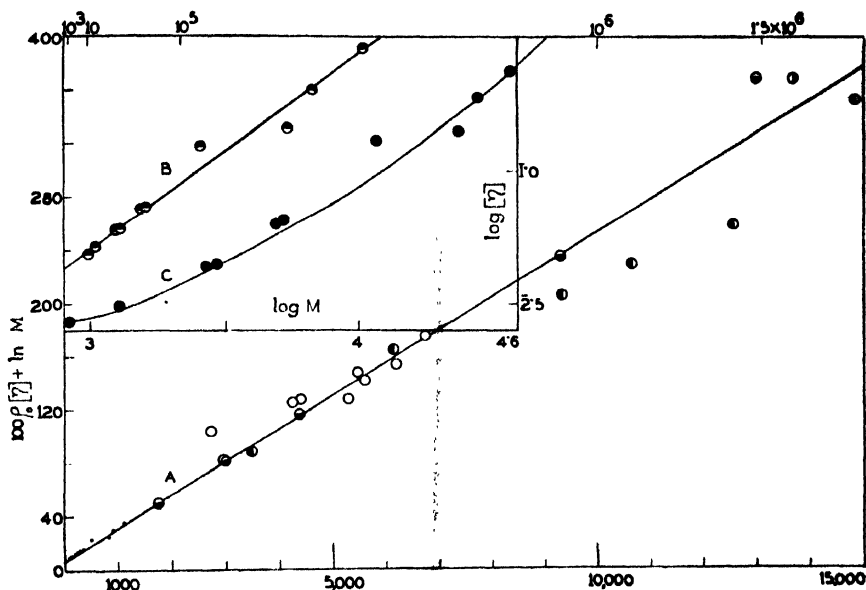


FIG. 4. Viscosity-molecular weight plot of polystyrene in toluene. Shaded circles are for Marzolph and Schulz (1954), lower half shaded circles for Bawn, et.al (1950), left half shaded circles for Alfrey et.al (1943), right half shaded circles for Bawn, Grimley and Wajid (1950), Unshaded circles for Frank, et.al (1951). Inset curve B shows the lowest data (Marzolph, et al, 1951) in a magnified plot, ordinate 6 times and abscissa 4 times magnified. Inset curve C is the conventional $\log [\eta]$ - $\log M$ plot of the same data.

a much wider range than that covered by the modified Staudinger equation. To demonstrate this point more clearly we have compared in Table II the calculated $[\eta]$ values from our least square equation with the experimental ones. It would be seen that the agreement is excellent in all cases and is certainly within the limits of experimental error of $[\eta]$. Similar comparison has also been made on the basis of modified Staudinger equation and it is clearly seen that the agreement is in no way better for the four fractions and is rather poor for the pure hydrocarbon.

It may be pointed out here that though $\ln M$ term in the ordinate is generally rather small in comparison with $100\rho_0[\eta]$, and its variation is comparatively very small in the usual high molecular weight range, it is comparatively quite a large term in the low molecular weight range as in the above case of polyethylenes. In fact, for the lowest point the $\ln M$ -term is more than three times the corresponding value of $100\rho_0[\eta]$, whereas for the highest point the former is only some twelve per cent of the latter. This demonstrates the reality of this term. Though the reality of the ' $\ln M$ ' term is thus demonstrated, in very many cases particularly for systems with comparatively high values of K_1 and over a narrow range and high values of molecular weight, it can be easily shown from our equation that $[\eta]$ would be practically linear with $M^{2/3}$ within the limits of our experimental accuracy of determining M . We have verified this by graphical

TABLE II

Comparison of the experimental and theoretical values for the intrinsic viscosity of polyethylene

M	New equation $100 \rho_0 [\eta] = 7.782 \times 10^{-2} M^{2/3} - \ln M + 4.045$ [η]			Modified Staudinger equation $[\eta] = 3.873 \times 10^{-4} M^{0.738}$ [η]		
	Observed	Calculated	Difference	Observed	Calculated	Difference
33,700	0.850	0.855	+0.005	0.850	0.848	-0.002
18,960	0.574	0.571	-0.003	0.574	0.557	-0.017
4,200	0.180	0.182	+0.002	0.180	0.183	+0.003
2,620	0.130	0.125	-0.005	0.130	0.129	-0.001
395	0.021	0.026	+0.005	0.021	0.032	+0.011

plotting in many cases specially for cellulose derivatives whose K_1 values are unusually high.

Data for polystyrene in toluene have been plotted in figure 4. Curve A is for viscosity data in toluene taken from different sources covering a wide range of molecular weight from below 10^3 to beyond 10^6 . It would be seen that the data upto $M \approx 10^6$ fall on practically the same straight line. The conventional $\log[\eta] - \log M$ plot of these data has been given by Marzolph and Schulz (1954) and they have found that the lowest points considerably deviate from a straight line, the slope falling off at a low range of molecular weight. This falling off at the low range has been shown in the inset curve C in the same figure along with our plot of the same data on a larger scale. Our plot is found to be linear, whereas the $\log[\eta] - \log M$ plot is seen to have a continually decreasing slope in this range. As would be seen later this decrease of slope is a necessary consequence of our equation in this case.

In figure 5 we have plotted the data for polystyrene in benzene from various authors according to our equation along with the conventional $\log[\eta] - \log M$ plot. It would be seen that the $\log[\eta] - \log M$ plot scatters very much more than our plot and in fact, the points from different authors show varied slopes and can hardly be accommodated on the same line, whereas the fit is much better with our equation at least upto a million molecular weight. However, for polystyrenes prepared at not too high temperatures we recommend use of our equation in toluene at 20°C , as the latter solvent shows greater consistency.

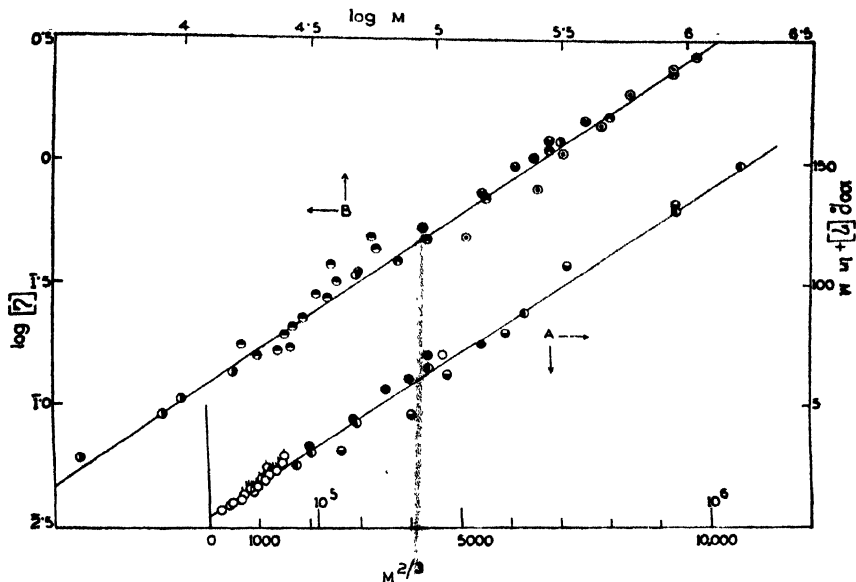


FIG. 5. Viscosity-molecular weight plot of polystyrene in benzene; Curve A is according to the new equation, curve B is the conventional $\log [\eta] - \log M$ plot. Data from Krigbaum et.al. (1952), Kern and Rugenstein (1953), Bueche (1949), Bawn, et.al (1950), Bawn, et.al. (1950).

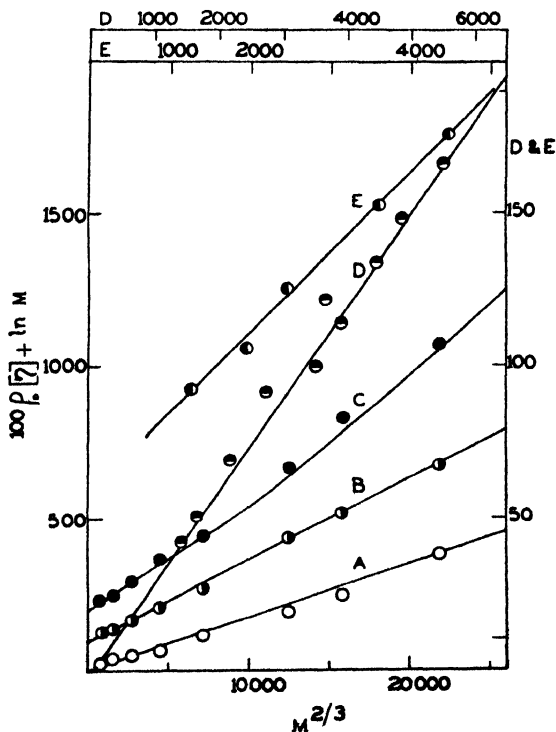


FIG. 6. Viscosity-molecular weight plot of polyacrylates according to the new equation. Curves A, B and C are for polymethyl methacrylates in acetone, benzene and chloroform respectively. Data from Baxendale, et. al (1946). Curve E for polymethyl acrylate (data from Sen, et. al., 1952).

In figure 6 we have plotted some recent data on acrylates and the plots in all cases except for methyl methacrylate in chloroform are found to be good straight lines in agreement with our equation. Our equation shows a definite rising tendency in chloroform for molecular weight of a few millions and onward, where the intrinsic viscosity is inordinately high. Such intrinsic viscosity values may not be useful for our equation as they are known to be strongly affected by shear gradient and this along with the uncertainty in molecular weight determination in this very high range may contribute to this deviation from our equation.

Sensitivity and Computational Error.

It might be surmised that in our equation M is much less sensitive to $[\eta]$ in comparison with the modified Staudinger equation. This is, however, not so, as can be seen from the calculations in Table II. This can, however, be theoretically demonstrated as below. By differentiating equation (7) with respect to $[\eta]$ and M , we can obtain the following equations:

$$d \ln [\eta] = d \ln M \times \frac{2}{3} \left(\frac{K_1 M^{2/3} - 1.5}{K_1 M^{2/3} + K_2 - \ln M} \right) \quad \dots \quad (11)$$

$$\frac{\partial \ln \eta}{\partial \ln M} = \frac{2}{3} \nu, \text{ where } \nu = \frac{K_1 M^{2/3} - 1.5}{K_1 M^{2/3} + K_2 - \ln M} \quad \dots \quad (12)$$

Hence, the calculated percentage accuracy of M is $3/2 \times 1/\nu$ times the percentage accuracy of $[\eta]$. As would be shown in a later section ν is very near to unity in the usual experimental range for most polymers and so the uncertainty of M is 1.5 times the uncertainty of $[\eta]$. This sensitivity compares very well with the value $1/\alpha$ which is the value of the above sensitivity for the modified Staudinger equation.

Though we have demonstrated above that the error in M for a given error in $[\eta]$ would be nearly the same in both the equations, there is, however, a very large source of error in the modified Staudinger equation. In the latter equation M is highly sensitive to α and it can be easily shown by proper differentiation of the modified Staudinger equation that for a given value of $[\eta]$, the calculated value of M would have an accuracy of $\ln M$ times that of α . Since α can be relied upon to an accuracy of about one per cent (generally the uncertainty is higher) we can never expect to calculate M at about 10^5 to an accuracy better than about 12 per cent.

The situation, however, is quite different with the new equation as M has no such disproportionate sensitivity with respect to the constants, K_1 and K_2 . It is easily shown that our calculated value of M in the useful region, viz, 10^4 to 10^6 , is generally of the order of, and very often better than, the accuracy of K_1 and K_2 . Further, the computed value of M becomes increasingly precise with increase in molecular weight, whereas the accuracy decreases with increase in molecular weight in the case of the modified Staudinger equation. This is the reason why a difference of even half a

million in molecular weight in the million range would not appear very much off the line in a $\log[\eta] - \log M$ plot, whereas it would be sharply brought out in our plot. It is no doubt true that equal difference does not also get equal weightage in our plot, but the M -values are certainly more widely spaced in our plot than in the conventional $\log [\eta] - \log M$ plot.

Deduction of Modified Staudinger Equation.

It is easy to see that under certain conditions particularly at high values M our equation reduces to the modified Staudinger equation. Thus, from equation (12) as written below

$$\frac{d \log [\eta]}{d \log M} = \frac{2}{3} \left\{ \frac{K_1 M^{2/3} - 1.5}{K_1 M^{2/3} + K_2 - \ln M} \right\} = \frac{2}{3} \nu$$

it is easy to see that for high values of M , ν tends to unity and so our equation reduces to the modified Staudinger equation with the exponent $\alpha = 2/3$. That the exponent α tends to be $2/3$ has already been noted by many previous workers (Carter, *et al*, 1946).

This is equivalent to neglecting the second and the third term on the right hand side of equation (8) as shown below,

$$[\eta] = K_1' M^{2/3} - \frac{0.023}{\rho_0} \log M + K_2'$$

$$[\eta] = K_1' M^{2/3} \approx K M^{2/3} \quad \dots (13)$$

We can, however, go one step further by calculating the order of the values of K_1' which is equal to the Staudinger constant, since our expression for K_1' does not contain any arbitrary constant. This we can do by putting $\gamma = 20$ and $\rho = 0.9$ in the expression for K_1' [equation (2)] which are fairly representative values for nonpolar compounds when we obtain $K_1' = 9 \times 10^{-4}$. We have thus arrived at a theoretical interpretation of the interesting observation that the modified Staudinger constant K is generally of the order of 10^{-4} .

Numerical Values of K_1 and K_2

Since our equation does not contain any adjustable parameter we can roughly compute the values of K_1 and K_2 and check if the experimental values are of the expected order. Taking the usual values as above, K_1 comes out to be near about 9×10^{-2} i.e. of the order of 10^{-2} for all high polymers. Table I shows how nicely this theoretical expectation is fulfilled by experimental data.

An instructive case of how K_1 in our equation always comes in the theoretically expected range whereas K of modified Staudinger equation shows a wide scatter can be studied from the data of Alfrey, Bartovics and Mark (1943). Their K -values for three samples of polystyrene prepared at 60° , 120° and 180°C are 1.6×10^{-2} , 6.6×10^{-3} and 4×10^{-4} respectively, thus showing a variation of about forty times. Our K_1 values, however,

are 2.3×10^{-2} , 3.7×10^{-2} and 3.6×10^{-2} , an extreme variation of merely 1.6 times in excellent corroboration of our theoretical expectation.

The calculation of K_2 requires a knowledge of the free volume per gram. We can write K_2 in the following form

$$K_2 = \ln h N + \frac{2}{3} \ln b_{sp}/v_{sp} + \frac{1}{3} \ln b_{sp}/\phi_{sp} + \ln 1/\phi_{sp} - \ln \eta_s \quad \dots (14)$$

where ϕ_{sp} is the free volume in cc per gram. Making the very drastic approximation that $b_{sp} \simeq v_{sp} \simeq 1$, we have to a first approximation

$$K_2 = \ln h N - \frac{4}{3} \ln \phi_{sp} - \ln \eta_s \quad \dots (15)$$

Taking that about one per cent is void inside liquids under usual conditions we get $K_2 \simeq 4$. Thus we find that K_2 has to be a small number whose value would be of the order of unity. This expectation is fairly confirmed experimentally as is seen from Table I. It seems from general consideration of our equation and the experimental figures that K_1 is related to the shape of the molecule and K_2 is related to compactness of packing inside the solvent, the K_1 values increasing with the stiffness and consequent approach to a rod shape of the chain molecule, and the K_2 values decreasing with increasing branching of the chain. However, this is only conjectural and a thorough understanding of the significance of these constants has to await further theoretical development in this line.

Slope of the log $[\eta]$ -log M curve According to our equation the slope of log $[\eta]$ -log M curve is given by equation (12) as below.

$$\text{Slope} = \frac{2}{3} \left\{ \frac{K_1 M^{2/3} - 1.5}{K_1 M^{2/3} - \ln M + K_2} \right\} = \frac{2}{3} \nu$$

It can be easily shown that for the usual values of K_1 and K_2 , ν tends to unity as M approaches 10^5 and higher, and therefore the log $[\eta]$ -log M slope is near about $2/3$ in this region. It is further to be noted that our expression for the slope is quite insensitive to a change of M in this usual range of M and this explains the observed approximate linearity of the log $[\eta]$ -log M curve over this range.

An examination of the variation of ν with change of K_1 and K_2 and M leads to a clear understanding of the observed behaviour of log $[\eta]$ -log M curve. From figure 3 it is seen that the log $[\eta]$ -log M line passes quite high above the point for the lowest molecular weight polyethylene ($C_{22}H_{44}$) which shows that at nearabout this region the log $[\eta]$ -log M curve has a decidedly higher slope. The behaviour of polystyrene, however, is just the opposite as can be easily seen from the figure given by Marzolph and Schulz (1954) who have collected much available data, and find that the log $[\eta]$ -log M curve has a continuously decreasing slope with lowering of molecular weight (figure 4, curve C).

The above behaviour is easily understood from figure 7 wherein we have plotted ν against log M for polystyrene and polyethylene, the data for K_1 and K_2 being taken from Table I. A value of $\nu = 1$ means that the log $[\eta]$ -log M

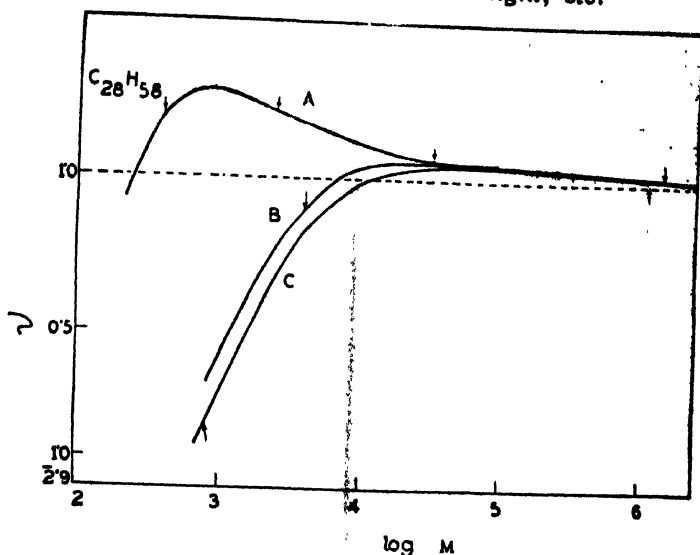


FIG. 7. Theoretical variation according to the new equation of slope of $\log [\eta] \cdot \log M$ plot with molecular weight. Curve A for polyethylene in decalin, B for polystyrene in benzene, C for polystyrene in toluene. The arrow heads mark range of molecular weights.

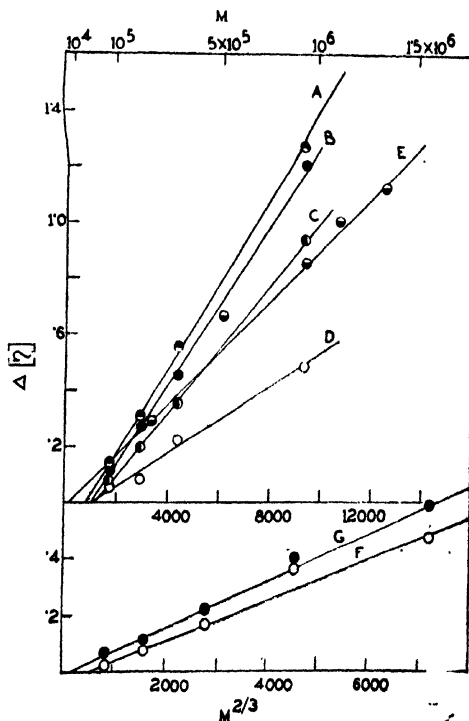


FIG. 8. Differential intrinsic viscosity-molecular weight plot of polystyrene, A: Benzene-M.E.K., B—toluene-toluene 50: heptane 50; C toluene-toluene 80: methanol 20, D—benzene: ethylbenzene, E—toluene-M.E.K. Data from Bawn, et. al (1950), Bawn et.al (1950) Goldberg, et. al, (1947); and of polymethyl methacrylate F—acetone; benzene; G—chloroform: acetone. Data from Schnitz et. al, (1953).

curve has a slope of $2/3$. On the graph for polyethylene we have indicated by dots the experimental points studied by Ueberreiter and coworkers (1952) and similarly we have marked off the regions of study for polystyrene by arrows.

It is easily seen from the trend in the value of ν in the above graph that for polystyrene the slope has to remain constant at nearabout $2/3$ in the usual experimental range, and has to fall off continuously in the low molecular weight region. It is to be pointed out that though the slope of the $\log [\eta]$ - $\log M$ line falls off in the low molecular weight region it is sensibly a straight line in our plot as expected. We, therefore, consider it unnecessary to invoke the concept of chain branching to explain the change of slope as has been done by Marzolph and Schulz (1954).

Equally evident is the reason why the lowest experimental point for polyethylene is below the curve and the slope there has to be high. The lowest experimental point happens to fall on a high value of ν and so has to be below the line. Further in the region investigated ν has an average value 1.13 and so the $\log [\eta]$ - $\log M$ slope should be $0.66 \times 1.19 = 0.736$ in agreement with the observed slope of 0.738.

Effect of a Change of Solvent on $[\eta]$. If $[\eta]_1$ and $[\eta]_2$ be the intrinsic viscosities of a polymer in two different solvents, it can be easily shown on the basis of our equation that they are related by the equation.

$$\rho_1[\eta]_1 - \rho_2[\eta]_2 = a'M^{2/3} + b' \quad \dots (16)$$

where a' and b' are constants given by $100a' = (K_1)_1 - (K_1)_2$ and $100b' = (K_2)_1 - (K_2)_2$. Since $\rho_1 \simeq \rho_2$, the above equation becomes

$$\Delta[\eta] = [\eta]_1 - [\eta]_2 = aM^{2/3} + b$$

where a is equal to a'/ρ . Thus we obtain the interesting result that the difference in viscosity is a linear function of $M^{2/3}$. That this is true is shown in figure 8 for polymethyl methacrylate and polystyrene in a number of solvent pairs. The usually quoted relation which directly follows from the modified Staudinger's equation that $\log [\eta]_1$ is linear in $\log [\eta]_2$ is also expected to be approximately true from our equation in the usual experimental range as can be easily seen by a calculation of $\partial \log [\eta]_1 / \partial \log [\eta]_2$ from our equation (9) being equal to ν_1/ν_2 .

A Critical Test between the two Equations—A critical test can be easily devised between the proposed equation and the modified Staudinger equation, success or failure of which can decide one way or the other. We write below our foregoing equation and also its counterpart based on the modified Staudinger equation.

$$\text{New equation :—} \quad \Delta[\eta] = [\eta]_1 - [\eta]_2 = aM^{2/3} + b \quad \dots (17)$$

Modified Staudinger equation :—

$$\Delta[\eta] = [\eta]_1 - [\eta]_2 = M^{2/3} \{K_1 M^{\alpha_1 - 2/3} - K_2 M^{\alpha_2 - 2/3}\} \quad \dots (18)$$

It can be easily seen that $\Delta[\eta]$ has to vanish absolutely at $M=0$, according to equation (18) whereas our equation expects a very small but

not necessarily zero value. The fact that both the equations cease to have a meaning long before M approaches zero is immaterial for the present purpose, and the extrapolated line has to pass through the origin in a $\Delta[\eta]$ versus $M^{2/3}$ (or for that matter any positive power of M) plot if equation (18) is valid. That this is not so is clearly seen from curves A and B of figure 8. In fact, some of these lines meet the $M^{2/3}$ -axis at quite a high value of M , viz. $M > 50,000$. This conclusively shows that there are inconsistencies in the modified Staudinger equation and so it cannot claim to be a true description of facts. At least, the algebraic form of the modified Staudinger equation is formally inadequate.

It is possible to design another subtle critical test based on equation (18). It is evident that since α is very near to 0.66 for most polymers, the quantity in bracket on the right hand side of equation (18) is simply $K_1 - K_2$ for low values of M and so the equation becomes

$$\Delta[\eta] \simeq M^{2/3}(K_1 - K_2) \quad \dots (19)$$

Thus, for such cases we should expect the slope of the $\Delta[\eta]$ versus $M^{2/3}$ line to be equal to $(K_1 - K_2)$. Frequently we observe not only a discrepancy with the above equation (19) but a positive slope is obtained where we should expect a negative slope.

Thus we cannot escape the conclusion that either the modified Staudinger equation is insufficient or that the K and α values are inconsistent. There is, however, no such difficulty with our equation as can be seen from the form of our equation. We feel that if the modified Staudinger equation is to be retained and has to serve any useful purpose, the above inconsistencies have to be removed, which seems to be an almost impossible task within the limits of two adjustable parameters.

Low Molecular Weight Liquids. Another important point in favour of the present equation is that this equation is not only true for polymers but the basic equation viz. equation 3, has been shown by the present author (Palit, 1952) to be very accurately followed by homologous liquids of low molecular weight. This is illustrated for hydrocarbons in figure 1 (curve C) where $\log(\eta M)$ is found to be accurately linear with $\gamma v_p^{2/3} M^{2/3}$ from C_3 to C_{12} alkanes with almost the theoretical slope in agreement with our equation (2). Other deductions from equation (2) have also been found (Palit, *loc. cit*) to be experimentally valid.

CONCLUSIONS

It is hence concluded that the proposed equation is in quantitative agreement with known facts, covers a wider range of molecular weight, is as sensitive as, if not more than, the current equation, answers satisfactorily the differential viscosity test, and has a theoretical background. Even considered as an empirical equation it scores over the modified Staudinger equation on many counts. The latter equation has also been demonstrated

to be formally inadequate from differential viscosity studies in two solvents. It is hoped that the proposed equation would be used in preference to the purely empirical modified Staudinger equation now in use in consideration of the above points.

REFERENCES

- Alfrey, T., Bartovics, A. and Mark, H., 1943, *J. Amer. Chem. Soc.*, **65**, 2319.
 Badgley, W. J. and Mark, H., 1947, *J. Phys. Coll. Chem.*, **51**, 58.
 Basu, S. and Roy, H. B., 1952, *J. Sci. Ind. Res.* **11B**, 94.
 Bartovics, A. and Mark, H., 1943, *J. Amer. Chem. Soc.*, **65**, 1901.
 Bawn, C. E. H., Grimley, T. B. and Wazid, M. A., 1950, *Trans. Farad. Soc.*, **46**, 1112.
 Bawn, C. E. H., Freeman, R. F. J. and Kamaliddin, A., 1950, *Trans. Farad. Soc.*, **46**, 1107.
 Baxendale, J. H., Bywater, S. and Evans M. G., 1946, *J. Polymer. Sci.*, **1**, 237.
 Bueche, A. M., 1949, *J. Amer. Chem. Soc.*, **71**, 1452.
 Brinkman, H. C., 1947, *Appl. Sci. Res. A.*, **1**, 27.
 " " 1947, *Physica.*, **13**, 447.
 Carter, W. C., Scott, R. L. and Magat, M., 1946, *J. Amer. Chem. Soc.*, **68**, 1480.
 Debye, P. and Bueche, A. M., 1948, *J. Chem. Phys.*, **16**, 573.
 Flory, P. J., 1943, *J. Amer. Chem. Soc.*, **65**, 372.
 Flory, P. J., 1949, *J. Chem. Phys.*, **17**, 303.
 Frank, H. P. and Breitenbach, J. W., 1951, *J. Polymer. Soc.*, **6**, 609.
 Glasstone, S., Laidler, K. J. and Lyring, H., 1947, *Theory of Rate Processes*, McGraw Hill, Ch. IX, p. 477.
 Goldberg, A. I., Hohenstein, W. P. and Mark, H., 1947, *J. Polymer. Sci.*, **2**, 503.
 Guth, R. and Gold, O. 1938, *Phys. Rev.*, **53**, 322.
 Houwink, R., 1950, *Elastomers and Plastomers*, Elsevier, Vol. 1, 441.
 Kern, W. and Rugenstein, M., 1953, *Macro. chemie*, **11**, 1.
 Kirkwood, J. G. and Riseman, J., 1948, *J. Chem. Phys.* **16**, 565.
 Krigbaum, W. R. and Flory, P. J., 1953, *J. Amer. Chem. Soc.*, **75**, 1775.
 Krigbaum, W. R., Mandelkern, L. and Flory, P. J., 1952, *J. Polymer Sci.*, **9**, 381.
 Kuhn, W., 1933, *Kolloid, Z.*, **62**, 269.
 Marzolph, H. and Schulz, G. V., 1954, *Makro. Chemie.* **13**, 120.
 Palit, S. R., 1952, *Ind. J. Phys.* **62**, 627.
 Partington, J. R., 1951, *An Advanced Treatise on Physical Chemistry*, Longman, Vol. 2, 115.
 Phillip, H. J. and Bjork, C. F., 1951, *J. Polymer Sci.*, **6**, 549.
 Roy Chowdhury, D. K., (unpublished work in this laboratory)
 Sakurda, I., 1934, *Kolloid, Z.*, **62**, 2
 Schulz, G. V., Cantow, H. J. and Meyerhoff, G., 1953, *J. Polymer Sci.*, **10**, 79.
 Sen, J. N., Chatterjee, S. R. and Palit, 1952, *J. Sci Ind Res*, **11B**, 90.
 Simha, R., 1940, *J. Phys. Chem.*, **44**, 25.
 Telang, S. S., 1949, *J. Chem. Phys.*, **17**, 536.
 Ueberreiter, K., Orthmann, H. J., and Sorge, G., 1952, *Makro. Chemie*, **8**, 21.

BETA ENERGETICS AND NUCLEAR SHELL STRUCTURE

BY S. N. GHOSHAI, AND A. N. SAXENA

INSTITUTE OF NUCLEAR PHYSICS, CALCUTTA-9

(Received for publication, November 27, 1954)

ABSTRACT. The occurrence of discontinuities in the binding energies of the last neutron or last proton in nuclei at magic numbers of neutrons or protons causes discontinuities to appear in the β^- -disintegration energies $E_\beta(A, Z)$ of radioactive nuclei. The difference $\epsilon_\beta(A, Z)$ between the observed values of $E_\beta(A, Z)$ and the values calculated from the Fermi-Weizsäcker mass formula for a series of isotopes ($Z=\text{constant}$) have been plotted against the neutron number N in these nuclei. Discontinuities are found to appear at $N=50, 82$ and 126 .

In order to show the nature of variation of the pairing energy term in the β^- -disintegration energy, the observed $E_\beta(A, Z)$ values have been plotted against Z for isobaric sequences for various odd values of A . The pairing energy terms have been derived from the $\epsilon_\beta(A, Z)$ values of these isobaric sequences and the corresponding values of B_1 , the slope of the isobaric line without the pairing energy term, have been deduced. The departure of the B_1 values from the calculated values are discussed. The effect of shell crossing on these isobaric lines is also discussed.

Evidences for the occurrence of discontinuity in the pairing energy term for even I nuclei have been observed.

1. INTRODUCTION

(One of the most direct evidences for the existence of shell structure within nuclei is the occurrence of discontinuities in the binding energies of neutrons and protons within the nuclei at the magic neutron and proton numbers. The sharp drop in these binding energies are revealed more clearly when the contributions to the binding energies from the bulk effect (i.e., the binding energies calculated by using Fermi-Weizsäcker mass formula) are subtracted from the observed values. This has been done by Harvey (1951) and Edmonds (1953) in the regions of neutron magic numbers.

The discontinuities occurring in the binding energies of neutrons and protons in nuclei at magic numbers will be reflected as discontinuities appearing in the β^- -decay energies of various nuclei if either the parent or the product nucleus contains a magic nucleon number. Recently, Way and Wood (1954) have plotted the experimental β^- -disintegration energies of the isotopes of a large number of elements throughout the periodic chart against neutron numbers and have observed discontinuities in the β^- -disintegration energy lines for the isotopes at the magic neutron numbers. They have made separate plots for the even and odd A nuclei, so that the

"spin effect," i.e. the pairing energy effect may not interfere with the observation of the discontinuities.

The plot of the differences between the experimental and calculated binding energies of nucleons within nuclei for a series of isotopes or isotonies against the corresponding nucleon numbers suggested that a similar plot of the β^- -disintegration energies of the various isotopes of an element against the neutron numbers of the nuclei would reveal the discontinuities at the magic neutron numbers more prominently than in the Way and Wood plots.

If we denote the experimental β^- -disintegration energies by $E_\beta^{(e)}(A, Z)$, and those calculated from the Fermi-Weiszäcker mass formula by $E_\beta^{(c)}(A, Z)$, then

$$\epsilon_\beta(A, Z) = E_\beta^{(e)}(A, Z) - E_\beta^{(c)}(A, Z) \quad \dots (1)$$

Using the notations used by Coryell (1953) in writing the mass formula, we have,

$$E_\beta^{(c)}(A, Z) = B_A(Z_A^* - Z - 0.5) \text{ for odd } A \text{ nuclei.} \quad \dots (2a)$$

$$= B_A(Z_A^* - Z - 0.5) \mp \delta_1 \text{ for even } A, \text{ odd } Z \text{ (plus) } \left. \begin{array}{l} \text{and even } Z \text{ (minus) nuclei.} \end{array} \right\} \quad \dots (2b)$$

Here

$$B_A = \frac{M_n - M_p + a_3}{Z_A^*}$$

$$Z_A^* = \frac{(M_n - M_p + a_3)A}{2a_3 + 6e^2 A^{2/3} / 5r_0}$$

where a_3 is the coefficient of the symmetry term in the mass formula (Bohr and Wheeler, 1939). δ_1 is the so-called spin-effect or the pairing energy term for the even A nuclei, given by $\delta_1 = 67/A^{3/4}$ Mev (Fermi, 1949).

Coryell (1953) has shown that the actual (observed) masses of the nuclei should be represented by a formula of the F-W type, though with different values of Z_A in the different shell regions. Besides, a pairing energy term for the odd A nuclei also should be introduced which is zero in the F-W mass formula. The observed β^- -disintegration energies should then be represented in the following manner :

$$E_\beta^{(e)}(A, Z) = B_A(Z_A - Z - 0.5) \mp (\pi - \nu) \text{ for } A \text{ odd, } Z \text{ even (minus) } \left. \begin{array}{l} \text{and } Z \text{ odd (plus) nuclei.} \end{array} \right\} \quad \dots (3a)$$

$$= B_A(Z_A - Z - 0.5) \mp (\pi + \nu) \text{ for } A \text{ even, } Z \text{ even (minus) } \left. \begin{array}{l} \text{and } Z \text{ odd (plus) nuclei.} \end{array} \right\} \quad \dots (3b)$$

We then have,

$$\epsilon_\beta(A, Z) = B_A(Z_A - Z_A^*) \mp (\pi - \nu) \text{ for odd } A \text{ nuclei.} \quad \dots (4a)$$

$$= B_A(Z_A - Z_A^*) \mp (\pi + \nu - \delta_1) \text{ for even } A \text{ nuclei} \quad \dots (4b)$$

Coryell (1953) assumed that for even A nuclei,

$$\pi + \nu \approx \delta_1$$

so that any observed discontinuity in the value of ϵ_β for even A isotopes would directly give the discontinuity in Z_A at shell crossing :

$$\Delta\epsilon_\beta(A, Z) = B_A \Delta Z_A \text{ for even } A \text{ nuclei.}$$

For odd A nuclei on the other hand, $\Delta\epsilon_\beta$ at shell crossing will include the discontinuity in $(\pi - \nu)$ value over and above the effect of Z_A discontinuity (Coryell, 1953).

II. DISCONTINUITY IN $\epsilon_\beta(A, Z)$ AT SHELL CROSSING

The experimental β^- -disintegration energy values of a fairly large number of nuclei are known or can be estimated [(Way, Fano, Scott and Thew (1950), Way, Wood and Thew (1951), Way, Fuller, Wood, Thew and Jurgens (1951), Way, Fuller, Wood, Thew and Jurgens (1952), Hollander, Perlman and Seaborg (1953), Way and Wood (1954), and new nuclear data lists of Nuclear Science Abstracts)]. Only those values have been selected in the present work which are fairly well established. In a few cases the β^- -energies have been extrapolated from the Way and Wood plots (1954). The calculated values were taken from the Table of Atomic Masses by Metropolis and Reitwiesner (1950). The differences $\epsilon_\beta(A, Z)$ for the isotopes of a number of elements in different shell regions are plotted against N in figures 1 to 3. The even and odd A isotopes have been separately plotted. The products $B_A(Z_A - Z_A^*)$ have also been plotted in these graphs (broken lines) using the Z_A values estimated by Coryell.

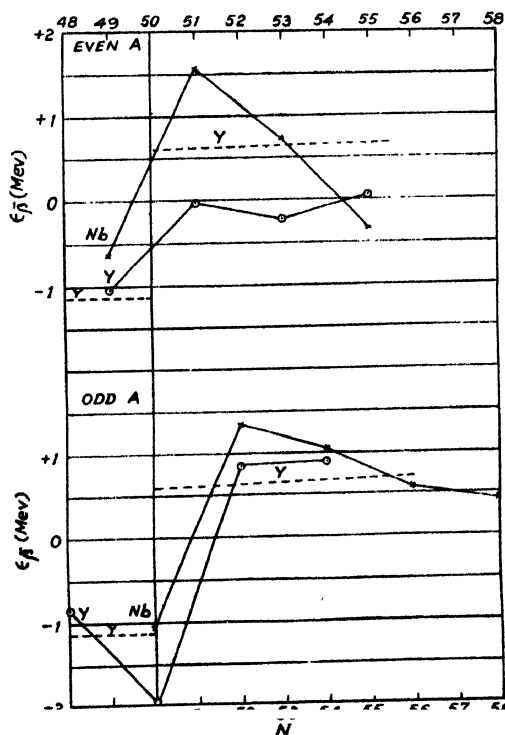


Fig. 1. Plot of ϵ_β^- against neutron number N for the isotopes of Nb and Y. $B_A(Z_A - Z_A^*)$ has been plotted as a dotted line.

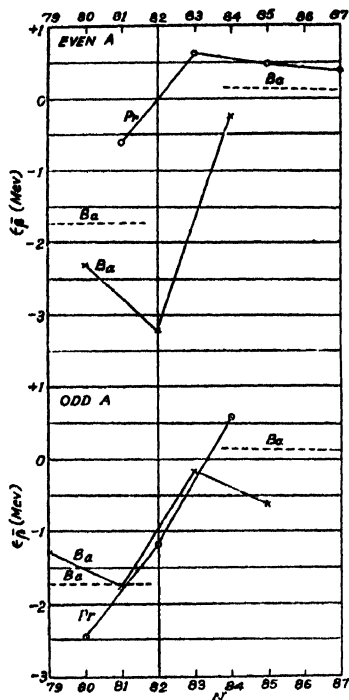


Fig. 2. Plot of ϵ_{β^-} against neutron number N for the isotopes of Ba and Pr. $B_A(Z_A - Z_A^*)$ has been plotted as a dotted line.

From equations (4a) and (4b) we observe that owing to the discontinuity in Z_A at shell crossing, there should be discontinuities in the slope as well as in the absolute magnitude of ϵ_{β^-} at the magic numbers of neutrons.

Since the plots of Z_A and Z_A^* against A are approximately parallel straight lines in the different shell regions, the difference $B_A(Z_A - Z_A^*)$ when plotted against A should be a straight line approximately parallel to the A -axis. Therefore the ϵ_{β^-} lines for a series of isotopes should be straight lines roughly parallel to the A -axis [(see eqns. 4(a) and 4(b)], if the pairing energy terms are assumed to be independent of A , with a discontinuity at shell crossing. From figure 3 we see that this is true for the crossing of the neutron shell at $N=126$. Further, the slopes of the ϵ_{β^-} lines in any shell region should approximately be the same for both even and odd A isotopes. This is also found to be true in the shell region above $N=126$. However, in the other shell regions, these criteria are not satisfied. For instance, for the isotopes of Nb ($Z=41$), the slope of the ϵ_{β^-} line above $N=50$ is not only considerably different from the predicted near-zero slope, but for the even and odd isotopes of this element, the slopes are distinctly different from one another (see figure 1). This probably indicates variation of the pairing energy term with mass number of the isotopes, not only for the odd A nuclei, ($\pi-\nu$ term), but also for the even A nuclei ($\pi+\nu-\delta_A$ term). The latter variation shows that the assumption of $(\pi+\nu)$ being approximately equal to the Fermi pairing energy term δ_A is not always valid. In fact, as we shall see later

in Section V, there are evidences that the $(\pi + \nu)$ terms show discontinuities similar to the $(\pi - \nu)$ terms at shell crossings.

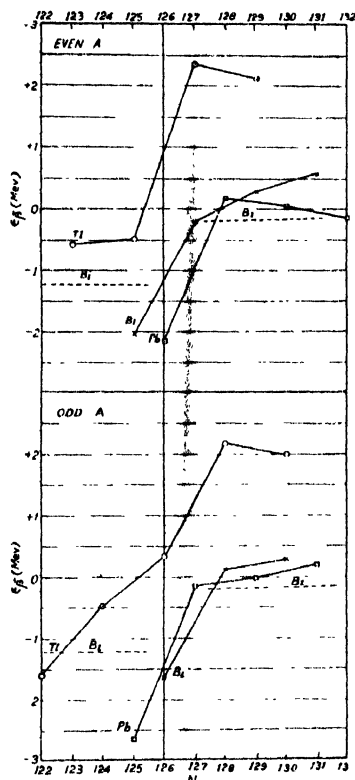


Fig. 3. Plot of ϵ_{β^-} against neutron number N for the isotopes of Tl, Pb and Bi $B_1(Z_A - Z_A^+)$ has been plotted as a dotted line.

III. EFFECT OF PAIRING ENERGY TERM ON ISOBARIC SEQUENCE

According to eqns. 2(a) and 2(b) the β^- -disintegration energies calculated from the F-W mass formula for *odd mass* isobaric sequence, when plotted against Z , should fall on a straight line whose slope is equal to B_1 . However, the observed β^- -energies for an isobaric sequence will not fall on a straight line due to the presence of the pairing energy term $(\pi - \nu)$. Since this term is added for the odd Z nuclei and subtracted for the even Z ones, the observed β^- -energies should fall on a zig-zag line when plotted against Z , the difference in $E_{\beta^-}(A, Z)$ between the even Z and the next higher odd Z nuclei being small compared to that between the odd Z and the next higher even Z nuclei, if $(\pi - \nu)$ is positive. If, however, $(\pi - \nu)$ is negative, the situation is reversed. Hence the plot of $E_{\beta^-}(A, Z)$ against Z for an isobaric sequence will not only reveal the presence of the $(\pi - \nu)$ effect in the β^- -disintegration energies, but will also give its sign by a mere inspection of the graph.

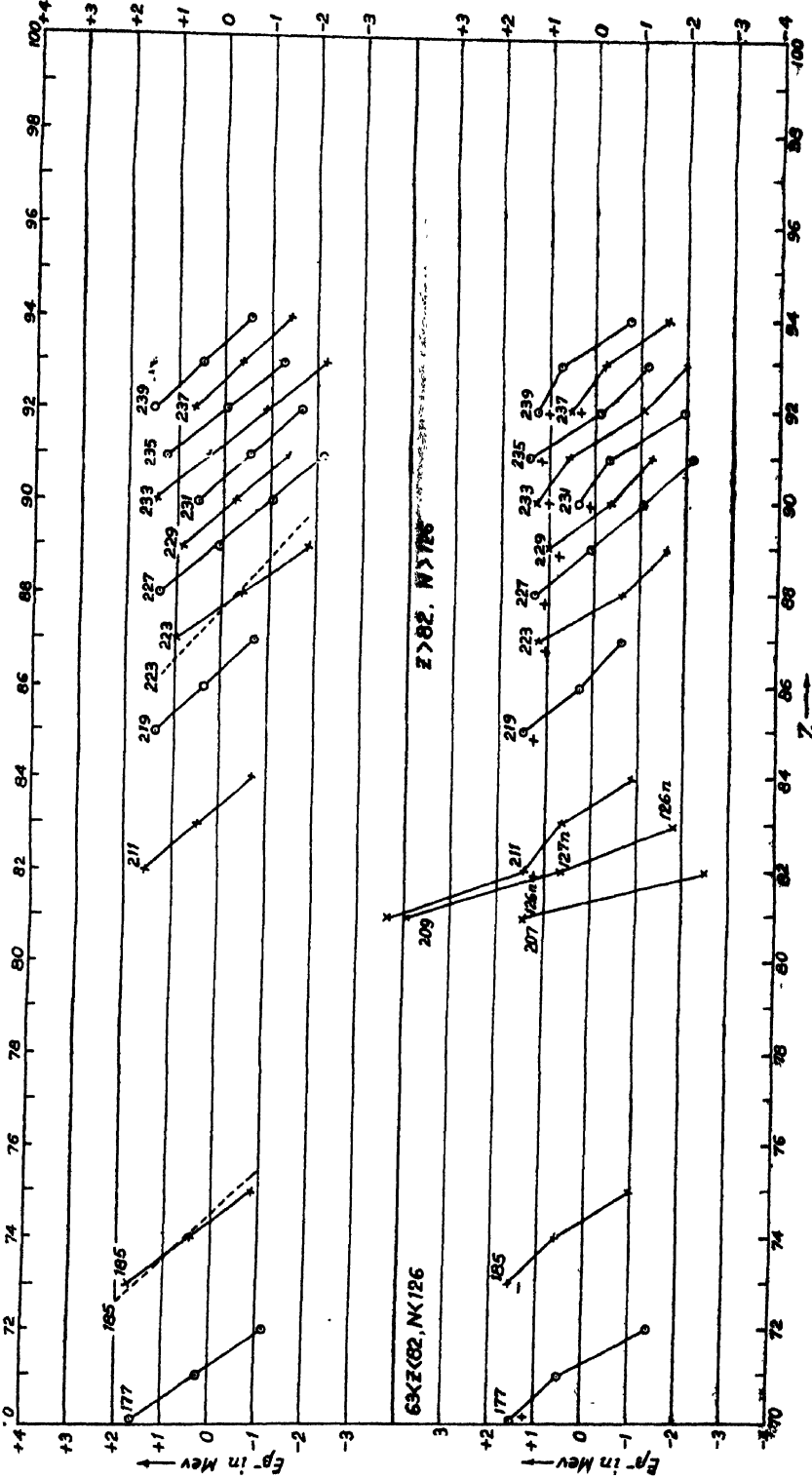


FIG. 4. (lower part)

TABLE I (contd.)

Shell region	Mass number	$(\pi - \nu)$
$Z > 50, N > 82$	141	+0.37
	143	+0.53
	151	+0.12
$63 < Z < 82, N < 126$	177	+0.25
	185	-0.15
$Z > 82, N > 126$	211	+0.18
	219	+0.07
	223	+0.22
	227	+0.01
	229	+0.11
	231	+0.24
	233	+0.21
	235	+0.15
	237	+0.17
	239	+0.23

If we take the difference between the eqns. 5(a) and 5(b) or eqns. (6a) and 6(b), we get,

$$\delta_{0p} - \delta_{r0} = A(\pi - \nu)$$

from which an average value of the pairing energy term for a given A can be derived. These values are listed in the third column of Table I.

If now the values of $(\pi - \nu)$ derived in this manner are subtracted from (for odd Z) or added to (for even Z) the observed β^- -disintegration energies and the points plotted against Z , we should get a straight line whose slope will give us the actual value of B_1 . The corrected points have been plotted in figure 4 (upper portion). It should be noted that the points lie on straight lines in almost all cases.

Values of B_1 for different A 's have derived from the observed slopes of these straight lines. These have been plotted in figure 5 where the solid line represents the B_1^* values calculated from the F-W formula. As is evident from this figure, the actual B_1 values are different from the calculated values, specially in certain regions. Coryell (1953) has briefly mentioned about such discrepancies in his review. The discrepancies observed by us are in substantial agreement with those observed by him (see figure 3 in Coryell's paper).

V. BEHAVIOUR OF $(\pi + \nu)$

Coryell has estimated the pairing energy term $(\pi + \nu)$ for different values of A for even A nuclei. As shown by him, these are not equal to the Fermi pairing energy term (Fermi, 1949). Suess and Jensen (1951) in their analysis of the pairing energy terms have formulated the following

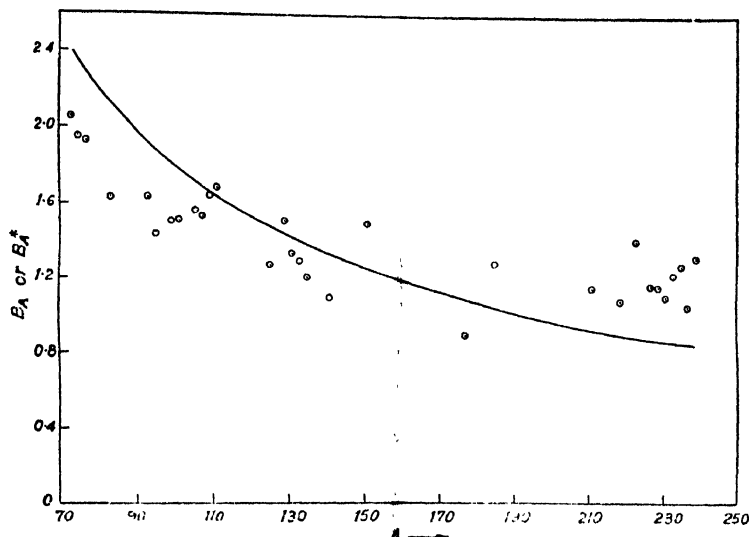


Fig. 5. Solid curve represents B_A^1 calculated from F-W mass formula. The points are B_A^1 values estimated from the slopes of the lines in the upper portion of figure 4.

rule: When one of the nucleon species crosses the magic number, the pairing energy of this species (π for protons and ν for neutrons)

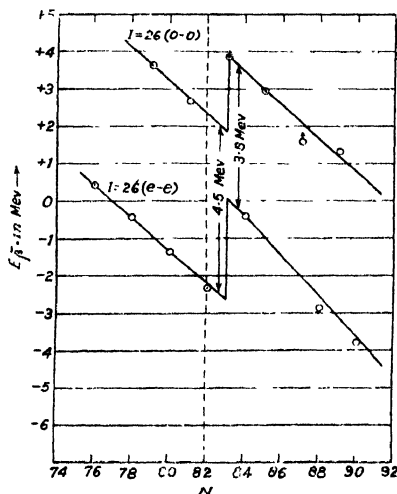


Fig. 6. Isodiapheric plot of the β^- -disintegration energies for $l=26$ (even l)

becomes smaller compared to that of the other species. This gives rise to the observed discontinuity in $(\pi - \nu)$, the pairing energy term in β^- -disintegration energies of odd A nuclei at the shell crossings. Since this term for even A nuclei is just the sum of the two terms π and ν , the discontinuities in π and ν at magic numbers should also be reflected in $(\pi + \nu)$, exactly in the same manner as in the case of $(\pi - \nu)$. Only, since in the present case the absolute magnitude of the pairing energy

term is much larger than in the odd A case, the effect of the discontinuity will be relatively small. We have searched for the presence of the discontinuity in $(\pi + \nu)$ by plotting the observed β^- -disintegration energies in isodiapheric sequences, following Suess and Jensen (1951). Since the effect is relatively small in the present case, the unambiguous presence of the discontinuity is discernible only in a few cases. One such case for $N=82$ has been shown in figure 6, where the isodiapheric plot for the $E_\beta(A, Z)$ values for $I=26$ is shown. As can be seen for this case, the difference between the even-even and odd-odd E_β lines just after the magic neutron number $N=82$ is equal to 3.8 Mev, as compared to the difference of 4.5 Mev just before $N=82$, the difference 0.7 Mev between the two being equal to twice the discontinuity in the neutron pairing energy ν . This is in agreement with that observed from the $(\pi - \nu)$ discontinuity (Suess and Jensen, 1951). The discontinuity in $(\pi + \nu)$ is not so marked in the other cases. More precise experimental data are needed in these cases.

VI. VARIATION OF PAIRING ENERGY TERM WITH I

Attempts have been made by various authors to estimate the pairing energies of nucleons from theoretical considerations. Mayer (1950) has assumed a simple δ -function interaction between two nucleons and has obtained the following expressions for the pairing energy of nucleons in the shell with total quantum number j , when there are n such nucleons in that shell.

$$\text{for } n=\text{even}, (J=0), E_0 = -\frac{n}{2} \cdot \frac{2j+1}{2} \cdot \frac{C}{A},$$

$$\text{for } n=\text{odd}, (J=j), E_j = -\frac{n-1}{2} \cdot \frac{2j+1}{2} \cdot \frac{C}{A}$$

since the last unpaired nucleon does not contribute to the pairing energy. C is a constant, and A is the mass number.

From these expressions, it is seen that the pairing energy associated with an even nucleon compared to that of an odd one will be given by

$$-\frac{2j+1}{2} \cdot \frac{C}{A} \quad (\text{Mayer, 1950}).$$

Since in general the "peripheral" protons and the neutrons are in shells of different j values, the pairing energy effect for the odd Z , odd A nuclei will be different from that for the odd N , odd A (same A) nuclei. This can be understood from the schematic diagram of figure 7, where the top-most line represents the energy of an odd Z -odd N nucleus. If a proton is added to it, the pairing energy of the the resulting even $(Z+1)$ -odd (N) nucleus is lowered by an amount

$$\pi = \frac{2j'+1}{2} \cdot \frac{C'}{A} \quad \left| \quad \text{If on the other hand, a neutron is added to the first odd-} \right.$$

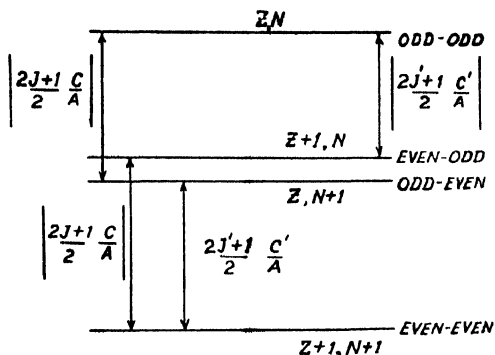


Fig. 7. Schematic diagram explaining the lowering of the pairing energy.

odd nucleus, the pairing energy of the resulting odd (Z)-even ($N+1$)

nucleus will be lowered by an amount $v = \frac{2j+1}{2} \cdot \frac{C}{A}$ which is different from

π . Finally, when a neutron and a proton are added to the original odd-odd nucleus, the pairing energy of the resulting even-even nucleus will be lowered by an amount $(\pi + v)$.

The above expressions for π and v show that the pairing energy terms should decrease with increasing mass number A . Fermi's empirical formula for even A nuclei gives an $A^{-3/4}$ dependence. Since the average j value for the peripheral nucleons also increases for heavier nuclei, the dependence of the pairing energy on A , as given by the above expressions, will not be very much different from that given by Fermi formula. The dependence of $(\pi + v)$ on A should also be of a similar nature. From Table I, it can be seen that at least for the shell region $Z < 50$, $N > 50$ the decrease of $(\pi + v)$ with increasing A is quite appreciable. The experimental data, of course, are not precise enough to permit any further detailed analysis of their behaviour at present. However, owing to the irregularities in the filling up of the nucleon shells (Klinkenberg, 1952), the variation of either $(\pi - v)$ or $(\pi + v)$ with A may also involve irregularities to a certain extent.

REFERENCES

- Bohr, N. and Wheeler, J. A., 1939, *Phys. Rev.*, **56**, 426
 Coryell, C. D., 1953, *Ann. Rev. Nuclear Sci.*, **2**, 395
 Edmonds, A. R., 1953, *Proc. Phys. Soc. (London)*, **66**, 7, 3
 Fermi, E., 1919, *Nuclear Physics*, notes by Oscar, J., Rosenfeld, A. H. and Schluttet, R. A., (Univ. of Chicago Press, Chicago, Ill), 249 pp.
 Harvey, J. A., 1951, *Phys. Rev.*, **81**, 353
 Hollander, J. M., Perlman, I. and Seaborg, G. T., 1953, *Rev. Modern Phys.*, **25**, 469
 Klinkenberg, P. F. A., 1952, *Rev. Mod. Phys.*, **24**, 63
 Mayer, M. G., 1950, *Phys. Rev.*, **78**, 22
 Metropolis, N. and Reitwiesner, G., 1950, U. S. Atomic Energy Commission Document NP-1980

Suess, H. B. and Jensen, J. H. D., 1951, *Arkiv. Föi Fysik*, **3**, 577

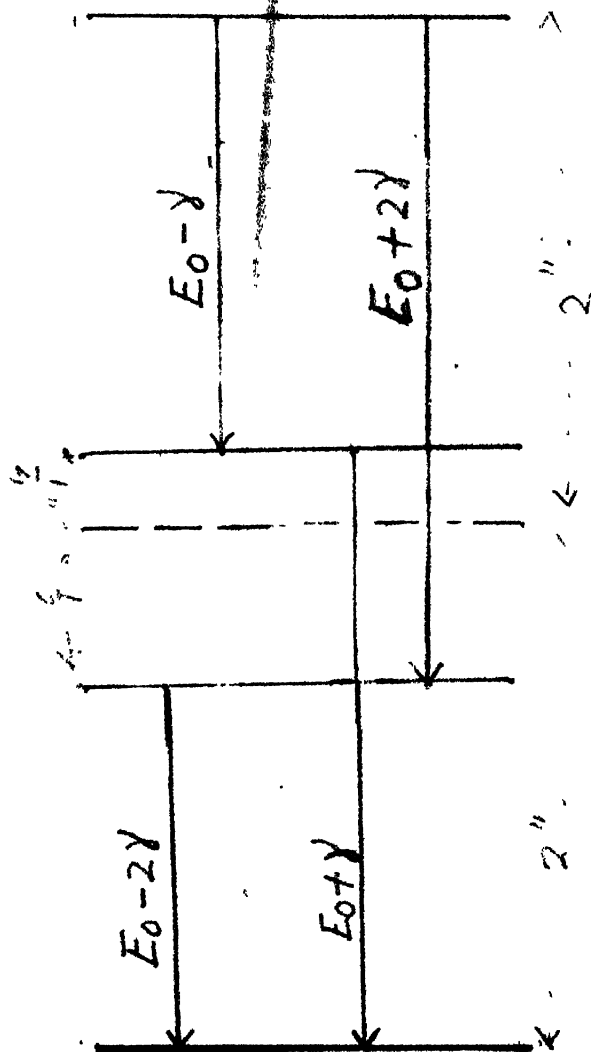
Way, K., Fano, L., Scott, M. R. and Thew, K., 1950, Nuclear Data, Natl. Bur. Standards (U. S) Circ. 499

Way, K., Wood, M. and Thew, K., 1951, Natl. Bur. Standards (U. S) Circ. 499, Suppl. 1.

Way, K., Fuller, G., Wood, M., Thew, K. and Jurgens, A., 1951, Natl. Bur. Standards (U. S) Circ. 499, Suppl. 2.

Way, K., Fuller, G., Wood, M., Thew, K. and Jurgens, A., 1952, Natl. Bur. Standards (U. S) Circ. 499, Suppl. 3.

Way, K. and Wood, M., 1954, *Phys. Rev.*, **94**, 119



ANALYSIS OF G-M COUNTER IMPULSES BY THE METHOD OF DELAYED COINCIDENCES

By SATYA PAL PURI AND P. S. GILL

DEPARTMENT OF PHYSICS, MUSLIM UNIVERSITY, ALIGARH

(Received for publication, December, 27 1951)

ABSTRACT. An interval analyzer circuit for studying the origin of spurious pulses in G-M counter tubes has been described. The method of delayed counts delay time has been employed in studying their time distribution. An expression for the probability that a real discharge creates an after discharge has been derived. The present investigations give :

- (i) An exponential decrease of dead and recovery times with overvoltage,
- (ii) The life of the petroleum ether filled counter and
- (iii) The values of coefficient of secondary emission. The coefficient of secondary emission seems to increase exponentially with overvoltage.

It is concluded that the alteration of the optimum gas composition by deterioration with use is the main cause responsible for the high values of this coefficient. The possibility of negative ion formation by molecular dissociation is also suspected.

INTRODUCTION

The plateau of a Geiger-Müller counter is defined as the voltage range over which the counting rate at a constant intensity of irradiation is substantially independent of voltage. No Geiger counter exhibits an ideally flat plateau characteristic for any considerable range about the threshold voltage. The increase in the counting rate with overvoltage is due to the increase in sensitivity but mainly to the occurrence of spurious counts. Since accurate measurements with Geiger counter require an essentially flat plateau, it was considered worthwhile to make a study of the spurious pulses.

Spurious counts result as a consequence of an earlier discharge and have been defined by Korff (1945) as those caused by any agency whatever other than the entity which it is desired to detect, or the normal contamination or cosmic ray background. When these spurious counts are few in number it is very difficult to distinguish them from genuine counts. The only method by which spurious counts are recognised is by studying their time distribution.

Were there no spurious counts, we would expect the counter to deliver randomly distributed pulses in time, modified only by the absence of intervals shorter than the dead time of the counter. The spurious counts, if present, may arise from a number of causes [Wilkinson (1950), Spatz (1943), Sanborn and Brown (1948), Sanborn et al (1950)]. In that case they will not be

randomly distributed but their times of occurrence will be related systematically to those of the pulses which caused them. Thus an excess of intervals of a particular range of the order of 10^{-4} sec shows the presence of spurious counts (Curran and Craggs, 1950). The delay of occurrence of a spurious pulse from a genuine one depends on the mechanism responsible for its production.

The method of time-interval analysis has been employed by a number of workers [Medicus (1936); Driscoll et al (1940); Roberts (1941); Ward (1942-43); Curran and Rae (1947); Putman (1948); Willard and Montgomery (1950); Guimaraes and Sampaio (1949); Kupperian et al (1951); Picard and Rogozinski (1953)]. In the present study the principle is similar to that employed by Curran and Rae (1947), but the resolving time of the coincidence circuit has been rendered discrete by the introduction of two shaping circuits, one in each of the two channels. Kupperian et al (1951) employed a multistage delay line for a similar investigation. The delay line has the disadvantage of its bulk and presents unavoidable distortion. In the present investigation a univibrator was used since its delay could be varied over wide limits, (Elmore and Sands, 1949). The circuit is simpler than the previous ones, but is based on the same principle as that of Curran and Rae (1947). The values of dead time and recovery time agree in a general way with those reported by earlier workers for a counter of these dimensions.

The circuit is extremely useful in studying the origin of spurious pulses. An equation has been developed for calculating the value of the coefficient of secondary emission caused by the impact of positive ions on the cathode surface, and it is shown that the value of K increases exponentially with overvoltage. This would be expected since the increase in overvoltage increases the number of positive ions per impulse and the probability that these positive ions will release secondary electrons at the walls becomes greater, (Stever, 1942). The results of the present paper show an exponential decrease of the dead and recovery times with overvoltage.

THE PULSE INTERVAL ANALYZER

The block diagram of the whole electronic circuitry is shown in figure 1.

The negative impulses from the counter are amplified by the pulse amplifier. These negative impulses from the amplifier feed simultaneously the shaping circuit I in the direct channel and the grid of the delay univibrator, which in its turn produces a square wave of variable duration. This gating pulse is differentiated into a negative and a positive part from its leading and trailing edges respectively; the positive part gives rise to a negative pulse at the plate of the inverter, which triggers the shaping circuit II in the delay channel. Thus the series of pulses from the shaping

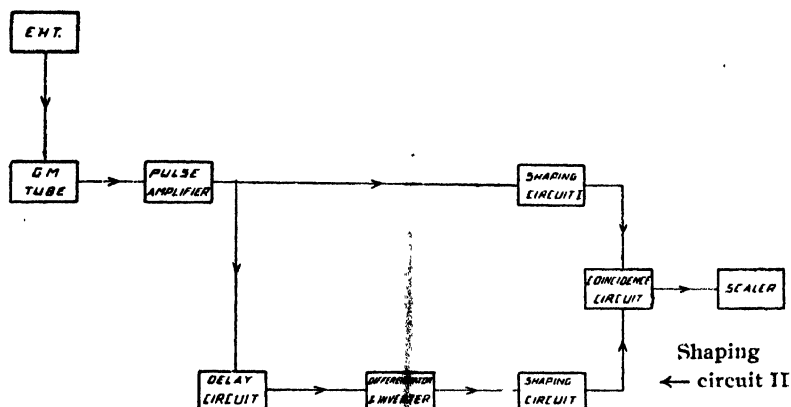


FIG. 1. Block diagram of the circuit

circuit II has no pulses spaced more closely than the time occupied by the gating pulse, which obviously depends on the setting of the fine and coarse controls of the delay multivibrator. These two series of pulses, one direct and the other from the delay channel are fed to the diode coincidence circuit. By measuring the rate of coincidences between a direct count and the delayed count as a function of delay, the time correlations in the ionizing events in the tube were determined.

I. *Cathode Input Amplifier.* Cathode input amplifier employs two (7C7) tubes, the first functioning as a cathode follower (power amplifier) and the second as voltage amplifier, with cathode coupling in between. The chief function of the amplifier is to increase the sensitivity of the apparatus and consequently the precision of measurement. Its input sensitivity is 0.2 volts and it furnishes very sharp negative pulses, which are fed simultaneously to the delay univibrator and the shaping circuit I.

II. *Delay Circuit.* The delay circuit also consists of two 7C7 tubes, which are cross-coupled to each other by condensers. In the normal condition the first 7C7 is conducting whereas the transconductance of the second is zero, since its grid is at a voltage beyond cut off, i.e. -15v .

As soon as it receives a negative pulse from the trigger amplifier, the circuit goes to a quasistable state whose duration is governed by the discharging time of C_1 through R_{13} which can be varied conveniently from 50 microseconds to 800 microseconds.

The negative rectangular signals (figure 3) of present duration are taken from the plate of the second 7C7 tube. Once the delay univibrator is flipped into operation, it is insensitive throughout the time occupied by the wave.

III. *Differentiator and Inverter.* The negative rectangular signal from the delay circuit is differentiated into negative and positive parts from its leading and trailing edges respectively. The negative pulse does not trigger the selector, since its grid is at -15v far beyond cut-off, thus it is the positive part which gives a negative pulse at its plate. It is in this

manner that a pulse whose delay is T_d is realized from the pulse from the counter.

Half of 6H6 has been used as coupling element, so that the operation of the next trigger circuit may not feed a signal back to the source.

IV. *Shaping Circuits I & II.* Two identical univibrators I and II are employed to put into form the direct and the delayed pulses respectively. The positive rectangular signals of duration t_1 and t_2 depend on the time constants R_7C_4 and $R_{21}C_{11}$. t_1 and t_2 can take all the values from 2 microseconds to 25 microseconds respectively, thus the resolving time of the succeeding coincidence circuit can be varied from 5 microseconds to 50 microseconds.

In order to render this time accurately determinate, it was thought necessary to incorporate these pulse shaping circuits both in the direct and delay channels; and it is an advantage over the previous circuits.

V. *Coincidence Circuit.* Two diodes are used to make a circuit which produces an output pulse only if its two input terminals are simultaneously excited by input pulses. The schematic diagram of the whole assembly is shown in figure 2.

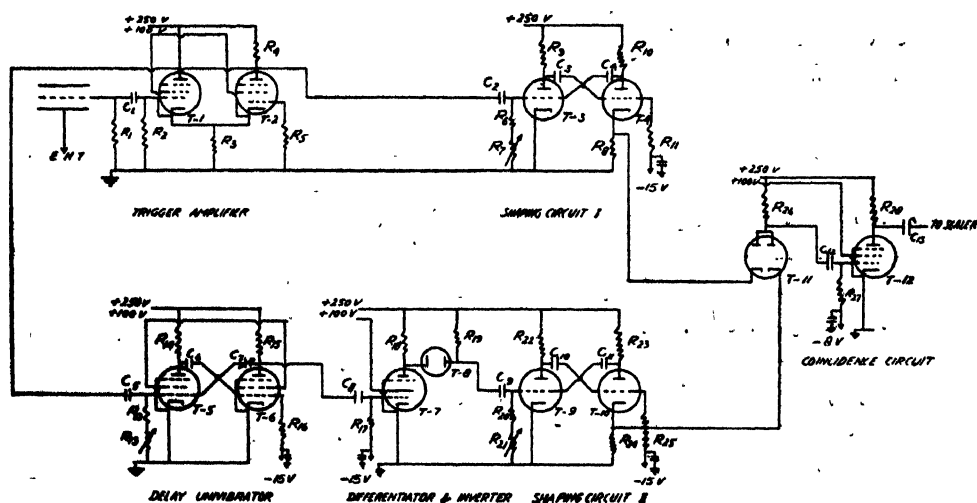


FIG. 2. Circuit of delayed coincidences. The values of components are listed below :

$$R_1 = 1M\Omega$$

$$R_2 = R_4 = R_{14} = R_{18} = R_{16}$$

$$= R_{26} = R_{27} = R_{28} = 100K$$

$$R_5 = R_9 = R_{17} = R_{23} = R_{11}$$

$$= R_{25} = 50K$$

$$R_7 = R_{31} = 100K, \text{ variable}$$

$$R_8 = 0.33K$$

$$R_6 = R_{10} = R_{20}, R_{23} = 5K$$

$$R_{12} = 10K$$

$$R_9 = R_{24} = 5K$$

$$R_{15} = R_{19} = 47K$$

$$C_1 = C_4 = C_5 = C_6 = C_9 = C_{11}$$

$$= 50pf$$

$$C_2 = 10pf$$

$$C_3 = C_8 = C_{10} = 5000pf$$

$$C_7 = 500 \rightarrow 1000pf, \text{ variable}$$

$$C_{12} = 2000pf$$

$$C_{13} = 1000pf$$

$$T_1 = T-2 = T-5 = T-6$$

$$= T-7 = 7C7$$

$$T-3 = T-4 = T-9 = T-10$$

$$= \frac{1}{2}6SL7$$

$$T-8 = \frac{1}{2}6H6$$

$$T-11 = 6H6$$

$$T-12 = 6AC7$$

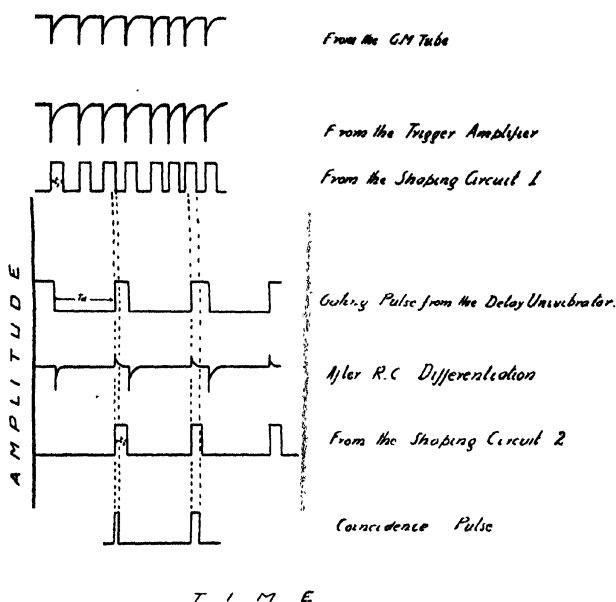


FIG. 3. Wave-shapes at different stages (not to scale)

3. THEORY OF THE METHOD OF RETARDED COINCIDENCES

Let n_r be the real number of particles entering the counter per sec,
 n_1' , the average number of particles recorded per second by the counter,
 n_1 , the average number of particles at the output of the amplifier per sec,
 τ , the dead time of the counter,
 τ' , the recovery time of the conventional amplifier. It is the minimum time interval that must elapse so that the amplifier amplifies the next pulse after the discharge of the G-M counter.

Then the loss of counting rate, incurred by the counter due to its finite dead time is $n_1' n_r \tau$.

Therefore $n_r - n_1' = n_1' n_r \tau$

so that $n_r = n_1' (1 + n_r \tau)$

Therefore the efficiency of the counter

$$\frac{n_1'}{n_r} = \frac{1}{1 + n_r \tau} \quad (1)$$

Now consider an interval of time τ' following an amplifier pulse at time zero. There can be no additional pulse from the counter within its dead time τ . The probability that none occurs in the interval τ to τ' can be computed as follows :

Let the probability that no pulse occurs in time $\tau' - \tau = \tau''$ be $P(\tau'')$. The probability that the amplifier will receive a pulse in additional time $\partial\tau''$ is $n_r \partial\tau''$; therefore the probability that no pulse is received in time $\partial\tau''$ will be $(1 - n_r \partial\tau'')$. The probability of not receiving a pulse in $\tau'' + \partial\tau''$ is $P(\tau'' + \partial\tau'')$.

$$P(\tau'' + \partial\tau'') = P(\tau'') \{1 - n_r \partial\tau''\}$$

Applying Taylor's theorem $P'(\tau'') = -P(\tau'') n_r$

therefore $P(\tau'') = C e^{-n_r \tau''}$.

But when $\tau'' = 0$, $P(\tau'') = 1$

Therefore $C = 1$

Hence $P(\tau'') = e^{-n_r(\tau' - \tau)}$

This then is the probability that the amplifier receives a next pulse after τ' . Hence the efficiency of the amplifier is

$$\frac{n_1}{n_r} = e^{-n_r(\tau' - \tau)} \quad \dots (2)$$

Therefore $n_1 = \frac{n_r}{1 + n_r} e^{-n_r(\tau' - \tau)} \quad \dots (2a)$

For small counting rates, $n_r(\tau' - \tau) \ll 1$, therefore, expanding $e^{-n_r(\tau' - \tau)}$ in power series and neglecting the higher terms

$$n_1 = \frac{n_r}{1 + n_r} \{1 + n_r \tau - n_r \tau'\}$$

$$n_r \left\{ 1 - \frac{n_r \tau}{1 + n_r \tau} \right\} \quad \dots (3)$$

But from (2a)

$$\frac{n_r}{1 + n_r \tau} = n_1 e^{n_r(\tau' - \tau)}$$

Substituting it in eq. 3, we obtain

$$n_1 = n_r \{1 - \tau' n_1 e^{n_r(\tau' - \tau)}\}$$

and since

$$n_r(\tau' - \tau) \ll 1$$

$$n_1 = n_r \left\{ 1 - \tau' n_1 \left[1 + n_r(\tau' - \tau) + \frac{n_r^2(\tau' - \tau)^2}{2!} + \dots \right] \right\}$$

$$= n_r \{1 - n_1 \tau' - n_r n_1 \tau'(\tau' - \tau) \dots\}$$

$$= n_r \{1 - n_1 \tau'\} \quad \dots (4)$$

Furthermore, these n_1 pulses are fed to the delay univibrator whose recovery time is T_d , which is the duration of the square wave. Strictly speaking, the recovery time of the delay circuit is slightly longer than T_d since C_7 is to get recharged through R_{15} with the consequence that the trailing edge of the pulse is not very sharp (figure 2).

If n_2 impulses per sec are given as output by the univibrator, then the efficiency

$$\frac{n_2}{n_1} = e^{-n_1(T_d - \tau')}$$

Therefore

$$n_2 = n_1(1 - n_1\tau')e^{-n_1(T_d - \tau')} \\ = n_1(1 - n_1\tau') \left\{ 1 - n_1(T_d - \tau') + \frac{n_1^2(T_d - \tau')^2}{2!} - \dots \right\}$$

Substituting from eq. (4) we get

$$n_2 = n_1 \{ 1 - n_1(T_d - \tau') \} \quad \dots (5)$$

If t_1 is the duration of the direct pulse after it has been put into form by the shaping circuit I and t_2 the duration of the retarded pulse from shaping circuit II, then the coincidence rate n_c is given by

$$n_c = n_1 n_2 (t_1 + t_2) \\ = n_1^2 \{ 1 - n_1(T_d - \tau') \} \quad \dots (6)$$

The two series of impulses, direct and retarded, are fed into the coincidence circuit, whose resolving time is $(t_1 + t_2)$. Since no pulse can occur during the dead time of the counter, no coincidence will be observed for time T_d less than τ' . Such a circuit is ideal for the rapid determination of τ' .

If any parasitic effect does not disturb the quasistatic distribution of the two series of pulses, the average frequency of coincidence n_c reduces to

$$n_c = n_1^2(t_1 + t_2)$$

which is the frequency of the coincidences for $T_d > \tau'$.

From the above equation n_c should have a constant value if there were no spurious effects present. The circuit detects the presence of the spurious pulses, if there is an excess of the intervals of short duration of the order of 10^{-4} sec. The circuit can be used for :

- (i) measuring the dead-time and recovery time of the counter.
- (ii) analysing its variation with overvoltage.
- (iii) detecting spurious pulses if present, and indicating their origin, and
- (iv) detecting and measuring the half life of a radio element of large disintegration constant, half life 50×10^{-6} sec. to 10^{-1} sec.

EVALUATION OF K, THE COEFFICIENT OF SECONDARY EMISSION

The after-discharges are systematically related in time to the impulses which generate them. The interval at which spuriousness occurs is roughly equal to the recovery time T of the counter in case of secondary emission caused by the impact of positive ions on the cathode, and is equal to $2T$ in case of negative ion formation at the cathode as in case of carbon dioxide-filled counters.

Let r be the rate of genuine discharges, n_1 , the observed rate and K , the probability that any discharge creates an after-discharge.

Then

$$n_1 = r + Kr + K^2r + K^3r + \dots$$

$$\frac{r}{1-K} \quad (7)$$

If n_p is the frequency of parasitic impulses [Curran and Rae (1947); Picard and Rogoziński (1953)],

$$\begin{aligned} n_p &= rK + rK^2 + rK^3 + \dots \\ &= \frac{rK}{1-K} \end{aligned} \quad (8)$$

Let us proceed to calculate the probability of the formation of the first peak, supposing there is a sequence of several parasitic impulses separated from each other by an interval of time T .

Actually the recovery time of the delay univibrator is more than T_d the imposed delay, a direct pulse giving a coincidence with a delayed pulse cannot itself initiate a delayed pulse. Consequently the coincidence will be between the alternate parasitic impulses.

For $T_d = T$, the probability of the formation of the first peak

$$\begin{aligned} K_1 &= K + K^3 + K^5 + \dots \\ &= \frac{K}{1-K^2} \end{aligned} \quad (9)$$

But, of the n_1 counts r are random, thus the frequency of real coincidences

$$r_e = r^2(t_1 + t_2) \quad (10)$$

The area A_1 under the first peak represents the contribution of the parasitic impulses whose probability of formation is K_1 . Normalizing this peak

$$A_1 = rK_1(t_1 + t_2) \quad (11)$$

Thus

$$\frac{A_1}{r_e} = \frac{K}{r(1-K^2)}$$

But

$$r = n_1(1-K) \text{ vide eq. (7)}$$

Therefore

$$\frac{A_1}{r_e} = \frac{K}{n_1(1-K^2-K+K^3)}$$

which reduces to

$$A_1 = r_e \frac{K}{n_1} \quad (\text{where } k \ll 4)$$

Thus

$$K = \frac{A_1}{r_e} n_1 \quad (12)$$

Putting the values of n_1 , A_1 and r_e , which are read out from the experimental curve, the coefficient of secondary emission and of any other mechanism which gives spurious count at $T_d = T$ can be evaluated.

OBSERVATIONS

1. *Determination of Dead and Recovery Times.* Figure 4 represents the plateau characteristic of the counter having a diameter of 1.5 cm and 13 cm long. The central wire had .003 inch diameter. The copper cathode was oxidized. It was filled with spectroscopically pure argon to a pressure of 9 cm of mercury, mixed with 1.1 cm of petroleum ether vapour (B. P. 40–60°C). It had already furnished 5×10^5 counts in its previous run and showed a slope of 7.04% per 100 volts.

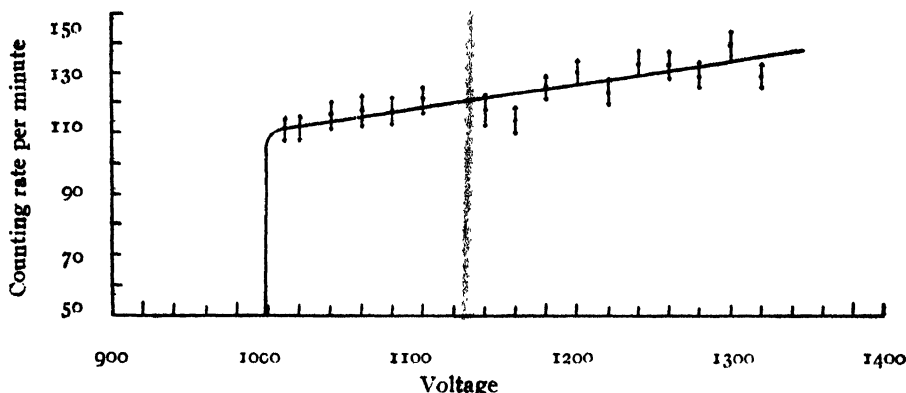


FIG. 4. Plateau characteristic of the counter investigated

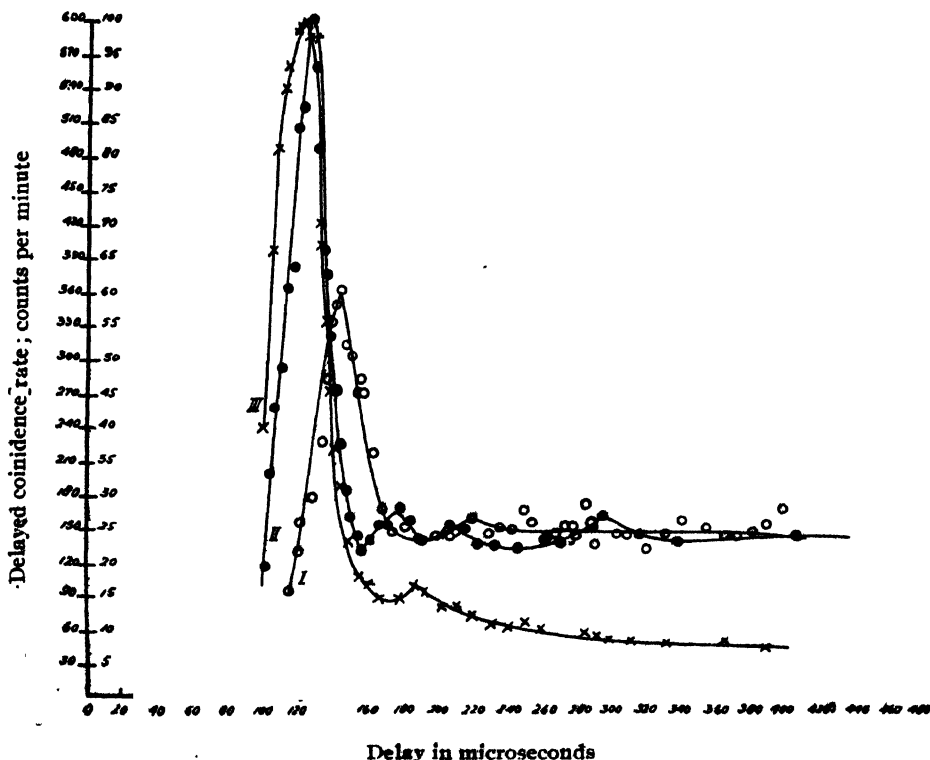


FIG. 5. Curves I, II and III represent the coincidence vs delay time for over-voltages of 30, 150 and 230 volts respectively. In each case the resolving time is $t_1 + t_2 = 40.50$ microseconds. The counting rates used for curves I, II and III were 9478, 9940 and 13, 120 per minute respectively

In figure 5 curves (I), (II), (III) represent the delayed coincidence rate (counts per minute) *vs* delay time for three different overvoltages of 30, 150, and 230 volts respectively. Counting rates of the order of 10,000 counts per minute were employed so that the spurious effects, if any, may become pronounced and thus afford a greater accuracy of measurement. The coincidence rate was recorded with a statistical accuracy of 4%.

In a counter with effective dead-time τ' , no interval less than τ' is found and there will not be any coincidence. The dead time τ' can be easily measured. The observed values of dead and recovery times are of the order of previously reported values, (Korff, 1946) for counters of these dimensions. The recovery time, that is, the time required for the transit of the positive ions from the central wire to the cathode can be read out under the peak of the curve, since it is at this value of $T_d = T$, that the maximum effects of the secondary emission from the cathode are expected.

Curves of figure 6 give plots of the variation of dead and recovery times with overvoltage. An exponential decrease with overvoltage is indicated.

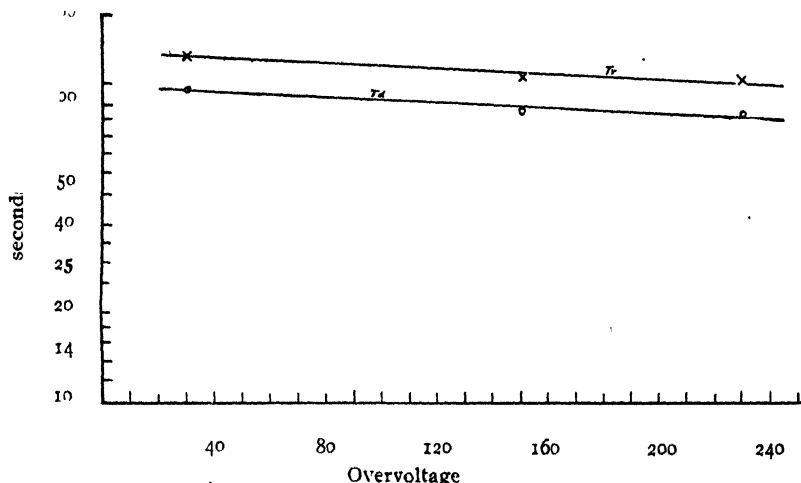


FIG. 6. Variation of dead and recovery times with over voltage. The curves may be represented by $T_d = 117 e^{-.00107(v-v_0)}$ and $T_r = 152 e^{-.00107(v-v_0)}$

2. *Investigation of Spuriousness.* Curves (I), (II), (III) of figure 5 represent coincidence rate *vs* delay time. All the three curves show a pronounced maximum which occurs at the time of transit of positive ions. The peaks show a shift towards the origin at higher overvoltages. This shift is due to the increased mobility of the positive ions with the increase of overvoltages and consequently less time is required to reach the cathode.

The values of K , the coefficient of secondary emission, as calculated by employing equation (12), give pretty high values for it. This would mean that G-M tube will give more and more spurious counts with higher and higher overvoltages. As a result a correction must be made to the

counting rate while carrying out precision measurements.

The values of K seem to increase exponentially with overvoltage (see figure 7). Curves (I) and (II) show that the spurious counts occur at the time of recovery whereas, curve (III) shows that some of them also occur at a later time, $T_d = 192$ microseconds. There is, however, an indication of second maxima in curve (II) as well. The counter under investigation was nearing its end, since it had furnished about 4×10^7 counts by the end of the present investigation. At the end, it was found to have the following characteristics :

- (i) that threshold had gone up by 150 volts.
- (ii) the plateau length diminished to about 40 volts only.

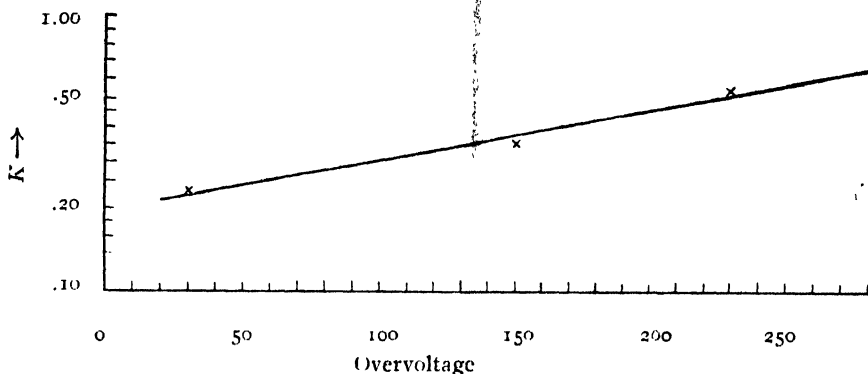


FIG. 7 Variation of coefficient of secondary emission with overvoltage. The curve may be represented by $K = 198 e^{0.00428(v-v_0)}$

DISCUSSION

The exponential decrease of dead and recovery times with overvoltage fits in with "Stevens" analysis of the motion of the positive ion sheath. As the overtension increases, the drift velocity of the sheath must increase and consequently the times required to travel to the critical radius and the cylinder must decrease. It is exponential, because the distributed capacity of the counter is to get recharged through the leakage resistance to the threshold from the starting voltage. If the final voltage to which it is to get charged is higher, as is the case at higher overvoltage, the time to reach the threshold falls exponentially.

Since the average life of a petroleum ether G-M tube is between 10^7 and 10^8 counts, it is concluded that the deterioration is due to the combination of two processes :

(i) Alteration in the optimum gas composition resulting from decomposition of petroleum ether into hydrogen, which is non-self-quenching and saturated and unsaturated hydrocarbons [Farmer and Brown (1948) ; Yaddanapalli (1942)].

(ii) The deposition on the cathode and anode of dielectric polymers formed from unsaturated hydrocarbons.

It is also evident from figure 5 that the spurious counts occur at the recovery time of the counter (Montgomery and Montgomery, 1940).

The high value of K may be arising from a number of causes. The most important cause seems to be that the insufficient amount of the self-quenching constituent is not acting as a complete trap for the vehicular gas positive ions. Only very few charge transfer collisions occur, with the consequence that some vehicular gas ions reach the cathode. Since the quenching resistance employed is only 1 meg, the secondary electrons resulting from the impact of positive ions on the cathode will re-ignite discharges and thus cause spurious counts.

In the case figure 5 curve (III), the presence of a second peak of spurious counts at $T_d = 192$ microseconds which is almost twice the recovery time is evident. The mechanism for the production of this peak may be :

(i) the cathodic emission and

(ii) the formation of negative ions as dissociation fragments at the wall or in the gas discharge and if formed will reach the vicinity of the wire after time $2T$.

The petroleum ether had not been subjected to its ionization and dissociation study by electron impacts, but in the case of methane, which is the parent hydrocarbon of petroleum ether, the negative ions had been detected (Smith, 1937).

The presence of spurious discharges cannot be explained by assuming the survival by a few metastable ions, of the dead-time; and ionization by positive ions, since both these hypotheses are unlikely and improbable for the observed effect.

ACKNOWLEDGMENT

One of the authors (S. P. P.) acknowledges the help of the Education Ministry of the Govt. of India for the award of a senior scholarship.

REFERENCES

- Curran, S. C., and Craggs, J. D., 1950, Counting Tubes, Butterworth's Scientific Publications.
- Curran, S. C., and Rae, E. R., 1947, *Rev. Sci. Inst.*, **18**, 871.
- Driscoll, R. L., Hodge, M. W., and Ruark, A., 1940, *Rev. Sci. Inst.*, **11**, 241.
- Elmore, W. C., and Sands, Matthew, "Electronics", 1949, McGraw Hill Book Company
- Farmer, F. C., and Brown, S. C., 1948, *Phys. Rev.*, **74**, 902.
- Guimaraes, Mari Alves, and Sampaio, P. A., 1943, *Rev. Sci. Inst.*, **20**, 485.
- Korff, S. A., 1946, Electron and Nuclear Counters, New York; Van Nostrand.
- Kupperian, J. E. Jr., Murray, P. C., and Feeny, H., 1951, *Rev. Sci. Inst.*, **22**, 60.
- Medicus, A., 1936, *Z. f. Phys.*, **103**, 76.
- Montgomery, C. G., and Montgomery, D. D., 1940, *Phys. Rev.*, **57**, 1030.
- Picard, E., and Rogozinski, A., 1953, *J. Phys. Radium*, **14**, 445.
- Putman, J. L., 1948, *Proc. Phys. Soc. (London)*, **61**, 312.
- Roberts, A., 1941, *Rev. Sci. Inst.*, **12**, 71.

- Sanborn, C. Brown, 1948, *Nucleonics*, 2-6, 10,
Sanborn, C. Brown and Claudine, Maroni, 1950, *Rev. Sci. Ints.*, 21, 241.
Smith, L. G., 1937, *Phys. Rev.*, 31, 263.
Spatz, W. D. B., 1943, *Phys. Rev.*, 64, 236.
Stever, H. G., 1932, *Phys. Rev.*, 61, 38.
Ward, A. G., 1943-45, *Proc. Roy. Soc.*, A181, 183.
Wilkinson, D. H., 1950, *Ionization Chambers and Counters*.
Willard D., and Montgomery, C. G., 1950, *Rev. Sci. Ints.*, 21, 520.
Yaddanapalli, L. M., 1942, *J. Phys. Chem.*, 46, 249.

TRANSFORMERS

IF YOU INSIST ON "QUALITY & ACCURACY"

PLEASE WRITE TO:—

INDIA RADIO MFG. Co.

ESTD 1937

GRAMS—CRESCENT

PHONE 34—2615

236, CHITTARANJAN AVENUE
CALCUTTA—6



INDEX BEAKERS AND FLASKS
ARE MADE OF SUCH THICKNESS
JUST TO STAND MECHANICAL AND
PHYSICAL STRAIN. THEY ARE
ALSO HEAT RESISTANT AS THE
COEFFICIENT OF EXPANSION IS
ONLY 3.4×10^{-6} , THUS THEY ARE.
PARTICULARLY SUITABLE FOR
RESPONSIBLE LABORATORY
WORK.

Sole Distributors :

GHARPURE & CO

P-36, Royal Exchange Place Extn
Calcutta 1

counting rate while carrying out precision measurements.

The values of K seem to increase exponentially with overvoltage (see figure 7). Curves (I) and (II) show that the spurious counts occur at the time of recovery whereas, curve (III) shows that some of them also occur at a later time, $T_d = 192$ microseconds. There is, however, an indication of second maxima in curve (II) as well. The counter under investigation was nearing its end, since it had furnished about 4×10^7 counts by the end of the present investigation. At the end, it was found to have the following characteristics :

- (i) that threshold had gone up by 150 volts.
- (ii) the plateau length diminished to about 40 volts only.

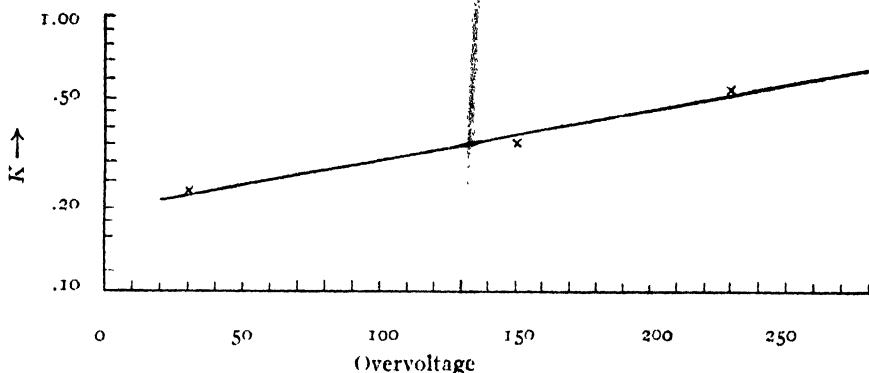


FIG. 7 Variation of coefficient of secondary emission with overvoltage. The curve may be represented by $K = 198 e^{0.00128(v-v_0)}$

DISCUSSION

The exponential decrease of dead and recovery times with overvoltage fits in with "Stevens" analysis of the motion of the positive ion sheath. As the overtension increases, the drift velocity of the sheath must increase and consequently the times required to travel to the critical radius and the cylinder must decrease. It is exponential, because the distributed capacity of the counter is to get recharged through the leakage resistance to the threshold from the starting voltage. If the final voltage to which it is to get charged is higher, as is the case at higher overvoltage, the time to reach the threshold falls exponentially.

Since the average life of a petroleum ether G-M tube is between 10^7 and 10^8 counts, it is concluded that the deterioration is due to the combination of two processes :

- (i) Alteration in the optimum gas composition resulting from decomposition of petroleum ether into hydrogen, which is non-self-quenching and saturated and unsaturated hydrocarbons [Farmer and Brown (1948); Yaddanapalli (1942)].

- (ii) The deposition on the cathode and anode of dielectric polymers formed from unsaturated hydrocarbons.

It is also evident from figure 5 that the spurious counts occur at the recovery time of the counter (Montgomery and Montgomery, 1940).

The high value of K may be arising from a number of causes. The most important cause seems to be that the insufficient amount of the self-quenching constituent is not acting as a complete trap for the vehicular gas positive ions. Only very few charge transfer collisions occur, with the consequence that some vehicular gas ions reach the cathode. Since the quenching resistance employed is only 1 meg, the secondary electrons resulting from the impact of positive ions on the cathode will re-ignite discharges and thus cause spurious counts.

In the case figure 5 curve (III), the presence of a second peak of spurious counts at $T_d = 192$ microseconds which is almost twice the recovery time is evident. The mechanism for the production of this peak may be :

(i) the cathodic emission and

(ii) the formation of negative ions as dissociation fragments at the wall or in the gas discharge and if formed will reach the vicinity of the wire after time $2T$.

The petroleum ether had not been subjected to its ionization and dissociation study by electron impacts, but in the case of methane, which is the parent hydrocarbon of petroleum ether, the negative ions had been detected (Smith, 1937).

The presence of spurious discharges cannot be explained by assuming the survival by a few metastable ions, of the dead-time; and ionization by positive ions, since both these hypotheses are unlikely and improbable for the observed effect.

ACKNOWLEDGMENT

One of the authors (S. P. P.) acknowledges the help of the Education Ministry of the Govt. of India for the award of a senior scholarship.

REFERENCES

- Curran, S. C., and Craggs, J. D., 1950, Counting Tubes, Butterworth's Scientific Publications.
- Curran, S. C., and Rac, E. R., 1947, *Rev. Sci. Inst.*, **18**, 871.
- Driscoll, R. L., Hodge, M. W., and Ruark, A., 1940, *Rev. Sci. Inst.*, **11**, 241.
- Elmore, W. C., and Sands, Matthew, "Electronics", 1949, McGraw Hill Book Company
- Farmer, F. C., and Brown, S. C., 1948, *Phys. Rev.*, **74**, 902.
- Guimaraes, Mari Alves, and Sampaio, P. A., 1943, *Rev. Sci. Inst.*, **20**, 485.
- Korff, S. A., 1946, Electron and Nuclear Counters, New York; Van Nostrand.
- Kupperian, J. B. Jr., Murray, P. C., and Feeny, H., 1951, *Rev. Sci. Inst.*, **22**, 60.
- Medicus, A., 1936, *Z. f. Phys.*, **103**, 76.
- Montgomery, C. G., and Montgomery, D. D., 1940, *Phys. Rev.*, **57**, 1030.
- Picard, R., and Rogozinski, A., 1953, *J. Phys. Radium*, **14**, 445.
- Putman, J. L., 1948, *Proc. Phys. Soc. (London)*, **61**, 312.
- Roberts, A., 1941, *Rev. Sci. Inst.*, **12**, 71.

- Sanborn, C. Brown, 1948, *Nucleonics*, 2-6, 10,
Sanborn, C. Brown and Claudine, Maroni, 1950, *Rev. Sci. Ints.*, 21, 241.
Smith, L. G., 1937, *Phys. Rev* , 31, 263.
Spatz, W. D. B., 1943, *Phys. Rev* , 64, 236.
Stever, H. G., 1932, *Phys. Rev.*, 61, 38.
Ward, A. G., 1943-45, *Proc. Roy. Soc.*, A181, 183.
Wilkinson, D. H., 1950, Ionization Chambers and Counters.
Willard D., and Montgomery, C. G , 1950, *Rev. Sci. Ints.*, 21, 520.
Yaddanapalli, L. M., 1942, *J. Phys. Chem* , 46, 249.

VIBRATIONAL ANALYSIS OF THE TANTALUM OXIDE BANDS

BY D. PREMASWARUP

PHYSICS DEPARTMENT, ANDHRA UNIVERSITY, WALT AIR

(Received for publication January 24, 1955)

Plates III A, B

ABSTRACT. Bands of the diatomic tantalum oxide molecule, TaO, in the region $\lambda 5000$ — $\lambda 3400$ are photographed with different instruments under various dispersions including that of a second order, 21-ft concave grating with 30,000 lines per inch. Complete data of the band heads lying in this region are given and compared with those given by earlier workers. All the more prominent bands are explained as forming members of two systems designated as A and C. The method of arriving at the vibrational analysis is discussed in detail. The vibrational constants ω_e and $x_e\omega_e$ for the ground and the two excited states involved are found to be 1040.0, 8.5; 901.4, 4.0 and 718.6, 2.2 cm^{-1} .

INTRODUCTION

The earliest report of a characteristic band spectrum attributable to the oxide of tantalum is that due to Kiess and Stowell (1934) who observed the bands in the course of their extensive work on the arc spectrum of tantalum. They photographed the arcs and sparks between metallic tantalum, the arcs being maintained by direct currents of 5 to 10 amperes supplied by 220-volt mains. It was mentioned in the work that the arc spectrum is always accompanied by an extensive band spectrum consisting of bands shaded towards the red from heads which are inconspicuous. This extensive band spectrum was ascribed by them to tantalum oxide. Whenever recognised as such, these heads were measured and their wavelengths reported.

From the table of wavelengths given by Kiess and Stowell there are a number of well separated regions in which the bands occur, two in the infrared from $\lambda 10050$ to $\lambda 7900$ and two or three in the visible and the ultraviolet from $\lambda 5600$ to $\lambda 3400$. The measured heads in the different regions are given in Table I.

* Communicated by Prof. K. R. Rao.

TABLE 1.

TaO band heads (Kiess and Stowell)

Wave-length	Int	Wave-number	Wave-length	Int	Wave-number
10043.27	5	9954.19	5566.99	4	17958.1
9989.75	5	10007.52	5520.21	2?	18110.2
9971.26	4	10026.08	5485.44	1?	18225.0
9957.94	4	10039.49	5385.25	3?	18564.1
9954.68	4	10042.77			
9919.90	8	10077.99	4901.57	3?	20396.0
9902.74	5	10099.45	4810.35	4	20782.7
9868.62	25	10130.35	4679.46	3	21364.0
9849.27	15	10150.15	4651.92	3	21490.5
9242.70	5	10816.38	4154.41	7	24064.1
9197.40	8	10869.66	4092.10	3	24430.5
9196.05	4	10871.25	4006.24	4	24954.0
			3896.43	4	25657.3
7921.65	1?	12620.16	3747.25	4	26678.7
			3625.68	4	27573.2
5589.04	1	17887.2	3429.33	2	29151.9

A band spectrum attributed to tantalum oxide was reported also by Krishnamurthy and Fernando (1949) in a short letter published in '*Current Science*'. The spectrum was excited in heavy current arcs in air between (1) tantalum rods, (2) carbon rods stuffed with tantalum oxide and also in arcs in an atmosphere of oxygen between tantalum rods. The bands were reported to be extending from $\lambda 5500$ — $\lambda 3900$ and the band heads were recorded to be 'not very prominent'. More than twenty of these bands were mentioned to have been arranged into a Deslandre's scheme and belonging to a system corresponding to the α system of zirconium oxide bands investigated by Francis Lowater (Herzberg 1951). Wavenumbers of only nine of these bands were published by the authors and the following values of the vibrational constants were reported:

$$\omega'_e = 712.7 \text{ cm}^{-1} \quad x'_e \omega'_e = 1.95 \text{ cm}^{-1}$$

$$\omega''_e = 1161.6 \text{ ''} \quad x''_e \omega''_e = 5.85 \text{ ''}$$

EXPERIMENTAL

Excitation of the Spectrum

In previous investigations on the band spectrum of columbium oxide in this laboratory it was found that the CbO bands occur in a number of sources, such as (a) the flame of a direct current arc between the metallic electrodes, (b) in the flame of a D.C. arc between graphite electrodes fed by columbium pentachloride and (c) in a heavy current discharge from a two kilowatt D.C. generator with pentachloride of columbium in a quartz discharge tube.

For the excitation of the zirconium or the titanium oxide bands the sources used were (1) the electric furnace of the type used by King, (2) arcs in air with iron or copper poles, the lower pole being fed by the oxide or some other compound of the metal such as ZrF_4 for zirconium oxide bands. By far the best source for zirconium oxide spectrum was found by Afaf to be the zirconium in moist hydrogen, the electrodes being the same as the ZrF_4 arc.

All the above-mentioned sources except that of the arc in moist hydrogen and the tube furnace have been employed in this investigation in the preliminary stages for obtaining the spectrum of tantalum oxide. The most convenient, simple and economical source which emitted almost completely the characteristic spectrum is found to be the D. C. arc between pure tantalum rods run at 220 volts and a current of 2–3 amperes. This lower value of the current helped in economising the metal. As observed by Kiess and Stowell the continuous maintenance of the arc in air was found to be somewhat difficult. It was frequently necessary to bring the electrodes into contact and strike the arc again, probably due to the poor conductivity of the oxide that might have been formed round the electrodes. With the higher dispersion instruments such as the 21-ft grating this simple source proved to be very convenient. The electrodes of the metal used were of the 'specpure' variety supplied by Johnson, Matthey and Company in the form of rods of 10 cm length and 4.5 mm diameter.

Instruments Used

Small and high dispersion instruments of the prism and grating types were used. The different instruments used were (1) a Fuess glass spectrograph having a dispersion of 28 Å/mm at $\lambda 5000$, (2) a two-prism Hilger glass Littrow instrument having a high resolution and a fairly high dispersion (36 Å/mm at $\lambda 6000$ and 7 Å/mm at $\lambda 4000$), (3) a Hilger E1 quartz Littrow spectrograph, specially for the region $\lambda 4000$ to $\lambda 3100$ (with a dispersion of 5 Å/mm at $\lambda 3000$), and (4) a 10-ft concave grating in Eagle mounting in the first order (dispersion 5.7 Å/mm). These instruments were found specially useful for obtaining spectrograms for the investigation of the vibrational analysis of the spectrum. Pictures with higher dispersion instruments were found less suitable.

Besides the above, the spectra were photographed in the first and second orders of a 21-ft concave grating with 30,000 lines per inch (dispersion 1.2 Å/mm and 0.6 Å/mm in the first and second orders respectively) and having a six inch ruled surface set up in the Paschen mounting. This grating is the one mounted in the Applied Physics Department of the University of Calcutta and the same as that used for the investigations on columbium oxide by Suryanarayana Rao.

The times of exposures for getting good photographs varied from 1 to 5 minutes with the smaller dispersion instruments while they extended up to three hours with the 21-ft grating, particularly in the second order.

The spectra were recorded on Ilford S. R. Panchromatic and Special Rapid ordinary plates, the maximum wavelength that was photographed being $\lambda 6500$. The infrared system could not be investigated. Special red sensitive plates of the 1N and other types have been ordered and the infrared region is proposed to be investigated shortly.

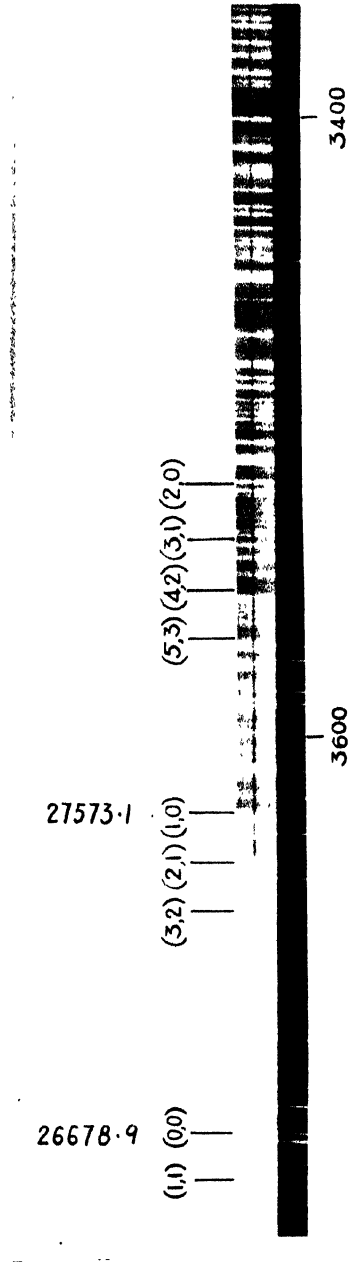
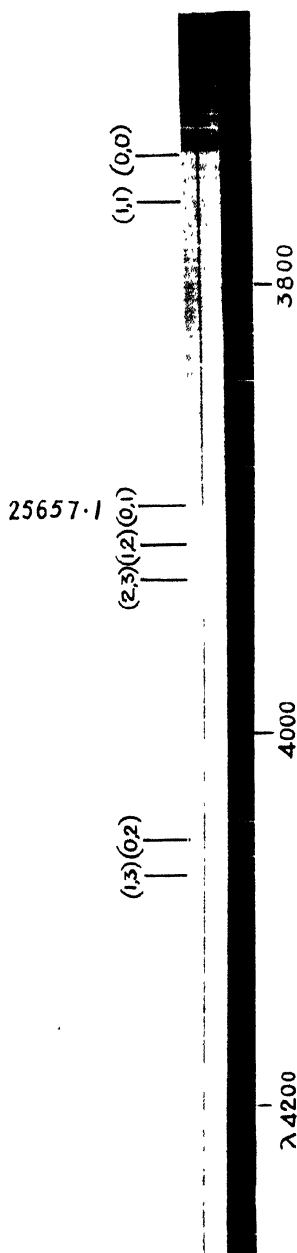
The spectra have been measured on a Hilger comparator employing the usual iron arc standards.

DESCRIPTION OF THE BANDS

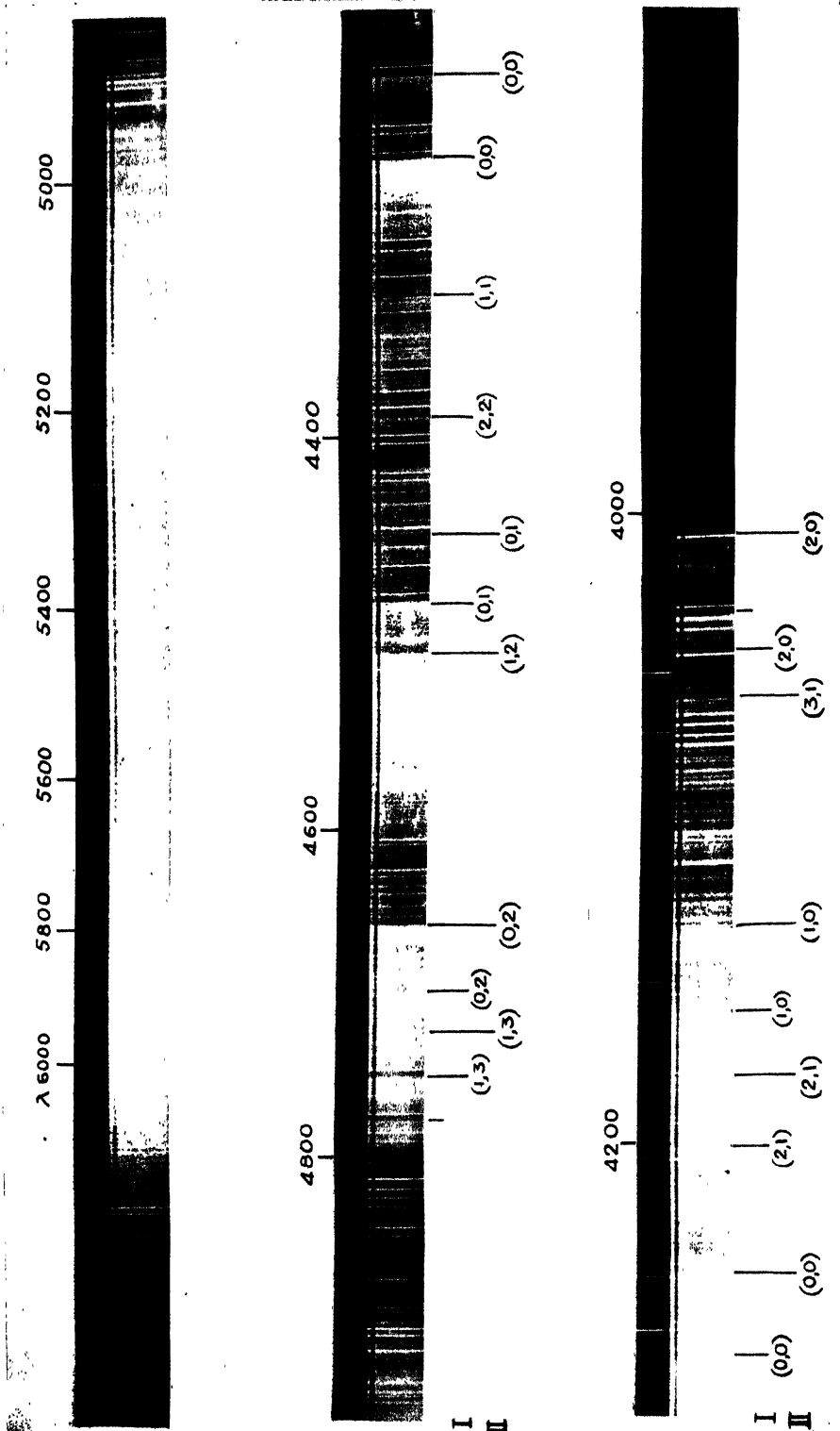
In the bands of columbium oxide in which three systems were recorded the structure differs conspicuously from system to system. There is an apparent partially open structure in the most refrangible system—system A, the structure being much less open in the other two systems. In vanadium oxide also the structure is rather open even under small dispersion in the case of the more refrangible system while in the infrared bands [as seen from the reproductions published by Keenan and Schroeder, (1952)] the rotational structure is just observable. Tantalum oxide presents similar appearance. In the case of many of the bands a rotational structure is observed even under small dispersion, but being very rich in lines the spectrum has presented considerable difficulty in the matter of location of the band heads. At times there is a confusion arising from the overlap of the atomic lines and the rotational structure as well as between the rotational structure of two different bands occurring close together. Besides this, in the sources in which the spectrum has been excited and particularly in the simple arc a continuous spectrum is superposed making the identification of the band heads more difficult. This feature of a strong continuum is very prominent between $\lambda 5100$ and $\lambda 6000$, where no band heads could at all be identified.

The entire spectrum is reproduced in Plates IIIA and IIIB. About 65 band heads are recorded in this region. The wavelength, intensity and wavenumber data for these heads are given in Table II. It will be seen that many of the band heads (more than twenty) have been marked as doubtful. It was found difficult to distinguish a band head from an accidental grouping of the rotational lines. This difficulty is noticed even in the case of bands with a reasonable intensity. The analysis is based on an attempt to assign the vibrational numbering in the case of only bands which are definitely noted as band heads. The most prominent bands of the spectrum are at $\nu 26679$, 25658 , 24063 , 23348 , 22199 , 21490 and 21070 cm^{-1} ,

PREMASWARUP



Tantalum oxide bands—system A (quartz Littrow)



Tantalum oxide bands—system C (glass Littrow)

TABLE II
Band head data for TaO

λ Kiess and Stowell	λ Krishna- murthy and Fernando*	λ Author	Int	ν	System and classifica- tion	ν_{obs} - ν_{calc}
		4952.8	4?	20184.9		
		28.2	5?	285.8		
	4909.7					
4901.57		4773.4	4?	943.5		
4810.35		44.7	6	21070.2	C I (1,3)	26.1
	4744.5	09.1	2?	229.6	C II (1,3)	9.0
		4693.4	5	300.9	C I (0,2)	18.2
		79.4	5	364.5		
4679.46		72.8	5?	394.4		
	4652.0	52.0	7	490.3	C II (0,2)	- 5.1
4651.02		10.0	3?	686.1		
		4595.2	2?	755.9		
	4590.9					
		84.9	4?	804.7		
		30.9	5?	22064.5		
		04.3	6?	194.6		
	4503.5	03.4	8	199.1	C II (1,2)	-10.5
		4495.0	5?	240.7		
		88.9	4?	270.9		
		82.2	4?	304.1		
		79.3	5	318.7	C I (0,1)	- 6.4
		45.3	1?	489.6	C II (0,1)	-11.8
	4415.7					
		4390.4	3	770.5	C I (2,2)	26.9
	4361.8					
		53.6	3?	963.3		
		38.6	4	23042.7	C I (1,1)	3.4
	4281.7	4281.8	8	348.1	C I (0,0)	0.0
		69.6	4?	23414.7		
		49.6	6	525.0	C II (0,0)	0.6
		01.7	4	793.2		
		4192.9	3?	843.1		
		77.0	3?	933.9	C II (2,1)	8.5
4154.41	4154.3	54.5	5	24063.4	C I (1,0)	1.1
		48.7	2?	097.0		
		25.3	3	233.7	C II (1,0)	- 4.9
4092.10		4093.1	2?	424.7		
		75.1	2?	532.5		
		71.6	2	553.5	A (1,3)	- 0.9
		58.1	2?	635.0	C II (3,1)	4.2
		54.2	2	658.7	A (0,2)	8.8
		37.2	2?	763.0	C I (2,0)	- 9.1
		28.4	3	816.6		
		14.8	2	901.1		
4006.24		06.3	4	953.7	C II (2,0)	5.3
		3995.3	2	25022.6		
		92.6	2	039.2		
		54.2	1	282.6		
		30.1	2	437.3	A (2,3)	- .62
		14.5	2	538.6	A (1,2)	- 4.8
3896.43		3896.4	5	657.7	A (0,1)	1.8
		12.1	0	26224.9		
		3778.2	2	456.1		
		65.5	3	549.3	A (1,1)	- 0.1

TABLE II (contd.)

λ Kiess and Stowell	λ Krishna- murthy and Fernando*	λ Author	Int	ν	System and classifica- tion	ν_{obs} — ν_{cal}
3747.25		47.2	8	678.9	A (0,0)	0.0
		3674.7	3	27205.2		
		61.6	2	302.7	A (3,2)	— 3.2
		43.5	4	428.1	A (2,1)	3.7
		3640.1	3	27464.3		
3025.68		25.7	6	573.1	A(1,0)	0.7
		17.3	6	637.3		
		3570.2	1	28002.0		
		64.1	0	049.5	A(5,3)	1.1
		50.9	2	153.6		
		48.6	2?	171.8	A(4,2)	4.1
		37.4	2	261.4		
		30.6	2	316.1	A(3,1)	3.7
		12.8	1	459.4	A(2,0)	1.5
		3429.3	1	29152.4		

* Wavelengths of Krishnamurthy and Fernando in this table are calculated from the wavenumbers given by them.

VIBRATIONAL ANALYSIS

The only published work on the analysis of tantalum oxide bands is that of Krishnamurthy and Fernando, who suggested ν' , ν'' values for nine band heads as shown in Table III

TABLE III

ν' \ ν''	0	1	2
0	22639.9	21490.0	20362.3
1	23348.7	22198.8	21071.1
2	24064.9	22920.0	21776.0

Of these, four bands 22639.9, 20362.3, 22920.0 and 21776.0 were not observed on the author's plates nor were they recorded by Kiess and Stowell. The absence of 22639.9 should be particularly noted. Comparing this scheme with the band head data obtained from the author's plates it is observed that there are many

prominent heads belonging to this molecule unassigned in this analysis. Further, the ω_e'' value is considered to be somewhat high. A complete revision of the analysis is therefore attempted.

For this purpose an initial survey of the characteristic systems of the oxide molecules of the heavier elements is considered useful. Table IV presents a comparison of this kind.

TABLE IV

	CaO		ScO		TiO		VO	
ω_e''	650		971		1008		1012	
$\nu_{0,0}$	F- 1Σ	28054	$2\Sigma^2\Sigma$	20579	$1\phi^1\Delta$	17841	$2^2\Delta^2\Delta$	17427
	$1\Pi^1\Sigma$	25191	$2\Pi^1\Sigma$	16444	$1\Pi^1\Delta$	1273		12539
	$1\Sigma^1\Sigma$	13682			$3\Pi^3\Pi$	19339		
	C- 1Σ	(18260)			$3\Sigma^3\Pi$	14030		
	$1\Sigma^1\Sigma$	15947						
	$1\Sigma^1\Sigma$	9491						
	SrO		YO		ZrO		CeO	
ω_e''	653		853		937		1003	
$\nu_{0,0}$	D-C	28532	$2\Sigma^2\Sigma$	20755	$1\Sigma^1\Sigma$	27151	$\Sigma\Sigma$	21321
	B- 1Σ	24636	$2\Pi^2\Sigma$	16304	$3\Pi^3\Pi$	33685	$2\Pi^1\Sigma$	14839
	$1\Sigma^1\Sigma$	10872			$3\Delta^3\Pi$	28512		
					$3\Pi^3\Pi$	21543		
					$3\Delta^3\Pi$	17484		
					$3\Sigma^3\Pi$	15443		
	BaO		LaO		HfO		TaO	
ω_e''	670		812				1040	
$\nu_{0,0}$	$1\Sigma^1\Sigma$	16722	D- 2Σ	28033	(23512)		$\Sigma\Sigma$	20679
			$2\Pi^2\Sigma$	22625	(19703)		$\Pi\Sigma$	23348
			$2\Sigma^2\Sigma$	17851				
			$2\Pi^2\Sigma$	12641				

Unfortunately the data for hafnium oxide are not known which would have made the estimation for the TaO bands easier. In order, if possible, to locate the approximate position of the ν_{00} bands of hafnium oxide systems a reference

is made to the excellent photographs of the hafnium arc published by Meggers in the course of his investigations on the HfI atomic spectrum. The identification from such a cursory examination is no doubt uncertain and may be misleading. Still the pictures suggest the possibility of considering the prominent head at ν 19073 and the other prominent head at ν 23512 as possible ν_{00} bands of different systems of hafnium oxide. The positions do not compare well with 12641 and 17851 band heads but correspond better with 17851 and 22625 of lanthanum oxide. Further investigation of the hafnium oxide bands in the red region is necessary.

In the spectrum of tantalum there is no evidence on the author's plates of the existence of prominent heads in the long wavelength region above λ 5000 (ν 19994). It might be that the strong continuous background (Plate IIIB) has masked the band heads, if any. Close scrutiny has been made of the plates in this region taken with shorter exposures. No prominent heads certainly were detected while those at 22199, 23348 and 26679 are very conspicuous. Kiess and Stowell, however, have recorded a number of bands between λ 5385 and λ 5589 and also further in the infrared although the data do not seem to be complete. This suggested that there may be several systems characteristic of the TaO molecule similar to those in lanthanum oxide, in zirconium oxide and also in columbium oxide. One or more systems may be expected among the bands measured by the author in the region below λ 5000 and additional systems may be expected in the red and infrared among Kiess and Stowell's measurements. A study of Table IV and extrapolation from vanadium and columbium on the one hand in the same vertical group and from barium and lanthanum in the same horizontal row on the other confirms this viewpoint.

A number of trials have been made based on the data recorded here, adopting successively the different prominent heads as the (0,0) band and trying to build up a vibrational array which would lead to an ω_e value of about 1000 cm^{-1} . The first clue which led to a starting point in the analysis is the existence of the strong band at 26679 with bands on either side fairly prominent and occurring at an interval of 1021 and 894. These three bands were recorded also by Kiess and Stowell. The 1021 interval is in the vicinity of 1000 which is of the anticipated order and the interval 894 is of the right magnitude for a red degraded band system. Further, four other pairs of bands are observed which approximately have the wavenumber difference of 1021 in the less refrangible region and one pair in the ultraviolet. This has pointed to the reality of the interval 1021. On this basis one band system (designated as system A analogous to system A of columbium oxide) could be readily built up, namely, that with 26678.9 as the (0,0) band. This system is shown in Table V. The occurrence of 26549.3 approximately in the calculated position of the (1,1) band was encouraging.

The search for another band system among the longer wavelength bands was next started. The four pairs of bands with 1020 interval which are mentioned

above may obviously form $v'' = 0$ and $v'' = 1$ progressions. The selection of the (0,0) band from among these gave rise to a difficulty for some time. There are five or six bands any of which might be considered as the (0,0). Arranging all the pairs in increasing order of frequency the one at 23348.1 and 23318.7 is found

TABLE V
Deslandre's scheme for system A of TaO bands

$v'' \backslash v'$	0	(1022.1)	1	(1007.7)	2	(985.1)	3
0	26678.9(8)	(1021.2)	25657.7(5)	(999.0)	24658.7(2)		
	(892.9)	(894.2)	(891.6)		(879.9)		
1	27573.1(6)	(1023.8)	26549.3(3)	(1010.7)	25538.6(2)	(985.1)	24553.5(2)
	(886.3)	(886.3)	(888.8)				(883.8)
2	28459.4(1)	(1021.3)	27438.1(4)				25437.3(2)
	(878.0)		(878.0)				
3			28316.1(2)	(1013.4)	27302.7(2)		
	(850.9)				(850.9)		
4					28171.8(2)		
5							28049.5(0)

to be having the smallest frequency. The possibility of treating 23348.1 as the (0,0) band is considered. The main difficulty had been that this band was not recorded by Kiess and Stowell although, as can be seen from Plate IIIB, this is one of the strongest and most unmistakable band on the spectrograms taken by the author. The interval involved, in this pair, namely, 1029.4 is also larger than the expected value 1021. The first point examined was the genuineness and the origin of the strong band at 23348. Reference to the published reviews of band head data such as Jevon's Report, Pearse and Gaydon's 'Identification of Molecular Spectra', Herzberg's 'Spectra of Diatomic Molecules', Eder and Valenta's 'Spectroscopic Atlas etc. etc.', has shown that there is no characteristic band for any molecule at 23348. The possible impurities in the tantalum rods supplied by Johnson, Matthey and Company are also considered. The report furnished by the suppliers indicated the possible presence of columbium, copper, magnesium and silicon etc. These of course could be present, if at all, in extremely minute traces. Known wavelength data of bands due to molecules with the above elements indicate that the band 23348 cannot be due to these impurities. It is believed that 23348 is genuine and is a characteristic band of tantalum

oxide although the author is unable to account why Kiess and Stowell failed to record it.

The possibility of taking 24063.4 as the (0,0) instead of 23348 is also considered since the former happens to be the strongest of all the bands in this region recorded by Kiess and Stowell with an intensity of 7. Further, this forms a pair with 23042.7 with an interval of 1020.7 agreeing very closely with 1021.2. Several alternative schemes have been examined at this stage. In every case, whenever 24063.4 is considered as the (0,0) band the strongest band at 23348 could not be included in the scheme and had to be left out without assignment. This is considered improbable as 23348 is observed to be an outstanding band with almost the largest intensity on the author's plates. Another point is that the expected region of occurrence as judged from Table IV of the ν_{00} band of the system is more satisfactory with 23348 than with 24063; but the difference may not be very much. Hence the question of the (0,0) band of the system is left open and a vibrational analysis could not be arrived at until more definite evidence is obtained from other considerations such as the study of the rotational analysis. This study has shown that $\nu_{26678.9}$ i.e., the (0,0) band of the more refrangible system and the two bands 23348 and 24063 which presumably belong to the less refrangible system have a common final state (Premaswarup, 1955)*.

Another important clue in arriving at the final vibrational analysis has been the observation of a recurring small interval of the order of 160 to 190 cm^{-1} between a number of bands probably belonging to the less refrangible system. This suggested the possibility of regarding this interval as the difference between the two components of a probable Π electronic state. The final vibrational scheme of this system (designated as C by analogy) arrived at on the basis of the above considerations is shown in Table VI. which is self-explanatory. For several members in this system two components are observed. These may be taken to represent the spin splitting of the upper electronic state.

CALCULATION OF THE VIBRATIONAL CONSTANTS

In order to calculate the vibrational constants of the two systems an equation, of the following type containing terms upto $(v + \frac{1}{2})^2$ has been assumed.

$$\nu = \nu_e + [\omega'_e(v' + \frac{1}{2}) - x'_e \omega'_e(v' + \frac{1}{2})^2] - [\omega''_e(v'' + \frac{1}{2}) - x''_e \omega''_e(v'' + \frac{1}{2})^2]$$

The values of ω_e and $x_e \omega_e$ are calculated from the equations

$$\Delta G(v + \frac{1}{2}) = G(v+1) - G(v) = \omega_e - 2(v+1)x_e \omega_e$$

and

$$\Delta_2 G(v) = \Delta G(v - \frac{1}{2}) - \Delta G(v + \frac{1}{2}) = 2x_e \omega_e$$

where $\Delta G(v + \frac{1}{2})$ and $\Delta_2 G(v)$ are first and second differences respectively of the vibrational levels of the same electronic state.

* Details of the rotational analysis will be published in a subsequent communication.

TABLE VI
Deslandre's scheme for system C of TaO bands

v'	v''	0	1	2	3
0		23348.1(8) 176.9 (1032.4) 23525.0(6) (712.0)	22318.7(5) 170.9 (1008.6) 22489.6(1) (724.0)	21300.9(5) 189.4 21490.3(7) (708.8)	
1		24063.4(5) 170.3 (1020.7) 24233.7(3) (709.8)	23042.7(4)	22199.1(8)	21070.2(6) 159.4 21229.6(2)
2		24763.0(2) 190.7 (1019.8) 24953.7(4)	23933.9(3) (701.1)	22770.5(3)	
3			24635.0(2)		

The values ω_r and $x_r\omega_r$ obtained for the three different states involved are given in Table VII

TABLE VII
Vibrational constants

	ω_p	$E_F\omega_p$
Ground state	1040.0 cm ⁻¹	8.5 cm ⁻¹
Excited state of ultraviolet system	901.4 ..	4.0 ..
Excited state of visible system	718.6 ..	2.2 ..

The ν_p values for the two systems are 26774.8 cm^{-1} and 23504.1, 23680.4 cm^{-1} .

ACKNOWLEDGMENTS

The author wishes to express his grateful indebtedness to Prof. K. R. Rao for his inspiring guidance in carrying out this work. His grateful thanks are due also to Prof. P. C. Mahanti who has generously given him permission and full facilities for recording the pictures on the 21-ft grating. The author would like to thank the Government of India for the award of a senior research scholarship.

REFERENCES

- Afif, M., 1950, *Proc. Phy. Soc.*, **63**, 1156.
- Herzberg, G., 1951, "Molecular Spectra and Molecular Structure", Vol. I, Diatomic Molecules.
- Keenan, P. C. and Schroeder, L. W., 1952, *Astroph. Jour.*, **115**, 82.
- Kiess, C. C. and Stowell, E. Z., 1934, *J. Res. Nat. Bur. Stand.*, **12**, 459.
- Krishnamurthy, S. G. and Fernando, I. G., 1949, *Curr. Sci.*, **18**, 371.
- Premaswarup, D., 1955, *Nature*, communicated.
- Ramakrishna Rao, V., 1950, *Ind. J. Phy.*, **24**, 35.
- Ramakrishna Rao, V. and Premaswarup, D., 1953, *Ind. J. Phy.*, **27**, 399.
- Suryanarayanan Rao, K., 1952, D.Sc. Thesis, Andhra University.
- „ 1954, *Nature*, **173**, 1240.
- „ 1955, *Proc. Nat. Inst. India*, (In course of publication).

A STUDY OF TRANSISTORS CONNECTED IN PARALLEL*

BY ANADI NATH DAW,

INSTITUTE OF RADIO PHYSICS AND ELECTRONICS, CALCUTTA UNIVERSITY.

(Received for publication, February, 18, 1955)

ABSTRACT. An analysis has been carried out of the problem of an amplifier using two transistors in parallel. It has been shown that the performance of the combination may be conveniently studied in terms of a single equivalent transistor whose parameters are related to those of the individual transistors in a simple manner. Expressions have been deduced for the gain and the input and the output impedances of the parallel combination for all the three basic modes of operation *viz.*, grounded base and grounded emitter and grounded collector connection. Results of experiments both for point contact and for junction transistors are found to be in good agreement with the results of the theoretical analysis.

1. INTRODUCTION

One of the main drawbacks of transistors as a substitute for vacuum tube amplifier is the small amount of power it can handle. This drawback may be overcome to some extent by using two transistors in pushpull or in parallel arrangement. The former may be used where efficiency of operation is an important consideration and the latter when this is not so. Pushpull operation, involving the use of transformers, however, enhances the cost and reduces the compactness of the equipment. To obviate this, one may use a transistor of p-n-p type in conjunction with another of n-p-n type. But this makes the power supply system complicated. A reasonable efficiency combined with large power handling capacity may be achieved with transistors connected in parallel, and study of the performance of transistors so arranged is thus of practical importance. This study has been made for both point contact and junction transistors and an account of the results obtained is presented in the paper. In section 2 is given a general analysis of the problem of a grounded base amplifier using two transistors in parallel and in section 3, a method by which the various working formulae for such an amplifier may be obtained by reducing the combination to a single equivalent transistor. This is followed in section 4 by results of experiments which support the theoretical deductions as given in section 3.

* Communicated by Prof. S. K. Mitra.

2. ANALYSIS OF GROUNDED BASE AMPLIFIER USING TWO TRANSISTORS IN PARALLEL

The equivalent circuit of a single point contact or junction transistor amplifier for grounded base operation is shown in figure 1. The symbols r_e , r_b & r_c denote respectively the emitter, base and collector resistances and $i_e r_m$ the active element introduced to take into account the current gain of the transistor. i_e and i_c represent the emitter and collector currents respectively and R_S and R_L denote the source and load resistances respectively.

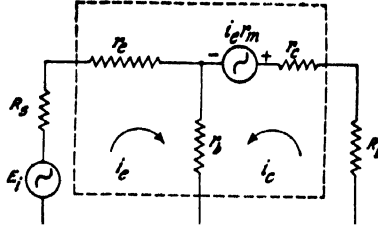


Fig. 1: Showing the equivalent circuit of a grounded base transistor amplifier.

It follows from figure 1 that for the case of a grounded base amplifier using two transistors in parallel, the equivalent circuit would take the form as shown in figure 2. The various resistances and currents of the second transistor are denoted by primed symbols in order to emphasize that the two transistors may not always be of identical characteristics.

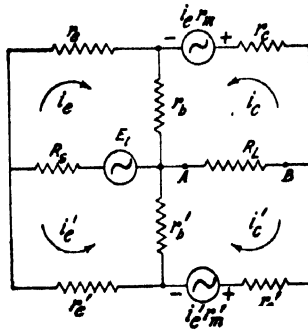


Fig. 2: Showing the equivalent circuit of a grounded base amplifier using two transistors in parallel.

Applying Kirchoff's laws to the 4 meshes of figure 2, the following equations are obtained :

$$\begin{aligned}
 (r_e + r_b + R_S)i_e + r_b i_c + R_S i_e' + 0 i_c' &= E_i \\
 R_S i_e + 0 i_c + (r_e' + r_b' + R_S')i_e' + r_b' i_c' &= E_i \\
 (r_b + r_m)i_e + (r_b + r_c + R_L)i_c + 0 i_e' + R_L i_c' &= 0 \\
 0 i_e + R_L i_c + (r_b' + r_m')i_e' + (r_b' + r_c' + R_L')i_c' &= 0
 \end{aligned} \tag{1}$$

These equations may be solved by standard methods. When this is done, i_e , i'_e , i_c and i'_c are found out to be given by:

$$\left. \begin{aligned} i_e &= E_i [-r'_{11}\{(r_{22}+R_L)(r'_{22}+R_L)-R_L^2\} + r'_{21}\{r_{12}R_L + r'_{12}(r_{22}+R_L)\}]/\Delta_p \\ i'_e &= E_i [-r_{11}\{(r_{22}+R_L)(r'_{22}+R_L)-R_L^2\} + r_{21}\{r_{12}(r'_{22}+R_L) + r'_{12}R_L\}]/\Delta_p \\ i_c &= E_i [-R_L r_{11}r'_{21} + r_{21}\{r'_{11}(r'_{22}+R_L) - r'_{12}r'_{21}\}]/\Delta_p \\ i'_c &= E_i [-R_L r'_{11}r_{21} + r'_{21}\{r_{11}(r_{22}+R_L) - r_{12}r_{21}\}]/\Delta_p \end{aligned} \right\} \dots (2)$$

where Δ_p = the circuit determinant

$$= -[(r_{11}r_{22} - r_{12}r_{21})(r'_{11}r'_{22} - r'_{12}r'_{21}) + R_L\{r_{11}(r'_{11}r'_{22} - r'_{12}r'_{21}) + r'_{11}(r_{11}r_{22} - r_{12}r_{21})\}] \dots (2a)$$

and r_{11} , r_{22} , r_{12} , r_{21} , r'_{11} , r'_{12} etc. are the open circuit parameters of the transistors defined by:

$$\left. \begin{aligned} r_{11} &= r_e + r_b, & r_{12} &= r_b; & r'_{11} &= r'_e + r'_b, & r'_{12} &= r'_b \\ r_{21} &= r_b + r_m, & r_{22} &= r_b + r_c; & r'_{21} &= r'_b + r'_m, & r'_{22} &= r'_b + r'_c \end{aligned} \right\} \dots (2b)$$

It is to be noted that the above solutions are obtained through the assumption that R_s is negligible—a condition which is always satisfied by a practical transistor amplifier circuit.

From (2), we readily get,
input impedance

$$Z_{in} = \frac{E_i}{i_e + i'_e} = \frac{\Delta\Delta' + R_L(r_{11}\Delta' + r'_{11}\Delta)}{r_{22}\Delta' + r'_{22}\Delta + R_L\{(r_{11} + r'_{11})(r_{22} + r'_{22}) - (r_{12} + r'_{12})(r_{21} + r'_{21})\}} \quad (3)$$

where $\Delta = r_{11}r_{22} - r_{12}r_{21}$ and $\Delta' = r'_{11}r'_{22} - r'_{12}r'_{21}$

The output impedance Z_{out} is given by the ratio of the voltage across the points *A* and *B* in figure 2, to the sum $i_c + i'_c$ with the generator E_i short-circuited. An analysis in exactly the same manner as carried out above gives

$$Z_{out} = \frac{\Delta\Delta'}{r_{11}\Delta' + r'_{11}\Delta} \dots (4)$$

The forward power gain ϕ is now readily obtained as

$$\phi = \frac{(i_c + i'_c)^2 R_L}{(i_e + i'_e)^2 Z_{in}} = Z_{in} R_L \left[\frac{r_{21}\Delta' + r'_{21}\Delta}{\Delta\Delta' + R_L(r_{11}\Delta' + r'_{11}\Delta)} \right]^2 \dots (5)$$

3. THE EQUIVALENT TRANSISTOR

Expressions for input and output impedances and gain of two transistors in parallel as deduced in the previous section may be easily obtained from the known

equations for a single transistor by deriving a single hypothetical transistor whose parameters are equivalent to those of the combination. Parameters of this equivalent transistor may be found out by applying elementary matrix consideration to the circuit shown in figure 2.

The 4-pole equations of a single transistor, taking $R_L = 0$, are

$$\begin{aligned} E_i &= i_e r_{11} + i_c r_{12} \\ 0 &= i_e r_{21} + i_c r_{22} \end{aligned} \quad \dots \quad (6)$$

Hence the impedance matrix is given by

$$[Z] = \begin{bmatrix} r_{11} & r_{12} \\ r_{21} & r_{22} \end{bmatrix} \quad \dots \quad (7)$$

from which by inverse operations, the admittance matrix is obtained as

$$[Y] = \begin{bmatrix} \Delta & -r'_{11} \\ -\Delta & \Delta' \end{bmatrix} \quad (8)$$

where $\Delta = r_{11}r_{22} - r_{12}r_{21}$

Equation (8) suggests that when two transistors are connected in parallel, the admittance matrix of the combination would be

$$[Y_0] = \begin{bmatrix} \left[\frac{r_{22}}{\Delta} + \frac{r'_{22}}{\Delta'} \right] & - \left(\frac{r_{12}}{\Delta} + \frac{r'_{12}}{\Delta'} \right) \\ - \left(\frac{r_{21}}{\Delta} + \frac{r'_{21}}{\Delta'} \right) & \left[\frac{r_{11}}{\Delta} + \frac{r'_{11}}{\Delta'} \right] \end{bmatrix} \quad \dots \quad (9)$$

where the primed elements refer to the second transistor. By inverse operations, the impedance matrix corresponding to $[Y_0]$ is found out, which after a little simplification is given by:

$$[Z_0] = \begin{bmatrix} \frac{r_{11}\Delta' + r'_{11}\Delta}{P} & \frac{r_{12}\Delta' + r'_{12}\Delta}{P} \\ \frac{r_{21}\Delta' + r'_{21}\Delta}{P} & \frac{r_{22}\Delta' + r'_{22}\Delta}{P} \end{bmatrix} \quad \dots \quad (10)$$

where $P = (r_{11} + r'_{11})(r_{22} + r'_{22}) - (r_{12} + r'_{12})(r_{21} + r'_{21}) \quad \dots \quad (10a)$

If now for the equivalent transistor, R_{11} , R_{12} , R_{21} and R_{22} denote the open circuit parameters given by

$$\begin{aligned} R_{11} &= R_c + R_b, & R_{12} &= R_b, \\ R_{21} &= R_b + R_m, & R_{22} &= R_b + R_c, \end{aligned}$$

where R_b , R_c , R_e and R_m are the equivalent circuit element values, its impedance matrix would be given by the expression

$$[Z_{eq}] = \begin{bmatrix} R_{11} & R_{12} \\ R_{21} & R_{22} \end{bmatrix} \quad (11)$$

Comparing equations (10) and (11), we obtain

$$\begin{aligned} R_{11} &= \frac{r_{11}\Delta' + r'_{11}\Delta}{P}; & R_{12} &= \frac{r_{12}\Delta' + r'_{12}\Delta}{P} \\ R_{21} &= \frac{r_{21}\Delta' + r'_{21}\Delta}{P} & R_{22} &= \frac{r_{22}\Delta' + r'_{22}\Delta}{P} \end{aligned} \quad (12)$$

from which the circuit element values are obtained as

$$\begin{aligned} R_e &= \frac{r_e\Delta' + r'_e\Delta}{P}; & R_b &= \frac{r_b\Delta' + r'_b\Delta}{P} \\ R_c &= \frac{r_c\Delta' + r'_c\Delta}{P} & R_m &= \frac{r_m\Delta' + r'_m\Delta}{P} \end{aligned} \quad (13)$$

To find out expressions for the input and output impedances and gain for the three modes of operation viz. grounded base, grounded emitter and grounded collector, a method suggested by Shekel (1952) is very helpful.

In this method, the impedance matrix $[Z_{eq}]$ as given in (11) is first converted to its admittance matrix $[Y_{eq}]$ given by

$$[Y_{eq}] = \begin{bmatrix} R_{22}/\Delta_0 & -R_{12}/\Delta_0 \\ -R_{21}/\Delta_0 & R_{11}/\Delta_0 \end{bmatrix} \quad (14)$$

where

$$\Delta_0 = R_{11}R_{22} - R_{12}R_{21}$$

A matrix $[Y^0]$ called the "indefinite admittance matrix" is then formed such that the sum of the elements in any row or column is zero. Thus

$$\begin{aligned} [Y^0] &= \begin{bmatrix} \frac{R_{22} - R_{12}}{\Delta_0} & \frac{R_{12} - R_{22}}{\Delta_0} & \frac{R_{12} - R_{22}}{\Delta_0} \\ R_{21} & R_{11} & R_{21} - R_{11} \\ \frac{R_{21} - R_{22}}{\Delta_0} & \frac{R_{12} - R_{11}}{\Delta_0} & \frac{R_{11} + R_{22} - (R_{12} + R_{21})}{\Delta_0} \end{bmatrix} \end{aligned} \quad (15)$$

From (15), the working equations for the different modes of operation are readily obtained by striking out certain rows and columns as shown below.

Grounded base operation: When the base is grounded, the third row and the third column are struck out and we have,

$$[Y_b] = \begin{bmatrix} -R_{22} & R_{12} \\ \Delta_0 & \Delta_0 \\ -R_{21} & R_{11} \\ -\Delta_0 & \Delta_0 \end{bmatrix}$$

where the subscript b refers to the grounded base mode of operation. The input impedance Z_{in_b} is then given by (Giacoletto, 1953), taking R_L the load resistance into consideration,

$$Z_{in_b} = \frac{R_L(r_{11}\Delta' + r'_{11}\Delta) + \Delta\Delta'}{r_{22}\Delta' + r'_{22}\Delta + R_L\{(r_{11} + r'_{11})(r_{22} + r'_{22}) - (r_{12} + r'_{12})(r_{21} + r'_{21})\}}$$

Similarly, output impedance

$$Z_{out_b} = \frac{\Delta\Delta'}{r_{11}\Delta' + r'_{11}\Delta}$$

and forward power gain

$$\phi_b = Z_{in_b} \cdot R_L \cdot \left[\frac{r_{21}\Delta' + r'_{21}\Delta}{\Delta\Delta' + R_L(r_{11}\Delta' + r'_{11}\Delta)} \right]^2$$

It will be noticed that these results are identical with those given by equations (3), (4) and (5).

Grounded emitter operation: When the emitter is grounded, the first row and the first column of the matrix $[Y^0]$ are struck out and then interchanging rows and columns, so that the new arrangement fits in with the grounded emitter circuit, we have,

$$[Y_e] = \begin{bmatrix} R_{11} + R_{22} - (R_{12} + R_{21}) & R_{12} - R_{11} \\ R_{21} - R_{11} & R_{11} \\ \Delta_0 & \Delta_0 \end{bmatrix}$$

where the subscript e refers to the grounded emitter mode of operation. Hence, input impedance

$$Z_{in_e} = \frac{R_L(r_{11}\Delta' + r'_{11}\Delta) + \Delta\Delta'}{(r_{11} + r_{22} - r_{12} - r_{21})\Delta' + (r'_{11} + r'_{22} - r'_{12} - r'_{21})\Delta + P \cdot R_L}$$

output impedance

$$Z_{out_c} = \frac{\Delta\Delta'}{r_{11}\Delta' + r'_{11}\Delta}$$

and forward power gain

$$\phi_c = Z_{in_c} \cdot R_L \cdot \left[\frac{(r_{21} - r_{11})\Delta' + (r'_{21} - r'_{11})\Delta}{(r_{11}\Delta' + r'_{11}\Delta)R_L + \Delta\Delta'} \right]^2$$

Grounded collector operation: When the collector is grounded, the second row and column of $[Y^0]$ are struck out and interchange of rows and columns are made. This gives input impedance

$$Z_{in_c} = \frac{R_L(r_{22}\Delta' + r'_{22}\Delta) + \Delta\Delta'}{(r_{11} + r_{22} - r_{12} - r_{21})\Delta' + (r'_{11} + r'_{22} - r'_{12} - r'_{21})\Delta + P \cdot R_L}$$

output impedance

$$Z_{out_c} = \frac{\Delta\Delta'}{r_{22}\Delta' + r'_{22}\Delta}$$

and forward power gain

$$\phi_c = Z_{in_c} \cdot R_L \cdot \left[\frac{(r_{12} - r_{22})\Delta' + (r'_{12} - r'_{22})\Delta}{(r_{22}\Delta' + r'_{22}\Delta)R_L + \Delta\Delta'} \right]$$

where the subscript c refers to the grounded collector mode of operation.

4. EXPERIMENTAL OBSERVATIONS

Expressions for equivalent parameters, as derived in section 3, were verified by experimental observations under static conditions. Transistors used for this purpose were the following :

Point contact: Philips OC 50 and OC 51.

Junction: Philips OC 70 and OC 71.

For point contact devices, the two transistors were first connected in parallel in the grounded base mode. Biases were then applied and the following observations made :

(i) Variation of collector voltage and emitter voltage with collector current, keeping emitter currents i_e and i'_e constant.

(ii) Variation of collector voltage and emitter voltage with emitter current, keeping collector currents i_c and i'_c constant.

Slopes of the curves obtained from observations (i) and (ii) gave R_{22} and R_{12} , and R_{21} and R_{11} respectively. These R -values and equation (2b) were then utilised to compute the elements of the equivalent T -configuration of the parallel combination. Results thus obtained are recorded in row 3, Table I.

The two transistors were then isolated and observations (i) and (ii) repeated on each one of them separately, keeping the values of the parameters (i_r , i'_e , i_c and i'_c) the same as those recorded when observations were made with the two transistors in parallel. These data and equation (2b) gave the values of the elements of the equivalent T-configurations of the individual transistors. Results thus obtained are recorded in rows 1 and 2, Table I. Theoretical R -values for the parallel configuration were then computed from these results with the help of equation (13). The computed values are given in row 4, Table I. These are found to be in close agreement with the experimental values obtained earlier.

TABLE I
Point contact transistors

Operating conditions : OC 50 : $i_r = 1.5 \mu a$; $i_c = -6 \mu a$.
: OC 51 : $i'_e = 0.6 \mu a$; $i'_c = -2.3 \mu a$.

Transistor under observation	$r_{e\Omega}$	$r_{b\Omega}$	$r_{c\Omega}$	$r_{m\Omega}$
1. OC 50	62	97	3.5 K	10.4 K
2. OC 51	90	147	5.5 K	15.3 K
3. OC 50 & OC 51 (experimental)	56.9	35.4	1.9 K	6.0 K
4. OC 50 & OC 51 (theoretical)	56.8	35	2.1 K	6.0 K

For junction transistors, the type of measurement described above gives rise to some difficulties. For these, measurement of the so called hybrid parameters defined by the following 4-pole equations is more convenient:

$$\begin{aligned} e_1 &= h_{11}i_r + h_{12}e_2 \\ i_r &= h_{21}i_r + h_{22}e_2 \end{aligned}$$

where h_{11} is an impedance, h_{22} an admittance and h_{12} & h_{21} are ratios.

Note : As in the case of point contact transistors, primed symbols, viz. h'_{11} , h'_{12} , h'_{21} etc. will be used here to denote the hybrid parameters of the other junction transistor and capital H letter symbols will be used to denote the hybrid parameters of the combination of the two transistors in parallel.

Unlike the case of the point contact transistors, the two junction transistors were connected in parallel in the grounded emitter mode which was the usual mode of operation for such transistors and base currents i_b and i'_b flowing through the individual transistors at a particular collector voltage V_{c_j} say, were noted. The following observations were thereupon made :

(i) variation of collector current and base voltage with collector voltage keeping base currents i_b and i'_b constant.

(ii) variation of collector current and base voltage with base current, keeping collector voltage V_{c_j} constant.

H_{22} and H_{12} were determined from observations (i) and H_{21} and H_{11} from observations (ii) by obtaining the slopes of the respective curves. These results were then utilised for obtaining the constants of the equivalent T-configuration for the parallel combination of the two transistors in the grounded base mode of operation by means of the following conversion formulae :

$$\left. \begin{aligned} R_e &= \frac{H_{12}}{H_{22}} ; & R_b &= H_{11} - \frac{H_{12}}{H_{22}} (1 + H_{21}) \\ R_c &= \frac{1}{H_{22}} (1 + H_{21}) ; & R_m &= \frac{1}{H_{22}} (H_{12} + H_{21}) \end{aligned} \right\} \quad \dots (16)$$

Results thus obtained are recorded in row 3, Table II.

Tests similar to those enumerated in (i) and (ii) above were thereafter made on the individual transistors with collector voltage maintained at V_{c_j} and base currents equal to i_b and i'_b respectively. These tests yielded h_{11} , h_{12} , h'_{11} , h'_{12} , etc. from which the elements of the T-equivalent circuit of the individual junction transistors were determined with the aid of expressions (16). These are given in rows 1 and 2, Table II. Theoretical R values for the parallel combination were then computed with the help of expression (13) and are recorded in row 4, Table II. Results are again found to agree fairly well with those obtained experimentally.

TABLE II

p-n-p Junction transistors

Operating Conditions : OC 70 : $V_{c_j} = -2$ volts, $i_b = -10\mu a$
 : OC 71 : $V_{c_j} = -2$ volts, $i'_b = -15\mu a$

Transistor under measurement	$r_{e_{\Omega}}$	$r_{b_{\Omega}}$	$r_{c_{\Omega}}$	$r_{m_{\Omega}}$
1. OC 70	50	450	2.05 M	2 M
2. OC 71	28.5	574	1.03 M	1 M
3. OC 70 & 71 (experimental)	17	289	.63 M	.61 M
4. OC 70 & 71 (theoretical)	18	286	.70 M	.67 M

5. CONCLUSION

The problem of two transistors connected in parallel may be analysed by ordinary method of circuit analysis. The analysis of the combination may be

further simplified by reducing it to a single equivalent transistor. The relations between the parameters of this hypothetical transistor and those of the two actual transistors appear in simple form and may be utilised for obtaining readily the expressions for input impedance, output impedance and power gain of parallel transistor amplifier working in any of the three basic modes viz. grounded base grounded emitter and grounded collector configuration. The analysis carried out is found to be essentially correct from the close agreement between some of the crucial theoretical results and those obtained from static experiments with both point contact and junction transistors.

Dynamic characteristics of the parallel combination under actual working condition are under investigation.

ACKNOWLEDGMENTS

The author wishes to thank Professor S. K. Mitra for giving him facilities for the work and constant encouragement, and the Ministry of Education, Government of India for providing him with a Research Training Scholarship. Thanks are also due to Shri S. Deb for suggesting the problem and for giving guidance in course of the work.

REFERENCES

- Giacoletto, 1953, *RCA Rev.*, **14**, 28.
Shea, R. F., 1953, *Principles of Transistor Circuits*, John Wiley, New York.
Shekel, Jacob, 1952, *Proc. I.R.E.*, **40**, 1493.

THERMAL DIFFUSION OF GAS MIXTURES AND DETERMINATION OF FORCE CONSTANTS*

S. C. SAXENA

INDIAN ASSOCIATION FOR THE CULTIVATION OF SCIENCE, CALCUTTA-32

(Received for publication, February 22, 1955)

ABSTRACT. The value for the force constant ϵ_{12} has been calculated from the observed variation of thermal diffusion factor with temperature to a higher approximation than before. These ϵ_{12} values have been combined with binary viscosity and inter-diffusion data to calculate r_{12} . Utilising these values of the force constants the thermal diffusion factor has been calculated for a number of binary gas mixtures and compared with the experimental data. It is found that the agreement between theory and experiment is quite satisfactory.

1. INTRODUCTION

Since the theory of transport phenomena developed by Enskog (1911, 1917) and by Chapman (1912, 1916, 1917), the influence of intermolecular forces on the transport properties of gases has been fully understood. Attempts have been made in recent years (Hirschfelder, Bird and Spotz, 1949; Srivastava and Madan, 1952*a*, 1952*b*, 1953*a*, 1953*b*) to utilise this Chapman-Enskog theory to obtain information about intermolecular forces from the temperature variation of the gaseous transport coefficients, as this is useful for predicting and correlating the various properties of gases, liquids and solids.

The Chapman-Enskog theory is based on the following assumptions: (1) the intermolecular force field is spherically symmetric; (2) only binary collisions between the molecules are important; (3) the binary collisions are elastic; and (4) molecular interactions are adequately described by classical mechanics. Thus the theory applies strictly to monatomic gases at moderate pressures and at sufficiently high temperatures so that the quantum effects are negligible. The theory has been fairly successful in accounting for the transport properties of most polyatomic gases so that the limitations imposed by conditions (1) and (2) do not appear to be very severe, and in most of the works these have been almost neglected.

For obtaining specific information about intermolecular forces from transport phenomena it is necessary to assume an analytical form for the intermole-

* Communicated by Prof. B. N. Srivastava.

cular potential. The most useful intermolecular potential for this purpose is the Lennard-Jones 12:6 potential energy function

$$E_{ij}(r) = 4\epsilon_{ij}[(r_{ij}/r)^{12} - (r_{ij}/r)^6] \quad \dots (1)$$

where ϵ_{ij} is the minimum potential energy (taken as positive) and r_{ij} the low velocity collision diameter.

The collision integrals for this potential have been calculated by a number of workers (Kihara and Kotani, 1943; Boer and Kranendonk, 1948; Hirschfelder, Bird and Spotz, 1948; Rowlinson, 1949), from which the various transport properties can be calculated, by utilising the formulae developed from Chapman-Enskog theory (Chapman and Cowling, 1952; Hirschfelder, Curtiss and Bird, 1954). It is well known that the coefficient of thermal diffusion is far more sensitive to the type of molecular interaction than the three elementary gas coefficients. Consequently, the force constants for the 12:6 model were calculated by Srivastava and Madan (1953a) for various gas mixtures from the data on the temperature variation of the thermal diffusion factor. In the present paper these calculations have been made more precise by taking a higher approximation and fairly accurate values have been obtained for the force constants ϵ_{12} and r_{12} for several pairs of molecules.

2. THEORY AND FORMULAE

The first approximation to the thermal diffusion factor for a mixture of two gases 1, 2 is given by

$$|\alpha|_1 = 5(c-1)g, \quad \dots (2)$$

where

$$\begin{aligned} g &= (S_1 y_1 - S_2 y_2) / (Q_1 y_1^2 + Q_2 y_2^2 + Q_3 y_1 y_2) \\ S_1 &= \frac{M_1}{5} \left(\frac{r_{11}}{r_{12}} \right)^2 \left[\frac{2(M_1 + M_2)^3}{M_2} \right]^{\frac{1}{2}} \left[\frac{W^2(2, kT/\epsilon_{11})}{W^1(1, kT/\epsilon_{12})} \right] \\ &\quad - 3M_2(M_2 - M_1) - 4AM_1M_2 \\ Q_1 &= \frac{1}{5} \left(\frac{r_{11}}{r_{12}} \right)^2 \left[\frac{2(M_1 + M_2)}{M_2} \right]^{\frac{1}{2}} \left[\frac{W^2(2, kT/\epsilon_{11})}{W^1(1, kT/\epsilon_{12})} \right] \\ &\quad \times [6M_2^2 + (5-4B)M_1^2 + 8AM_1M_2] \\ Q_3 &= 3(M_1 - M_2)^2(5-4B) + 4AM_1M_2(11-4B) \\ &\quad + \frac{4}{25} \left(\frac{r_{11}r_{22}}{r_{12}^2} \right)^2 \left[\frac{(M_1 + M_2)^3}{(M_1M_2)^{\frac{1}{2}}} \right] \left[\frac{W^2(2, kT/\epsilon_{11}) \cdot W^2(2, kT/\epsilon_{22})}{\{W^1(1, kT/\epsilon_{12})\}^2} \right] \end{aligned}$$

with similar expressions for S_2 and Q_2 . M_i is the molecular weight of the i th species, y_i is the mole fraction. A , B , C are functions of kT/ϵ_{12} , and $W^l(n, kT/\epsilon_{ij})$ are the collision integrals.

In the previous paper (Srivastava and Madan, 1953a) the values of the force parameter ϵ_{12} were calculated by attributing the temperature variation of α to the factor $(C-1)$ alone, while the temperature variation of the factor g was ignored. Here we have taken into account this small variation of g as well, but for doing so we require the force parameters both for like and unlike molecules. The force constants used for like molecules are those obtained from thermal diffusion viscosity and self-diffusion (Srivastava and Madan, 1953b; Hirschfelder, Bird and Spotz, 1949; Srivastava and Madan 1952a and 1952b) and are reported in a previous paper (Madan, 1953).

For the binary mixture, the formulae for the first approximation to the viscosity is given by

$$[\eta_{12}]_1 \times 10^7 = \frac{R_1 + R_2 + R_3 + (E/H_1) + (E/H_2)}{(R_1/H_1) + (R_2/H_2) + (E/H_1 H_2) + (R_4/E)} \quad \dots (3)$$

in which

$$R_1 = (y_1/y_2)(2/3 + A M_1/M_2)$$

$$R_2 = (y_2/y_1)(2/3 + A M_2/M_1)$$

$$R_3 = 2[2/3 - A]$$

$$R_4 = 2A(M_1 + M_2)^3/3M_1M_2$$

$$H_i = 266.93(M_i T)^{1/2}(r_i)^{-2}/W^2(2, kT/\epsilon_i)$$

$$E = 37.75[(M_1 + M_2)^3 T / (M_1 M_2)]^{1/2}(r_{12})^{-2}/W^1(1, kT/\epsilon_{12})$$

Here H_i are simply the first approximations to the viscosity of the i th component, while the other quantities have their usual meaning.

The second approximation for the coefficient of diffusion is given by the the following equation

$$[D_{12}]_2 = \frac{0.00092916 T^{3/2} [(M_1 + M_2)/M_1 M_2]^{1/2}}{p r_{12}^2 W^1(1, kT/\epsilon_{12})(1 - \Delta)} \quad \dots (4)$$

in which D_{12} is the coefficient of diffusion in $\text{cm}^2 \text{sec}^{-1}$, p the pressure in atmosphere, and Δ is a small quantity defined by

$$\Delta = 5(c-1)^2(P_1 y_1^2 + P_2 y_2^2 + P_{12} y_1 y_2)/(Q y_1^2 + Q_2 y_2^2 + Q_{12} y_1 y_2)$$

in which

$$P_1 = M_1^3 [M_1 + M_2]^{-2} (2/3 V_0) ([D_{12}]_1 / [\eta_{11}]_1) (273.16 p / T)$$

$$P_{12} = [3(M_1 - M_2)^2 + 4A M_1 M_2] / (M_1 + M_2)^2$$

$$Q_1 = (P_1 / M_1^2) (6M_2^2 + 5M_1^2 - 4M_1^2 B + 8A M_1 M_2)$$

$$Q_{12} = [3(5 - 4B)(M_1 - M_2)^2 / (M_1 + M_2)^2 + 4A M_1 M_2 (11 - 4B) / (M_1 + M_2)^2 + 2P_1 P_2 (M_1 + M_2)^4 / M_1^2 M_2^2]$$

With similar expressions for P_2 and S_2 , $[D_{12}]_1$ is the first approximation to D_{12} and is related to $[D_{12}]_2$ by the relation

$$[D_{12}]_2 = [D_{12}]_1 / (1 - \Delta) \quad (5)$$

and V_0 is the molar volume under standard conditions, and $[\eta_1]_1$ and $[\eta_2]_1$ are the calculated first approximations to the viscosity of the pure component.

Equations (3) and (4) can be utilised to calculate r_{12} when ϵ_{12} is known.

3. CALCULATION OF ϵ_{12} AND r_{12}

As already mentioned equation (2) was utilised in a previous paper (Srivastava and Madan, 1953a) to calculate the force constant ϵ_{12} by treating g as constant, actually, however, g is slightly temperature dependent. These ϵ_{12} values may therefore be slightly in error. To obtain a more accurate value of ϵ_{12} it is desirable to calculate g at the different temperatures for which experimental data on α are available and to take into account the observed variation of g . For this purpose the values of ϵ_{11} , ϵ_{22} , r_{11} , r_{22} as given by Madan (1953) were utilised and r_{12} was calculated from equations (3) and (4) by utilising the experimental data on binary viscosity and inter-diffusion. The values of r_{12} so obtained are given in Table II.

For Ne-Kr, Ne-Xe and Ar-Xe mixtures there are no experimental data on viscosity or interdiffusion. Hence for these r_{12} was calculated from the relation

$$\epsilon_{12} r_{12}^6 = 2(\epsilon_{11} \epsilon_{22} r_{11}^6 r_{22}^6) (I_1 I_2)^{1/2} / (I_1 + I_2) \quad \dots \quad (6)$$

The values so obtained are given in Table III.

TABLE I (a)

Values of g

$T(^{\circ}\text{K})$	$\text{H}_2 - \text{N}_2$	$\text{H}_2 - \text{O}_2$	$\text{H}_2 - \text{CO}$	$\text{H}_2 - \text{A}$
83	0.5110	—	0.4978	—
93	—	0.5199	—	—
108	—	—	—	0.5862
123	0.4999	0.5094	0.4842	0.5819
173	0.4955	0.5008	0.4786	0.5706
223	0.4935	0.4971	0.4761	0.5654

Utilising these ϵ_{12} , r_{12} values and the values of the force constants for like molecules the values of the factor g are calculated at various temperatures for a number of gas pairs. These values are recorded in Table I. Next the factor

α/g is plotted (instead of α) against the corresponding temperature and ϵ_{12} is calculated in a similar manner as done previously. The values of ϵ_{12} so obtained are given in Table II, column 3 and are seen to be about 4% higher than the previous values. These precise first approximation values of ϵ_{12} were recombined with the inter-diffusion and binary viscosity data to yield r_{12} and these are collected in Table II, columns 5 and 7 respectively. These two sets of values of r_{12} are seen to be in agreement among themselves as well as those obtained with the help of equation 6 (vide column 11 table II). The first approximation values for the pairs Ne-Kr, Ne-Xe, and A-Xe are given in Table III.

TABLE I (b)
Values of g

$T(^{\circ}\text{K})$	He-A	Ne-A	Ne-Kr	Ne-Xe	A-Xe
117	0.5971	0.3284	0.5325	---	---
147	0.5955	0.3290	0.5245	---	---
185	0.5931	0.3238	0.5191	---	---
233	0.5926	0.3195	0.4865	0.5990	0.4658
293	0.5923	0.3164	0.5111	0.5950	0.4586
369	---	---	---	0.6054	0.4511
464	---	---	---	0.5887	0.4462
585	---	---	---	0.5876	0.4422

TABLE II
Force constants for unlike molecules

Gas pair	$\epsilon_{12}/k(^{\circ}\text{K})$ from thermal diffusion (first approximation)		$r_{12}(\text{\AA})$ from viscosity (first approximation)		$r_{12}(\text{\AA})$ from inter- diffusion (first approximation)		$r_{12}(\text{\AA})$ mean (first approximation)		$r_{12}(\text{\AA})$ from equation 6	
	Rough calculation	Precise calculation	from col. 2	from col. 3	from col. 2	from col. 3	from col. 2	from col. 3	from col. 2	from col. 3
H ₂ -N ₂	46.53	48.05	3.364	3.355	3.341	3.332	3.353	3.344	3.395	3.377
H ₂ -O ₂	59.81	62.51	3.244	3.229	3.198	3.183	3.221	3.206	3.205	3.181
H ₂ -A	56.06	57.29	3.200	3.195	3.242	3.237	3.221	3.216	3.258	3.249
H ₂ -CO	51.33	52.45	3.267	3.263	3.365	3.361	3.316	3.312	3.345	3.341
He-A	26.65	27.91	3.083	3.071	3.046	3.035	3.065	3.053	3.049	3.025
Ne-A	65.35*	67.60	3.102	3.090	---	---	3.102	3.090	3.098	3.079

* This value has been calculated from the experimental data of Grew *et al.* (1954) and therefore differs from that given by Srivastava and Madan (1953a) as they calculated from the older data of Grew (1947) which differs appreciably from that given in his recent work.

TABLE III
Force constants for unlike molecules

Gas pair	$\epsilon_{12}/k(^{\circ}\text{K})$ from thermal-diffusion (first approximation)		$r_{21}(\text{\AA})$ from equation (6)	
	Rough calculation	Precise calculation	From column (2)	From column (3)
Ne—Kr	62.09	64.88	3.311	3.287
Ne—Xe	69.01	71.99	3.485	3.460
A—Xe	166.5	168.9	3.725	3.716

4. CALCULATION OF THERMAL DIFFUSION FACTOR

Thus knowing the force constants for unlike molecules purely from experimental data we can test the adequacy of the 12:6 model by finding how well it reproduces the experimental data on the various transport properties. The phenomenon of thermal diffusion has been utilised here in view of its greater sensitiveness to the force between molecules. With the help of Table II and equation (2) the thermal diffusion factor α has been calculated at various temperatures and concentrations. These are recorded in Tables IV, V and VI along with the experimentally observed values. These tables also give the percentage of the lighter component. The data for the variation of α with concentration is taken from Atkins, Bastick and Ibbs (1939), while that for the variation with temperature on inert gas mixtures is taken from the work of Grew (1947), with the single exception of Ne-A which has been taken from his more recent work (Grew, 1954). The data on $\text{H}_2\text{—A}$, $\text{H}_2\text{—O}_2$, $\text{H}_2\text{—N}_2$ and $\text{H}_2\text{—CO}$ is that given by Ibbs, Grew and Hirst (1929). The assignement of temperature to the experimental values of Atkins et. al. (1939) is done by utilising the Brown's formula,

$$T_r = \frac{T_1 T_2}{T_2 - T_1} \ln (T_2/T_1) \quad \dots (7)$$

where T_2 and T_1 are the temperatures between which the thermal diffusion has been measured. In each case the smoothed experimental values have been reported.

TABLE IV
Thermal diffusion of gases

% of the lighter component	Gas pair	A—He		A—Ne		Ne—Kr		Tempera- ture °K
		α exp.	α theor.	α exp.	α theor.	α exp.	α theor.	
10		0.278	0.290	×	×	×	×	327
20		0.298	0.310	0.146	0.158	0.203	0.239	327
30		0.314	0.334	0.161	0.165	0.212	0.255	327
40		0.338	0.363	0.170	0.173	0.233	0.273	327
50		0.372	0.395	0.183	0.182	0.267	0.293	327
60		×	×	0.195	0.192	0.306	0.317	327

TABLE V
Thermal diffusion of gases

Tempera- ture °K	Gas- Pair	A—He		A—Ne		Ne—Kr		Ne—Xe		A—Xe	
		51.2%		52.0%		53.0%		54.2%		56.4%	
		α exp.	α theor.	α exp.	α theor.	α exp.	α theor.	α exp.	α theor.	α exp.	α theor.
117		0.329	0.331	0.0847	0.0807	0.152	0.139	—	—	—	—
147		0.349	0.357	0.108	0.111	0.180	0.186	—	—	—	—
185		0.369	0.377	0.136	0.139	0.212	0.231	0.260	0.245	0.0490	0.0235
233		0.381	0.389	0.159	0.160	0.249	0.250	0.282	0.285	0.0708	0.0660
293		0.387	0.398	0.179	0.177	0.292	0.292	0.306	0.319	0.0981	0.110
369		0.393	0.401	—	—	0.313	0.312	0.334	0.350	0.137	0.153
464		0.399	0.403	0.196	0.199	0.323	0.324	0.367	0.371	0.175	0.193
585		0.399	0.405	—	—	0.339	0.332	0.404	0.385	0.212	0.223
736		—	—	0.196	0.207	—	—	—	—	—	—
1167		—	—	0.196	0.207	—	—	—	—	—	—

TABLE VI
Thermal diffusion of gases

Temperature °K	H ₂ -N ₂ (29.4% H ₂)		H ₂ -O ₂ (29.8% H ₁)		H ₂ -A (47.0% H ₂)		H ₂ -CO (24.0% H ₂)	
	α exp.	α theor.	α exp.	α theor.	α exp.	α theor.	α exp.	α theor.
83	0.121	0.123	—	—	—	—	0.115	0.102
93	—	—	0.0956	0.0900	—	—	—	—
108	—	—	—	—	0.144	0.162	—	—
123	0.154	0.202	0.133	0.152	0.164	0.194	0.177	0.179
173	0.207	0.256	0.206	0.219	0.219	0.265	0.249	0.237
223	0.241	0.285	0.229	0.256	0.266	0.302	0.272	0.266
273	0.241	0.303	0.229	0.279	0.266	0.329	0.280	0.284

5. DISCUSSION OF RESULTS

The method of calculating the force parameter ϵ_{12} from the temperature variation of the thermal diffusion factor α is theoretically preferable as the large change in α is directly attributable to the term containing ϵ_{12} , while in the case of the other transport properties a large portion of the change is brought about by an explicit dependence on the temperature and only a small part is attributable to ϵ_{12} term. The thermal diffusion method, however, suffers from the drawback that only the first approximation formula for α is known.

Recently (1955), however, we have worked out the formula for the second approximation to α for the Lennard-Jones 12:6 model in the case of a mixture of heavy isotopes and have shown that the maximum difference between the first and second approximations (in the range studied there) is about 3%. In the absence of any precise knowledge of the difference between the first and second approximations to α for the case of binary mixtures, we can make the plausible assumption that for this also the difference is of the same order as for isotopes. With this assumption we can make an estimate of the order of error involved in our computed values of ϵ_{12} . Calculation shows that this effect of the second approximation is not likely to change the value of ϵ_{12} by more than 3% and may be even much less.

The values of the force parameter r_{12} found here are sufficiently accurate and reliable. We have utilised the binary viscosity also in addition to inter-diffusion, in view of the fact that the experimental determination of the former is capable of greater accuracy, though calculation for this involves the pure gas parameters which might be in error and might thereby vitiate the results. However, in most of the cases investigated here the agreement between the values obtained from the two properties is quite satisfactory and it is difficult to establish the supremacy of one over the other.

It will be seen from the tables that the agreement between the calculated and experimental values of α is fairly good, being excellent in certain cases. The slight discrepancies observed in a few cases may be due to slight errors in the assumed values of ϵ_{11} , ϵ_{22} , ϵ_{12} and r_{11} , r_{22} , r_{12} ; the limitations under which the theory of transport phenomena has been developed by Chapman and Enskog, and the possible errors involved in the experimental measurements. The experimental data for A—Xe are less accurate due to the insensitiveness of the gauge and slight impurity of xenon employed.

6. ACKNOWLEDGMENTS

The author wishes to acknowledge his deep indebtedness to Prof. B. N. Srivastava, D.Sc., F.N.I., for his invaluable guidance in carrying out this work. This work has been done under a research scheme financed by the Council of Scientific and Industrial Research, New Delhi, to whom the author is deeply indebted for this award.

REFERENCES

- Atkins, B. E., Bastick, R. E., and Ibbs, T. L., 1939, *Proc. Roy. Soc. A*, **172**, 142.
 deBoer, J. and van Kranendonk, J., 1948, *Physics*, **14**, 442.
 Chapman, S., 1912, *Trans. Roy. Soc. (London)*, A, **211**, 433.
 1916, *ibid.*, **216**, 279.
 1917, *ibid.*, **217**, 115.
 Chapman, S. and Cowling, T. G., 1952. The mathematical theory of non-uniform gases, second edition, Cambridge University Press, England.
 Enskog, D., 1911, *Physik, Z.*, **12**, 56, 533.
 1917, Inaug. Diss, Upsala.
 Grew, K. E., 1947, *Proc. Roy. Soc. A.*, **189**, 402.
 „, 1954, *Proc. Roy. Soc. A.*, **224**, 513.
 Hirschfelder, J. O., Bird, R. and Spotz, E. L., 1948, *J. Chem. Physics*, **16**, 968.
 „, 1949, *Chem. Rev.*, **44**, 205.

- Hirschfelder, J. O., C.F. and Cutiss, Bird, R. B., 1954. The molecular theory of gases and liquids, John Wiley and Sons, Inc., New York.
- Ibbs, T. L., Grew, K. E., and Hirst, A. A., 1929, *Proc. Phys. Soc.*, **41**, 456.
- Kihara, T. and Kotani, M., 1943, *Proc. Phys. Math. Soc., Japan*, **25**, 602.
- Madan, M. P., 1953, *Proc. Nat. Inst. Sci.*, **19**, 5, 713.
- Rowlinson, J. S., 1949, *J. Chem. Physics*, **17**, 101.
- Saxena, S. C. and Srivastava, B. N., 1955. (In the course of publication).
- Srivastava, B. N. and Madan, M. P., 1952a, *Phil. Mag.*, **7**, 43, 968.
- „ 1952b, *Proc. Nat. Acad. Sci.*, **21**, III-VI, 254.
- „ 1953a, *Proc. Phys. Soc. A.*, **66**, 277.
- „ 1953b, *J. Chem. Phys.*, **21**, 807.

A STUDY OF A. C. RESISTIVITY OF CALCUTTA SOIL*

S. P. BHATTACHARYYA

DEPARTMENT OF APPLIED PHYSICS, CALCUTTA UNIVERSITY

(Received for publication, January 13, 1955)

ABSTRACT. The paper deals with the a.c. resistivity of soils in and around the city of Calcutta and its variations with temperature and moisture content of the soil.

INTRODUCTION

In a previous communication (Bhattacharyya and Mahanti, 1953) the results of study of d.c. resistivity of soil in and around the city of Calcutta and its variation with time, temperature and humidity were reported. The effect of endosmosis was also ascertained. In the present paper are reported the results of measurement of its a.c. resistivity.

It has been stated (Bhattacharyya and Mahanti, 1953) that all previous workers have studied the a.c. resistivity of Indian soils at only high frequencies. But as the values of electrical constants of a soil are not the same at different frequencies and since the frequency of a.c. power supply in Calcutta is 50 cycles per second, it was thought desirable to obtain data of a.c. resistivity of Calcutta soil at such power frequency.

The method of measurement was the same as that employed for measurement of d.c. resistivity. For the present purpose the a.c. voltage applied across the test samples was of magnitude 120 volts and was taken from an a.c. supply of 220 volts through an auto-transformer.

The same samples of soil as used for the measurement of d.c. resistivity were used, and the same technique also employed in preparing the test samples.

EXPERIMENTAL RESULTS

Table I contains the data of a.c. resistivity of different samples of soil at a room temperature of 30° C and with a moisture content of 15 per cent. For comparison, the data of their d.c. resistivity are also included in the table.

*Communicated by Prof. P. C. Mahanti

TABLE I

Soil taken from	a.c. Resistivity (ohm-cm)	d.c. Resistivity (ohm-cm)
East Calcutta (Boliaghata)	2778	3250
Central Calcutta (Science College)	2650	2850
West Calcutta (Dockyard)	1379	1450
North Calcutta (Sinthoe)	1375	1415
South Calcutta (Tollygunge)	1350	1400
Ganges Silt	1312	1365

It will be seen from Table I that the value of a.c. resistivity of soil of a particular locality is lower than that of its d.c. resistivity. This difference is attributed to the polarisation effect accompanying direct current. Similar results have been obtained also by the previous workers (Higgs, 1930; Smith-Rose, 1934) on soils of other countries.

TIME CURRENT CHARACTERISTICS

A steady a.c. voltage was applied across a sample of soil having a definite value (16 per cent) of moisture content and the reading of the ammeter at suitable intervals was noted until the current attained a constant value. The results are shown graphically in figure 1. It is seen that the current at first increases to a maximum value and then decreases to a minimum. This is unlike what one would

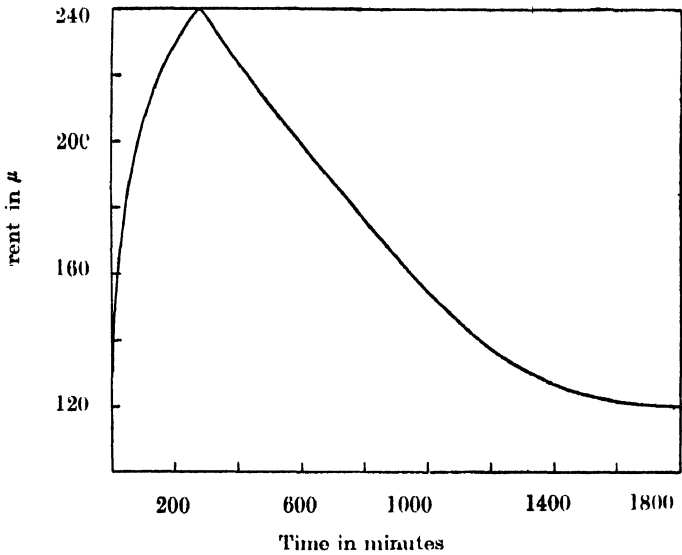


Fig. 1

expect when a current passes through a sample of soil containing many electrolytic salts in its composition since the coefficient of electrical conductivity of such a soil should be positive. But the nature of the curve is found nearly identical with that of the corresponding curve obtained with direct current passing through the sample of soil. In the latter case, the predominance of the heating effect over the effects of polarisation and endosmosis or vice versa determines the total resistance of the sample at any instant. The last two effects tend to increase the resistance of the soil. But with alternating current the polarisation effect is absent. Moreover, as the moisture moves in the direction of the current flow, the effect of endosmosis is also negligible. Hence the nature of the time-current characteristics will depend on the heating effect alone. To confirm this it was thought of interest to study the temperature gradient across the sample when carrying alternating current. For this purpose a sample of soil (Central Calcutta) having a given moisture content (14 per cent) was taken in the experimental cylinder and on its surface three equidistant holes, one at the middle and two near the ends, were bored vertically through its axis. Three sensitive thermometers were introduced into the soil through these three holes. The two outer thermometers would give the temperature of the soil section nearest to the electrodes while the temperature of the middle section would be recorded by the third thermometer. A constant a.c. voltage was applied across the electrodes and the current allowed to flow continuously until it was found to attain a constant value. At suitable intervals the readings of the voltmeter, the ammeter and the thermometer were recorded. Finally when thermometer readings were steady, the percentage of the moisture content of the soil in the immediate neighbourhood of the thermometer bulbs was determined and found to be as shown in Table II.

TABLE II

Position of the thermometer along the tube	Temperature °C	Per cent of moisture content
End 1	45	13.0
Middle	55	11.1
End 2	46	12.9

Curves showing the variations of temperature recorded by each thermometer with time are given in figure 2, which also includes the corresponding values of current flowing through the sample.

Form the curves it is seen that the temperature of each section first rises and then diminishes to a minimum value although temperatures of these sections are different from one another. It is further seen that the temperature of the middle

section is always higher than that of each outer section. Electrodes, being in contact with the atmosphere, radiate their heat to the surroundings and the temperature of each soil section adjacent to electrodes is, therefore, of lower value than that of the middle section. A temperature gradient is thus set up in the

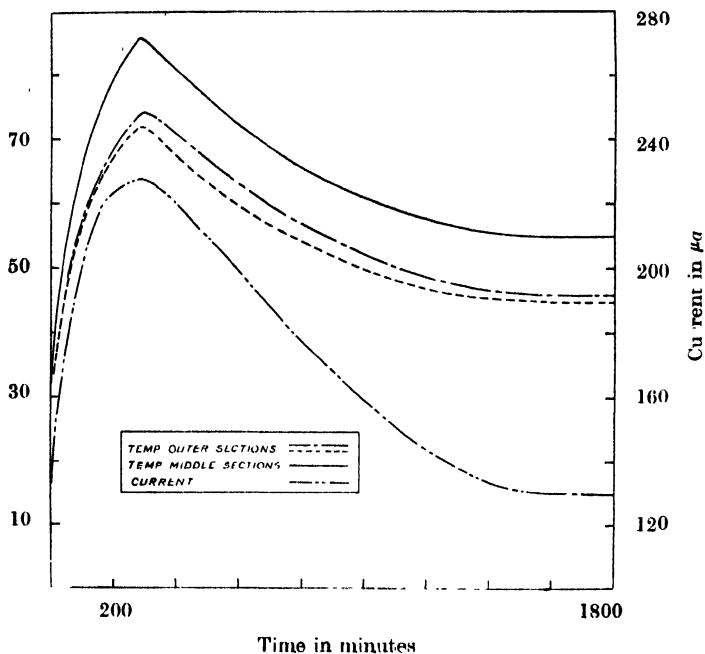


Fig. 2

sample of the soil from the central plane to either electrodes and the moisture moves along this gradient. Thus the distribution of moisture content in the soil is disturbed, the moisture having a tendency to accumulate more near the outer electrodes than at the centre. After sometime heat radiates from the outer surface of the porcelain tube and the temperature of the whole system therefore decreases till a steady state is reached.

The effect of temperature gradient on the current distribution in the body of the soil in the experimental cylinder was also studied. When the applied voltage is kept constant the voltage drop across any section depends on its moisture content as well as on its temperature. The drop across each of the three sections of the sample of soil was obtained in a similar manner as was obtained previously (loc. cit) to study the effect of endosmosis. The results are shown graphically in figure 3. From these curves it is seen that with time the voltage drop across the middle section first decreases and then increases to a maximum value while the drop across each of the outer sections first increases and then diminishes to a minimum. This is due to the fact that a moisture content gradient sets

in the soil along with the temperature gradient. At any instant their additive effects, so long the applied voltage remains constant, determine therefore the value of the total resistance of any section and hence the voltage drop across it.

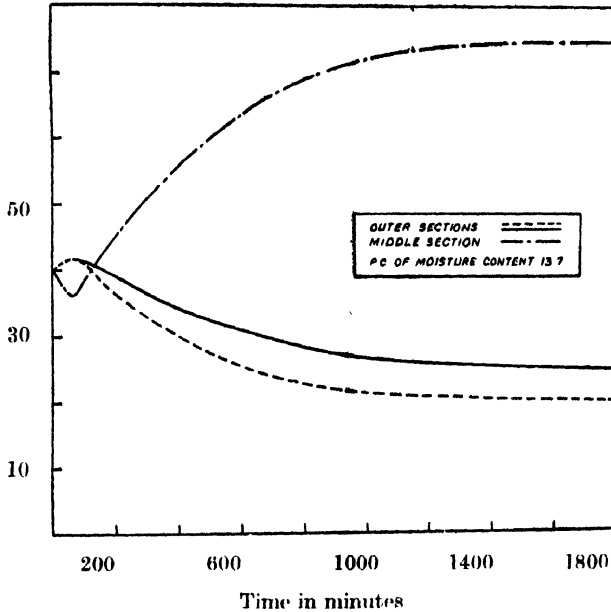


Fig. 3

Effect of moisture content as well as effect of temperature on different soil samples were studied separately and found to yield almost the same results as those obtained in the d.c. measurement, the only difference being that for the same moisture content and for the same temperature, the a.c. resistivity is always lower than the d.c. resistivity.

For ascertaining the effect of polarisation in the soil an experimental arrangement was set up as shown in figure 4. A steady d.c. voltage was applied across a sample of soil of known moisture content and the reading of the ammeter at suitable intervals was noted until the current attained a constant value. Along

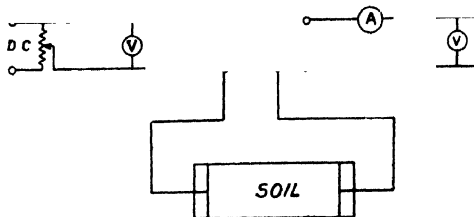


Fig. 4

with each ammeter reading, the temperature of the test sample was also recorded with the help of a sensitive thermometer introduced into it through a hole along

the axis of the cylinder. Switch over from d.c. to a.c. was made at regular intervals as quickly as possible and the a.c. ammeter was read. Results are shown graphically in figure 5, which also includes the corresponding values of resistivity, both d.c. and a.c., of the sample. From the figure it is seen that both d.c. and a.c. resistivity curves show the same characteristics. It is further seen that d.c.

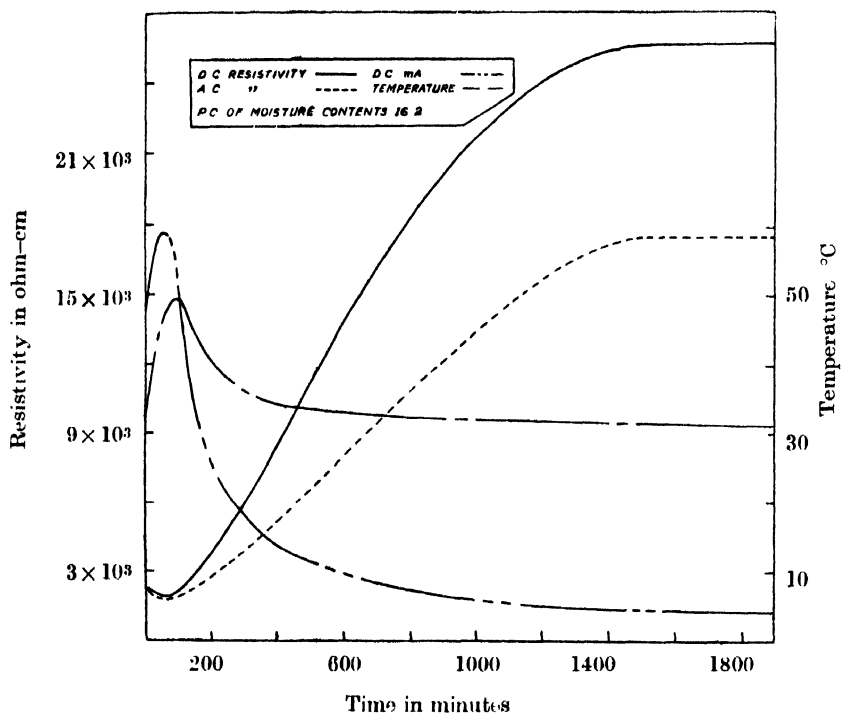


Fig. 5

resistivity increases more rapidly than a.c. resistivity with time but finally they become constant. This difference is attributed to the absence of the effect of polarisation when alternating current is used. So the difference in the values of a.c. and d.c. resistivities may give an idea of the degree of polarisation at any instant. The effect of endosmosis is not taken into account as at any instant the distribution of moisture set up by the flow of direct current will remain unaltered if the readings on a.c. side be taken quickly.

ACKNOWLEDGMENTS

The author acknowledges with pleasure his best thanks to Prof. P. C. Mahanti for his valuable guidance and also to Dr. A. K. Sen Gupta for helpful discussions during the course of the investigation.

REFERENCES

- Bhattacharyya, S. P. and Mahanti P. C. 1953, *Ind. Jour. Phys.*, **27**, 615.
 Higgs, 1930, *Jour. I.E.E.*, **68**, 736.
 Smith-Rose, 1934, *Jour. I.E.E.*, **75**, 221.

FORCE CONSTANTS FOR SUBSTITUTED GERMANES.

PART I. GeH_3Cl and GeD_3Cl

BY S. L. N. G. KRISHNAMACHARI

PHYSICS DEPARTMENT, ANDHRA UNIVERSITY, WALTAIR

(Received for publication, January 24, 1955)

ABSTRACT. A set of force constants are determined for GeH_3Cl and GeD_3Cl molecules using the Wilson F G matrix method. This set reproduces the frequencies of the GeH_3Cl molecule to the nearest wavenumber and those of the GeD_3Cl molecule to within a mean error of 0.81%.

INTRODUCTION

Force constants for the halogen derivatives of methane and silane are worked out to a considerable extent. There is yet no systematic work on the force constants for germane and its halogen derivatives excepting that for GeCl_4 and GeBr_4 , the force constants are determined by the use of approximate methods. In view of this, the author has undertaken the calculation of the force constants of the halo-germanes and to start with, of the molecules monochlorogermane and monochlorogermane- D_3 . The infrared spectra of these compounds are investigated in the vapour state by Lord and Steese (1954); but there is yet no report on the force constants for these molecules.

CALCULATIONS

A normal coordinate treatment is carried using the Wilson F-G matrix method as for methylecyanide and methylisocyanide in a previous paper by the author (1954). The two molecules belong to the C_{3v} point group. Each has three totally symmetric A_1 vibrations and three degenerate type E vibrations. All are infrared and Raman active. In the infrared, the three A_1 vibrations appear as parallel and the three E type vibrations appear as perpendicular bands. In Raman effect the three A_1 type vibrations appear as polarised and the three E type vibrations appear as depolarised lines.

The symmetry coordinates that are constructed from the internal coordinates are the same as those employed by Cleveland and Meister (1946) for the case of CH_3Cl . The potential energy function employed in the present case is

$$\begin{aligned}
 2V = & f_D(\Delta D)^2 + f_d\{\Delta d_1^2 + \Delta d_2^2 + \Delta d_3^2\} + 2f_{dd}\{\Delta d_1 \cdot \Delta d_2 + \Delta d_1 \cdot \Delta d_3 + \Delta d_2 \cdot \Delta d_3\} \\
 & + f_\alpha\{d^2(\Delta\alpha_{12}^2 + \Delta\alpha_{13}^2 + \Delta\alpha_{23}^2)\} + f_\beta\{d^2(\Delta\beta_1^2 + \Delta\beta_2^2 + \Delta\beta_3^2)\} \\
 & + 2f_{\alpha\beta}\{d^2\{\Delta\beta_1(\Delta\alpha_{12} + \Delta\alpha_{13}) + \Delta\beta_2(\Delta\alpha_{23} + \Delta\alpha_{21}) + \Delta\beta_3(\Delta\alpha_{31} + \Delta\alpha_{32})\}\} \\
 & + 2f_{\alpha\alpha}\{d^2(\Delta\alpha_{12} \cdot \Delta\alpha_{13} + \Delta\alpha_{12} \cdot \Delta\alpha_{23} + \Delta\alpha_{13} \cdot \Delta\alpha_{23})\} \\
 & + 2f_{\beta\beta}\{d^2(\Delta\beta_1 \cdot \Delta\beta_2 + \Delta\beta_1 \cdot \Delta\beta_3 + \Delta\beta_2 \cdot \Delta\beta_3)\} \\
 & + 2f_{D\alpha}\{\Delta D\{d(\Delta\alpha_{12} + \Delta\alpha_{13} + \Delta\alpha_{23})\}\} \\
 & + 2f_{D\beta}\Delta D \cdot d(\Delta\beta_1 + \Delta\beta_2 + \Delta\beta_3).
 \end{aligned}$$

The nature of these constants is shown in the first column of Table 1.

From the potential energy matrix and the matrix formed from the coefficients of the internal coordinates, as obtained from the symmetry coordinates, the following F matrices are obtained.

A_1

$$\begin{array}{l}
 F = \\
 E \\
 F =
 \end{array}
 \begin{array}{|c|cc}
 & f_D & 0 & \sqrt{\frac{3}{2}}d(f_{D\alpha} - f_{D\beta}) \\
 & & f_d + 2f_{dd} & 0 \\
 & & & \frac{d^2(f_\alpha + f_\beta + 2f_{\alpha\alpha} + 2f_{\beta\beta} - 4f_{\alpha\beta})}{2} \\
 & f_d - f_{dd} & 0 & 0 \\
 & & d^2(f_\beta - f_{\beta\beta}) & -d^2f_{\alpha\beta} \\
 & & & d^2(f_\alpha - f_{\alpha\alpha})
 \end{array}$$

The G matrices are the same as those for CH_3Cl but for the fact that in the present case μ_{Cl} replaces μ_{C} . The bond lengths and interbond angles employed in these calculations are determined from microwave spectra due to Mays and Dailey (1952). The observed bond angles are not however employed in the present calculations; instead, tetrahedral angles are assumed.

The potential energy function contains ten different force constants, all of which cannot be separately determined. $f_{\alpha\alpha}$ and $f_{\beta\beta}$ occur as combinations and f_α , $f_{\alpha\alpha}$, f_β , $f_{\beta\beta}$, $f_{D\alpha}$ and $f_{D\beta}$ occur as differences in the F matrices, leaving only eight independent constants which are f_D , f_d , f_{dd} , $(f_{D\alpha} - f_{D\beta})$, $(f_\alpha - f_{\alpha\alpha})$, $(f_\beta - f_{\beta\beta})$ and $(f_{\alpha\alpha} + f_{\beta\beta})$. The values of these constants were then systematically adjusted

until they reproduced the observed frequencies of GeH_3Cl to the nearest wave-number. The final set so obtained is shown in the third column of Table I. The agreement between the calculated and observed frequencies for GeH_3Cl is shown in Table II.

TABLE I
Force constants

Nature of the force constant	Representation	Value $\times 10^5$ dynes/cm.
Ge—Cl bond stretch	f_D	2.545
Ge—H bond stretch	f_d	2.648
Ge—H, Ge—H interaction	f_{dd}	0.0063
H—Ge—H bending and H—Ge—H, H—Ge—H interaction	$f_\alpha - f_{\alpha\alpha}$	0.1793
H—Ge—Cl bending and H—Ge—Cl, H—Ge—Cl interaction	$f_\beta - f_{\beta\beta}$	0.2308
H—Ge—H, H—Ge—H interaction H—Ge—Cl, H—Ge—Cl interaction	$f_{\alpha\alpha} + f_{\beta\beta}$	0.0341
H—Ge—H, H—Ge—Cl interaction	$f_{\alpha\beta}$	0.0250
Ge—Cl, H—Ge—H, H—Ge—Cl interaction	$f_{D\alpha} - f_{D\beta}$	-0.0200

TABLE II
Calculated and observed frequencies of GeH_3Cl (cm^{-1})

	Calculated	Observed
ν_1	2121.0	2121.1
A_1 ν_2	848.0	847.7
ν_3	423.0	422.6
ν_4	2129.0	2129.4
E ν_5	875.0	874.6
ν_6	604.0	604.1

These force constants are then used to calculate the frequencies of GeD_3Cl . The F and G matrices are the same as above, excepting that in this case μ_D replaces μ_H . The calculated and observed frequencies for GeD_3Cl are shown in Table III.

TABLE III

Calculated and observed frequencies of GeD_3Cl (cm^{-1})

		Calculated	Observed	% error
	ν_1	1505	1520	1.13
A_1	ν_2	613	614	0.17
	ν_3	419	421	0.50
	ν_4	1520	1530	0.70
E	ν_5	623	630	1.15
	ν_6	439	434	1.20

The small discrepancies between the calculated and observed values in the case of GeD_3Cl can be considered as due to the anharmonicity of the vibrations which effects the two molecules differently.

The individual values of the force constants which occur as sums or differences in the present case can be obtained from a similar work on other chlorides of germanium. Work on the trichlorogermane is under progress.

ACKNOWLEDGMENTS

The author wishes to express his deep indebtedness to Prof. K. R. Rao for for his valuable guidance throughout the work. The author is grateful to the Government of India for the award of a senior research scholarship.

REFERENCES

- Cleveland, F. F. and Meister, A. G., 1946, *Amer. J. Phys.*, **14**, 13.
 Krishnamachari, S. L. N. G., 1954, *Ind. J. Phys.*, **28**, 463.
 Lord, R. C. and Stease, C. M., 1954, *J. Chem. Phys.*, **22**, 542.
 Mays, J. M. and Dailey, B. P., 1952, *J. Chem. Phys.*, **20**, 1695.
 Wilson, Jr., E. B., 1939, *J. Chem. Phys.*, **7**, 1047.
 „, 1941, *J. Chem. Phys.*, **9**, 76.

A WIDE-BAND FREQUENCY MODULATED SYSTEM WITH ASYMMETRICAL 3-PHASE OSCILLATOR

BY P. KUNDU,

INDIAN INSTITUTE OF TECHNOLOGY KHARAGPUR

(Received for publication, August 26, 1954)

ABSTRACT. In this paper, the possibilities of a 3-phase R. C. oscillator of asymmetrical type have been discussed, and optimum operating conditions have been derived with particular reference to its capability to produce wide-band frequency modulation. A comparative study of the symmetrical and asymmetrical systems has also been made in regard to the linearity of modulation, modulation sensitivity and frequency stability.

INTRODUCTION

Optimum performance of frequency modulated LC oscillator by the conventional reactance tube method is limited due to the smaller frequency range over which it can be used and also due to the non-linearity of the system where wide band frequency modulation is required.

These limitations can be avoided in a resistance-capacitance oscillator and modulation can be achieved at the maximum obtainable frequency of the system by varying one of the resistances in the frequency selective coupling net work.

A symmetrical 3-phase oscillator due originally to Van der Pol (1934), have been subsequently studied and report of faithful wide band modulation has been published (Rakshit and Sarkar, 1950).

In this communication an analytical study of an asymmetrical type of a 3-phase oscillator has been made and conditions for optimum operation have been derived with particular reference to wide band frequency modulation from the point of view of linearity of modulation, modulation sensitivity and frequency stability.

DESCRIPTION

In the 3-phase system mentioned above, the symmetry of the three stages have been maintained and all the three anode resistances are adjusted to have identical values at the centre carrier frequency as shown in figure. 1 Frequency

modulation is produced by varying the tuning resistance of one of the oscillator stages by the modulating voltage.

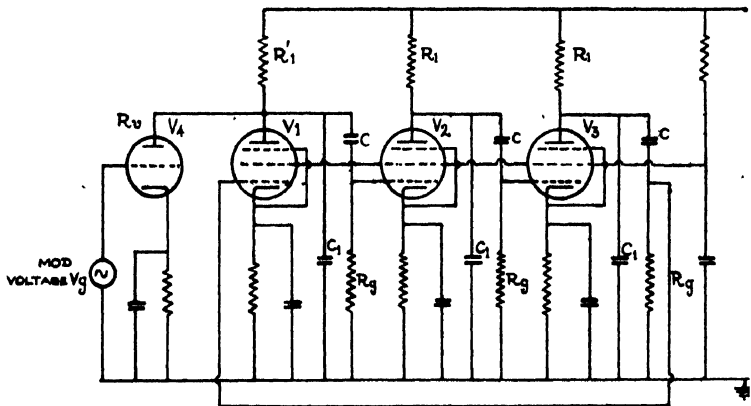


Fig. 1: Frequency modulated symmetrical system.

In the asymmetrical system, the asymmetry has been introduced in the anode load in so far as the value of resistance of one stage differs to a great extent from the other two which are similar to each other. Here, unlike the previous case, simultaneous variation of two anode resistances which are similar to each other have been considered to generate frequency-modulated oscillations, as shown in figure 2.

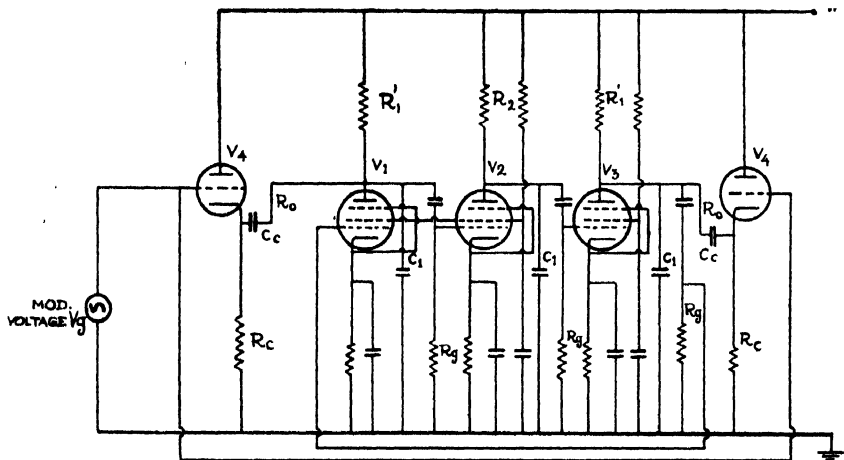


Fig. 2: Frequency modulated asymmetrical system.

THEORETICAL CONSIDERATIONS

In the asymmetrical type, the gain and phase shift due to two similar stages will be the same while those will be different from the remaining one.

Let $A_1 e^{j\phi_1}$ and $A_2 e^{j\phi_2}$ be the gains and phase shifts due to each of the two similar stages and the remaining stage respectively, then the overall gain due to the three stages will be

$$A = A_1^2 A_2 e^{j\phi},$$

where

$$\phi = 2\phi_1 + \phi_2.$$

From the circuit analysis it can be shown from figure 2. that

$$A_1 = \frac{g_m R_1}{1 + jx_1}$$

where

$$x_1 = \omega C_1 R_1$$

and

$$R_1 \ll r_p \text{ and } R_g$$

and

$$A_2 = \frac{g_m R_2}{1 + jx_2}$$

$$\text{where } x_2 = \omega C_1 R_2$$

$$\therefore |A| = A_1^2 A_2 = \frac{g_m^2 R_1^2}{(1 + \omega^2 C_1^2 R_1^2)} \cdot \frac{g_m R_2}{(1 + \omega^2 C_1^2 R_2^2)^{1/2}} \quad \dots (1)$$

and

$$\phi = 2 \tan^{-1} \omega C_1 R_1 + \tan^{-1} \omega C_1 R_2.$$

or

$$\phi = \tan^{-1} \frac{2\omega C_1 R_1 + \omega C_1 R_2 (1 - \omega^2 C_1^2 R_1^2)}{1 - \omega^2 C_1^2 R_1^2 - 2\omega^2 C_1^2 R_1^2} \quad \dots (2)$$

Conditions for maintenance of oscillations:

$$(I) \quad \phi = 2\pi$$

$$(II) \quad |A| \geq 1$$

Condition (I) is satisfied if

$$2\omega C_1 R_1 + \omega C_1 R_2 (1 - \omega^2 C_1^2 R_1^2) = 0$$

when

$$\omega = \frac{1}{C_1 R_1} \sqrt{1 + \frac{2R_1}{R_2}} \quad \dots (3)$$

And the overall gain of the system at the frequency of resonance

$$|A| = \frac{g_m^2 R_1^2 R_2}{2 \left(1 + \frac{R_2}{R_1}\right) \left(1 + \frac{R_2}{R_1}\right)}$$

$$\text{or, } |A| = \frac{g_m^2 R_1^2 R_2}{2 \left(2 + \frac{R_1}{R_2} + \frac{R_2}{R_1}\right)} \quad \dots (4)$$

Symmetrical Case:

In the symmetrical case as in figure 1, the oscillator has been adjusted to have the same load (R_1) in all the three stages at the centre frequency,

$$\text{i.e. when } R_1 = R_2$$

$$\omega = \frac{\sqrt{3}}{C_1 R_1} \quad \dots (5i)$$

$$\text{and } |A| = \frac{g_m^3 R_1^3}{8} \quad \dots (5ii)$$

The effective anode load of the modulated stage V_1 is $R_1 = \frac{R'_1 R_v}{R'_1 + R_v}$, where R_v is the anode-cathode resistance of V_4 and is a function of its control grid voltage. For frequency modulation the effective value of R_1 has been varied by varying R_v and let the new value be R_2

i.e. when $R_2 \neq R_1$ (i.e. R_2 varying slightly above and below its initial value R_1)

$$\text{then } \omega = \frac{1}{C_1 R_1} \sqrt{1 + 2 \frac{R'_1}{R_2}} \quad \dots (5iii)$$

$$\text{where } R_2 = \frac{R'_1 R_v}{R'_1 + R_v}$$

$$\text{and } |A| \approx \frac{g_m^3 R_1^3}{8} \quad \dots (5iv)$$

Similar relations for the symmetrical case have also been obtained by Rakshit and Sarkar (1950) in which frequency modulation was produced by slightly varying one of the three equal anode resistances by varying the grid bias of the modulator value as shown in the figure. 1.

Asymmetrical Case :

In this case two of the equal anode load resistances (R_1) are always much less than the remaining one (R_2)

$$\text{i.e. } R_2 \gg R_1$$

$$\text{Then } \omega = \frac{1}{C_1 R_1} \left(1 + \frac{R_1}{R_2} \right) \quad \dots (6i)$$

$$\approx \frac{1}{C_1 R_1}$$

$$\text{and } |A| = \frac{g_m^3 R_1^3}{2 \left(1 + 2 \frac{R_1}{R_2} \right)} \quad \dots (6iii)$$

The above equations show that the maximum obtainable frequency is limited by the optimum value of the anode load obtained from the relation $A \gg 1$, and higher the value of mutual conductance of the oscillator valves, higher will be the maximum obtainable frequency. With the same types of valves, the maximum frequency that can be generated depends on the minimum anode load required to satisfy the condition of gain.

For 'S' case :

$$g_m^2 R_1^2 = 8$$

i.e.,

$$R_{1S\min} = \frac{2}{g_m} \quad \dots \quad (7i)$$

when

$$\omega_{S\max} = \frac{\sqrt{3}}{2} \frac{g_m}{C_1} = 0.866 \frac{g_m}{C_1} \quad \dots \quad (7ii)$$

For 'A' case

$$g_m R_{1A\min} = 2^{1/2} \quad \dots \quad (8i)$$

$$\omega_{A\max} = 0.8 \frac{g_m}{C_1} \quad \dots \quad (8ii)$$

The relative values of anode load required to generate the same frequency in the above cases:

$$\omega = \frac{\sqrt{3}}{C_1 R_{1S}} = \frac{1}{C_1 R_{1A}} \\ \therefore R_{1S} = \sqrt{3} R_{1A} \quad \dots \quad (9)$$

Here suffixes indicate the respective system i.e. 'S' for symmetrical, and A for asymmetrical.

It is seen that while the maximum frequency that can be generated is higher in case I, the resistance R_1 required in the former is more than the latter to generate the same frequency.

METHOD OF MODULATION

In an RC oscillator frequency modulation can be achieved by the variation of either a tuning resistance or a capacity. In the symmetrical type, one of the tuning resistances was varied by shunting it with a valve. The variation was obtained by the variation of the anode-cathode resistance of the shunting valve with modulating voltage. Some adverse effects have been reported to be associated with this type of modulation. The anode-cathode resistance is dependent on the plate voltage and is essentially non-linear. Consequently, any variation of the anode voltage affects the centre frequency stability; and the presence of r.f. voltages at the plate of the modulator valve should be very small compared to the

anode current of the modulated valve so that the optimum operating condition of the oscillator is not disturbed. Another disadvantage is the presence of the amplified modulating voltage at the anode of the oscillator superimposed upon the carrier.

Better performance can be obtained by shunting the tuning resistance with the output impedance of a cathode follower which is a pure resistance with resistive load and is related as

$$R_0 = \frac{1}{\frac{1}{r_p} + \frac{1}{R_c} + g_m} \approx \frac{1}{R_c + g_m}$$

In a valve having a square law relation between $i_p \sim v_g$ characteristic, the value of the mutual conductance g_m varies linearly with the control grid voltage v_g .

With a cathode follower the operation of the modulating circuit will be more linear and the valve parameter less dependent on the H.T. voltage due to the inherent negative feedback in the cathode, while the presence of modulating signal can be made negligible due to the presence of the coupling capacity C_c .

Conditions for Faithful Modulation :

The superiority of performance between the two systems can be judged from the three important conditions for faithful wide band modulation which are listed as follows :

1. High modulation sensitivity which can be defined as the ratio of the total frequency deviation to the centre frequency, i.e. $\Delta f/f_0$
2. A linear relationship between the frequency deviation and the modulating voltage.
3. Inherent centre frequency stability.

Degree of Linearity:

The degree of linearity of modulation can be studied from the slope of the frequency and tuning resistance curve.

For the 'A' case $f_o = \frac{K_1}{C_1 R_1} = \frac{K_A}{R_1}$ where $K_A = \frac{K_1}{C}$

and $\frac{1}{R_1} = \left(\frac{1}{R'_1} + \frac{1}{R_c} \right) + g_m = \frac{1}{R_{1A}} = \alpha_A + g_m$

i.e. $f_o = K_A(\alpha_A + g_m)$

Then $\delta f / \delta g_m = K_A \quad \dots \quad \dots \quad \dots \quad (10)$

For perfect linearity $\delta f / \delta g_m$ should be constant and the equation shows that the degree of linearity of an asymmetrical system is only limited by the $g_m \sim v_g$ curve.

With proper selection of valve and with the restriction of the grid swing, the $g_m \sim v_g$ curve can be practically linear over the range of operation.

For linearity of modulation in the symmetrical case, it is required that

$$f \propto a_1 + b_1 v_g, \text{ but } f_0 = K_s \sqrt{\alpha_s + \beta_s g_m} \quad \text{where } K_s = \frac{1}{2\pi C_1 R_1}$$

$$\text{i.e.} \quad \alpha_s + \beta_s g_m = K(a_1 + b_1 v_g)^2 \quad \dots \quad (11i) \quad \alpha_s = 1 + 2R_1 \left(\frac{1}{R'_1} + \frac{1}{R_c} \right)$$

$$\text{i.e.} \quad g_m = a + b v_g + c v_g^2. \quad \dots \quad (11ii) \quad \beta_s = 2R_1 = 2R_{1s}$$

Hence the modulator valve should be so selected and adjusted that there is a square law relation between g_m and v_g as in equation (11ii)

For the optimum performance in linearity in each case, the valves should be selected accordingly and in the latter case the grid swing may be made conveniently larger for wider frequency deviation. However, it has been observed by Rakshit & Sarkar (1950) that it is better to have variation of R_r (i.e. g_m) slowly with v_g from the point of view of frequency stability. So it may be preferable to work with a system in which g_m should vary linearly with v_g .

MODULATION SENSITIVITY

Assuming that the mean frequency f_0 and the variation of mutual conductance Δg_m corresponding to the modulating voltage v_g are same in both the cases,

'A' Case.

$$f_0 = K_A (\alpha_A + a + b v_g)$$

since

$$g_m = a + b v_g$$

and

$$f_0 + \Delta f_A = K_A (\alpha_A + a + b v_g + b \Delta v_g)$$

$$\therefore D_A = \frac{\Delta f_A}{f_0} = \frac{b \Delta v_g}{\alpha_A + g_m} \quad \dots \quad (12)$$

'S' Case.

$$f_0 = K_s \sqrt{\alpha_s + \beta_s g_m}$$

$$= K_s \sqrt{\alpha_s + \beta_s (a + b v_g + c v_g^2)}.$$

Since for linearity, g_m must be equal to $a + b v_g + c v_g^2$.

in this case.

$$\therefore f_0 + \Delta f_s = K_s \sqrt{\alpha_s + \beta_s (a + b v_g + c v_g^2) + \beta_s \Delta v_g (b + 2c v_g + c \Delta v_g)}$$

Hence
$$D_S = \frac{\Delta f_S}{f_0} = \frac{1}{2} \frac{\beta_S \Delta v_g (b + 2cv_g + c\Delta v_g)}{\alpha_S + \beta_S(a + bv_g + cv_g^2)} \quad (13)$$

$$\therefore \frac{D_A}{D_S} = \frac{2(\alpha_S + \beta_S g_m)}{(\alpha_A + g_m)\beta_S} \cdot \frac{b}{b + 2cv_g + c\Delta v_g}$$

But usually $b \gg c$

$$\therefore \frac{D_A}{D_S} = \frac{2(\alpha_S + \beta_S g_m)}{(\alpha_A + g_m)\beta_S} \quad (14i)$$

Substituting the values of the constants, we have

$$\begin{aligned} \frac{D_A}{D_S} &= \frac{2 \left[1 + 2R_1 \left(\frac{1}{R_1} + \frac{1}{R_c} + g_m \right) \right]}{\left(\frac{1}{R_c} + \frac{1}{R_c} + g_m \right) 2R_1} \\ &= \frac{2 \left[1 + \frac{2R_{1S}}{R_{2S}} \right]}{2 \frac{R_{1S}}{R_{1A}}} \end{aligned}$$

Since

$$R_{1S} \simeq R_{2S}$$

then

$$\frac{D_A}{D_S} = 3 \frac{R_{1A}}{R_{1S}} = \sqrt{3} \quad \dots \quad (14ii)$$

The above relation shows that the modulation sensitivity in the A case may be as much as $\sqrt{3}$ times the S case. Nevertheless Δf_{max} will depend also upon the permissible Δg_m , but it may be better to get more frequency variation with less Δg_m , to avoid amplitude modulation.

FREQUENCY STABILITY

In LC oscillator, the Q of the LC circuit is the figure of merit in determining the constancy of frequency and the purity of waveform. The value of Q can be made reasonably high for r.f. oscillations. In a simple RLC parallel circuit as shown in figure 3.,

Fig. 3: A parallel RLC circuit.

$$Z = \frac{1}{\frac{1}{R} + j\omega c + \frac{1}{j\omega L}}$$

Then the phase angle ϕ between the voltage developed and the current when the circuit is fed from a constant current source is as

$$\tan \phi = \frac{R}{\omega L} - \omega CR$$

Substituting $\frac{\omega}{\omega_0} = a, \quad \omega_0 = \frac{1}{\sqrt{LC}} \quad \text{and} \quad Q = \frac{R}{\omega_0 L}$

we get $\tan \phi = \frac{R}{a\omega_0 L} - a\omega_0 CR = \frac{Q}{a} - aQ$

$$\therefore \left(\frac{d\phi}{da} \right)_{a=1} = -2Q \quad \dots (15i)$$

The equation shows that higher the Q , higher is the rate of change of phase angle near the resonance with fractional change of frequency and consequently higher is the stability of the circuit. The magnitude of Q can be expressed as

$$Q = \frac{1}{2} \left(\frac{d\phi}{da} \right)_{a=1} \quad \dots (15ii)$$

The equivalent Q of a RC frequency selective network can be found out similarly by evaluating the value of $\left(\frac{d\phi}{da} \right)_{a=1}$ for the particular type.

For symmetrical case, the loop phase shift

$$\phi = 3 \tan^{-1} \omega C_1 R_1 = 3 \tan^{-1} \sqrt{3} a$$

Therefore, $\left(\frac{d\phi}{da} \right)_{a=1} = 1.28 \quad \text{whence} \quad Q_s = 0.64.$

For asymmetrical case when $R_1 = \frac{R_2}{10}$ and $\omega = \frac{1}{C_1 R_1}$

the loop phase shift $\phi = 2 \tan^{-1} \omega C_1 R_1 + \tan^{-1} \omega C_1 R_2$
 $= 2 \tan^{-1} a + \tan^{-1} 10a$

$$\left(\frac{d\phi}{da} \right)_{a=1} = 1.1 \quad \text{where} \quad Q_A = 0.55.$$

This shows that the equivalent Q for both the cases are less than unity and which is almost always the case with RC frequency selective circuits. This is the fact due to which RC oscillator is inherently less stable than LC oscillator, and is required to be maintained critically for distortionless waveform. The dissipative nature of the network which lacks the quality of storing up of energy of LC

circuit is responsible for the low Q . As a result the effect of Q on the frequency stability becomes of secondary importance, while the effect due to the variation of temperature, H.T. voltage and valve parameters becomes a major factor in maintaining the constancy of frequency. The effects of these variations on the frequency of a 3-phase oscillator have been studied quantitatively by Rakshit and Sarkar (1950). It has been shown that lower the value of R_1/r_p higher will be the stability against the variation of r_p . For the same frequency $R_{1S} > R_{1A}$ so that the effect due to the variation of temperature and H.T. is less in the asymmetrical case. This advantage may be offset due to the fact $R_{2A}/r_p \gg R_{1S}/r_p$ and hence the centre frequency stability may therefore be practically the same in each case.

CONCLUSIONS

Normal reactance tube method of frequency modulation of LC circuit at very high frequency is not suitable due to non-linearity of modulation and low impedance reflected across the oscillatory circuit. Consequently desired frequency modulated carrier is obtained by a series of frequency multiplication. On the other hand wide-band modulation can be obtained at the maximum obtainable frequency by RC oscillator in a much more simplified manner. Reports of a symmetrical system looks encouraging for its use as frequency modulated carrier system. It has been shown here that in an asymmetrical system, when two of the tuning resistances are varied simultaneously, similar performance can be achieved with greater modulation sensitivity.

ACKNOWLEDGMENTS

The author's grateful thanks are due to Dr. J. C. Ghosh, Director, I.I.T., for his kind interest in the work and also to Dr. K. K. Bose, Dept. of Communication Engineering, I.I.T., for helpful discussions. Thanks are also due to Dr. H. Rakshit, B.E. College, Howrah, for his valuable suggestions.

REFERENCES

- Rakshit, H. and Sarkar, N. 1950, *Ind Jour. Phys.*, **24**, 107.
 Van der M. and Van der B. Pol. 1934, *Physica*, **1**, 437

ABSORPTION OF MICROWAVES AND U. H. F. RADIO WAVES IN PHENOL, CYCLOHEXANOL AND 1-BROMO 2-CHLOROETHANE*

DILIP KUMAR GHOSH

OPTICS DEPARTMENT, INDIAN ASSOCIATION FOR THE CULTIVATION OF SCIENCE,
JADAVPUR, CALCUTTA-32

(Received for publication, March 28, 1955)

ABSTRACT. The absorption of U.H.F. radiowaves in the range 250-800 Mc/sec. and 3.18 cm microwaves in phenol and cyclohexanol and the absorption of 3.18 cm microwaves in 1-bromo 2-chloroethane have been studied by the direct optical method by avoiding formation of stationary waves. Maximum absorption of 3.18 cm microwaves has been exhibited by phenol, cyclohexanol and 1-bromo 2-chloroethane at temperatures 80°C, 95°C and 10°C respectively. In the case of phenol and cyclohexanol these absorption maxima are found to be due to rotation of the substituent OH group about an axis, which coincides in the case of phenol with the diameter of the benzene ring passing through the carbon atom to which the OH group is attached. In the case of 1-bromo 2-chloroethane the absorption maximum may be due to rotation of one half of the molecule about the C-C axis.

No absorption maxima have been observed in the case of phenol and cyclohexanol in the U.H.F. region, but there is indication of occurrence of peaks beyond 850 Mc/sec. and these are found to be due to rotation of the substituent OH group in the case of cyclohexanol and of the single molecule in the case of phenol.

INTRODUCTION

The presence of rotational freedom of some groups in substituted benzenes was inferred by Fischer (1949) from the values of dielectric loss observed in the solution of some substituted benzenes in the metre wavelength region. It has been actually observed by the present author (Ghosh, 1954a, 1954b) that some substituted benzenes with substituent groups having rotational freedom show absorption peak corresponding to rotation of the substituent group about a diameter of the benzene ring passing through the point of substitution. The values of radius of the rotors calculated from Debye's theory with the help of the observed results lie between 1.25\AA and 1.5\AA which correspond to those of the substituent group rotating about an axis. It has also been observed (Ghosh, 1954b) that other substituent groups which do not have rotational freedom do not exhibit absorption maxima in the 3.18 microwave region at any temperature. Both these types of molecules, however, exhibit usually two absorption maxima in the U.H.F. region and the radii of rotors calculated on Debye's theory come out approximately as those of the monomeric and dimeric molecules (Ghosh, 1954a, 1954b). If this interpretation of the results be correct it is expected that molecules having similar substituent groups should show absorption in the microwave

* Communicated by Professor S. C. Sirkar.

region only at those temperatures at which the viscosity is of the proper value. In the case of 1,2-substituted ethanes also such absorption of microwaves is expected to take place at suitable temperatures so that the radius of the rotor corresponds to the rotation of one half of the molecule about the C-C axis as observed in the case of ethylene dichloride. The present work was undertaken to find out whether these expectations are fulfilled. Some molecules with OH as a substituent have been chosen in order to find out whether these molecules show any absorption in the microwave region inspite of having very high viscosity.

EXPERIMENTAL

The liquids studied in the present investigation are cyclohexanol, phenol and 1-bromo 2-chloroethane. The liquids studied were all of chemically pure quality. They were all distilled in vacuum after proper dehydration. Phenol and cyclohexanol were supplied by B.D.H. 1-bromo 2-chloroethane was supplied by Fisher Scientific Company, New York. The experimental arrangement used in the present investigation was the same as that reported previously (Ghosh, 1953*a*, 1953*b*, 1954*a*). The absorption in these liquids of microwaves of wavelength 3.18 cm and U.H.F. radiowaves in the region 250-800 Mc/sec was studied for different temperatures of the liquid.

RESULTS

The absorption curves for the microwave region observed with phenol, cyclohexanol, 1-bromo 2-chloroethane are given in figures 1, 2, and 3. The absorption observed in the U.H.F. region in the case of phenol and cyclohexanol is given in figures 4 and 5.

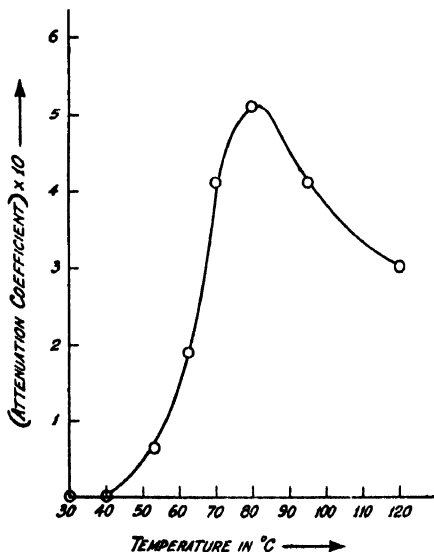


Fig. 1

Phenol. $f=9415$ Mc/sec. Thickness of the liquid 1 cm.

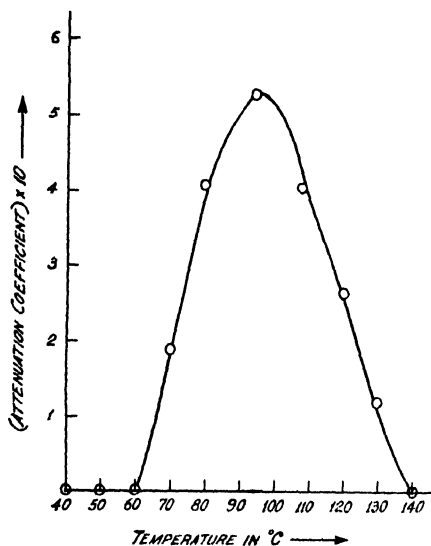


Fig. 2

Cyclohexanol. $f = 9415$ Mc/sec. Thickness of the liquid 1 cm.

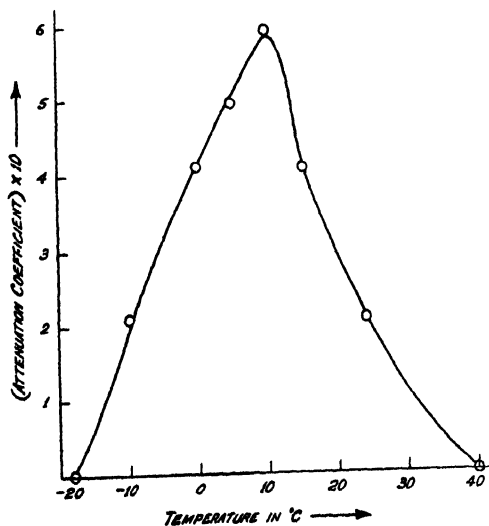


Fig. 3

1-Bromo 2-chloroethane. $f = 9415$ Mc/sec. Thickness of the liquid 1 cm.

The frequencies of absorption peaks, the corresponding temperatures, the values of a^3 and τ calculated from Debye's theory and the different constants involved in this calculation are shown in Table I.

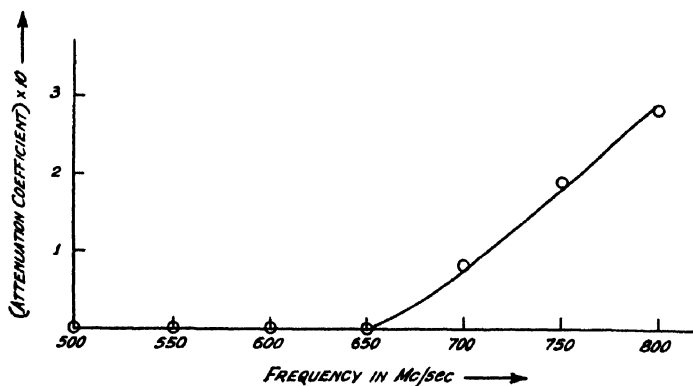


Fig. 4

Phenol at 40°C. Thickness of the liquid 3.5 cms.

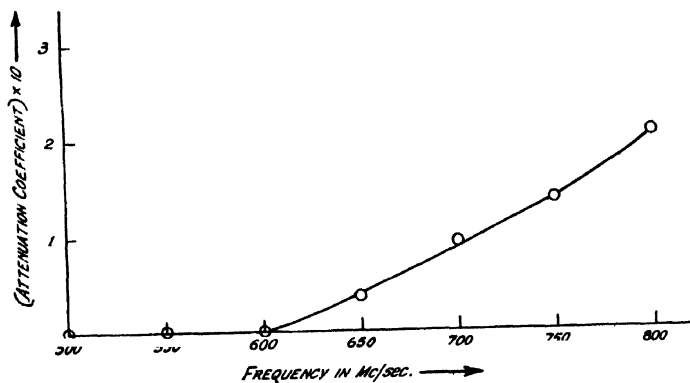


Fig. 5

Cyclohexanol at 40°C. Thickness of the liquid 3.5 cms.

TABLE I.

Liquid	$\omega/2\pi$ in Mc/sec.	$T^{\circ}\text{K}$ for max. absorption	ϵ_0	ϵ_1	$\eta \times 100$	$\tau \times 10^{11}$	$\alpha \times 10^8$ c.m.
Cyclohexanol	900 (approx.)	313	2.13	13	20	12.02	1.27
	9415	368		7.8	2.2	1.34	1.36
Phenol	900 (approx.)	313	2.37	15	4.8	28.64	2.72
	9415	353		6.8	1.59	1.4	1.49
1-bromo 2-chloro ethane.	9415	283	2.19	7.34	.993	1.37	1.61

The values of η are obtained from the results reported in the International Critical Table. The value of η for 1-bromo 2-chloroethane was not found in published literature and, therefore, it was determined by comparing its viscosity with that of CCl_4 by the capillary flow method at the temperature of the maximum absorption. The values of ϵ_1 have been obtained from the table of dielectric constants of pure liquids published by National Bureau of Standards, United States, Department of Commerce and also from the International Critical Tables. The values of ϵ_0 have been assumed to be equal to square of n , the refractive index at 20°C for sodium D-line. The value n the refractive index at 35°C of 1-bromo 2-chloroethane was measured by the author by means of an Abbe refractometer.

DISCUSSIONS

The results obtained in the present investigation show that both cyclohexanol and phenol having large values of viscosity do not show any absorption in the microwave region below 50°C , but as the temperature is further raised gradually the liquids show absorption of 3.18 cm microwaves. An absorption maximum is observed at 95°C in the case of cyclohexanol and at 80°C in the case of phenol. The absorption diminishes at higher temperatures and in the case of cyclohexanol no absorption is exhibited by the liquid above 140°C .

It can be seen from Table I that all the three liquids exhibit maximum absorption of 3.18 cm microwaves at suitable temperatures and the radii of the rotors are 1.49, 1.36 and 1.61×10^{-8} cm in the case of phenol, cyclohexanol and 1-bromo 2-chloroethane respectively. As the radii of the molecules in the case of phenol and cyclohexanol are much larger than these values the rotors cannot be the whole molecules. These absorption maxima are evidently due to rotation of the substituent OH group about an axis which coincides in the case of phenol with diameter of the benzene ring passing through the carbon atom to which the OH group is attached. Since the radius of the rotor is the same and the frequency of the microwaves is also kept constant, maximum absorption due to such rotation of the OH group is expected to take place only for particular value of the viscosity. Actually the absorption maxima for cyclohexanol and phenol are observed at temperatures at which the viscosities of the two liquids are almost identical. This shows the correctness of the assumption that OH group is the rotor in these two cases.

In the case of 1-bromo 2-chloroethane the observed absorption peak may be due to rotation of one half of the molecule about the C-C axis and the observed radius of the rotor supports such a hypothesis.

As regards the absorption in the U.H.F. region in the case of phenol and cyclohexanol it may be pointed out that although the absorption maxima have not been actually observed there is indication of the occurrence of peaks beyond 850 Mc/sec. Assuming a peak at about 900 Mc/sec., the radii of the rotors are 1.27 \AA and 2.72 \AA in the case of cyclohexanol and phenol respectively. In the case of

cyclohexanol the value of the radius of the rotor corresponding to absorption maximum in the U.H.F. region comes out to be almost equal to that corresponding to the absorption in the microwave region. This may indicate that the absorption maximum in both the cases is due to the same type of rotor and it changes with change of temperature from the U.H.F. region to the microwave region. The rotor is evidently the substituent OH group. In the case of phenol the radius of the rotor corresponding to the absorption at 40°C in the U.H.F. region is found to be 2.72\AA which is of the order of the radius of the single molecule. The absorption peak due to OH group and for the liquid at 40°C lies probably in a region having frequencies higher than 900 Mc/sec. No absorption due to single molecule of cyclohexanol at 40°C was observed in the region 250 Mc/sec—600 Mc/sec and such absorption maximum may be exhibited by the liquid at frequencies lower than 250 Mc/sec.

It would be interesting to find out whether all molecules having the OH group as substituent exhibit absorption maxima at suitable regions so as to yield the same value of radius of the rotor according to Debye's theory. Such a programme of work has been undertaken and the result will be reported later.

ACKNOWLEDGMENT

The author's grateful thanks are due to Professor S.C. Sirkar, D.Sc., F.N.I. for kindly suggesting the problem and for his constant guidance during the progress of the work.

REFERENCES

- Fischer, Von. E., 1949, *Z. Naturforsch.*, **4a**, 707.
Ghosh, D. K., 1953a, *Ind. J. Phys.*, **27**, 285.
Ghosh, D. K., 1953b, *ibid.*, **27**, 511.
Ghosh, D. K., 1954a, *ibid.*, **28**, 191.
Ghosh, D. K., 1954b, *ibid.*, **28**, 485.
Sirkar, S. C., and Ghosh, D. K., 1953, *J. Chem. Phys.*, **21**, 1614.

ANALYSIS OF SKY-WAVE FIELD INTENSITY—PART I

S. N. MITRA

AND

R. B. L. SRIVASTAVA

RESEARCH DEPARTMENT, ALL INDIA RADIO, NEW DELHI

(Received for publication, March 30, 1955)

ABSTRACT. The paper presents a statistical analysis of field intensity of the internal short wave stations of All India Radio over the period of a complete solar cycle (1942-52). The yearly, seasonal and monthly variations of the field intensity and their correlation with sunspot numbers have been shown in a series of graphs. An interesting feature of the analysis is that the night-time field intensity has been found to be correlated with solar activity. This is rather inexplicable since no ionospheric absorption is usually assumed for the night-time propagation.

1. INTRODUCTION

It is known that over long distances of propagation, short wave radio communication is carried out *via* the ionosphere and is, therefore, influenced by the variable conditions occurring therein. It is generally observed that short wave radio signal varies in its intensity both on a short term as well as on a long term basis. At present, it is rather difficult to explain the exact nature and cause of such variations, mainly due to our inadequate knowledge of the ionosphere and its effect on short wave radio communication. However, an indirect attempt to study the nature of such varying conditions can be made by correlating the field intensity observations with known variable parameters as are associated with the characteristics of the ionosphere.

This paper presents the results of some statistical studies of the observed values of field intensity of the internal short wave stations of All India Radio over a period of a complete solar cycle (1942-1952). The measurements of field intensity of Bombay, Calcutta and Madras transmitters are made at regular intervals at Delhi. The stations use frequencies in the 3, 4, 5, 6, 7 and 9 Mc/s bands for their internal services. Sufficient data are available for the various frequencies at different times of the day and night. The analysis has been carried out with a view to studying the monthly, seasonal and sunspot cycle variation of field intensity.

In Part II of the paper, a comparison will be made between the observed values of the field strength and those calculated from known methods. The various assumptions in the methods of calculation will also be discussed.

2. METHOD OF ANALYSIS

Measurements of field intensity made by All India Radio at Delhi on frequencies in the 3, 5, 7 and 9 Mc/s bands from each of the three transmitting stations at Bombay, Calcutta and Madras at different times of the day and night, have been used for the analysis. In order to find out how the ionospheric absorption influences propagation of these frequencies, two representative times have been considered. The periods are (a) between 1200 and 1400 hours IST which is considered to correspond to the period of maximum absorption and (b) between 2000 and 2200 hours IST, which corresponds to the minimum absorption. IST (Indian Standard Time) is $5\frac{1}{2}$ hours ahead of GMT. In order to find out the monthly value of the field intensity, all the measurements between 1200 and 1400 IST on any frequency for any of the three stations for a particular month are grouped together and the average value is called the *midday* field intensity for the month. Similarly, the average value between 2000 and 2200 IST is calculated and is called the *night-time* field intensity.

It has been found that there is not much difference in the value of field intensity on a particular frequency at 1200 from its value at 1400 IST on a particular day and similarly the field intensity at 2000 is very nearly the same as at 2200 IST. The day-to-day variation in the field strength on any of the frequencies at any hour between 1200 and 1400 IST is not large, while the same between 2000 and 2200 IST is sometimes appreciable. It has, however, been observed that the ratio between the maximum and the minimum for the period 2000 to 2200 IST hardly exceeds 3 to 4 db. During the period 1200-1400 IST, the ratio is much less.

The monthly mean values of field intensity are thus arrived at for the midday and night-time periods on 3, 5, 7 and 9 Mc/s bands for the transmitters at Bombay, Calcutta and Madras for the period 1942-1952. These monthly mean values represent the 'Upper Decile' figures of the field intensity. For convenience of analysis, the upper decile values have been reduced by 13.3 db to arrive at the corresponding lower decile figures. It may be pointed out that in practical problems on radio transmissions, the lower decile value is usually of greater interest than the upper decile figure. Thus, all field intensity values shown in the paper in the form of curves etc., represent the lower decile figures.

The measurements of field intensity of the internal short wave stations of All India Radio at Bombay, Calcutta and Madras which are analysed in this paper were carried out at Delhi. The distance of the receiving centre from the transmitting stations and their location are given below:—

- (i) Bombay (Lat. $19^{\circ} 0' N$, Long: $73^{\circ} 0' E$), distance from receiving station: 1140 kms.
- (ii) Calcutta (Lat. $22^{\circ} 30' N$, Long: $88^{\circ} 30' E$), distance from receiving station: 1320 kms.

- (iii) Madras (Lat: $13^{\circ} 0' N$, Long: $80^{\circ} 15' E$), distance from receiving station: 1760 kms. Receiving station: Delhi (Lat: $28^{\circ} 35' N$, Long: $77^{\circ} 5' E$)

The transmitters at all the different stations are identical and radiate a power of 10 kw. The transmitting aerial is mostly a horizontal dipole situated $7/16\lambda$ above the ground.

The following analyses have been carried out:

- (i) Correlation with sunspot number.
- (ii) Monthly variation of field intensity.
- (iii) Yearly variation of field intensity for different seasons.

The results of the analysis are presented graphically wherein the values shown for the field intensity are in decibels above one microvolt per metre.

3. (i). CORRELATION WITH SUNSPOT NUMBER

To study the effect of the sunspot number on the variation of field intensity, yearly averages of all the mean values for the midday and night-time periods, and the relative sunspot number for the years have been plotted. This analysis is particularly interesting for the night-time period since theoretically it is assumed that during the night the ionospheric absorption is usually negligible and for all practical purposes of calculations, it is taken to be zero. A correlation with sunspot activity would indicate that the ionospheric absorption cannot be neglected during the night and a proper allowance should be made. This will further be discussed later in the paper.

3 (ii). MONTHLY VARIATION OF THE FIELD INTENSITY

An analysis has been made to indicate the variation of field intensity from month to month over the period 1942-1952. The mean values of field intensities for a particular month over the 11 year period have been grouped together and averages arrived at. The average field intensity for different months is plotted for different frequencies and transmitting stations. The resulting curve would, therefore, indicate the average variation in the field intensity that would be expected from month to month during a complete solar cycle. A better method of representing this monthly variation would have been to plot separate system of curves for each sunspot index, e.g., maximum, medium and minimum and indicate the average monthly variation during different phases of sunspot activity. Such a system would have been of more practical interest since one would be able to compute from these curves the changes in the monthly values of field intensity associated with solar activity. We have not included such analysis in the present paper since sufficient measurements of field intensity in different months are not available for any frequency for any of the transmitting stations for different phases of solar activity.

3 (ii). YEARLY VARIATION OF FIELD INTENSITY

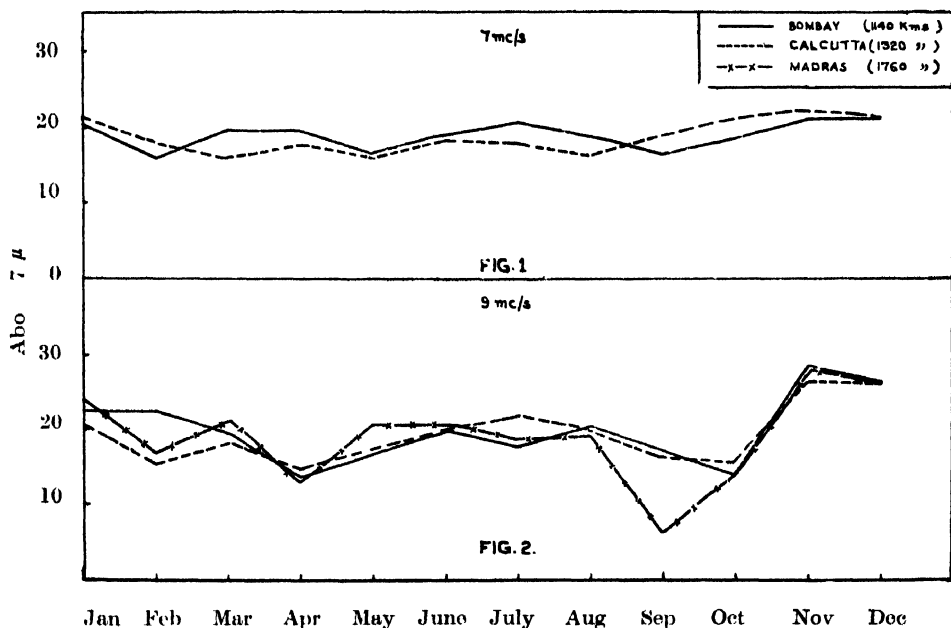
In order to study the yearly variation of field intensity in different seasons and its correlation with sunspot number, the monthly mean values have been grouped together for the three seasons namely, summer (May to August), winter (November to February) and equinox (March, April, September and October). The average field intensity for any season has, then been plotted for different years. The yearly average sunspot number is also indicated in the same figure to show correlation of field intensity with solar activity. Separate curves have been plotted for separate frequencies and for different transmitting stations.

4. RESULTS OF THE ANALYSIS

The three types of analysis described above have been made for all operating frequencies of the stations (Bombay, Calcutta and Madras), in the 3, 5, 7 and 9 Mc/s bands during midday and night-time periods. The results of the analysis are discussed below for midday and night-time periods separately.

(a) *Midday Period (1200-1400 IST)*

7 and 9 Mc/s have mostly been used at Bombay, Calcutta and Madras for the period 1942-1952. No attempt has been made to correlate the yearly variation of field intensity with sunspot number, since sufficient data are not available in



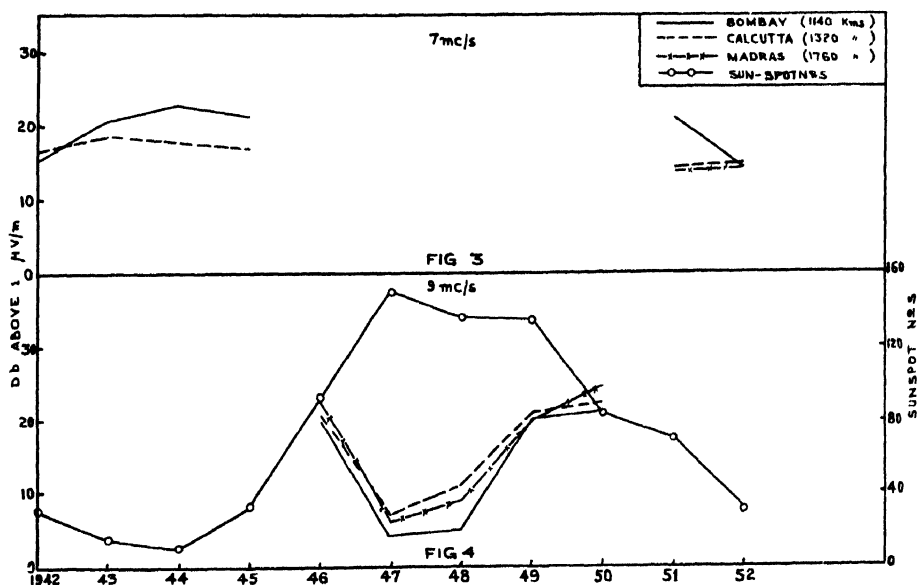
Figs. 1 & 2. Monthly variation of field intensity (mid-day period).

each year on either 7 or 9 Mc/s. This is because partly 7 and partly 9 Mc/s was used during the midday period over the 11 years.

The monthly variation of the field intensity (Sec. 3-ii) has been shown in figures 1 and 2 for 7 and 9 Mc/s respectively. It will be seen from figure 1 that on 7 Mc/s there is not much variation in the field intensity from month to month. The maximum to minimum variation for Bombay is from 21 to 16 db above $1\mu\text{V/m}$, the average being about 18 db. For Calcutta, the maximum to minimum variation is roughly the same and the average is somewhat lower than that of Bombay. For Madras, measurements for sufficient number of years are not available for an analysis to be made. So far as the seasonal variation is concerned, it is interesting to note that there is no appreciable difference in the field intensity from summer to winter.

9 Mc/s has been more extensively used in the midday period. Figure 2 shows that the monthly variations of the field intensity for Bombay, Calcutta and Madras are not much different from one another. Higher values have been obtained in November and December as expected. The average value for most of the months is about 18 db above $1\mu\text{V/m}$.

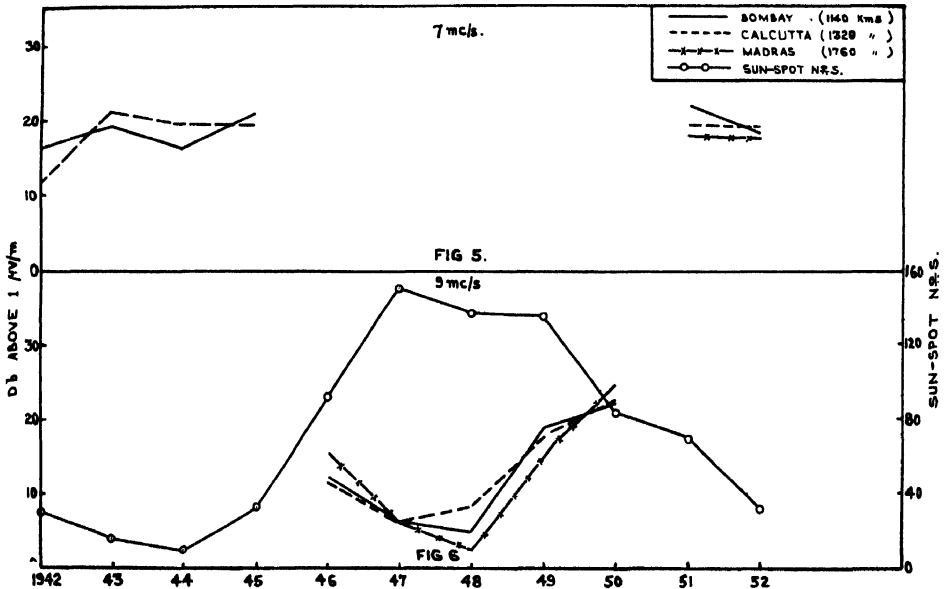
Figures 3 and 4 show the yearly variation of the field intensity (see Section 3-iii) on 7 and 9 Mc/s for summer. The sunspot number has also been shown for correlation. It will be seen from these figures that 7 Mc/s has been used in low sunspot period and 9 Mc/s in high sunspot activity. The variations of field



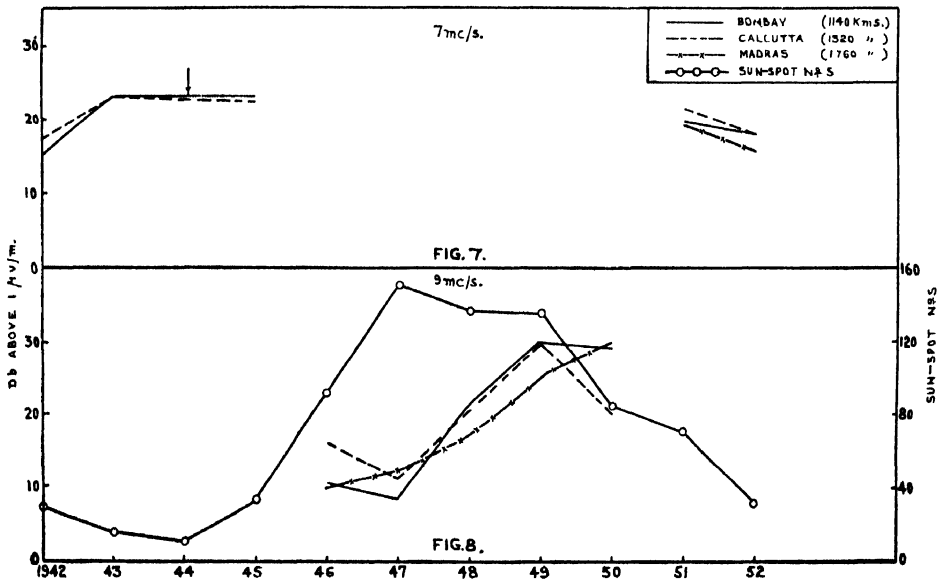
Figs. 3 & 4. Yearly variation of field intensity (mid-day period) for summer.

intensity are well correlated with the sunspot activity: the field intensity is low on high sunspot activity and vice versa. This is expected since the ionospheric absorption (non-deviative) is supposed to have a linear relationship with sunspot number.

Figures 5 to 8 show similar variation of field intensity for equinox and winter. While in equinox there is a close correlation with sunspot activity, in winter it will be seen that for Calcutta and Bombay, the field intensity is lower in low



Figs. 5 & 6. Yearly variation of field intensity (mid-day period) for equinox.



Figs. 7 & 8. Yearly variation of field intensity (mid-day period) for winter. ↓ indicates interpolated values.

sunspot activity period. It is too early to suggest any reason for this apparent discrepancy; more data are required.

(b) Night-Time Period (2000-2200 IST).

3 and 5 Mc/s have mostly been used at Bombay, Calcutta and Madras for the period 1942-1952. Figure 9 shows the correlation with sunspot activity (See. 3-i) of the yearly average of the field intensity on 5 Mc/s for the transmitters at Bombay, Calcutta and Madras. It will be noted that the yearly variation of field intensity is more or less well correlated with sunspot numbers, although for Madras, the correlation is not so well defined. The analysis indicates that it is not correct to assume specular reflection from the ionosphere during night with zero

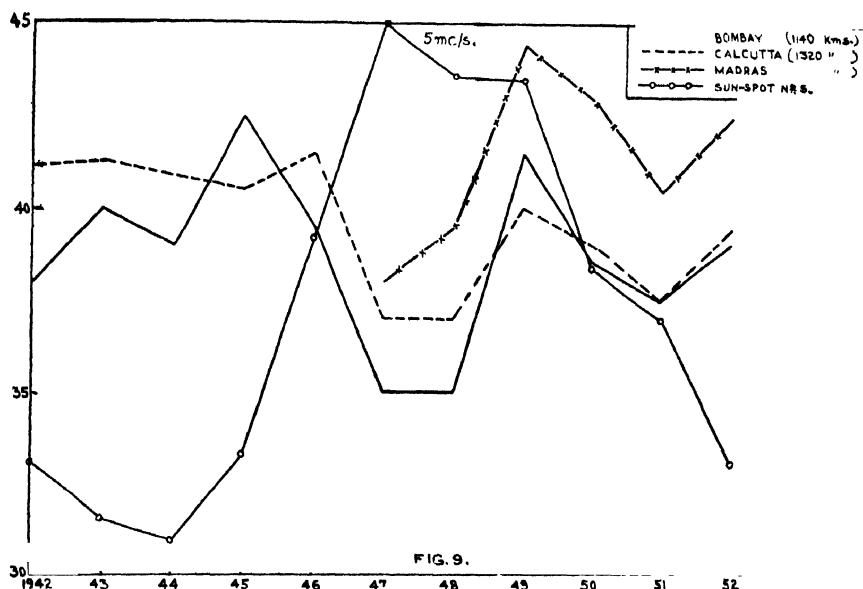
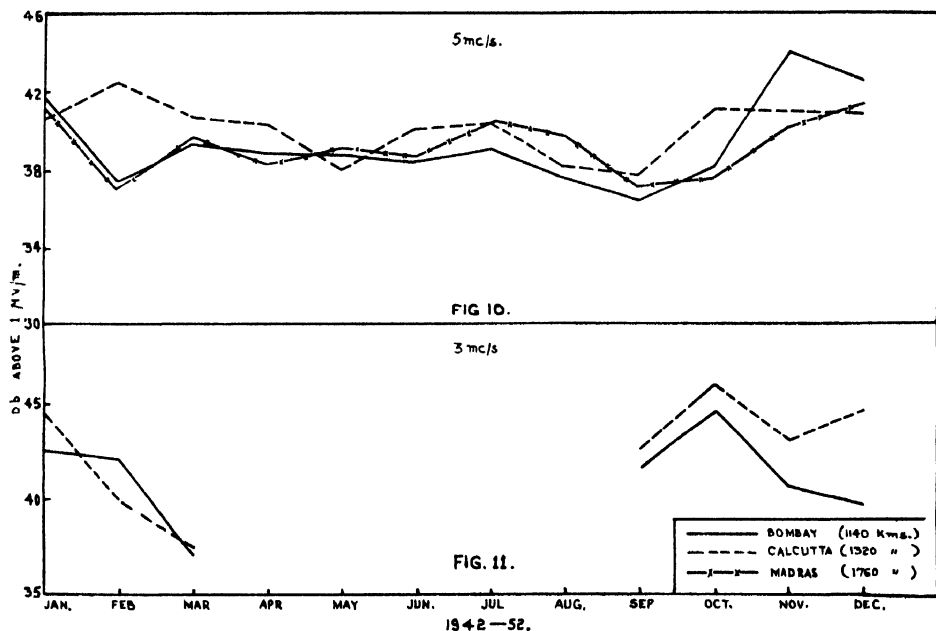


Fig. 9. Correlation with sunspot activity (night-time).

absorption. The sunspot cycle has a distinct effect on ionospheric propagation during the night; the exact mechanism of its effect on the absorption at night is, however, not clearly understood. But it is apparent that due allowance should be made for the sunspot cycle when theoretical calculation of field intensity on long distance propagation during night is undertaken. No attempt is made to evolve an empirical formula for such absorption since the data at our disposal are not considered sufficient.

Figures 10 and 11 show the monthly variation of field strength (Sec. 3-ii) on 5 and 3 Mc/s respectively. 3 Mc/s has not been used for the months April to August, the frequency being well below the optimum frequency of operation. The Madras transmitter has also used 3 Mc/s very infrequently and the monthly variation of its field intensity has, therefore, not been shown in figure 11.

It will be seen from figure 10 that the monthly variation of field intensity in respect of the transmitters at Bombay, Calcutta and Madras follow one another during most of the months. There are, however, significant variations during the winter months. Calcutta figures are higher than the corresponding ones for Bombay and Madras during the months of January and February. Similarly, the Bombay figures are higher in the months of November and December than the corresponding ones for Calcutta and Madras. These variations can to some extent be explained to be due to the different distances of transmissions involved



Figs. 10 & 11. Monthly variation of field intensity (night-time).

and the difference in the orientation of the aerials at the three transmitting stations with respect to the receiving station at Delhi. The downward monthly trend for Bombay and Madras figures for the months of January and February is inexplicable since one would expect the field intensity to be higher during the winter month. Calcutta figures, however, show an upward trend. It was earlier seen in figure 1, that on 7 Mc/s during midday there was no significant difference between the field intensities from month to month. In figure 10, it is seen that although the field intensities for the three stations during the period March to October do not vary much, the average being of the order of 40 db, the variations for the winter months are quite significant. Insufficient data are available regarding field intensity on 3 Mc/s (figure 11).

Figure 12 shows the yearly variation of the field intensity (Sec. 3-iii) on 5 Mc/s for summer. The sunspot number has also been shown for correlation. It will be seen from this figure that there is some correlation between the field intensity and solar activity. The field intensity is quite low during high sunspot activity and high during low sunspot numbers. There is also a close correlation between the field intensity variations for Bombay, Calcutta and Madras from year to year. The trend is nearly the same for all the three stations.

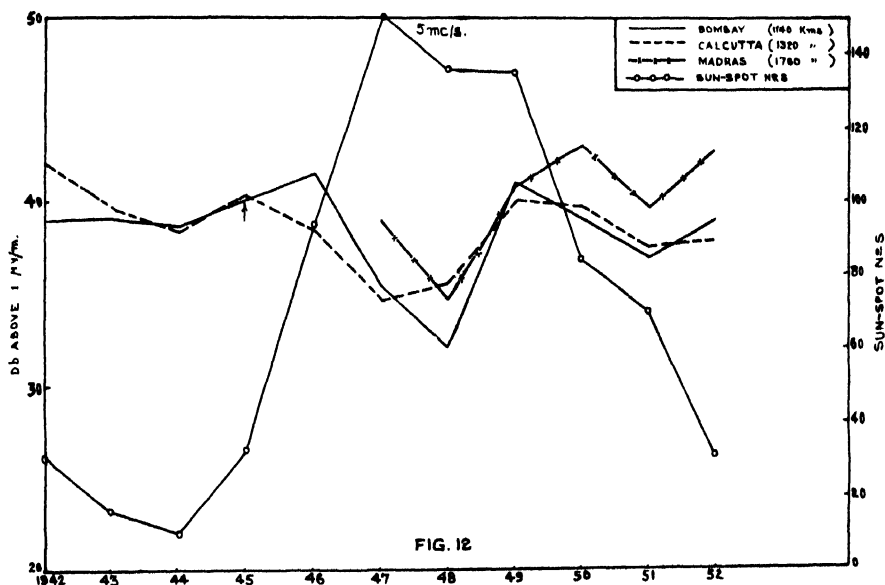


Fig. 12. Yearly variation of field intensity (night-time) for summer. ↓ indicates interpolated values.

Figure 13 shows the yearly variation of the field intensity on 5 Mc/s for equinox. While there is some correlation between the field intensity and sunspot activity in summer for all the stations (figure 12), it will be seen from figure 13 that the variation of field intensity for Madras shows an inverse correlation with sunspot numbers in equinox during the year 1942-45. So far as Bombay and Calcutta are concerned, they do show some correlation. The peculiar behaviour for Madras is not readily understandable.

Figure 14 shows the yearly variation of the field intensity on 5 Mc/s for winter. Here again the Madras field intensity shows an inverse correlation with sunspot numbers (1946-49) as in the case of equinox. It is significant to note that the field intensity variations for Madras indicate inverse relationship with sunspot activity both for equinox and winter seasons, whereas in summer the position is as one would expect.

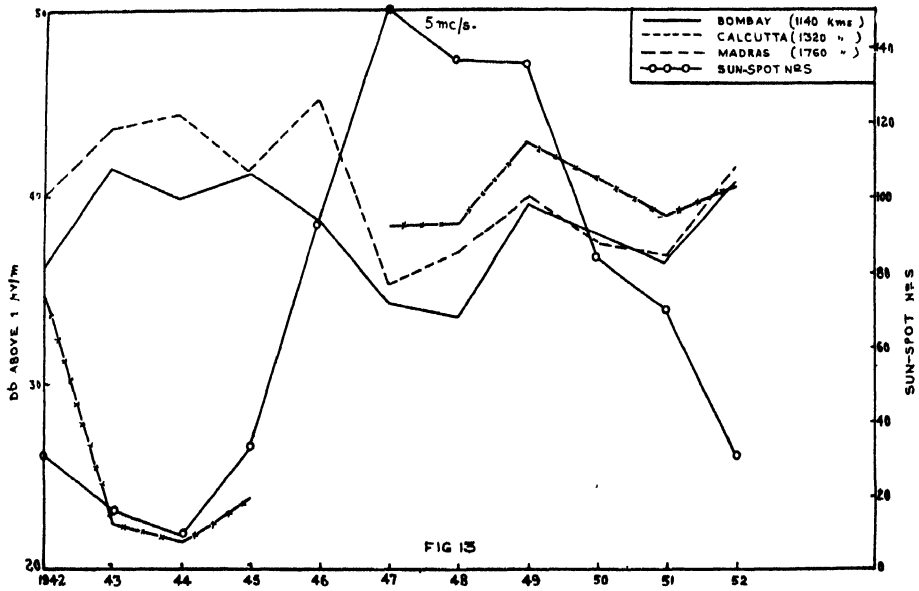


Fig. 13. Yearly variation of field intensity (night-time) for equinox.

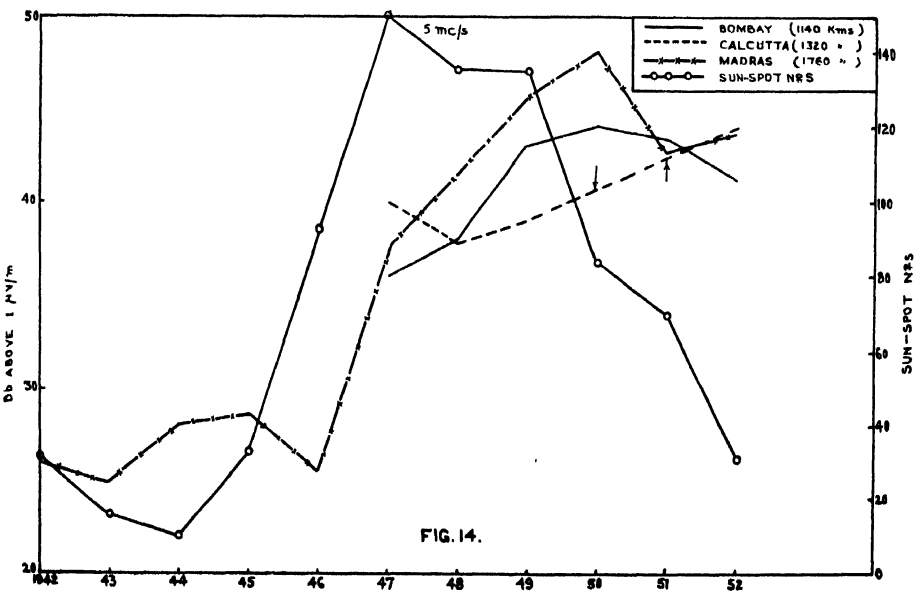


Fig. 14. Yearly variation of field intensity (night-time) for winter. ↓ indicates interpolated values.

As already indicated, sufficient measurements are not available on 3 Mc/s. This band has mostly been used in winter and the yearly variations for Bombay

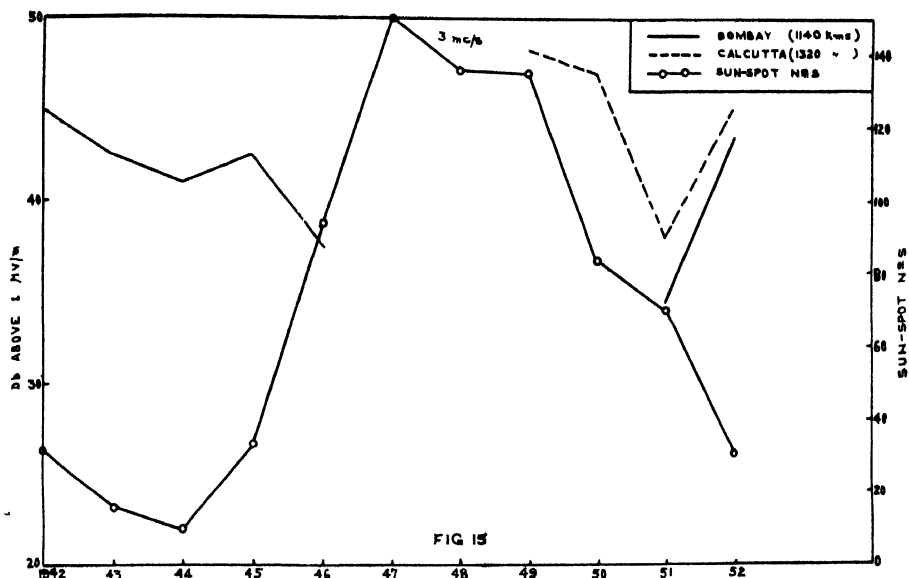


Fig. 15. Yearly variation of field intensity (night-time) for winter.)

and Calcutta are shown in figure 15. Even with the limited data, it is seen that the field intensity variations show some correlation with sunspot activity.

5. SUMMARY AND CONCLUSION

We note from figures 1 to 8 that both the monthly and yearly variations of the field intensity for different seasons during midday as observed at Delhi for transmitters at Bombay, Calcutta and Madras radiating on 9 Mc/s follow the sunspot activity rather closely. The values calculated from the CRPL and the SPIM (1952) methods are somewhat higher which we shall discuss in Part II of this paper.

Figure 9 indicates correlation of night-time field intensity with sunspot numbers. Figure 10 to 15 indicate monthly and yearly variations of the field intensity for different seasons during the night-time period as observed at Delhi for transmitters at Bombay, Calcutta and Madras radiating on 3 and 5 Mc/s. The interesting feature of this analysis is that there appears to be a close correlation with sunspot numbers even during the night-time. Absorption seems to be higher on high sunspot activity and lower on the low values of sunspot numbers. This indicates a possibility that there is a residual D- and E-layer ionisation during the night-time on higher sunspot numbers. The recombination rate may also be insufficient to eliminate at night all the D- and E-layer ionisation as produced during the day-time. This may be due to a higher ion-density during the day for which the collisional frequency is not sufficient as to produce a complete recombination during the night.

ACKNOWLEDGMENTS

The work described in this paper was undertaken for investigating a few questions submitted by the C.C.I.R. for its VIIIth Plenary Assembly. The paper in a modified form was published as an Indian document in the proceedings of the C.C.I.R. (London, 1953). The authors wish to thank Mr. B. V. Baliga, Officer on Special Duty, Ministry of Defence, Mr. M. L. Sastry, Deputy Chief Engineer, Mr. S. S. Aiyar, Director of Frequency Assignment and Mr. S. Thiruvengkatachari, Research Engineer, All India Radio for helpful discussions. Thanks are also due to the Engineers at the Todapur Receiving Centre, Delhi for taking field strength measurements. The authors are grateful to Mr. A. C. Ramchandani, Chief Engineer, All India Radio, for permission to publish this paper.

REFERENCES

- C. R. P. L., 1949, Ionospheric Radio Propagation, U.S. Department of Commerce, National Bureau of Standards, Circular 462.
Rawer, K., 1952, *Wir. Engr.*, **29**, 287.

RAMAN SPECTRA OF ORTHO AND META DICHLOROBENZENE IN DIFFERENT STATES AND AT DIFFERENT TEMPERATURES*

By D. C. BISWAS

OPTICS DEPARTMENT, INDIAN ASSOCIATION FOR THE CULTIVATION OF SCIENCE, JADAVPUR,
CALCUTTA-32

(Received for publication, March 18, 1955)

Plates IV A, B

ABSTRACT. The Raman spectra of ortho and meta dichlorobenzene in different states and at different temperatures have been photographed and compared with each other and with that due to *p*-dichlorobenzene. In the case of the ortho compound two lines at 468 and 487 cm^{-1} due to the mode ϵ'_{η} coalesce to form one intense line at 478 cm^{-1} and the line at 433 cm^{-1} becomes weaker when the substance is solidified and cooled down to -180°C . These changes have been explained by attributing the line at 487 cm^{-1} to a carbon ring vibration in a single molecule while the line at 468 cm^{-1} to the same vibration in a dimer. In the case of the meta compound some of the lines disappear with solidification and these results have been also explained by assuming the presence of dimers as well as monomers in the liquid state and only dimers in the solid state of the substance. The Raman lines due to C—H valence oscillation become sharper with solidification so that the lines 3062 and 3080 cm^{-1} are resolved from each other.

The new lines in the low-frequency region are different for the two substances. At a temperature of -60°C , the crystal of ortho dichlorobenzene produces a single new line at 25 cm^{-1} while the crystal of *m*-dichlorobenzene produces two broad bands at 56 and 81 cm^{-1} respectively. When the temperature is lowered to -180°C , the line at 25 cm^{-1} of *o*- $\text{C}_6\text{H}_4\text{Cl}_2$ crystal disappears but three new lines appear at 68, 81 and 92 cm^{-1} respectively. For similar change of temperature of the meta compound a new line appears at 35 cm^{-1} , the band at 56 cm^{-1} splits up into two lines at 50 and 61 cm^{-1} and the line 81 cm^{-1} shifts to 89 cm^{-1} . It is pointed out that although these two molecules have smaller number of symmetry elements than the *p*-dichlorobenzene molecule, the number of the new lines in the low frequency region is much larger in the latter case. The significance of these results has been discussed.

INTRODUCTION

The Raman spectra of paradichlorobenzene in the solid state have engaged the attention of a large number of workers (Vuks, 1936; Sirkar and Gupta, 1936; Venkateswaran, 1938; Rousset, 1948; Korshunov, 1950; Narain and Saksena, 1951 and Ray, 1951). Rousset (1948) assigned the new lines in the low-frequency

* Communicated by Prof. S. C. Sirkar.

region to the different modes of angular oscillation of the molecules about three axes in the crystal lattice. Korshunov (1950) attributed the origin of three of the nine such lines observed by him to the translational oscillations which are ordinarily forbidden at room temperature but appear at low temperature, while Narain and Saksena (1951) postulated the existence of two different crystal modifications to explain the origin of two different sets of low-frequency lines observed by them in the case of two specimens. In one of these modifications they assumed the existence of free rotation of the molecules about an axis. Ray (1951) observed that the Raman spectrum in low-frequency region of *p*-dichlorobenzene crystal is identical for an approximately single crystal and a polycrystalline mass of the substance, but the spectrum is altered if the crystal is once cooled down to a few degrees below 0°C and then brought back to room temperature again. On analysing the data given by different authors, Ray (1951) concluded that these low-frequency lines of *p*-C₆H₄Cl₂ crystal cannot be attributed to the angular oscillations of molecules in the field of simple Van der Waals' force of crystal lattice. The results of ultraviolet absorption spectra of this compound obtained by Sirkar and Swamy (1953) lend further support to the conclusion arrived at by Ray (1951). The absorption bands of crystals of *p*-C₆H₄Cl₂ become extremely sharp at low temperatures. They concluded from these results that angular oscillations of the molecules cease at low temperature. The intensity of the low-frequency lines does not diminish, however, with lowering of temperature. From a comparison of the results of the investigations on the Raman spectra with those on ultraviolet absorption spectra, Swamy (1953) concluded that the low-frequency lines in the case of *p*-C₆H₄Cl₂ cannot be due to the angular oscillations of the molecules in the crystal lattice.

The suggestion put forward by Korshunov (1950) can be tested by studying the Raman spectra in the low-frequency region of a few suitably chosen substituted benzene compounds. If his interpretation for the origin of three low-frequency lines be correct, we would expect the number of low-frequency lines to be larger in the Raman spectra of crystals of ortho and meta dichlorobenzene than in the case of *p*-dichlorobenzene in the solid state, because in the former two cases the unit cell has no centre of symmetry and the translational oscillations of the lattice are allowed. On the other hand, Sirkar and Swamy (1952) observed, while studying the ultraviolet absorption spectra of *o*-dichlorobenzene at low temperatures, that the influence of intermolecular field on the molecules of this substance is strong enough to split up the electronic energy levels into three components. In the case of *m*-dichlorobenzene also similar results are expected. Further, the Raman spectra of these two substances in the vapour state have been studied by Sponer and Kirby-Smith (1941). The data published by them indicate that some of the strong lines due to molecular vibrations of these two compounds are absent in the Raman spectra of the substances in the vapour state.

Microphotometric records of Raman spectra

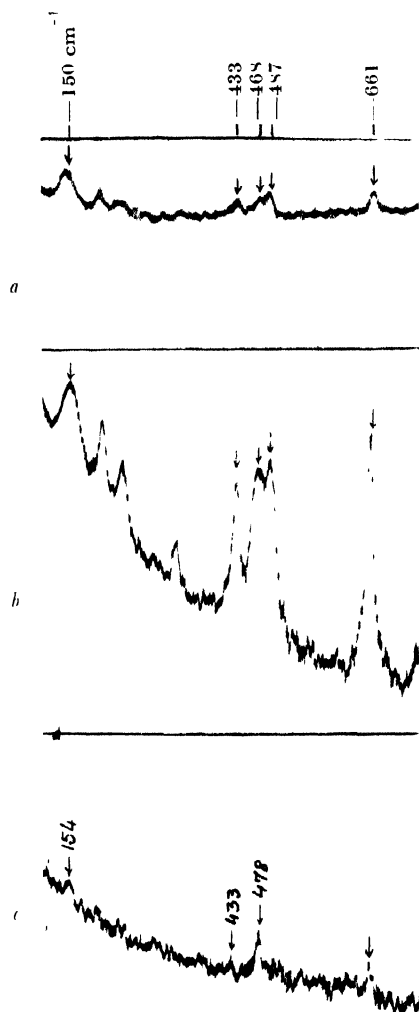


Fig. 1

Ortho dichlorobenzene

(a) Liquid at 110°C

(b) Liquid at 28°C

(c) Solid at -180°C

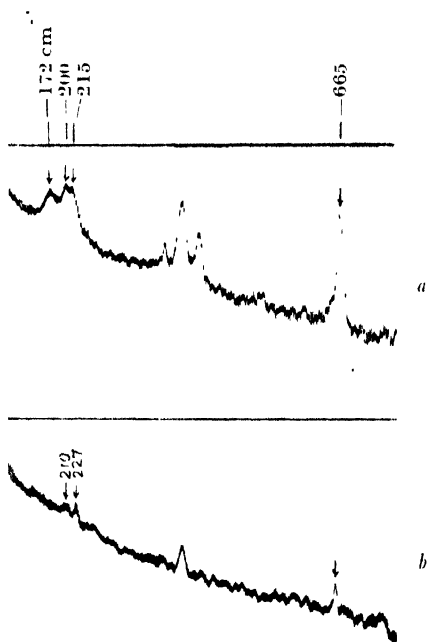


Fig. 2

Meta dichlorobenzene

(a) Liquid at 28°C

(b) Solid at -180°C

Microphotometric records of Raman spectra

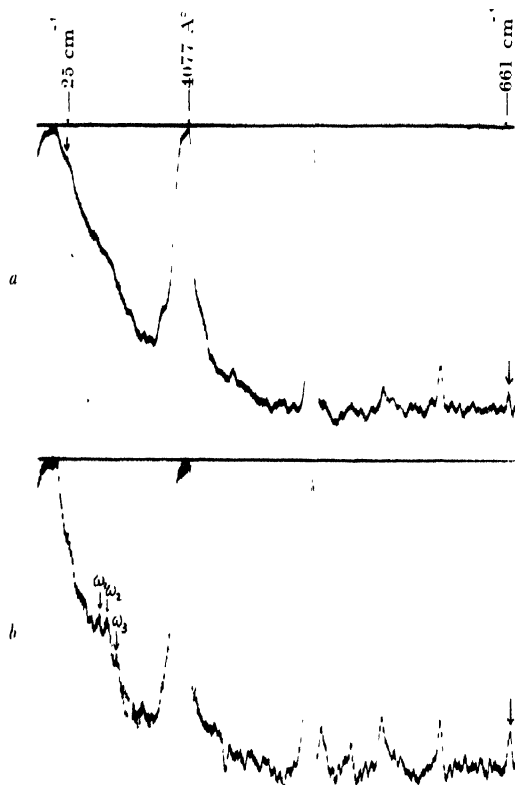


Fig. 3

Ortho dichlorobenzene

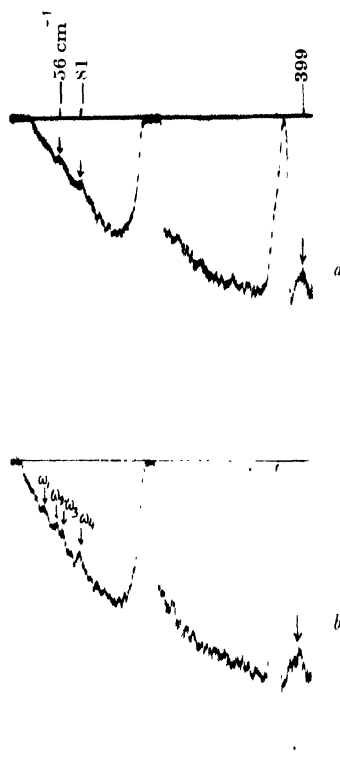
(a) Solid at about -60°C (b) Solid at -180°C $w_1 = 68\text{ cm}^{-1}$, $w_2 = 81\text{ cm}^{-1}$, $w_3 = 92\text{ cm}^{-1}$ 

Fig. 4

Meta dichlorobenzene

(a) Solid at about -60°C (b) Solid at -180°C $w_1 = 35\text{ cm}^{-1}$, $w_2 = 50\text{ cm}^{-1}$ $w_3 = 61\text{ cm}^{-1}$, $w_4 = 89\text{ cm}^{-1}$

The object of the present investigation was to find out whether similar changes take place in the Raman spectra of the two substances with the change from liquid to solid phase and whether the relative positions of the two halogen atoms in the molecule have any influence on the number and intensity of the new lines which appear in the low-frequency region with the solidification of these substances.

EXPERIMENTAL

The liquids ortho and meta dichlorobenzene were supplied by B. D. H. Laboratory and Schuchardt Co. Ltd. respectively and they were of chemically pure variety. They were again distilled in vacuum before every exposure. The Raman lines of these liquids were, as usual, compared with those obtained by previous workers in order to test the purity of the samples. The Raman spectra of the substances in the solid state at different low temperatures were recorded in the same way as described in previous papers (Biswas, 1954*a*, 1954*b*). In all cases the spectra were photographed on Ilford Zenith plates with the help of a Fuess glass spectrograph having dispersion of about 11 \AA° in the 4047 \AA° region. The microphotometer records were taken with a Kipp and Zonen type self-recording Moll microphotometer.

RESULTS AND DISCUSSION

Tables I and II contain the calculated Raman shifts of the substances both in the liquid state and in the solid state at different low temperatures. The tables also include for comparison the Raman shifts of the substances in the liquid phase as observed by Swaine and Murray (1933). Microphotometric records showing the intensities of the low-frequency lines in relation to that due to some molecular vibration and also showing the relative intensities of some of the molecular vibrations in different states have been reproduced in figures 1,2,3 and 4 (Plates IVA, IVB).

(a) *Intramolecular oscillations:*

From Table I it is found that the lines at 698 (0), 780 (1), 934(0), 1070 (0) and 1460 (0) cm^{-1} observed in the present investigation for the liquid state of ortho dichlorobenzene have not been reported by the previous workers. Similarly Table II shows that meta dichlorobenzene in the liquid state yields a few extra Raman lines at 744 (0), 773 (3), 872 (0), 891 (1) 934 (1) and 2983 (1) cm^{-1} . The spectrograms of the present investigation have been probably exposed for a longer period and hence some feeble lines have appeared in them. The extra line at 773 cm^{-1} is, however, quite intense and it is difficult to understand why it was not reported earlier. On the other hand, a few feeble lines reported by earlier workers in the case of meta dichlorobenzene cannot be traced in the spectrograms obtained in the present investigation. These lines are at 1018 (0), 1456 (0), 1544 (0) and 1625 (0) cm^{-1} respectively.

TABLE I
Orthodichlorobenzene, $o\text{-C}_6\text{H}_4\text{Cl}_2$
 $\Delta\bar{\nu}$ in cm^{-1}

Vapour Sponer & Smith (1941)	Liquid		Solid (Present author)	
	Swaine & Murray (1933)	Present author	At about -60°C 25 (3) k	At -180°C
				68 (2) k 81 (3) e,k 92 (1b) k
	154 (10)	150 (10b) \perp e,k	154 (3) e,k	157 (4) e,k
194 (w)	203 (3)	204 (4) \perp e,k	200 (1) e	200 (1) e
	239 (1b)	243 (3b) \perp e, \perp k	251 (1b) e,k	251 (1b) e,k
300 (m)	330 (0b)	333 (3) \perp e,k	335 (0) e,k	335 (0) e,k
434 (vw)	430 (1)	433 (6) \perp e,k,i	433 (2) e,k	433 (1) e,k
	469 (1)	468 (5b) \perp e,k	478 (3b) e,k	478 (4) e,k
487 (m)	483 (2)	487 (7b) e,k		
664 (m)	658 (5)	661 (8) \perp e,k,i 698 (0) e	661 (3) e,k	661 (3) e,k
760 (w)	756 (0b)	750 (2b) e,k 780 (1) e,k 855 (0) e 934 (0) e	750 (0) e,k 780 (0) e	750 (0) e,k 780 (0) e
	1020 (1)	1021 (3b) e,k	1021 (0) e,k	1021 (0) e,k
1035 (st)	1041 (10)	1041 (10) e,k 1070 (0) e	1041 (4) e,k	1041 (6) e,k,i
1133 (st)	1129 (5)	1134 (8) e,k,i	1134 (3b) e,k	1134 (4b) e,k
	1160 (1b)	1159 (3) e,k	1159 (0b) e,k	1159 (1b) e,k
1271 (w)	1274 (1b)	1276 (3) e,k 1382 (1) e,k 1460 (0) e	1276 (0) e,k	1276 (0) e,k
=				
1598 (w)	1577 (4)	1574 (8) e,k	1574 (3) e,k	1574 (4) e,k
	1607 (0b)	1601 (0) e		
	2994 (1)	3004 (0) e,k	3004 (0) e,k	3004 (1) e,k
3082 (st)	3073 (10)	3067 (8) e,k,i	3070 (6) e,k,i	3070 (8b) e,k,i
3150 (w)	3146 (3)	3145 (1) e,k	3145 (0) e,k	3145 (0) e,k

(The letters w, m, st, vw within brackets indicate weak, medium, strong and very weak intensity respectively.)

TABLE II
m-Dichlorobenzene, *m*-C₆H₄Cl₂
 $\Delta\bar{\nu}$ in cm⁻¹

Vapour	Liquid		Solid (present author)	
Sponer & Smith (1941)	Swaine & Murray (1933)	Present author	At about - 60° C	At - 180° C
				35 (1)e,k
			56 (4b)e,k	50 (3)e,k
				61 (4)e,k
			81 (4b)e,k	89 (4)e,k
	178 (3)	172 (5)±e, ±k		
205 (wb)	202 (3)	200 (7)±e, ±k	210 (1)e	210 (1b)e
	216 (2)	215 (6)±e, ±k	227 (3)e,k	227 (4)e,k
356 (w)	366 (1)	367 (2)e,k	367 (0)e	367 (0)e
399 (m)	399 (4b)	399 (11)±e,k,i	399 (5)e,k	399 (6)e,k
	428 (2)	430 (4)±e,k,i	430 (1)e,k	430 (1)e,k
613 (vw)	530 (0)	531 (2)e,k		
665 (m)	666 (4)	665 (9)e,k,i 744 (0)e 773 (3)e,k 872 (0)e 891 (1)e,k 934 (1)e	665 (4)e,k	665 (5)e,k
998 (st)	999 (10) 1018 (0)	990 (15)e,k,i	990 (7)e,k,i	990 (8)e,k,i
1056 (m, vb)	1070 (3b) 1109 (2)	1067 (5)e,k,i 1108 (3)e,k	1067 (1)e,k 1108 (0)e,k	1067 (2)e,k 1108 (0)e,k
1129 (m)	1126 (4) 1240 (0) 1425 (0) 1456 (0) 1544 (0)	1130 (9)e,k,i 1159 (3)e,k 1253 (2)e,k 1415 (2)e,k	1130 (2)e,k 1159 (0)e 1253 (0)e 1415 (0)e	1130 (4)e,k 1159 (0)e 1253 (0)e 1415 (0)e
1590 (m)	1579 (5b) 1625 (0)	1582 (10)e,k 2983 (1)k	1583 (4)e,k	1583 (6)e,k
3090 (st)	3076 (10)	3068 (12b)e,k,i	3065 (8)e,k,i 3080 (0)e	3062 (9)e,k,i 3080 (3)e,k
3169 (w)	3152 (2)	3150 (2)e,k	3150 (0)e	3150 (0)e,k

(The letters w, m, st, vw, etc., within brackets indicate weak, medium, strong and very weak intensity respectively; and letter b indicates broad).

When liquid $o\text{-C}_6\text{H}_4\text{Cl}_2$ is solidified and cooled down to a temperature of -60°C , the Raman lines at 150, 204, 243 and at 3067 cm^{-1} are found to shift respectively to 154, 200, 251 and 3070 cm^{-1} . The microphotometric records reproduced in figure 1 show that the intensities of these lines also undergo changes when the liquid is solidified and cooled down to different low temperatures. The intensity of the line at 150 cm^{-1} increases while the line at 433 cm^{-1} becomes weaker at -180°C . The most remarkable change, however, takes place in the pair at 468 and 487 cm^{-1} . Both these lines are fairly strong in the case of the liquid, but with solidification and cooling down of the solid to -60°C , these two lines are replaced by a single line at 478 cm^{-1} . This line is much stronger than any individual member of the pair (vide fig. 1) and has a frequency-shift intermediate between those of the two lines mentioned above. We can, therefore, conclude that the two lines merge into one another in the case of the crystal at low temperatures. The Raman spectra of ortho and meta dichlorobenzene in the vapour state were studied previously by Sponer and Kirby-Smith (1941). They observed only the line at 487 cm^{-1} while the line 468 cm^{-1} was absent in the case of the vapour. In order to find out whether the change in this doublet takes place gradually with rise of temperature of the liquid, the Raman spectrum of liquid $o\text{-C}_6\text{H}_4\text{Cl}_2$ at 110°C was also studied. The microphotometric records reproduced in figure 1 show that the line at 468 cm^{-1} becomes weaker when the liquid is heated to 110°C . These results can be explained on the assumption that the line at 468 cm^{-1} is due to dimers and the line 487 cm^{-1} is due to the monomers present in the liquid and that the number of dimers diminishes with rise of temperature and the dimers disappear in the vapour state. In the case of the solid state, however, the dimeric molecules are under uniform intermolecular field and this may change the frequency a little so that a line at 478 cm^{-1} is produced.

The line 487 cm^{-1} was assigned to the carbon ring vibration of symmetry e_g^+ (Nordheim and Sponer, 1943). It has been concluded now that the line 468 cm^{-1} is also due to such a mode in the dimer formed by the association of molecules in the liquid. The presence of permanent electric moment seems to be responsible for this type of influence, because in the case of para dichlorobenzene no such change is observed in the corresponding line at 330 cm^{-1} . In the liquid the molecules can orient freely and it appears that strongly associated pairs can be formed in the liquid. In the case of the solid state of $o\text{-C}_6\text{H}_4\text{Cl}_2$ the influence of regularly arranged dipoles around each dipole acts in opposition and the resultant influence is less than that in the case of an isolated associated pair of dipoles.

One of the strong lines at 150 cm^{-1} of $o\text{-C}_6\text{H}_4\text{Cl}_2$ in the liquid state has not been detected by Sponer and Kirby-Smith (1941) on the spectrogram for the vapour state of the substance. In the solid state, this line becomes more

intense and shows an increase in the frequency-shift. Hence the origin of this line should also be attributed to dimers formed by the polar molecules of $o\text{-C}_6\text{H}_4\text{Cl}_2$ in the liquid state. This line due to deformation oscillation in the dimer is totally depolarised probably due to the presence of a symmetry element.

In the case of *m*-dichlorobenzene, the line at 215 cm^{-1} shifts to 227 cm^{-1} and becomes relatively stronger when the substance is solidified and cooled down to different low temperatures. The first line at 172 cm^{-1} of the liquid $m\text{-C}_6\text{H}_4\text{Cl}_2$ seems to disappear completely in the solid state while the line at 200 cm^{-1} shifts to 210 cm^{-1} and becomes diffuse and weaker with solidification of the substance. The photometric records of these lines due to molecular vibration of the substance in different states have been reproduced in figure 2. The line at 172 cm^{-1} which disappears with solidification and the line at 200 cm^{-1} which has a very small intensity in the solid state may be both due to some deformation vibration in the single molecule and the line 215 cm^{-1} may be due to similar vibration in the associated group or a dimer. In the solid state most of the molecules form associated groups and the line at 215 cm^{-1} due to this mode in the associated group becomes stronger while the other two become weaker. Further, in the case of *m*-dichlorobenzene we get a broad line at 3068 cm^{-1} due to the C-H valence oscillation of the molecules in the liquid phase, while in the solid state at -180°C we get, instead, a pair of relatively sharp lines at 3062 and 3080 cm^{-1} respectively. These two lines are broad in the liquid phase and appear as a single broad band, while in the solid state they are sharp and are resolved into two distinct lines.

The substances studied in the present investigation are both polar and the principal changes in the vibrations take place at a temperature not much below their freezing points. This result is in agreement with that obtained by Swamy (1953), who noticed that some changes occur in the absorption bands of *o*-dichlorobenzene even at a temperature of -50°C of the solidified mass.

(b) *Low-frequency lines :*

The microphotometric records reproduced in figure 3 show that *o*-dichlorobenzene in the solid state at -60°C gives rise to a single and intense new line at 25 cm^{-1} in the low-frequency region. With lowering of temperature of the solidified mass to -180°C , this line at 25 cm^{-1} disappears while three other new lines appear at 68 , 81 and 92 cm^{-1} respectively. The line at 81 cm^{-1} has intensity comparable to that of some of the intense lines due to molecular vibrations. The microphotometric records given in figure 4, show the low-frequency lines exhibited by the meta compound in the solid state at -60°C and

-180°C . At -60°C the crystal produces broad and intense Raman lines at 56 and 81 cm^{-1} respectively. When the polycrystalline mass is gradually cooled down to -180°C , the broad band at 56 cm^{-1} splits up into two intense and sharp lines at 50 and 61 cm^{-1} , while the band at 81 cm^{-1} shifts to 89 cm^{-1} and becomes more intense and sharper. Also a new line at 35 cm^{-1} appears with the lowering of temperature to -180°C .

It would be interesting to compare these results with those observed in the case of *p*-dichlorobenzene, because such a comparison would reveal the influence of relative positions of the same substituent atoms in the molecule on the nature of the Raman spectrum in the low-frequency region. The low-frequency lines exhibited by the crystals of these three isomers at different temperatures are given in Table III. The frequencies for *p*-dichlorobenzene crystal are taken from the results reported by Ray (1951).

TABLE III

 $\Delta\nu$ in cm^{-1}

<i>o</i> - $\text{C}_6\text{H}_4\text{Cl}_2$ crystal		<i>m</i> - $\text{C}_6\text{H}_4\text{Cl}_2$ crystal		<i>p</i> - $\text{C}_6\text{H}_4\text{Cl}_2$ crystal	
at about 60°C	at -180°C	at about 60°C	at -180°C	at about 28°C	at -180°C
25 (3)			35 (1)	17 (3)	11 (3)
				40 (2)	30 (4)
		56 (4b)	50 (3)	50 (2)	55 (3)
68 (2)			61 (4)		61 (4s)
81 (3)		81 (4b)	89 (4)	83 (2b)	106 (3s)
92 (1b)					127 (0)

The results given in Table III can be used to test the correctness of the suggestion put forward by Korshunov (1950). According to the explanation offered by him some of the faint lines observed in the low-frequency region in the case of *p*-dichlorobenzene are due to translational oscillations which are forbidden in the case of centro-symmetrical crystals. In the Raman spectra of the asymmetric molecules of *o*- and *m*- $\text{C}_6\text{H}_4\text{Cl}_2$ these lines are expected to be much stronger than in the case of symmetric molecules of the para compound, but contrary to this expectation the number of new lines in the low-frequency region in the crystals

of para compound is much greater than those yielded by the ortho or the meta compound. Hence, the explanation for the origin of three faint Raman lines at low temperature due to $p\text{-C}_6\text{H}_4\text{Cl}_2$ offered by Korshunov (1950) does not seem to be correct. The data given in Table III further show that the lowering of temperature of the crystals of these isomeric compounds always increases the number of new lines in the low-frequency region and that the maximum number of such lines is exhibited by the crystal of $p\text{-C}_6\text{H}_4\text{Cl}_2$ at -180°C . The ultraviolet absorption spectra of ortho and para dichlorobenzene have already been studied by Sirkar and Swamy (1952) and by Swamy (1953). The results indicate that the angular oscillations of the molecules of these dichlorobenzenes cease at low temperatures. The increase in the number, and sometimes in the intensity of the low-frequency Raman lines, therefore, definitely contradicts the hypothesis that most of these new lines should originate from the angular oscillations of the molecule in the crystal lattice. On the other hand, a consistent explanation for the changes in these new Raman lines in the low-frequency region can be found by attributing them to the vibrations of groups of molecules formed by association in the solid state. In such a group of molecules the number of low-frequency lines can increase at lower temperatures due to association with next neighbours. Such association with next neighbours at lower temperatures disturbs the symmetry of the associated group and brings about a change in the polarisability of the group during any of its resulting vibrations. This can satisfactorily account for the change in intensity of some of the low-frequency lines with lowering of temperature of the crystal. Further, the appearance of larger number of new Raman lines in the low-frequency region in the case of the crystals of the para compound may be due to the fact that the Cl-atoms are at the two extreme ends of the benzene ring and this probably helps in the formation of larger intermolecular complexes in the case of the para compound. The enhancement in the frequency-shifts of some of these new Raman lines in the low-frequency region with lowering of temperature is evidently due to the increase in the strength of some of these virtual bonds at lower temperature. The above discussion on the low-frequency Raman spectra of these three isomeric molecules clearly shows that the new Raman lines in the low-frequency region in these crystals primarily originate from the vibrations in associated groups of molecules formed through virtual bonds in the solid state and that no other hypothesis can satisfactorily explain all the observed facts regarding the Raman spectra of these substances.

ACKNOWLEDGMENT

The author is indebted to Professor S. C. Sirkar, D.Sc., F.N.I. for his kind interest and guidance during the progress of this work.

REFERENCES

- Biswas, D. C., 1954a, *Ind. J. Phys.*, **28**, 85.
Biswas, D. C., 1954b, *Ind. J. Phys.*, **28**, 303.
Biswas, D. C., 1954c, *Ind. J. Phys.*, **28**, 423.
Korshunov, A. V., 1950, *Doklady Acad. Nauk. S.S.S.R.*, **74**, 691.
Nordheim, G. and Sponer, H., 1943, *J. Chem. Phys.*, **11**, 253.
Narain, H., and Saksena, B. D., 1951, *Ind. J. Phys.*, **25**, 79.
Ray, A. K., 1951, *Ind. J. Phys.*, **25**, 459.
Rousset, A., 1948, *Jour. de Phys.*, **9**, 101.
Sirkar, S. C. and Gupta, J., 1936, *Ind. J. Phys.*, **10**, 473.
Sirkar, S. C. and Swamy, H. N., 1952, *J. Chem. Phys.*, **20**, 1177.
Sirkar, S. C. and Swamy, H. N., 1953, *Proc. Ind. Sc. Cong., Abstracts Part III*, 158.
Sponer, H., and Kirby-Smith, J. S., 1941, *J. Chem. Phys.*, **9**, 667.
Swaine, J. W. and Murray, J. W., 1933, *J. Chem. Phys.*, **1**, 512.
Swamy, H. N., 1953, *Ind. J. Phys.*, **27**, 119.
Venkateswaran, C. S., 1938, *Proc. Ind. Acad. Sc.*, **8A**, 448.
Vuks, M., 1936, *Comptes Rendus (Doklady)*, **1**, 73.

ON THE QUANTITATIVE RELATION BETWEEN ISOTOPIC BETA RADIATION AND ITS PHOTOGRAPHIC RESPONSE

By R. K. PODDAR

BIOPHYSICS DIVISION, INSTITUTE OF NUCLEAR PHYSICS, CALCUTTA-9

(Received for publication, February 26, 1955)

ABSTRACT. The photographic action of the continuous beta spectrum as emitted by the radioisotopes has been studied. It has been deduced theoretically that the optical density, D , produced by the beta particles in any photographic emulsion should approximately vary, directly as the number, Q , of the beta particles striking it per unit area and inversely as the average energy, E , of the beta spectrum of the isotope concerned, i.e., in short, $(D \times Q)/E = \text{a constant}$. This relation has been experimentally verified in the case of Au-198, I-131 and P-32, three isotopes frequently used in biophysical investigations. It has also been found that the values of the number of beta particles/cm² necessary to produce a density of 0.6 above background in the photographic emulsion used are 2.8×10^8 , 1.7×10^8 and 6.5×10^8 , respectively in the case of Au-198, I-131 and P-32.

INTRODUCTION

Auto-radiography, or the technique of detection of the site of a localised radioisotope by means of the photographic action of its emitted radiations, is now being extensively applied in the fields of biology, medicine, geology, etc. All the artificial radioisotopes used in auto-radiography emit beta particles. Hence, to estimate the concentration of the localised radioisotope, the knowledge of quantitative relation between the number of beta particles incident on the photographic emulsion and the response of the latter is essential. Many authors have studied the effects of mono-energetic electrons on the photographic emulsions (Baker, Ramberg and Hillier, 1942; Cranberg and Halparen, 1949). But Cobb and Solomon (1948) first made a quantitative study of the photographic action of the beta-spectrum as emitted by a radioisotope.

This paper reports on a method for determination of the relation between the number of beta particles from a radioisotope striking a photographic emulsion and

the optical density they produce in it. An approximate theoretical expression has also been derived connecting the optical density with the incident number of beta particles and the average energy of the beta spectrum. This expression has been verified in the case of Au-198, I-131 and P-32, the three isotopes very frequently used in biophysical investigations.

THEORY

The photographic emulsion layer, whether the ordinary optical type or the nuclear track type, consists of a large number of tiny grains of silver bromide embedded in gelatine, the grain-size varying from 0.1 to 3μ (Mees, 1954). If an electron passes through such an emulsion it loses energy as a result of interactions of various types with the atoms of the emulsion medium lying near its path. The most important of these interactions in the case of the isotopic beta radiation, having energies up to 1 or 2 Mev only, is the collision with orbital electrons of these atoms. Because of such collisions, the orbital electrons may be ejected from atoms (ionisation) or raised to some excited levels (excitation). The ionisation and excitation produced in the silver bromide grains of the emulsion by the passage through them of a fast moving electron may render them developable. (Beiser, 1952). Hence if a photographic plate after exposure to a stream of beta particles from a radioisotope be developed, the regions through which the electrons have passed will be blackened due to the developed silver bromide grains. An expression connecting the blackening of the emulsion and the number of beta particles producing it can be derived as follows:

Let Q be the total number of beta particles passing through the emulsion per unit area (hereinafter termed as 'Exposure'), I_{col} the mean energy lost due to collision by a beta particle per unit thickness of the emulsion, and d , the total emulsion thickness, then the total collision-loss in the emulsion, ϵ , will be given by

$$\epsilon = Q.I_{col}.d \quad \dots (1)$$

Since the energies of the beta particles from a radioisotope are distributed over a wide range, actually from zero to a certain characteristic maximum, E_{max} , and the collision-loss depends on the energy of the beta particle, an accurate evaluation of I_{col} is hardly possible; however, an approximate estimate may be made by assuming that all the beta particles would have lost the same amount of energy due to collision even if each of them had an energy, E , equal to the average energy of the beta spectrum of the isotope under consideration. It has been experimentally found (Whitehouse and Putman, 1953) that the collision-loss approximately varies inversely as the kinetic energy of electrons upto about 1 Mev.

Since the average energies of the artificial radioisotopes used in tracer experiments are not greater than 1 Mev. we can rewrite equation (1) as

$$\epsilon = A.Q.d/E \quad \dots (2)$$

where A is a constant depending on the nature of the emulsion.

Now let G be the total number of silver bromide grains in the emulsion per unit area. At any particular instant during the exposure of the emulsion to the beta particles, a number of these grains would have already suffered collisions with them, thereby absorbing an amount of energy, ϵ say, and thus been rendered developable; let this number be g' . During the next infinitesimal interval, let there be an increment in the absorbed collision-loss energy by an amount, $d\epsilon$. Then the corresponding increase in the number of developable grains will be

$$dg' = k(G - g')d\epsilon$$

Here k is a constant which gives the probability that a grain will be rendered developable per unit increase in the absorbed energy and $(G - g')$ is the number of silver grains still remaining undevelopable. Such a relation is suggested by the nature of the absorption of the beta particles by matter. On integration it yields

$$g' = G(1 - e^{-k\epsilon}) \\ \approx G.k.\epsilon, \quad \text{when } k\epsilon \text{ is small.}$$

A definite fraction of developable grains will be actually developed. Thus the number of developed grains for unit area of the emulsion, g will be proportional to g' , and hence from the above equation it can be shown that $g = B.\epsilon$, where B is another constant. Substituting for ϵ from equation (2) one gets

$$g = C.Q.d/E, \text{ (putting } C = A.B) \quad \dots (3)$$

To measure the photographic density, D , of the blackened region of the developed plate, a pencil of light is sent through that region. Consider an infinitesimal portion of area, dx , of the blackened region through which the light rays are passing. The number of grains in this portion is gdx . We now associate with each of the developed grain an area, σ , such that any photon that may come within this area will either be absorbed or scattered so as not to be transmitted. Evidently σ will depend on the grain-size and hence will be approximately constant for a particular emulsion type. Now the total of such areas in the section dx is $\sigma.g.dx$. We can then assume that the ratio of the reduction of intensity dI , to the incident intensity, I , will be given by $-(dI/I) = \sigma.g.dx$. This expression,

on integration between the limits $I = I_0$ to $I = I_t$, and $\alpha = 0$ to $\alpha = 1$ gives $I_t = I_0 \cdot e^{-\sigma g}$, where I_0 and I_t , are the intensities of the light pencil before and after transmission. Since, by definition, the optical density of the blackened region, D , is $\log_{10} (I_0/I_t)$, it is easily seen that $D = \sigma \cdot g/2.3$. Substituting for g from equation (3) one gets

$$D = C \cdot \sigma \cdot d \cdot Q/2.3E \quad \dots (4)$$

For a particular emulsion with a given thickness, σ , C , and d are constants. Hence, in words, one can write:

$$(\text{Density} \times \text{average energy})/\text{exposure} = \text{a constant.}$$

MATERIAL AND METHODS

(a) *The method of exposing the photographic plate to beta particles:*

Radioactive solutions were spread over thin copper planckets. The planckets were then dried and subsequently used as the sources of beta particles in the experiment. By varying the strength and/or the amounts of the radioactive solutions on the planckets, sources of different strengths were obtained. Then a thick brass plate was taken and several equispaced, circular holes, each $\frac{1}{4}$ " in diameter, were bored into it. On one side of the plate, concentric with each hole, was scooped out a circular area of same diameter and thickness as those of a plancket. This brass plate will be referred to as the 'collimator'.

The collimator was then placed on the photographic plate such that its side containing scooped-out areas was on the top and the plane side was in contact with the photographic emulsion. The Kodak medium lantern slide plates were used. The source-planckets were then fitted into the scooped-out areas, their sides with radioactive residue facing the photographic emulsion through the holes of the collimator. The thickness of the collimator (5mm) was sufficient to stop all beta particles except those that pass through the holes. The photographic plate with the collimator above it was placed on another thick brass plate so that, sandwiched between two heavy brass plates, it was immune to slight mechanical disturbances during the period of exposure. The whole arrangement was then kept in a light-tight box in a cool, dry place at room temperature for the desired exposure time. Figure 1(b) shows the experimental set-up.

(b). *Determination of Exposure Q:*

For this purpose, the source-plancket covered with an absorber, having a concentric circular hole of the same dimension as in the collimator, was placed under

an end-window beta counter. The beta counter was so arranged that its window occupied the same position as the emulsion of the photographic plate did during

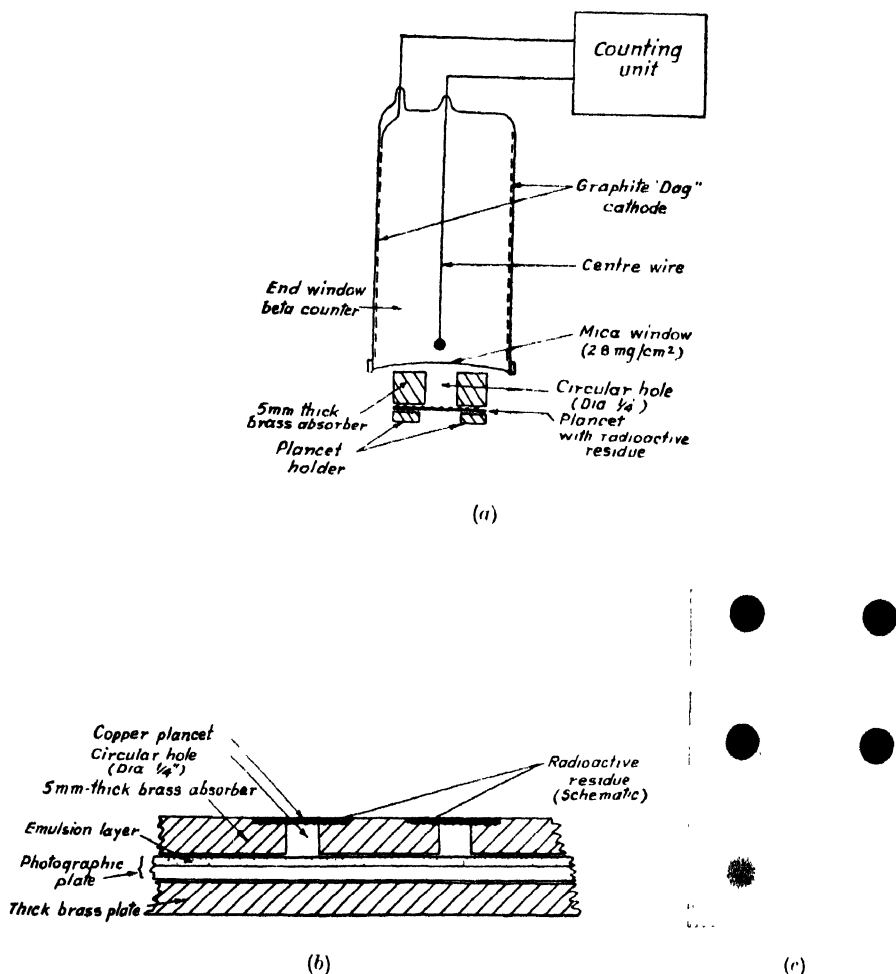


Fig. 1.

its exposure to the beta particles from the same source as shown figure 1(a). The initial counting rate, i.e. the number of beta particles from the source recorded by the counter per min. before exposing it to the photographic plate, was determined. Since the efficiency of the counter for beta particles is $\sim 100\%$ and that for gamma rays is negligible (see Discussion), this observed initial counting rate was only corrected for (1) the dead time of the counter, (2) background counts, and (3) the absorption of beta particles by the counter window, and thus the true initial counting rate R_0 , say, was obtained. Now, if within the source spread over the area A of the collimator-hole, N_0 and N were the total number of radioactive

atoms just before and after the time of exposure t , then the exposure, Q , is evidently $(N_0 - N)/A$. But since $N = N_0 e^{-\lambda t}$, where λ is the decay constant of the isotope and $R_0 = -(dN/dt)_{t=0} = \lambda N_0$ it is easily seen that

$$Q = (R_0/A\lambda)(1 - e^{-\lambda t}) \quad \dots \quad (5)$$

Thus knowing R_0 , A , λ and t , the exposure Q was calculated out from equation (5).

(c) *The processing of the exposed photographic plate and the measurement of the optical density:*

After proper exposure, the photographic plates were developed in Kodak D72E, diluted 1:2 with water, for 3 minutes at 65° F and fixed in Kodak F5 fixer at the same temperature for 6 minutes. The plates were then washed and dried. The exposed parts appeared as blackened spots on the processed plates. Some of the spots are shown in the figure 1(c). The optical densities of the spots were measured by means of a photovolt transmission densitometer. The mean density of the regions not occupied by the spots was taken as the back ground density for the plate concerned. The density of a spot above back ground gave the effect of the beta particles only, that of the associated gamma rays, if any, being negligible (see Discussion).

RESULTS

Of the three radioisotopes used, P-32 emits a simple beta spectrum with the maximum energy (E_{\max}) of 1.7 Mev and disintegrates to S-32, its half-life being 14.3 days. I-131 decays to Xe-131 by means of two competitive beta disintegrations—one (86 %) with $E_{\max} = 0.60$ Mev and the other (14 %) with $E_{\max} = 0.32$ Mev—and has a half-life of 8.0 days. The beta emission is associated with four gamma rays, with quantum energies as follows: 0.64 Mev (14%), 0.36 Mev (80%), 0.28 Mev (6%) and 0.08 Mev (6%) percentage giving probability of emission. Au-198 has a half-life of 2.7 days only and decays to Hg-198, emitting a beta spectrum with $E_{\max} = 0.96$ Mev and an associated gamma ray of quantum energy, 0.41 Mev (N.B.S. circular, 1950). The average energies, \bar{E} , of the beta particles from P-32, I-131 and Au-198 are 0.7 Mev, 0.2 Mev and 0.32 Mev respectively. (Marinelli et al, 1948).

Altogether 8 different exposures were made with each isotope. The experimental data are shown in Table 1. The true initial counting rate of the sources before exposure, R_0 , (column 2) was converted to the exposure, Q , (column 4) by means of the equation (5); column 5 contains the corresponding optical density above back-ground. In the last column are shown the product (density, $D \times$ average energy, \bar{E})/exposure, Q . The exposure-density relations for all the three isotopes are also shown graphically in the figure 2.

DISCUSSION

From the study of Table I and the curves of figure 2, it is found that for a given exposure beta particles from P-32 produce the least density, those from

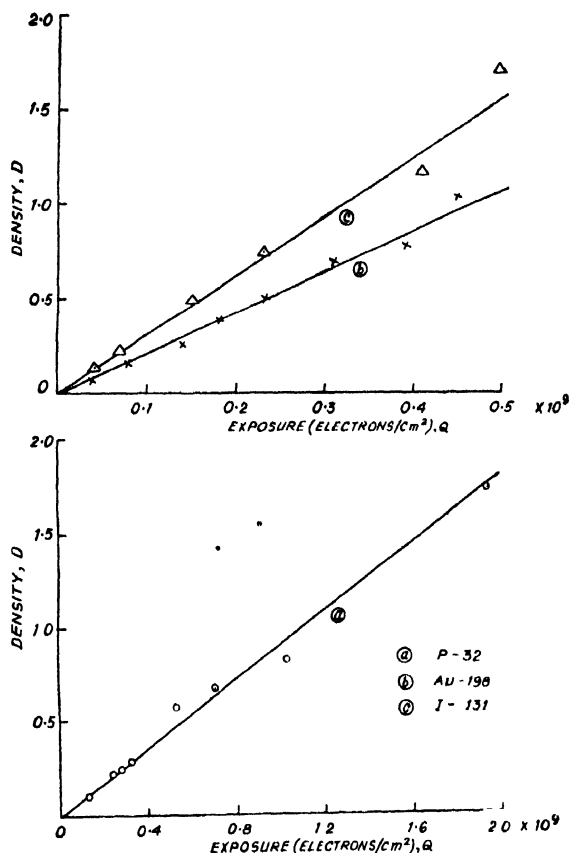


FIG 2 DENSITY-EXPOSURE RELATIONS

I-131 the maximum density and those from Au-198 an intermediate one. It is also seen that between the exposures of 10^7 – 10^9 electrons/cm², the optical density is approximately linearly related to the exposure and varies inversely as the average energy of beta particles. The values of the number of the beta particles/cm² necessary to produce a density of 0.6 above background in the photographic emulsion used are 6.5×10^8 , 2.8×10^8 and 1.7×10^8 , respectively, in the case of P-32, Au-198 and I-131. These values compare well with those quoted by Herz (1951).

TABLE I

Density—exposure relations

Isotope	Exposure, $Q = (R_0/4\lambda) (1 - e^{-\lambda t})$: [$A = 0.317 \text{ cm}^2$]			Mean density, D , (above back ground)	$(D \times E/Q)$, in Mev-cm ² electron $\times 10^{-10}$
	Initial counts per min, $R_0, \times 10^3$	Exposure time, t , in days	electrons per sq. cm $\times 10^9$		
P-32	222	2	1.93	1.75	6.3
$E = 0.70 \text{ Mev}$	235	1	1.03	0.82	5.6
$\lambda = 0.048 \text{ day}^{-1}$	55.6	3	0.70	0.67	6.7
	61.5	2	0.53	0.58	7.6
	25.4	3	0.32	0.30	6.5
	65.0	1	0.29	0.25	6.2
	27.9	2	0.24	0.22	6.4
	29.4	1	0.13	0.10	5.4
I-131	41.3	3	0.50	1.75	7.0
$E = 0.20 \text{ Mev}$	49.2	2	0.41	1.20	5.9
$\lambda = 0.087 \text{ day}^{-1}$	53.6	1	0.23	0.75	6.5
	12.6	3	0.15	0.50	6.7
	15.0	2	0.13	0.35	5.4
	16.4	1	0.07	0.22	6.2
	4.32	3	0.05	0.18	6.9
	5.14	2	0.04	0.12	5.6
Au-198	46.8	3	0.44	1.00	7.2
$E = 0.32 \text{ Mev}$	54.9	2	0.39	0.80	6.3
$\lambda = 0.257 \text{ day}^{-1}$	22.2	3	0.31	0.67	6.9
	32.6	2	0.23	0.50	7.0
	41.4	1	0.17	0.35	6.4
	14.9	3	0.14	0.25	5.7
	11.5	2	0.08	0.16	6.2
	4.22	3	0.04	0.08	6.5

The relative efficiency of the gamma rays with respect to the beta particles from any artificial radioisotope in activating a detector may be roughly taken to be μ_γ/μ_β , where μ_γ and μ_β are the total real mass absorption coefficients of the gammas and the betas from the same isotope within the detecting medium. The values of μ_γ for different quantum energies in various materials have been compiled by Johns (1953) and Mayneord (1950). The μ_β can be obtained directly from absorption measurement. Of the three isotopes we used, only I-131 and Au-198 emit gamma rays in addition to beta particles. For these two isotopes, the relative gamma efficiency in the counter gas ($Z_{eff} \sim 2$) or in the photographic emulsion ($Z_{eff} \sim 4$) is less than 1% and hence negligible compared to the experimental error which is about $\pm 5\%$.

The chief advantages of this method over those using the biological tissues or other similar specimens incorporated with radioactive substances as the activating sources are that the accurate determination of the number of beta particles striking the plate is possible and that no correction for geometry is necessary in this method. Again since uniformly dark spots are obtained after exposure the density measurements are much more accurate. When a particular photographic plate has been calibrated by this method and the same plate has been used in the auto-radiography, the actual concentration of the isotope in the specimen can be determined from measurement of the densities on the plate.

ACKNOWLEDGMENTS

This work was aided by a grant from the Ministry of Education, Govt. of India. The author expresses his indebtedness to Prof. N. N. Das Gupta for his valuable guidance and to Prof. M. N. Saha, F.R.S., for his kind interest in this work.

REFERENCES

- Baker, R. F., Ramberg, E. G. and Hillier, J., 1942, *J. App. Phys.*, **13** (7), 450.
Beiser, A., 1952, *Rev. Mod. Phys.*, **24**, 273.
Cobb, J. and Solomon, A. K., 1948, *Rev. Sci. Inst.*, **19**, 441.
Craneberg, L. and Halparen, J., 1949, *Rev. Sci. Inst.*, **20**, 641.
Herz, R. H., 1951, *Nucleonics*, **9** (3), 24.
Johns, H. E., 1953, In "The Physics of Radiation Therapy" published by C. C. Thomas, Springfield, Illinois, U.S.A., p. 44

- Marinelli, L. D., Quimby, E. H. and Hine, G. J., 1948, *Nucleonics*, **2** (April, 1948), 66.
- Mayneord, W. V., 1950, *Brit. J. Radiol. Suppl.*, **2**.
- Mees, C. E. K., 1954, In "The Theory of Photographic Process", Macmillan & Co., New York, Revised Edition, p. 303.
- N. B. S. (U.S.A.), Circular, 1950, *Nuclear Data*.
- Whitehouse, W. J. and Putman, J. L., 1953, In "Radioactive Isotopes", O. U. P., London, p. 76.

FERMI'S STATISTICAL THEORY OF MULTIPLE PION PRODUCTION

By K. K. SINGH

PHYSICS DEPARTMENT, DELHI UNIVERSITY, DELHI

(Received for publication, October 20, 1954)

ABSTRACT. The probability for emission of N pions in a nucleon-nucleon collision is calculated on Fermi's model by applying relativistic classical thermodynamics to the 'pion gas'. In Section II relative probabilities for various numbers of pions produced in a nucleon-nucleon collision are computed.

Fermi's (1950) statistical theory of multiple pion production in high energy nucleon-nucleon collisions has aroused considerable interest in recent years. The theory has two apparently different procedures for dealing with the problem. One approach amounts to assuming the probability for the creation of N pions proportional to the density of final states in a small volume $\Omega \sim (4\pi/3)(h/2\pi\mu c)^3$ in which the energy of the colliding nucleons is supposed to be suddenly liberated, while, the other (suited to extremely high energies) consists in applying Bose-Einstein statistics to the pion gas in Ω . For a given energy W in the centre-of-mass system, the first approach yields for the most probable number of pions produced:

$$N_{\text{prob}} = 2.1[(w-2)/w^{1/3}] - 1/6, \\ w = W/Mc^2, \quad \dots \quad (1)$$

whereas, the thermodynamic theory gives

$$N'_{\text{prob}} = 2.6(w-2)^{3/4}/w^{1/4} \quad \dots \quad (2)$$

As Fermi has pointed out, these different expressions for the number of pions produced arise, because, in deriving (1) the statistical correlations of the particles are completely ignored. In this note the 'pion gas' in Ω is treated according to classical statistical thermodynamics. The probability for the production of N pions is taken proportional to $\exp \{S(N)/k\}$ where $S(N)$ is the entropy of N pions and k , the Boltzmann's constant. It is found that if one does not omit the factor $N!$ in the expression $N!/\pi_i(n_i!)$ for the weight of a state in evaluating the entropy, the result is the same as that obtained by Fermi. One might consequently conclude that when the number of pions produced is large, the

correlations of the particles are taken into account by dividing Fermi's expression by $N!$. The formula for the most probable number of particles produced then agrees with (2) except for a small difference in the numerical factor.

In Section II, relative probabilities for various numbers of particles produced in a nucleon-nucleus collision are computed using Fermi's model. The average number of pions produced in such an event is seen to be substantially higher than that in the corresponding nucleon-nucleon collision.

I. The basic assumptions of the statistical theory are: (i) the pions are produced in a small volume given by

$$\Omega = (4\pi/3)(\hbar/2\pi\mu c)^3(2Mc^2/W), \quad \dots \quad (3)$$

where μ is the pion rest-mass and W the total energy of the colliding nucleons in the centre-of-mass system; and (ii) the probability that in the final state N particles are present is proportional to

$$(\Omega/\hbar^3)^{N-1} dQ_{N-1}/dW, \quad \dots \quad (4)$$

where $Q_{N-1}(W)$ is the volume of the momentum space containing all those states for which the energy is less than or equal to W .

In the case of an event in which the final state consists of N pions (together with the two nucleons), (4) yields the following expression for the relative probabilities:

$$P_N(w) = K \cdot [(251/w)(w-2)^3]^N / (3N+1/2)!, \quad \dots \quad (5)$$

where

$$w = W/Mc^2 \text{ and } K \text{ is a constant.}$$

We treat the 'pion gas' in Ω according to relativistic classical statistical thermodynamics. The partition function for the assembly is (without omitting the factor $N!$):

$$\begin{aligned} Z &= \sum_{\{n_s\}} [N!/\prod_i (n_i!)] \exp [-(\sum_s n_s \epsilon_s)/kT]; \quad \sum_s n_s = N \\ &= [\sum_s \exp (-\epsilon_s/kT)]^N \end{aligned} \quad \dots \quad (6)$$

The entropy of the pion gas is

$$\begin{aligned} S &= k \ln Z + E/T \\ &= kN \ln [\sum_s \exp (-\epsilon_s/kT)] + E/T, \end{aligned} \quad \dots \quad (7)$$

where

$$E = \text{energy of the pion gas} = (W - 2Mc^2).$$

The density of single particle states in Ω is

$$(\Omega/h^3)4\pi p_s^2 dp_s = (4\pi\Omega/c^3h^3)\epsilon_s^2 d\epsilon_s$$

since,

$$p_s = \epsilon_s/c.$$

therefore,

$$\begin{aligned} \sum_s \exp(-\epsilon_s/kT) &= (4\pi\Omega/c^3h^3) \int_0^\infty \epsilon^2 \exp(-\epsilon/kT) d\epsilon \\ &= (4\pi\Omega/c^3h^3) \cdot 2(kT)^3. \end{aligned}$$

The average number of particles in energy level ϵ_s is

$$\begin{aligned} n_s &= -kT \partial/\partial\epsilon_s (\ln Z) \\ &= N \exp(\epsilon_s/kT) / \sum_s \exp(-\epsilon_s/kT), \end{aligned}$$

and the total energy

$$\begin{aligned} E &= \sum_s n_s \epsilon_s \\ &= (N/2(kT)^3) \int_0^\infty \epsilon^3 \exp(-\epsilon/kT) d\epsilon \\ &= 3NkT. \end{aligned}$$

Substitution in (7) yields

$$\begin{aligned} S/k &= -N \ln [(27/8\pi\Omega)\{ch/(W-2Mc^2)\}^3 N^3] + 3N \\ &= -3N \ln (N/N_0) + 3N. \end{aligned} \quad \dots (8)$$

where

$$N_0 = (8\pi\Omega/27)^{1/3} \{(W-2Mc^2)/ch\} = 2.1(w-2)/w^{1/3} \quad \dots (9)$$

is the value of N that makes S maximum.

The probability for the production of N pions is proportional to

$$\exp[S(N)/k] = (N_0/N)^{3N} \exp(3N),$$

or, since N is large, the probability is proportional to

$$(3N_0)^{3N}/(3N)! = [(251/w)(w-2)^3]^N/(3N)!, \quad \dots (10)$$

which agrees with the Fermi expression (5).

It is thus clear that if the average value of N is large, Fermi's approach is equivalent to applying classical thermodynamics to the pion gas without omitting

the 'Gibbs-Paradox' factor $N!$. Correct results are consequently obtained by dividing (5) by $N!$.

The most probable value of N obtained from (10) after division by $N!$ (and also introducing the weight factor 3 for pions) is

$$N_{\text{prob.}} = 2.3(w-2)^{3/4}/w^{1/4}.$$

This may be compared with the value

$$N'_{\text{prob.}} = 2.6(w-2)^{3/4}/w^{1/4}$$

obtained by Fermi by applying Bose-Einstein statistics to the pion gas.

II. NUCLEON-NUCLEUS COLLISION

Suppose the nucleus contains n nucleons. The velocity of the centre of mass is (in units of c)

$$(\gamma^2 - 1)^{1/2}/(\gamma + n)$$

and the Lorentz contraction factor

$$1/\gamma_c = (2n\gamma + n^2 + 1)^{1/2}/(\gamma + n). \quad \dots (11)$$

rMc^2 is the energy of the bombarding nucleon in the laboratory system. The total energy available in the c.m. system is (in units of Mc^2)

$$w = (2n\gamma + n^2 + 1)^{1/2}.$$

The volume Ω in which the mesons are produced may be taken as (Cocconni, 1954)

$$\Omega = n\Omega_0/\gamma_c, \quad \Omega_0 = (4\pi/3)(h/2\pi\mu c)^3. \quad \dots (12)$$

With this assumption, Fermi's theory gives the following expression for the weight of a state consisting of N pions and $(n+1)$ nucleons:

$$W(n+1;N) = [251\{wn^2/(w^2+n^2-1)\}(w-n-1)^2]^N \times 1/(3N+3n/2-1)!. \quad \dots (13)$$

As before, this should be divided by $N!$ to take into account the statistical correlations of the pions.

In going through a nucleus of atomic weight 100, the primary nucleon interacts with not more than 4 or 5 nucleons; the numerical calculations have,

therefore, been made for $n = 5$. Table I gives the relative probabilities for five different values of γ . In each row the first line gives the results obtained from (13) and the second line those obtained after division by $N!$. The results may be compared with Fermi's results (reproduced in Table II) for the nucleon-nucleon collision for the same values of γ . The multiplicities in the case of the composite collision are much higher.

TABLE I

γ	$N=$	0	1	2	3	4	5	6	7	8	9	10	11	12	13	N
2.1		55	35	9	1											0.6
		58	37	5												0.5
3.5		2	12	27	30	19	8	2								2.8
		6	36	40	15	3										1.7
5.1				2	9	18	25	23	14	6	2	1				5.4
				8	29	37	20	5	1							2.9
7.0					2	6	13	20	22	18	11	5	2	1		8.0
				1	8	25	34	22	8	2						4.0
11.5		—		—	—	—	—	—	—	—	—	—	—	—	—	—
					3	11	24	29	20	9	3	1				6.0

TABLE II

γ	$N=$	0	1	2	3	4	5	6	7	N
2.1		49	47	4						0.6
3.5		9	59	30	2					1.2
5.1		2	31	46	18	3				1.9
7.0			13	40	33	11	2			2.5
11.5			2	15	34	31	14	3	1	3.5

TABLE I shows relative probabilities for the production of various numbers N of pions in a nucleon-nucleus collision. In each row the first line gives results obtained from equation (13) and the second line those obtained after division by $N!$.

TABLE II shows Fermi's results for the nucleon-nucleon collision. N is the average number of pions produced.

ACKNOWLEDGMENTS

It is a pleasure to express my thanks to Prof. D. S. Kothari and Dr. F. C. Auluck for suggesting the problem and for helpful advice.

REFERENCES

- Cocconni, G., 1954, *Phys. Rev.*, **93**, 1107.
Fermi, E., 1950, *Progr. Theoret. Phys.*, **5**, 570.

THE EMISSION SPECTRUM OF BROMINE

By P. B. V. HARANATH AND P. TIRUVENGANNA RAO

DEPARTMENT OF PHYSICS, ANDHRA UNIVERSITY, WALTAIR

(Received for publication, April 7, 1955)

Plates V A-B

ABSTRACT. The emission spectrum of bromine as excited by a high frequency high power oscillator is photographed in the visible region, λ 6400 to λ 4400 and is found to consist of as many as 300 bands as against only 80 bands reported previously by Uchida and Ota in the region λ 8700 to λ 5000. Tentative vibrational analysis of the bands on the basis of two systems suggested by Uchida and Ota are considerably extended to include all the bands down to λ 4400. This has led to a redetermination of the following vibrational constants

	ω'_e	$x'_e\omega'_e$	ω''_e	$x''_e\omega''_e$	ν_e
System I	190.0	1.0	376.0	1.25	19290.0
System II	152.0	0.35	376.0	1.25	18782.0

The vibrational assignments are well supported by an extensive study of the bromine isotope effect.

INTRODUCTION

The emission spectra of chlorine and bromine in the visible region are well known. Uchida and Ota (to be referred to as UO) (1928) first reported three systems in the emission spectrum of chlorine. Later Elliot and Cameron (1938) reinvestigated these bands and offered a different analysis from the one proposed earlier by UO, on the basis of two systems ascribed to the transition $^2\text{II} - ^2\text{II}$. From the even multiplicity of the systems involved they considered that the emitting molecule may be the ionised molecule Cl_2^+ . In view of the uncertainty in the analysis proposed earlier and the number of systems involved in the spectrum of Cl_2^+ , Howell (1953) suggests that the main difficulty in the analysis of the emission bands of Cl_2^+ is due to the fact that the ^2II separation of the ground state is of the same order of magnitude as the ground state vibrational frequency. Hence he concludes that a study of the spectrum of Br_2^+ would be more helpful in determining the nature of electronic levels and the relative order of values of ω'_e and ω''_e . In the light of this suggestion it is considered worthwhile to undertake a detailed study of the emission band spectrum of bromine.

UO (1928) were the first to suggest the vibrational analyses of the emission bands of bromine in the region λ 6700— λ 5000 as belonging to two systems. The following vibrational quantum formulae were derived from the analyses.

$$\begin{aligned} \text{System I} \quad \nu &= 17325.80 + 191.45n' - 1.05n'^2 - 360.65n'' + 0.65n''^2 \\ \text{System II} \quad \nu &= 16105.00 + 152.40n' - 0.40n'^2 - 361.70n'' + 1.62n''^2 \end{aligned}$$

It is noteworthy that the intensity distribution in both the systems is of the open Franck-Condon parabola type which is normally to be expected for such divergent values of ω_e' and ω_e'' . However, they admit that the quantum numbering of the bands is quite arbitrary as the assignments were not supported by bromine isotope effect. The bands in these two systems, as in the case of chlorine, bear no relationship with absorption bands of the neutral bromine molecule. The present paper describes the results of the authors obtained on the emission spectrum of bromine which is found to consist of as many as 300 bands in the region $\lambda 6700$ down to $\lambda 4400$.

EXPERIMENTAL

UO excited the spectrum through an induction coil discharge generating bromine by heating silver bromide. In the present work the spectrum of bromine was excited in an electrodeless discharge from a high frequency high power oscillator. For photographing the bands a pure sample of cupric bromide was spread uniformly in the middle of the tube. The discharge tube was made of pyrex glass of length 30 cm and diameter 1.6 cm and was drawn into an adapter at one end for evacuation by a Cenco Hyvac pump. The other end was fitted with a glass window by means of shellac. The heat of the electrodes was found sufficient to maintain a steady column of bromine vapour. The discharge which appears rose-red in colour could be maintained for several hours free from any traces of either the usual impurity bands or those of CuBr. The design of the discharge tube was slightly altered when the spectrum was excited using pure fuming liquid bromine. In this case the tube having the same diameter was closed at one end and was provided with two side limbs to one of which was connected a small bulb containing pure liquid bromine. The pressure of bromine inside the discharge tube was regulated by adjusting a pinch-cock attached to the pressure tubing connecting the bromine container to the discharge tube. The other limb was connected to a Cenco Hyvac pump through a liquid air trap. It was found that at some optimum pressure the development of the spectrum was more satisfactory than in the case of cupric bromide.

Photographs of the spectra were taken both on Fuess and three-prism glass Littrow spectrographs, using Ilford Special Rapid panchromatic plates. Exposures varying from one to two hours were found necessary to obtain the bands on the Fuess instrument while longer exposures of six hours were necessary on the Littrow instrument. The development of the spectrum which extends from $\lambda 6400$ — $\lambda 4400$ was found to be better in the region below $\lambda 5000$ in the Fuess spectrograms. Hence measurements of band heads in the region $\lambda 6400$ to $\lambda 5000$ were made on Littrow plates and below 5000 on Fuess plates. A number of plates were measured and the mean wavelengths were deduced using international iron arc standards. Measurements on different plates seldom differ by more than two wave number units. Table I records the band head data and assignments.

TABLE I

Authors		Uchida, Ota, Wave- number	Int	Assignment	
Wave- length	Wave- number			System I ν', ν''	System II ν', ν''
6604.1		15137.9			3,11
6579.0		15195.7			
6540.7		15284.6			4,11
6519.7		15333.9			2,10
6499.6		15381.7		1,11	0,9
6476.6		15435.9			5,11
6455.1		15487.3			3,10
6435.9		15533.5			1,9
6421.2		15569.1		2,11	
6413.7		15587.3		4,12	6,11
6403.0		15613.3			
6392.8		15638.2			4,10
6372.1		15689.0			2,9
6366.8	15702i		1		
6357.5	15725	15725.1	2	1,10	
6343.4	15760		1	3,11	
6338.1	15773		1	5,12	
6333.0	15786	15786.4	2		5,10
6314.8	15831	15829.9	0		
6310.5	15842	15841.9	2		3,9
6299.5	15870		1		
6290.0	15894	15893.6	2	0,9	
6282.2	15914	15914.1	3	2,10	
6273.6	15935	15935.1	4	4,11	6,10
6268.1	15949	15949.1	2	6,12	
6259.1	15972i	15970.0	1		
6251.3	15992	15991.7	2		4,9
6244.7	16009i		1		
6225.5	16058i		1		
6217.3	16080	16080.4	4	1,9	7,10

TABLE 1 (*contd.*)

Authors		Uchida, Ota Wave-number	Int	Assignment	
Wave-length	Wave-number			System I v', v''	System II v', v''
6106.6	16107	16107.3	3	3,10	
6105.0	16112i		1		
6200.5	16123	16123.0	2	5,11	
6194.5	16139	16139.1	3		5,9
6188.0	16156i		1		
6182.5	16170	16172.0	0		
6152.1	16250		1	0,8	
6145.0	16269	16269.4	3	2,9	
6140.8	16280i		3		
6137.7	16288	16287.7	3	4,10	6,9
6133.3	16300	16300.4	4	6,11	
6127.0	16317i	16316.1	2		
6122.0	16330i		1		
6115.8	16347	16344.4	3		4,8
6110.1	16362i		2		
6089.1	16418i		3		
6083.2	16434	16434.4	8	1,8	7,9
6077.3	16450i		3		
6074.7	16457	16457.4	8	3,9	
6068.1	16475	16474.8	8	5,10	
6060.0	16497		4		5,8
6055.3	16510i		1		
6033.4	16570i		4		
6028.0	16585	16585.2	8		8,9
6021.7	16602i	16601.7	3		
6013.0	16626	16625.7	4	2,8	
6008.0	16641	16640.9	1		6,8
6004.7	16649	16649.2	4	4,9	
5999.1	16665		2		
5980.2	16716i		4		

TABLE 1 (*contd.*)

Authors		Uchida, Ota Wave- number	Int	Assignment	
Wave- length	Wave- number			System I ν', ν''	System II ν', ν''
5976.1	16729	16729.5	7		9,9
5972.4	16739i		4		
5959.4	16776i		4		
5954.5	16789		8		7,8
5950.0	16802i		4		
5945.7	16814	16814.2	4	3,8	
5940.8	16828	16828.3	4	5,9	
5935.4	16843		3		
5909.6	16917i		5		
5905.0	16930	16930.1	8		8,8
5901.2	16941i		5		
5891.1	16970		5		
5885.6	16986		4	2,7	
5879.7	17000	17000.3	6	6,9	6,7
5876.5	17012i		3		
5855.4	17073i		2		
5852.3	17083	17083.1	5		9,8
5848.7	17093i		3		
5830.2	17147		8		7,7
5826.5	17158i		5		
5821.2	17174	17178.2	6	3,7	
5818.3	17182		8	7,9	
5814.0	17195		2		
5804.6	17223	17223.2	4		10,8
5801.3	17233i		4		
5776.1	17308		2		
5770.4	17325		2		
5762.7	17348i		3		
5758.4	17361	17361.4	7	6,8	6,6
5754.7	17372i		2		

TABLE 1 (*contd.*)

Authors		Uchida, Ota Wave- number	Int	Assignment	
Wave- length	Wave- number			System I v', v''	System II v', v''
5731.8	17442	17442.3	4		9,7
5728.6	17451i		2		
5711.3	17504i		2		
5708.7	17512		3		7,6
5703.6	17528		4	9,9	
5699.6	17540	17539.3		7,8	
5697.0	17548i		3		
5690.6	17568i		2		
5684.7	17586	17586.2	4		10,7
5679.0	17604i		2		
5666.4	17643		1		
5662.7	17654i	17650.5	2		
5660.0	17663		4		8,6
5657.7	17670i		2		
5644.9	17710	17710.8	4	8,8	
5642.2	17718	17718.6	5	6,7	
5639.9	17726i		3		
5620.2	17788		1		
5615.3	17804		2		9,6
5602.0	17846		3		
5594.2	17871		4		7,5
5589.4	17886		3	9,8	
5586.0	17897	17896.6	5	7,7	
5583.2	17906		2	5,6	
5575.2	17932		0		
5571.4	17944		1		10,6
5548.1	18019		1		8,5
5543.3	18035		1		
5532.5	18070	18070.3	1	8,7	
5529.1	18081	18080.7	1	6,6	

TABLE I (contd.)

Authors		Uchida, Ota, Wave- number	Int	Assignment	
Wave-length	Wave-number			System I v', v''	System II v', v''
5525.6	18093		1		11,6
5504.1	18163		1		9,5
5483.6	18231		1		12,6
5480.0	18243	18243.1	2	9,7	
5476.3	18255	18254.7	2	7,6	
5460.0	18310		1		10,5
5434.4	18396		2	12,8	
5428.6	18416	18415.8	2	10,7	
5425.9	18425		2		
5424.2	18431		2	8,6	
5420.4	18444		2	6,5	
5417.4	18454		0		11,5
5388.3	18554		1		
5377.2	18592	17592.5	1		12,5
5373.3	18604	18604.3	1	9,6	
5368.1	18623		1	7,5	
5355.9	18666		1		10,4
5341.0	18718		0		
5335.6	18737		1		13,5
5330.6	18754		1	12,7	
5325.1	18774	18774.1	1	10,6	
5318.7	18796	18788.6	1	8,5	
5314.0	18813		1		11,4
5309.4	18829		1		
5304.2	18848		1		
5296.3	18876		2		14,5
5290.7	18896		2		
5285.2	18915	18914.4	4	13,7	
5277.3	18944	18944.5	4	11,6	
5273.3	18958		3		12,4

TABLE I (contd.)

Authors		Uchida, Ota Wave- number	Int	Assignment	
Wave- length	Wave- number			System I <i>v',v''</i>	System II <i>v',v''</i>
5271.1	18966		3	9,5	
5266.3	18983	18981.9	2		
5264.9	18988		2	7,4	
5261.2	19001		1		
5256.3	19019		2		15,5
5249.5	19044		1		
5242.5	19070		1		
5234.1	19100		2		13,4
5280.8	19112	19112.5	3	12,6	
5224.6	19135		2	10,5	
5211.9	19181		2		11,3
5196.1	19240		2		14,4
5191.2	19258		2		
5186.6	19275		3	13,6	
5178.9	19304	19304.1	2	11,5	
5173.3	19325		3		12,3
5170.0	19337	19341.4	3	9,4	
5156.2	19386		1		15,4
5155.2	19392i		1		
5153.6	19398		2	16,7	
5142.8	19439	19440.7	4	14,6	
5138.7	19455		2		
5134.1	19472	19471.8	4	12,5	13,3
5126.2	19502		1	10,4	
5119.6	19527		1	8,3	
5113.4	19551		2		11,2
5105.3	19582		4		
5099.9	19603	19599.7	4	15,6	14,3
5096.0	19618		1		
5089.2	19644		2	13,5	

TABLE I (contd.)

Authors		Uchida, Ota Wave- number	Int	Assignment	
Wave- length	Wave- number			System I v', v''	System II v', v''
5081.2	19675		2	11,4	
5075.5	19697		3		12,2
5073.9	19703i		3	9,3	
5066.1	19733		2		
5061.9	19750		3		
5059.7	19758		5	16,6	15,3
5049.1	19800		4	14,5	
5038.9	19840		4	12,4	13,2
5032.5	19865		4	10,3	
5024.9	19895		4	8,2	
5020.4	19913		3	17,6	
5018.2	19922		4		11,1
5016.2	19930i		3		
5008.3	19961		5	15,5	
4996.5	20008		2	13,4	
4988.4	20041		2	11,3	
4972.8	20104		0		
4968.5	20121		2	16,5	
4966.4	20130		1		15,2
4963.8	20140i		1		
4957.7	20165		0	14,4	
4945.7	20214		6	12,3	13,1
4941.1	20233		3	10,2	
4933.4	20264i		4		
4930.8	20275		5	17,5	15,2
4928.3	20285i		4		
4923.5	20305		1		
4910.7	20358		2		14,1
4905.5	20380		3	13,3	
4898.2	20410		3	11,2	

TABLE I (*contd.*)

Authors		Uchida, Ota Wave- number	Int	Assignment	
Wave- length	Wave- number			System I v', v''	System II v', v''
4891.0	20440		3		
4885.1	20465		3		
4878.5	20492		2	16,4	
4875.7	20504		3		15,1
4872.8	20516i		2		
4866.9	20541		4	14,3	
4858.0	20579		4	12,2	
4855.3	20590		8		13,0
4852.5	20603i		3		
4848.7	20618		3		
4845.0	20634i		1		
4842.3	20646		2	17,4	16,1
4839.3	20658i		1		
4830.5	20696i		2		
4828.8	20703		3	15,3	
4827.2	20710i		2		
4824.4	20722i		4		
4821.9	20733		4		14,0
4818.8	20746i		4	13,2	
4810.5	20782		1	11,1	
4797.0	20841		2		
4792.5	20860		3	16,3	
4790.3	20870i		2		
4788.0	20880		3		15,0
4782.6	20903		0	14,2	
4780.2	20914i		0		
4768.9	20963		1		
4766.7	20973i		0		
4756.0	21020		5	17,3	16,0
4747.8	21056i		2		

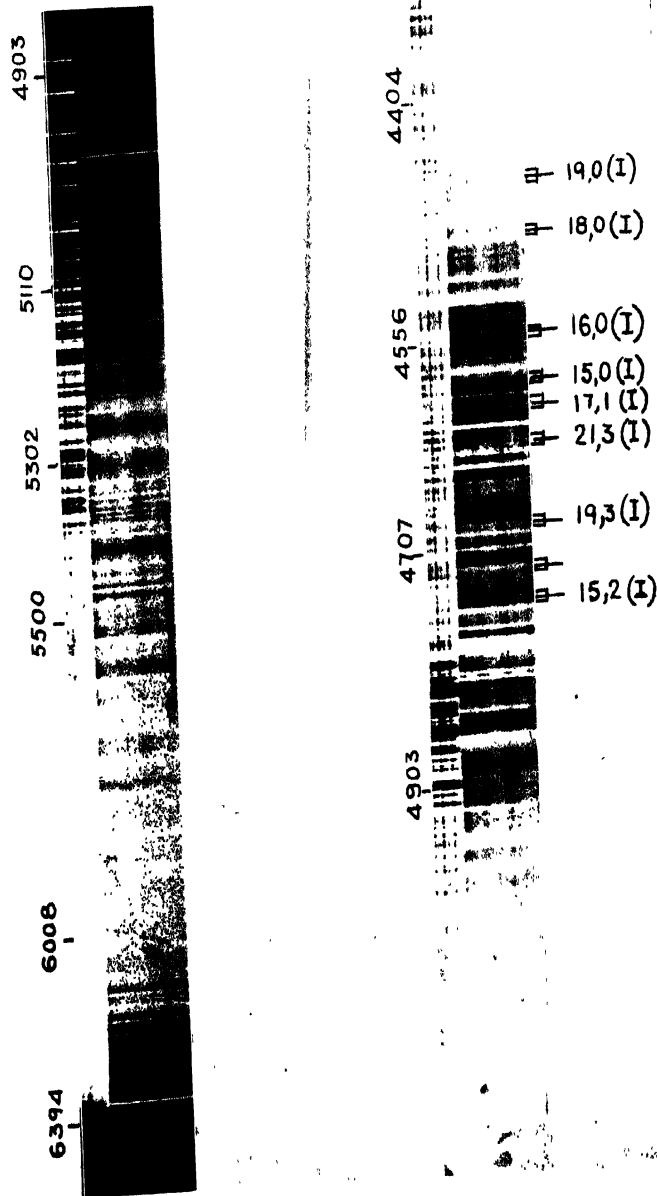
TABLE I (contd.)

Authors		Uchida, Ota Wave- number	Int	Assignment	
Wave- length	Wave- number			System I v', v''	System II v', v''
4745.9	21065		3	15,2	
4743.2	21077i		2		
4734.8	21114		2	13,1	
4726.4	21152		3	11,0	
4722.2	21171		4	18,3	
4713.0	21212		0		
4708.8	21231		1	16,2	
4706.5	21241i		0		
4698.8	21276		1	14,1	
4695.7	21290i		0		
4691.3	21310i		2		
4689.1	21320		4	19,3	
4686.2	21333i		2		
4673.9	21389		2	17,2	
4670.6	21404i		1		
4664.6	21432i		2		
4662.3	21443		4	15,1	
4659.4	24156i		2		
4656.4	21470		4	20,3	
4653.9	21481i		3		
4652.4	21488		2	13,0	
4647.9	21509		2		
4640.5	21543		3	18,2	
4627.6	21603		3	16,1	
4625.1	21615		3	21,3	
4622.2	21629i		2		
4619.2	21643i		1		
4616.3	21656		1	14,0	
4608.9	21691		0	19,2	
4606.3	21703i		0		

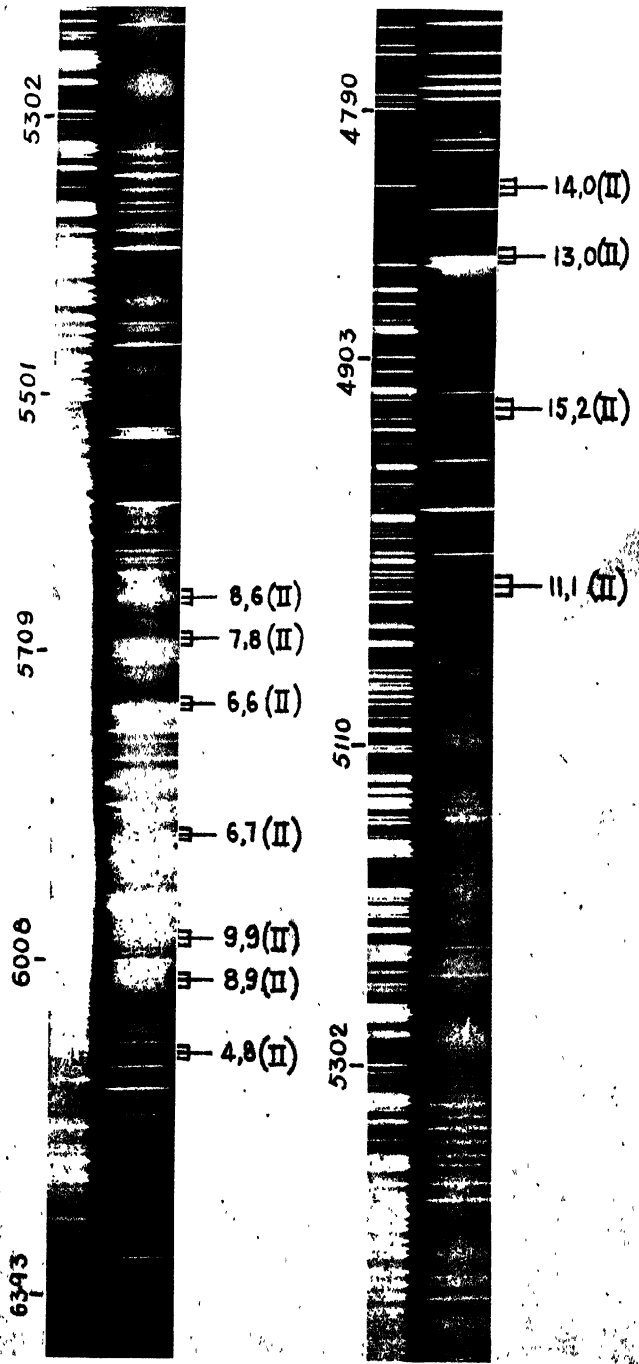
TABLE I (*contd.*)

Authors		Uchida, Ota Wave- number	Int.	Assignment	
Wave- length	Wave- number			System I v', v''	System II v', v''
4596.8	21748i		1		
4594.3	21760		2	17,1	
4590.4	21778i		1		
4587.1	21791		0		
4584.6	21806i		1		
4581.8	21819		2	15,0	
4578.5	21835i		1		
4567.1	21890i		2		
4563.6	21906		3	18,1	
4560.4	21992i		1		
4556.8	21939		1		
4553.1	21957i		1		
4549.7	21973		2	16,0	
4546.0	21991		2	21,2	
4542.5	22008i		1		
4536.9	22035		1		
4532.4	22057		1		
4520.6	22115i		2		
4517.2	22131		3	17,0	
4515.8	22138		3	22,2	
4507.3	22180		3		
4504.1	22196i		1		
4500.8	22212		4	20,1	
4492.7	22252		2		
4489.0	22270i		2		
4485.8	22286		3	18,0	
4482.1	22305 i		2		
4469.8	22366		0	21,1	
4463.1	22400		1		
4458.8	22421i		1		

HARANATH & RAO



Emission bands of bromine-1 Fues spectrograms. Isotopes for some of the bands are bracketed. The longer limbs represent the component due to the abundant molecule.



Emission bands of bromine (Littrow spectrograms). Isotopes for some of the bands are bracketed. Longer limbs represent the component due to the abundant molecule.

TABLE I (contd.)

Authors		Uchida, Ota Wave- number	Int	Assignment	
Wave-length	Wave-number			System I v', v''	System II v', v''
4455.5	22438		2	19,0	
4451.9	22456i		1		
4449.1	22470		1		
4447.2	22480		1		
4444.7	22492		1		
4433.5	22549		1		
4430.6	22564i		1		
4427.3	22581		2	20,0	
4419.5	22621		1		
4416.7	22635		1		
4414.2	22648		1		
4394.8	22748		1		

Note : The wavenumbers marked with the letter "i" are the isotopic components of the neighbouring bands.

P L A T E S

The spectrum extending from λ 6700 to λ 4400 consists of more than 300 bands as against only 80 bands reported by UO in the region λ 6700 to λ 5000. Plate VA is a reproduction of the Fuess spectrogram and is shown in two strips. Among these some are red degraded, some are diffuse and others appear line-like. There is a gradual fall in the intensity of the spectrum towards the shorter wavelengths. Bands on the less refrangible side appear unresolved, probably due to the lower dispersion. Below λ 5300 the bands appear sharp and well resolved. Below λ 4400 there appears a continuum overlaid by perhaps, two or three groups of discrete bands.

Plate VB is the reproduction of the spectrum in the region λ 6400 to λ 4800 recorded on the glass Littrow instrument and is shown in two strips.

TABLE II
System I
Vibrational scheme due to Uchida and Ota

$\begin{smallmatrix} v'' \\ \backslash \\ v' \end{smallmatrix}$	0	1	2	3	4	5	6
0					15893.6		15195.7
1				16434.4	16080.4	15725.1	15381.7
2				16625.7	16269.4	15914.1	15569.1
3				16814.2	16457.4	16107.3	
4				16993.1	16649.2	16287.7	
5				17178.2	16828.3	16474.8	16123.0
6		18080.7	17718.6	17361.4	17000.3		16300.4
7		18254.7	17896.6	17539.3			
8			18070.3	17710.8			
9		18604.3	18243.1				
10		18774.4	18415.8				
11	19304.1	18944.5	18584.2				
12	19471.8	19112.5	18749.1				
13			18914.4				
14		19440.7					
15		19599.7					

TABLE III
System II
Vibrational scheme due to Uchida and Ota

$\begin{smallmatrix} v'' \\ \backslash \\ v' \end{smallmatrix}$	0	1	2	3	4
0			15381.7		
1			15533.5		
2			15689.0	15333.9	
3			15841.9	15478.3	15137.9
4			15991.7	15638.2	15284.6
5			16139.1	15786.4	15435.9
6		16640.9	16287.7	15935.1	15587.3
7		16789.4	16434.4	16080.4	
8		16930.1	16585.2		
9	17442.3	17083.1	16729.5		
10	17586.2	17233.2			

ANALYSIS

As has already been mentioned the bands obtained by UO in the region $\lambda 6700$ to $\lambda 5000$ were analysed into two systems which are shown in Tables II and III. With the prominent band heads among the 80 bands they formed a small number of genuine progressions. The vibrational formulae derived from the analyses are given in the introduction. The lower state is common for both the systems. The intensity distribution in the two systems is of an open Franck-Condon parabola type which is in keeping with such divergent values of ω'_e and ω''_e . However, the vibrational assignments were not supported by the study of bromine isotope effect and are quite arbitrary.

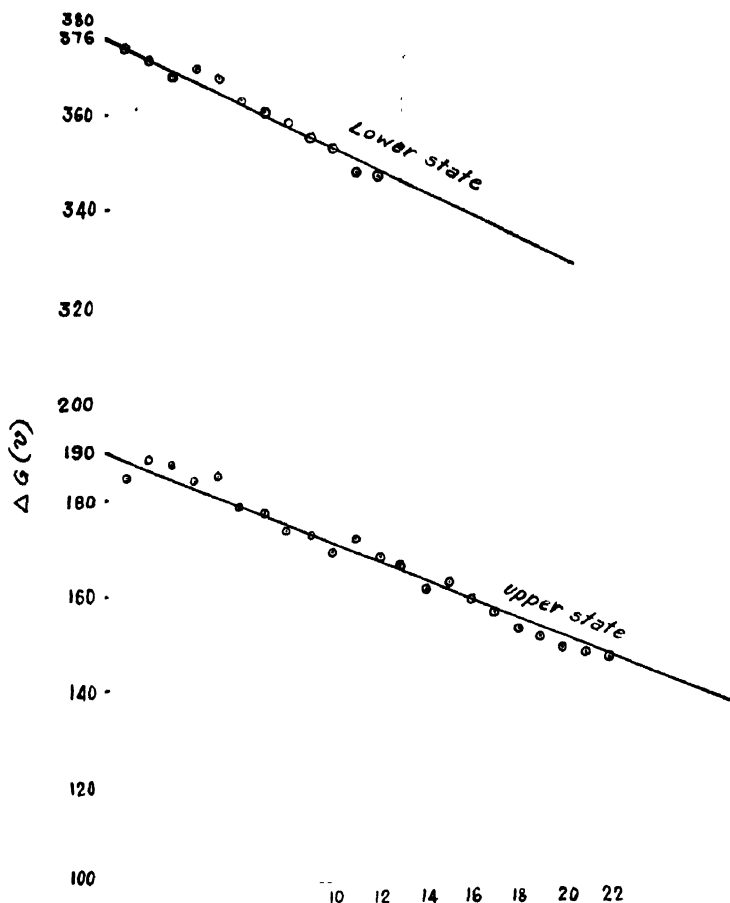


Fig. 1 System I

With the present data of more than 300 bands in the extensive region $\lambda 6700$ to $\lambda 4400$ it is found possible to extend the above two analyses considerably.

Not only some of the previous progressions are considerably extended, but, many more new progressions could be developed in both the systems. The newly formed vibrational schemes are shown in Tables IV and V. This extension has necessitated a renumbering of the bands and also a redetermination of the vibrational constants. The constants are extrapolated by drawing the usual $\Delta G(v)-v$ curves which are found to be linear. These curves are shown in figures 1 and 2.

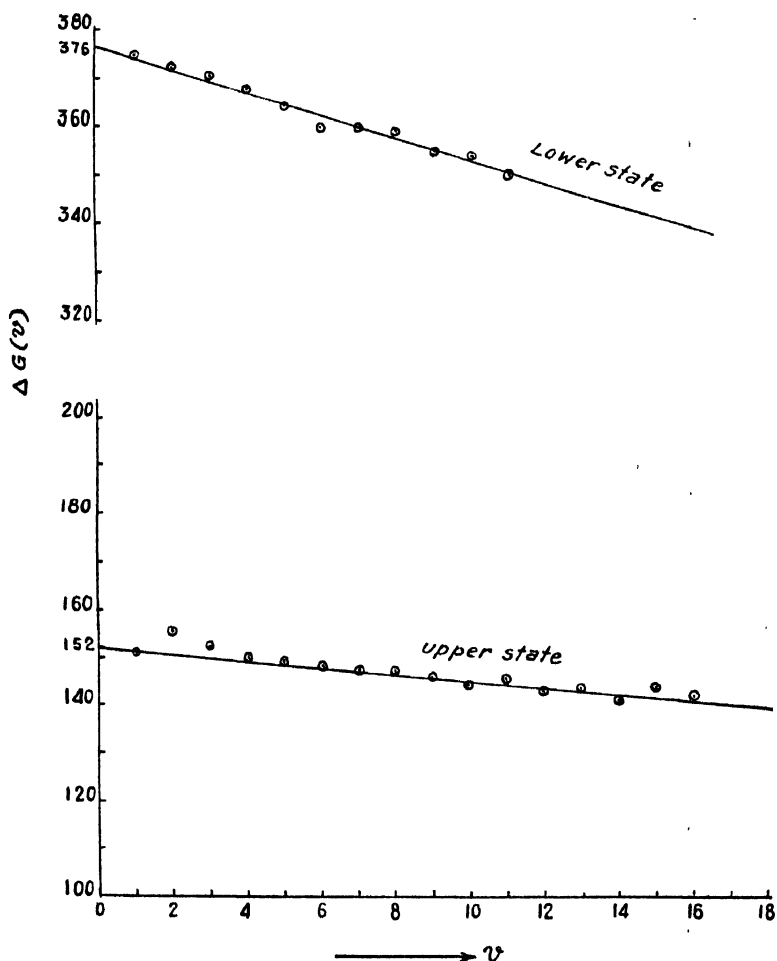


Fig. 2. System II

The following vibrational formulae represent the two systems.

$$\text{System I } \nu = 19290 + 190.0(v' + \tfrac{1}{2}) - 1.0(v' + \tfrac{1}{2})^2 - 376.0(v'' + \tfrac{1}{2}) + 1.25(v'' + \tfrac{1}{2})^2$$

$$\text{System II } \nu = 18782 + 152.0(v' + \tfrac{1}{2}) - 0.35(v' + \tfrac{1}{2})^2 - 376.0(v'' + \tfrac{1}{2}) + 1.25(v'' + \tfrac{1}{2})^2$$

TABLE IV

λ	0	1	2	3	4	5	6	7	8	9	10	11	12
0									16250	15894		15196	
1									16434	16080	15725	15382	
2								16986	16626	16269	15914	15569	
3								17174	16814	16457	16107	15760	
4								17361	17003	16649	16288	15935	15587
5							17906	17540	17182	16828	16475	16123	15773
6					18444	18081	17719	17361*				16300	15949
7			18988		18623	18255	17897	17540*					
8					18796	18431	18070	17710					
9			19895	19527	19337	18966	18604	18243	17886				
10			×		19502	19135	18774	18416					
11		20782	20410	20041	19675	19304	18944						
12		21320	20579	20214	19840	19472	19112	18754					
13		21488	20746	20380	20008	19644	19275	18915					
14		21656	21276	20903	20541	20165	19800	19439					
15		21819	21443	21065	20703	×	19861	19603					
16		21973	21603	21231	20860	20492	20121	19758					
17		22131	21760	21389	21020	20646	20275	19913					
18		22286	21906	21543	21171	×							
19		22438	×	21691	21320*								
20	22581	22212		21470									
21			21991	21617									
22			22138	×	21404								

Note: The bands marked with (*) occur twice. The places marked × are superposed by atomic lines.

TABLE V

	0	1	2	3	4	5	6	7	8	9	10	11
0										15382		
1										15533		
2										15689	15334	
3										15842	15487	15138
4									16347	15992	15638	15285
5									16497	16139	15786	15436
6							17361	17003	16641	16288	15935	15587
7						17871	17512	17147	16789	16434	16080	
8						18019	17663	×	16930	16585		
9					×	18163	17804	17442	17083	16729		
10					18666	18310	17944	17586	17223			
11		19922	19551	19181	18813	18454	18093					
12		×	19697	19325	18958	18592	18231					
13	20590	20214	19840	19472	19100	18737						
14	20733	20358	×	19603	19240	18876						
15	20880	20504	20130	19758	19386	19019						
16		20646	×									

Note : The places marked × are superposed by atomic lines.

The lower state 376.0 is again common for both the systems. The intensity distribution in both the systems is still of open Franck-Condon parabola type and is consistent with the order of ω'_e and ω''_e values obtained above. An examination of the vibrational arrays shown in Tables IV and V reveals that there are bands common to both the systems. This is a feature which can also be seen from the vibrational arrays of UO shown in Tables II and III.

ISOTOPE EFFECT

Further confirmation of these analyses could be obtained from a study of the bromine isotope effect. It is well known that bromine has got two isotopes of mass numbers 79 and 81, out of which three components due to the three molecules are to be observed in its molecular spectrum. The three molecules are $(\text{Br}^{79}\text{Br}^{79})$, $(\text{Br}^{79}\text{Br}^{81})$, $(\text{Br}^{81}\text{Br}^{81})$. The relative abundance ratio of these molecules is as 1:2:1 respectively. In the band spectrum of Br_2 , for bands on the violet side of the system origins, i.e. with $v > v_e$ the separation of the isotopic component $(\text{Br}^{79}\text{Br}^{79})$ with respect to the component of the more abundant molecule $(\text{Br}^{79}\text{Br}^{81})$ is positive and the corresponding separation for the component of $(\text{Br}^{81}\text{Br}^{81})$ is negative. For the bands on the red side of the system origins, i.e., with $v < v_e$ the opposite is the case. The isotope separations with respect to the more abundant molecule, $\Delta\nu$, are calculated according to the formula

$$\nu^i - \nu = (\rho - 1) [\omega'_e(v' + \frac{1}{2}) - \omega''_e(v'' + \frac{1}{2})] - (\rho^2 - 1) [x'_e \omega'_e(v' + \frac{1}{2})^2 - x''_e \omega''_e(v'' + \frac{1}{2})^2].$$

An examination of the vibrational schemes shown in Tables IV and V, reveals bands with large differences in the values of v' and v'' . For such bands the isotope separations for the less abundant molecules calculated from the above formula are found to be large and may be expected to be resolved even under the low dispersion of the Fuess instrument. For example, the calculated separations of the two components for 15,0 band in system I are 16.2 and 13.8. The isotopic components for some of these bands are expected to coincide with the position of the main bands assigned to the same system. In Table I, some of the main bands occur as isotopic heads of the neighbouring bands belonging to the same system.

For a large number of the bands the agreement between the observed³ and calculated separations as can be seen from Table VI is quite satisfactory. On Plates VA and VB the isotopic components are bracketted for some of the bands.

TABLE VI

Isotope effect

SYSTEM I.						SYSTEM II.					
(Br ⁷⁹ Br ⁸¹) ν' ν''		(Br ⁷⁹ Br) ⁷⁹ Cal. Obs.		(Br ⁸¹ Br ⁸¹) Cal. Obs.		(Br ⁷⁹ Br ⁸¹) ν' ν''		(Br ⁷⁹ Br ⁷⁹) Cal. Obs.		(Br ⁸¹ Br ⁸¹) Cal. Obs.	
15,	0	16.2	16	13.8	13	13,	0	13.0	13	11.3	11
16,	0	17.0	18	14.8	16	14,	0	14.0	13	12.2	11
17,	0	18.0	*	15.8	16	11,	1	8.2	8	7.1	9
18,	0	18.7	19	16.8	16	15,	1	12.4	12	10.8	12
19,	0	19.6	18	16.8	17	16,	1	13.4	12	11.7	12
20,	0	20.3	*	17.8	17	15,	2	9.9	10	8.6	9
15,	1	13.5	13	11.5	11	16,	2	10.9	11	9.5	11
16,	1	14.3	14	12.5	*	6,	6	9.7	13	8.4	11
17,	1	15.3	18	13.5	12	7,	6	8.6	8	7.4	*
18,	1	16.0	16	14.5	16	8,	6	7.5	9	6.5	7
20,	1	17.6	*	15.5	16	6,	7	12.1	15	10.6	11
14,	2	10.1	13	8.8	*	7,	7	11.0	*	9.6	11
15,	2	11.0	12	9.3	9	9,	7	8.9	9	7.8	9
19,	2	14.4	12	12.3	*	4,	8	16.4	17	14.5	15
21,	2	15.9	17	13.3	13	6,	8	14.4	15	12.7	*
15,	3	8.4	7	7.0	7	7,	8	13.3	13	11.7	13
19,	3	11.8	13	10.0	10	8,	8	13.3	13	10.8	11
20,	3	12.5	11	11.0	14	9,	8	11.2	10	9.9	10
21,	3	13.3	14	11.5	12	10,	8	10.2	10	8.8	10
2,	7	15.7	16	13.8	17	4,	9	18.9	20	16.5	17
4,	7	13.2	13	11.6	11	5,	9	17.9	17	15.5	17
5,	7	12.0	12	10.5	8	6,	9	16.9	19	14.7	*
6,	7	10.8	9	9.4	7	8,	9	14.7	15	12.8	17
7,	7	10.0	11	8.5	9	9,	9	13.7	13	11.9	10
8,	7	8.6	*	7.5	11	6,	10	19.1	21	16.8	14

TABLE VI (Contd.)

SYSTEM I				SYSTEM II	
(Br ⁷⁹ Br ⁸¹) <i>v'</i> <i>v''</i>		(Br ⁷⁹ Br ⁷⁹) Cal. Obs.		(Br ⁸¹ Br ⁸¹) Cal. Obs.	
2,	8	18.0	*	15.9	15
3,	8	16.8	*	14.7	14
4,	8	15.5	17	13.7	13
6,	8	13.1	13	11.5	11
7,	8	12.3	12	10.6	10
0,	9	23.0	24	20.1	20
1,	9	21.8	22	18.9	*
2,	9	20.5	19	17.9	19
3,	9	19.3	23	16.7	18
4,	9	18.0	23	15.7	16
5,	9	16.8	14	14.6	15
1,	10	24.0	22	21.0	*
2,	10	22.7	20	20.0	21
3,	10	21.5	27	18.8	16
5,	10	19.0	18	16.7	22
5,	11	21.4	16	18.7	16
6,	11	20.2	20	17.6	17

Note : The places marked (*) are superposed by atomic lines.

CONCLUSIONS

In the foregoing pages, the vibrational analyses of the emission bands of bromine, as belonging to two different systems, are reported. As has already been pointed out, these emission bands do not bear any relationship with the absorption bands due to the neutral bromine molecule. Further, the vibrational frequency 376 cm^{-1} which is common to both the above systems does not correspond to any one of the vibrational frequencies known till now to the neutral molecule. It is also interesting to note that this frequency comes nearer to the value 361 cm^{-1} predicted by Mulliken (1934) as the most probable value of the ground state of the ionised molecule Br_2^+ . The above considerations will lead one to con-

jecture that the emitter of the above two systems may be the ionised molecule Br_2^+ . However, confirmation of this view can only be obtained by a study of the rotational analysis of some of these bands which will also lead to a clear understanding of the nature of the levels involved. Work in this direction is in progress.

ACKNOWLEDGMENT

The authors wish to express their grateful thanks to Prof. K. R. Rao for his kind interest in the work.

REFERENCES

- Elliot, A., and Cameron, W. H. B., 1937, *Proc. Roy. Soc. A.*, **158**, 681.
" 1938, *Ibid* **164**, 531.
Howell, H. G., 1953, *Proc. Phys. Soc. A.*, **66**, 759.
Mulliken, R. S., 1934, *Phys. Rev.*, **46**, 549.
Uchida, Y., and Ota, Y., 1928, *Jap. J. Phys.*, **5**, 53.
" *Ibid* **5**, 59.

ANALYSIS OF SKY-WAVE FIELD INTENSITY—PART II

By S. N. MITRA AND R. B. L. SRIVASTAVA

RESEARCH DEPARTMENT, ALL INDIA RADIO, NEW DELHI

(Received for publication, April 2, 1955)

ABSTRACT. In Part I of this paper, we have presented a statistical analysis of the field intensity of the internal short wave stations of All India Radio over the period of a complete solar cycle (1942–52). In this paper we have compared the results of our observations with theoretical deductions as described in the C.R.P.L. publication and Rawer's paper. It has been pointed out that both the theoretical methods are not strictly applicable to the calculation of sky-wave field intensity as observed in tropical countries. A modified method applicable to tropical conditions has yet to be developed.

1. INTRODUCTION

Accurate theoretical methods of calculating sky-wave field intensity and their verification by experimental observations are not available. In the theoretical calculations, one has to assume a number of parameters in order to arrive at a workable formula for calculating absorption in the ionosphere. Similarly, in experimental observations, difficulties often arise in eliminating some parameters which vitiate accurate determination of ionospheric absorption. The main draw-back in a theoretical calculation appears to lie in our inadequate knowledge of the ionosphere and the experimental observations become inaccurate due to difficulties in separating the sources of error. Since, our present day knowledge of the ionosphere does not permit accurate prediction of ionospheric absorption, it is only by experimental observations that one may approach the problem of verifying the accuracy of calculating the sky-wave field intensity. Sufficient experimental data are required so that a statistical analysis can be made and agreement with theoretical prediction attempted.

In this paper, an attempt has been made to compare the observed values of field intensity of internal short wave stations of All India Radio with the corresponding calculated values. The calculations have been made by two published methods namely, (1) C.R.P.L. method, as published by the National Bureau of Standards, Washington in their Circular No. 462 and (2) the S.P.I.M. method published by Rawer (1952). The two methods are not essentially different, except in the assumption of certain constants. We shall not attempt to evolve a theoretical formula for calculating the sky-wave field intensity. However, the results of calculations by the two methods mentioned above have been compared with the observed values of field intensities of certain A.I.R.

Stations, and few conclusions have been drawn therefrom. In Part I (Mitra and Srivastava, 1955) of this paper, we have presented a statistical analysis of the observed field intensities. We shall utilise some of the results contained in Part I.

2. THEORETICAL CONSIDERATION

We shall first describe the various factors involved in calculating the sky-wave field intensity. It is known that the most important aspect in all calculations of field intensity is the attenuation that a wave suffers in its path of propagation. The important factors which are to be taken into account in calculating the sky-wave field intensity are given below:

- (a) Spatial attenuation due to propagation through free space.
- (b) Non-deviative absorption in the ionosphere: This is the absorption that the wave suffers due to the portion of its path in the D-region and which is non-deviative. The reflection of the wave usually occurs at the E- or F-region. Experimental measurements have, however, shown that maximum absorption takes place in the D-region.
- (c) Deviative absorption: This is the absorption in the process of reflection of the wave. It is usually small except when the wave frequency approaches the maximum frequency that can be reflected by the layer.
- (d) Losses due to ground reflection: On multi-hop transmissions, some loss is likely to occur due to the reflection of the wave at the surface of the earth. The loss is, however, small at oblique incidence when the reflection coefficient approaches unity.
- (e) Losses due to Es: The nature of sporadic E ionisation is not yet known. Sometimes, Es behaves as a 'thin layer' producing partial reflection of the wave going through it; at other times, it reflects completely and the F-layer is 'blanketted out'. The effect of Es is not essentially one of absorption but the incident wave gets 'spread out' and an additional distribution of the wave-field in the system of reflected waves is produced.
- (f) Absorption during S.I.D.'s: The occurrence of irregular bursts of solar radiation and solar corpuscular emissions produce sudden ionospheric ionisation causing high absorption in the sky-wave field intensity. Similarly, there is an abrupt increase in E-region ionisation during meteoric showers. The effect of S.I.D. may, however, be neglected as all practical measurements are taken on quiet days.
- (g) Effect of fading: Fading of the received wave is one of the predominant factors in making absorption measurements most difficult. In practical measurements, one is mostly interested in short-term fading and the

effect of long-period fluctuation may be neglected. There are several types of fading of which the 'interference fading', 'polarisation fading' and 'skip fading' are predominant in producing rapid fluctuation of the received signal. It is difficult to assess the 'loss' in the signal strength due to fading since the origin of the phenomenon is not definitely known. In India 'surge' and 'flutter' types of fading are often present which, due to their very rapid nature, render measurements of the received signal strength more difficult than during interference or polarisation fading.

3. CALCULATION OF SKY- WAVE FIELD INTENSITY

We shall now briefly describe the two methods of calculating the sky-wave field intensity. In order to arrive at a workable formula, both the C.R.P.L. and the S.P.I.M. methods have considered mostly the effect of only spatial attenuation and non-deviative absorption. The C.R.P.L. method has, however, taken into account the effect of fading.

For spatial attenuation the C.R.P.L. method considers a reduction of field intensity according to an approximately inverse distance law. This may, perhaps, be applicable to short distance of propagation only, but for long distances the curvature of the ionospheric reflecting and refracting layers may have some effect. Rawer's (1952) S.P.I.M. method has taken into account an additional 'increase' of field intensity caused by such curvature of the ionospheric surface. This increase is due to what is called the 'focussing' effect of the reflecting layers on long distance circuits. The variation of field intensity with distance assumed in the S.P.I.M. method shows higher values than in the C.R.P.L. one. We shall compare in the following sections the observed values of field intensity with those calculated by the C.R.P.L. and S.P.I.M. methods. For this purpose, we shall consider only the night-time measurements of field intensity since in these calculations the D-layer absorption has been assumed to be negligible and the incident field intensity has been assumed to depend only upon spatial attenuation. It will be seen later in the paper that this view point is not strictly correct since the variation of the observed field at night is correlated with sunspot numbers. In other words, it appears that there are other controlling factors in addition to spatial attenuation in estimating the field intensity at night.

According to the C.R.P.L. method, the absorption is given by $S_o JQK_d$ where,

S_o is a function of frequency, J is the seasonal variation factor, Q is the solar cycle variation factor, K_d is the average value of diurnal absorption for the transmission path d .

The important assumptions in the C.R.P.L. method are :

(a) The diurnal variation factor K is related to the solar zenith angle χ by the relation

$$K = 0.142 + 0.858 \cos \chi$$

(b) The solar cycle variation factor Q is related to the sunspot number R by the relation :

$$Q = 1 + 0.005R.$$

(c) The seasonal variation factor J has the same value for different months in any particular season, namely, summer, winter and equinox.

The theoretical basis of the above assumptions is not known. The advantage of this method over the other lies in the quick way of calculating the sky-wave field intensity from readily available charts and nomograms.

The S.P.I.M. method of Rawer is, on the other hand, based on theoretical considerations and analysis of observations. Rawer considers two predominant causes for losses in ionospheric propagation. One is called the spatial attenuation δ_1 which also takes into account the focussing effect of the curved ionospheric layer on long distance propagation. δ_1 is independent of frequency and gives higher values of field intensity than what is obtained from the approximately $d^{-1.4}$ law as adopted by the C.R.P.L. The other factor δ_2 takes into account the non-deviative absorption in the ionosphere. According to Rawer

$$\delta_2 = \frac{p.430(1 + .0035\bar{R}) \cos^{3/4}\chi \sec \alpha_D}{(f \pm f_L)^2}$$

where p = number of multiple paths in a single mode of propagation.

\bar{R} = yearly average of the sunspot number,

χ = solar zenithal angle,

α_D = angle of incidence of the wave with the D-region,

f = wave frequency,

f_L = longitudinal component of the gyro-frequency.

\pm signs are for the ordinary and the extraordinary components.

The above formula is valid for quasi-longitudinal mode of propagation.

The total loss is, therefore, $\delta_1 + \delta_2$. The main difference between the C.R.P.L. and S.P.I.M. methods lies in the following :

- (i) The diurnal variation factor varies linearly with $\cos \chi$ in the C.R.P.L. method, whereas, it is $\cos^{3/4}\chi$ in the S.P.I.M. method. Rawer has taken this factor from the British observations lasting for about 10 years (Piggott, 1953). It may incidentally be mentioned that Appleton (1937) has earlier considered non-deviative absorption as due to the ionisation in a simple Chapman layer formed in an exponential atmosphere (Appleton-Beynon, 1940) and found that when $\nu^2 \ll (f \pm f_L)^2$, the diurnal variation factor is proportional to $(\cos \chi)^{3/2}$

- (ii) The solar cycle variation factor has been assumed to be $(1+0.005R)$ and $(1+0.0035\bar{R})$ in the C.R.P.L. and the S.P.I.M. methods respectively. Here again the assumption of the latter is based on the British observations.

Both the methods consider only the spatial attenuation and the non-deviative absorption. It may be pointed out, however, that the deviative absorption in the E-layer cannot always be assumed to be negligible specially for long distances of propagation. The C.R.P.L. method has assumed certain values to take into account the effect of short term fading. Piggott (1953) has suggested different ones.

In general, both the C.R.P.L. and the S.P.I.M. methods of calculating the incident sky-wave field intensity have certain limitations. Accurate determination of ionospheric absorption will depend upon a more precise knowledge of the mechanism of ionospheric propagation and the various factors contributing to the cause of ionospheric absorption.

4. EXPERIMENTAL OBSERVATIONS

We have so far dealt with the theoretical considerations involved in the calculation of field intensity. We shall now present an analysis of our measurements and compare them with theoretical calculations based on the C.R.P.L. and the S.P.I.M. methods.

Observed values of field intensity of the internal short wave stations of All India Radio at Bombay, Calcutta and Madras, are available for a complete solar cycle (1942-1952) on frequencies in the 3, 5, 7 and 9 Mc/s bands. The measurements have been taken at Delhi (Lat. $28^{\circ}35'N$; Long $77^{\circ}5'E$). The location and distances of transmitting stations from Delhi are given below:

Bombay	: Lat. $19^{\circ}0'N$	Long. $73^{\circ}0'E$.	Distance 1140 km.
Calcutta	: Lat $22^{\circ}30'N$	Long. $88^{\circ}30'E$.	Distance 1320 km
Madras	: Lat. $13^{\circ}0'N$	Long. $80^{\circ}15'E$.	Distance 1760 km.

The transmitters at all the stations are identical and radiate a power of 10kw. The aerial used is mostly a horizontal dipole situated $(7/16)\lambda$ above the ground.

In the analysis, two representative periods namely 1200-1400 and 2000-2200 IST, corresponding to periods of maximum and minimum absorption, have been considered. IST (Indian Standard Time) is $5\frac{1}{2}$ hours ahead of GMT. In order to arrive at the monthly value of field intensity, all measurements during 1200-1400 IST and 2000-2200 IST have been grouped together for each frequency and station and the average worked out. The values for the two periods are called the *midday* and *night-time* field intensities respectively. These monthly mean values

are the 'Upper Decile' values of field intensity. For convenience of analysis and comparison, these values have been reduced by 13.3 db. to convert them to their respective 'Lower Decile' figures. In practical problems on radio communication, the lower decile value is usually of greater interest. The method of analysis has been described in Part I. In this report we shall utilise the analyses of the yearly variation of field intensity for different transmitting stations for different frequencies both during the midday and night-time periods. The analyses are shown by a series of graphs. The values are given in db. above $1\mu\text{v/m}$.

In order to find out the yearly variation of field intensity in different seasons the monthly mean values have been grouped together for summer, winter and equinox. The average field intensity for any season has been plotted for different years.

5. CALCULATION OF INCIDENT FIELD INTENSITY

We first take up the unabsorbed field intensity in the night. Since the night-time field intensity has been assumed to depend only upon the spatial attenuation and the focussing effect caused by the curvature of the ionospheric layer, the field intensity will have a constant value for different years, seasons and frequencies for a given distance of propagations. The night-time field intensity has thus been calculated both by the C.R.P.L. and the S.P.I.M. methods.

For the calculation of midday field strength the following points have been taken into consideration for the C.R.P.L. and the S.P.I.M. methods:

(a) *C.R.P.L. Method:*

- (i) The centre points of the three transmission paths between Delhi and the transmitters at Bombay, Calcutta and Madras lie close to one another and average value of absorption index K representing the absorption index for the three circuits for the period 1200-1400 IST is determined. The maximum error involved in this approximation is within 5 to 10 per cent. Such values of K are read for all the months from January to December.
- (ii) $A(=JQK)$ is then worked out for summer, winter and equinox for average sunspot numbers 10, 40, 70, 120 and 150.

(b) *S.P.I.M. Method:*

The attenuation of a wave is due to $\delta_1 + \delta_2$. The values of δ_1 are read from the curves shown in Rawer's (1952) paper.

$$\delta_2 = \frac{p.430(1 + .0035\bar{R}) \cos^{3/4}\chi \sec \alpha_D}{(f \pm f_L)^2}$$

assumptions are made in the above form

- (i) The effect of the extraordinary component has been neglected.

- (ii) An average value of 1.0 Mc/s has been taken for f_1 for all calculations.
- (iii) $\cos^{3/4}\chi$ has been taken as equal to the value of K of the C.R.P.L. formula as there is not much difference in practice between $\cos^{3/4}\chi$ and that assumed in the C.R.P.L. publication.
- (iv) For p , only 1F and 2F have been assumed.
- (v) \bar{R} has been taken as 10, 40, 70, 120 and 150.
- (vi) δ_1 and δ_2 are thus added and the sum subtracted from 110 db to arrive at the actual field intensity.

The calculations of field intensity for the three circuits have been made for the two modes of propagation only, namely, 1F and 2F. Higher modes are also possible. Some experiments were carried out at Delhi in 1941 to verify the actual mode of propagation using pulsed transmissions from Bombay and Madras with similar transmitters and aeriels (Rao, 1942). Observations of down-coming angles were made at Delhi. It was found that for 3 and 5 Mc/s during night, the most predominant mode of propagation from Bombay and Madras was by one or two hop F. The values have, therefore been calculated for 1F and 2F.

The aerial directivity loss i.e. the loss due to the deviation of the receiving station from the direction of maximum field for the aerial has been worked out from the polar diagram of the aerial in question for 1F and 2F. The gain of the aerial used over that considered in the C.R.P.L. method is approximately 3 db. The gain of the transmitter is taken as 10 db. The total gain, thus arrived at, is added to the field due to 1kw calculated by the two methods for 1F and 2F. The 1F and 2F fields are then added in quadrature to give the resultant field intensity. As these values represent the median field intensity, they have been reduced by 8.2 db to arrive at the lower decile value for the purpose of comparison.

In the above calculations, the heights of E-and F-layers have been assumed to be the same as those contained in the C.R.P.L. and S.P.I.M. publications. The ionospheric heights in India are somewhat different from those at temperate latitudes.

6. COMPARISON WITH EXPERIMENTAL RESULTS

We now present the comparison between the measured and calculated values of field intensity.

(a) Night-time field intensity on 3 and 5 Mc/s.

Figures 1 to 3 show the yearly variation of field intensity for summer, winter and equinox. The corresponding values calculated from the C.R.P.L. and the

S. P. I.M. methods are also shown in the figures. It will be seen from the figures that the S.P.I.M. method gives a higher value of field intensity than the C.R.P.L. one. The difference is of the order of 9 to 10 dbs. The observed values do not

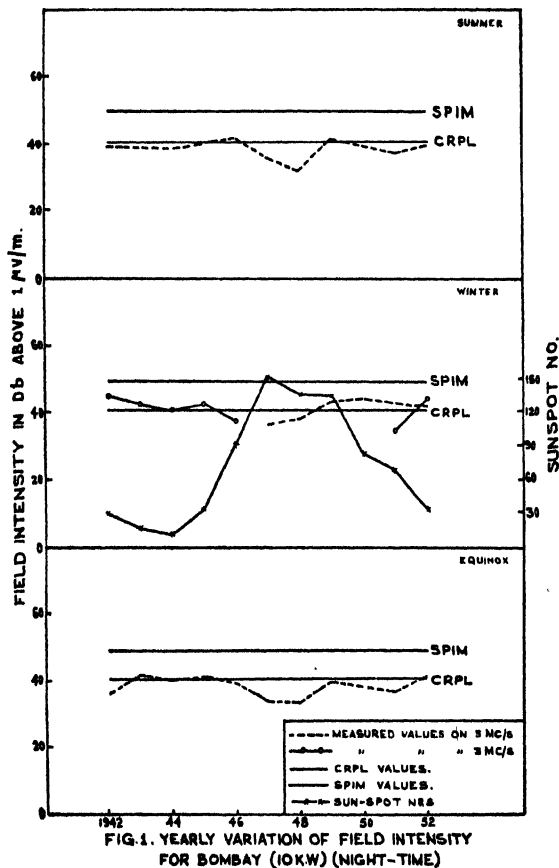


Fig. 1

agree with the values calculated by the S.P.I.M. method. On the other hand, as is evident from the figures 1 and 2, there appears to be a better correlation of the observed values for Bombay and Calcutta with the values calculated by the C.R.P.L. method during all the three seasons. For Madras (figure 3), however, there appears to be some amount of correlation between the observed and calculated (C.R.P.L.) values during the period 1947-1952. There is a large divergence in the values during the earlier period, i.e. 1942-1946, which is difficult to interpret.

An interesting point to note is that the observed values of field intensity in the night show variations which are to some extent correlated with the sunspot number. Higher fields have been observed during low sunspot activity and lower during high sunspot numbers. Theoretically, the non-deviative absorp-

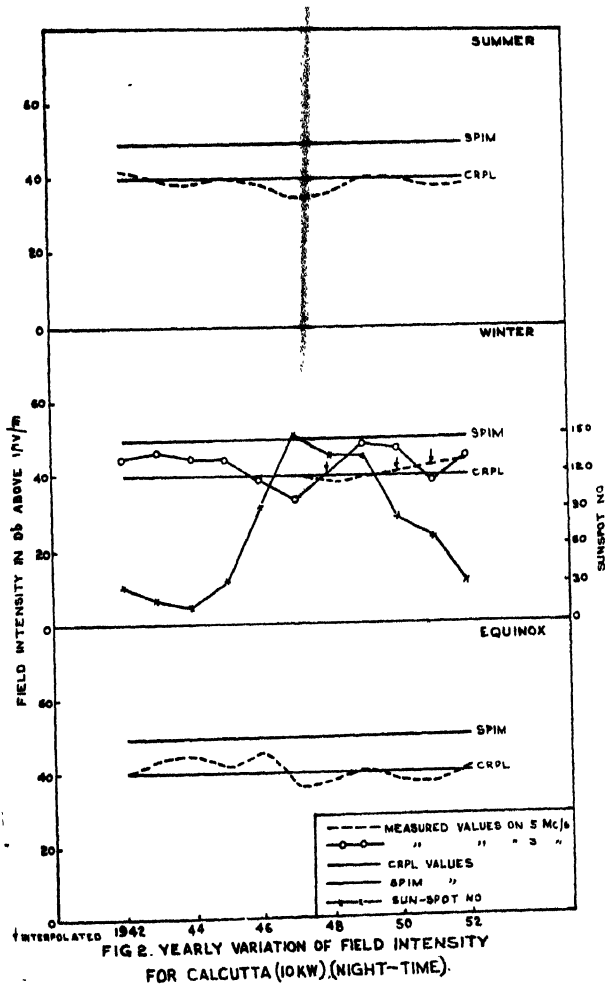


Fig. 2

tion in the D-layer is negligible during the night. The observations, however, show that apart from spatial attenuation during night, there is an 'additional absorption factor' which varies with sunspot activity. It may also be noted that the dip in the value of the observed field intensity for Bombay and Calcutta at sunspot maximum is roughly of the same order for all seasons. This indicates that the sunspot variation factor may be more important than the seasonal variation factor. It is not known, whether, such a phenomenon is observed

elsewhere also. A relationship could, therefore, be worked out between the night-time field and the sunspot number when sufficient data are available. The physical processes involved in having a sunspot cycle effect on the night-time field intensity is not clear. It may be due to a residual ionisation in the non-deviating layer at night during periods of high sunspot activity.

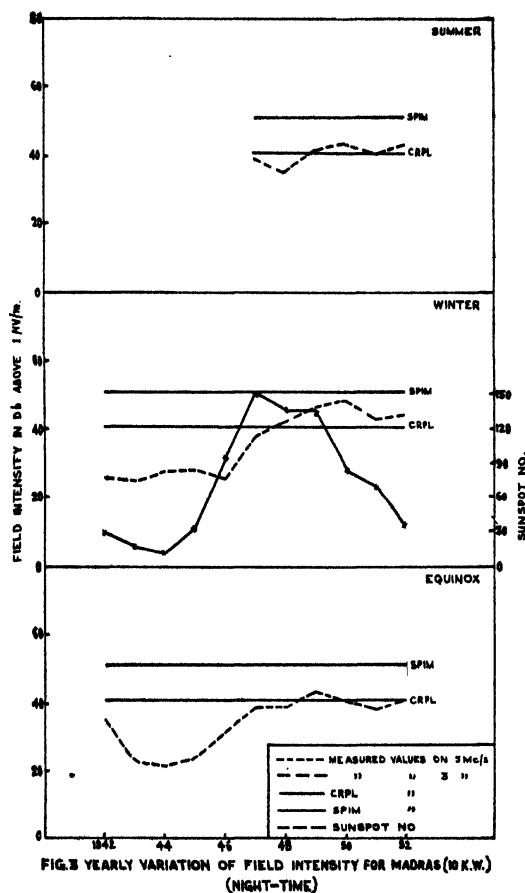


Fig. 3

The measurements of Madras (figure 3) show an interesting inverse correlation with sunspot activity. The field intensity during winter and equinox, for which data are available, (for the entire period 1942-1952), is low at low sunspot activity and high at high sunspot activity. The reason for such a peculiar behaviour is not clear.

(b) Day-time field intensity on 7 and 9 Mc/s.

The yearly variation of the midday field intensity on 7 and 9 Mc/s are shown in figures 4 to 6. The values calculated by the C.R.P.L. and the S.P.I.M. methods are also shown. It will be seen here also that the S.P.I.M. method gives a higher value of field intensity.

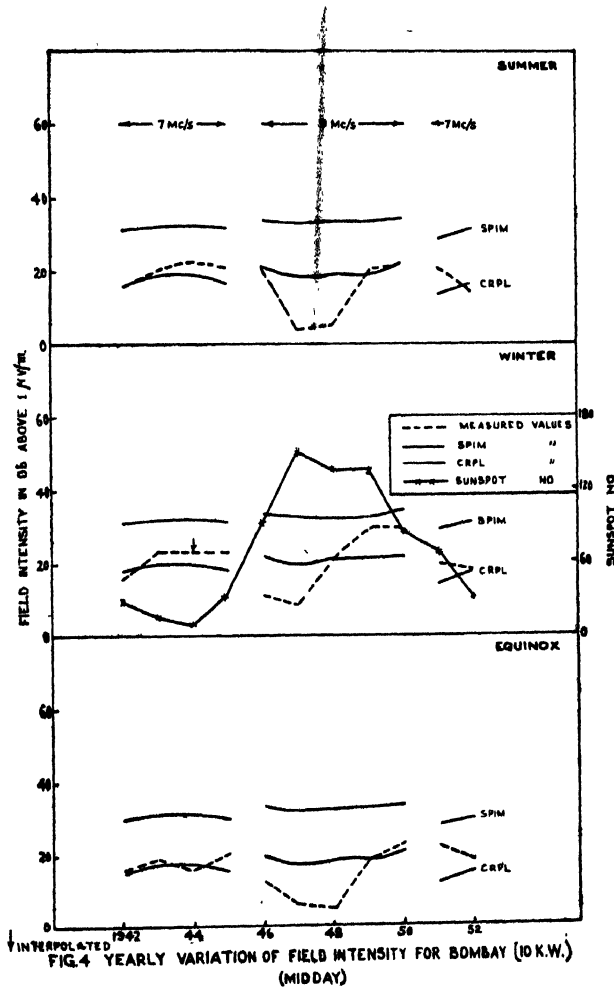


Fig. 4

The observed values of field intensity on 7 Mc/s during low sunspot activity appear to agree with the values calculated by the C.R.P.L. method. But on 9 Mc/s, the observed values are not represented by either of the two methods,

although C.R.P.L. one appears to give somewhat better agreement than the S.P.I.M. These results indicate that further detailed investigations are necessary for arriving at a better theoretical formula. The factors that are required to be

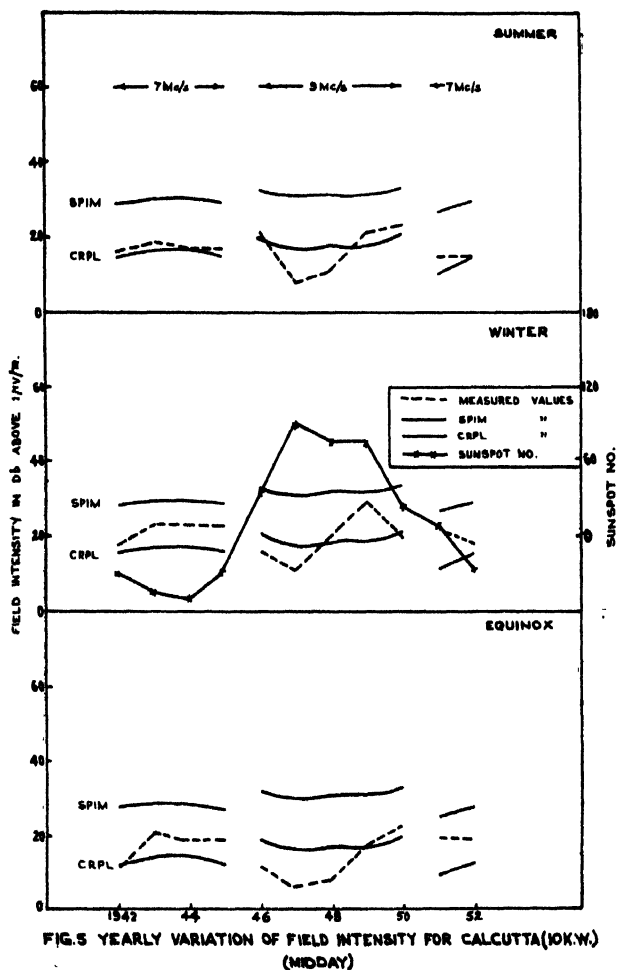


Fig. 5

studied are the effect of deviative absorption in the E-layer, the sunspot cycle variation and the contribution due to diurnal variation in the non-deviative region. The S.P.I.M. method is based upon British observations over a long period

but the ionospheric conditions over Great Britain are different from those over India. It is quite likely that the above factors will have different values when applied to tropics.

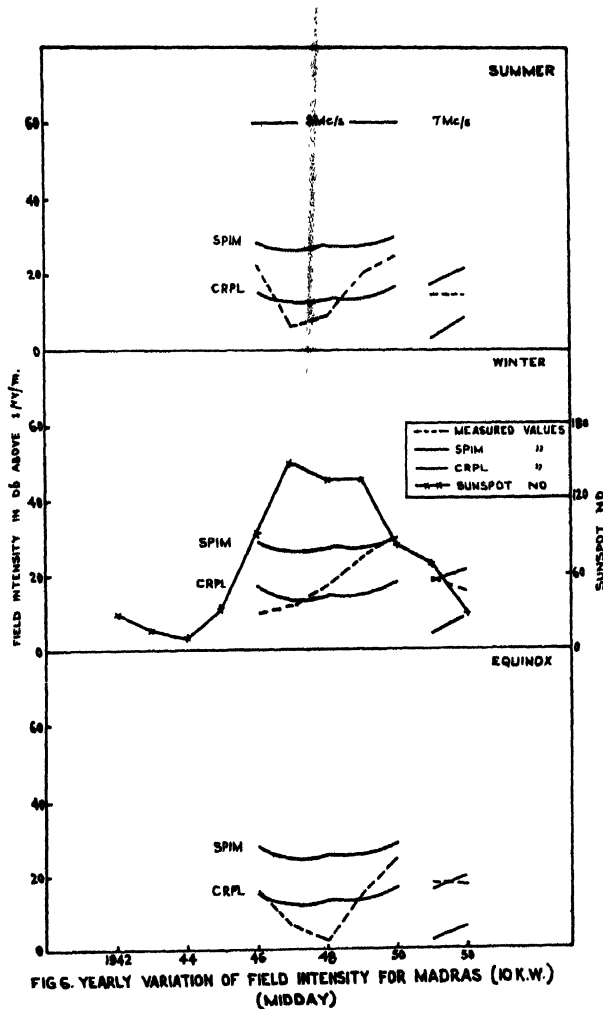


Fig. 6

Figure 7 shows the comparison between the values calculated by the C.R.P.L. and the S.P.I.M. methods at different sunspot numbers for different seasons for transmitters at Bombay, Calcutta and Madras working on 7 and 9 Mc/s during midday. The set of curves shows that the values obtained by the S.P.I.M. method

are higher than those obtained by the C.R.P.L. one. Rawer has indicated that the difference is mainly due to lower values of the spatial attenuation due to

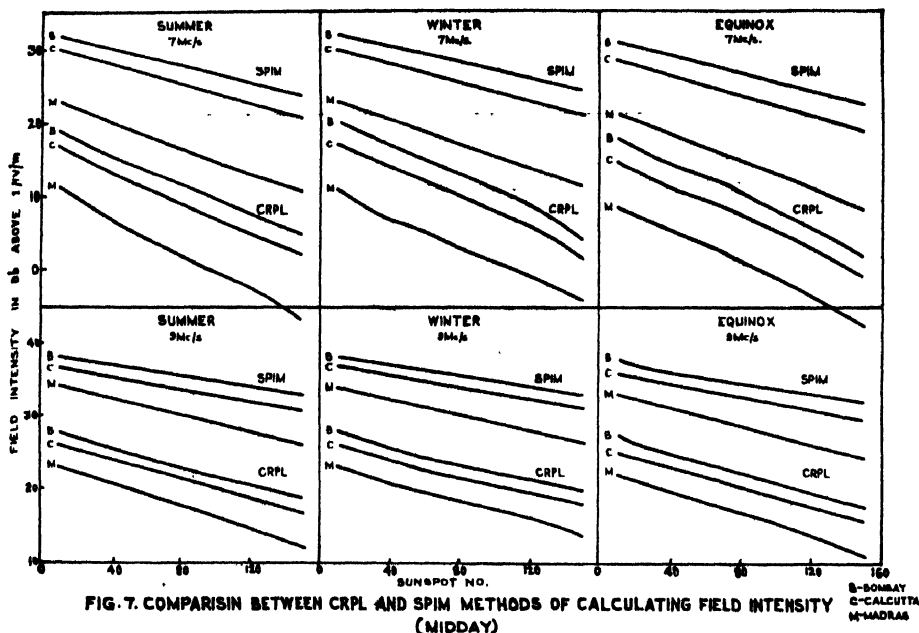


Fig. 7

increase in the field intensity attributed to the focussing effect of the curved ionosphere. It has also been shown that this increase in field intensity becomes quite large for long distances of propagation.

7. SUMMARY AND CONCLUSION

Accurate knowledge of absorption in the ionosphere and the characteristics of ionospheric propagation are not available. The two published methods of calculating the sky-wave field intensity have not been found to be strictly applicable to Indian conditions. Since an approach to the problem of calculating sky-wave field intensity entirely on theoretical grounds is a difficult one due to our insufficient knowledge of the mechanism of the formation of ionospheric layers and their diurnal and seasonal variations, any method of calculation at the present stage will be somewhat empirically based on statistical analysis of long series of absorption and field intensity measurements. A modified method has yet to be evolved based on such analysis for the tropical countries. A few of the salient discrepancies observed when applying the C.R.P.L. and the S.P.I.M. methods of calculation to Indian measurements are given below:

At night, the field intensity has been observed to be influenced by the sunspot cycle variations, the exact nature of the influence of which is not known. The non-deviative absorption in the night is omitted in the calculations since the D-layer has been assumed to be non-existent at that time. There is little experimental evidence to show that the D-layer does not exist in the night. The D-layer has been observed to occur in two types. One has been called the normal type which is effective in the day time. Theoretical estimate of absorption of waves passing through the normal D-layer may be obtained by assuming a Chapman distribution of ion density. This type of D shows a diurnal, seasonal and solar cycle variation of absorption. The other type has been called the sporadic D and has been observed mainly in the tropics at a height of about 60 kms. in the frequency range of 1 to 3.5 Mc/s. This type was first observed by the Indian workers, Mitra and Syam (1935) and has since been reported by other observers and have been summarised by Ellyett (1940). He has concluded from his observations at Pitcairn Islands that the sporadic D shows a minimum both in the summer and winter. It has also been reported that this type of D is appreciably absorbing. Anderson (1931) has observed night-time echoes from sporadic D. Thus, in order to understand the solar cycle variation of field intensity at night, further observations on D-region at night in the tropics are very necessary. If, on the other hand, this extra absorption in the night is due to residual ionisation in the E-region during high sunspot activity periods, it is only by further experimental observations, that a confirmation (or otherwise) may be obtained.

For the day-time field intensity the results of the measurements show that both the C.R.P.L. and the S.P.I.M. methods require suitable modifications. Rawer, has indicated that when the focussing effect is neglected, the S.P.I.M. and the C.R.P.L. methods agree with each other. We have made some calculations of field intensity according to the S.P.I.M. method where the unabsorbed field has been taken from the C.R.P.L. publication and only δ_2 has been added to it. We find that the S.P.I.M. field intensity is reduced by about 8 to 10 db by this method and its variation fits more or less with the C.R.P.L. calculations. It is difficult to verify by experiment whether the focussing effect causes an actual increase in the field intensity. One way to verify the focussing effect would be by observing the amplitude of incident sky-wave at different distances from the transmitter working on a frequency away from the maximum usable frequency for the layer. However, the measurement of the spatial attenuation and the focussing effect is likely to be affected by other factors modifying the resultant amplitude of the received wave.

It has been indicated earlier, that in order to arrive at a better theoretical formula for calculating the field intensity, the diurnal, seasonal and sunspot cycle variation factors require further study and modifications to suit condition in the tropics. It will be seen from figures 4 to 6 that while the theoretical calculations give a slowly varying function of field intensity, the observed varia

tions are rather rapid. Unfortunately, measurements of absorption in the tropics are not available for arriving at a suitable formula.

Till now, the effect of deviative absorption has not been applied in the calculation of field intensity. There is reason to believe that on long distance transmissions, over 400 kms and on frequencies away from maximum usable frequency for the layer, there will be some amount of deviative absorption. The calculation is rather complicated and experimental observation difficult due to other factors influencing the absorption in the path. The effect of fading has, however, been taken into account in the C.R.P.L. method which considers a reduction of the median field by 1.6 db for interference fading and 3.0 db for polarisation fading. On the other hand, Piggott (1953) has mentioned that the effect of short term fading, due to the existence of ionospheric irregularities tends to increase the median field intensity by a factor of about 2.5 db. Further detailed investigations in the tropics are, therefore, desirable and necessary.

ACKNOWLEDGMENTS

The work described in this paper was undertaken for investigating a few questions submitted by the C.C.I.R. for its VIIth Plenary Assembly. The paper in a modified form was published as an Indian Document in the proceedings of the C.C.I.R. (London 1953). The authors wish to thank Mr. B. V. Baliga, Chife Engineer, Mr. M. L. Sastry, Deputy Chief Engineer, Mr. S. S. Aiyar, Director of Frequency Assignment and Mr. S. Thiruvengkatachari, Research Engineer, All India Radio, for helpful discussions. Thanks are also due to the engineers at the Todapur Receiving Centre for taking field strength measurements. The paper is published by permission of the Chief Engineer, All India Radio.

REFERENCES

- Anderson, C. N., 1931, *Proc. I. R. E.*, **19**, 1150.
 Appleton, E. V., 1937, *Proc. Roy. Soc., A*, **162**, 451.
 Appleton, E. V., and Beynon, W. J. G., 1940, *Proc. Phys. Soc.*, **52**, 518.
 Do. 1947, *Proc. Phys. Soc.*, **59**, 58.
 C. R. P. L., 1948, Circular No. 462.
 Ellyett, C. D., 1947, *Terr. Mag. Atmos. Elect.*, **52**, 1.
 Mitra, S. K., and Syam, P., 1935, *Nature*, **135**, 953.
 Mitra, S. N., and Srivastava, R. B. L., 1955, *Ind. J. Phys.*, **29**, 167.
 Piggott, W. R., 1953, *Proc. I. E. E.*, Pt. III, **100**, 61.
 Rao, M. R., 1942, *Ind. J. Phys.*, **16**, 347.
 Rawer, K., 1952, *Wir. Engng.*, **29**, 287.

BARYON MESON SYSTEM IN PAIS FORMALISM : THE SCATTERING MATRIX

BY S. P. MISRA

MATHEMATICS DEPARTMENT, RAVENSHAW COLLEGE, CUTTACK 3

(Received for publication, December 29, 1954)

ABSTRACT. We have given here an explicit formulation of the scattering matrix in a formalism introduced by Pais. We have considered only the baryon meson system, and have started from an equation similar to Tomonaga's equation. Some selection rules for different processes or Feynman graphs are obtained.

1. INTRODUCTION

One of the well-established facts about nuclear forces is their charge independence. The theoretical foundations of this fact was first given by Kemmer (1938) by a symmetrical theory. This was further discussed by Heitler (1946) from a purely algebraic point of view. According to this hypothesis, the theory of such short range nuclear forces remains invariant under rotations in a hypothetical space called the isotopic spin space. The success of these methods and some other considerations led Pais (1953a) to assume that the wave functions do not depend only on the space-time variables x , but on ω -variables as well, where ω denotes points on the isotopic spin space (or ω -space as we shall call it; vide Pais (1953a, b)). This isotopic spin space is defined only for rotations of a three dimensional Euclidean space and may be considered as points on a unit sphere of such a space. The theory thus developed gives a natural relationship between the nucleons and V_1 -particles, and describes the nucleon meson system as a part of a larger system of particles, some of which have charge greater than one. The antiparticles exist in this theory as in previous theories of the nucleons. However, that these particles of higher charges are not observed is attributed to their short life times.

We have not done here any numerical calculations, since the divergencies introduced in this formalism have not been removed, and also as the coupling constant remains as large as before, making second order calculations unreliable. We have only derived some qualitative results from an equation similar to Tomonaga's relativistic wave equation by proceeding according to the well known methods of Feynman, Schwinger, and Dyson.

2. GENERAL FORMULATION

Let the baryon field be denoted by $\psi = \psi(x, \omega)$ and the meson field by $\phi = \phi(x, \omega)$. For definiteness and since in ordinary theory this is renormalisable

(Mathews and Salam, 1951) we consider pseudoscalar mesons (spin zero, odd space parity) with pseudoscalar or direct coupling. Also, in ω -space we take this system as having isotopic spin 1, which corresponds to the charge symmetric theory of Kemmer with interactions through positive, negative and neutral mesons. We proceed to obtain the scattering matrix for the interaction of these two systems of particles. It should be noted that according to the present theory, ψ has eight components, four of which are obtained in the usual Dirac electron theory with the wave function splitting up into a pair of spinors, and each of these components further splitting up into two, corresponding to an isotopic spin $\frac{1}{2}$ of the baryons. Corresponding to isotopic spin 1, ϕ has three components, each of which is pseudoscalar in space-time and is taken to be real.

We take the hamiltonian density of the field as

$$H = H_0 + H_1 \quad \dots (1),$$

where, H_0 gives the sum of the hamiltonian densities of the baryon system and the meson system without interaction, and H_1 is the interaction hamiltonian density. Here by hamiltonian density we mean the function which is to be integrated over the whole of ω -space and then over the space variables alone of space-time to give the usual hamiltonian function.

We choose a representation that corresponds to interaction representation in the ordinary formalism. We take $\hbar = c = 1$, and after Tomonaga or Schwinger, write,

$$i \frac{\delta \Psi(\sigma)}{\delta \sigma(x, \omega)} = H_1(x, \omega) \Psi(\sigma) \quad \dots (2)$$

Here $\Psi(\sigma)$ is the general wave function corresponding to the state vector of both the systems, defined over a surface σ in the six-dimensional manifold, with the restriction that the surface is space-like in space-time. $H_1(x, \omega)$ is the interaction hamiltonian density assumed to be invariant under Lorentz transformations and rotations in ω -space. $\frac{\delta}{\delta \sigma(x, \omega)}$ denotes the functional derivative at (x, ω) generalised to the six-dimensional space; i.e.

$$\frac{\delta \Psi(\sigma)}{\delta \sigma(x, \omega)} = \lim_{\substack{\delta x \rightarrow 0 \\ \delta \omega \rightarrow 0}} \frac{\Psi(\sigma') - \Psi(\sigma)}{\delta x \delta \omega}$$

where δx stands for the four dimensional volume element in space-time, and $\delta \omega$ stands for the two-dimensional volume element in ω -space. σ' and σ are surfaces of the nature mentioned which differ only in the neighbourhood of the point (x, ω) and $\delta x \delta \omega$ is the volume enclosed by the two surfaces.

Equation (2) can be seen to be equivalent to

$$\Psi(\sigma) = U(\sigma)\Psi_0 \quad \dots (3)$$

where $U(\sigma)$ satisfies the differential equation.

$$i \frac{\delta U(\sigma)}{\delta \sigma(x, \omega)} = H_1(x, \omega) U(\sigma) \quad \dots (4)$$

In equation (3) we take the constant state vector Ψ_0 as the state vector at infinite past, both in the interaction representation and in the Heisenberg representation; i.e. we assume that the interaction is switched off when the surface lies at infinite past. This procedure is justified only in the consideration of scattering phenomena and not in the consideration of bound state problems (see Gellman and Low, 1951). This understanding adds to equation (4) the boundary condition

$$U(-\infty) = 1. \quad \dots (5)$$

Here $U(-\infty)$ means the value of the operator for any surface at infinite past. Now proceeding in a way similar to Dyson (1949a), we write $U(\sigma_0)$ as,

$$U(\sigma_0) = 1 + (-i) \int_{-\infty}^{\sigma_0} H_1(x_1, \omega_1) dx_1 d\omega_1 + (-i)^2 \int_{-\infty}^{\sigma_0} dx_1 d\omega_1 \int_{-\infty}^{\sigma(x_1, \omega_1)} H_1(x_1, \omega_1) H(x_2, \omega_2) dx_2 d\omega_2 + \dots$$

Hence introducing Dyson's time ordering P -product, the scattering matrix $U(\infty)$ is given as

$$U(\infty) = 1 + S_1 + S_2 + \dots + S_n + \dots \quad \dots (6)$$

where

$$S_n = (-i)^n / n! \int_{-\infty}^{\infty} dx_1 d\omega_1 \int_{-\infty}^{\infty} dx_2 d\omega_2 \dots \int_{-\infty}^{\infty} dx_n d\omega_n P\{H_1(x_1, \omega_1) H_1(x_2, \omega_2) \dots H_1(x_n, \omega_n)\}. \quad \dots (7)$$

We now want to show that S_n , the contribution of the S -matrix of a definite order, is the sum of the contributions of a number of processes corresponding to a number of Feynman graphs generalised to the six dimensional space. For this purpose we proceed according to Wick (1950). We know that Dyson's P -product and T -product of Wick can differ only in sign. Proceeding as in the paper

of Wick, it is easily seen that no significant change occurs in the process of calculation except in the values of non-zero contractions, contractions being defined as in Wick (1950). For example, for this purpose we develop $\psi(x, \omega)$ as

$$\psi(x, \omega) = \sum_A \psi_A(x) \chi_A(\omega)$$

where $\psi_A(x)$ is an ordinary wave function belonging to mass M_A , and $\chi_A(\omega)$ is the eigenfunction of the mass operator in ω -space belonging to the eigenvalue M_A . Now we can expand as usual $\psi_A(x)$ in terms of positive and negative energy states and thus finally obtain

$$\psi(x, \omega) = u(x, \omega) + \bar{v}(x, \omega); \quad \bar{\psi}(x, \omega) = \bar{u}(x, \omega) + v(x, \omega).$$

Here $u(x, \omega)$ is the sum of positive energy states (i.e. they annihilate the Dirac particles) and $\bar{v}(x, \omega)$ is the sum of negative energy states (i.e. they create the antiparticles). Similarly $\bar{u}(x, \omega)$ and $v(x, \omega)$ respectively create the particles and annihilate the antiparticles. Here we rather have a family of particles and antiparticles corresponding to the different mass levels of the baryon system. Thus we have,

$$\dot{\psi}(x, \omega) \dot{\bar{\psi}}(x', \omega') = [u(x, \omega), \bar{u}(x', \omega')]_+ = \sum_{m>} \dot{\psi}_m(x, \omega) \dot{\bar{\psi}}_m(x', \omega') \quad \text{when } x_0 > x'_0, \quad \dots \quad (8a)$$

$$= -[\bar{v}(x, \omega), v(x', \omega')]_+ = - \sum_{m<} \dot{\psi}_m(x, \omega) \dot{\bar{\psi}}_m(x', \omega') \quad \text{when } x_0 < x'_0, \quad \dots \quad (8b)$$

In the above the dots denote contraction, $[,]_+$ denotes the anticommutator, and $\sum_{m>}$ denotes summation over positive energy states, and $\sum_{m<}$ summation over negative energy states.

Similarly the other non-zero contraction $\dot{\phi}(x, \omega) \dot{\phi}(x', \omega')$ can be determined by expanding $\phi(x, \omega)$ in terms of mass eigenstates. We shall deduce it in detail in the next section for the case under consideration.

Since the P -product or the T -product can be broken up into the sum of all possible contractions (this is proved exactly as in Wick, 1950), we obtain that the contribution to the S -matrix of a given order can be broken up into the sum of a number of parts each of which corresponds to definite virtual or real physical process and a definite Feynman graph. The contracted terms correspond to internal lines, and the free operators, the external lines. There may be other terms, such as γ_s or τ_s whose significance will be explained later. These will correspond to vertices. Thus corresponding to internal lines, external lines and vertices, we have definite terms of the S -matrix. This proves our proposition.

3. DISCUSSIONS OF PAIS EQUATION

We now proceed to discuss Pais equation of the baryon system itself and its interactions with the meson field. We start with the Dirac equation describing the baryon system :

$$(\gamma_i \frac{\partial}{\partial x_i} + \frac{\tau \cdot K}{\Lambda} + M) \psi(x, \omega) = 0 \quad \dots (9)$$

Here the notations are the same as in Pais (1953a, b). We can expand $\psi(x, \omega)$ in terms of the eigenfunctions of equation (9). Then we have,

$$\psi(x, \omega) = \sum_{r, A, n} \vec{\psi}_{rAn}(x) \chi_{A, n}(\omega) e^{-iE_{rA}t} \quad \dots (10)$$

Here A stands for (k, ϵ) , where k is the isotopic spin space orbital angular momentum and $\epsilon = I - k$, I being the total angular momentum in ω -space. n is the component of the total ω -space angular momentum in a fixed direction, here taken as the direction $(0, 0, 1)$ in that space. We can easily see that ' A ' as taken in the last article, denotes the definite mass states of the baryons. When the electromagnetic field is present, n is interpreted to give the charge, thus making

charge degenerate with respect to mass. In the above, $\vec{\psi}_{rAn}(x)$ are the four component Dirac spinors belonging to the mass level M_A . The eigenstates belonging to different momenta are given by the r 's, taken as enumerable assuming as usual a periodicity in space. $\chi_{A, n}(\omega)$, written in full as $\chi_{k, n}^{(\epsilon)}(\omega)$ in Pais (1953b) has two components and is an eigenstate of $\vec{\tau} \cdot \vec{K}$ belonging to the eigenvalue k when $A = (k, \frac{1}{2})$ and, $-(k+1)$ when $A = (k, -\frac{1}{2})$.

Let us now obtain the propagation function deduced in (8). As before we keep the spin and isotopic spin indices implicit; thus the propagation function becomes an 8×8 matrix. Then for $x_0 > x'_0$, $x_0 = t$, we obtain,

$$\dot{\psi}(x, \omega) \dot{\bar{\psi}}(x', \omega') = \sum_{r > A, n} \vec{\psi}_{rAn}(x) \chi_{A, n}(\omega) e^{-iE_{rA}x_0} \bar{\psi}_{rAn}(x') \chi_{A, n}^*(\omega') e^{-iE_{rA}x'_0} \dots (11)$$

$$= \sum_{A, n} K_{+A}(x, x') \chi_{A, n}(\omega) \chi_{A, n}^*(\omega'). \quad \dots (12)$$

Here $K_{+A}(x, x')$ is the ordinary Feynman propagation function for a Dirac particle of mass M_A , and is a 4×4 matrix. $\chi_{A, n}^*(\omega)$ is the hermitian conjugate of $\chi_{A, n}(\omega)$. It is also clear that the same relation holds when $x_0 < x'_0$. Let us now denote the point (x_{μ_1}, ω_1) where x_{μ_1} represents the space time coordinates, by 1, and by 2 the point (x_{μ_2}, ω_2) , the points laying in the underlying manifold over which the wave functions are defined. Let us take

$$\dot{\psi}(1) \dot{\bar{\psi}}(2) = K_+(2, 1). \quad \dots (13)$$

The form (11) then easily shows us, on proceeding as in Feynman (1949) and remembering that $\chi_{A,n}(\omega)$ are normalised, that,

$$\psi(2) = \int_{t_1=0} K_+(2, 1) \beta \psi(1) d^3x_1 d\omega_1 - \int_{t'_1=\tau} K_+(2, 1') \beta \psi(1') d^3x_1', \quad 0 < t_2 < T \quad \dots \quad (14)$$

which gives us that $K_+(2, 1)$ is the propagation function or the Feynman kernel in the six dimensional space.

To obtain the propagation function for the meson system, we proceed as in Pais (1953b) and take $\eta_{k,n}^{(\epsilon)}$ and $H_{k,n}^{(\epsilon)}$, the former occurring in the expansion of the real ϕ and the latter, in that of complex Φ . The calculation is trivial; thus using the results of Wick (1950) and Pais (1953b) and their notations, we obtain,

$$\begin{aligned} \dot{\phi}(x, \omega) \dot{\phi}(x', \omega') &= T(\phi(x, \omega) \phi(x', \omega')) - : \phi(x, \omega) \phi(x', \omega') : \\ &= \sum_{A,n,A',n'} \eta_{A,n}(\omega) \eta_{A',n'}(\omega') [T(\phi_{A,n}(x) \phi_{A',n'}(x')) - : \phi_{A,n}(x) \phi_{A',n'}(x') :] \\ &= \sum_{A,n,A',n'} (-1)^{n'} \eta_{A,n}(\omega) \eta_{A',n'}(\omega') [T(\phi_{A,n}(x) \phi_{A',-n'}^*(x')) - \\ &\quad : \phi_{A,n}(x) \phi_{A',-n'}^*(x') :] \\ &= \sum_{A,n} (-1)^n \eta_{A,n}(\omega) \eta_{A,-n}(\omega') \Delta_{FA}(x, x'). \quad \dots \quad (15) \end{aligned}$$

In the above as usual $A = (k, \epsilon)$ gives the mass states. We have written $\phi_{A,n}(x)$ for $\phi_n^{(\epsilon)}(x)$ of Pais and similarly for $\eta_{A,n}(\omega)$, and have used the result $\phi_{A,n}^*(x) = (-1)^n \phi_{A,-n}(x)$. $\Delta_{FA}(x)$ is the usual Δ_F function belonging to the mass μ_A of the meson. It should be noted that $H_{k,n}^{(\epsilon)}(\omega)$ are eigenfunctions of $\vec{T} \cdot \vec{K}$ belonging to the eigenvalues $k, 0$, and $-k$ for ϵ equal to $1, 0$, and -1 respectively.

We have assumed that the mass operator is a function of $\vec{T} \cdot \vec{K}$ and \vec{K}^2 as taken in Pais (1953b).

Now we proceed to consider some particular cases of the S -matrix corresponding to simple Feynman graphs.

For this purpose we note that the interaction hamiltonian density H_1 is given as

$$H_1 = -ig \bar{\psi} \gamma_5 \tau_a \psi \phi_a$$

Here summation is to be taken over $a = 1, 2, 3$, where

$$\tau_1 = \begin{pmatrix} 0 & 1 \\ 1 & 0 \end{pmatrix}, \quad \tau_2 = \begin{pmatrix} 0 & -i \\ i & 0 \end{pmatrix}, \quad \tau_3 = \begin{pmatrix} 1 & 0 \\ 0 & -1 \end{pmatrix}.$$

The nature of the interaction hamiltonian density obviously shows that the difference of the number of particles and antiparticles of the baryon system remains the same.

We can also easily deduce now the fact that the charge and the parity of ω -space orbital angular momentum are conserved at any vertex. Here we use the same notation as Pais (1953b) except that we take

$$S = \begin{pmatrix} -\frac{1}{\sqrt{2}} & +\frac{i}{\sqrt{2}} & 0 \\ 0 & 0 & 1 \\ \frac{1}{\sqrt{2}} & \frac{i}{\sqrt{2}} & 0 \end{pmatrix}$$

such that

$$\Phi = S\phi = \begin{pmatrix} -\frac{1}{\sqrt{2}} & (\phi_1 - i\phi_2) \\ 0 & \phi_3 \\ \frac{1}{\sqrt{2}} & (\phi_1 + i\phi_2) \end{pmatrix}$$

Clearly S is unitary, and

$$S^{-1} = \begin{pmatrix} -\frac{1}{\sqrt{2}} & 0 & \frac{1}{\sqrt{2}} \\ -\frac{i}{\sqrt{2}} & 0 & -\frac{i}{\sqrt{2}} \\ 0 & 1 & 0 \end{pmatrix}$$

Hence we have

$$\begin{aligned} \vec{\tau} \cdot \phi &= (\tau_1, \tau_2, \tau_3) S^{-1} \begin{pmatrix} \Phi_1 \\ \Phi_2 \\ \Phi_3 \end{pmatrix} \\ &= \left[-\frac{1}{\sqrt{2}} \begin{pmatrix} 0 & 2 \\ 0 & 0 \end{pmatrix}, \begin{pmatrix} 1 & 0 \\ 0 & -1 \end{pmatrix}, \frac{1}{\sqrt{2}} \begin{pmatrix} 0 & 0 \\ 2 & 0 \end{pmatrix} \right] \cdot \Phi \\ &= \sum_{A,n} \phi_{An}(x) H_{k,n}^{(c)}(\omega) \cdot \left[-\frac{1}{\sqrt{2}} \begin{pmatrix} 0 & 2 \\ 0 & 0 \end{pmatrix}, \begin{pmatrix} 1 & 0 \\ 0 & -1 \end{pmatrix}, \frac{1}{\sqrt{2}} \begin{pmatrix} 0 & 0 \\ 2 & 0 \end{pmatrix} \right] \end{aligned}$$

Now let us consider for simplicity a baryon with k, n, ϵ in ω -space absorbing meson with k'', n'', ϵ'' , at the vertex (x, ω) and changing into another baryon, k', n', ϵ' (see figure 1a).

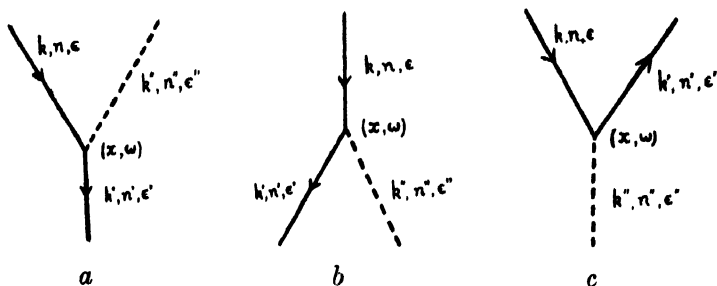


Fig. 1

Then the ω -dependent terms will separate as

$$\chi_{k', n'}^{(\epsilon')*}(\omega) \left[-\frac{1}{\sqrt{2}} \begin{pmatrix} 0 & 2 \\ 0 & 0 \end{pmatrix}, \begin{pmatrix} 1 & 0 \\ 0 & -1 \end{pmatrix}, \frac{1}{\sqrt{2}} \begin{pmatrix} 0 & 0 \\ 2 & 0 \end{pmatrix} \right] \cdot H_{k'', n''}^{(\epsilon'')}(\omega) \chi_{k, n}^{(\epsilon)}(\omega).$$

But using the expressions for $\chi_{k, n}^{(\epsilon)}(\omega)$ and $H_{k, n}^{(\epsilon)}(\omega)$ given by Pais (1953b) we can see that the integration over ω is the sum of the following integrals multiplied by certain constants depending on the k 's, n 's and ϵ 's. The integrals are

$$(1) \int Y_{k', n' - \frac{1}{2}}^*(\omega) Y_{k'', n'' - 1}(\omega) Y_{k, n + 1}(\omega) d\omega,$$

$$(2) \int Y_{k', n' - \frac{1}{2}}^*(\omega) Y_{k'', n''}(\omega) Y_{k, n - 1}(\omega) d\omega,$$

$$(3) \int Y_{k', n' + \frac{1}{2}}^*(\omega) Y_{k'', n''}(\omega) Y_{k, n + 1}(\omega) d\omega,$$

$$(4) \int Y_{k', n' + \frac{1}{2}}^*(\omega) Y_{k'', n'' + 1}(\omega) Y_{k, n - 1}(\omega) d\omega.$$

Replacing $d\omega$ by $\sin\theta d\theta d\phi$ (this angle ϕ should not be confused with the wave function ϕ), and integrating with respect to ϕ , we get that all the above integrals vanish except when

$$n' = n'' + n.$$

This gives the conservation of charge at any vertex. Also, since the parity of $P_{k, n}(\mu)$ for a certain variable μ changed to $-\mu$ is $(-1)^{k+n}$, here ($P_{k, n}$ are the associated Legendre polynomials), the above conservation of charge gives that also the parity of the k 's or of the total ω -space orbital angular momentum must be conserved.

If we have a meson created at the vertex instead of being annihilated, then $\phi_{k,n}^{(n)}(x) = (-1)^n \phi_{k,-n}^{(n)}(x)$ is to be taken and hence n is replaced by $-n$, thus again giving conservation of charge. The same also holds for antiparticles, since the creation operators of the negative energy states of the particles are the annihilation operators of the antiparticles and similarly the creation operators of the antiparticles are the annihilation operators of the negative energy states of the particles. (For this and the above case, see figures 1 b, c)

It is also clear from the propagation functions (12) and (15) that also when one or more of the lines are internal lines, the charge as well as ω -space total orbital angular momentum parity must be conserved at any vertex.

On integrating over x , we can easily see that the total energy momentum four vector of the particles considered remains the same (see Dyson, 1949b). However, it should be noted that the rest mass of the baryons need not remain unaltered and will in general change, consistent with the conservation rules. This will give as a particular case the decay of higher mass baryons.

If one of the baryons is a nucleon, then $\chi_{0,n}^{(-\frac{1}{2})}$ does not exist. Here the proton and neutron states are given respectively as $\chi_{0,\frac{1}{2}}^{(\frac{1}{2})} = \begin{pmatrix} 1 \\ 0 \end{pmatrix}$, and $\chi_{0,-\frac{1}{2}}^{(\frac{1}{2})} = \begin{pmatrix} 0 \\ 1 \end{pmatrix}$. Since here one of the spherical harmonics is a constant, the orthogonality of the other pair gives that, besides the conservation of charge, the ω -space total orbital angular momentum must be conserved as well. Thus if a baryon having (k, n) in ω -space decays with one of the decay products a nucleon, then on the first approximation (i.e. without any intermediate state) the decay meson will have in ω -space $(k, \mp \frac{1}{2})$ according as whether the nucleon is a proton or a neutron. Similarly also total k is conserved when one of the decay products is a π -meson. But when the next higher order approximations are important and are to be considered, this conservation of ω -space orbital angular momentum does not necessarily hold even in these particular cases (see figure 2).

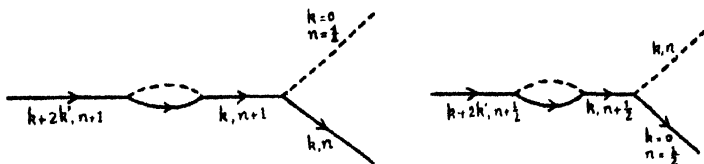


Fig. 2

Also it is interesting to note that any change in the cases of meson nucleon or nucleon nucleon scattering in this formalism with higher order corrections, i.e. with the introduction of vertex or self-energy parts to the lowest order graph, will occur only when the energies of the particles are sufficiently higher to allow for transitions to higher mass states. These correspond to the lowest resonance

levels given in Pais (1953a). However, by what we have stated above, there will be no difference for these processes between this formalism, and what we previously had without the introduction of the ω -space, unless we take into account these higher order radiative corrections (see figure 3).

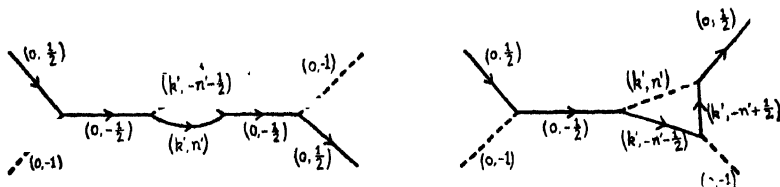


Fig. 3. Here (a, b) means $k=a, n=b$

4. DISCUSSIONS

It has been widely believed for some time that our present theories may be 'open' instead of being 'closed'. We should expect, as has been pointed out by Heisenberg (1953), that our wave functions should describe families of particles instead of there being different wave functions for all the distinct particles. The present particle-fields should be given as particular cases of such wave functions. However, these theories ought to be closed and should give a more convincing method of renormalisation than what we have at present. The theory we have discussed does not at all help us in this direction and it has not been possible to renormalise the ω -divergencies as well. That this formalism does not give a new colour to the divergency problem is to be attributed to the fact that the ω -space and the ordinary Lorentz space are completely independent except for the mass depending on the ω -space. The apparent fusion that is made by starting from an equation similar to Tomonaga's relativistic wave equation is spoilt, because we require the interaction hamiltonian to be invariant under the transformations of the Lorentz group and rotations in the ω -space separately. It is, however, necessary to discuss such attempts in detail in so far as we have not been able to succeed in any of our local theories, and we expect that some such extension of the basic manifold where the wave functions may depend on variables other than only space-time variables and which give systems of particles coordinating the experimentally observed selection rules may help us in this direction.

ACKNOWLEDGMENTS

The author wishes to express his sincere thanks to Professor H. J. Bhabha for his guidance while working under him and to Dr. K. K. Gupta and Mr. E. C. George for some illuminating discussions.

R E R E N C E E S F

- Dyson, F. J., 1949a, *Phys. Rev.*, **75**, 486;
 " " 1949b, *Phys. Rev.*, **75**, 1436.
Feynman, R. P., 1949, *Phys. Rev.*, **76**, 749.
Gellman, M. and Low, Francois, 1951, *Phys. Rev.*, **84**, 350.
Heisenberg, W., 1953, *Physica*, **19**, 897.
Heitler, W., 1946, *Proc. Royal Irish Academy*, Sec. A, **51**, 33.
Kemmer, N., 1938, *Proc. Camb. Phil. Soc.*, **34**, 354.
Mathews, P. T. and Salam, A., 1951, *Rev. of Mod. Phys.*, **23**, 311.
Pais, A., 1953a, *Physica*, **19**, 869; 1953b, *Prog. of Theor. Phys.*, **10**, 457.
Wick, G. C., 1950, *Phys. Rev.*, **80**, 268.

Letters to the Editor

RAMAN SPECURUM OF *O*-CHLOROETHYLBENZENE

The Raman spectrum of *o*-chloroethylbenzene was obtained in the liquid state. Mercury 4358 Å radiation, filtered through the Du Pont Rhodamine 5GDN extra dye in *p*-nitrotoluene-methylalcohol solution, was used for excitation.

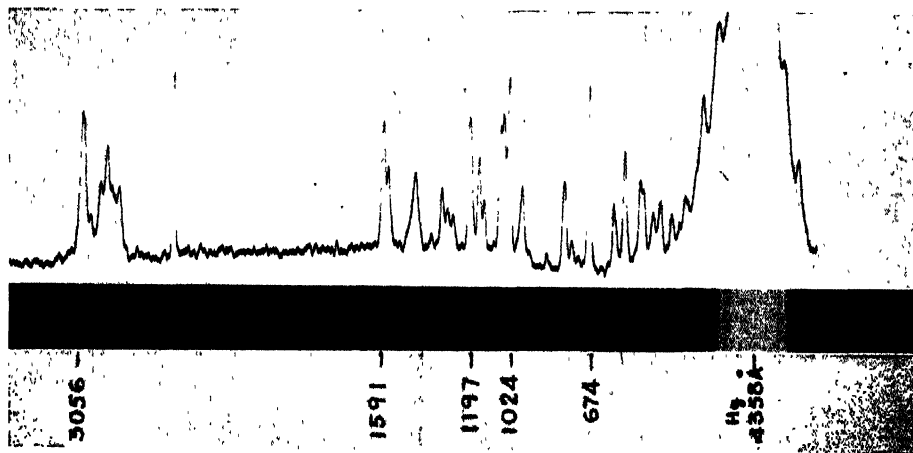


Fig. 1

About 35 Raman lines were recorded and the Raman shifts are given in Table I. Lines marked with an asterisk were obtained as Stokes and anti-Stokes lines. Semi-quantitative relative intensities (in the scale 0–10) are obtained from a microphotometer curve and given in Table I.

The Raman spectrum along with the microphotometer curve is reproduced in figure 1.

TABLE I

Raman frequencies of *o*-chloroethylbenzene

$\Delta\nu$ (cm^{-1})	Int	$\Delta\nu$ (cm^{-1})	Int
137*	4	1061	4
196*	3	1130	2
265*	1	1155	3
323*	1	1197	6
369*	2	1273	1
401	2	1299	2
440*	2	1321	2
456*	2	1367	1
522*	4	1441	2
566*	2	1566	3
674*	10	1591	4
720		2869	2
746	1	2902	2
856	1	2933	4
778	3	2965	2
964	2	3012	1
1024	10	3056	6
1044	5	—	—

S. L. N. G. KRISHNAMACHARI
V. RAMAKRISHNA RAO

Physics Department,
Andhra University,
Waltair.
12 April 1955.

RAMAN SPECTRA AND FLUORESCENCE OF A FEW SUBSTITUTED TOLUENES IN THE SOLID STATE AT DIFFERENT LOW TEMPERATURES*

BY D. C. BISWAS,

OPTICS DEPARTMENT, INDIAN ASSOCIATION FOR THE CULTIVATION OF SCIENCE,
JADAVPUR, CALCUTTA 32.

(Received for publication, April 12, 1955)

ABSTRACT. The Raman spectra of *m*-CH₃C₆H₄Cl, *m*-CH₃C₆H₄Br and *o*-, *m*- and *p*-CH₃C₆H₄OH in the liquid state and in the solid state at different temperatures were studied. Each of the liquids has yielded a few new feeble lines not reported by previous workers. It is found that except in the case of *p*-cresol, a strong line in the neighbourhood of 200 cm⁻¹ disappears in each case when the liquid is solidified. An explanation has been offered for this change. Similar to the case of other substituted benzenes, a few Raman lines appear in the low-frequency region when the substances are solidified. Changes in the frequency-shifts, as well as in the intensities of these new lines, are observed on lowering the temperature of the crystals to -180°C. An attempt has been made to interpret these results.

INTRODUCTION

Previous investigations on the Raman spectra of a few disubstituted benzene compounds in the solid state at different temperatures have shown that when these substances are solidified, a few new Raman lines appear in the low-frequency region in each case and the change which they undergo with change of temperature of the solidified mass is different for different compounds. Further, it has been observed previously (Sanyal, 1953; Biswas, 1954) that certain substituted toluenes exhibit two broad fluorescence bands in the visible region when they are solidified and cooled to -180°C and that this appearance of fluorescence bands in the solid state is accompanied by an appreciable diminution in the intensity of a Raman line due to C = C vibration of the molecules. Sometimes it is also found that a strong Raman line observed in the case of the liquid phase of some disubstituted benzenes disappears when the substances are solidified (Biswas, 1955). One of such compounds is *o*-dichlorobenzene which shows a splitting in its ultraviolet absorption bands in the solid state (Sirkar and Swamy, 1952) at low temperatures. This splitting up of the absorption bands and also the disappearance of some strong Raman lines in the solid state can both be accounted for by assuming

* Communicated by Prof. S. C. Sirkar.

the existence of a strong intermolecular field in the solid state of the substance produced by the formation of virtual bonds amongst the neighbouring molecules. The data available so far are not, however, adequate to lead to a general conclusion regarding the behaviour of these Raman lines with change of temperature. It was, therefore, thought worthwhile to study a few more disubstituted benzene compounds the ultraviolet absorption spectra of which show similar splitting of the absorption bands in the solid state or show any other peculiarities. With these objects in view, the present investigation on the Raman spectra of meta chloro- and meta bromotoluene and also of the three isomeric *o*-, *m*- and *p*-cresols in the solid state at low temperatures was undertaken. The ultraviolet absorption spectra of these compounds (excepting *m*-bromotoluene) have been studied by Swamy (Swamy, 1952*a*; Swamy, 1952*c*). The cresols were particularly chosen to find out whether the replacement of the halogen atoms of chloro- or bromotoluenes by the hydroxyl group brings about any fundamental change in the Raman spectra of these substances in the solid state in the low-frequency region.

EXPERIMENTAL

The liquids meta chlorotoluene and meta bromotoluene were supplied by Schuchardt Co. Ltd. and City Chemical Corporation, N.Y. respectively, while ortho cresol was secured from May and Baker Ltd., England. Meta and para cresol were obtained from B. D. H. Ltd. and were of 98% pure variety. The two halogen substituted toluenes were distilled in vacuum once before every exposure, but some special care was taken to purify the cresol compounds. The cresols were fractionated under vacuum successively for five or six times, each time rejecting the first and last fractions of the distillate. The Raman spectra of all these compounds in the liquid phase were recorded and compared with the results given by previous workers. Further, for unequivocal assignment of the lines, the Raman spectra of ortho and para cresol in the liquid state were also recorded using the 4358Å line of mercury only as the exciting radiation by cutting off the 4047 Å group with a filter of rhodamine 6 GBM solution mixed with solution of *p*-nitrotoluene in suitable proportions. The polarisation of the Raman lines of the two halogen substituted toluenes in the liquid phase was estimated in the usual manner by photographing simultaneously both the vertical and the horizontal components of the Raman lines produced by interposing a double-image prism just in front of the slit of the spectrograph. The Raman spectra of these substances in the solid state at different low temperatures were recorded in the same way as described earlier (Biswas, 1954*a*; 1954*b*). In all cases the spectra were photographed on Ilford Zenith plates with a Fuess glass spectrograph having a dispersion of about 11Å° per mm in the region of 4047Å°. The microphotometer records were taken with a Kipp and Zonen type self-recording Moll microphotometer.

RESULTS AND DISCUSSION

The Raman shifts of the different substances in the liquid and solid states at different temperatures are given in Tables I-V. The data on the Raman spectra of all these substances in the liquid state as given in the Annual Tables of Constants and Numerical Data (Magat, 1936) are also included for comparison. The polarisation of these compounds were studied previously by different workers, but as the data were not available we redetermined qualitatively the polarisation of the Raman lines of the two halogen substituted toluenes in the liquid state. In Tables I and II the capital letter P or D against any particular Raman line indicates whether the line is polarised or depolarised to the extent 6/7.

(a) RAMAN LINES DUE TO INTRAMOLECULAR VIBRATIONS

(i) *Metachlorotoluene.*

The data given in Table I show that two extra weak lines at 884(0) and 948(0) cm^{-1} recorded in the present investigation in the liquid phase of *m*-chlorotoluene, are not given by previous authors. On the other hand, the lines 613(4)? and 3031(4) cm^{-1} reported by previous authors are not observed in the present investigation. The spectrogram obtained in the present investigation is a well-exposed one and the lines are definitely absent. Again, each of the lines 231 and 1216 cm^{-1} reported by previous workers is actually split up into two lines. These are at 222(5) and 247(5) cm^{-1} in the former case and at 1209(1) and 1219(4) cm^{-1} in the latter case.

A group of three intense lines at 187, 222 and 247 cm^{-1} respectively shows some remarkable change with the change from the liquid to the solid phase. The first line at 187 cm^{-1} seems to disappear while the second line shifts a little towards the Rayleigh line when the substance is solidified and cooled down to -70°C . The line at 2926 cm^{-1} due to C-H stretching vibration of the molecule in the liquid shifts to 2919 cm^{-1} in the solid state at -70°C and a new broad weak line at 2849 cm^{-1} is observed. On further lowering the temperature of the solidified mass to -180°C , two more new lines at 2910 and 2953 cm^{-1} have been observed. Moreover, the intensities of both the lines 1571 and 1601 cm^{-1} of the liquid seem to decrease with solidification of the substance as these two lines are more intense than the line 1383 cm^{-1} in the case of the liquid while they are weaker than the same line in the spectrogram due to the solid at -180°C .

(ii) *Metabromotoluene:*

In the case of metabromotoluene in the liquid state also we observe a few feeble extra Raman lines not reported by earlier workers (Magat, 1936). These are at 467(00), 862(1), 892(1) and 943(0) cm^{-1} respectively. Further, the line at 1206(4) cm^{-1} is resolved into two lines at 1205(1) and 1211(4) cm^{-1} respectively

TABLE I
m-Chlorotoluene (*m*-Cl.C₆H₄CH₃)
 $\Delta\bar{\nu}$ in cm⁻¹

Liquid		Solid (Present author)	
Magat (1936)	Present author	At about -70°C	At -180°C
		43 (2) e,k	50 (1) e,k
		125 (1) e,k	129 (3) e,k
187 (6)	187 (5) \pm e, +k D	—	—
231 (7)	222 (5) \pm e, \pm k D	218 (1b) e,	218 (1b) e
	247 (5) \pm e, \pm k D	247 (1) o,k	247 (1) e,k
387 (1)	394 (1) e,k P		
417 (7)	419 (6) \pm e,k P	419 (2) e,k	419 (2) e,k
522 (6)	522 (6) \pm e,k P	522 (2) o,k	522 (2) e,k
613 (4)?			
683 (7)	683 (7) \pm e,k P	683 (3) e,k	683 (3) o,k
771 (2)	775 (2) e,k		
855 (3)	861 (3) e,k P		
	884 (0) o		
	948 (0) o		
996 (10)	998 (10) e,k,i P	998 (5) e,k	998 (5) e,k
1046 (1)	1042 (1) e,k		1042 (0) o,k
1080 (3)	1077 (4) e,k P	1077 (1) e,k	1077 (1) e,k
1097 (1)	1102 (2) e,k		1102 (0) o,k
1165 (1)	1160 (2) e,k		
1216 (4)	1209 (1) e,k		
	1219 (4) e,k P	1219 (2) e,k	1219 (2) e,k
1379 (3)	1383 (2) e,k P	1380 (0) o	1380 (0) e,k
1582 (3)	1574 (3) e,k D	1574 (0) o	1574 (1) e,k
1600 (4)	1601 (4) e D	1601 (0) o	1601 (0) e,k
2862 (2)		2849 (1b) k	2849 (1b) k
			2910 (1) k
2921 (7b)	2926 (6b) e,k P	2919 (2b) e,k	2919 (2) e,k
3031 (4)		2953 (1) k	2953 (1) k
3060 (7b)	3062 (10b) e,k,i P	3066 (6) e,k,i	3066 (6) e,k,i

TABLE II
m-Bromotoluene (*m*-Br.C₃H₄CH₃)
 $\Delta\bar{\nu}$ in cm⁻¹

Liquid		Solid (Present author)	
Magat (1936)	Present author	At about -80°C	At -180°C
		33 (2) k	33 (1) k
		120 (1) o,k	126 (3) o,k
171 (7)	173 (7b) \pm e, \pm k D	—	—
197 (5)	200 (5) \pm e, \pm k D	203 (5b) e	203 (5b) e
225 (6)	224 (6b) \pm e, \pm k D	242 (2) o,k	242 (2) o,k
306 (9)	308 (9) \pm o,k,i P	314 (5) o,k	314 (5) o,k
378 (0)	381 (0) o		
	467 (00) o		
518 (6)	522 (6) \pm e,k P	522 (2) o,k	522 (2) o,k
667 (7)	671 (7) \pm o,k,i P	671 (4) o,k	671 (4) o,k
770 (0.5)	774 (1) o,k		
789 (0.5)			
831 (3)	835 (3) o,k P	835 (0) o,k	835 (0) o,k
	862 (0) o		
	892 (1) o		
915 (1)			
	943 (0) o		
990 (10)	998 (11) e,k,i P	998 (6) o,k	998 (6) o,k
1022 (2)	1029 (2) o,k P	1029 (0) o,	1029 (0) o
1065 (5)	1070 (5) o,k P	1070 (2) o,k	1070 (2) o,k
1162 (1)	1166 (1) o,k		
1206 (4)	1205 (1b) o		
	1211 (4) o,k P	1211 (2) o,k	1211 (2) o,k
1365 (3)			
	1383 (4) o,k P	1383 (1) o	1383 (1) o,k
1411 (0)			
1567 (4)	1571 (5) o D	1571 (1) o,k	1571 (1) o,k
1593 (4)	1601 (5) o D	1601 (0) o,k	1601 (0) o,k
2874 (1)	2865 (2) o,k P	2865 (0) k	2865 (0) k
2923 (3)	2926 (7b) e,k P	2915 (4b) o,k	2915 (4) o,k
			2932 (0) k
3051 (4b)	3062 (9b) P	3065 (6b) o,k,i	3067 (6) o,k,i

TABLE III

Orthocresol. (*o*-CH₃C₆H₄OH) $\Delta\bar{\nu}$ in cm⁻¹

Liquid		Solid (present author)	
Magat (1936)	Present author	At about -30°C	At -180°C
		45 (1b) k	40 (1) k
			68 (1) k
		90 (2b) k	85 (1b) k
190 (6)	190 (5) ± e, k	—	—
274 (5)	275 (5) ± e, k	280 (0)	280 (0)
305 (0)	316 (1) e, k		
445 (0)	445 (2) e, k		
530 (5)	531 (4) e, k	531 (0) e	531 (0) e
584 (6)	587 (7) ± e, k	587 (1) e, k	587 (1) e, k
	646 (0) e		
	695 (0) e		
	711 (0) e		
749 (12)	749 (12) ± e, k, i	749 (4) e, k	749 (4) e, k
847 (2)	845 (2) e, k		
989 (3)	992 (3) e, k	992 (0) e, k	992 (0) e, k
1044 (7)	1040 (10) e, k, i	1040 (3) e, k	1040 (4) e, k
	1094 (1) e		
1110 (0)	1109 (1) e		
1156 (3)	1155 (4) e, k	1155 (1) e, k	1155 (1) e, k
1238 (4)	1235 (1) e	1240 (1) e, k	1240 (1) e, k
1256 (4)	1258 (6) e, k	1258 (2) e, k	1258 (2) e, k
1380 (3)	1383 (3) e, k	1383 (1) e, k	1383 (1) e, k
1438 (1)	1444 (2) e, k		
	1471 (1) e		
	1510 (1) e		
1588 (2)	1597 (4) e, k	1597 (2) e, k	1597 (1) e, k
1614 (4)	1619 (6) e, k	1619 (1) e, k	1619 (0) e
2920 (7)	2920 (6) e, k	2920 (3) e, k	2920 (3) e, k
		2948 (2) k	2948 (2) k
3057 (7)	3063 (8b) e, k	3063 (3b) e, k	3063 (3b) e, k
3203 (1)			

TABLE IV

Metacresol ($m\text{-CH}_3\text{C}_6\text{H}_4\text{OH}$) $\Delta\bar{\nu}$ in cm^{-1}

Liquid		Solid (represent author)	
Magat (1936)	Present author	At about -40°C	At -180°C
			95 (1b) k
214 (6)	216 (6b) \pm e,k	219 (0) e	219 (0) e
239 (6)	245 (7b) \pm e,k	249 (0) e	249 (1) e
307 (0)	305 (1b) e		
	450 (0) e		
521 (5)	518 (6) e,k	518 (0) e,k	518 (1) e,k
541 (5)	543 (6) e,k	543 (0) e,k	543 (1) e,k
563 (0.5)	569 (2) e,k		
735 (8)	734 (12) e,k,i	734 (3) e,k	734 (4) e,k
777 (0)	779 (1) e		
833 (0)	848 (0) e		
	956 (0) e		
998 (10)	1002 (15) e,k,i	1002 (5) e,k	1002 (6) e,k
1084 (4)	1085 (5) e,k	1084 (1) e,k	1088 (1) e,k
1160 (2)	1166 (4) e,k	1166 (0) e,k	1166 (0) e,k
1277 (5)	1276 (5b) e,k	1276 (2b) e,k	1276 (2b) e,k
1378 (3)	1383 (5) e,k	1383 (1) e,k	1383 (1) e,k
1448 (0)			
	1460 (0) e,k		
1592 (3)	1593 (5) e,k	1593 (0) e	1593 (0) e
1610 (3)	1616 (4) e,k	1616 (0) e	1616 (0) e
2923 (6)	2920 (6b) e,k	2920 (2b) k	2920 (3b) k
			2949 (0) k ?
3051 (9)	3052 (7b) e,k,i	3052 (3b) e,k	3052 (4b) e,k

TABLE V
Paracresol ($p\text{-CH}_3\cdot\text{C}_6\text{H}_4\text{OH}$)
 $\Delta\bar{\nu}$ in cm^{-1}

Liquid		Solid (present author)	
Magat (1936)	Present author	At about -30°C	At -180°C
		47 (1b) k	47 (1) k
		90 (0b) k	90 (1b) k
	282 (0b) e		
337 (6)	338 (6b) \pm e,k	343 (1b) e,k	343 (2) e,k
	406 (0) e		
464 (6)	462 (6) \pm e,k	467 (1) e,k	467 (1) e,k
507 (0)	513 (1) e		
646 (5)	644 (6) \pm e,k	644 (1) e,k	644 (2) e,k
700 (1)	698 (2) e,k		
736 (1)	742 (2) e,k		
	809 (0) e		
825 (4)	829 (5b) e,k,i	829 (1) e,k	829 (2) e,k
841 (9)	845 (11) \pm e,k,i	840 (5) e,k	840 (6) e,k
	969 (0) e		
	1032 (0) e		
1170 (3)	1167 (3) e,k	1167 (0) e	1167 (0) e,k
	1205 (2) e,k		
1213 (4)	1219 (5) e,k	1211 (1) e,k	1211 (2) e,k
	1253 (3b) e,k	1253 (1) e,k	1253 (2) e,k
1296 (0)	1295 (1) e,k		
1380 (3)	1383 (4) e,k	1383 (0) e,k	1383 (1) e,k
1450 (0)	1460 (1) e		
	1517 (0b) e		
	1597 (4) e,k	1588 (0) e,k	1588 (1) e,k
1608 (4)	1613 (6) e,k	1600 (1) e,k	1600 (2) e,k
2866 (2)	2864 (3b) e,k	2864 (0) k	2864 (0) k
2921 (5)	2920 (4b) e,k	2912 (2b) e,k	2912 (2b) e,k
3018 (0)	3012 (2) e,k	3012 (0) k	3012 (0) k
	3048 (2) e,k	3048 (0) k	3048 (0) k
3055 (7)	3063 (6) e,k,i	3058 (5) e,k	3058 (6) e,k
3189 (1)	3201 (1) k		

in the present investigation. On the other hand, the lines $789(0.5)$, $915(1)$ and $1411(0)$ cm^{-1} reported by previous workers are not observed in the dense spectrogram obtained in the present investigation. Corresponding to three lines below 300 cm^{-1} of *m*-chlorotoluene, this substance also yields a group of three intense lines with frequency shifts $173(7b)$, $200(5)$ and $224(6)$ cm^{-1} respectively. The microphotometer records showing the relative intensities of these lines observed in the liquid state as well as in the solid state at -180°C are reproduced in figure 1. It can be seen from the records that the first line at 173 cm^{-1}

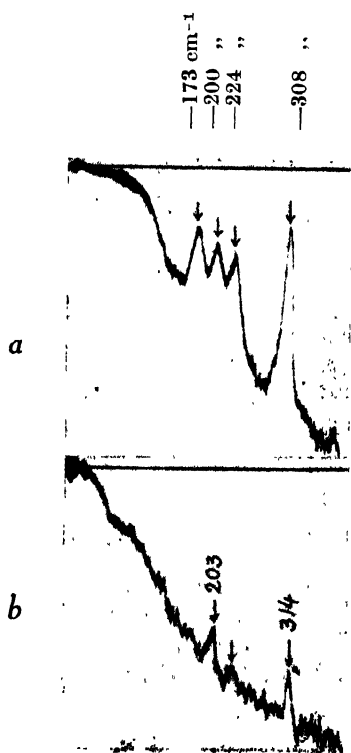


Fig. 1

Microphotometric records of the Raman spectra

Fig. 1. Metabromotoluene

- (a) Liquid at room temp,
(b) Solid at -180°C

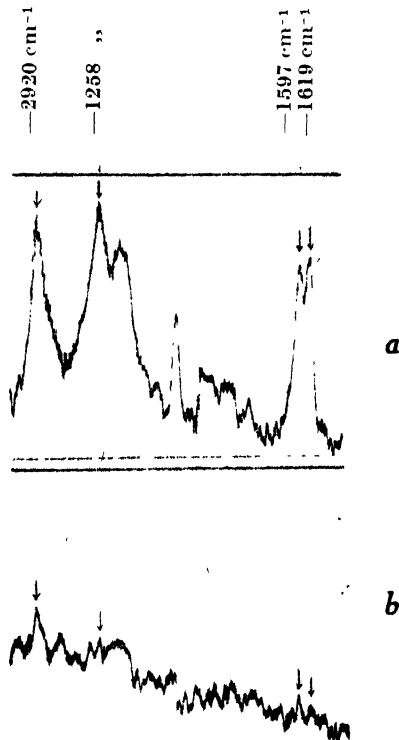


Fig. 2

Fig. 2. Orthocresol

- (a) Liquid at room temp,
(b) Solid at -30°C

disappears while the line at 224 cm^{-1} becomes sharper and shifts by about 18 cm^{-1} away from the exciting line at -180°C . The line at 200 cm^{-1} which is relatively weak in the liquid phase becomes very intense in the case of the solid state. Further, the width of the line also increases considerably with the solidification of the liquid. In addition to the above changes, the line at 2926 cm^{-1} shifts to 2915 , a new fainter line appears at 2932 cm^{-1} and the

doublet at about 1600 cm^{-1} becomes relatively weaker when the substance is solidified and cooled down to -180°C .

It is thus seen from the results discussed above that the lines 187cm^{-1} and 173 cm^{-1} of *m*-chlorotoluene and *m*-bromotoluene respectively disappear almost completely with the solidification of the liquids, while the intensity of the line 200 cm^{-1} of the latter compound increases with solidification. In order to understand the significance of these changes, it is necessary to make correct assignment, of these lines which are observed to be totally depolarised. In the molecules of *m*-chlorotoluene and *m*-bromotoluene, the vibrations involving bending of the C-Cl or C-Br and the C-(CH₃) bond in the plane of the molecule are expected to give rise to the Raman shifts in the neighbourhood of 200 cm^{-1} if the assignment made by Sponer and Kirby-Smith (1941) in the case of some lines in this region due to ortho dichlorobenzene be assumed as correct. However, in the case of the ortho- or meta compounds studied in the present investigation, we can expect only two such modes producing only polarised Raman lines, because there is no two-fold axis of symmetry. Actually, however, three totally depolarised lines are observed in either of these liquids. So it is difficult to assign the lines to any mode involving bending of the C-CH₃ and C-Cl or C-Br bonds in the plane of the molecules. On the other hand, neglecting the hydrogen atoms in the CH₃ group, we can assume that these molecules have a plane of symmetry and these lines may be due to some displacements at right angles to the plane of the molecule. Mere bending of the C-CH₃ or C-Cl or C-Br bonds at right angles to the plane of the molecules however, gives rise to lines of much higher frequency-shifts. Hence the lines are to be assigned to some mode in which both the carbon atom and the halogen atom attached to it are displaced at right angles to the plane of the molecule. Probably these are of the type $E_{2u}(\nu_{20})$, given by Herzberg (1946).

We can expect, however, two totally depolarised lines due to such modes. The third line which vanishes almost completely when the liquids are solidified cannot therefore be attributed to any mode of the single molecule. Probably one of these modes in some of the molecules in the liquid state is affected by the field of the neighbouring molecules so that the frequency diminishes a little. This can happen if due to random orientation of the molecules in the liquid some of the molecules are suitably oriented and are sufficiently close to each other to form associated groups of molecules. In the crystalline state, however, the molecules become regularly arranged and the resultant field of neighbouring molecules may counterbalance the effect of the virtual bond so that the frequency of the particular mode becomes almost the same as that of the single molecule. Actually, however, the frequency-shift of one of the two lines observed in the case of the solid is slightly smaller than that in the liquid state.

In the case of ortho- and metadichlorobenzene also some of the lines in this region are probably due to the mode E_{2u} as suggested above for the case of

chloro- and bromotoluene and if such an assumption is made, the difficulty pointed out by Sponer and Kirby-Smith (1941) does not arise.

(iii) *Orthocresol*.

From Table III it can be seen that the extra weak lines observed in the case of this liquid at 646(0), 695(0), 711(0), 1094(1), 1471(1) and 1510(1) cm^{-1} respectively were not reported by previous workers. When the substance is solidified and cooled down to different low temperatures, the strong line at 190 cm^{-1} observed in the case of the liquid disappears completely while the intensity of the line 275 cm^{-1} diminishes. Further, with solidification, a new strong line appears at 2948 cm^{-1} and the line 1240 cm^{-1} becomes almost as intense as the line 1258 cm^{-1} . Also, the relative intensities of the lines at 1597 and 1619 cm^{-1} seem to be reversed with the solidification and cooling down to lower temperature (figure. 2).

The lines at 190 and 275 cm^{-1} are probably due to some modes involving displacements at right angles to the plane of the molecule and correspond to the mode E_{2v} (ν_{20}) of the benzene molecule as pointed out earlier. Now in one of these modes all the atoms move at right angles to the plane of the molecule and probably on solidification strong virtual bonds are formed between neighbouring molecules so that the frequency becomes much smaller and the corresponding line shifts towards the region within 100 cm^{-1} from the exciting wavelength. The appearance of the new line at 2948 cm^{-1} due to the C-H valence oscillation and the increase in intensity of the line due to C-H bending vibration probably supports the view that the molecules become strongly associated in the solid state causing shift of the line at 190 cm^{-1} .

(iv) *Metacresol*.

Data given in Table IV show that the feeble lines at 450(0) and 956(0) cm^{-1} observed in the present investigation are not reported by earlier authors (Magat, 1936). The weak line at 1460(0) cm^{-1} may probably correspond to the weak line at 1448 (0) cm^{-1} reported by previous workers. When the liquid is solidified, the lines at 216 and 245 cm^{-1} shift to 219 and 249 cm^{-1} respectively, but unlike the corresponding lines of the ortho compound these lines persist in the solid state. The appearance of the new line at 2948 cm^{-1} in the case of the ortho compound is probably connected with the diminution in the intensity of the lines 190 and 275 cm^{-1} . In the case of the meta compound no change takes place in the relative intensities of the two lines 216 and 239 cm^{-1} probably because no strong hydrogen bonding takes place through the hydrogen atom of the C-H group.

(v) *Paracresol*.

In the case of paracresol (Table V) also a few extra lines are observed in the liquid phase of this substance. They are at 282(0), 406(0), 809(0), 969(0), 1032(0), 1253(3b), 1517(0) and 3048(2) cm^{-1} respectively. Amongst these

extra lines, the lines at 1253 and 3048(2) cm^{-1} are not very weak. The lines at 1213 and 1608 cm^{-1} reported by earlier authors (Magat, 1936) are resolved in the present investigation into doublets at 1205 and 1219 cm^{-1} and at 1597 and 1613 cm^{-1} respectively. The lines at 338, 462, 845, 1219, 1597, 1613 and 2920 cm^{-1} shift respectively to 343, 467, 840, 1211, 1588, 1600 and 2912 cm^{-1} when the substance is solidified. Moreover, excepting the line at 2920 cm^{-1} all of the broad lines produced in the liquid phase of this substance become sharp in the solid state at -180°C .

The lines 1597 and 1613 cm^{-1} are due to deformations in the benzene ring in which the displacements take place in the plane of the molecule and we seldom notice any decrease in the frequency-shifts of these lines with solidification of the substance. In this particular case, therefore, such a diminution in the Raman shifts of these lines indicates that the strength of the bond amongst the atoms of the benzene ring is probably slightly weakened in the solid state. The slight decrease on solidification in the frequency-shift of the strongest line at 845 cm^{-1} which is probably due to the breathing vibration of the substituted ring also corroborates this statement.

(b) NEW RAMAN LINES IN THE LOW-FREQUENCY REGION IN THE SOLID STATE

The microphotometer records of figures 3 and 4 show the number and relative intensities of the new Raman lines in the low-frequency region produced by the two halogen substituted toluenes studied in the present investigation. Metachlorotoluene in the solid state at -70°C gives rise to two new lines at 43 and 125 cm^{-1} respectively. With lowering of temperature to -180°C these lines shift to 50 and 129 cm^{-1} respectively. The change in their intensities with change of temperature of the solidified mass is, however, more prominent than the change in frequency. The relative intensities of these two lines change from the ratio 2:1 to 1:3 with change of temperature from -70°C to -180°C . The low-frequency Raman spectrum of solidified metabromotoluene has similar appearance for the two temperatures -80°C and -180°C , but the frequency-shifts are slightly smaller. The behaviour of these lines with change of temperature is also similar to that of *m*-chlorotoluene. In the case of cresols at least one of the new lines in the low-frequency region is very broad even at -180°C . The change in the relative positions of the OH and CH_3 groups seems to alter the low-frequency lines considerably. The meta compound in the solid state yields only one new broad line in the low-frequency region while the para and ortho compounds yield respectively two and three such lines at -180°C . A comparison of the changes in the ultraviolet absorption spectra of the three cresols with similar changes in the temperatures of the substances (Swamy, 1952) shows that in the case of the para compound the bands become sharper at -180°C while in the case of the other two compounds the bands do not become very sharp even when the substances are cooled down to -180°C . The new Raman lines, however, are sharper and more intense in

the case of the para compound than in the case of the meta compound. This comparison shows that the angular oscillation of molecule in the crystal lattice cannot be mainly responsible for the origin of low-frequency lines in crystals, because

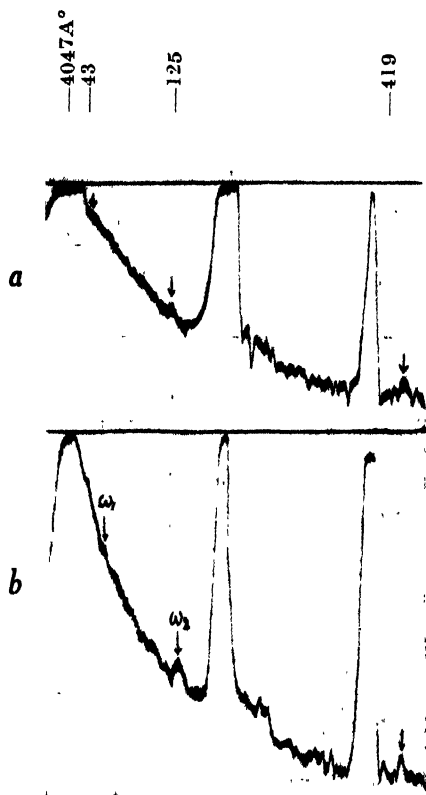


Fig. 3

Microphotometric records of the Raman spectra

Fig. 3. Metachlorotoluene

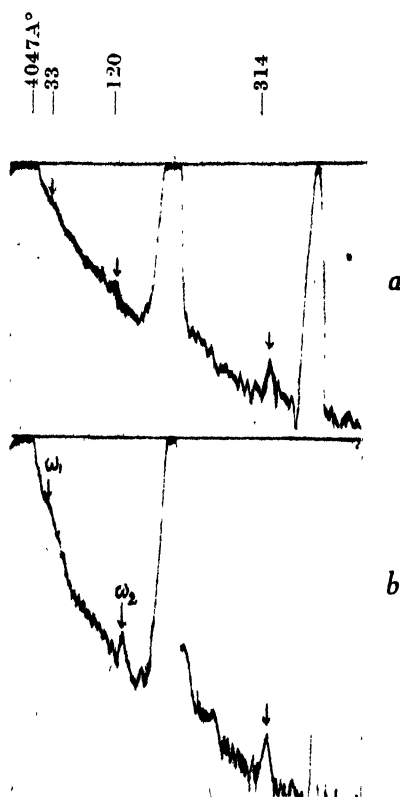
(a) Solid at -70°C (b) Solid at -180°C $(\omega_1 = 50\text{cm}^{-1}; \omega_2 = 129\text{cm}^{-1})$ 

Fig. 4

Fig. 4. Metabromotoluene

(a) Solid at -80°C (b) Solid at -180°C $(\omega_1 = 33\text{cm}^{-1}, \omega_2 = 126\text{cm}^{-1})$

the new lines in the low-frequency region are intense and greater in number in the case of paracresol than in the case of the meta compound while the ultra-violet absorption spectra indicates that the angular oscillation nearly ceases in the solid state at low temperature in *p*-cresol and such angular oscillations at least partially persist in the solid state at -180°C in meta cresol.

It would be interesting to compare the low-frequency Raman spectra of all the three isomers of chlorine and bromine substituted toluenes in the solid state, because such a comparison would show the influence of change in the relative positions of the substituents and of the mass of the substituents on the number and positions of the new lines. The low-frequency Raman lines of these compounds

are given in Table VI. The figures in parentheses in the table indicate the visually estimated intensities of these lines.

It appears from Table VI that there is no correlation between the frequency-shifts of the new lines and the mass of the substituent atoms in the same type of isomer, because the line 50 cm^{-1} is present in the spectra of all the chlorotoluenes

TABLE VI

 $\Delta\nu$ in cm^{-1}

Chlorotoluenes at -180°C			Bromotoluenes at -180°C		
Ortho (Sanyal, 1953)	Meta (Present author)	Para (Sanyal, 1953)	Ortho (Biswas, 1954)	Meta (Present author)	Para (Biswas 1954)
36 J (0)		38 (2)	36 (2)	30 (1)	
50 (1)	50 (1)	50 (1b)			52 (1)
78 (0)		85 (1b)			
102 (2)			100 (4b)		94 (3b)
	129 (3)			126 (3)	
					133 (4)
					162 (1)

and parabromotoluene. Again, it is observed that the line at about 126 cm^{-1} in the case of the meta compounds is extremely weak when the substances are solidified and cooled to about -80°C , but when the temperature is lowered to -180°C the intensity of the line increases to three times its value at -80°C in the case of both metachlorotoluene and metabromotoluene. This observation precludes the possibility of attributing this line to any mode of angular oscillation about an axis of the molecule, because in that case the intensity would not increase at low temperatures. Further, the increase in the frequency-shifts of the lines with lowering of temperature cannot be explained by any other hypothesis except that of the formation of virtual bonds and strengthening of these bonds at lower temperatures.

(c) FLUORESCENCE SPECTRA

Both metachlorotoluene and metabromotoluene produce two broad fluorescence bands in the visible region in the solid state at -180°C . Amongst the cresols, only the ortho compound produces one broad fluorescence band under similar conditions. The fluorescence bands in all the above three compounds are, however, weak. The approximate position for the centres of the bands, the interval between two successive bands in any compound as well as their visually estimated intensities are given in Table VII.

TABLE VII
Fluorescence spectra

Compound (solidified & cooled to -180°C)	No. of bands	1st band		2nd band		Band interval in cm^{-1}
		Position in cm^{-1}	Intensity	Position in cm^{-1}	Intensity	
<i>m</i> -Chlorotoluene	2	23211	1	21611	1	1600
<i>m</i> -Bromotoluene	2	23195	1	21592	1	1603
<i>o</i> -Cresol	1	20419	2	—	—	—

The interval between the two successive fluorescence bands of the two halogen substituted toluenes is about 1600 cm^{-1} which may correspond to the frequency of $\text{C}=\text{C}$ vibration in these molecules. It appears from such coincidence that the electronic state of the benzene ring itself is responsible for this fluorescence. Swamy (1952) observed that the ν_0 band of *m*-chlorotoluene shifts from 36315 cm^{-1} to 37015 cm^{-1} with solidification and lowering of temperature to -180°C . Whether this band is responsible for the fluorescence or a new band that appears on the longer wavelength side is not known.

ACKNOWLEDGMENT

The author is indebted to Professor S. C. Sirkar, D. Sc., F.N.I. for his kind help and guidance during the progress of this work.

REFERENCES

- Biswas, D. C., 1954a, *Ind. J. Phys.*, **28**, 85.
 Biswas, D. C., 1954b, *Ind. J. Phys.*, **28**, 303.
 Biswas, D. C., 1954c, *Ind. J. Phys.*, **28**, 423.
 Biswas, D. C., 1955, *Ind. J. Phys.*, **29**, 179.
 Herzberg, G., 1946, *Infra red and Raman spectra of Polyatomic molecules*, p. 118.
 Magat, M., 1936, *Annual Tables of constants and Numerical data*, pp. 74 and 77.
 Sanyal, S. B., 1953, *Ind. J. Phys.*, **27**, 447.
 Sirkar, S. C., and Swamy, H. N., 1952, *J. Chem. Phys.*, **20**, 1177.
 Sponer, H., and Kirby-Smith, J. S., 1941, *J. Chem. Phys.*, **9**, 667.
 Swamy, H. N., 1952a, *Ind. J. Phys.*, **26**, 119.
 Swamy, H. N., 1952c, *Ind. J. Phys.*, **26**, 445.

SPIN-ECHO MODULATION DUE TO MAGNETIC DIPOLE INTERACTION BETWEEN A CLOSELY INTERACTING PAIR OF NUCLEI IN CRYSTALS*

T. P. DAS* AND S. K. GHOSH ROY

INSTITUTE OF NUCLEAR PHYSICS, CALCUTTA,

(Received for publication, February 15, 1955)

ABSTRACT. It is shown that the strong interaction between a closely interacting pair of nuclei subject to resonance simultaneously produces a modulation of the spin-echo pattern for these nuclei. It is discussed how we can obtain information regarding the structure of the crystal from an analysis of this modulation pattern.

INTRODUCTION

Previous work by Hahn and others [Hahn and Maxwell (1952), Gutowsky et al (1949), McNeil et, al. (1951), Bloom and Norberg (1954), Hahn and Herzog (1954), Das and Saha (1954)] have shown that the causes which give rise to a splitting of the resonance line-shape in steady experiments produce a modulation of the echo-envelope in spin-echo experiments. Among the causes which have been already analysed by these authors are chemical-shift, J -coupling, weak-quadrupole interaction of the resonant nuclei with the surroundings in the presence of a strong external magnetic field and interaction with a weak external applied magnetic field in the presence of strong quadrupole interaction of the nuclei with the surroundings (the magnetic splitting of pure quadrupole resonance lines). In the present paper we shall discuss the effect of the magnetic dipole interaction between a closely interacting pair of nuclei on their spin-echo pattern. Examples of such two spin systems are the proton pairs in a molecule of crystals, the water of crystallization of CaSO_4 , $2\text{H}_2\text{O}$ and KF , $2\text{H}_2\text{O}$ (Pake, 1948) and the proton pair in each CH_2Cl group of $\text{CH}_2\text{Cl}-\text{CH}_2\text{Cl}$. We can take the closely interacting pair of protons as virtually isolated from the other neighbouring nuclei in considering the effect of this interaction on their spin-echo pattern. The interaction with the neighbouring nuclei causes a distribution about the fine-structure components arising out of the magnetic dipole interaction between the interacting pair. In the echo experiment we expect it to merely cause a damping of the echo and free induction signals. Also, we assume the crystal to be perfectly rigid so that we do not have to take account of the presence of any spin-lattice relaxation effects. In Section I, we deduce the expressions for the amplitudes of free-induction, primary and stimulated echo signals for a closely interacting pair of nuclei of spin $1/2$. In Section II, we discuss how the observation of the modulation pattern on the free-induction signals and the echo-envelopes can yield structural informations

* Present address : Chemistry Department, Cornell University, U. S. A.

such as the length and orientation of the radius vector joining the two closely interacting nuclei.

I. THE FREE-INDUCTION AND ECHO-SIGNAL AMPLITUDES FOR AN ASSEMBLY OF CLOSELY INTERACTING PROTON PAIRS

The Hamiltonian for a pair of closely interacting protons in the presence of a strong magnetic field H_z is

$$H = H_0 + H'$$

where

$$H_0 = -\gamma\hbar(I_{z1} + I_{z2})H_z, \quad \dots (2)$$

$$\begin{aligned} H' = & -\hbar\left\{PI_{z1}I_{z2} - \frac{P}{4}(I_{-1}I_{+2} + I_{+1}I_{-2})\right. \\ & -Q(I_{+1}I_{z2} + I_{+2}I_{z1}) - Q^*(I_{-1}I_{z2} + I_{-2}I_{z1}) \\ & \left. + RI_{+1}I_{+2} + R^*(I_{-1}I_{-2})\right\}, \quad \dots (3) \end{aligned}$$

with $I_{\pm} = I_x \pm iI_y$, the suffixes 1 and 2 referring to the two nuclei of the pair, γ is the magnetogyric ratio of the proton, P , Q and R are given by

$$\begin{aligned} P &= \frac{\gamma^2\hbar}{r^3} (1 - 3 \cos^2\theta), \\ Q &= \frac{3\gamma^2\hbar}{2r^3} \sin\theta \cos\theta e^{-i\phi}, \quad \dots (4) \\ R &= \frac{3\gamma^2\hbar}{4r^3} \sin^2\theta e^{-2i\phi} \end{aligned}$$

r representing the length of the radius vector joining the two interacting nuclei, θ the angle it makes with the Z -axis and ϕ its azimuth taking the rf -field direction as X -axis.

The free precession matrix describing the transformation of the states of the spin system in the absence of rf pulses will be given as usual by

$$D(t_0 \rightarrow t) = \exp\left[-\frac{i}{\hbar}(H_0 + H')(t - t_0)\right] \quad \dots (5)$$

We can work with the product kets as basis viz. $\alpha_1\alpha_2$, $\beta_1\beta_2$, $\alpha_1\beta_2$ and $\alpha_2\beta_1$ (α and β referring respectively to the kets corresponding to the states of a proton with its spin respectively parallel or anti-parallel to the applied magnetic field), but with such a selection of basis, there is a degeneracy in the energy levels corresponding to the states $\alpha_1\beta_2$ and $\alpha_2\beta_1$ even in the first order. On the other hand,

if we work with the kets $\alpha_1\alpha_2$, $\frac{\alpha_1\beta_2 + \alpha_2\beta_1}{\sqrt{2}}$, $\beta_1\beta_2$ and $\frac{\alpha_1\beta_2 - \alpha_2\beta_1}{\sqrt{2}}$ as basis (corresponding to the basis of the irreducible representations characterised by the

values 1 and 0 of the total spin), this degeneracy is removed. We shall retain terms correct to the second order in the exponents of the matrix elements of D so that the modulation effects that we shall estimate will be correct to second order.

Next we have to find the Rabi-Bloch matrix in the presence of the rf -pulses (Bloch and Rabi, 1945). We have, designating the states $\alpha_1\alpha_2, \frac{\alpha_1\beta_2+\alpha_2\beta_1}{\sqrt{2}}, \beta_1\beta_2$ and $\frac{\alpha_1\beta_2-\alpha_2\beta_1}{\sqrt{2}}$ by 1, 2, 3 and 4 respectively and using the conventional Rabi-Bloch expression,

$$\left. \begin{aligned} R_{11} &= \cos^2 \xi/2 & R_{13} &= R_{31} = -\sin^2 \xi/2 \\ R_{22} &= \cos \xi & R_{12} &= R_{21} = \frac{i}{\sqrt{2}} \sin \xi \\ R_{33} &= \cos^2 \xi/2 & R_{23} &= R_{32} = \frac{i}{\sqrt{2}} \sin \xi \\ R_{n4} &= R_{4n} = 0 & n &\neq 4 \\ R_{44} &= 1 \end{aligned} \right\} \quad (6)$$

Using these R and D matrices, we can find the master-matrix S after a number of applied pulses given by [cf. Das et al (1954)]

$$S = D_n R_n D_{n-1} R_{n-1} \dots D_1 R_1 \quad (7)$$

the suffixes 1, 2, ... n representing the successively applied pulses. We then have, as in our previous papers [Das et al (1954), Das and Saha (1954)], the transformed density matrix for a spin-system after a number of pulses as

$$\rho(t) = S\rho(0)S^{-1} \quad \dots (7a)$$

$\rho(0)$ is the initial density matrix representing a Boltzmann distribution, viz.

$$\begin{aligned} \rho(0) &= \frac{N}{2I+1} \exp \left[-\frac{\hbar\omega_z}{k\Theta} (I_{z1} + I_{z2}) \right] \\ &\approx \frac{N}{2I+1} \left[1 - \frac{\hbar\omega_z}{k\Theta} (I_{z1} + I_{z2}) \right], \quad \dots (8) \end{aligned}$$

where I takes up the $(2I_1+1)$ values $2I_1$ to 0, which in the present case are only two in number. N is the number of such interacting pairs of nuclei in a system.

We then have the expectation value of the X -component of the magnetisation of the spin-system, after a number of pulses, as proportional to

$$\langle I_{x_1} + I_{x_2} \rangle = - \frac{N\hbar\omega_z}{(2I+1)k\Theta} T_r \left(S(I_{z_1} + I_{z_2}) S^{-1}(I_{x_1} + I_{x_2}) \right)$$

Using equations (7a), (8) and (9) we have calculated the expectation values of $I_{x_1} + I_{x_2}$, viz. $\langle I_{x_1} + I_{x_2} \rangle$ for an isochromatic group (Hahn, 1950) characterised by $\Delta\omega = \omega_z - \omega$ after the application of one, two and three applied pulses respectively as shown in figure 1. We have, correct to second order in the frequencies involved,

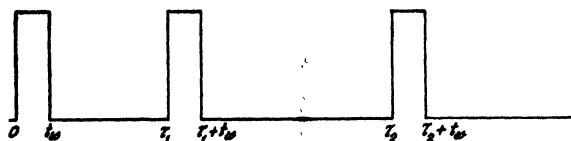


Fig. 1. Applied rf-pulses

Single pulse :

$$t > t_w$$

$$\langle I_{x_1} + I_{x_2} \rangle = - \frac{4N\hbar\omega_z}{3k\Theta} \cos \xi/2 \sin \xi/2 \cos \frac{3Pt}{4} \sin (\omega_z + S)t$$

Two pulses :

$$t > \tau_1 + t_w$$

$$\begin{aligned} \langle I_{x_1} + I_{x_2} \rangle = & \frac{4N\hbar\omega_z}{3k\Theta} \cos \xi/2 \sin^3 \xi/2 \left\{ \cos^2 \xi/2 \cos \frac{3P}{4} (t - 2\tau_1) \right. \\ & \left. - \cos \xi \cos \frac{3P}{4} t \right\} \times \sin \{(\omega_z + S)(t - 2\tau_1)\} \end{aligned}$$

Three pulses :

$$t > \tau_2 + t_w$$

$$\begin{aligned} \langle I_{x_1} + I_{x_2} \rangle = & - \frac{8N\hbar\omega_z}{3k\Theta} \cos^3 \xi/2 \sin^3 \xi/2 \sin \{(\omega_z + S)(t - \tau_2 - \tau_1)\} \\ & \times \left\{ 2(\cos^6 \xi/2 + \sin^6 \xi/2) \left[2 \cos \frac{3P}{4} (t - \tau_2 - \tau_1) - \cos \frac{3P}{4} (t - \tau_2 + \tau_1) \right] \right. \\ & + 3 \cos^2 \xi/2 \sin^2 \xi/2 \left[\cos^3 \xi/2 \cos \frac{3P}{4} (t - \tau_2 + \tau_1) \right. \\ & \left. \left. + \sin^2 \xi/2 \cos \frac{3P}{4} (t - \tau_2 - \tau_1) \right] \right\} \quad (12) \end{aligned}$$

where

$$S = \frac{QQ^* + RR^*}{2\omega_z} \dots\dots \quad (13)$$

In the latter two cases, viz. those of two and three applied pulses we have only given the terms involving $\omega_z(t - 2\tau_1)$ and $\omega_z(t - \tau_1 - \tau_2)$ respectively, which lead to

the primary and stimulated echoes. We have to integrate these expressions over Gaussian distributions in $(\omega_z + S) - \omega$ to get the contributions from all the isochromatic groups. The r.m.s. width of the distribution, according to Hahn

(1950) will be given by $T_2'' = \frac{T_2 T_2^*}{T_2 + T_2^*}$ where T_2 represents the spin-spin relaxation

time due to interaction with other neighbours and T_2^* the r.m.s. width of the distribution in external field inhomogeneity. The expressions $\sin(\omega_z + S)t$, $\sin(\omega_z + S)(t - 2\tau_1)$ and $\sin(\omega_z + S)(t - \tau_2 - \tau_1)$ in the above expressions then get replaced by

$\exp\left(-\frac{t^2}{2T_2''^2}\right)$, $\exp\left\{-\frac{(t-2\tau_1)^2}{2T_2''^2}\right\}$ and $\exp\left\{-\frac{(t-\tau_1-\tau_2)^2}{2T_2''^2}\right\}$ respectively show-

ing the occurrence of free induction primary echo and stimulated maxima at $t = 0$, $2\tau_1$ and $\tau_2 + \tau_1$ respectively. It is evident that the second order terms embodied in S do not give rise to any modulation of the echo pattern, they only cause a shift in the resonance frequency as in the case of weak electric quadrupole interaction in the presence of a strong magnetic field (cf. Volkoff, 1953). The first order effect causes a modulation of the free induction signal due to the presence of the $\cos 3Pt/4$ terms, and also gives rise to both "echo modulation" and "envelope modulation" [cf. Das and Saha (1954)] of the primary and stimulated echo signals. The envelope modulation term both in the primary and stimulated echoes is $\cos 6P\tau$. Thus in the case of stimulated echo, we only get a modulation of the envelope obtained by varying τ_1 , the interval between the first pair of pulses and not τ_2 , that between the second pair.

II. STRUCTURAL ANALYSIS FROM THE ABOVE MODULATION EFFECTS IN POWDERS:

The above modulation effects can give us information on both the unknown r and θ . We obtain from an analysis of the modulation patterns and this is seen to involve both r and θ viz.

$$P = \frac{\gamma^2 \hbar}{r^3} (3\cos^2\theta - 1)$$

If we now rotate the crystal about an axis perpendicular to the Z -field through an angle θ_1 , the modulation pattern with the new orientation will give us the new values of P , viz.

$$P' = \frac{\gamma^2 \hbar}{r^3} \{3 \cos^2(\theta + \theta_1) - 1\}. \quad \dots (15)$$

Using these two equations, we can obtain the two unknowns r and θ . We thus need only one rotation of the crystal to obtain the required information.

In the case of powders, we shall have a distribution in θ and we have to integrate the expressions (10), (11) and (12) over the entire range of θ , viz, 0 to π . Thus

considering the free induction signal alone, the modulation term is $\cos 3Pt$ which, for an orientation θ with respect to the Z -field, we write as $\cos \frac{3}{4}P(\theta)t$. Hence the net signal from the powder, involving a distribution in θ , will involve

$$\begin{aligned} M &= \frac{1}{2} \int_0^\pi \cos \frac{3}{4} P(\theta)t \, d\theta \sin \theta \\ &= \frac{1}{2} \int_0^\pi \cos \{qt(3 \cos^2 \theta - 1)\} d\theta \sin \theta \end{aligned} \quad (16)$$

where

$$= \frac{3\gamma^2 \hbar}{4r^3}.$$

M can be put in the form,

$$\begin{aligned} M &= \frac{1}{2} \left[\int_0^1 \cos 3z^2 qt \cos qt \, dz + \int_0^1 \sin 3z^2 qt \sin qt \, dz \right] \\ &= \sqrt{\frac{\pi}{6qt}} \left[\int_0^{\sqrt{6qt/\pi}} \cos \frac{\pi x^2}{2} \cos qtdx + \int_0^{\sqrt{6qt/\pi}} \sin \frac{\pi x^2}{2} \sin qtdx \right] \\ &= \sqrt{\frac{\pi}{6qt}} [C(\sqrt{6qt/\pi}) \cos qt + S(\sqrt{6qt/\pi}) \sin qt] \end{aligned} \quad (17)$$

with $C(x)$ and $S(x)$ representing the Fresnel's integrals (cf. Jahnke and Emde, 1938). Now t must correspond to at least a full period of the modulation if the modulation pattern is to be visible, we therefore have

$$\sqrt{\frac{6qt}{\pi}} \approx \sqrt{\frac{12\pi}{\pi}} \approx 3.5.$$

From the curves for $C(x)$ and $S(x)$ [Jahnke and Emde (1938)] we have

$$M = \frac{1}{3.5} [0.33 \cos qt + 0.62 \sin qt] \approx \frac{1}{10} \cos (qt - \epsilon) \quad (18)$$

where $\epsilon = \tan^{-1} 2$. This shews that the modulation frequency in powders is $q = \frac{3\gamma^2 \hbar}{4r^3}$ as is to be expected from Pake's (1948) analysis of the steady resonance splitting in powders due to this type of interaction. It is thus evident that we can only get information of r from observations on powders.

CONCLUSION

The above analysis does not take into account the effects of hindered motion inside the crystals; such hindered motions, if present, lead to a reduction in the splitting as observed by Gutowsky and others (1949). To take account of these motions, we have to incorporate their effects in the final density matrix after the passage of pulses and therefore in the D matrix. We shall discuss this point in a later paper.

ACKNOWLEDGMENTS

The authors are grateful to Prof. M. N. Saha, F.R.S. and Dr. A. K. Saha for their keen interest in our work. We are also grateful to Mr. D. K. Roy for some helpful discussions.

REFERENCES

- Bloom, M. and Norberg, R. E., 1954, *Phys. Rev.*, **93**, 638.
Das, T. P. and Saha, A. K., 1954, *Phys. Rev.*, in press.
Das, T. P. Saha, A. K. and Roy, D. K., 1954, *Proc. Roy. Soc. A.*, in press.
Gutowsky, H. S., Kistianowsky, Pake, G. E. and Purcell, E. M., 1949, *J. Chem. Phys.*, **17**, 972.
Hahn, E. L., 1950, *Phys. Rev.*, **80**, 580.
Hahn, E. L. and Herzog, B., 1954, *Phys. Rev.*, **93**, 639.
Jahnke, E. and Emde, E., 1938, *Tables of Functions*, p. 37, Dover Publications, New York.
McNeil, Gutowsky and Slichter, 1951, *Phys. Rev.*, **84**, 1245.
Pake, G. E., 1948, *J. Chem. Phys.*, **16**, 327.
Volkoff, G. M., 1953, *Can. H. Phys.*, **31**, 820.

ELECTRONIC COLLISIONAL FREQUENCY IN THE F-REGION OVER CALCUTTA*

By S. DATTA

INSTITUTE OF RADIO PHYSICS AND ELECTRONICS, UNIVERSITY OF CALCUTTA

(Received for publication, May 18, 1955)

ABSTRACT. Results of measurements of the effective electronic collisional frequency in the F-region of the ionosphere over Calcutta (geographic latitude $22^{\circ}33'$; geomagnetic latitude $13^{\circ}N$) are described. The measurement was based upon the theoretical formula of Appleton (1935), relating the reflection coefficient of an ionospheric region with the difference between the group and optical paths within the region. The collisional frequency is found to be of the order 3.8×10^3 per sec. per electron in the F-region of the ionosphere. An attempt is also made to find out the variation of the same with height in the F-region.

1. INTRODUCTION

A knowledge of the value of electronic collisional frequency in the different ionospheric regions is indispensable for the estimation of total attenuation suffered by radio waves in their passage through the ionosphere. The knowledge is also helpful for the estimation of temperature and pressure in the height range 100 km to 400 km.

Unfortunately, measurement of the electronic collisional frequency does not generally form a part of the programme of the observations carried out in an stations ionospheric observatory. The remark is particularly applicable to low latitude for which collisional frequency data are very meagre. In view of this, measurement of the collisional frequency in the F-region has recently been carried out at Calcutta. For this purpose, Appleton's theoretical expression relating the mean effective electronic collisional frequency with deviative absorption in the region as a function of probing radio frequency has been utilised.

2. THEORETICAL CONSIDERATIONS

It can be shown that the coefficient ρ of radio wave reflection from an ionospheric region is related to the mean collision frequency ν_{ω} in the region over the deviative path by the equation,

$$\log_e \rho = - \frac{\nu_{\omega}}{2c} [P' - P] \quad \dots (1)$$

assuming $\nu_{\omega}^2 \ll f^2$, where $c = 3 \times 10^{10}$ cms/sec.,

$P' = \int \frac{ds}{\mu}$ is the group path, $P = \int \mu ds$ is the optical path, and f is the radio

* Communicated by Prof. S. K. Mitra.

wave frequency. As shown by Appleton, equation (1) may conveniently be expressed in the differential form,

$$\nu_{\omega} = -2c \cdot \frac{\delta(f \log_e \rho)}{f \delta P'} \quad \dots (2)$$

ν_{ω} and its variation with altitude may therefore be estimated from the above relation, when $f \log_e \rho$ has been determined experimentally as a function of P' . Since $\nu_{\omega}^2 \ll f^2$ in the F-region, Equation (2) may be utilised for the determination of electron collision frequency.

3. EXPERIMENTAL ARRANGEMENT

Measurements of the reflection coefficient ρ and the group path P' were carried out with the semi-automatic ionospheric equipment of the Ionosphere Laboratory of the Institute of Radio Physics and Electronics of the Calcutta University.

The characteristics of the equipment are as follows:

Pulse frequency—50 per sec,

pulse width—200 micro-seconds,

accuracy of measuring group path— ± 15 km,

peak power output of the transmitter—500 Watts.

The receiver was of communication type, capable of receiving the band width of the transmitted pulse. The reflection coefficient was obtained by measuring the relative amplitudes of reflected echoes (assuming the reflection coefficient of the ground to be unity).

Thus $\rho = \frac{(n+1) \cdot I_{n+1}}{n \cdot I_n}$ where I_n and I_{n+1} correspond to the n th and $(n+1)$ th

order echo amplitudes respectively. The echo amplitudes were measured by comparison with a scale on the oscilloscope screen, care being taken to measure only echoes of such amplitude as lay within the linear range of the receiver. The linearity characteristics of the receiver, when the output is taken from the second detector load are shown in figure 1. Generally, only the first and the second order echo amplitudes were measured. Effect of random fading phenomenon of the reflected signal was eliminated by averaging the fluctuations. Observations were made at intervals of 10 seconds and, in order that the results could be assumed to be related to a definite ionospheric condition, each set of observations was completed within 15 minutes.

It is to be noted that the reflected radio wave, besides suffering absorption in the deviating F-region, also suffers absorption in passing and re-passing the underlying non-deviative D-and E-regions.

However, the effect of these absorptions is negligible in the morning and evening hours when the non-deviative absorptions are small and do not vary much

with change of the frequency of measurement. The actual hours of measurements were chosen from the theoretical curves drawn from Appleton's (1937)

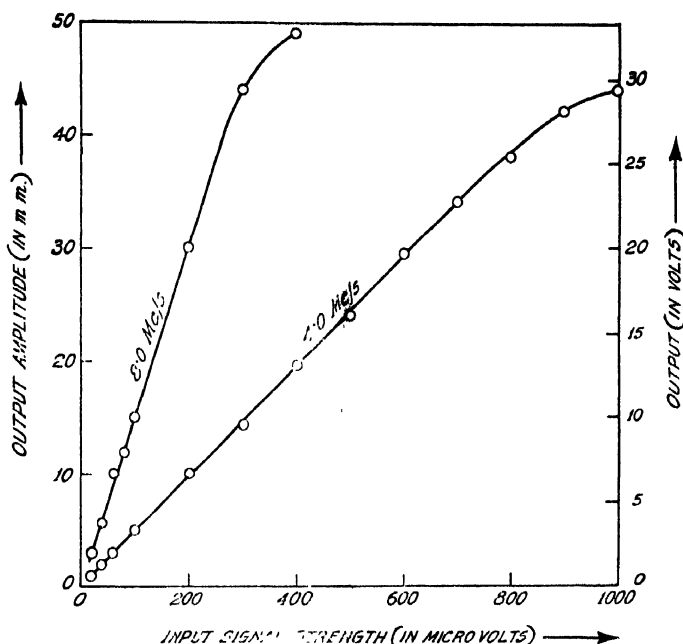


Fig. 1. Linearity characteristics of the receiver at 8.0 Mc/s and 4.0 Mc/s.

formula depicting the variation of the hourly values of the non-deviative absorptions in the E-region over Calcutta for the months of observations at the frequencies of measurements.

TABLE I

Electronic collisional frequency in the F-region

Date	Hour of observation (L.M.T.)	Exploring wave frequency (Mc/s)	Maximum electron number density per e.c.	Equivalent path in km.	Approximate altitude in km.	Collisional frequency per second per electron
1954						
April 15	18.30	8.40	1.05×10^6	390	280	3.8×10^3
April 20	09.45	8.22	0.92×10^6	360	305	5.8×10^3
	18.30	9.65	1.30×10^6	360	285	7.5×10^3
May 1	09.30	8.00	0.90×10^6	390	300	1.7×10^4
May 11	10.30	7.70	1.12×10^6	480	355	3.3×10^3
	19.30	7.40	1.04×10^6	460	345	4.5×10^3
May 12	09.45	7.60	0.86×10^6	480	355	5.8×10^3
May 14	10.30	8.10	0.96×10^6	465	330	3.0×10^3
	18.15	8.65	1.00×10^6	405	225	6.4×10^3
May 24	20.30	5.50	0.60×10^6	450	290	1.3×10^3

True height reached by the radio wave at the frequency of measurement was calculated on the assumption of a parabolic distribution of electron number density with height near the region of maximum ionisation.

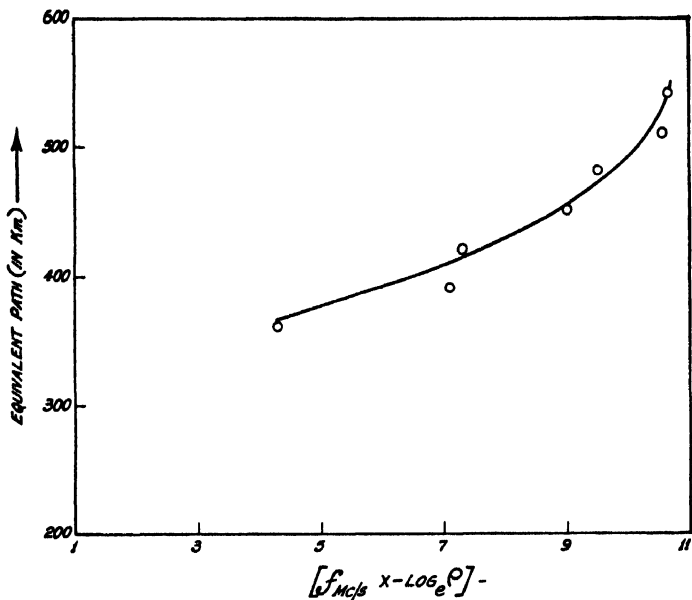


Fig. 2. (a) Variation of $[f_{Mc/s} \times -\log_e p]$ with the equivalent path on 28th April, 1954 at 21 hours and 45 min. L.M.T.

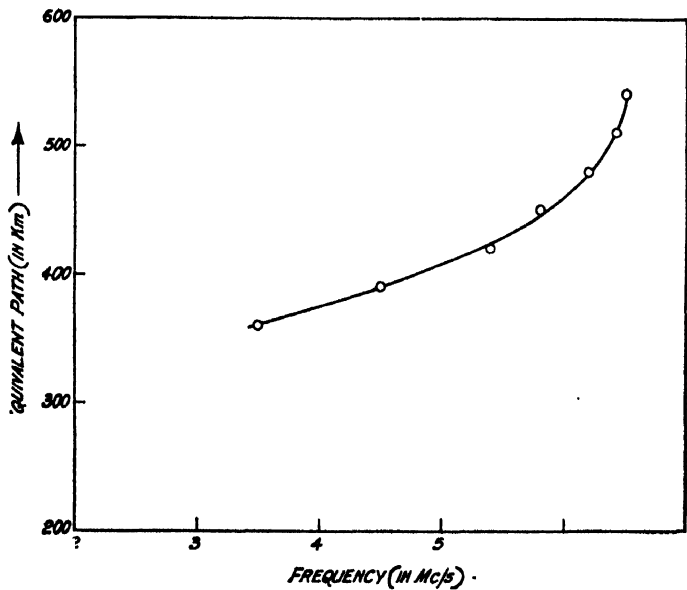


Fig. 2 (b) Corresponding equivalent height-frequency curve.

Table I shows the values of the collisional frequency in the F-region over Calcutta as obtained experimentally.

The most probable value of the F-region collision frequency over Calcutta as obtained from Table I is thus 3.8×10^3 /sec. per electron. An attempt was also made to find out how the collisional frequency varies with height. Obviously, such measurements are possible at the hours when the equivalent path varies rapidly with frequency. Results of observations made on April 28, 1954 with this purpose are shown in Table II.

TABLE II

April 28, 1954.

21.45 L.M.T.

Maximum electron number density— 0.57×10^6 /c.c.

Frequency of measurement (Mc/s)	Equivalent path in km.	Approximate altitude in km.	Collisional frequency per second per electron
6.50	540	390	1.5×10^3
6.20	480	375	3.7×10^3
5.40	420	350	7.2×10^3

It will be noted from the Table that the collisional frequency decreases with altitude.

4. CONCLUDING REMARKS

The values of collisional frequency as obtained by the author may be compared with the values obtained by other workers as shown in Table III.

TABLE III

Height (km)	Electronic collisional frequency (per sec.)	Author
250	5×10^3	White and Brown (1936)
250-400	$5 \times 10^3 - 1.2 \times 10^3$	Vilbig (1944) Farmer and Ratcliffe (1935b)
265	$3.6 \times 10^3 - 1.6 \times 10^3$	Eckersley (1935) Farmer and Ratcliffe (1935a)
300	3.0×10^3	Ginsburg and Alpert (1944)

(NOTE: Recently, Rawer, Bibl and Argence (1952) obtained experimentally from the night time observations an abnormally low value, $\nu = 2 \times 10^2$ per sec.).

It is to be noted that the collisional frequency ν as measured is the sum of the various collisional frequencies given by,

$$\nu = \nu_i + \nu_{N_2+N} + \nu_0 + \nu_e$$

where ν_i is the frequency of electron-ion collision, ν_{N_2+N} is the frequency of electron nitrogen particles collision, ν_0 is the frequency of electron-atomic oxygen collision and ν_e is the frequency of electron-electron collision. In the F-region, the contribution of ν_i is much larger than those of ν_{N_2+N} , ν_0 and ν_e . Theoretical analysis by Nicolet (1953), and by Gerson (1951) of Majumdar's (1937) expression for ν_i , shows that the value of ν_i is dependent on electron concentration and very strongly on the temperature. The theoretical expression for ν_i given by Nicolet is

$$\nu_i = \left[34 + 8.36 \log_{10} \frac{T^{3/2}}{n_e^{1/2}} \right] n_e T^{-3/2} \quad \dots (3)$$

where T is the absolute temperature and n_e is the concentration of the electrons. The wide scatter of the values of electronic collisional frequency in the F-region as obtained by different workers, may thus be due partly to the experimental difficulties (for the accurate measurements of the deviative absorptions) and partly to the fact that the representative values, refer to different electron densities and different temperatures.

ACKNOWLEDGMENTS

The author's grateful thanks are due to Professor S. K. Mitra for his kind guidance and help. The author is also indebted to Dr. S. S. Baral for suggesting the experimental investigation and for helpful suggestions. Thanks are also due to the Scientific Man Power Committee, Government of India, for providing the author with a scholarship.

REFERENCES

- Appleton, E. V., 1935, *Nature*, **135**, 618.
 Appleton, E. V., 1937, *Proc. Roy. Soc. A.*, **162**, 451.
 Mitra, S. K., 1948, *The Upper Atmosphere*, The Asiatic Society of Bengal, Calcutta.
 Eckersley, T. L., 1935, *Nature*, Lond., **135**, 435.
 Farmer, F. T. and Ratcliffe, J. A., 1935a, *Nature*, **135**, 585.
 Farmer, F. T. and Ratcliffe, J. A., 1935b, *Proc. Roy. Soc. A.*, **151**, 370.
 Gerson, N. C., 1951, *Reports on Progress in Physics.*, **14**, 316.
 Ginsburg, V. L. and Alpert, I. L., 1944, *Izvestiia Akad. Nauk. S.S.S.R., Seriiia Fizi-cheskaia*, **8**, 42.
 Majumdar, R. C., 1937, *Z. Phys.*, **107**, 599.
 Nicolet, M., 1953, *Jour. Atoms. & Terr. Phys.*, **3**, 200.
 Rawer, K., Bibl, K. and Argence, E., 1952, *Soc. Roy. Sc., Lie'ge, Me'moires*, **12**, 269.
 Vilbig, H. F., 1944, *Lehrbuch der Hochfrequenztechnik*, I (Leipsig : Akad Verlagsgesellschaft), p. 338.
 White, F. W. G. and Brown, L. W., 1936, *Proc. Roy. Soc.*, **153**, 639.

SPECTROSCOPIC CONSTANTS OF MOLECULES. IV SIMILARITIES IN GROUND STATE VIBRATION FREQUENCIES OF ISOELECTRONIC DIATOMS

By Y. P. VARSHNI AND K. MAJUMDAR,

DEPARTMENT OF PHYSICS, ALLAHABAD UNIVERSITY, ALLAHABAD

(Received for publication, March 21, 1955)

ABSTRACT. Resemblances in ground state vibration frequencies of isoelectronic diatoms belonging to the same molecular group and having "reversed" closed shells, have been investigated.

INTRODUCTION

In the broadest meaning of the term, "isoelectronic molecules" signifies molecules having equal number of total electrons. Isoelectronic atoms and ions are known to show very regular behaviour. However, for tracing regularities among isoelectronic molecules, the term in its widest sense is not useful, it is too general. For example, it would be insignificant to put together LiI and SBr, though both are iso-electronic (51 electrons). It is only in restricted classes of molecules having similar structure, that we can expect regularities. Usually the term signifies molecules having equal number of valence electrons and belonging to the same molecular period.

Bärwald, Herzberg and Herzberg (1934) pointed out the close resemblance in CP, SiN and CN, N_2^+ . Clark (1935) divided the isoelectronic molecules in three types, orthostere, metastere and parastere and traced regularities in them. Sharma (1945a, 1945b) showed the similarities in ($SnTe$, Sb_2) and ($PbTe$, $BiSb$). Other workers have also drawn attention to such regularities (Glockler, 1948, 1950; Vago and Barrow, 1946 etc.).

It is easy to understand theoretically the similarities between such molecules from a consideration of electron configurations (Herzberg, 1951). The electron configurations and the resulting electronic energy levels of molecules with not too different nuclei are determined essentially by the number of valence electrons and are therefore very similar for iso-electronic molecules (see also Coulson, 1952).

In order to substantiate this similarity of electronic configuration for such molecules, attention has frequently been directed towards the similarity that exists between certain physical properties, e.g. boiling point, critical constants etc. However, Long and Walsh (1947) have rightly emphasised that this argument is not logical, since many of the properties cited go to show similar molecular volumes and similar external fields of force rather than similar electronic arrangements, (see also Syrkin and Dyatkina, 1950).

Long and Walsh (1947) also pointed out the fact that the molecules N_2 and CO differ in a very significant way. When the N_2 molecule ionises to give N_2^+ the bond is weakened, as shown by increase in r_e and decrease in ω_e . On the other hand, when CO ionises to give $(CO)^+$ the bond is strengthened, as shown by decrease in r_e and increase in ω_e . Such examples clearly show that, even when the number of valence electrons in iso-electronic molecules is same, there may be significant differences in structures of the two.

In the present paper we would be concerned with a very restricted class of neutral diatoms, such isoelectronic molecules which belong to the same molecular group and have reversed closed shells (e.g., SiBr and GeCl). It will be shown that vibration frequencies for such diatoms are very close to each other. This fact enables us to estimate the vibration frequency of such diatoms which have not been investigated so far. Clark (1935) has also studied such molecules, however, his metasteres embrace a wider range of molecules, some of which do not show very close similarities. For example, NaBr and CuCl which are both metasteres have widely different vibration frequencies viz. 315 and 416.9 respectively.

The available experimental data (sources given in Part III, Varshni and Majumdar, 1955) have been collected in Table I together with some estimated values by the method of previous paper (Varshni and Majumdar, 1955). The estimated values by the method of this paper are followed by an "e". The molecule with lesser reduced mass (μ_A) has been placed first.

D A T A

The data have been taken from the sources given in Part III (Varshni and Majumdar, 1955) and those indicated in notes below the tables.

TABLE I

Group	Total number of electrons	Diatom	ω_e	Corresponding diatom	ω_e	Percentage difference
1a—7b	20	LiCl	~600 ee	NaF	465eV ₄ 477eR ₂	
	72	KI	200	RbBr	180	—10
1b—7b	82	CuI	264.8	AgBr	247.72	— 6.5
2a—6b	20	BeS	820 e	MgO	785.1	
2a—7b	21	BeCl	846.6	MgF	717.6	—15.2
	73	CaI	242	SrBr	216.5	—10.5
2b, 7b	83	ZnI	223.4	CdBr	230	+ 3.0
	115	ZnAt	180 e	HgBr	186.25	
	133	CdAt	130 e	HgI	125.6	

TABLE I (contd.)

Group	Total number of electrons	Diatom	ω_e	Corresponding diatom	ω_e	Percentage difference
3b-6b	21	BS	1173.6	AlO	978.2	- 16.7
	39	BSe	~ 700 e	GaO	767.7	
	57	BT ₆	~ 650 e	InO	703.1	
3b-7b	22	BCl	839.12	AlF	814.5	- 2.9
	40	BBr	684.31	GaF	623.8	- 8.8
	58	BI	570 eV ₄	InF	534.7	
	90	BAt	480 e	TlF	475	
	48	AlBr	378	GaCl	365	- 3.4
	66	AlI	316.1	InCl	317.4	+ .4
	98	AlAt	285 e	TlCl	287.47	
	84	GaI	216.4	InBr	221	+ 2.1
	116	GaAt	185 e	TlBr	192.1	
	134	InAt	145 e	TH	150	
4b-5b	21	CP	1239.7	SiN	1151.7	- 7.1
4b-6b	22	CS	1285.1	SiO	1242	- 3.3
	40	CSe	1036	GeO	985.7	- 4.9
	58	CTe	860 eV ₄	SnO	822.4	
			~ 875			
	90	CPo	740 e	PbO	721.8	
	48	SiSe	580	GeS	575.8	- .7
	66	SiTe	481.2	SnS	487.68	+ 1.3
	98	SePo	420 e	PbS	428.14	
	84	GeTe	323.4	SnS	331.2	+ 2.4
	116	GePo	270 e	PbS	277.6	
	134	SnPo	205 e	Pb ₂	211.8	
	21	CCl	846	SiF	856.7	+ 1.3
	41	CBr	670 eV ₄	GeF	665.2	
	59	CI	570 eV ₄	SnF	582.9	
	91	CA ₂	500 e	PbF	507.2	
	49	SiBr	425.4	GeCl	407.6	- 4.2
	67	SiI	360 e	SnCl	352.5	

TABLE I (contd.)

Group	Total number of electrons	Diatom	ω_e	Corresponding diatom	ω_e	Percentage difference
340 eV ₄						
	99	SiAt	300 e	PbCl	303.8	
	85	GeI	240 e	SnBr	247.7	
230 eV ₄						
	117	GeAt	200 e	PbBr	207.5	
	135	SnAt	160 e	PbI	160.5	
5b-6b	23	NS	1220	PO	1230.6	+ .9
	41	NSe	970 e	AsO	967.4	
1000 eV ₄						
	59	NTe	820 e	SbO	817.2	
880 eV ₄						
	91	NPo	700 e	BiO	695.9 B ₂	
	49	PSe	770 e	AsS	767	
	67	PTe	420 e	SbS	411	
	99	PPo	380 e	BiS	386	
	85	AsTe	330 e	SbSe	326	
	117	AsPo	260 e	BiSe	264.7	
	135	SbPo	210 e	BiTe	208.5	
5b-7b	42	NBr	(693)	AsF	(700) e	
	60	NI	600 e	SbF	614.2	
	92	NAt	500 e	BiF	510.7	
	68	PI	370 e	SbCl	369	
	100	PAt	310 e	BiCl	308	
	86	AsI	225 ee	SbBr	225 eV ₄	
	118	AsAt	200 e	BiBr	203.34	
	136	SbAt	160 e	BiI	163.9	
6b-7b	43	OBBr	713	SeF	720 e	
	61	OI	(687)	TeF	(690) e	
7a-7b	78	MnI	(240)	MaBr	(250) e	

Notes on Table I

'e' denotes an estimated value. 'e' not followed by any reference indicates that the value has been estimated by the method of this paper. 'ee' signifies that this value depends on another estimated value. B₂—Bridge and Howell (1954), R₂—Rittner (1951), V₄—Varshni and Majumdar (1955)

DISCUSSION

The average percentage difference for the 20 pairs for which data are available is 5.3, which shows that this method is reliable for predicting unknown vibration frequencies. Usually it is only in the case of lighter molecules that the differences are large. Thus, barring some individual cases, correct values can be expected to be within $\pm 6\%$ of the estimated values.

For most of the pairs, the molecule with higher reduced mass has a lower frequency, though it is not a strict rule and the reverse behaviour is also noticed in several cases. The restriction of 'reversed' shells is necessary, otherwise the differences are much larger. We may quote the case of (GeSe—406.5, SnS—487.68) and (GeO—985.7, SiS—749.5), which though belong to the same molecular group do not have "reversed" closed shells.

It will further be observed that in many cases (e.g. the pairs BI, InF; CBr, GeF, etc.) the values estimated by the previous method (Part III) fit very well in this scheme. In some cases there are small differences in the values predicted by the two methods. We may discuss the case of the pair SiI, SnCl. The experimental value for SnCl is 352.5, the predicted value for SnI by the previous method is 340. However, $\mu_A(\text{SiI}) < \mu_A(\text{SiCl})$ and it is expected that $\omega_e(\text{SiI})$ would be somewhat higher than $\omega_e(\text{SiCl})$, thus a value 360 is to be preferred.

For applying the method of Part III, it is necessary that at least two points be available for drawing the straight line. But in many cases only one point is available or none at all. The predicted values in Table I can be used in conjunction with the method of Part III to make further estimates. These are given in Table II. The probable error for these would be somewhat larger, because these values are based on estimated values. The compound average error, however, would not be larger than 8%.

Lithium and arsenic compounds require special mention. For lithium there is only one pair available satisfying the above requirements—that of LiCl and NaF. For estimating the value for LiCl, we require the value for NaF. But no experimental value is available for NaF; however, the method of Part III predicts a value 465 which is in good agreement with Rittner's theoretical value 477. This suggests that the correct value is not far from 480, and we may place an upper limit at 500. We expect the value of LiCl to be higher than this, however, caution has to be exercised as the reduced mass of the two molecules are much different, being $\mu_A(\text{LiCl}) = 5.806$ and $\mu_A(\text{NaF}) = 10.405$. In analogy with other light molecule pairs, the value for LiCl may be much higher, a safe estimate would be 600. If we assume this value for LiCl, it is expected that $\omega_e(\text{LiI})$ would not be higher than 500. However, this argument need not be given too much weight because LiCl and NaF are very light molecules and there is great difference in their reduced masses, and thus the possibility that the vibration frequency of LiCl may be higher than 600 cannot be completely ruled out. Van Leeuwen's (1930)

theoretical calculations give a value 509 for LiI. The observed value for LiI is 450, which is too low from the trend of force constants of alkali iodides. This has been discussed in Part III. Thus the position of ω_e values of Li compounds is very fluid.

TABLE II

Group	Diatom	Estimated
1a—7b	LiF	~700 eee
	LiBr	520 eee
2b—7b	HgAt	90 ee
3b—7b	TlAt	125 ee
4b—6b	PbPo	170 ee
4b—7b	PbAt	130 ee
5b—6b	PS	870 ee
	AsS	550 ee
	AsSe	400 ee
	BiPo	160 ee
5b—7b	PF	~950 ee
	PCl	~700 ee
	PBr	550 ee
	AsCl	430 eee
	AsBr	270 eee

Notes on Table II—If there n number of e, this denotes that the given value depends on $(n-1)$ previous estimations.

We have mentioned in Part III that As gives an anomalous line and that either of the values of AsO or AsS is in error. This is supported by considerations of this paper. We compare AsTe and SbSe. The experimental value for SbSe is 326. In view of the fact that the molecules are heavy, this suggests a value not too different, near 330 for AsTe. As line in Part III gives a value 660. The difference is very wide and cannot be explained as due to the limitations of the two methods. We can make some conjectures about AsO and AsS. If we assume isoelectronic value for AsTe, viz. 330 and the observed value 767 for AsS, the line through the two has a slope higher than that of N line which is again anomalous. On the other hand, the points for AsTe (isoelectronic value 330) and AsO (observed 967.4) give a normal line. Thus it seems that the observed AsS value may not be quite correct. On the basis of the normal line the estimated values for the other two molecules viz. AsS and AsSe are 550 and 400 respectively.

The predicted values for $5b-6b$ and $5b-7b$ groups are much uncertain as they are based on very limited data.

We have considered above the vibration frequencies of iso-electronic diatoms of a restricted class. Similar considerations apply for the other molecular constants, but a few points may be noted. Force constant K_e is given by $4\pi^2\mu c^2\omega_e^2$. In view of the fact that μ_A for the two diatoms are often not very near and ω_e is involved as square, the force constants for isoelectronics show large differences. The scanty data available for r_e values shows good similarities. This is supported by the following argument. In a molecular group $K_e \propto r_e^{-n}$ (Guggenheimer, 1946) where $n \sim 3$. In other words, $r_e \propto (\mu_A\omega_e^2)^{1/n}$. In view of the higher power of the exponent, similarities in r_e values would follow.

ACKNOWLEDGMENT

The authors are thankful to the Council of Scientific and Industrial Research for the financial assistance.

REFERENCES

- Bärwald, H., Herzberg, G. and Herzberg, L., 1934, *Ann. Phys.*, **20**, 369
 Bridge, N. K. and Howell, H. G., 1954 *Proc. Phys. Soc.*, **A67**, 44.
 Clark, C. H. D., 1935, *Trans. Farad. Soc.*, **31**, 1017.
 Coulson, C. A., 1952, Valence, Oxford University Press, p. 106.
 Glockler, G., 1948, *J. Chem. Phys.*, **16**, 602
 Glockler, G., 1950, *J. Chem. Phys.*, **18**, 1518
 Guggenheimer, K. M., 1946, *Proc. Phys. Soc.*, **58**, 456.
 Herzberg, G., 1951, Spectra of Diatomic Molecules, (D. van Nostrand Co., Inc., New York)
 Long, L. H. and Walsh, A. D., 1947, *Trans. Farad. Soc.*, **43**, 342.
 Rittner, E., 1951, *J. Chem. Phys.*, **19**, 1030.
 Sharma, D., 1945a, *Proc. Nat. Acad. Sci. India*, **A14**, 257.
 Sharma, D., 1945b, *Proc. Nat. Acad. Sci. India*, **A14**, 275.
 Syrkin, J. K. and Dyatkina, M. E., 1950, "Structure of Molecules and the Chemical Bond", Butterworths Scientific publications.
 Vago, E. E., and Barrow, R. F., 1946, *Proc. Phys. Soc.*, **58**, 538.
 Van Leeuwen, H. J., 1930, *Z. Phys.*, **66**, 241.
 Varshni, Y. P., and Majumdar, K., 1955, *Ind. J. Phys.*, **29**, 38.

ANALYSIS OF SOME INDIAN ORES AND MINERALS BY BENT MICA CRYSTAL SPECTROGRAPH*

By PRABHAT KUMAR BHATTACHARYYA

KHAIRA LABORATORY OF PHYSICS, UNIVERSITY COLLEGE OF SCIENCE, CALCUTTA-9

(Received for publication, April 26, 1955)

ABSTRACT. A transmission type bent mica crystal X-ray spectrograph has been constructed in which each wavelength chooses its own Bragg angle, and X-ray spectrum from Fe to U could be taken in one set-up. With the help of this instrument the presence of trace elements in some Indian ores and minerals has been studied, and some new results have been obtained.

INTRODUCTION

To detect the presence of the unknown trace elements in ores and minerals with the help of a plane crystal Bragg spectrograph, a large number of X-ray spectral photographs are to be taken by setting the crystal at different sets of Bragg angles corresponding to K_α , L_α , etc., lines of the different elements in question. The time of exposure should be of considerable length in each case. Replacing the traditional Bragg spectrograph by a bent mica crystal spectrograph designed by Mille Cauchois, we overcome these two difficulties, because in the latter case each wavelength chooses its own Bragg angle, and the time of exposure less than a minute is equivalent to one hour exposure with the usual Bragg method. Thus, on a single photograph we get a complete X-ray spectrum within a very short period of time from FeK_α to SbK_α . By chemical analysis and by optical spectroscopic methods, trace elements are usually detected; but chemical analysis is a lengthy and laborious process and optical spectroscopic methods are sometimes too laborious. Whereas, in the method described here, if once the line $K_{\alpha_2\alpha_1}$ of a particular element is determined, then there is no ambiguity about the presence of the element in the ore. Compared to optical methods, identification of lines is very easy in this case.

EXPERIMENTAL TECHNIQUE

The spectrograph was constructed following the outlines sketched by Mille Y. Cauchois, (Cauchois, 1932). The grating had a radius of curvature of 50 cms, and that of the film holder was 25 cms. The bent crystal holder and the cassette have been locally constructed and the final finishing of the cylindrical surface of the bent crystal holder was done by hand-lapping to eliminate the ghost lines. The whole system was placed on a circular disc resting on three adjustable screws. The circular disc was graduated in degrees. The grating holder was

* Communicated by Prof. S. N. Bose.

rigidly fixed with it, while the film holder could be moved to different regions, to get the spectrum of that particular region.

On a copper target some known elements e.g., Ni, Zn etc. are rubbed to get $K_{\alpha_2, \alpha_1, \beta_1}$ lines of the elements. The absorption edges of Br and Ag also appear

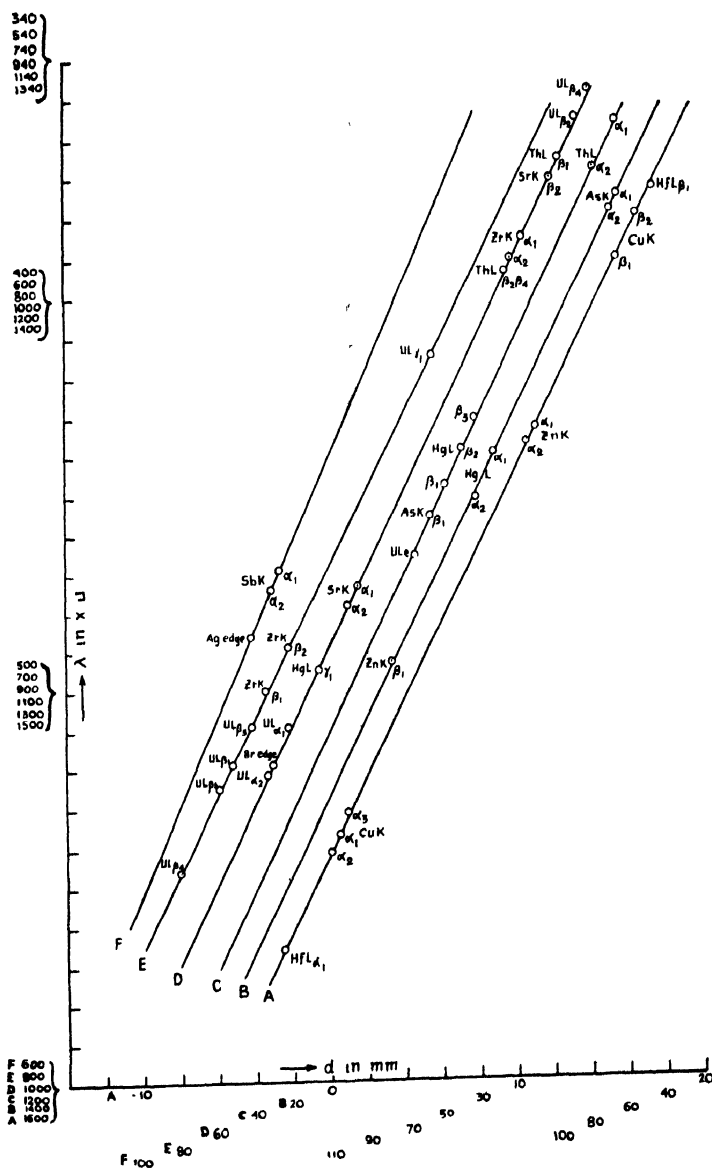


Fig. 1

Abscissa—distance measured in mm from CuK_α line

Ordinate— λ in XU.

on the X-ray film. Distances d in mms of different characteristic wavelengths are measured from $\text{CuK}\alpha_2$ to each of these lines or edges, and wavelengths for

each case being known from Seigbahn's data considering order correction, a graph is drawn, plotting d on one axis and λ on the other. The graph is very nearly a straight line (figure 1).

Now for each ore in question, the same process is repeated; and due to the presence of all the elements having atomic numbers greater than 26, characteristic lines are obtained. Measuring the distance of each line from $\text{CuK}\alpha_2$, with the help of the d - λ graph originally drawn, the λ is determined. The dispersion obtained by the instrument used is approximately 10XU/mm on the photo-film.

The main beauty of this method of analysis lies in the fact that one should never fail to detect the presence of any element between 26 and 92 in the unknown ores and minerals, even if they be present in traces.

Pure ZrO_2 was analysed and with an exposure of about 4 hours the minute trace of Hf was clearly detected. The period of exposure was too high because the operating voltage had to be kept low at 14 kv. for reasons explained below.

Sometimes it has been felt necessary to control the voltage of the X-ray tube so as to avoid the overlapping of emission lines of two different elements, as for example Hf L_{α_1} (= 1566) and Zr K_{α_1} , in second order (= 1568). So, to obtain Hf L_{α_1} , the voltage applied was kept below the K-excitation potential of Zr.

SETTING OF THE SPECTROGRAPH

By different screw-adjustments the grating-holder could be given all sorts of movements and inclinations. In order to get photographs, the axis of the cylinder containing the grating-holder and that of the cylinder containing the film-holder must be parallel to each other. The different screw adjustments mentioned above serve this purpose. By using a spirit level and a plumb-line first of all the axes of these two cylinders were made parallel, each being perpendicular to the horizontal level. Then the diameters of the two cylinders were made coincident by optical methods. Mica was used for the crystal. A clean, optically flat mica piece was chosen for this purpose, and a particular plane in the mica which makes an angle $\alpha = 10^\circ 19' \pm 1'$ with the split plane, was used as the Bragg reflecting plane. The orientation of this particular plane was determined by taking a Laue photograph of the mica piece. Then the mica was cut in proper size and was pressed inside the crystal holder, taking care that the curvature was perfect. For mica $d = 2.554 \pm 0.005\text{\AA}$ and $\text{Cu K}\alpha$ lines were expected at an angle of about 56° from the direct beam. Although in one set-up a full X-ray spectrum is obtained in this case due to divergent beam used,—when trace elements are searched, it is desirable that the spectral lines due to the presence of these trace elements be of considerable intensity. As such, instead of taking the photograph in one set-up, sometimes two or three X-ray spectral photographs were necessary, the whole spectroscope including the grating-holder was differently oriented in each case, with respect to the direct beam.



Fig. 2
Bent mica crystal X-ray spectrograph

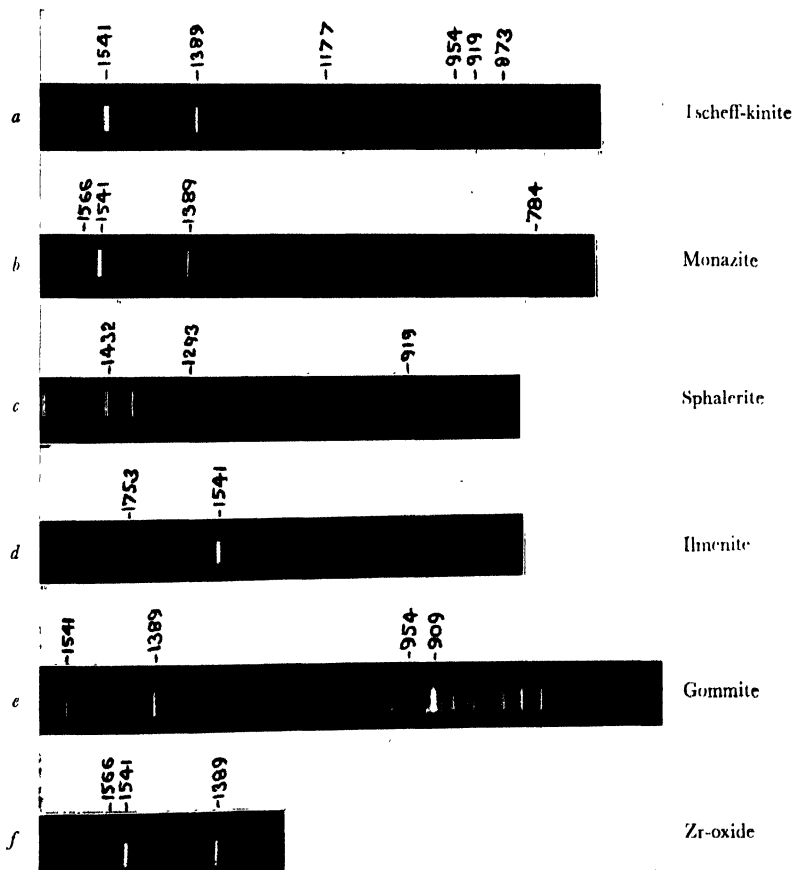


Fig. 3

RESULTS

The first X-ray photograph was obtained by using a clean Cu-target.. The original $d-\lambda$ graph was drawn from the following lines :

$\text{CuK}\alpha_1$ ($\lambda 1541$ XU), $\text{CuK}\alpha_1$ (1537), $\text{CuK}\alpha_2$ (1531), $\text{ZnK}\alpha_2$ (1436), $\text{ZnK}\alpha_1$ (1432), $\text{CuK}\beta_1$ (1389), $\text{CuK}\beta_2$ (1378), $\text{ZnK}\beta_1$ (1293), HgLa_2 (1250), HgLa_1 (1239), $\text{HgL}\beta_1$ (1047), $\text{HgL}\beta_2$ (1038), $\text{HgL}\beta_3$ (1030), Br-edge (919), and Ag-edge (486).

The $d-\lambda$ graph (figure 1) is split up into six graphs in order to magnify the scales. One small scale division is equal to one XU and the identification of different lines are correct to ± 1 XU.

With the help of $d-\lambda$ graph thus obtained the unknown spectral lines of several ores and minerals were determined, as shown in Table I.

TABLE I

Serial No.	Name of ore	Tubo voltage kv	Tube curr. ma	Time of exp. hours	Identified lines with λ
1	Tschoff-Kinite (Orissa)	32	5 -7	1	As $\text{K}\alpha_2\alpha_1\beta_1$ (1177, 1173, 1055) Th $\text{La}_2\alpha_1\beta_2\beta_1\beta_1$ (966, 954, 792, 764) Sr $\text{K}\alpha_2\alpha_1\beta_2$ (878, 873, 769)
2	Monazite (Travancore)	30	5	1	Hf $\text{La}_1\beta_1$ (1566, 1371) Zr $\text{K}\alpha_2\alpha_1\beta_1\beta_2$ (789, 784, 700, 689)
3	Sphalerite (Jawar mines, Udaypur)	32	5—7	1	Zn $\text{K}\alpha_2\alpha_1\beta_1\beta_2$ (1436, 1432, 1293, 1281) Sb $\text{K}\alpha_2\alpha_1$ (474, 469)
4	Ilmenite (Sumji, Singbhum)	32	5—7	1	Fe $\text{K}\beta_1$ (1753)
5	Gommitte (?) (Rajputana)	32	6—8	2	U $\text{La}_1\alpha_2\alpha_1\beta_2\beta_1\beta_3\beta_1\beta_3\gamma_1$ (1065, 921, 909, 753, 746, 725, 719, 709, 614) Th $\text{La}_2\alpha_1$ (966, 954)
6	Zr -oxide (pure)	14	5	4	Hf La_1 (1566) Zr $\text{K}\alpha_2\alpha_1\beta_1\beta_2$ (789, 784, 700, 689)

A few interesting spectrograms are reproduced in figure 3 and the photograph of the spectrograph is reproduced in figure 2.

CONCLUSION

A thorough analysis of quite a large number of Indian ores and minerals have been undertaken and it is interesting to note that in many cases we are getting definite proof of the presence of certain elements in ores and minerals which have not been reported earlier by their chemical or spectroscopic analysis.

ACKNOWLEDGMENTS

The author is grateful to Prof. S. N. Bose for his kind help and encouragement. His thanks are due to Dr. K. Das Gupta for his valuable guidance and for introducing him to the technique. Thanks are also due to Dr. R. K. Datta Roy for his kind co-operation.

REFERENCES

Cauchois, Y., 1932, *J. de Physique*, **3**, 320.

THE EFFECT OF FLUID MOTION ON HEAT TRANSMISSION

PART III, SOLIDS OF DIFFERENT SHAPES AND SIZES

BY D. G. KAPADNIS*

NATIONAL PHYSICAL LABORATORY OF INDIA, NEW DELHI

(Received for publication, August 9, 1954)

ABSTRACT. A detailed experimental study of the effect of a unidirectional stream of air on the rate of heat dissipation from solids of different shapes and sizes by forced convection has been made in a limited range of Reynolds numbers from 10^3 to 10^5 . The experimentally derived values of the constants B and n in the Nusselts equation (employed for air)

$$\left(\frac{1}{A \Delta \theta} \frac{dQ}{dT} \frac{D}{K} \right) = B \left(\frac{VD}{\xi} \right)^n$$

(the symbols have their usual meaning) are respectively 0.505 and 0.516 for horizontal cylinders with ellipsoidal nosepiece, 0.033 and 0.783 for the same with plane blunt nose-piece; 0.78 and 0.517 for spheres; 0.12 and 0.654 for rectangular parallelopipeds placed in face-on position; and 0.24 and 0.576 for the same placed in edge-on position. Finally the experimental data have been compared with those of other investigators.

INTRODUCTION

The interchange of heat between a hot solid and a moving stream of relatively cool fluid or vice versa is a subject of considerable technical importance, and also not devoid of scientific interest. A considerable amount of work has been done on the cooling of solids at rest in moving fluids. Compared to the abundant experimental work on heat transfer in tubes and ducts relatively little has been done concerning the flow of the fluid parallel or perpendicular to a heating or a cooling surface when the fluid is not bounded by the walls of a tube or a channel. Moreover, our knowledge of the complex mechanism of heat dissipation by convection is as yet, especially from the theoretical standpoint, incomplete. More experimental evidence is necessary for the satisfactory understanding of the thermodynamics of heat-interchange between the solid and the surrounding stream of fluid under different ambient conditions. The experiments of heat dissipation from vertical cylinders (Kapadnis, 1953) were, therefore, extended to solids of various shapes and sizes with a view to throwing some light on this problem of convection in these cases.

EXPERIMENTAL ARRANGEMENT

The experimental arrangement used by the present author (1953) in studying the heat dissipation from vertical cylindrical vessels of different sizes filled with

* Now at Kamerlingh Onnes Cryogenic Laboratory of The State University of Leiden, The Netherlands.

hot water and placed in a current of air under different ambient conditions was completely modified in these investigations. A vessel *A* (figure 1) containing hot water was placed at a distance of about 90 cm from an electric fan *F* and a stream of air proceeding from the fan was directed on this vessel after allowing it to pass through a wire grid *G* situated at a distance of about 18 cm from the fan. The purpose of the grid was to change the divergent stream of air issuing from the fan into uniform parallel stream giving natural conditions resembling a wind tunnel

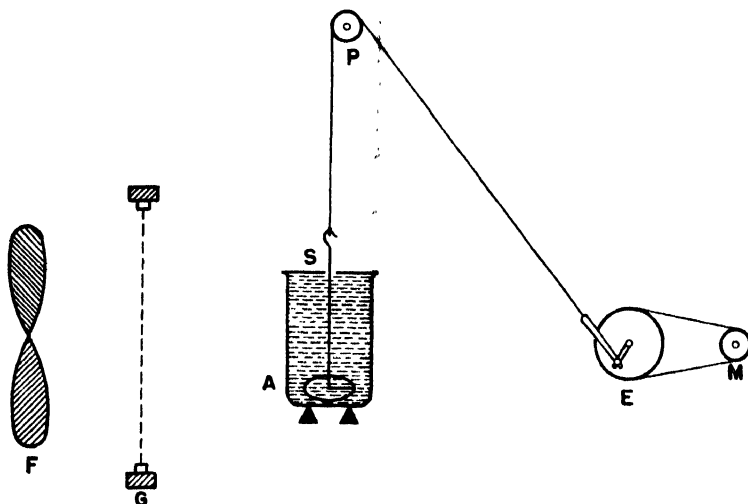


Fig. 1.

of infinite dimensions. The top of the vessel was closed by a lid having a hole in it. Through this hole a stirrer *S* was kept working up and down in the vessel by connecting it to a string passing over a pulley *P*. The other end of the string was connected to an eccentric arrangement *E* attached to slow-speed electric motor *M*, thus ensuring a vertical motion of the stirrer in the vessel. A uniform temperature was thus maintained throughout the whole mass of water at any instant. The usual precautions were taken to minimize heat losses due to conduction, radiation and evaporation. Separate experiments in still air were also performed in order to calculate the losses due to natural or free convection. All subsequent observations were corrected for losses due to radiation and natural convection. Under these circumstances the heat dissipation, when the vessel was subjected to air stream, was due to forced convection alone.

The fan was made by attaching four steel blades to the axle of the three-phase motor, the speed of which could be regulated by a rotor rheostat and by varying the voltage of the alternator supplying the current. A good range of wind velocity was thus obtained. The values of air velocity used by the author in the previous investigation were preferred in this work for the sake of convenience in calculations. The velocity of the air currents produced by the fan was measured

by means of a cyclometer pattern type four-cup anemometer supplied by the Indian Meteorological Centre. This anemometer was arranged to indicate the run of the wind which had passed in any desired interval, by a simple system of gears terminating in a counting mechanism. This instrument measures the linear velocity but fails to measure the eddying motion of air produced near an obstacle in the turbulent region, therefore, the values of air velocity were checked up by means of a silvered Kata thermometer measuring the air movement by the cooling effect of the wind. Both of these instruments were previously calibrated.

Four copper-constantan thermocouples, having a potentiometer as an auxiliary measuring device, were used as temperature-measuring device in these experiments. The potentiometer circuit is shown in figure 2. Only one cold junction b common to all the four hot junctions a_1, a_2, a_3 and a_4 of the thermocou-

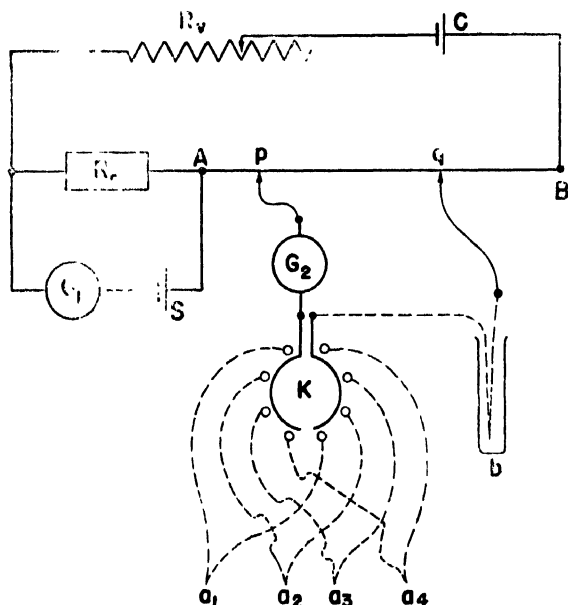


Fig. 2

ples was connected to each of them one by one through a multiple switch K . An accumulator C caused the current to pass round the circuit through the variable resistance R_v , the fixed standard resistance R_s and the potentiometer wire AB . The current was standardized by adjusting the variable resistance R_v until the voltage drop across R_s was just equal to the electromotive force of the standard cell S , as indicated by a zero reading of the galvanometer G_1 . The potentiometer tappings p and q were then adjusted until the electromotive force of the thermocouple was balanced by the voltage drop along the potentiometer wire between them, indicated by a zero reading of the galvanometer G_2 . The thermocouples were calibrated with a standard thermometer and a graph of temperature difference against the length of the segment of the potentiometer wire was plotted directly

and this plot was used in subsequent experiments. The hot junctions of the thermocouples were soldered to the outer surface of the vessel for the measurement of its surface temperature. The method used by Kapadnis and Gogate (1952) was followed in calculating the rate of heat dissipation. The cylindrical vessels used were all circular. The diameters of the cylindrical and spherical vessels were taken as characteristic linear dimension in subsequent calculations. But in the case of rectangular vessels the diameter of the circular cylindrical vessel of equal exposed surface was used as the characteristic dimension. The density, viscosity and conductivity of the surrounding stream of air were taken at the mean film temperature.

A detailed study of convective heat transmission from vessels filled with warm water to the surrounding air stream was made with vessels of three different shapes used in five ways—horizontal cylinders in two positions, spheres and rectangular parallelepipeds placed in face-on as well as edge-on position. The velocity of the air current was varied from 80 cm per second to 1095 cm per second. The experiments were repeated for vessels of four different sizes of each shape, a typical set of observations being recorded in Table I.

TABLE I

Shape of the vessel	Characteristic dimension of the vessel in cm	Air velocity in cm/sec	Rate of heat transmission in cal/cm ² /sec/°C $\times 10^4$	$\frac{VD}{\xi} \times 10^3$	$\frac{1}{A\Delta\theta} \frac{dQ}{dT} \frac{D}{K}$
Horizontal cylinder	5.2	80	3.06	2.6	27.7
		242	5.79	7.9	52.3
		405	7.70	13.2	69.5
		563	8.88	18.4	80.3
		721	9.82	23.6	88.7
		882	11.48	28.8	103.7
		967	11.71	31.6	105.9
		1095	12.22	35.7	110.4
	10.7	80	2.27	5.4	42.1
		242	3.94	16.3	73.3
		405	5.27	27.2	97.9
		563	6.42	37.8	119.3
		721	7.09	48.5	131.8
		882	7.72	59.2	143.5
		967	8.32	64.9	154.7
		1095	8.98	73.5	167.0
	15.0	80	1.92	7.5	50.0
		242	3.45	22.8	90.0
		405	4.27	38.1	113.9
		563	5.61	53.0	146.3
		721	5.96	68.0	155.2
		882	6.75	83.1	175.8
		967	7.16	91.0	186.7
		1095	7.49	103.0	195.2

TABLE I (contd.)

Shape of the vessel	Character- istic dimension of the vessel in cm	Air velocity in cm/sec	Rate of heat transmission in cal/cm ² /sec/°C × 10 ⁻⁴	$\frac{VD}{\xi}$ × 10 ³	$\frac{1}{A\Delta\theta} \frac{dQ}{dT} \frac{D}{K}$
Sphero	21.8	80	1.64	11.0	62.0
		242	2.80	33.1	106.0
		405	3.65	55.4	138.2
		563	4.34	77.0	164.4
		721	4.99	98.9	188.9
		882	5.60	120.7	212.3
		967	6.10	132.3	231.1
		1095	6.72	149.8	254.6
	4.8	80	5.74	2.4	47.9
		242	9.98	7.3	83.2
		405	13.15	12.2	109.6
		563	14.42	17.0	120.2
		721	16.18	21.7	134.9
		882	17.34	26.6	144.5
		967	19.91	29.1	166.0
		1095	21.33	33.0	177.8
	10.3	80	3.07	5.2	55.0
		242	6.27	15.6	112.2
		405	8.46	26.2	151.4
		563	10.17	36.4	182.0
		721	11.95	46.6	213.8
		882	13.10	57.0	234.4
		967	13.41	62.5	239.5
		1095	15.04	70.8	269.2
	15.8	80	2.71	7.9	74.1
		242	5.27	24.0	144.5
		405	6.63	40.2	182.0
		563	7.79	55.9	213.8
		721	9.58	71.5	263.0
		882	10.27	87.5	281.8
		967	10.75	95.9	295.1
		1095	11.00	108.6	302.0
	20.4	80	2.52	10.2	89.1
		242	4.37	31.0	154.9
		405	6.17	51.9	218.8
		563	6.62	72.1	234.4
		721	8.33	92.3	295.1
		882	8.52	112.9	302.0
		967	9.78	123.8	346.7
		1095	10.97	140.3	389.0
Rectangular parallelopiped (Face-on position)	5.4	80	2.51	2.7	23.6
		242	4.63	8.2	43.5
		405	6.44	13.7	60.4
		563	8.53	19.1	63.5
		721	8.95	24.4	84.0
		882	10.99	29.9	103.0
		967	12.27	32.8	115.1
		1095	13.34	37.1	125.0
		80	1.96	5.1	34.8
		242	3.75	15.5	66.5
		405	5.12	25.9	90.8

TABLE I (contd.)

Shape of the vessel	Characteristic dimension of the vessel in cm	Air velocity in cm/sec	Rate of heat transmission in cal/cm ² /sec/°C × 10 ⁻⁴	VD × 10 ³	$\frac{1}{A\Delta\theta} \frac{dQ}{dT} \frac{D}{K}$
Rectangular parallelopiped (Edge-on position)	10.2	563	6.52	36.1	115.6
		721	7.36	46.2	130.6
		882	8.36	56.5	148.3
		967	9.23	61.9	163.7
		1095	10.69	70.1	189.7
	15.2	80	1.80	7.6	41.2
		242	3.02	23.1	79.8
		405	4.27	38.7	112.7
		563	5.66	53.7	149.6
		721	6.78	68.8	179.1
	20.1	882	7.73	84.2	204.2
		967	8.36	92.3	220.8
		1095	9.38	104.5	247.7
	5.4	80	1.56	12.7	62.8
		242	2.97	30.5	103.8
		405	3.92	51.1	136.8
		563	5.09	71.0	177.8
		721	5.81	91.0	202.8
	10.2	882	6.89	111.3	240.4
		967	7.40	122.3	258.2
		1095	8.55	138.2	298.5
	15.2	80	2.51	2.7	23.5
		242	4.60	8.2	43.2
		405	5.90	13.7	55.3
		563	7.46	19.1	70.0
		721	9.00	24.4	84.3
	20.1	882	9.38	29.9	87.9
		967	10.47	32.8	98.2
		1095	11.07	37.1	103.8
	5.4	80	1.88	5.1	33.4
		242	3.34	15.5	59.3
		405	4.75	25.9	84.3
		563	5.70	36.1	101.2
		721	6.05	46.2	107.4
	10.2	882	7.26	56.5	128.8
		967	8.04	61.9	142.6
		1095	8.09	70.1	143.5
	15.2	80	1.59	7.6	38.9
		242	2.98	23.1	78.7
		405	3.79	38.7	100.2
		563	5.04	53.7	133.0
		721	5.25	68.8	138.7
	20.1	882	6.32	84.2	167.1
		967	6.82	92.3	180.3
		1095	7.46	104.5	197.2
	5.4	80	1.47	12.7	55.3
		242	2.55	30.5	89.1
		405	3.61	51.1	125.9
		563	3.97	71.0	138.7
		721	4.66	91.0	162.6
	10.2	882	5.50	111.3	191.9
		967	6.01	122.3	209.9
		1095	6.62	138.2	231.2

RESULTS AND DISCUSSION

The method of dimensional analysis gives for forced convection the following simplified equation in the case of gases:

$$\left(\frac{1}{A\Delta\theta} \cdot \frac{dQ}{dT} \cdot \frac{D}{K} \right) = B \left(\frac{VD}{\xi} \right)^n \quad \dots (1)$$

where $\frac{dQ}{dT}$ is the rate of heat transmission;

A the area of the solid exposed;

D the characteristic dimension of the solid;

$\Delta\theta$ the excess of the surface temperature of the solid over that of the surrounding air stream;

V the velocity of the air stream;

K the heat conductivity of air;

ξ the ratio of viscosity of air to its density;

and B and n are constants to be determined from the experimental data.

A logarithmic plot of the quantities in the parentheses of the above equation against each other should give a straight line having a slope equal to n and an intercept on the axis equal to B . Figures 3 to 6 represent such logarithmic plots in all the cases of vessels tried for different air velocities; the experimental data for differently shaped vessels are plotted in different figures, thus each figure corresponds to a particular shape of the vessel. All these curves satisfy equation (1), the constants B and n having different values for differently shaped vessels. The values of these constants revealed by the various curves are recorded in Table II. It is seen from all these figures that the experimental data for vessels of different shapes and sizes exposed to various streams of air current lie reasonably close to the straight lines (thick continuous lines in the figures), the slopes and intercepts on the axes of which give the values of n and B respectively. It is evident that the values of B and n change with the shape of the vessel, but they remain practically constant when the size of the vessel or the velocity of the air stream is changed. The logarithmic plot of the experimental data for cylinders given by various investigators slightly concaves upwards, suggesting a variation of B and n with the Reynolds number—mainly with the fluid velocity and the characteristic dimension of the solid. A very slight variation of B and n in some of the present investigations which were carried out in a limited range of Reynolds number (from 2.5×10^3 to 1.5×10^5) is insignificant. The experimental data of the present author for this limited range are, therefore, represented almost within the limits of experimental error by straight lines.

Equation (1) gives (Kapadnis, 1953)

$$\Delta \log \left(\frac{1}{A \Delta \theta} \frac{dQ}{dT} \right) = n \Delta \log V \quad (2)$$

$$\Delta \log \left(\frac{1}{A \Delta \theta} \frac{dQ}{dT} \right) = (n-1) \Delta \log D \quad \dots \quad (3)$$

Equation (2) represents the effect of changing the velocity of the fluid stream alone on the rate of heat transmission, all other factors remaining unchanged;

TABLE II

Constants of Nusselts equation for forced convection from solids of various shapes (according to different investigators)

Shape of the solid	Observer	Reynolds number		B	n
		From	To		
Vertical cylinders	Kapadnis	2000	40000	0.56	0.517
		40000	130000	0.185	0.62
Horizontal cylinders	Jakob and Dow	40000	100000	0.590	0.5
		100000	1500000	0.028	0.8
	Kapadnis	2600	150000	0.505	0.516
		22000	150000	0.033	0.783
Spheres	Williams (cor-related data)	20	150000	0.33	0.60
	Nottage and Boelter	1000	100000	0.70	0.52
	Kapadnis	2400	140000	0.78	0.517
Rectangular parallelopiped (Face-on position)	Hilpert	5000	100000	0.092	0.675
	Reiher	2500	8000	0.160	0.699
	Kapadnis	2700	140000	0.12	0.654
Rectangular parallelopiped (Edge-on position)	Hilpert	5000	100000	0.222	0.588
	Reiher	2500	7500	0.261	0.624
	Kapadnis	2700	140000	0.24	0.576

while equation (3) gives the effect of changing the characteristic dimension of the vessel alone on the rate of heat dissipation. The experimental values of the slope n found in all the cases of differently shaped vessels are less than unity. Therefore,

equation (2) expressed qualitatively for all these cases means that the rate of heat dissipation does not increase quite so fast as the air velocity. The values of n substituted in equation (3) give negative slopes, each less than unity. Therefore, as the characteristic dimension of the vessel is reduced the rate of convective heat transfer increases, of course, not quite so fast. The experimental data for these two cases when represented graphically (rate of heat dissipation against air velocity) give a family of curves for vessels of different sizes but of the same shape. The general nature of the various families of curves corresponding to various shapes of the vessels is similar to that obtained for vertical cylinders in the previous investigations (figure 2, Kapadnis, 1953). In all these cases as the air velocity increases the curves rise steadily with a continuous decrease in slope, the curves for vessels bigger in size lie below those for the smaller ones, showing a good agreement with equations (2) and (3). The two equations can also be used as an approximate check to the observations of the new set in which either the velocity of the air stream or the characteristic dimension of the vessel is changed. For example, when the velocity of the air stream increases from 450 to 882 cm per second—2.178 fold—the expected increase in the rate of heat dissipation as per equation (2) is 1.663 fold for a specific case of a rectangular vessel of 10.2 cm diameter. The experimentally observed and calculated values for the rate of heat loss per unit area per unit excess of temperature are 8.356×10^{-4} and 8.513×10^{-4} units respectively, the latter being about 1.9 percent higher than the former. Similarly, when there is a twofold increase in the characteristic dimension of the rectangular vessel for a constant velocity of 721 cm per second, the decrease in the heat dissipation should according to equation (3), be 1.265 fold; the calculated and observed values for the rate of heat loss per unit area per unit excess of temperature in this case are 5.821×10^{-4} and 5.808×10^{-4} units, the former being less than one percent higher than the latter.

The horizontal cylinders used were ellipsoidal at one end. The observations were taken by keeping the ellipsoidal edge facing the stream of air. The experimental results can be satisfactorily represented by equation (1) with $n = 0.516$ and $B = 0.505$, the logarithmic plot of which has been shown by a thick continuous line in figure 3. The dotted line has been drawn as per Pohlhausen's (1921) theoretical equation (employed for air) which has been confirmed by the experiments of Jakob and Dow (1946) except for a slight difference in the value of B . The slight deviation of the experimental results of the present author from Pohlhausen's equation might be due to less homogeneous air stream used. A few observations (not recorded in the table), were also taken by keeping the plane blunt edge of the cylinder facing the air stream. Because of the setting of turbulence higher values were obtained in this case. The values arrived at have been represented in figure 3 by broken line giving $n = 0.783$ and $B = 0.033$ for Reynolds numbers from 2×10^4 to 1.6×10^5 . The experiments of Jakob and Dow (1946) led to $n = 0.80$ and $B = 0.028$, but for Reynolds numbers higher than 10^5 .

The experimental data for spheres satisfies equation (1) with $n = 0.517$ and $B = 0.78$. The data have been represented by thick continuous line in figure 4. The values obtained are a bit higher than those arrived at for the same limited range of Reynolds number by Nottage and Boelter (1940). Their values shown in the figure by dotted line give $n = 0.52$ and $B = 0.70$. The broken line represents the data correlated by Williams (1942) in the range of Reynolds number from 20 to 1.5×10^5 . The values obtained by the present author for Reynolds numbers higher than 10^4 are in close agreement with the data correlated by Williams.

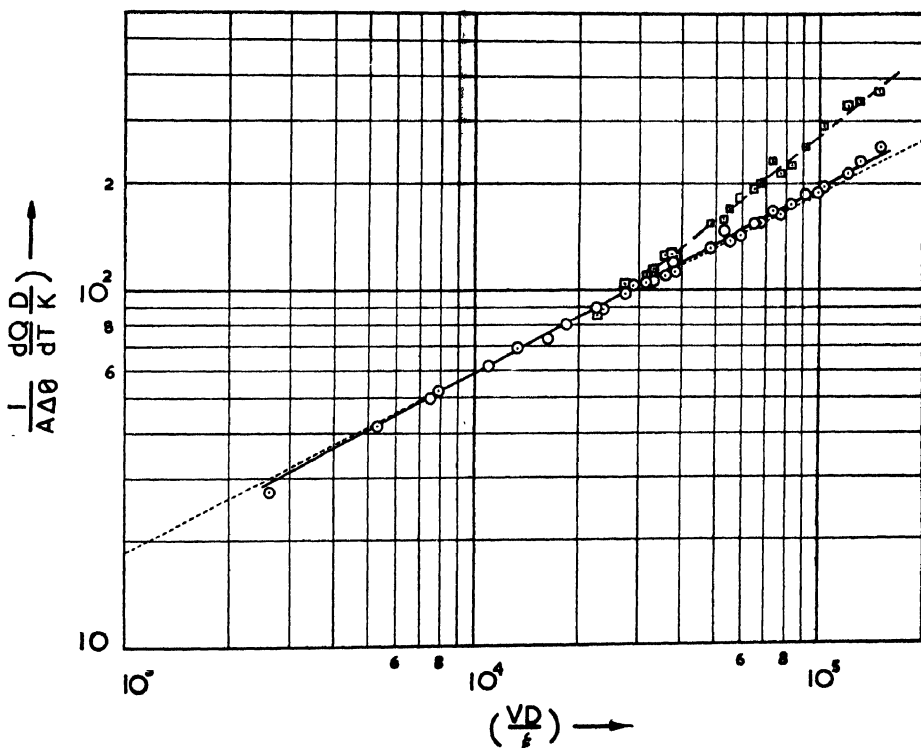


Fig. 3

The thick continuous lines in figures 5 and 6 represent the experimental data for rectangular vessels with face-on and edge-on positions respectively. The data lead to $n = 0.654$ and 0.576 and $B = 0.12$ and 0.24 respectively. The values are in agreement with those of Hilpert (1933), shown by broken lines in both the figures. The slight deviation might be due to the use of less homogeneous stream of air by the present author. Reiher's (1925) data are represented by dotted lines in both the cases. The values obtained by Reiher are much higher in comparison with those of Hilpert and of the present author, but they are limited to a small

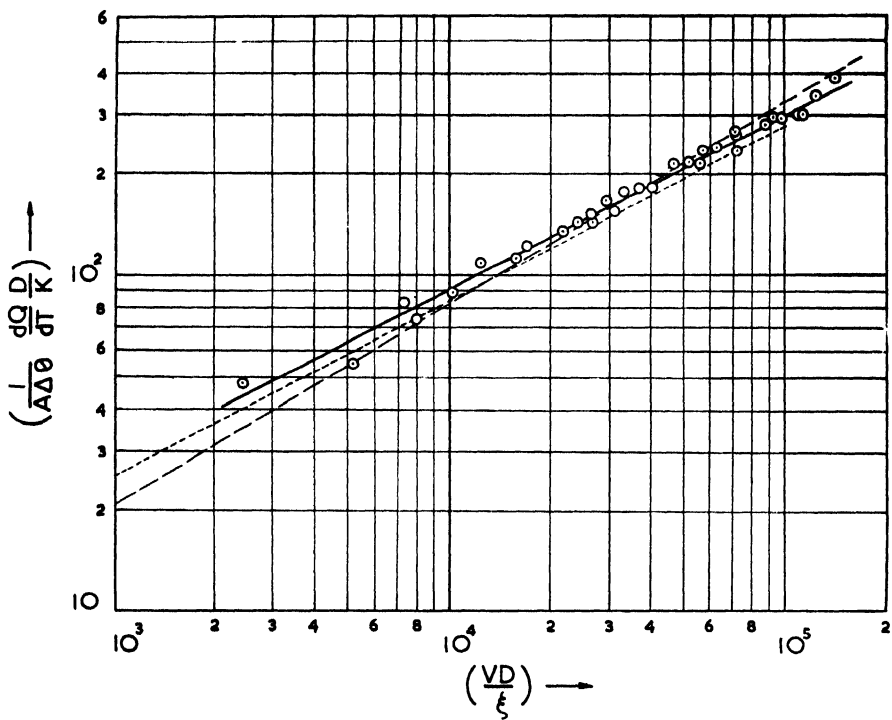


Fig. 4

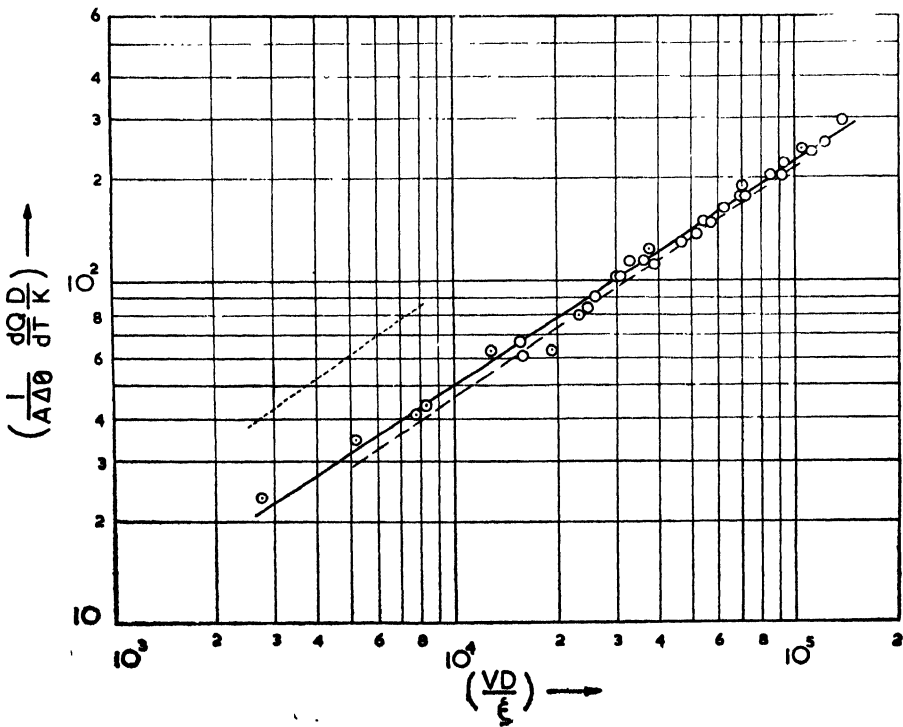


Fig. 5

range of Reynolds number which was not so exhaustively studied in the present investigations.

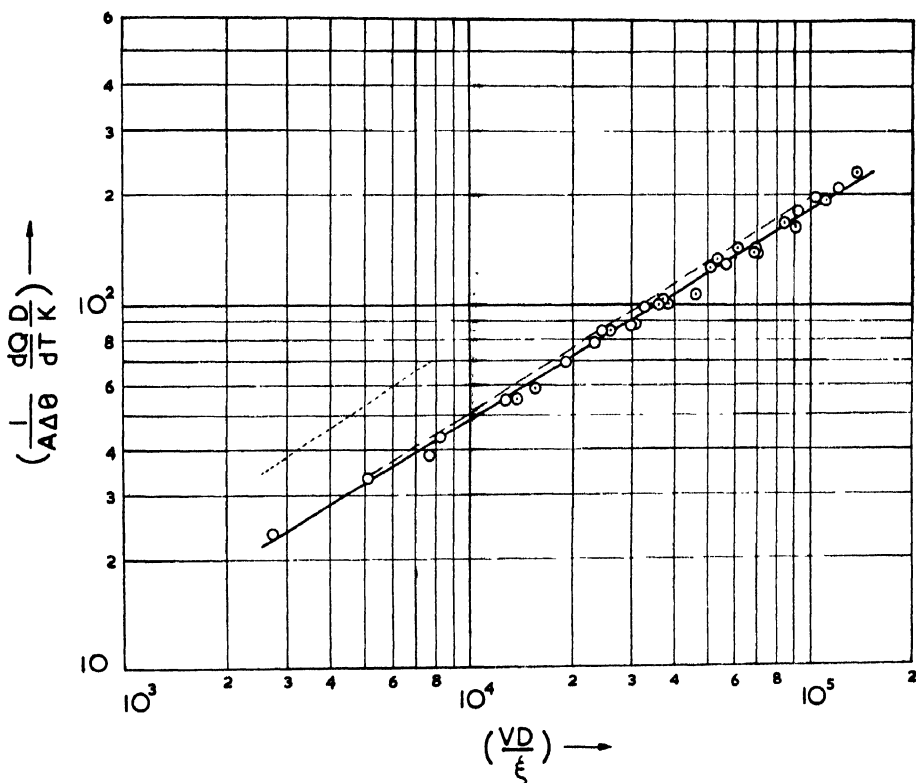


Fig. 6

A careful study of the author's (1953) experimental data on vertical cylinders shows a bend indicating a change in the character of the flow at Reynolds number 4×10^4 which escaped notice of the author at that time. The new values for n and B for Reynolds numbers higher than 4×10^4 are, therefore, 0.62 and 0.185 respectively, while the previously published values of n and B hold good for Reynolds numbers from 10^3 to 4×10^4 . As the observations taken for Reynolds numbers less than 5×10^3 were very few in those investigations it is difficult to attribute the deviations of the values calculated from those observations to a less pronounced bend somewhere there. These newly calculated results have been also included in Table II.

For the sake of comparison at a glance the data, according to different investigators, discussed in the preceding paragraphs have been collected in Table II.

ACKNOWLEDGMENTS

The author wishes to express his grateful thanks to the Director of the National Physical Laboratory, for his kind permission to publish this paper. He further wishes to express his deep indebtedness to Dr. Ghai, assistant Director of

Heat and Power division; to Shri Joglekar, assistant Director of the division of Industrial Physics; and to Shri N. V. Ganpule from INSDOC for constant encouragement, numerous helpful discussion and valuable suggestions.

It is a deep pleasure to express gratitude to The Maharaja Sayajirao University of Baroda, for award of a research scholarship to pursue this research.

REFERENCES

- Hilpert, R., 1933, *Forschg. Geb. Ing. Wes.*, **4**, 215.
Jakob, M. and Dow, W. M., 1946, *Trans. Am. Soc. Mech. Engrs.*, **68**, 123.
Kapadnis, D. G., 1953, *Ind. J. Phys.*, **27**, 77.
Kapadnis, D. G. and Gogate, D. V., 1952, *Ind. J. Phys.*, **26**, 171.
Nottage, H. B. and Boelter, L. M. K., 1940, *Trans. Am. Soc. Heating, Ventilating Engrs.*, **46**, 41.
Pohlhausen, E., 1921, *Zeitschr. f. angew. Math. U. Mech.*, **1**, 252.
Reiher, H., 1925, *Mitt. ub. Forsch. d. Ver. deutsch. Ing. Heft.*, p. 269.
Williams, G. C., in McAdams, W. H., 1942, *Heat Transmission*, (McGraw Hill Book Co., New York), 2nd edition, p. 237.

FREDHOLM THEORY AND HANKEL TRANSFORM OF THE SCHRÖDINGER EQUATION*

By S. N. BISWAS

DEPARTMENT OF THEORETICAL PHYSICS,
INDIAN ASSOCIATION FOR THE CULTIVATION OF SCIENCE, JADAVPUR, CALCUTTA-32

(Received for publication, May 18, 1955)

ABSTRACT. The Fredholm theory of integral equation has been applied to the Hankel transform of the radial part of the Schrödinger wave equation for the determination of phase shifts corresponding to the S ., P . D . etc. waves. The numerical results of the S -wave phase shift have been compared with similar ones obtained by other approximate methods. The Hankel transform of the Schrödinger equation is parallel to the Fourier transform of the same as investigated by Bethe and Salpeter.

INTRODUCTION

It has been mentioned by Salpeter (1951) that in a number of nuclear problems, the Fourier transform of the function has many advantages, hence it may be of some interest to study the Hankel transform of the wave function for the problem of neutron-proton scattering by a nuclear potential. The choice of Yukawa potential is motivated merely by its obvious theoretical interest.

It is well known that for low and intermediate energies the Born approximation method does not hold good, the phase method is the only course at our disposal. The determination of the phase shift requires that the radial part of the scattered wave will differ asymptotically from the radial part of the corresponding incoming wave only by a phase shift. This radial part of the differential equation has been converted into an integral equation by using the Hankel transform.

It will be seen that the asymptotic behaviour of the wave function in the coordinate space is characterised by the singular nature of the integral equation satisfied by the wave function in the transformed space. Hence the determination of the phase shift depends entirely on the study of the singular nature of the integral equation.

The Fredholm theory of integral equation has been applied for the explicit calculation of the phase-shift in the spherically symmetric scattering by a central force. This type of scattering is considered as the simplest collisional process. We consider here this case for which the partial wave analysis requires the determination of the asymptotic phases. Jost and Pais (1951) have considered

* Communicated by Dr. D. Basu.

the necessity of Fredholm solution in view of the unsuitability of Born's approximation. They have however, not considered the determination of the phase shifts. Consequently in the present paper we investigate the advantages of the Fredholm solution to estimate the phase shifts.

A successive approximation based on the iterative procedure has been developed by Salpeter (1951) in connection with the bound state problem. He has also applied the same method to the scattering of neutrons by protons, but the method has not been extended beyond the first iteration.

The perturbation formulae, as commonly developed, may be shown to have a finite radius of convergence, however the series diverges when the radius of convergence exceeds that finite value. Hence it will be useful to find a method for improving the convergence for large values of the coupling constant, that is, it provides the analytic continuation of the iterative perturbation formula beyond its radius of convergence. This Fredholm perturbation formula is most easily described if the theory is discussed in terms of operators and vectors in an abstract vector-space (Smithies, 1941).

In this paper the calculations are carried out to the second approximation. The numerical results thus deduced are compared with earlier approximate results.

A simple generalisation is given to obtain the phase shifts corresponding to P -, D , etc. states.

2. SCATTERING BY A CENTRAL POTENTIAL

In this section we treat the problem of scattering of a non-relativistic particle of energy E , by a fixed central potential of the type $\lambda e^{-\mu r}/r = V(r)$. It is well known that the Schrödinger equation of angular momentum $l = 0$

$$\left[-\frac{d^2}{dr^2} + V(r) - k^2 \right] \psi(r) = 0, \quad \dots (2.1)$$

where $k^2 = \frac{M_n E}{\hbar^2}$, with M_n the nucleon mass and E the energy of the incident particle, with the boundary conditions, $\psi(0) = 0$,

$$\lim_{r \rightarrow \infty} \psi(r) = \sin kr + \tan \eta \cos kr \quad \dots (2.2)$$

where η is the phase shift for the S -wave scattering.

We now transform (2.1) to an integral equation with the aid of Hankel transform. For this we introduce the following,

$$\psi(r) = \sqrt{\frac{\pi}{2}} \int_0^\infty (p.r)^{\frac{1}{2}} J_{\frac{1}{2}}(pr) \phi(p) dp \quad \dots (2.3)$$

Whence $\phi(p)$ is the Hankel transform of $\psi(r)$

$$\text{and} \quad \lambda V(p, p') = \lambda V(p', p) = \int_0^{\infty} (pr)^{\frac{1}{2}} J_{\frac{1}{2}}(pr) V(r) \cdot (p'r)^{\frac{1}{2}} J_{\frac{1}{2}}(p'r) dr \quad \dots \quad (2.4)$$

and noting that

$$\int_0^{\infty} (pr)^{\frac{1}{2}} J_{\frac{1}{2}}(pr) (p'r)^{\frac{1}{2}} J_{\frac{1}{2}}(p'r) dr = \delta(p-p') \quad \dots \quad (2.5)$$

we get the integral equation,

$$(p^2 - k^2)\phi(p) + \lambda \int_0^{\infty} V(p, p')\phi(p')dp' = 0 \quad \dots \quad (2.6)$$

This is similar to the non-relativistic Bethe-Salpeter equation (1952).

But the phase-shift η will be obtained from the asymptotic behaviour of $\psi(r)$, so we consider (2.3) for large values of r . It appears from (2.3) that

$$\lim_{r \rightarrow \infty} \sqrt{\frac{\pi}{2}} \int_0^{\infty} (pr)^{\frac{1}{2}} J_{\frac{1}{2}}(pr) \phi(p) dp \rightarrow 0$$

if $\phi(p)$ be a regular function of its argument (see Titchmarsh, Fourier series and integrals; Riemann—Lebesgue theorem). Hence to obtain the required value of $\lim_{r \rightarrow \infty} \psi(r)$ we should expect that $\phi(p)$ must not be a regular function. Thus the

singularity of $\phi(p)$ will determine the asymptotic nature of $\psi(r)$. Hence we re-write (2.6) as

$$\phi(p) = \delta(p-k) - (p^2 - k^2)^{-1} \lambda \int_0^{\infty} V(p, p')\phi(p')dp' \quad \dots \quad (2.7)$$

Since the integral on the right hand side is a regular one, so we write (2.7) as

$$\phi(p) = \delta(p-k) - (p^2 - k^2)^{-1} \cdot B(p). \quad \dots \quad (2.8)$$

where $B(p)$ is free from singularity.

Now taking the Hankel transform of (2.2) we get

$$\phi(p) = \delta(p-k) + \left(\frac{2}{\pi}\right) \tan \eta \cdot (p^2 - k^2)^{-1},$$

which on comparison with the singular integral equation for $\phi(p)$ (2.7) gives

$$B(p) = -\frac{2p}{\pi} \tan \eta$$

Since the phase-shift is characterised by the singular nature of (2.7) so the phase shift is determined by the value of $B(p)$ at the point $p = k$

$$\text{Hence} \quad \tan \eta = -\pi B(k)/2k \quad \dots \quad (2.9)$$

From (2.7) and (2.8)

$$B(p) = \lambda \int_0^{\infty} V(p, p')\phi(p')dp' \quad \dots \quad (2.9A)$$

Now putting the value of $\phi(p)$ from (2.7) in (2.9A) i.e.

$$B(p) = \lambda \int V(p, p') \left[\delta(p' - k) - \frac{B(p')}{p'^2 - k^2} \right] dp'$$

$$\text{we get} \quad B(p) = B_0(p) - \lambda \int V(p, p') (p'^2 - k^2)^{-1} B(p') dp' \quad \dots (2.10)$$

$$\text{where} \quad B_0(p) = \lambda V(p, k)$$

Eq. (2.10) is an integral equation for $B(p)$ which from (2.9) yields the asymptotic phase.

The solution of (2.10) according to the modified Fredholm theory of integral equation is given by Smithies (1941),

$$B(p) = - \int \frac{D(\lambda, p, p')}{d(\lambda)} B_0(p') dp' \quad \dots (2.11)$$

$$\text{where, writing} \quad k(p, p') \text{ for } V(p, p') / (p'^2 - k^2)$$

we have

$$D(\lambda, p, p') = \sum_{n=0}^{\infty} \lambda^n D_n(p, p'); \quad D_n(p, p') = \frac{(-1)^n}{n!} \begin{vmatrix} \delta(p-p') & n & 0 \dots 0 \\ K(p, p') & \sigma_1 & n-1 \dots 0 \\ \vdots & \vdots & \vdots \\ K^n(p, p') & \sigma_n & \sigma_{n-1} \dots \sigma_1 \end{vmatrix}$$

$$d(\lambda) = \sum_{n=0}^{\infty} \lambda^n d_n; \quad d_0 = 1; \quad d_n = \frac{(-1)^n}{n!} \begin{vmatrix} \sigma_1 & n-1 & \dots & 0 \\ \sigma_2 & \sigma_1 & \dots & 0 \\ \vdots & \vdots & \ddots & \vdots \\ \sigma_n & \sigma_{n-1} & \dots & \sigma_1 \end{vmatrix}$$

$K^n(p, p')$ stands for iterated Kernels and

$$\sigma_n = \text{trace } K^n = \int K^n(p, p) dp$$

Also from the well known property of $d(\lambda)$ it is written alternatively as $d(\lambda) = \exp[\text{trace log } (1 - \lambda K)]$

$$\text{From (2.11), } B(p) = -B_0(p) \frac{\left[1 + \lambda \Delta_1(p) - \lambda \sigma_1 + \lambda^2 \Delta_2(p) - \frac{\lambda^2}{2} \sigma_2 + \dots \right]}{\exp \left(-\lambda \sigma_1 - \frac{\lambda^2}{2} \sigma_2 - \dots \right)} \quad \dots (2.12)$$

$$\text{where} \quad \Delta_1(p) = \frac{1}{B_0(p)} \int V(p, p') \frac{dp'}{p'^2 - k^2} V(p', k)$$

$$\Delta_2(p) = \frac{1}{B_0(p)} \int \int V(p, p') \frac{dp'}{p'^2 - k^2} V(p', p'') \frac{dp''}{p''^2 - k^2} V(p'', k)$$

$$\sigma_1 = \int_0^{\infty} V(p, p) (p^2 - k^2)^{-1} dp;$$

$$\dots \quad \sigma_2 = \int \int V(p, p') V(p', p) (p^2 - k^2)^{-1} (p'^2 - k^2)^{-1} dp dp'$$

$$\text{with } V(p, p') = \sqrt{pp'} \int J_1(px) J_1(p'x) e^{-\mu x} dx$$

we get the value of the asymptotic phase from (2.12) and (2.9) with the help of the following results (see § 13.22, 13.23(1), 13.53(4) of Waston's Bessel functions)

$$\Delta_1(k) = [B_0(k)]^{-1} \left[\frac{\lambda^2}{2k\pi} \left\{ \log \left(1 + 4 \frac{k^2}{\mu^2} \right) \times \sum_{n=1}^{\infty} \left(\sec^n \theta \frac{\sin n\theta}{n^2} - \cos^n \theta \frac{\sin n\theta}{n^2} \right) \right\} \right]$$

$$\left(\theta = \arctan \frac{2k}{\mu} \right)$$

The series $\sum_{n=1}^{\infty} \left(\sec^n \theta - \cos^n \theta \right) \frac{\sin n\theta}{n^2}$ can be easily put to in the form

$$\int_{\cos \theta}^{\sec \theta} \frac{dy}{y} \tan^{-1} \frac{y \sin \theta}{1 - y \cos \theta}, \text{ which is numerically evaluated by using Simpson's}$$

rule (Ince. ordinary Diff. eq.)

$$\sigma_1 = \frac{\pi}{2k} \arctan \frac{2k}{\mu}$$

$$\sigma_2 = \frac{1}{2\pi k^2} [(\log \sec^2 \theta)^2 + \pi^2/4]$$

$$V(k, k) = \frac{1}{\pi} Q_0 \left(1 + \frac{\mu^2}{2k^2} \right);$$

$$\frac{\lambda}{\mu} = \left(\frac{M_n}{\mu} \right) f^2$$

Q_0 is the Legendre function of the second kind, and M_n = nucleon mass, λ = meson mass, f^2 = coupling constant, $\hbar = c = 1$. The phase shifts are now determined from (2.12) and (2.9). The differential cross section for the n-p scattering is given by

$$\sigma_{np}(\theta) = \left| \frac{1}{k} \sum_{l=0}^{\infty} (2l+1) e^{i\eta_l} \sin \eta_l P_l(\cos \theta) \right|^2$$

and the total cross section by

$$\sigma_{np} = \int_0^{\pi} \sigma_{np}(\theta) \sin \theta d\theta = \frac{4\pi}{k^2} \sum_{l=0}^{\infty} (2l+1) \sin^2 \eta_l$$

As only the s -wave scattering is of importance in the low energy limit (Blatt and Weisskopf, 1952) so the total cross section can be written for the s -wave as

$$\sigma_{np} = \frac{4\pi}{k^2} \sin^2 \eta_0$$

where η_0 is obtained from (2.12) and (2.9).

3. THE SCATTERING BY A CENTRAL POTENTIAL FOR ANGULAR MOMENTUM $l > 0$

Extension to higher angular momentum.

The radial Schrödinger Eq. for angular momentum, l , is

$$\left(-\frac{d^2}{dx^2} + V(x) + \frac{l(l+1)}{x^2} - k^2 \right) \psi(x) = 0 \quad \dots (3.1)$$

with the boundary condition that

$$\lim_{x \rightarrow \infty} \psi(x) = kx [j_l(kx) - \tan \eta_l n_l(kx)] \quad \dots (3.2)$$

where

$$j_l(kx) = \sqrt{\frac{\pi}{2kx}} J_{l+1/2}(kx) \sim \frac{\sin(kx - \pi l/2)}{kx}$$

$$n_l(kx) = \sqrt{\frac{\pi}{2kx}} J_{-l-1/2}(kx) \sim \frac{\cos(kx - \pi l/2)}{kx}$$

and η_l is the phase shift corresponding to the angular momentum l .

We transform (3.1) into an integral equation with the aid of generalised Hankel transform of order $\nu = l + \frac{1}{2}$.

If $\phi(p)$ be the Hankel transform of $\psi(x)$ then the inverse relation is

$$\psi(x) = \int_0^\infty (px)^{\frac{1}{2}} J_\nu(px) \phi(p) dp$$

and writing

$$\lambda V_l(p, p') = \frac{2}{\pi} \int_0^\infty (px)^{\frac{1}{2}} J_\nu(px) V(x) (p'x)^{\frac{1}{2}} J_\nu(p'x) dx$$

with

$$V(x) = \lambda e^{-\mu x}/x.$$

We obtain finally

$$(p^2 - k^2) \phi(p) + \lambda \int_0^\infty V_l(p, p') \phi(p') dp' = 0, \quad \dots (3.3)$$

(3.3) is the integral equation formalism of (3.1). In obtaining (3.3) we have made use of the following result :

$$\int_0^\infty (px)^{\frac{1}{2}} J_\nu(px) (p'x)^{\frac{1}{2}} J_\nu(p'x) dx = \delta(p - p')$$

The asymptotic behaviour of (3.3) is given by the singular solution of $\phi(p)$ and is given by

$$\phi(p) = \delta(p-k) - (p^2 - k^2)^{-1} \lambda \int_0^\infty V_l(p, p') \phi(p') dp' \quad \dots (3.4)$$

It may easily be verified that (3.4) is satisfied by (3.2) provided

$$\tan \eta_l = - \frac{\pi \lambda}{2k} \int_0^\infty V_l(k, p') \phi(p') dp' \quad \dots (3.5)$$

As in Section 2 we may easily construct an equivalent integral equation for $B_l(p)$ as given in (2.9),

where
$$B_l(p) = \lambda \int_0^\infty V_l(p, p') \phi(p') dp'$$

and we write

$$B_l(p) = B_{l,0}(p) - \lambda \int_0^\infty V_l(p, p') (p'^2 - k^2)^{-1} B_l(p') dp' \quad \dots (3.6)$$

where
$$B_{l,0}(p) = \lambda V_l(p, p')$$

The Fredholm solution of (3.6) is given as

$$B_l(p) = -B_{l,0}(p) \frac{[1 + \Delta_1^l(p) - \lambda \sigma_1^l + \dots]}{\exp \left(-\lambda \sigma_1^l - \frac{\lambda^2}{2} \sigma_2^l \dots \right)} \quad (3.7)$$

Hence as in the last section we have for the phase shift of P, D, F , etc. states the following result

$$\tan \eta_l = \frac{\pi}{2k} V_l(k, k) \left[\lambda - \lambda^2 \sigma_1^l + \lambda^2 \Delta_1^l(k) + \dots \right] \exp (\lambda \sigma_1^l + \dots) \dots (3.8)$$

where
$$\Delta_1^l = \frac{1}{V_l(k, k)} \int_0^\infty V_l(k, p') (p'^2 - k^2)^{-1} V_l(p', k) dp' \quad \dots (3.9)$$

$$\sigma_1^l = \int_0^\infty V_l(p, p) (p^2 - k^2)^{-1} dp \quad \dots (3.10)$$

The results of (3.8), (3.9) and (3.10) are given in what follows. (3.8) gives the asymptotic phase for any value of l . The s -wave phase is obtained by putting $l = 0$ in (3.8), (3.9) and (3.10).

$$\begin{aligned}
 & \int_0^{\infty} V_l(k, p')(p'^2 - k^2)^{-1} V_l(p', k) dp' \\
 &= \frac{2^{2\nu+1}}{\pi} (k/\mu)^{2\nu+2} \frac{\Gamma(2\nu + \frac{1}{2})}{\Gamma(\frac{1}{2})} \sum_{n=0}^{\infty} I_n \frac{\mu^{n+2\nu+1}}{\Gamma(4\nu + n + 1)} \cdot \frac{(-1)^{n+2\nu+1}}{12} \left\{ \frac{\partial}{\partial \mu} \right\}^{n+2\nu+1} \\
 & \quad \times \left[(\mu^2 + 4k^2)^{-\frac{1}{2}} + \frac{4 \cos \frac{\nu\pi}{2}}{\sqrt{\mu^2 + 4k^2}} + \frac{\cos \nu\pi}{\mu} \right] \\
 & + \frac{1}{12\pi^2} \cdot Q_{\nu-1} \left(1 + \frac{\mu^2}{2k^2} \right) \left[(\mu^2 + 4k^2)^{-\frac{1}{2}} + 4 \cos \frac{\nu\pi}{2} \cdot (\mu^2 + 2k^2)^{-\frac{1}{2}} + \cos \nu\pi \cdot \mu^{-1} \right] \\
 & - \frac{2}{\pi} \left(\frac{k}{\mu} \right)^2 \sum_{n=0}^{\infty} I'_n \frac{\mu^{n+1}}{(n+1)\Gamma(n+1)} \left\{ \frac{k^{2\nu}}{\mu^{n+2}} - \frac{\Gamma(2\nu + n + 1)}{\Gamma(2\nu + 1)} \cdot \frac{\pi}{6} \right. \\
 & \quad \left. {}_2F_1 \left(\frac{n+2\nu+2}{2}, \frac{n+2\nu+3}{2}, \nu+1, -\frac{2k^2}{\mu^2} \right) \right\} \\
 \text{with } I_n &= \int_0^{\pi/2} \cos^{2\nu}\phi \left(1 + 4 \frac{k^2}{\mu^2} \cos^2\phi \right)^{n/2+\nu} C_n^{2\nu+1} \left(\sqrt{\frac{-\mu}{\mu^2 + 4k^2 \cos^2\phi}} \right) d\phi \\
 I'_n &= \int_0^{\pi/2} \cos 2\nu\phi \left(1 + 4 \frac{k^2}{\mu^2} \cos^2\phi \right)^{n/2} C_n^{\frac{1}{2}} \left(\sqrt{\frac{-\mu}{\mu^2 + 4k^2 \cos^2\phi}} \right) d\phi \\
 \text{and } \sigma_1^l &= \frac{\pi^2}{12} \left[(\mu^2 + 4k^2)^{-\frac{1}{2}} + \frac{4 \cos \nu\pi/2}{\sqrt{\mu^2 + 2k^2}} + \frac{\cos \nu\pi}{\mu} \right]
 \end{aligned}$$

In evaluating the above two integrals we have utilised Simpson's rule to find

out, $\int_0^{\pi/2} \cos 2\nu\phi (\mu^2 + 4k^2 \cos^2\phi)^{-\frac{1}{2}} d\phi$. For particular values of ν these can be easily integrated.

4. COMPARISON WITH OTHER APPROXIMATE RESULTS

We now give below in a tabular form the theoretical values as derived from (2.12) and 2.10). The numerical values obtained from the Fredholm series (eqs. 2.12) has been compared with different results as obtained from Born's approximation, and variational approximations. The values of the Born's are taken from Kälén (1949) and the variational calculation of Hulthén (1943).

TABLE I

f^2		.0416	.0832	.1248	.1664	.2080	.2496
k/μ							
2.0	1st Born	.088500	.17100	.25600	.35	.43	.51000
	2nd Born	.090000	.18300	.27900	.38	.48	.59000
	2nd Fredh	.096650	.18300	.27919	.38045	.48015	.59305
	Hult	.090800	.18600	.28700	.39000	.50000	.62000
1.5	1st Born	.19000	.19000	.29	.38	.48000	.58000
	2nd Born	.20000	.20000	.31	.42	.54000	.67000
	2nd Fredh	.20006	.20006	.31031	.42115	.54311	.67671
	Hult	.22000	.22000	.32000	.50000	.65000	.80000
1.0	1st Born	.10100	.20100	.30200	.40000	.50	.60
	2nd Born	.10500	.21900	.34200	.47000	.62	.77
	2nd Fredh	.10501	.21929	.34353	.47462	.63296	.80142
	Hult	.10400	.21800	.34500	.49000	.68000	.92000
.5	1st Born	.0866	.173	.26000	.35	.43	.52
	2nd Born	.0934	.202	.32000	.46	.61	.78
	2nd Fredh	.0943	.20293	.32451	.47571	.65360	.89790
	Hult	.0944	.20900	.35000	.55000	.84000	1.33000

The table supplies the theoretical s -wave phase shift as determined by the Fredholm approximation.

5. CONCLUSION

It appears from the table of numerical results that for small values of the coupling constant the Fredholm second order approximation is larger than the corresponding Born's approximation. This is a desirable feature of the Fredholm perturbation method as the experimental data demand values of the phase shifts larger than that given by the Born approximation. However, Hulthén's variational treatment is still a better approximation.

ACKNOWLEDGMENT

The author wishes to thank Dr. D. Basu for suggesting the problem and for his valuable help in the preparation of the manuscript.

REFERENCES

- Blatt, J. M. and Weisskopf, V., 1952, *Theoretical Nuclear Physics*. John Wiley and Sons.
- Hulthén, L., 1948, *Ark. for mat. Astr. och. fys.*, Bd. 35A, No. 25.
- Ince, 1926, *Ordinary Diff. Equation*. Dover Publication.
- Jost, R. and Pais, A., 1951, *Phys. Rev.*, **82**, 840.
- Källén, G., 1951, *Ark. For. Fys.*, 2 nr. 6, 33.
- Kohn, W., 1951, *Phys. Rev.*, **84**, 429.
- Salpeter, E. E., 1951, *Phys. Rev.*, **84**, 1226.
- Smithies, F. J., 1941, *Duke. Mathe. Jour.*, **8**, 107.
- Titchmarsh, E. C., 1948, *Theory of Fourier Integral*, Oxford.
- Watson, G. N., 1948, *Bessel functions*, Cambridge, Second Edition.

ON THE DEVIATION OF MAGNETIC MOMENTS OF S NUCLEI FROM THE SCHMIDT LIMITS*

By M. L. CHAUDHURY

DEPARTMENT OF THEORETICAL PHYSICS,

INDIAN ASSOCIATION FOR THE CULTIVATION OF SCIENCE, CALCUTTA-32

(Received for publication, May 26, 1955)

ABSTRACT. The present attempt to explain the deviations of the magnetic moments of the $S_{\frac{1}{2}}$ -nuclei from the Schmidt limits, is based on the assumption that this deviation is essentially due to the change in the intrinsic magnetic moment of the last odd particle as a result of exchange of vector mesons between it and the adjacent nucleons of the core.

The exchange moment has been calculated by the usual perturbation method. The agreement with experimental findings is discussed in the paper.

INTRODUCTION

It is well-known that the single-particle shell model of Mayer (1950), and Haxel, Jensen and Suess (1950) interprets the various nuclear properties, such as isomerism, β -decay probabilities, magic numbers, nuclear spins etc. with remarkable success. According to this model, for odd- A nuclei the nuclear properties are to be explained in terms of the last odd particle only, which occupies the state of binding corresponding to an independent particle motion in the averaged field of the core formed by the other nucleons. This description of the nucleus which bears a close analogy to that of atomic structure, presents considerable difficulties in explaining the magnetic moments, quadrupole moments, and gamma-transitions of electric quadrupole type. In a plot of the magnetic moments against the nuclear spin I , this model leads to two different pairs of lines, known as the Schmidt (1937) lines; one pair of lines being for the odd-proton and the other pair for the odd-neutron nuclei; and one line of each pair corresponds to the particle state with orbital angular momentum $l = I + \frac{1}{2}$ and the other to the state with $l = I - \frac{1}{2}$. On the other hand, the experimental values of the magnetic moments are found to be scattered within the Schmidt limits except for the cases of H^3 , He^3 , C^{13} and N^{15} , the values of which fall outside the limits.

Various modifications have been suggested to improve the situation but none of them is satisfactory. Of the different suggestions, one that provides a natural basis for the observed values of the magnetic moments being intermediate between the Schmidt limits, assumes that the state of the last odd particle is a mixture of

* Communicated by Dr. D. Basu.

the two states with $l = I + \frac{1}{2}$ and $l = I - \frac{1}{2}$. However, this mixture theory requires arbitrary percentages of the component states and as pointed out by Foldy and Milford (1950) and others, such mixtures of widely separated energy states are hardly justifiable.

Bohr and Mottelson (1953) postulate a mechanical deformation of the core and a sharing of angular momentum between the core and the last odd particle through surface tides. This, so-called quasi-atomic model, it is admitted, fails to account for the deviations of the moments in the cases of the $S_{\frac{1}{2}}$ -nuclei. Further, as pointed out by previous authors, though this model gives for small l values a general closing up of the Schmidt limits, various types of couplings between the core and the last particle are required for the individual nuclei.

Another modification of Mayer's single particle hypothesis has been to consider all the nucleons in the last unfilled shells to be coupled amongst themselves. Hence assuming $j-j$ coupling Mizushima and Umezawa (1952), Kurath (1952-53) and Flowers (1952) have obtained agreement between the calculated and observed moments of various nuclei. But for the $S_{\frac{1}{2}}$ -nuclei the values of magnetic moments obtained by them are very nearly the same as the Schmidt values.

Thirdly, Bloch (1951) has suggested that, the intrinsic moment of the last odd-nucleon may be affected by its binding to the core and hence may differ appreciably for different nuclei.

Miyazawa (1951), however, introduces the idea that the above change in the intrinsic moment of the last particle is due to the fact that the possible virtual states of the last odd nucleon are limited by the occupied states of the nucleons of the core. His theory, like that of Bohr et al, (1953) gives a general closing up of the Schmidt limits, but does not explain the individual variations of the nuclei.

Finally, prior to the suggestion of Bloch, Villars (1947) has considered similar deviation due to exchange of meson currents in the cases of H^3 and He^3 nuclei.

In the following we shall assume that the deviation of the magnetic moment of a nucleus from the Schmidt value is essentially due to the change in the intrinsic moment of the last odd particle as a result of exchange of mesons between the last odd particle and those of the core, which also gives the binding of the last nucleon to the core as suggested by Bloch (loc. cit).

Extending the definition of magnetic moment of a *free* nucleon given by Heitler, Kemmer and Fröhlich (1938) to the case of a *bound* nucleon we propose that the virtual meson, may in addition to being self-absorbed, be also absorbed by the nucleons constituting the core.

We shall use the perturbation method (cf. Fröhlich, Heitler, Kemmer (loc. cit)) for calculating the exchange moment for a single pair and then sum for all such appropriate pairs. The expression obtained for the magnetic moment due

to the exchange of mesons between two unlike nucleons, involves the mutual distance, r_{AB} . To find r_{AB} for any nucleus, we shall plot r_{AB} against binding energy per particle, ϵ/A . The theoretical values of r_{AB} are worked out for H^2 and H^3 . It is not possible to calculate the same for heavier nuclei with higher ϵ/A , because the wave functions are very much complicated. So for the latter nuclei, comparison of the theory with experiment is made with the help of a curve showing the variations of r_{AB} against ϵ/A .

SECTION 1

We assume that the meson has the spin value 1 and is represented by the vector field. In the case of a *free* nucleon, the anomalous moment of the proton or the neutron has been attributed by Fröhlich, Heitler and Kemmer (1938) to the additional moment of the meson during the interval between emission and self-absorption. To extend this idea to the case of a *bound* nucleon, one has to consider in addition to self-absorption, the effect of absorption by neighbouring nucleons. Because, as soon as the last odd proton (or neutron) dissociates into a neutron (or proton) and a positive (or negative) meson, there is a competition between the probabilities of self-absorption and absorption by the other adjacent nucleons. Since neutral mesons are excluded, we are to consider exchange only between unlike nucleons.

The matrix elements for the emission and absorption of the transverse mesons, are as follows :

$$H'_{n_i^+, n_{i+1}^+} = - \sum_{i,j,a} f^* \sqrt{\left(\frac{\hbar c (n_i^+ + 1)}{2V(\chi^2 + k_i^2)^{\frac{1}{2}}} \right)} \cdot \tau_a^A \left(\vec{\sigma} \cdot \text{curl } \vec{l}_{ij} \cdot e^{+ik_i \cdot \vec{r}_A} \right) \quad \dots (1)$$

and

$$H'_{n_{ij+1}^+, n_{ij}^+} = + \sum_{i,j,a} f \sqrt{\left(\frac{\hbar c n_{ij}^+}{2V(\chi^2 + k_i^2)^{\frac{1}{2}}} \right)} \cdot \tau_a^B \left(\vec{\sigma} \cdot \text{curl } \vec{l}_{ij} \cdot e^{-ik_i \cdot \vec{r}_B} \right) \quad \dots (2)$$

Where V is the volume in which the field is confined, k_i is the wave number, \vec{l}_{ij} represents unit vector in the direction of polarisation, subscript i indicates all possible values of k_i . For the transverse meson $j = 2$ and 3 where k_i is in the direction of l_{ij} and $\chi = m_0 c / \hbar$, where m_0 = mass of π meson.

Now we have for the second order perturbation energy

$$W^2 = \frac{H'_{01} H'_{10}}{(E_0 - E_1)} = - \frac{ff^* \hbar^2 c^2}{2V} \sum_{i,j,a} \left(\tau_a^A \tau_a^B \right) \cdot \left(\vec{\sigma}_A \cdot \vec{l}_{ij} \times \vec{k}_i \right) \left(\vec{\sigma}_B \cdot \vec{l}_{ij} \times \vec{k}_i \right) \cdot e^{+ik_i \cdot \vec{r}_{AB}} \quad (3)$$

where E_0 and E_1 are the total energies of the system in the initial and intermediate states respectively. The difference of E_0 and E_1 is equal to the energy of the emitted meson ϵ_i .

Replacing the summation over by integration and remembering that the emitted meson is subjected to a weak magnetic field, one obtains from (3)

$$W^2 = + \sum_a \left(\tau_a^A \tau_a^B \right) \frac{ff^*}{16\pi^3} \int d\Omega \int dk \frac{k^2 \cdot e^{+ik \cdot r_{AB}}}{\left((\chi^2 + k^2)^{\frac{1}{2}} - \frac{eH}{2m_0 c^2} \right)^2} \{ (\vec{\sigma}_A \cdot \vec{k})(\vec{\sigma}_B \cdot \vec{k}) - k^2 (\vec{\sigma}_A \cdot \vec{\sigma}_B) \} \dots \quad (4)$$

Now we expand the denominator, neglect H^2 term as being small and multiply both the numerator and the denominator by

$$\left((\chi^2 + k^2) + \frac{eH(\chi^2 + k^2)^{\frac{1}{2}}}{m_0 c^2} \right).$$

Hence we can write from (4)

$$W^2 = \sum_a \left(\tau_a^A \tau_a^B \right) \frac{ff^*}{16\pi^3} \int d\Omega \int_0^\infty dk \frac{k^2 ((\chi^2 + k^2) + eH(\chi^2 + k^2)^{\frac{1}{2}}/m_0 c^2)}{(\chi^2 + k^2)^2} \times \{ (\vec{\sigma}_A \cdot \vec{k})(\vec{\sigma}_B \cdot \vec{k}) - k^2 (\vec{\sigma}_A \cdot \vec{\sigma}_B) \} \cdot e^{+ik \cdot r_{AB}} \dots \quad (5)$$

To find the magnetic moment due to exchange we expand the perturbation energy in a series in powers in H :

$$W^2 = c - \mu_{ex}^{AB} \cdot H + \dots \quad (5.1)$$

We are interested in the term involving H only, and from (5) and (5.1) we obtain,

$$\mu_{ex}^{AB} = - \sum_a \left(\tau_a^A \tau_a^B \right) \cdot \frac{ff^* e}{16\pi^3 m_0 c^2} \cdot \int d\Omega \int dk \frac{k^2 e^{+ik \cdot r_{AB}}}{(\chi^2 + k^2)^{3/2}} \times \{ (\vec{\sigma}_A \cdot \vec{k})(\vec{\sigma}_B \cdot \vec{k}) - k^2 (\vec{\sigma}_A \cdot \vec{\sigma}_B) \} \dots \quad (6)$$

Now for the convenience of integration we split up $(\vec{\sigma}_A \cdot \vec{k})(\vec{\sigma}_B \cdot \vec{k}) = (\sigma_x^A \cdot k_x + \dots)(\sigma_x^B \cdot k_x + \dots)$ and make r_{AB} coincide with the z -axis such that $k_x^2 = k^2 \sin^2 \theta \cos^2 \phi$, and from the 1st part of (6), contribution to the magnetic moment due to x -component of \vec{k} is as follows:

$$\left(\mu_{ex}^{AB} \right)_{Ix} = - \sum_a \left(\tau_a^A \tau_a^B \right) \frac{ff^* e (\sigma_x^A \sigma_x^B)}{16\pi^3 m_0 c^2} \int_0^\infty dk \frac{k^4}{(\chi^2 + k^2)^{3/2}} \int_0^\pi e^{+ik r_{AB} \cos \theta} \sin^2 \theta d\theta \dots \quad (6.1)$$

Now by integrating one gets (dropping the subscript AB)

$$\begin{aligned} \left(\mu_{ex}^{AL} \right)_{Ia} = & - \sum_a \left(\tau_a^A \tau_a^B \right) \cdot \frac{ff^* e (\sigma_x^A \sigma_x^B)}{16\pi^2 m_0 c^2} \cdot \left[-\frac{4}{r^2} \cdot \frac{\partial}{\partial r} \cdot \left\{ \frac{r}{\chi} K_1(r\chi) \right\} \right. \\ & \left. + \frac{4}{r^2} \cdot \frac{\partial^2}{\partial r^2} \cdot \left\{ \frac{r}{\chi} K_1(r\chi) \right\} \right] \quad \dots (7) \end{aligned}$$

Since

$$\int_0^\infty dk \frac{\cos kr}{(\chi^2 + k^2)^{3/2}} = \frac{1}{2} \cdot \int_{-\infty}^{+\infty} \frac{e^{ikr} dk}{(\chi^2 + k^2)^{3/2}} = \frac{r}{\chi} \cdot K_1(r\chi) \quad \dots (7.1)$$

K_n is the modified Hankel functions of order n and in this case $n = 1$. On using the recurrence formula for K_n , the differentiation in (7) yields,

$$\begin{aligned} \left(\mu_{ex}^{AB} \right)_{Ia} = & - \sum_a \left(\tau_a^A \tau_a^B \right) \frac{ff^* e (\sigma_x^A \sigma_x^B)}{16\pi^2 m_0 c^2} \\ & \times \left[\frac{\chi}{r} (3K_1 + K_3) - \frac{2}{r^2} (K_0 + K_2) - \frac{4}{\chi r^3} K_1 \right] \quad \dots (8) \end{aligned}$$

Since $k_y^2 = k^2 \sin^2 \theta \sin^2 \phi$, the contribution of k_y^2 to the 1st part of (6) is similar to (8) excepting for the factor $(\sigma_y^A \cdot \sigma_y^B)$. The contribution of k_z is slightly different and proceeding as before.

$$\begin{aligned} \left(\mu_{ex}^{AB} \right)_{Ia} = & - \sum_a \left(\tau_a^A \tau_a^B \right) \frac{ff^* e (\sigma_x^A \sigma_x^B)}{8\pi^2 m_0 c^2} \\ & \times \left[\frac{\chi}{r} (3K_1 + K_3) - \frac{\chi^2}{4} (3K_0 + 4K_2 + K_4) + \frac{2}{r^2} (K_0 + K_2) + \frac{4}{\chi r^3} K_1 \right] \dots (9) \end{aligned}$$

On summing for all the three components and integrating the second part in (6) as above, we have for the total magnetic exchange moment as

$$\begin{aligned} \mu_{ex}^{AB} = & - \sum_a \left(\tau_a^A \tau_a^B \right) \frac{ff^* e}{16\pi^2 m_0 c^2} \left\{ \left(\vec{\sigma}_A \cdot \vec{n} \right) \left(\vec{\sigma}_B \cdot \vec{n} \right) - \frac{1}{3} \left(\vec{\sigma}_A \cdot \vec{\sigma}_B \right) \right\} \\ & \times \left\{ \frac{12}{\chi r^3} K_1 + \frac{6}{r^2} (K_0 + K_2) - \frac{\chi^2}{2} (3K_0 + 4K_2 + K_4) \right\} \\ & - \frac{2}{3} \left(\vec{\sigma}_A \cdot \vec{\sigma}_B \right) \cdot \left\{ \frac{3\chi}{r} (3K_1 + K_3) - \frac{\chi^2}{2} (3K_0 + 4K_2 + K_4) \right\} \quad \dots (10) \end{aligned}$$

Where \vec{n} is the unit vector in the z -direction. We further assume that the contribution of the tensor force term is negligible. So finally the expression for the exchange magnetic moment of a proton A interacting with a neutron B , is

$$\left(\mu_{ex}^{AB}\right)_p = + \left(\frac{ff^* \chi^2}{8\pi\hbar c}\right) \frac{M_p}{\pi m_0} \left(\frac{e\hbar}{2M_p c}\right) \frac{2}{3} (\vec{\sigma}_A \cdot \vec{\sigma}_B).$$

$$\sum_a \left(\tau_a^A \tau_a^B\right) \left\{ \frac{3}{\chi r} (3K_1 + K_3) - \frac{1}{2} (3K_0 + 4K_2 + K_4) \right\} \dots \quad (11)$$

If, however, the last odd particle is a neutron, a similar calculation is to be carried out, the only difference being that the neutron emits a negative meson, the magnetic energy of which has the sign opposite to that in the case of the proton, so that $(\mu_{ex}^{AB})_n$ is exactly similar to (11) with a negative sign. Taking the values of $ff^*\chi^2/8\pi\hbar c = 0.122$ and $\chi = 7.14 \times 10^{+12}$ (cf. Basu 1952), we give below the variation of μ_{ex}^{AB} with r_{AB} in Table I

TABLE I

$r_{AB} \times 10^{+13} \text{ cm.}$	(χr)	$\frac{(\mu_{ex}^{AB})_P}{\left[(\sum_a \tau_a^A \tau_a^B) (\vec{\sigma}_A \cdot \vec{\sigma}_B) \right]}$
1.259	0.9	+0.21300
1.399	1.0	+0.12400
1.545	1.1	+0.06730
1.679	1.2	+0.03010
1.818	1.3	+0.00582
1.958	1.4	-0.00998
2.098	1.5	-0.01990
2.239	1.6	-0.02590
2.378	1.7	-0.02910
2.519	1.8	-0.03060

It may be noted that the above values in Table 1 are for the odd—proton nuclei. For the odd neutron nuclei the values are the same but the sign is opposite in each case. In both cases the values of $[(\mu_{ex}^{AB})/(\sum_a \tau_a^A \tau_a^B) (\vec{\sigma}_A \cdot \vec{\sigma}_B)]$ change sign at $r_{AB} = 1.868 \times 10^{-13} \text{ cm.}$ This explains qualitatively the sign of the deviations of the magnetic moments of extremely light nuclei with small binding, and $r_{AB} >$

1.862×10^{-12} , being opposite to that of the rest of the nuclei which have larger binding and $r_{AB} < 1.862 \times 10^{-12}$ cm.

The formula (11) gives μ_{ex}^{AB} in terms of internucleonic distance r_{AB} which is not known. To find r_{AB} for all the $S_{\frac{1}{2}}$ -nuclei, it is intended to plot a curve showing $\langle r_{AB} \rangle_{AV}$ against average binding per particle ϵ/A . $\langle r_{AB} \rangle_{AV}$ is worked out for H^2 and H^3 with the wave functions given by Wilson (1938).

On taking the value of the meson mass as $276m_e$ and the binding energy of H^2 as 2.19 Mev, $\langle r_{AB} \rangle_{AV}$ comes out to be 2.503×10^{-12} cm. For H^3 , Wilson's wave function is $\psi_3 = \exp\{-\frac{1}{2}\alpha(\xi_1 + \xi_2 + \xi_3)\}$ where $\xi_1 = \chi r_{23}$, $\xi_2 = \chi r_{13}$ and $\xi_3 = \chi r_{12}$. On using elliptic coordinates due to Hylleraas (1929) i.e. $s = \xi_1 + \xi_3$, $t = \xi_3 - \xi_1$ and $u = \xi_2$ and the volume element $d\tau = ds du dt u(s^2 - t^2)$, we have for the normalization factor $D = 2\alpha^3/\sqrt{7}$.

$$\text{and } \langle r_{AB} \rangle_{AV} = \frac{1}{\chi} \langle \xi_2 \rangle_{AV} = \frac{D^2}{\chi} \int_0^\infty ds \int_0^s du \int_0^u dt u^2(s^2 - t^2) e^{-\alpha s - \alpha u} = 2/\chi\alpha \quad (12)$$

Following Wilson and taking the above mentioned value of meson mass, $\alpha = 1.41$. Hence for H^3 the value of

$$\langle r_{AB} \rangle_{AV} = 1.985 \times 10^{-12} \text{ cm.} \quad \dots (12.1)$$

The theoretical calculations of r_{AB} for heavier nuclei are exceedingly complicated. So for comparison of the formula (11) with experimental data in the cases of heavier nuclei, we assume that (11) is correct and find out those values of r_{AB} which would make the theoretical and experimental values of magnetic moments of F^{19} and Te^{125} agree with each other. On taking these values of r_{AB} and the corresponding values of average binding per particle ϵ/A , a curve is drawn. With the help of this curve and the relation (11), we see how much agreement is obtained for other nuclei.

For drawing ϵ/A vs. r_{AB} curve, we have taken ${}^9F^{19}$ and ${}^{52}Te^{125}$. The reason for this choice is that if F^{19} is excluded, no other pair of nuclei gives the form of the ϵ/A vs. r_{AB} curve near the intermediate values of ϵ/A . Secondly Te^{125} represents the group of nuclei with high average binding energy, i.e. about 8.5 Mev. Any other nucleus can be taken instead of Te^{125} and the results will not be much affected.

This procedure, however, can be applied only for those nuclei for which μ_{ex}^{AB} depends only on r_{AB} , other factors remaining the same. Of the thirteen $S_{\frac{1}{2}}$ -nuclei there are nine nuclei for which the number of interacting pairs in the last proton and neutron shells, is the same. The reason for taking pairs of only unlike nucleons has already been stated. Now the justification for taking the neutrons and

protons occupying only the last shells, is that μ_{ex}^{AB} depends sensitively on the mutual distance r_{AB} and would necessarily be negligible for the nucleons excepting those in the last shell. From the shell structure of F^{19} and Te^{125} it can be seen that in both the cases, the number of interacting pairs of unlike nucleons in the last shells, is two. Further, let the last odd nucleon A (proton or neutron) be interacting with two adjacent nucleons B_1 and B_2 (neutrons or protons), the spins of which should be in the opposite direction. If the pair AB_1 is in the singlet state, then the pair AB_2 will be in the triplet state. Therefore

$$(\sum_{\alpha, B_1 B_2} \tau_{\alpha}^A \tau_{\alpha}^B)(\sigma_A \sigma_B) = -8 \quad \dots (13)$$

From what has been said above, the required values of r_{AB} and other data can be arranged in Table II

TABLE II

Element	ϵ/A Mev	$r_{AB} \times 10^{13}$ cm.
${}_1H^2$	1.090	2.503
${}_1H^3$	2.800	1.985
${}_9F^{19}$	7.745	1.729
${}_{52}Te^{125}$	8.450	1.393

With the above data two curves, one in the low energy region and the other in the high energy region, are drawn. From these curves, r_{AB} of any nucleus of which ϵ/A is known, can be found and used in the relation (11) for comparison with experiment.

COMPARISON WITH EXPERIMENT

For comparison of the present theory with experiment, one has to remember that by our definition, the magnetic moment of a whole nucleus is the sum of the exchange moment of the last odd nucleon A and its magnetic moment observed in the free state, which is $+2.792$ for a proton and -1.913 for a neutron in unit of a nuclear magneton (n.m.). Again the formula (11) gives the exchange moment of a single pair AB , and for the whole nucleus we shall have to sum the values of all such interacting pairs formed by the last odd proton (or neutron) and the neutrons (or protons) in the last neutron (or proton) shell. The results of calculations are shown in the Table III. We have taken shell-structure from Mayer's scheme. ϵ/A is taken either from the Table of atomic nuclei or is estimated from the ϵ/A vs. A curve given by Rosenfeld (1948). Observed values of μ are taken from the Table of Klinkenberg (1952); μ_{sp} represents the values of moments

expected on the single-particle model. In each case of the following the number of interacting pairs formed by nucleons in the last shells, is seen to be only two.

TABLE III

Element	Shell-structure		ϵ/A	r_{AB} $\times 10^{13}$	$\sum_B \mu_{\pi AB}$	μ theor.	μ obs.	μ_{sp}
	Proton	Neutron	Mev	gms.		n.m.	n.m.	n.m.
${}^3_1\text{H}^3$	$(s_{\frac{1}{2}})^1$	$(s_{\frac{1}{2}})^2$	2.800	1.985	+0.100	+2.892	+2.978	+2.792
${}^3_2\text{He}^3$	$(s_{\frac{1}{2}})^2$	$(s_{\frac{1}{2}})^1$	2.550	2.058	-0.144	-2.057	-2.127	-1.913
${}^{31}_{15}\text{P}^{31}$	$(\pi)(d_{5/2})^6(s_{\frac{1}{2}})^1$	$(\bar{\pi})(d_{5/2})^6(s_{\frac{1}{2}})^2$	8.484	1.375	-1.088	+1.700	+1.311	+2.792
${}^{115}_{50}\text{Sn}^{115}$	$(4\bar{8})(p_{\frac{1}{2}})^2$	$(\bar{6}4)(s_{\frac{1}{2}})^1$	8.490	1.372	+1.096	-0.820	-0.918	-1.913
${}^{117}_{50}\text{Sn}^{117}$	$(4\bar{8})(p_{\frac{1}{2}})^2$	$(\bar{6}6)(s_{\frac{1}{2}})^1$	8.490	1.372	+1.096	-0.820	-0.999	-1.913
${}^{119}_{50}\text{Sn}^{119}$	$(4\bar{8})(p_{\frac{1}{2}})^2$	$(\bar{6}\bar{8})(s_{\frac{1}{2}})^1$	8.497	1.368	+1.112	-0.800	-1.046	-1.913
${}^{123}_{54}\text{Te}^{123}$	$(5\bar{0})(g_{7/2})^2$	$(\bar{7}0)(s_{\frac{1}{2}})^1$	8.450	1.393	+1.024	-0.890	-0.736	-1.913

DISCUSSIONS

It can be seen from Table III that the theoretical values of magnetic moments of ${}^3_1\text{H}^3$ and ${}^3_2\text{He}^3$ agree quite well with the observed values. In these two cases, r_{AB} is known theoretically and hence comparison is unambiguous and satisfactory, particularly because, as mentioned in the Introduction, these two $S_{\frac{1}{2}}$ -nuclei belong to the small group of four exceptional nuclei which have their sign of deviations of magnetic moments from the Schmidt limits being opposite to that of all the other odd- A nuclei.

It is also seen that for the other nuclei the opposite sign follows correctly from the formula. As regards quantitative agreement for these nuclei, the theoretical values, though not close to the observed ones may be considered satisfactory, in view of the uncertainties involved in the values of r_{AB} taken. These uncertainties arise from several causes. Firstly, in finding r_{AB} we have used average binding ϵ/A . But the actual binding in the last shell would differ from ϵ/A to a certain extent. Secondly, the slightly higher value in the case of ${}^{15}\text{P}^{31}$ is probably due to the fact that this is an odd-proton nucleus and its binding is further affected by coulomb repulsion.

Correction to the above theoretical values, is also necessary because the interacting nucleons are not always in the $s_{\frac{1}{2}}$ -states which affect the symmetry property and hence the value given in (13).

ACKNOWLEDGMENT

It is a pleasure to acknowledge my indebtedness to Dr. D. Basu Ph.D. for suggesting the problem and helpful discussions and guidance during the progress of the work.

REFERENCES

- Basu, D., 1952, *Ind. J. Phys.*, **28**, 291.
Blöch, F., 1951, *Phys. Rev.*, **83**, 839.
Bohr, A. and Mottelson, 1953, *Det. Kgl. Danske. Sels. Mat. fys.*, **27**, no. 16.
Flowers, B. H., 1952, *Phil. Mag.*, **43**, 1330.
Flody, L. L., and Milford, F. T., 1950, *Phys. Rev.*, **80**, 751.
Fröhlich, H., Heitler, W., Kemmer, N., 1938, *Proc. Roy. Soc. Lond. A.*, **166**, 154.
Haxel, O., Jensen, J. H. D., and Suess, H. E., 1950, *Z. f. Phys.*, **128**, 295.
Hylleraas, E. A., 1929, *Z. f. Phys.*, **54**, 347.
Klinkenberg, P. F. A., 1952, *Rev. Mod. Phys.*, **24**, 63.
Kurath, D., 1952, *Phys. Rev.*, **88**, 804.
„ 1953, *Phys. Rev.*, **91**, 1430.
Mayer, M. G., 1950, *Phys. Rev.*, **78**, 16.
Miyazawa, H., 1951, *Prog. Theor. Phys.*, **6**, 801.
Mizushima, M., and Umezawa, M., 1952, *Phys. Rev.*, **83**, 463.
Rosenfeld, L., 1948, "Nuclear Forces".
Schmidt, T., 1937, *Z. f. Phys.*, **106**, 358.
Villars, F., 1947, *Helv. Phys. Acta.*, **20**, 476.
Wilson, A. H., 1938, *Proc. Camb. Phil. Soc.*, **34**, 365.

ON THE ENERGY RESPONSE AND RESOLUTION OF A SCINTILLATION COUNTER

BY SOBHANA DHAR

INSTITUTE OF NUCLEAR PHYSICS, UNIVERSITY COLLEGE OF SCIENCE, CALCUTTA

(Received for publication, May 31, 1955)

Plate VII

ABSTRACT. The experimental investigations on the energy response, resolution and figure of merit of a scintillation counter using different phosphors are reported. The observations have been taken with the help of a 180° M-F spectrometer set up as an energy selector and the results are obtained for the phosphors NaI-Tl, anthracene, stilbene, terphenyl and plastifluor* B (plastic phosphor) under excitation by monoenergetic electrons ranging from nearly 100 kev to 1.1 Mev. From the experimental data, sodium iodide shows a linear behaviour in the entire energy range investigated while anthracene, stilbene and terphenyl seem to give linear responses above 160 kev, 120 kev and 240 kev respectively. The plastic phosphor is non-linear upto about 800 kev. The relative responses of the different phosphors to monoenergetic electrons are obtained under similar experimental conditions. The pulse height distributions for all the phosphors are found to be approximately of Gaussian nature. With the help of experimental data, the figure of merit and the energy required to produce one photon have been calculated for different phosphors. The pulse height resolutions for the phosphors have been computed from the experimental results and the inverse pulse height resolutions are plotted against pulse heights. The relative response curves and the inverse resolution versus pulse height curves reveal the comparative value and the usefulness of a particular phosphor in the spectrometry of nuclear radiations.

1.1 INTRODUCTION

The scintillation counter has proved to be an extremely useful tool in the detection of the nuclear radiations and an important application of it is found in the spectrometry of nuclear radiations. The scanning of the heights of the scintillation pulses provides a simple and efficient method of measuring the energy of the incident radiations and hence of elucidating the complex decay schemes of radioactive nuclei. In such investigations, it is essential to have a thorough knowledge of the nature of the response and resolution of the scintillation counter unit to the incident radiation. The response will naturally depend on certain factors, such as, the luminescence process in the phosphor material, the photo-multiplier tube, optical geometry of the system and the nature and energy of the incident radiation. All these considerations will decide the suitability of a scintillation counter assembly to the particular use concerned.

It is, therefore, evident that detailed studies on the energy response and resolution are necessary before one may use it successfully in the spectrometry

of beta and gamma radiations. Since for most of the artificial radioactive sources, the energies of gamma rays lie within the range from 0 to 1.5 Mev and occasionally upto 3 Mev, the data for this range will be most useful. We have chosen to perform our experimental investigations on energy response and resolution of a scintillation counter in the region from nearly 100 kev to 1.1 Mev. The measurements on energy response to electrons have been reported by some earlier workers (Taylor et al, 1951; Hopkins, 1951; and some others) who have used sodium iodide, anthracene and stilbene and for certain energy regions. In the present investigations, we aim at extending the knowledge of energy response for the above-mentioned phosphors as well as for some more phosphors, like terphenyl and plasti-fluor* B (plastic phosphor). Moreover, the studies on the nature of the pulse height distribution curves, the energy spent for the production of one photon and the resolution obtained with different phosphors are included.

1.2 EXPERIMENTAL ARRANGEMENT

The different factors involved in the energy response and resolution measurements have been discussed previously by Dhar (1955). In the present experimental investigations, monoenergetic electrons have been used as the exciting radiation. The selection of monoenergetic beam of electrons is made with the help of a 180° M-F β -ray spectrometer developed for the purpose. Since the resolving power of a β -ray spectrometer is very high, the spread in the output pulse amplitude for monoenergetic electrons can be attributed to be almost wholly due to the scintillation counter assembly.

The details of the experimental arrangement are dealt with in this section. The different parts of the spectrometer assembly and the electronic circuits are also described in brief.

(a) *Source*: It is well known that the monoenergetic beam of electrons can be obtained by accelerating electrons by means of highly stabilised D.C. voltages, but it is limited by the stability and the maximum value of the high voltage supply. The simpler and easier method is, therefore, to select a beam of electrons of known energy from the continuous β -ray spectrum using a β -ray spectrometer as an energy selector. The 180° M-F type β -ray spectrometer is chosen specially for its high resolving power compared to other types.

RaE source is used for the purpose to get energies upto 1.1 Mev and the selection of a monoenergetic beam of electrons is effected by the 180° M-F type spectrometer with variable magnetic field and a slit system.

(b) *Spectrometer Chamber*: The spectrometer assembly consisting of the source holder, lead shield, defining slit, exit (detector) slit etc., is mounted on a $3/8$ " thick brass plate and the whole assembly is enclosed in a rectangular chamber *B* made of $1/4$ " thick brass sheets joined by soft soldering. The over-all dimensions of the chamber are: length 19 cms. width 6.5 cms. and height 10.5 cms. The top rectangular flange supports the soft rubber gasket,

The source holder is a thin perspex plate resting on four brass screws (so that the height is adjustable), on which the source tube ($1\text{ cm} \times 0.2\text{ cm}$) is fixed by wax (figure 1).

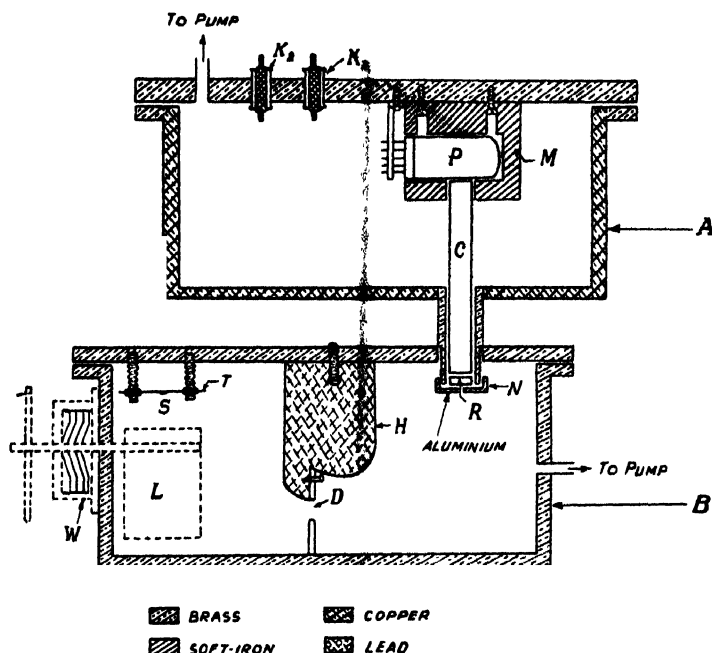


Fig. 1. Sectional diagram of spectrometer assembly.

A lead block *H* fixed on the top plate *A* by two screws shields the detecting counter from direct radiations from the sample. The central defining slit is made out of thick brass plate and is rectangular ($2\text{ cm.} \times 1\text{ cm.}$) in shape. *L* is a lead plate fitted to a brass rod passing through the Wilson seal arrangement and it serves the purpose of a shutter to shield the source when measuring the background due to cosmic rays and local radioactivity with magnetic field. There is an opening leading to the pump, manometer and discharge tube. The pressure within the chamber is maintained at about 10^{-3} cm of Hg. The diameter of the central circle passing through the centres of the source plate, central slit and exit slit is 13 cms.

A hollow brass tube, screwed and soft soldered to the top brass plate, communicates the lower chamber *B* to the upper chamber *A* containing photomultiplier assembly. The end of the brass tube is covered by an aluminium cap provided with a rectangular slit $1\text{ cm.} \times 0.2\text{ cm.}$, the width of which can be adjusted, whenever necessary.

A spectrometer of similar type was used by Das and Saha (1946) for the study of the beta radioactivity of Co^{60} . Considering the transmission curve for the spectrometer (Saha, 1945), the optimum service is expected when the source slit and the detector slit are of the same width $1\text{ cm.} \times 0.2\text{ cm.}$

The whole assembly is represented in figure 1. The lower chamber is placed within the pole pieces of the magnet. The upper chamber is made out of a copper cylinder and a $\frac{1}{2}$ " thick brass plate carrying the photomultiplier assembly has been placed at the top. The 1P21 photomultiplier tube together with the voltage dividing network is enclosed within the chamber. A soft iron enclosure round the photomultiplier tube (leaving only the photocathode surface exposed) shields it from stray magnetic fields. To ensure complete shielding from any external magnetic disturbances, the upper chamber is again wrapped round with a number of soft iron sheets.

The incident radiation entering the exit (detector) slit falls on the phosphor and the emitted light quanta are conducted to the photocathode surface through a perspex light conductor; the high voltage supply is fed to 1P21 tube through a spark plug K_2 and the output pulse from the collector plate is led to the cathode follower unit through a similar plug K_1 .

From the spectrometer constants and assuming the standard relation for the resolution (Cavanagh, 1950) of a 180° M-F type β -ray spectrometer, the resolution $\frac{\Delta p}{p}$ is obtained as

$$\frac{\Delta p}{p} = \frac{1}{2} [(s+\omega)/\rho + \alpha^2] \quad \dots (1)$$

where s and ω denote the exit slit width and source width respectively, 2ρ is the diameter of the path of the trajectory and α the semi-angle of the defining aperture.

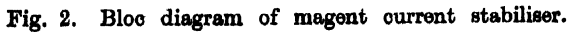
The relation (1) applied to the particular spectrometer assembly used by us, yields a resolution of 3.2 per cent which is quite satisfactory for our purpose.

(c) *Magnet Current Stabiliser*: The spectrometer magnet used in the present case is an electromagnet of iron-core type. For the proper selection of the mono-energetic beam of electrons and to minimise the fluctuations in energy, the stabilisation of the energising current of the magnet becomes essential. This demand is met by constructing a current stabiliser suited to the purpose.

The stabiliser unit described here is similar to that reported by Sen (1950). The schematic bloc diagram for the current stabiliser unit is shown in figure 2. The magnet current is obtained from the 220 volts D.C. mains through the final amplifier. The final amplifier is actuated by the pre-amplifier. For currents more than one ampere, the final amplifier is shunted by a suitable resistance which passes all the current required except about 500 milliamperes which is supplied by the final amplifier.

Since there is no D.C. connection between the final amplifier and the pre-amplifier, and the controlling signal is fed to the final amplifier over a radio-frequency carrier, the whole assembly is made extremely flexible. As the final amplifier operates as a separate unit independent of any D.C. reference point, the magnet can be connected to either the live side or the earth side of the D.C. line and the D.C. supply can be drawn from +220 as well as from -220 volts.

The more detailed descriptions of the individual units and their operations have been discussed by Sen (1950).



(d) *Recording Arrangement:* The photomultiplier tube 1P21 is selected out of a number of tubes of the same type, so as to yield the optimum signal to noise ratio. The tube, together with the voltage dividing network, is mounted properly within the upper chamber (figure 1). In order to shield the tube from external magnetic disturbances and the field of the spectrometer magnet, it is kept enclosed within a block of soft iron leaving only the photocathode surface exposed. To ensure complete magnetic screening, the upper chamber is also covered with sheets of soft iron. The detection of any variation in the number of noise counts with the change of magnetic field will check the adequateness of the shielding arrangement.

The photomultiplier voltage is supplied from a highly stabilised supply; the voltage per dynode stage is kept within the range of 75 to 100 volts, which can be varied whenever necessary.

The scintillation pulses at the output of the photomultiplier tube 1P21 are fed to the grid of the cathode follower through the spark plug K_1 (figure 1). The cathode follower is again followed by two three-stage feed-back amplifier loops a single channel pulse height analyzer (Model 510—Atomic Instrument Co.) and the scanned pulses are finally recorded with a Model 162 scaler (Nuclear Instrument Co.) and a mechanical recorder. Stabilised power supplies are used for running the electronic recording circuits. The A.C. mains supply is also stabilised by a magnetic stabiliser. The stabilised high voltage supply used by us for the photomultiplier tube has been described earlier (Dhar, 1951); the stabilisation has been measured and the variation is found to be ~ 0.1 volt. in 1200 volts.

The gain of the amplifier is variable and it has a band-width of 3 megacycles. Before taking each observation, the amplified pulses are checked visually in an oscilloscope to be sure that the amplifier is not overloaded.

For each setting of the magnet current, the differential distribution of the signal pulses are taken, subtracting the counts due to background at each stage. The magnetic field corresponding to each current setting is measured with the fluxmeter and the relation between the magnetic field and the mean energy of the electrons incident on the scintillator is obtained from the expression

$$\sqrt{\frac{\chi^{10^8}}{1 - \frac{1}{[1 + \chi/m_0c^2]^2}}} = \frac{1}{2} H\rho c$$

where χ denotes the energy of the electron in volts,

$$\rho = 6.5 \text{ cms.},$$

$$m_0c^2 = 5 \times 10^5 \text{ ev}$$

Before taking any observations, it is found essential to warm up the electronic circuits for a few hours. The H.V. supply unit for photomultiplier tube is switched on after allowing the mechanical pump to run for several hours so as to ensure proper vacuum within the chamber, failing which discharge may pass causing damage to the dynode pins. Adequate measures are taken to make the electronic circuits shock-proof and practically free from extraneous pick-ups.

(e) *Light Collection*: Though the photomultiplier tube is provided with adequate magnetic shielding, yet it is advisable to keep the tube, as far as possible, away from the intense magnetic field within the pole-pieces. Hence arises the question of transmitting the light quanta from the scintillator (near the detector slit) to the distant photocathode surface. This can be achieved by introducing a light conductor of suitable material in between the phosphor and the photo-

multiplier tube. The desirable characteristics of the light conductor are: (i) the light conductor should be transparent in the band of wave-lengths covering the emission from the phosphor, (ii) it should not scintillate with the incident radiation during the experiment, (iii) a high refractive index of the light conductor is desirable at the conductor vacuum or conductor-air interface so as to obtain large total internal reflection, (iv) the light guides should be capable of being formed in any useful shape. The most useful materials satisfying all these requirements to a reasonable extent are quartz and polymethyl methacrylate (perspex, lucite). Timmerhaus, et al (1950) have studied on the light transmission of different materials and found perspex, lucite to be the most suitable light conductors for general application.

For our purpose, we have used a perspex rod (1" in diameter) as light conductor. To increase the fraction of light quanta reaching the photocathode, the sides of the perspex rod are covered with highly polished aluminium foils and the front surface of the phosphor facing the detector slit as well as the sides are also covered with a very thin (0.5μ) aluminium foil.

1.3 BEHAVIOUR OF CRYSTALS IN VACUUM

A phenomenon, which is interesting from the experimental point of view, has been noted by us regarding the behaviour of crystals in vacuum. The organic crystals like anthracene, stilbene are found to evaporate fairly rapidly in a vacuum system and the surface layers of NaI-Tl crystal tend to get cloudy under similar conditions. This situation is evidently an unhappy and undesirable one and it has been remedied in our case, by coating the organic crystals with a thin layer of silicone grease which serves as a protective measure and also seems to increase the optical efficiency of the system due to better optical contact between the crystal and the light conductor. As has been already mentioned, all the surfaces of the phosphors (except that in contact with the perspex light conductor) are covered with thin aluminium foils (0.5μ) and the thin layer of silicone grease round the phosphor helps the foils sticking to the phosphor surface. However, for a NaI-Tl crystal, which is hygroscopic, the coating of DC 200 silicone fluid proves to yield better results; of course, the sodium iodide crystal still needs periodical cleaning of the surfaces in a dry atmosphere when in continuous use for a long interval of time.

As an illustration of evaporation of organic crystals in vacuum, the picture of a stilbene crystal with a crater-like hole in it produced when kept as such in the vacuum system of the spectrometer for a few days, is shown in figure 3. (Plate VII)

1.4 LUMINESCENCE SPECTRA OF THE PHOSPHORS USED

For the studies on energy response to monoenergetic electrons we have used the phosphors NaI-Tl, anthracene, stilbene, terphenyl and plastic phosphor (plastifluor* B).

The emission band for NaI-Tl lies in the range 3700\AA° – 4550\AA° , while those for anthracene and stilbene are found to be 4250\AA° – 4600\AA° and 3980\AA° – 4180\AA° respectively (manufacturer's data; Chatterjee, 1951).

The luminescence spectra of terphenyl and plastifluor* B are shown in figures 4(a) and 4(b) in Plate VII. Plastifluor* B is a solid solution of *p*-terphenyl and tetraphenyl butadiene in the plastic base of polyvinyltoluene. The emission band of this phosphor peaks around 4600\AA° and that of terphenyl lies in the range 3900\AA° – 4300\AA° .

In the investigations reported here, RCA 1P21 photomultiplier tube has been used, because among the smaller RCA tubes, this seems to be best suited to the spectral responses of all the scintillators used.

1.5 RESULTS AND DISCUSSION

With the experimental arrangements described earlier, the pulse height distribution curves are taken for different settings of the magnetic field and the normalised counts are plotted against pulse heights. Since the exciting radiation is obtained from Ra E β -source, the range of investigation is limited nearly from 100 kev. to 1.1Mev.

The statistical variation in the counting rates has been reduced to a minimum by taking a large number of counts and the accuracy of the experimental points is within 2%.

(a) *Energy Response*: The notable difference in the behaviour of organic and inorganic phosphors is the relatively poor response of organic phosphors to heavily ionising radiations such as α -particles, protons etc. Another distinguishing feature of the inorganic phosphors is the proportionality between the light output and the energy absorbed by the phosphor over a very wide energy range for both lightly and heavily ionising radiations. The organic phosphors, on the other hand, show non-linear response in the lower energy region and exhibit a saturation effect for heavily ionising rays. While it appears that the energy transfer process is the same for heavily and lightly ionising particles, different explanations have been offered for the change of fluorescence efficiency with the energy and nature of the incident radiation, and some standard books may be referred to in this connection (Birks, 1953; Curran, 1953; Swank, 1954). The readings for NaI-Tl are taken with a crystal of thickness 1.3 cm. and diameter 2.4 cm. A few typical pulse height distribution curves for NaI-Tl are shown in figures 5(a) and 5(b). The pulse height versus energy curves are given in figure 6. In the pulse height versus energy curves, the peak values of the distribution curves are plotted against electron energies. The two lines indicate the readings obtained with two different settings of the amplifier gain. Both the curves seem to pass nearly through the origin when extrapolated to zero pulse height. Taylor et al (1951) obtained a non-linear behaviour of NaI-Tl below 1000 ev. However, it being not



Fig. 3
Picture illustrating the evaporation of a stilbene crystal in vacuum.



Fig. 4

- (a) Luminescence spectrum of terphenyl.
(b) Luminescence spectrum of plastiflor with monoenergetic electrons.

practicable to extend the range of the present investigation to that low energy region, further checking in the range extrapolated by us is not possible.

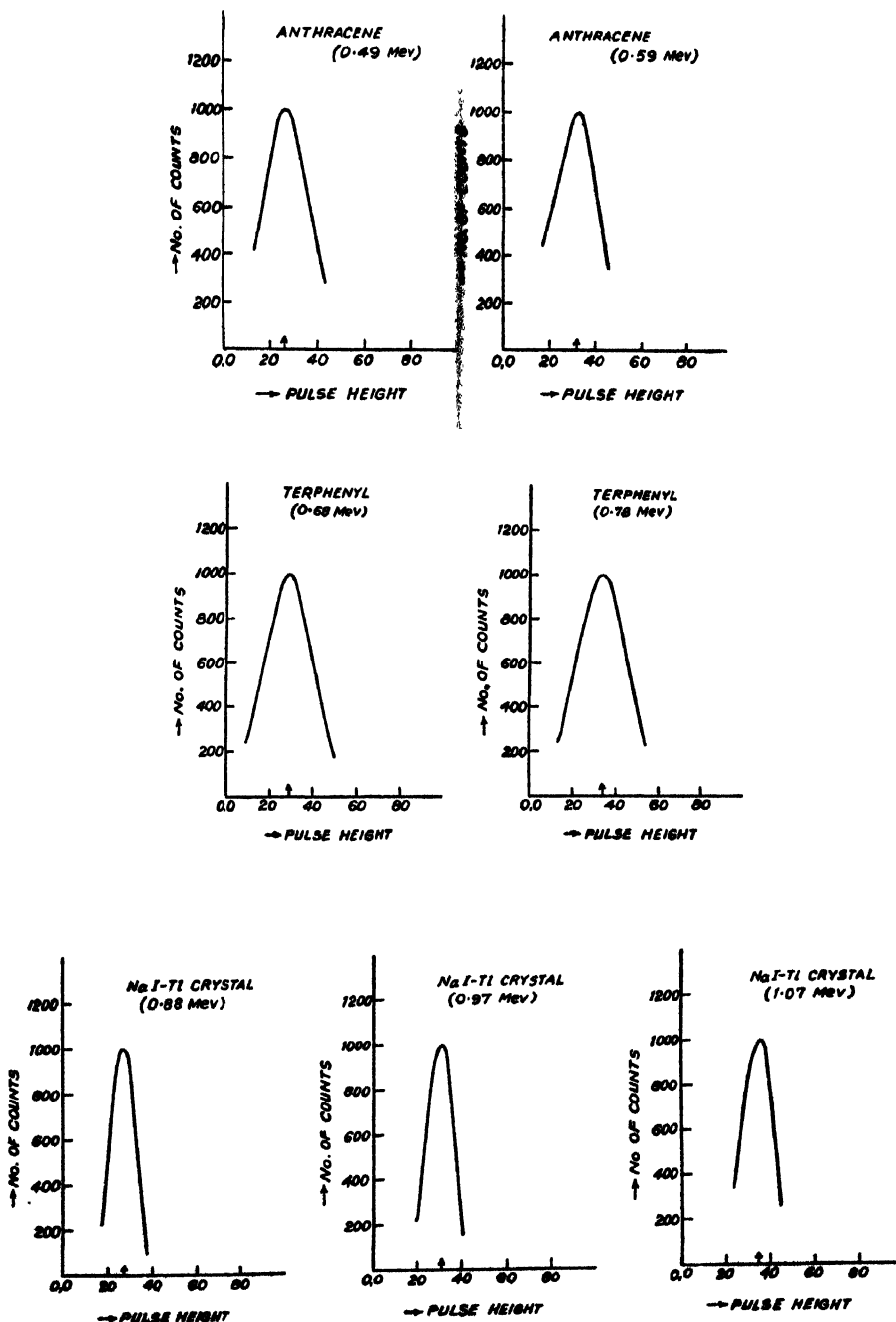


Fig. 5(a) and 5(b). Pulse height distribution curves for NaI-Tl with monoenergetic electrons.

Anthracene is, perhaps, the most widely used organic scintillator and the behaviour of anthracene may be taken to be typical of the organic crystals in

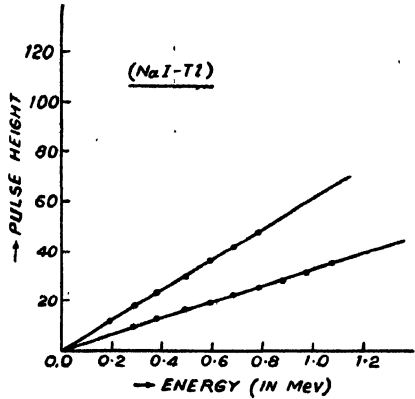


Fig. 6. Pulse height versus energy curve for NaI-Tl.

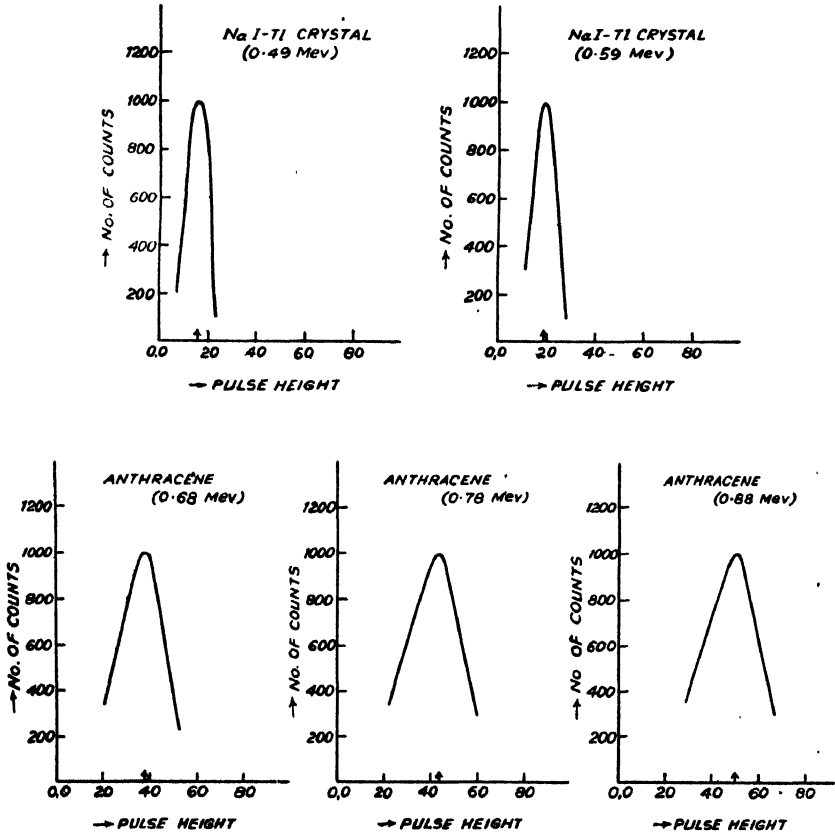


Fig. 7. Pulse height distribution curves for anthracene with monoenergetic electrons.

general. The pulse height distribution curves for the organic crystals are taken with an anthracene crystal of area $1.4 \text{ cm.} \times 1.7 \text{ cm}$ and thickness 0.6 cm , a stilbene crystal of area $1.5 \text{ cm} \times 1.3 \text{ cm}$ and thickness 1 cm and a terphenyl crystal of diameter 2.5 cm and thickness 1.1 cm . The results are plotted in figures 7 to 9. Taylor, et al (1951) and Hopkins (1951) have obtained the linear response for anthracene above 100 kev and 125 kev respectively. In the present case, anthra-

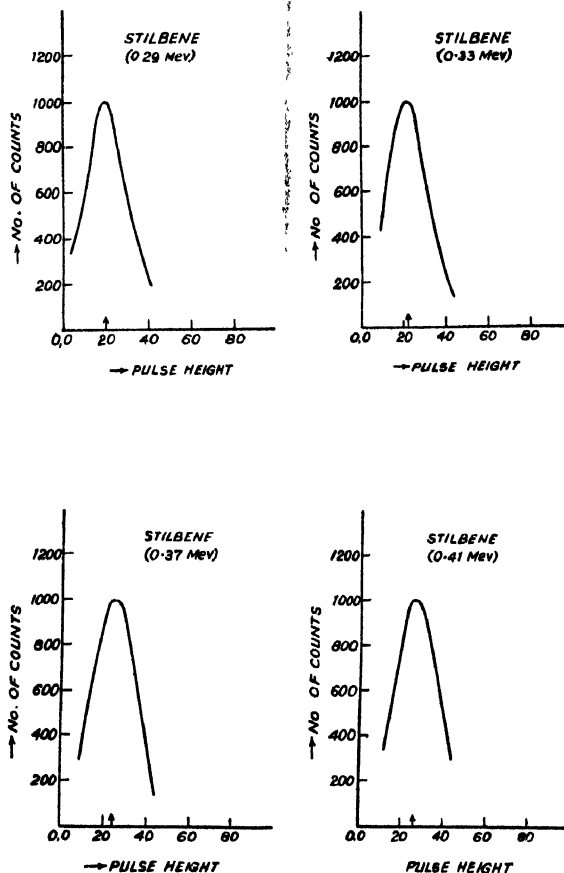


Fig. 8a. Pulse height distribution curves for stilbene with monoenergetic electrons.

cene yields a linear response above nearly 160 kev , in fair agreement with the results of the previous authors. The pulse height versus energy curves for anthracene and stilbene crystal are represented in figures 10 and 11; stilbene shows

linearity above nearly 120 kev. which is compatible with the results reported by Taylor, et al (1951). From the pulse height versus energy studies, NaI-Tl proves definitely superior to the organic crystals, due to its linear response over a wider range and even in the region of fairly low energies; but, anthracene and stilbene scintillation counters can also be utilised successfully in the spectroscopy of nuclear radiations, except in the very low energy region.

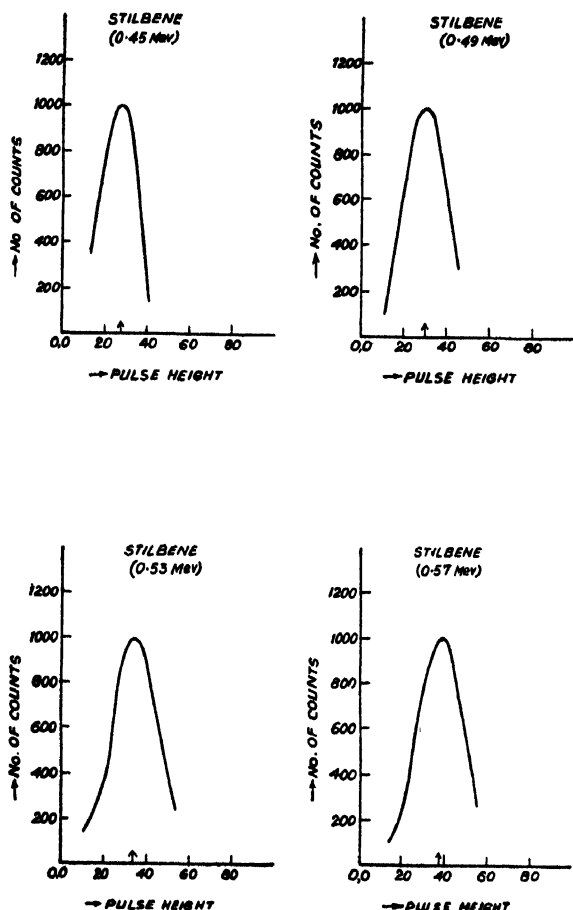


Fig. 8b. Pulse height distribution curves for stilbene with monoenergetic electrons.

The behaviour of terphenyl in this respect seems to be less prospective, since from the present investigations, the crystal is found to show a non-linear response below 240 kev (figure 12). No detailed data for the energy response of a terphenyl crystal seem to have been reported so far. Some typical distribution curves for terphenyl are shown in figure 9.

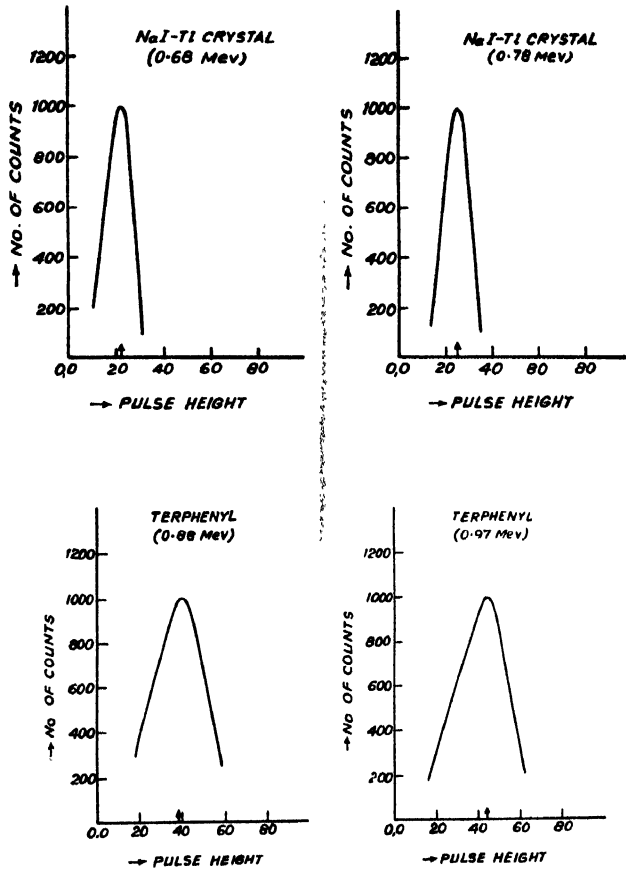


Fig. 9. Pulse height distribution curves for terphenyl with monoenergetic electrons.

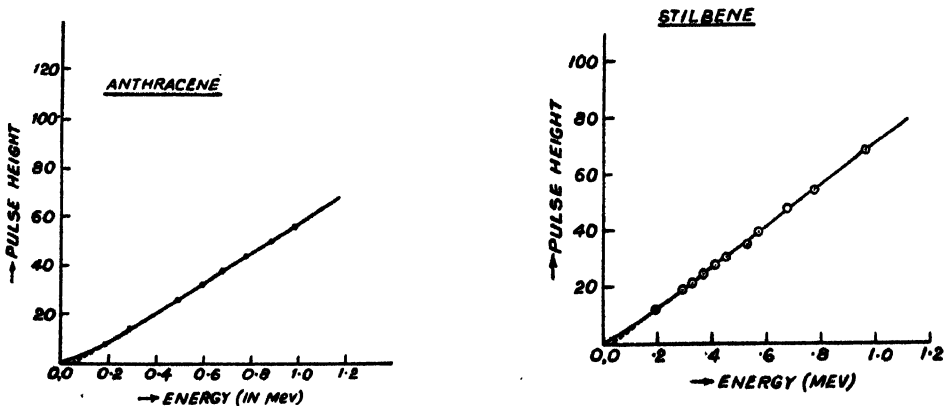


Fig. 10. Pulse height versus energy curve for anthracene.

Fig. 11. Pulse height versus energy curve of stilbene.

In addition to the inorganic and the organic phosphors mentioned above, measurements have also been made with an organic plastic phosphor (plastifluor* B) the distribution curves for which are shown in figure 13. The pulse height versus

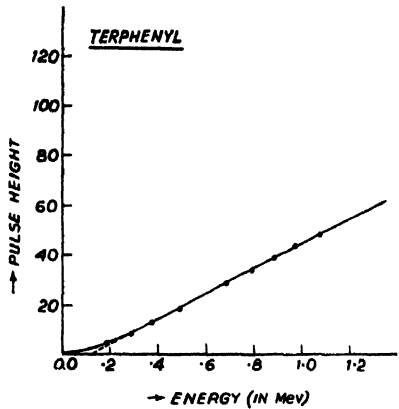


Fig. 12. Pulse height versus energy curve for terphenyl.

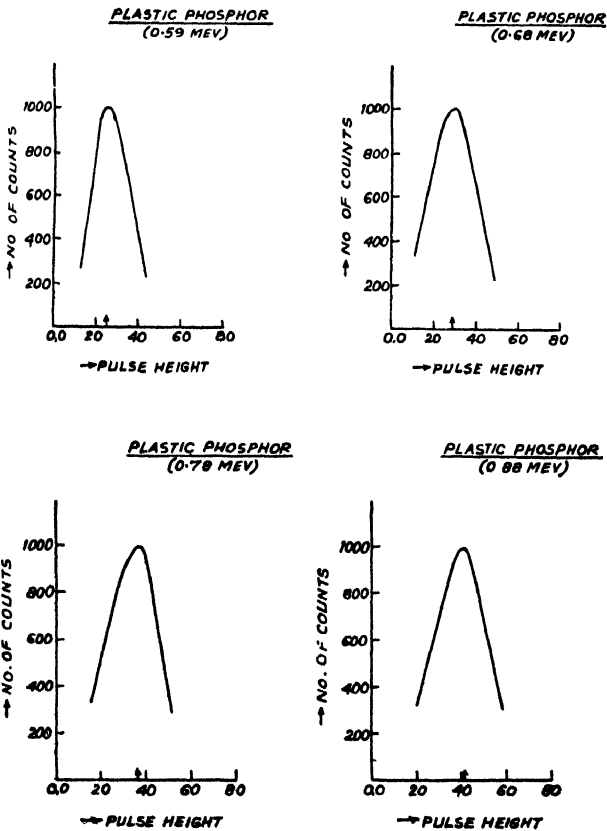


Fig. 13. Pulse height distribution curves for plastifluor.

energy data (figure 14) shows that the response of this phosphor is not linear in a major part of the energy region examined. From figure 14, however, it is found that the linearity of response improves at energies above 800 kev; but since the observations are not extended beyond 1.1 Mev, the predictions regarding the linear behaviour cannot be made conclusively. It appears that the plastic phosphor will not render very useful service in radiation spectroscopy; its main advantages seem to be fully exploited in problems involving fast detection without energy evaluation, since the decay constants of the organic plastic phosphors are very

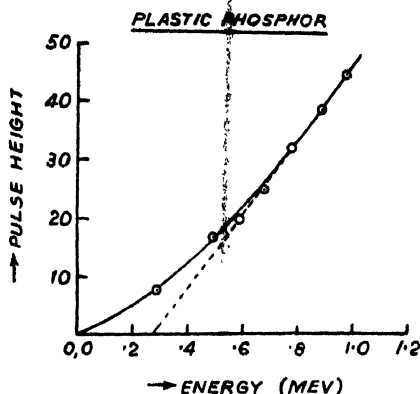


Fig. 14. Pulse height versus energy curve for plastifluor.

small, of the order of 10^{-9} sec. Moreover, whereas the growing of appreciably large transparent and flawless crystals (organic or inorganic) presents a complicated and uncertain technique, the low cost plastic scintillators may be moulded to quite large volumes with very high transparency and can be machined according to specifications. These facts indicate the potentialities of the plastic phosphors as robust detectors of short resolving time which can be employed in coincidence arrays, such as those used in cosmic ray experiments. The relative efficiencies of a number of plastic scintillators containing different kinds and varying concentrations of solute phosphor have been reported by Koski (1951), Schorr and Torney (1950), Buck and Swank (1953), and Swank (1954). But much remains to be done in order to exploit the advantages of the plastic scintillators to the fullest extent.

The pulse height distribution curves shown in figures 5, 7 to 9 and 13 are taken with different amplifier gains for different phosphors. This is found necessary because for the same energy of incident radiation, different phosphors produce pulses of amplitudes varying over a considerably wide range and the amplifier with a constant gain fails to amplify all these pulses faithfully.

In order to facilitate a comparison of the response of the different phosphors used, the data for all the phosphors are again taken under identical conditions of the optical assembly and the electronic circuits,

The points plotted in figures 15 are taken with the amplifier gain of 1.3×10^3 and the photomultiplier tube being operated at 83 volts per stage. For the same energy of electrons, the pulses with the sodium iodide crystal are of much greater heights than the pulses from other phosphors; hence for sodium iodide, the

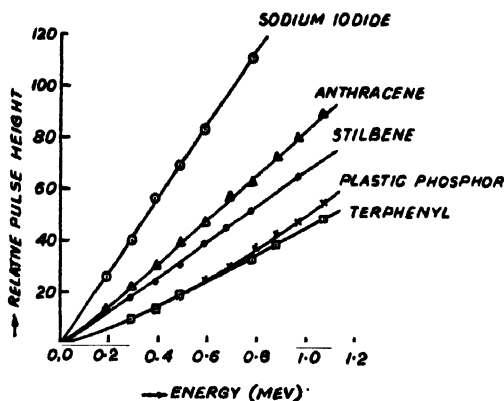


Fig. 15. Relative response of different phosphors to monoenergetic electrons.

readings taken with a known lower gain of the amplifier are multiplied by a constant ratio so as to correspond to the readings for the gain of 1.3×10^3 .

As is obvious from figure 15, sodium iodide undoubtedly exhibits the best response of all the phosphors tried in the present investigations; the next best is anthracene and the response of stilbene is comparable to that of anthracene. Terphenyl yields much inferior results compared to anthracene and in fact, upto about 600 kev, the response curves due to terphenyl and plastifluor* B are practically coincident. At the higher energy region, the response of the plastic phosphor even tends to be better than that due to the terphenyl crystal. Thus, according to the relative scintillation efficiencies of the phosphors used, they can be arranged in the order NaI-Tl, anthracene, stilbene, plastifluor* B and terphenyl.

The measurements on the scintillation response of the same kind of phosphors by different workers may differ in some cases and this can be accounted for by the slight difference in quality of the phosphors obtained from different manufacturers. The organic crystal phosphors are found to be very sensitive to traces of impurities which may quench the fluorescence due to the photon energy exchange process. For example, the relative efficiency of stilbene is reported by various authors to be 60%, 40% and in one case (Bittman et al, 1951) even more than 100% compared to anthracene. Similarly for terphenyl, some observers report a scintillation efficiency of 65% of that of anthracene, while values as low as 30% are obtained by others (Sangster, 1951).

(b) *Nature of the Pulse height distribution:* Referring to pulse height distribution curves in figures 5, 7 to 9 & 13 obtained with different phosphors, it is found that all the curves show \bar{x} distributions of Gaussian nature within the

statistical variation in the counting rates. The half-widths of the distribution curves are, however, different for different phosphors.

For monoenergetic electrons of energy E , Hopkins (1951) has assumed a distribution equation of the form

$$N(E) = A \exp \left[-\left(\frac{\Delta E}{a} \right)^2 \right] \quad \dots (2)$$

where $N(E)$ represents the number of counts for an energy differing from the mean energy by an amount ΔE and a is the half-width at $1/e$ of maximum. The constant A is such that when $\Delta E = 0$, $N(E)$ becomes equal to the number of counts at the mean energy.

Assuming the distribution equation represented in relation (2), an attempt has been made to fit that relation to the experimental curves obtained by us. An excellent agreement is observed between the experimental results and the theoretically computed values. This is illustrated in figure 16 with random selection of a distribution curve for each phosphor. The solid lines indicate the distribution curves obtained from experimental studies and the points marked by dotted circles are the calculated values of $N(E)$. It is concluded that the pulse height distribution curves with all the phosphors are of Gaussian nature.

(c) *Figure of Merit*: The figure of merit of a scintillation counter is usually defined as the energy required to produce one effective photo-electron at the cathode and can be denoted by E/N where N is the number of photo-electrons produced by a particle of energy E . If one desires to get the best possible values of E/N , the following factors are of importance:

(i) the phosphor should have a high efficiency of conversion of particle energy to photons;

(ii) as large a fraction as possible of the photons emitted should be channeled on to the photocathode of the multiplier tube; and

(iii) the photomultiplier tube should have an efficient photocathode for converting photons to photo-electrons.

Hopkins (1951) described two methods of determining E/N for a scintillation counter assembly; he obtained a value of nearly 2 kev/photo-electron for anthracene crystal using RCA 5819 tube. For the NaI-Tl crystal used with EMI5311 tube, Pringle and Standil (1950) reported a value of 1.5 kev per photo-electron, while Hofstadter and McIntyre (1950) and West et al (1951) found values between 0.66 and 1.0 kev per photo-electron.

A rough estimate of the value of E/N may be obtained from experimental data and under certain assumptions. If one obtains a mean pulse height V for a monoenergetic particle of energy E , then the number N of photoelectrons produced at the photocathode can be expressed as :—

$$N = \frac{VC_0}{G_A M_e}, \quad \dots (3)$$

where G is the gain of the amplifier, M the gain of the photomultiplier corresponding to the particular operating voltage, e the electronic charge and C_0 the capacity at the collector plate including the capacity introduced due to the cathode follower unit and wiring system.

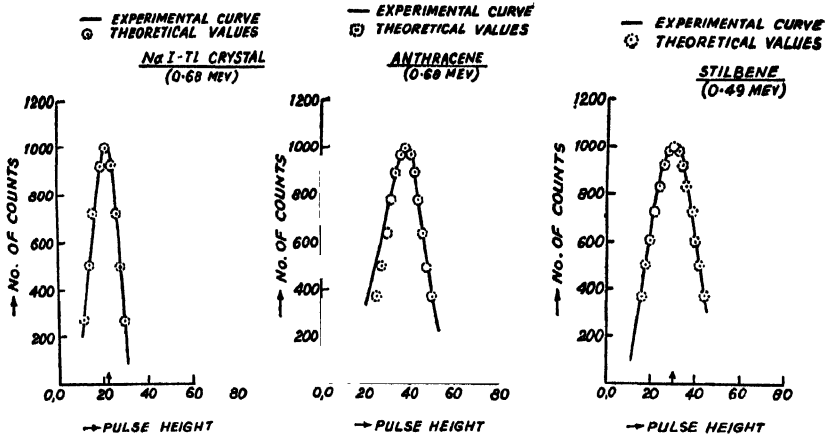


Fig. 16(a) The correlation between theoretical and experimental pulse height distribution curves for NaI-Tl.
Fig. 16(b) The correlation between theoretical and experimental pulse height distribution curves for anthracene.
Fig. 16(c) The correlation between theoretical and experimental pulse height distribution curves for stilbene.

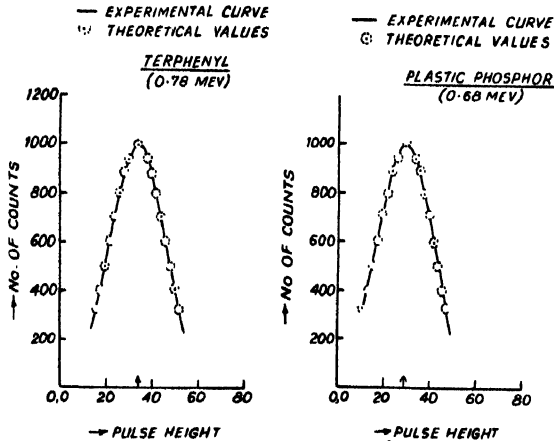


Fig. 16(d) The correlation between theoretical and experimental pulse height distribution curves for terphenyl.
Fig. 16(e) The correlation between theoretical and experimental pulse height distribution curves for plastiflour*B.

The values of V and G_A are fairly accurately known from experimental observations; and C_0 is of the order of $20 \mu\mu F$; M is determined from the gain versus interstage potential curves for the 1P21 tube.

Thus, the energy expended per photo-electron is given by

$$\frac{E}{N} = \frac{EeMG}{VC_0} \quad \dots (4)$$

Let us take a concrete example. The mean pulse height V for monoenergetic electrons of energy 0.49 Mev is 69 volts with a NaI-Tl crystal. The amplifier gain is 1.3×10^2 ; and for an operating voltage of 830 volts, the over all gain of 1P21 tube is 6×10^5

Hence, from equation (3),

$$N = \frac{69 \times 20 \times 10^{-12}}{130 \times 6 \times 10^5 \times 1.6 \times 10^{-19}} = \frac{23000}{208}$$

$$\text{and } \frac{E}{N} = \frac{490 \times 208}{23000} \text{ kev/photoelectron} = 4.4 \text{ kev/photo-electron.}$$

This value is higher than the expected value. The reason may be sought in the facts that:

(i) In expression (4), the optical geometry factor of the phosphor assembly (including the light conductor) has not been considered. With a good reflecting material and very small loss of light at the phosphor-conductor interface, the factor usually lies between 0.5 and 1.0.

(ii) Secondly, because of the nature of the location and the shape of the photocathode surface in a 1P21 tube, it is unlikely that all the light transmitted through the perspex conductor will be incident on the photocathode. Even with the best attainable value of the optical geometry factor, this second factor cannot be avoided. Thus, the scintillation light incident on the photocathode surface is only a fraction of the total light conducted through the perspex rod; and this fraction can be taken to be equal to the ratio of the photocathode area to the face area of the light conductor. In our case, it comes out to be 0.37.

Taking into account the error introduced in the expression (4) due to the above-mentioned factors, E/N reduces to 1.6 kev/photo-electron, which is in fair agreement with the values between 0.66 and 1.5 kev per photo-electron reported by others. The optical geometry factor has been taken to be 1.0. It is obvious that better results can be expected with improved types of photomultiplier tubes.

From the above considerations, it is natural to expect that for different geometry (i.e. with different sizes of the light piper and different types of photomultipliers), E/N will be different. It is better to compare the values for energy required to produce one photon obtained by different workers.

For NaI-Tl, energy required for the production of one photon become 0.16 kev, assuming 10% photon conversion efficiency for the photocathode of a 1P21 tube. From similar calculations, the value for anthracene is 0.28 kev. As the

calculations involve some assumptions, the agreement between our value and the value of 0.24 kev reported by Hopkins (1951) for anthracene is fairly satisfactory.

The 'figure of merit' and the energy required to produce one photon are calculated for all the phosphors used by us and the results are given in Table I.

TABLE I

Phosphor	Mean value of E/N (kev/photoelectron)	Mean value of energy required to produce one photon (kev/photon)
NaI-Tl	1.6	.16
Anthracene	2.8	.28
Stilbene	3.4	.34
Terphenyl	5.8	.58
Plastic phosphor	5.6	.56

(d) *Pulse Height Resolution* : The spread of the output pulse distribution in a scintillation counter produced by monoenergetic particles is due to the statistical fluctuations in the various processes by which the incident energy is converted into the output pulse; and the width of this spread will primarily decide the degree to which the counter system is capable of distinguishing two different energies of the same kind of radiation.

Swank and Buck (1952) have examined the nature of the dependence of the pulse height resolution (defined as the reciprocal of the fractional mean square deviation of the output pulse amplitudes resulting from a series of identical scintillations) on the cathode emission and the first dynode voltage for a number of RCA 5819 tubes. They have also shown that the resolution R varies with pulse height at small pulse heights levelling off towards a saturation value at larger pulse heights.

According to the usual convention followed in the case of β -ray spectrometers, we define the pulse height resolution of the scintillation counter assembly as the ratio $\Delta V/V$, where ΔV denotes the half-width (at $1/e$ of maximum) of the pulse height distribution and V the mean pulse height. Since the contributions due to the phosphor and the photomultiplier tube have not been taken into account separately, both the factors are naturally responsible for the spread in the pulse size distribution curves. In all the discussions that follow, $\Delta V/V$ is referred to as the 'resolution', and the 'inverse resolution' as the 'resolving power'.

The pulse height resolution for a particular phosphor can be computed from the half-width of the distribution. The inverse of the resolution thus found is plotted against the corresponding mean pulse height in figure 17. The solid lines indicate the region of experimental investigations and when extrapolated, these curves (broken lines) appear to pass through the origin. The inverse resolution versus pulse height curves for the inorganic and organic phosphors have a monotonous

rise tending to attain a saturation value. With the plastic phosphor, however, the curve appears almost flattened near the higher pulse height end. The limiting saturation value, if there be any, will naturally represent the intrinsic resolution for a particular scintillation counter assembly due to the source concerned and to various optical asymmetries which are not of a statistical nature.

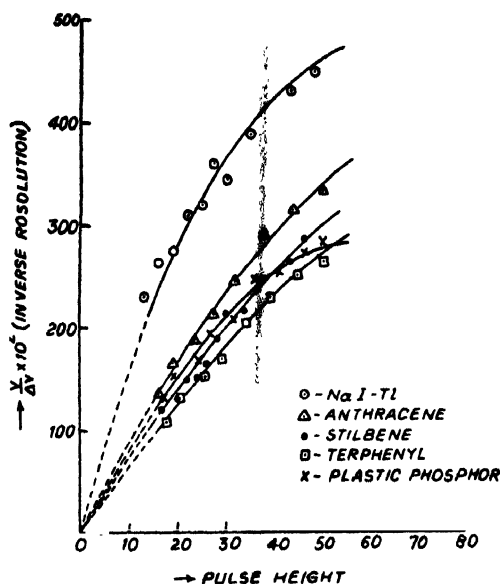


Fig. 17. Inverse resolution versus pulse height curves for different phosphors.

The results obtained by us for the response and the resolving power of the different phosphors along with their emission bands and decay times are summarised in Table II.

TABLE II

Phosphor	Emission band (Å°)	Relative scintillation pulse height			Decay constant (10 ⁻⁸ sec.)	Resolving power (relative)
		(With electrons of energy)				
		300 kev	600 kev	900 kev		
NaI-Tl	3700—4560	57	115	173	250 (Manufacturer's data)	136
Anthracene	4250—4600	31	65	100	30 (Manufacturer's data)	100
Stilbene	3980—4180	26	54	81	8 (Sangster)	88
Terphenyl	3900—4300	14	34	54	12 (Sangster)	80
Plastiflour* B	Peaks around 4600	14	35	58	{ 8 (Manufacturer's data) 4 (Swank and Buck).	81

In the investigations reported here, the resolving powers actually obtained for the phosphors appear to be somewhat lower than the expected values. This is due to the fact that some broadening of the output pulse amplitudes is caused by the use of smaller 1P21 tubes and the insertion of a light conductor of nearly 13 cms. length in between the phosphor and the photocathode surface. Both these factors may tend to lower the optical geometry factor resulting in a poorer resolution. However, the results obtained by us are definitely satisfactory, keeping in mind that smaller photomultiplier tubes have been used. The replacement of 1P21 tube by bigger RCA tube (5819 type) and the exclusion of the light conductor are sure to improve the situation and will increase the resolving power of the scintillation counter unit. In the photomultiplier tubes with flat semitransparent photocathodes, the phosphor (or the light conductor with it) can be directly mounted on the photocathode surface with an intervening thin layer of canada balsam or silicone grease. The better optical contact, in this case, ensures higher light collection efficiency and improved resolution.

The applicability of a scintillation counter in radiation spectroscopy is determined primarily by the resolution expected from it; and in this respect, the organic crystals are largely superseded by the alkali halides. The higher conversion efficiencies combined with better resolution factors prove the inorganic phosphors to be specially suitable in beta and gamma ray spectroscopy. The fast response time and reasonably high detection efficiencies of the organic scintillation counters will, however, make them indispensable for the studies of short-lived nuclear isomers and artificially produced mesons.

ACKNOWLEDGMENTS

The author acknowledges her gratitude to Prof. M. N. Saha, F.R.S., for his keen interest and encouragement in the work. She is also grateful to Prof. B. D. Nag for his kind supervision and valuable discussions. The author is indebted to Prof. S. C. Sircar for the luminescence spectra of the plastic phosphor and the terphenyl crystal.

REFERENCES

- Birks, J. B., 1953, *Scintillation Counters* (Pergamon Press).
- Bittman, L. *et al*, 1952, *Phys. Rev.*, **87**, 83.
- Buok, W. L. and Swank, R. K., 1953, *Nucleonics*, **11**, No. 11, 48.
- Cavanagh, P. E., 1950, *Progress in Nuclear Physics*, Vol. 1.
- Chatterjee, A., 1951, D.Phil. Thesis, Calcutta University.
- Curran, S. C., 1953, *Luminescence and the Scintillation Counters* (Butterworths Scientific publications).
- Das, S. and Saha, A. K., 1946, *Proc. Nat. Inst. Sci. Ind.*, **12**, 227.
- Dhar, S., 1951, P. R. S. Thesis, Calcutta University.
- „ 1955, D. Phil. Thesis, Calcutta University.
- Hofstadter, R. and McIntyre, J. A., 1950, *Phys. Rev.*, **80**, 631.

- Hopkins, J. I., 1951, *Rev. Sci. Inst.*, **22**, 29.
- Koski, W. S., 1951, *Phys. Rev.*, **82**, 230.
- Pringle, R. W. and Standil, S., 1950, *Phys. Rev.*, **80**, 762.
- Saha, A. K., 1945, *Ind. J. Phys.*, **19**, 97.
- Sangster, R. C., 1952, M. I. T. Tech. Rep., **55**.
- Schorr, M. G. and Torney, F. L., 1950, *Phys. Rev.*, **80**, 474.
- Sen, S. K., 1950, D. Phil. Thesis, Calcutta University.
- Swank, R. K., 1954, Annual Review of Nuclear Science, Vol. **4**, 111.
- Swank, R. K., and Buck, W. L., 1952, *Nucleonics*, **10**, No. 5, 51.
- „ 1955, *Rev. Sci. Inst.*, **26**, 15.
- Taylor, C. J., *et al*, 1951, *Phys. Rev.*, **84**, 1034.
- Timmerhaus, K. D. *et al*, 1950, *Nucleonics*, **6**, No. 6, 37.
- West, H. I. *et al*, 1951, *Phys. Rev.*, **81**, 141.

ULTRASONIC ABSORPTION IN SOLUTIONS

BY BIBHUTI BHUSAN DEO

RAVENSHAW COLLEGE, CUTTACK

*(Received for publication, October, 20, 1954,**Received after revision, March, 31, 1955)*

ABSTRACT. Equations have been derived for the excess ultrasonic absorption in solutions due to occurrence of chemical reaction accompanied by a change of volume. Modifications for aqueous solutions of electrolytes have been worked out. The results explain some of the anomalous values of sound absorption in bivalent sulphate solutions.

Freedman (1953) has derived equations for ultrasonic absorption and relaxation frequency due to relaxing specific heat of chemical reaction. His theory is remarkably successful for acetic and propionic acids. Freedman assumes no change in volume; most chemical reactions are, however, accompanied by both changes of volume and temperature. If change of volume ΔV , alone, in a chemically reacting solution with n_i moles of the i th species, is taken into consideration, we can analogously deduce, that the reaction compressibility is

$$\beta_0^* = \frac{(\Delta V)^2}{VRT} \frac{D}{1+i\omega \frac{D}{U}} = \frac{\beta_0^r}{1+i\omega\tau}$$

$$\text{where } \beta_0^r = \frac{D(\Delta V)^2}{VRT} ; D = \left[\sum \frac{a_i^2}{n_i} - \frac{(\sum a_i)^2}{n_i} \right]^{-1} ;$$

a_i is the stoichiometric coefficient of the i th reaction component;

U is the gross reaction rate and $d\tau = \frac{D}{U}$ is the time lag.

Writing the effective compressibility as

$$\beta_0^e = \beta_0^s + \frac{\beta_0^r}{1+i\omega\tau}$$

we can deduce by well known methods that for a frequency ν , the absorption coefficient per cm. is given by

$$\frac{\alpha}{\nu^2} = 2\pi^2\nu\rho \frac{\beta_0^r\tau}{1+\omega^2\tau^2} \text{ where } \nu \text{ is the velocity}$$

so that the relaxation frequency is

$$\nu_m = \frac{1}{2\pi\tau} = \frac{1}{2\pi} \frac{U}{D}$$

and the intensity absorption per wavelength

$$\mu = 2\alpha\lambda = 2\pi\rho v^2\beta_0^* \frac{\omega\tau}{1+\omega^2\tau^2}$$

μ has therefore a maximum for $\omega\tau = 1$, the maximum value being given by

$$\mu_m = \pi\rho v^2\beta_0^* = \pi\rho \frac{D(\Delta V)^2}{VRT}$$

In a first order reaction < like $A \rightleftharpoons A^*$ or $A \rightleftharpoons B$ it can be easily shown that

$$\mu_m = \frac{\pi}{V} \frac{(\Delta V)^2}{\beta_0^* RT} \alpha(1-\alpha)$$

where α is the degree of formation of A^* or B .

For a second order reaction like $AB \rightleftharpoons A+B$

$$\mu_m = \frac{\pi}{V} \frac{(\Delta V)^2}{\beta_0^* RT} \frac{\alpha}{2} (1-\alpha^2)$$

The above theory assumes an ideal solution where the components exist in their pure phases. To apply thermodynamics to solutions of electrolytes, for example, the activity must be considered. Activity will determine the rate and rate constants. Further, in most chemical reactions of physicochemical interest, the solvent is in such great excess, that its concentration does not change appreciably as the reaction proceeds to completion.

Writing the equilibrium constant as

$$K = \Pi(n_i f_i)^{\alpha_i}$$

f_i denoting the activity coefficient of i th component, we use the thermodynamic relationship

$$\frac{\partial}{\partial p} \log K = - \frac{\Delta V^0}{RT}$$

where ΔV^0 is the change in molar volume referred to a standard state.

But
$$\frac{\partial}{\partial p} \log K = \sum \frac{a_i}{n_i} \frac{\partial n_i}{\partial p} + \sum \frac{a_i}{f_i} \frac{\partial f_i}{\partial p}$$

We can always write f_i as a function of n_i , so that

$$\delta f_i = \frac{\partial f_i}{\partial n_i} \delta n_i$$

$$\therefore \frac{\partial}{\partial p} \log K = \left[\sum \frac{a_i^2}{n_i} + \sum \frac{a_i^2}{f_i} \frac{\partial f_i}{\partial n_i} \right] \frac{\partial Z}{\partial p} = \frac{1}{D^*} \frac{\partial Z}{\partial p}$$

where $\delta n_i = a_i \delta Z$

and $D^* = \left[\sum \frac{a_i^2}{n_i} + \sum \frac{a_i^2}{f_i} \frac{\partial f_i}{\partial n_i} \right]^{-1}$

so that $\beta_0^r = \frac{D^*(\Delta V^0)^2}{VRT}$

The gross reaction rates can be written as

$$U_f = k_f \pi (n_i f_i)^{-a_i} \quad a_i < 0$$

$$U_b = k_b \pi (n_i f_i)^{+a_i} \quad a_i > 0$$

and the dynamic compressibility can be deduced to be

$$\beta_0^* = \frac{(\Delta V^0)^2}{VRT} \frac{D^*}{1 + i\omega D^*/U} = \frac{\beta_0^r}{1 + i\omega \tau}$$

where $\tau = \frac{D^*}{U}$

giving $\mu_m = \frac{\pi}{V} \frac{D^*(\Delta V^0)^2}{\beta_0^r RT}$

where V is the total volume of the solution. Thus absorption will depend on both degree of dissociation and activity coefficients. Both should be known and also the nature of variation of activity coefficient with concentration.

1-1 electrolytes, like NaCl and KBr etc., are very nearly cent per cent dissociated and their activity coefficients approximate unity. So dissociation reaction has negligible contribution to ultrasonic absorption. The negative absorption (less than water) observed in higher concentrations of these salts is due to the depolymerising effect on water; the three bonded structure becoming less and less numerous with increase of concentration.

Of great theoretical interest is the excess absorption in bivalent sulphates in the low frequency region. Absorption per wavelength gives two clear maxima in some sulphates, one in the 1-10 megacycle range and another in 100 megacycle range. The values of μ_m are strictly proportional to concentration and ν_m is independent of concentration in the range 0.01 to 0.1 M. Concentration-independence of the relaxation frequency indicates at the outset a first order reaction. If c is the concentration of the electrolyte in moles per litre and α the degree of dissociation or hydration; $D^* = D = \alpha(1-\alpha)c$

$$\frac{\mu_m}{c} = \frac{\pi}{1000} \frac{(\Delta V)^2}{\beta_0 RT} \alpha(1-\alpha)$$

Taking a minimum volume change of 20 c.c. the value of α should be very nearly one to explain the experimental results.

From recent experiments (1952) it has been found that the degree of dissociation of bivalent sulphates is nearly constant in the same concentration range and is due to the activity coefficients being inversely proportional to the square root of concentration.

$$f_i \propto \frac{1}{\sqrt{c_i}} \quad \therefore \quad \frac{1}{f_i} \frac{\partial f_i}{\partial n_i} = -\frac{1}{2\alpha c} \quad \text{for ions}$$

$$\text{and} \quad \frac{1}{f_i} \frac{\partial f_i}{\partial n_i} = 0 \quad \text{for undissociated molecules}$$

$$\text{whence} \quad \frac{\mu_m}{c} = \frac{\pi (\Delta V^0)^2}{1000 \beta^0 RT} \propto (1-\alpha)$$

So $\frac{\mu_m}{c}$ is expected to be constant so long as α is constant. Further

$$U_f = k_f (\alpha c) \cdot (\alpha c) f_{R^{++}} \times f_{SO_4^{--}} = \text{const. } k_f \alpha^2 c$$

$$\text{and} \quad U_b = k_b (1-\alpha)c$$

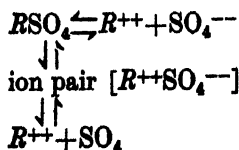
If α is constant, at equilibrium, the net gross reaction rate U is proportional to the concentration. Since

$$v_m = \frac{1}{2\pi} \frac{U}{D^*} = \frac{1}{2\pi} \frac{U}{\alpha(1-\alpha)c}$$

v_m is also independent of concentration.

Although the dissociation reaction $RSO_4 \rightleftharpoons R^{++} + SO_4^{--}$ explains the results qualitatively, the quantitative agreement is poor. Taking the experimental value $\alpha = 0.9$ for, say, $MgSO_4$, we must take $(\Delta V^0)_1 = 5$ e.c. and $(\Delta V^0)_2 = 10$ e.c. to explain the two maxima. In any case, the high degree of dissociation of sulphates does not indicate such a low value of ΔV^0 .

The only plausible and satisfactory picture is to consider a mechanism of the type



The undissociated RSO_4 is in simultaneous equilibrium with a biwise dissociation reaction, some of it directly dissociating to bivalent ions, while others break their electronic linkages forming the so called ion pairs of Bjerrum, which further dissociate to the ions. If the net measured concentration of each ion be αc and if α' be the degree of formation of the ion pair, then the

concentration of undissociated molecules is $(1-\alpha)(1-\alpha')c$ and of pair $\alpha'(1-\alpha)c$. However, for explaining the values of activation energies the total step



may be taken to be responsible for the absorption of the lower maximum. Of these the step $RSO_4 \rightleftharpoons [R^{++}SO_4^{--}]$ is associated with a considerable change of volume and contributes to β_0^r ; whereas the subsequent step $[R^{++}SO_4^{--}] \rightleftharpoons R^{++} + SO_4^{--}$ is accompanied with no change of volume and, hence, does not contribute to β_0^r .

So, whereas
$$\frac{\mu_m}{c} = \frac{\pi}{1000} \cdot \frac{(\Delta V)^2}{\beta_0^r RT} \alpha'(1-\alpha')(1-\alpha);$$

the dissociation constant for the total step is $K = K_{obs}^{(RSO_4)} \times \frac{\alpha'^2}{1-\alpha'}$. With a value of $\alpha' = 0.05$ nearly, along with the observed values of α , it is possible to explain all the results of Kurtze and Tamm (1953); including the values of free energy change from the equation $\Delta F = -RT \log K$. It has been tacitly assumed that the ion pair dissociates just like the neutral molecule. In spite of the many uncertainties involved, this mechanism seems to be responsible for the absorption. The explanation of the second maxima is not possible, unless accurate values of μ_{m_2} and ν_{m_2} are available experimentally.

ACKNOWLEDGMENT

Author's sincere thanks are due to Dr. A. K. Dutta. D.Sc., F.N.I. for the close interest he has shown in the present work.

REFERENCES

- Freedmann, 1953, *J. Chem. Phys.*, **21**, 1784.
 Kurtze and Tamm, 1953, *Acoustica*, **33**, 3.
 Wicke and Eigen, 1952, *Naturwiss*, **39**, 545.

AN X-RAY STUDY ON BIVALENT SILVER AND COPPER NICOTINATE COMPOUNDS*

BY D. M. CHACKRABURTTY,

DEPARTMENT OF GENERAL PHYSICS, X-RAYS AND MAGNETISM,
INDIAN ASSOCIATION FOR THE CULTIVATION OF SCIENCE, CALCUTTA-32

AND

B. BANERJEE

DEPARTMENT OF INORGANIC CHEMISTRY,
INDIAN ASSOCIATION FOR THE CULTIVATION OF SCIENCE, CALCUTTA-32.

(Received for publication, June 8, 1955)

ABSTRACT. The X-ray diffraction data on bivalent silver and copper nicotinate compounds are given and the results are discussed in full details.

1. INTRODUCTION

The argentic compound of picolinic acid, an isomer of nicotinic acid, was prepared by Barbieri (1934). This compound along with the copper picolinate was studied by the X-ray diffraction method by Cox, Wardlaw and Webster (1936). The X-ray data for both the compounds were analyzed in detail, and it was concluded that the bivalent silver and copper compounds of picolinic acid were isomorphous.

Here in this communication we are extending our work to bivalent silver and copper nicotinates ($\text{Ag}[\text{C}_6\text{H}_4\text{O}_2\text{N}]_2$ and $\text{Cu}[\text{C}_6\text{H}_4\text{O}_2\text{N}]_2$) in order to obtain complete preliminary X-ray diffraction data, and then to analyze the data to see how the compounds are interlinked in their structural aggregation.

2. PREPARATION OF COMPOUNDS

To prepare copper nicotinate the aqueous solution of potassium nicotinate (7.0 gm in 20 c.c.) was added to a hot aqueous copper acetate solution (4.0 gm in 60 c.c.) with constant stirring. On cooling, the precepitate of copper nicotinate separated, which was filtered, and dried at 110°C . The cupric nicotinate was obtained as bluish white powder. The amount of copper estimated was 20.6% which agrees well with the theoretically calculated value, namely 20.66%. Argentic nicotinate has been prepared by Banerjee and Roy (1955) by a special process and it is brick red in colour and microcrystalline in nature.

The bivalent compounds of silver and copper are paramagnetic. The magnetic behaviour of these two substances were also studied and were found out to be paramagnetic. The μ_B values for argentic and cupric nicotinates were 1.74 and 1.89 respectively.

* Communicated by Prof. B. N. Srivastava.

3. X-RAY DIFFRACTION RESULTS

The X-ray pictures were taken in copper radiation at 35 kv. and 15 mA. in a cylindrical camera of radius 4.13 cm., the radius being standardised with the help of known spacings of aluminium lines. The glancing angles θ 's of the X-ray pictures of silver and copper nicotinate were calculated in the usual way and the spacings ' d ' were obtained from the Bragg equation. The ' d ' values are given in kX units (1 kX unit = 1.002Å). The data are tabulated in Tables I and II, and θ , d and visually estimated intensities of the lines are given side by side. As far as possible the spacing for Cu β lines are eliminated.

TABLE I
Argentite nicotinate ($\text{Ag}[\text{C}_6\text{H}_4\text{O}_2\text{N}]_2$)

No. of lines	θ	d in kX units	Intensity
1	6°.330	6.982	v.s.
2	8°.932	4.958	v.s.
3	10°.49	4.233	s.
4	11°.45	3.879	m.s.
5	12°.75	3.489	m.s.
6	14°.05	3.172	m.
7	14°.83	3.007	s.
8	16°.82	2.662	m.
9	17°.86	2.505	m.
10	19°.51	2.305	m.w.
11	20°.46	2.203	v.s.
12	21°.43	2.108	w.
13	22°.28	2.032	m.
14	23°.13	1.960	s.
15	23°.93	1.898	v.w.
16	24°.62	1.848	w.
17	25°.66	1.778	m.w.
18	26°.91	1.701	w.
19	28°.62	1.608	m.
20	29°.31	1.573	m.w.
21	30°.09	1.536	w.
22	32°.51	1.433	w.

TABLE I (contd.)

No. of lines	θ	d in kX units	Intensity
23	33°.3	1.403	w.
24	34°.68	1.353	w.
25	35°.46	1.327	w.
26	36°.76	1.286	w.
27	37°.71	1.259	w.
28	39°.96	1.199	v.w.
29	42°.32	1.144	v.w.
30	43°.18	1.126	v.w.
31	45°.44	1.081	v.w.
32	46°.13	1.068	v.w.
33	47°.17	1.050	v.w.
34	47°.68	1.041	v.w.
35	48°.64	1.026	w.
36	50°.46	.9986	m.w.

TABLE II

Cupric nicotinate ($\text{Cu}[\text{C}_6\text{H}_4\text{O}_2\text{N}_2]_2$)

No. of lines	θ	d in kX unit	Intensity
1	6°.501	6.801	v.s.
2	7°.803	5.671	m.s.
3	8°.670	5.110	m.s.
4	10°.06	4.411	s(broad)
5	11°.36	3.823	m.s.
6	12°.48	3.563	v.s.
7	13°.53	3.291	m.s.
8	14°.85	2.997	s.
9	16°.99	2.636	m.s.(broad)
10	19°.04	2.361	v.s.
11	21°.76	2.077	m.
12	22°.72	1.994	m.s.(broad)
13	25°.49	1.789	m.
14	32°.60	1.429	w.

4. DISCUSSION OF RESULTS

From Tables I and II it appears that the silver salt of nicotinic acid is a better crystalline substance than copper nicotinate. Also there are certain X-ray lines in copper nicotinate which are broad and are likely to be due to disorder in lattices. If the d values are compared, it will be seen that certain spacings of both the tables are similar. The similar spacings are tabulated in Table III.

TABLE III

d in $k\lambda$ unit (Silver nicotinate)	d in $k\lambda$ unit (Copper nicotinate)
6.98	6.80
4.96	5.11
3.88	3.82
3.49	3.56
3.17	3.29
3.01	3.00
2.66	2.64
2.31	2.36
3.01	3.00
2.66	2.64
2.03	2.08
1.96	1.99
1.78	1.79
1.43	1.43

This similarity of spacings of both the substances suggests that copper and silver nicotinates may be isomorphous. Practically line to line spacings of copper compound have similarity with those of silver compound. The extra lines appearing in both the pictures, particularly the argentic nicotinate, are either due to better degree of crystallinity in certain direction or in whole of the aggregates. This type of isomorphism is quite likely. In fact in the paper of Cox, Wardlaw and Webster (1936) certain extra lines appeared in both copper and silver salts (more lines in silver salt) of picolinic acid, an isomer of nicotinic acid, but their general X-ray patterns, as in our case, agreed quite well.

Due to different atomic scattering factors of copper and silver, the intensities of all the similar lines are not identical.

Further X-ray studies are being undertaken by one of the authors (D. M. C.) and a detailed interpretation of the lines from the lattice structure will be published later.

ACKNOWLEDGMENTS

The authors are greatly indebted to Prof. B. N. Srivastava for his valuable guidance and constant advice during the progress of the work and to Prof. P. Ray for much help and encouragement.

REFERENCES

- Banerjee, B. and Ray P. 1955, *Science and Culture*, **20**, 613.
 Barbieri, 1934, *Chemical Abstract*, **28**, 2291.
 Cox, Wardlaw and Webster, 1936, *J. Chem. Soc.*, 776.

ON THE RAMAN SPECTRA OF ETHYLENE CHLORHYDRIN AND *n*-PROPYL CHLORIDE IN THE VAPOUR STATE*

BY MONOMOHAH MAZUMDER

OPTICS DEPARTMENT, INDIAN ASSOCIATION FOR THE CULTIVATION OF SCIENCE, CALCUTTA-32.

(Received for publication, June 28, 1955)

Plate VIII

ABSTRACT. The Raman spectra of ethylene chlorhydrin and *n*-propyl chloride in the vapour state at different temperatures above the boiling points, and in the liquid state at room temperature and at temperatures nearly equal to those of the vapour of corresponding liquids have been studied and compared with those reported for the solid state at low temperatures by previous workers. It is observed that the intensity-ratio of the two lines in 750 cm^{-1} and 662 cm^{-1} changes abruptly with the change from liquid to vapour phase in the case of ethylene chlorhydrin, and the same changes from about 1.0 to about 5.0 when the vapour at 130°C . is heated to 180°C . This intensity-ratio, however, changes only very slightly with change of temperature of the liquid from 30°C . to 130°C . In the case of *n*-propyl chloride the change in the intensity-ratio of the corresponding two lines is much smaller than that observed in the case of ethylene chlorhydrin, but the line 1452 cm^{-1} becomes much weaker and the frequency-shifts of the lines 728 cm^{-1} and 648 cm^{-1} increase to 742 cm^{-1} and 663 cm^{-1} respectively with vaporization of the liquid. It has been pointed out that the abrupt change in the intensity-ratio with vaporization of the liquid mentioned above cannot be explained on the assumption that two types of molecules co-exist in the liquid, the relative population of the molecules depending on their energy difference, and that a strong interaction between molecules in the liquid state is to be postulated to explain the above facts. It is also pointed out that the lines 742 cm^{-1} and 663 cm^{-1} observed in the case of *n*-propyl chloride in the vapour state are due to the single molecule and associated molecule respectively and the line 716 cm^{-1} observed in the case of the solid state is due to the associated molecules surrounded by regularly arranged neighbours.

INTRODUCTION

It was pointed out previously by the author (Mazumder, 1953) that the ratio of the intensity of the two lines 654 cm^{-1} and 755 cm^{-1} of ethylene dichloride in the vapour state at 135°C is 1 : 4.5 while this ratio has the value 1 : 5.0 at 170°C according to Morino *et al* (1942). These results indicated that the energy difference between the two forms of molecules in the vapour state was almost the same as that in the liquid state. This conclusion was contradictory to that arrived at earlier by Mizushima *et al* (1949). It was observed, however, that as the liquid at 130°C was transformed into vapour

* Communicated by Prof. S. C. Sirkar.

at 135°C the ratio of the intensities of the two lines changed from 1 : 2 to 1 : 4.5 and it was concluded that the ratio of the two forms of the molecule changes abruptly with vaporization of the liquid, and that a strong interaction between the neighbouring molecules taking place in the liquid state is responsible for this abrupt change. When the substance is solidified the line 654 cm^{-1} disappears and it was concluded by Mizushima *et al* (1938) that in the solid state the molecules are only of the 'trans' configuration. Similar phenomenon was also observed in the case of ethylene chlorhydrin and *n*-propyl chloride (Mizushima *et al*, 1940). They observed that the line 750 cm^{-1} of ethylene chlorhydrin disappears at low temperatures, and assuming that this line is given by the gauche form, they concluded that the molecules of ethylene chlorhydrin in the solid state are all of the 'trans' form, while in the case of *n*-propyl chloride in the solid state they are of the 'gauche' form, and that in the liquid state molecules of both trans and gauche forms are present. Recently, Mizushima *et al* (1951) investigated the Raman and infra red spectra of ethylene chlorhydrin in liquid and vapour states at different temperatures and attributing the line 750 cm^{-1} to the trans form they concluded that the molecules of the trans configuration increase in number with rise of temperature in the case of the vapour. So, according to this new assignment, the solid state of ethylene chlorhydrin would consist of molecules of gauche form only. The frequencies of vibration of different modes of the skeleton Cl-C-C-O have also been calculated for both the forms by these authors but although the calculated frequencies agree with observed frequencies in the case of gauche form, the agreement in the case of the trans form is poor. Mizushima *et al* (1951) measured the relative densities of the absorption bands 760 cm^{-1} and 669 cm^{-1} in the case of the vapour of ethylene chlorhydrin at different temperatures but similar data regarding the Raman spectrum of the substance were not available. On the other hand, the conclusion about disappearance of one of the two forms of the molecule with solidification was drawn by previous workers from the study of the Raman spectra. It was, therefore thought worthwhile to study the Raman spectra of ethylene chlorhydrin in the liquid and vapour states at high temperatures to find out whether in this case also any abrupt change takes place in the relative intensities of the two Raman lines 750 cm^{-1} and 662 cm^{-1} with vaporization of the liquid. As the Raman spectrum of *n*-propyl chloride also show some changes with solidification of the liquid, the Raman spectra of the compound in the liquid and vapour states at high temperatures have also been investigated for comparison.

EXPERIMENTAL

The experimental arrangement was similar to that used by the author in his previous investigation (Mazumder, 1953), excepting a little modification in the illuminating system. The liquids ethylene chlorhydrin and *n*-propyl chloride were distilled several times in vacuum before being introduced in the thickwalled Wood's

tube of special design (Mazumder, 1954). The temperature of the tube containing requisite quantity of the liquid was raised to about 180°C in the case of ethylene chlorhydrin (B. P. 128.8°C) and 100°C in the case of *n*-propyl chloride (B.P. 46.6°C), and the pressure developed inside the Wood's tube at those temperatures of the vapours of the corresponding liquids was about four atmospheres in each case. The liquid still left in the bulb at the tail after vaporization was not more than 1 c.c. in volume. Two long glass tubes of diameter 6 cms. filled with distilled water were placed between the mercury arcs and the heater to focus the long mercury arcs on the axis of the Wood's tube. Two cylindrical reflectors of highly polished aluminium sheets were used to reflect back the light proceeding away from the Wood's tube, and this light also was focussed on to the axis of the Wood's tube. This improvement in the arrangement for illumination enhanced the intensity of the incident light so much that the time of exposure could be reduced to five days only.

The Adam Hilger two prism spectrograph used in the previous investigations was used in the present experiment also. Iford Zenith plates were used to photograph the spectra. In both the cases the Raman spectra of the liquids at room temperature and at temperatures nearly equal to those of the vapours were also photographed for comparison. At least two spectrograms were obtained for the vapour phase of each of the two compounds in order to verify the changes observed in the first spectrogram in each case, and in the case of ethylene chlorhydrin spectrograms for the vapour at 130°C and 180°C were obtained.

RESULTS AND DISCUSSION

The Raman frequencies in wave number units are given in Tables I and II, in which the data for the solid state are also included for comparison. The spectrograms due to the substances in the vapour state at high temperatures and in the liquid state at temperatures much above the boiling points are reproduced in Plate VIII.

It can be seen from Table I that in the case of ethylene chlorhydrin the ratio of the intensity of the two lines 662 cm^{-1} and 750 cm^{-1} changes abruptly as the liquid at 130°C is transformed into vapour at 130°C . This result is in complete disagreement with that reported by Mizushima *et al* (1951). They observed that the ratio of the densities of the absorption bands I_{760}/I_{669} increases from 0.55 to 0.68 as the temperature of ethylene chlorhydrin vapour is raised from 82°C to 155°C . In the case of Raman spectrum, however, the ratio I_{750}/I_{662} changes from 0.5 to about 0.6 when the temperature of the liquid is raised from 30°C to 130°C , but in the case of vapour at 130°C the ratio becomes almost equal to unity and at 180°C the ratio becomes about 5.0. It appears, therefore, that there is abrupt change in the ratio of the intensity of the two lines with vaporization of the liquid at 130°C , and a great change takes place again in the same intensity

TABLE I

Ethylene chlorhydrin, $\text{Cl}.\text{CH}_2.\text{CH}_2.\text{OH}$. $\Delta\nu$ in kayser.

Liquid state		Mizushima <i>et al</i> (1940) Solid state	Vapour state	
at 30°C.	at 130°C.	at (Ca.-100°C.)	at 130°C.	at 180°C.
295 (1b) e	295 ($\frac{1}{2}$ b) e	311 (0) e		
396 (2) e,k	396 (1) e,k			
476 (1) e,k	476 ($\frac{1}{2}$) e,k	471 (0) e		
662 (10) e,k	662 (5) e,k	659 (8) e,k,(i), f,g	662 (1) e,k	662 (0b) e,k
750 (5) e,k	750 (3) e,k		750 (1) e,k	750 (4) e,k
852 (3) e,k	852 (1) e,k	849 (3) e,k		825 (0) e
940 (2) e,k	940 ($\frac{1}{2}$) e,k	939 (3) e,k		
1034 (4) e,k	1034 ($\frac{1}{2}$ b) e,k	1036 (3) e,k		
1078 (0) e,k		1083 (1) e,k		
		1130 (0) e,k		
		1171 (0) e,k		
1244 (4b) e,k		1246 (0) k		
		1387 (0) e,k		
1458 (6) e,k	1458 (2b) e,k	1451 (2) e,k		
2880 (2) e,k	2880 (1) e,k			
2928 (1) e,k		2934 (6) e,k,i		2928 (0) e,k
2958 (5b) e,k	2958 (3) e,k	2960 (8) e,k,i	2960 (3) e,k	2960 (6) e,k
3010 (3) e,k	3010 (1) e,k	3013 (5) e,k		

ratio when the temperature of the vapour is raised from 130°C to 180°C. If we assume that the two lines 662 cm^{-1} and 750 cm^{-1} are due to two configurations of the molecule then this great change in the ratio of the intensity of the two lines with change of temperature from 130°C to 180°C would indicate a large energy difference between the two forms of the molecule, but the small change in the intensity-ratio observed with the rise of temperature of the liquid, however, does not indicate such a large energy difference in the liquid state. So this postulate that the relative populations of the two types of molecules depend on the temperature is not supported by the observed facts. Also the abrupt change in the ratio of the intensity of the two lines with vaporization of the liquid at 130°C indicates

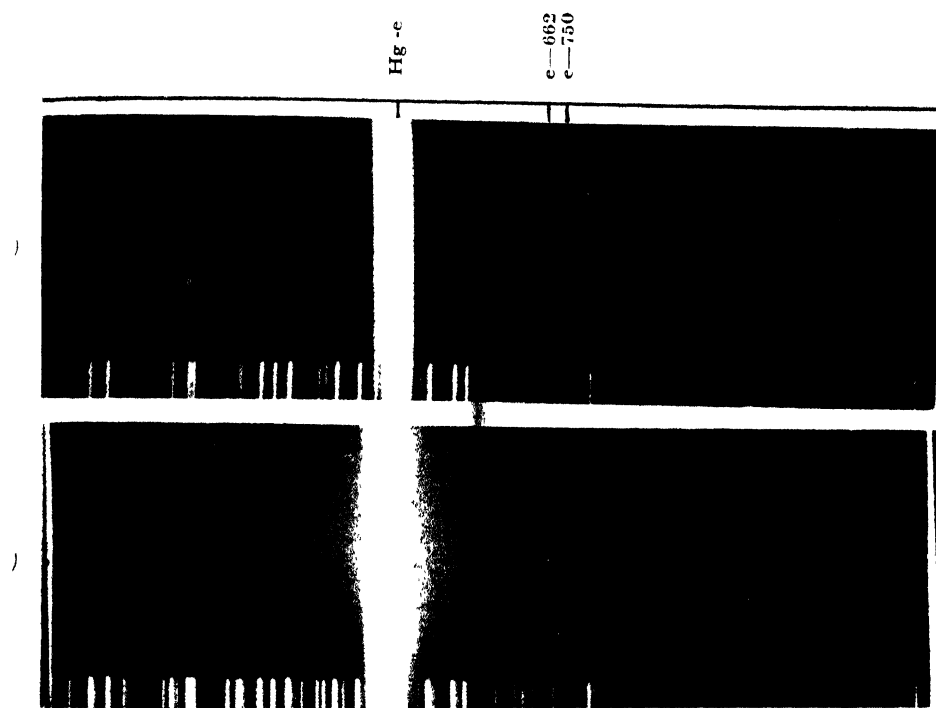


Fig. 1

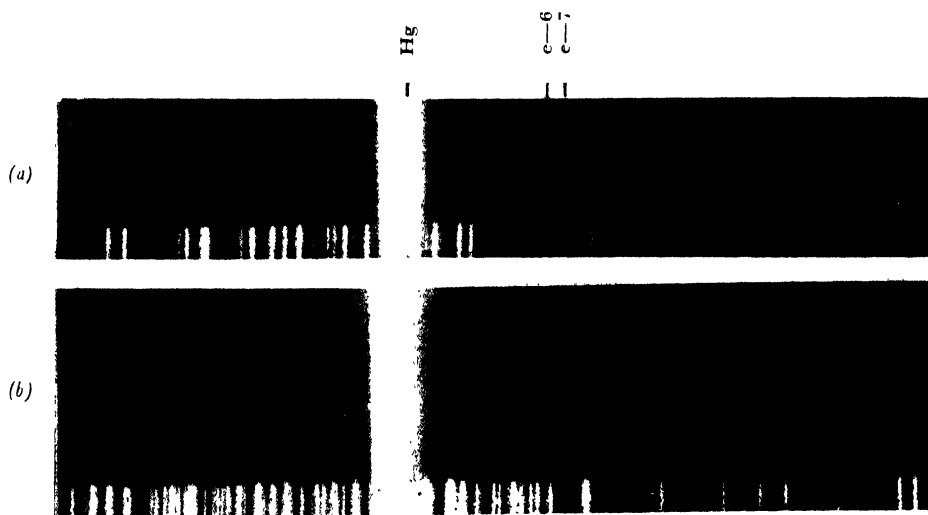


Fig. 2

Fig. 1. Ethylene chlorhydrin

(a) Liquid at 130°C

(b) Vapour at 180°C

Fig. 2. *n*-Propyl chloride

(a) Liquid at 100°C

(b) Vapour at 100°C

TABLE II

n-Propyl chloride, $\text{CH}_3\text{CH}_2\text{CH}_2\text{Cl}$. $\Delta\nu$ in kayser

Liquid state		Mizushima <i>et al</i> (1940) Solid state	Vapour state
at 30°C.	at 100°C.	at (Ca.-150°C.)	at 100°C.
140 (0) e			146 (0b) e
		229 (0) e,(k)	
295 (1) e,k			
366 (7) e,k	366 (4) e,k	363 (5) e,(k)	368 (1) e,k
424 (1) e,k	424 (0) e,k		
648(10) \pm e,k	648 (6) e,k	716 (7) e,k,i	663 (3) e,k
728 (5) e,k	728 (3) e,k		742 (2) e,k
791 (4) e,k	791 (2) o,k		
854 (2) e,k	854 (1) e,k		
894 (2) e,k	896 (1) e,k		
1026 (6) e,k	1026 (3) e,k	1029 (5) e,k	1030 (0b) e,k
1255 (3) e,k	1255 (1) o,k		
1452 (8b) e,k	1452 (4b) e,k	1441 (2) e,k	
2878 (6) e,k	2878 (4b) e,k	2870 (5) (e),k	2880 (2) e,k
		2894 (1) k	
2915 (3) e,k	2915 (2) e,k	2908 (1) (e),k	2915 (1) e,k
2937 (5) e,k	2937 (4) e,k	2941 (6) e,k	2959 (1) e,k
2960 (5) e,k	2960 (4) e,k	2975 (0) e,k	2970 (4) e,k
		2997 0) e,k	

that the intermolecular field in the liquid state is largely responsible for the creation of the two types of molecules in the liquid, and one of these two types may be a single molecule and the other an associated group of molecules. In the solid state the latter giving rise to the line 659 cm^{-1} is predominant. Thus these results clearly indicate that in the case of the molecules in the vapour state there is only one stable configuration and a second configuration is formed only in the state of

aggregation. In the liquid state both these configurations are present, while in the solid state the molecules are all in associated groups forming the second configuration.

In the case of *n*-propyl chloride, however, the situation seems to be more complicated. The change in the relative intensities of the lines 648 cm^{-1} and 728 cm^{-1} with change of temperature in the liquid is negligible and when the liquid at 100°C is vaporized at that temperature the ratio I_{728}/I_{648} increases very slightly. The line 1452 cm^{-1} which is more intense than the line 728 cm^{-1} in the case of the liquid at 100°C is absent in the case of the vapour at 100°C and the lines 2937 cm^{-1} and 2960 cm^{-1} shift respectively to 2959 cm^{-1} and 2970 cm^{-1} . This shows that the latter spectrum is due to the vapour only. On the other hand, as observed by Mizushima *et al* (1940), the line 649 cm^{-1} disappears when the liquid is solidified and cooled down to -150°C . Hence from these results they concluded earlier that in the solid state the *n*-propyl chloride molecules are all of gauche form and the ethylene chlorhydrin molecules are all of trans form and attributed the lines 649 cm^{-1} and 728 cm^{-1} of *n*-propyl chloride to trans and gauche configuration respectively and the corresponding lines 662 cm^{-1} and 750 cm^{-1} of ethylene chlorhydrin to the gauche and the trans configuration. They have, however, reversed their assignment recently (Mizushima *et al*, 1951) and have attributed the lines 750 cm^{-1} and 662 cm^{-1} of ethylene chlorhydrin to trans and gauche configuration respectively. So, according to this new assignment in the case of *n*-propyl chloride in the solid state all the molecules will be of trans configuration and both liquid and vapour states should consist of molecules of both the configurations. Evidently, the presence of the OH group in ethylene chlorhydrin molecule is responsible for this difference in behaviour of the two types of molecules. As both the lines 648 cm^{-1} and 728 cm^{-1} are polarised (Bishui, 1948) they are certainly due to the C-Cl vibration in two different types of molecules. If these two types are rotational isomers, the energy difference must be very small in the liquid and vapour states, as the relative intensities do not change very much with rise of temperature of the liquid. But the disappearance of one of these lines at 150°C cannot be due to the change of temperature alone, because the energy difference is very small. If on the other hand we assume that the associated molecules and the single molecule are the two types which produce these two lines, it is difficult to understand how the line 728 cm^{-1} increases in intensity both at low temperatures in the solid state and at high temperatures in the vapour state. Probably, the change in the value of the frequencies of the lines with change of state may provide some clue for the understanding of this phenomenon. The frequency of the Raman line 728 cm^{-1} observed at 30°C remains the same when the liquid is heated to 100°C , but it increases to 742 cm^{-1} when the liquid at 100°C is vaporized and apparently diminishes to 716 cm^{-1} when the liquid is solidified and cooled down to -150°C . No such shifts are observed in the case of ethylene chlorhydrin. So, it appears that since in the case of ethylene chlorhydrin the

C-Cl frequency is not affected appreciably by the intermolecular field the association between neighbouring molecules takes place through the OH group in the liquid state, while in the case of *n*-propyl chloride such association takes place through the Cl atom. If we now attribute the line 742 cm^{-1} to vibration in the single molecule and 663 cm^{-1} to that in the associated molecule in the vapour state, the influence of intermolecular field lowers these frequencies to 728 cm^{-1} and 648 cm^{-1} respectively in the liquid state. With solidification, however, further change takes place in the intermolecular field, as each C-Cl bond is surrounded by regularly arranged C-Cl groups in the lattice. The influence of these groups may be opposite to that of the formation of associated groups through the Cl atom. In that case we would expect a frequency of C-Cl vibration intermediate between the frequencies of C-Cl vibration in the single molecule and the associated molecule respectively. This may be the reason why in the case of *n*-propyl chloride in the solid state the frequency of C-Cl vibration is observed to correspond to 716 cm^{-1} which is less than 742 cm^{-1} observed in the case of the single molecule and greater than 663 cm^{-1} given by the associated molecule in the case of vapour. It may be pointed out here that when association takes place through the Cl atom, the virtual bond may be much stronger than that formed through OH group. This may be the reason why in the case of *n*-propyl chloride associated molecules persist even in the vapour state, while in the case of ethylene chlorhydrin in the vapour state almost all the molecules are monomeric.

The C-Cl vibration frequencies observed in the case of *n*-propyl chloride in the vapour state agree closely with those observed in the case of ethylene chlorhydrin in the vapour state. This proves conclusively that the C-Cl stretching vibration in a single molecule has frequencies corresponding to 742 cm^{-1} and 750 cm^{-1} in the case of *n*-propyl chloride and ethylene chlorhydrin respectively. Any normal coordinate treatment should give this frequency as one of the normal modes of vibration. Since Misushima *et al* (1951) obtained 704 cm^{-1} as the calculated value for the 'trans' configuration of ethylene chlorhydrin molecule the potential constants used by them are not correct. Attempts have been made to find new potential constants for the obtained frequencies of the C-Cl vibration and the results will be published in a separate communication.

ACKNOWLEDGMENTS

The author is indebted to Professor S. C. Sirkar, D.Sc., F.N.I., for his kind interest and helpful guidance throughout the the progress of the work and to the Government of India for the award of a Senior research scholarship.

REFERENCES

- Bishui, B. M., 1948, *Ind. J. Phys.*, **22**, 333.
Mazumder, M., 1953, *Ind. J. Phys.*, **27**, 405.

- Mazumder, M., 1954, *Ind. J. Phys.*, **28**, 297.
- Mizushima, S. and Morino, Y., 1938, *Proc. Ind. Acad. Sc.*, **8**, 315.
- Mizushima, S., Morino, Y. and Nakamura, S., 1940, *Sc. Papers Inst. Phys. Chem. Research (Tokyo)*, **37**, 205.
- Mizushima, S., Morino, Y., Watanabe, I., Simanouti, T. and Yamagauchi, S., 1949, *Jour. Chem. Phys.*, **17**, 592.
- Mizushima, S., Shimanouchi, T., Miyazawa, T., Abe, K. and Yasumi, M., 1951, *Jour. Chem. Phys.*, **19**, 1477.
- Morino, Y., Watanabe, I. and Mizushima, S., 1942, *Sc. Papers. Inst. Phys. Chem. Research (Tokyo)*, **29**, 396.

PULSE TECHNIQUES FOR ACOUSTICAL MEASUREMENTS IN BROADCAST STUDIOS

By RAM K. VEPA AND N. K. TRIVEDI

RESEARCH DEPARTMENT, ALL INDIA RADIO, NEW DELHI.

(Received for publication, January 8, 1955; received after revision, July 6, 1955)

Plate IX

ABSTRACT. In recent years, the concept of reverberation time as the sole criterion of good acoustics in a test enclosure has yielded to an emphasis on the manner of sound decay in the enclosure. New techniques using short impulse sounds have been developed for this purpose, and this paper describes the particular method employed in All India Radio for the acoustic testing of broadcast studios. Results obtained in a typical studio in the Broadcasting House, New Delhi, are described and are interpreted on the basis of the acoustical treatment employed in it. Finally, a discussion of the advantages and limitations of the new techniques are given, together with a summary of the latest advances in the subject in other countries.

1. INTRODUCTION

The concept of reverberation time, introduced first by Wallace Sabine almost fifty years ago, was, till very recently, considered as the sole criterion of good acoustics in any enclosure. Since then, various "optimum" reverberation time curves have been drawn empirically by several investigators, showing the dependence of this quantity on such parameters as the volume of the enclosure, the frequency employed, and the nature of sound generated. For broadcast studios, there is an additional factor since the pick-up chain is monaural as contrasted with the binaural hearing in concert halls or other public buildings where a live audience is present.

2. REVERBERATION TIME AND ROOM ACOUSTICS

In recent years, however, the absolute validity of the reverberation time as the *only* criterion of satisfactory acoustics, has been challenged. Almost a decade ago, Mason and Moir found in the case of cinema halls that the mere attainment of an optimum value of the reverberation time was no guarantee of a satisfactory acoustical condition and that in some cases, such halls did not just "sound" right (Mason and Moir, 1944). And since the human ear is the final arbiter of what is good acoustics, this observation—corroborated by other investigators—could not be lightly dismissed. Mason and Moir concluded that this discrepancy was due to the fact that conventional reverberation time measurements were often conducted with continuous tones (either pure or warbled) which were switched off, after a steady state has been attained in the test enclosure. Most sounds,

in practice, are, however, pulsatory in nature, and this is true of speech even more than of music. In music itself, there is a marked difference between the sharp staccato rhythms of a drum and the sonorous flowing music of an organ. It is reasonable to assume that the sound field produced by these pulsatory sounds is, in a sense, different from that produced by continuous sounds.

Another observation made by Mason and Moir at the same time is also of great interest. They found that good listening in the cinema auditoria was associated with a number of image sources, distributed at random, which radiate the incident sound so as to reach the ears of the listener after a very short time delay. This has been strikingly confirmed by the experiments conducted by Haas at Gottingen during the war, (the results of which have been reported only recently) on the effect of a time-delayed single echo on the intelligibility of speech (Haas, 1951). Haas reported that echoes with time delays of the order of 1-30 milliseconds are not heard separately but, actually, enhance the pleasing quality of speech. He has further shown that there is a critical time delay which is a function of echo intensity, frequency of the source, and reverberation of the test enclosure. Good acoustics, which is a harmonious combination of both the functional and aesthetic aspects, is now, therefore, associated with a number of randomly distributed virtual sound images that reflect the incident sound wave with the right intensity and optimum time delay.

The emphasis has therefore been shifting slowly to the manner of sound decay, rather than merely on the time taken by the sound to decay by a certain arbitrary ratio (as reverberation time actually is). Mayo has expressed this cogently when he says that "the acoustical properties of a studio do not depend on the mere presence or absence of standing wave patterns but on the nature of these patterns" (Mayo, 1951). Sound sources at present normally used in reverberation time measurements merely indicate whether standing waves have been set up in the enclosure but cannot provide any information about their characteristics. It is obviously impossible to locate with a continuous tone the virtual sound sources that make up the resonance in an enclosure. Such a method merely indicates the response of the enclosure to sound in the steady state but does not reveal as to how the sound is built up, which is, however, vital to a complete knowledge of the acoustical behaviour of the test enclosure. One solution is to sweep the entire audio frequency spectrum in interval before the first reflections begin to arrive, (i.e. within about 50 milliseconds, according to Haas) but this has many limitations in practice. Besides, it is doubtful if steady state conditions are attained in so short a time for any frequency.

3. THE PULSE TECHNIQUE

An alternative method, employed in All India Radio, uses pulse bursts of adjustable length (of the order of a few milliseconds) and the response of the studio.

to these impulse sounds is displayed as a luminous pattern on the screen of a CRO. The frequency spectrum of the impulse is similar to that of 'white' noise where the amplitudes of component frequencies are nearly all equal.

It may be mentioned here that many of the investigations reported in literature deal primarily with concert halls and auditoria of large dimensions, of the order of 200,000 cu. ft., (Somerville, 1949) but here in this paper, results obtained in a broadcast studio of comparatively small volume (of the order of 15,000 cu. ft.) are reported. In fact, one of the principal aims of the present investigation was to ascertain whether such pulse techniques could be employed for determining the acoustical characteristics of test enclosures, such as broadcast studios.

Before the investigations are described in detail, it is instructive to form a physical picture of what happens when an impulse sound is produced in any enclosure. Mayo provides such a picture (Mayo, *loc. cit.*) by drawing what he calls the "echo-time diagram" (figure 1a). The ordinates of PQR are inversely proportional to the time elapsed after the generation of the pulse. The actual magnitudes of the echoes are smaller than that given by curve PQR due to absorption and reflection losses. A is the point where the time base of the CRO starts and B is the time when the direct sound has reached the microphone. C, D are the first order echoes due to image sources distributed on the boundaries of the enclosure. The cluster at E represent the second order echoes and later bunches are due to higher order echo returns. The abscissa values of time correspond to the distances of the real and image sources from the microphone. If now the source emits the tone continuously, the resulting diagram would be a complex one depending on the phase at which these echoes return to the microphone. This

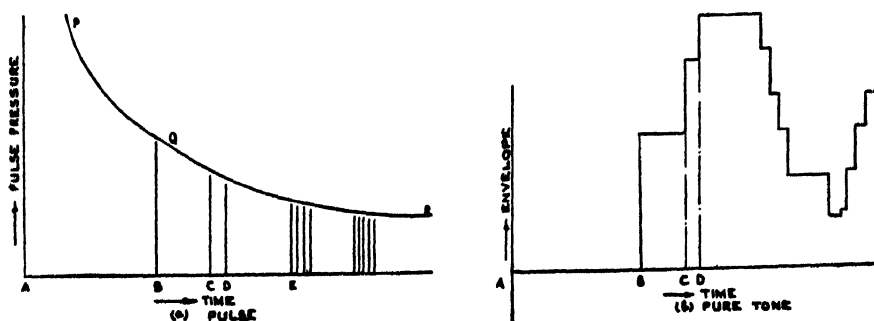


Fig. 1. Variation of total sound pressure at any point with time.

is in turn dependent on the distance travelled by the sound wave, and hence on the time delay of the echo—as obtained from the echo time diagram. Such a diagram is shown in figure 1(b) where the time delay obtained from the echo time diagram has been used to compute the phase and add, vectorially, the direct and the reflected sound. The envelope diagram shown in figure 1(b) thus represents the build-up transient of the sound in the enclosure and a similar

diagram can be constructed for the switch-off transient. It is obvious from this picture, that if a continuous sound source is used, there is an interference between the direct sound and the first order reflections and the analysis of such a pattern becomes virtually impossible.

The physical picture of the behaviour of a sound pulse can be given thus: In the first stage, are discrete echoes, few in number and sometimes of considerable magnitude. In the second stage are numerous echoes, small in magnitude and due to sets of virtual sources distributed in several planes. Finally, in the third stage when the echoes arrive in groups, which Mayo (*loc. cit*) believes represents the steady state response of the enclosure. This last stage is not reached till the sound is almost 30 to 40 db below the initial level. If this point of view is correct, it would mean that the real eigen tones are established only after a lapse of time and that the second 30 db of decay is comparatively more significant in indicating the steady state characteristics of the enclosure, such as reverberation time. This is contrary to the present practice of giving greater weightage to the first 30 db decay in computing the effect on the human ear. Whether Mayo's view is correct or not, the physical picture he has provided of the behaviour of a pulse in an enclosure, emphasises the superiority of the new technique in studying the acoustical characteristics of the enclosure.

In an irregular auditorium where the echo returns have a random phase, the envelope of sound decay should have a nearly exponential characteristic. This would imply that no high intensity echoes arrive at large time delays to violate Haas' condition for good acoustics. In a rectangular room, however, the normal modes come out as regularities in the pattern indicating unsatisfactory diffusion. Diffusion is such an important characteristic of broadcast studios, particularly in regard to microphone placement, that it is useful to have facilities to study it.

4. CIRCUIT DETAILS

Figure 2 is a block schematic of the set-up for conducting pulse measurements in a broadcast studio. The pulsing unit generates short pulses of variable

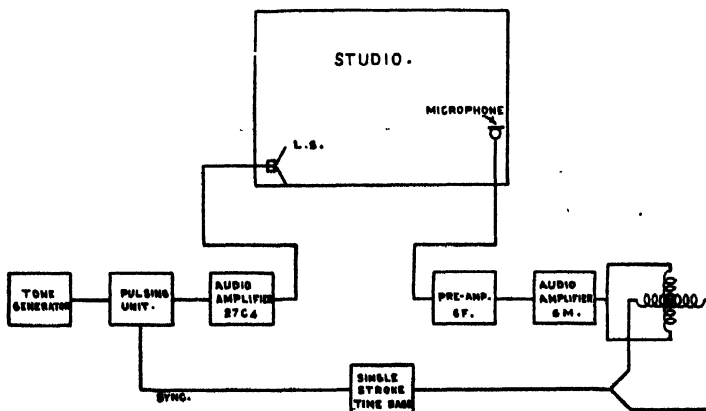


Fig. 2. Block schematic of the pulse study of a studio,

length which, after amplification are, applied to a loudspeaker located in the test studio. A microphone suitably located picks up the sound, amplifies it before feeding it to the vertical plates of a CRO, whose horizontal plates are connected to a time base circuit that is synchronized with the impulse switch. These pulses are so short (of the order of a few millisees) and applied at intervals long enough for the direct sound to decay to a very small value. A more detailed description of the equipment is given below:

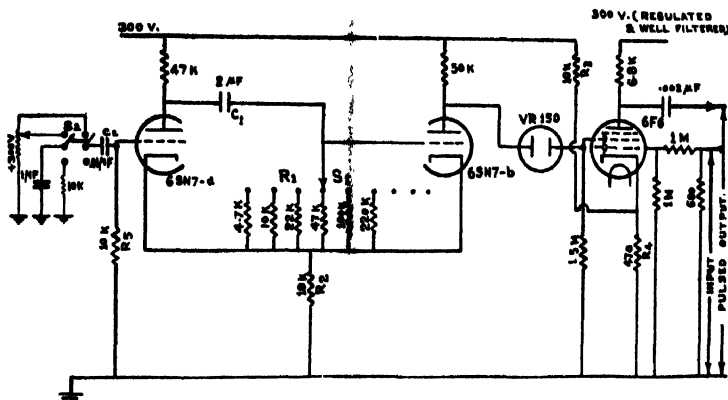


Fig. 3. Pulsing unit.

4.1. *Source*: Various types of pulsing sources have been tried by several investigators and it was preferred to have an electronic source, both for its simplicity and reliability. A uni-stroke multivibrator circuit was chosen to provide approximately square wave pulses whose length can be varied between 5 and 200 millisees by varying resistance R_1 , in the time constant circuit C_1R_1 (figure 3). The square wave output of the multivibrator is applied to the screen grid of a 6F6 tube through a voltage regulator tube of proper voltage rating. The signal from the tone generator, which has to be modulated by the square wave, is applied to the grid of the 6F6 tube and the output is taken from the anode through a .003 mfd condenser. With this method of modulation, and rise and fall of the pulse is sharp and is limited by the operating time constants of the VR tube only.

A simple method of synchronisation is obtained by applying a high voltage impulse through a condenser to the 6SN7 grid (figure 3) which starts the square wave. One pair of a DPDT switch (S_2) applies this impulse while the other pair of the same switch starts the charging of a condenser for time base circuit (Sec. 4.3). In one position of the switch S_2 , the voltages are applied and the square wave and time sweep start simultaneously, while in the other position of S_2 , the time base condenser is discharged through a suitable resistor so as to be ready for next stroke when S_2 is flipped back.

4.2. *Indicator:* The microphone output, after amplification, is applied to the vertical plates of a CRO. For ease of visual observation as well as for photographic work, the need for a long persistence tube is obvious. A 5FP7 tube was chosen for the purpose and the h.t. in the anode was a rectified RF of the order of 12 k.v. Controls to adjust the focus and brilliancy of the pattern were also provided.

4.3. *Time Base Circuit:* The requirements of a suitable time base for the experiment are: (i) it should be single stroke (ii) it should be capable of being synchronised with the pulse generation (iii) it should cover the face of the tube in varying intervals from 0.1 to 2 secs, since the reverberation times of most broadcast studios are well within this range, and (iv) it should be reasonably linear. In the circuit, adopted after trial and error, a condenser in the grid circuit is charged by the supply voltage through any of the three resistances that can be chosen by a switch. The maximum voltage on the condenser for full sweep is not larger than 50v, which is only 20% of the supply voltage, and hence the non-linearity is well within the limits of tolerance. Finer sweep control is available by controlling the charging voltage, which should be kept as high as possible. The time base is calibrated by disconnecting the vertical plates from the output of the microphone and applying a 50 cycle mains frequency.

5. EXPERIMENTAL DETAILS

A typical studio of Broadcasting House, New Delhi, (Studio 1) is chosen for conducting pulse measurements. Studio 1 is moderate sized (Vol: 13,5000 cu.ft.) and is used primarily for concert music, both Indian and Western. It has a slightly asymmetric plan with non-parallel walls, purposely so designed to improve the sound diffusion in the studio and, in particular, to avoid any "flutter". Only walls is treated with 2 layers of glass wool quilts (of $\frac{1}{2}$ " thickness each) faced with one of the side a perforated transite board. The other three walls are untreated and the facing material is laid directly on 2" battens on the bare wall. Five pilasters (each of width 4' 3") similarly treated with $1\frac{1}{2}$ " thick glass wool quilts and transite board (with an air gap of about $7\frac{1}{2}$ " behind the glass wool) are distributed on two of the side walls. The ceiling is also treated with the transite board-glass wool combination while the floor is covered with linoleum. Figure 4 shows a plan of the studio as also some of the structural details described above.

The measured values of reverberation time in the studio are found to be considerably lower than the optimum at the low frequencies below 500 cycles (100 c/s : 0.58 sec; 500c/s:0.52 sec.). At 800 c/s, the measured reverberation time curve crosses the desired optimum curve, and at frequencies above 1500 c/s, the measured values are much greater than the optimum values (2000 c/s:0.86 sec; 4000 c/s: 0.96 sec.).

In these measurements, a 25W loudspeaker set in a bass-reflex baffle was used and was located in one of the corners, as shown in figure 4. The microphone

was an omni-directional type and was mounted on a stand about five feet above the floor. The position of the microphone was varied during the experiment and the four positions used in these investigations are shown in fig. 4.

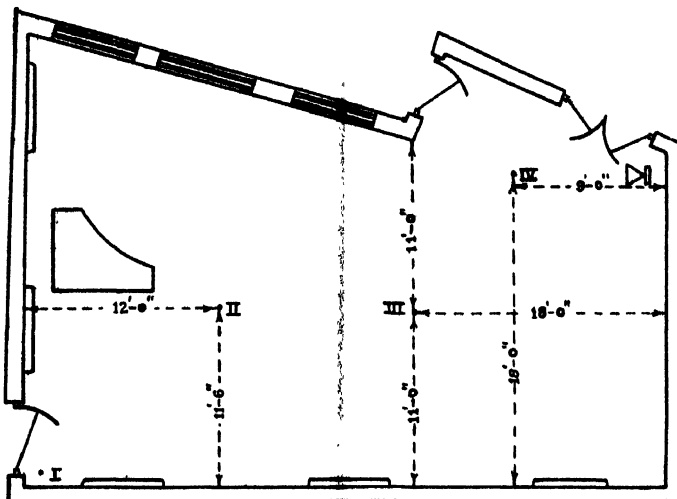


Fig. 4. Studio no. 1. Broadcasting house, New Delhi.

The positions of the microphone were chosen so as to provide the most useful information from the point of view of the acoustic analysis of the studio. For instance, the corner position (marked I in figure 4) is never used in normal broadcast practice, and yet is of great interest since it is the position where the largest number of room resonances have their pressure maxima. Hence, a measurement at such a location would help to analyse the intrinsic behaviour of the enclosure.

In actual practice, however, microphone positions are primarily chosen on other considerations. Thus, for instance, the microphone must be so located that the largest possible pick-up space is utilised; this is, in turn, dependent on the type of programme broadcast and the characteristic of the microphone being employed. In a drama programme, for instance, where a bi-directional microphone is used, there should be ample space on both the "working faces" of the microphone. In a musical concert on the other hand, where an omni-directional or uni-directional microphone is utilised, the space utilisation is somewhat different and depends to a large extent on the balancing of musical instruments. Another important consideration for the position of the pick-up microphone is that it should be fully visible from the control booths attached to the studio to enable the producer and announcer to have a clear view of what is going on in the studio. In the studio under investigation, it is seen from figure 4, that position II satisfies this criterion adequately and is hence used in normal practice.

Pulse patterns were at first obtained with varying pulse lengths and photographed with the oscillograph camera. It was noticed that for an enclosure of

this size, extremely short pulse lengths were necessary for obtaining a well defined picture. Otherwise, the patterns tend to become "fuzzy" and besides, interference between the direct sound and the echo returns occurs, resulting in an envelope that is extremely difficult to analyse. In the results reported here, a pulse length of 5 millisecs has been employed with corroboration from 20 millisecs pulses, wherever necessary.

It was noted that the patterns were repeatable enough to warrant a detailed study of the new technique. The patterns obtained are unique for the microphone position, test frequency and pulse length.

At each position of the microphone, patterns were obtained with ten frequencies: 90, 120, 150, 210, 300, 400, 500, 1000, 2000, and 4000 c/s. The lower frequencies were chosen so as to be near some of the prominent low-order modes as indicated by the transmission-frequency characteristic.

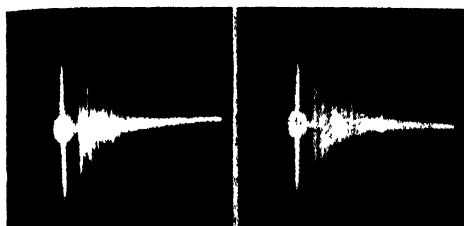
6. RESULTS

The exact interpretation of the pulse patterns is somewhat complicated but, undeniably, they afford a visual picture of the acoustical performance of the studio. The photographs were examined particularly for three details: (a) general decay of the pulse (b) prominent echo returns of the pulse (c) and the time interval at which these echo returns occur.

(a) *Position I*: Though this position is never used in practice, it is of interest as being the location where the largest number of modes have their pressure maxima. Figure 5 shows the patterns obtained at 150 c/s and 1000 c/s. It can be seen that the decays are in general smooth and even, and there are no long delayed returns marring the acoustics of the studio.

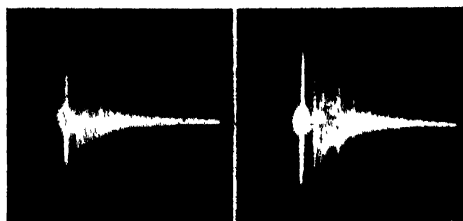
(b) *Position II*: This is the normal broadcast position as it is near the piano and has a good view of the announcer and control booths. Figure 6 shows the patterns obtained at 90 c/s and 1000 c/s. The low frequency decay is smooth but at the mid frequency, there are prominent returns with a delay of 90 and 150 millisecs., the former being the stronger of the two. The pattern at 1000 c/s is interesting in indicating the presence of strong short path initial reflections. According to Potwin and Maxfield, the presence of short path reflections contributes to satisfactory acoustics (Potwin and Maxfield, 1939) and it is gratifying to note that this is fulfilled in the position used normally for broadcasting.

(c) *Position III*: This is a position almost at the centre of the studio. Figure 7 shows the decay curves at 150 c/s, 300 c/s and 1000 c/s. In the patterns at 150 c/s and 1000 c/s, the decays are found to be jagged and non uniform. For the low frequency pattern, the envelope of decay deviates markedly from an exponential characteristic. It is to be noted also that no strong first order reflections are present here as in position II. In the case of 1000 c/s, there are prominent echo returns at 60 and 100 millisecs. The former has a large amplitude and



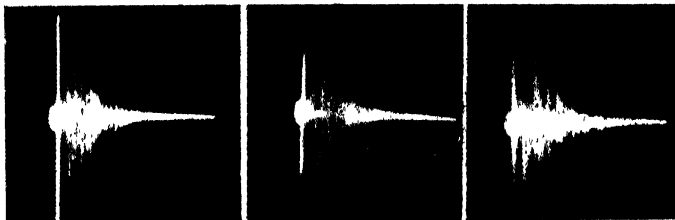
150 c/s 1000 c/s

Fig. 5. Position I



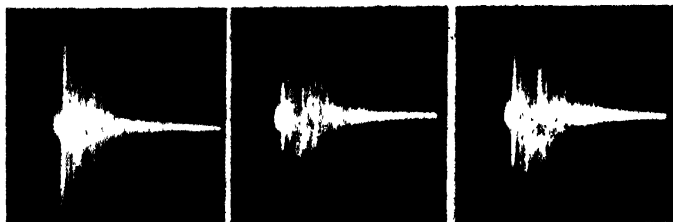
90 c/s 1000 c/s

Fig. 6. Position II



150 c/s 300 c/s 1000 c/s

Fig. 7 Position III



90 c/s 500 c/s 1000 c/s

Fig. 8. Position IV

is expected to affect the acoustics of the studio. The patterns indicate that this position of the microphone is an unsatisfactory one.

(d) *Position IV*: This is a position adjacent to the source and can be expected to show uneven decay. This is borne out by figure 8 which shows the patterns obtained at 90 c/s, 500 c/s and 1000 c/s. In the middle range of frequencies, a 75 millisees. delay and echo is noticed. At lower frequencies, there were prominent returns at shorter time delays.

It is seen from the above, that the task of analysing the patterns is, indeed, a formidable one.* It is difficult at this stage to draw more than tentative conclusions of the acoustical behaviour of the studio under test. However, with experience, imagination and a certain intuitiveness, it is possible by this method to construct a visual picture of the progress of a sound wave in the studio.

The pulse technique has shown that the smooth decay of sound at any frequency is associated with the presence of a large number of small amplitude echoes, random in phase and direction, rather than a small number of discrete echoes from large flat surfaces.

The pulse patterns are particularly invaluable for detecting long delayed echoes that mar the intelligibility of speech and, generally, the acoustics of the enclosure. However, the practical problem of locating the surfaces responsible for the unwanted reflections is a complicated one. One method, which is suitable in this connection is to use an omni-directional microphone to obtain the pulse patterns like those described earlier in this section. The relative echo amplitudes give an indication of the intensity of the individual echoes from the different boundary surfaces in the studio. From the delay time, the path lengths can be calculated from which the surfaces responsible for the echoes can be guessed. For a more precise knowledge, a highly directional microphone like the tubular microphone (Mason and Marshall, 1939) can be used to locate the offending surfaces with reasonable accuracy.

Once the reflecting surfaces are located, there are two alternatives to remedy the situation: (i) to alter the subtended angles by breaking the surface into smaller areas at divergent angles to the plane or (ii) to apply acoustic treatment to the surfaces as to make the intensity of the wave reflected from that surface as small as possible.

7. RECENT DEVELOPMENTS

It is interesting to speculate whether it is possible to evaluate the reverberation time from the pulse patterns but a little thought will suggest two objections: (i) The pulse lengths are too short to be certain that steady state conditions are obtained in the enclosure which is a necessary condition for valid measurement of reverberation time. (ii) Since the sound pressure amplitudes are applied to the plates of the CRO in a linear scale, the variation of sound level in the pattern is

too limited (not more than 20 db at the maximum) to permit any reliable computation of reverberation time.

Both the objections are overcome in an interesting method developed by Mayo and Beadle at the BBC (Mayo and Beadle, 1951). They use relatively long pulses (200 millisees) to ensure steady state condition in the studio and they have further incorporated a logarithmic stage before applying the microphone output to the oscilloscope. A linear decay curve similar to the one on the graphic level recorder with a mechanical stylus, is obtained and there is a goniometer arrangement whereby the R. T. can be computed directly by adjusting the slope of the decay curves to coincide with one of the lines inscribed on a graticule attached to the goniometer.

While the equipment is undoubtedly an ingenious adaptation of the pulse technique, it is useful to enquire whether there is any considerable advantage in this method over the conventional graphic level recorder for measuring reverberation time. The comparatively long pulse lengths rob the method of its ability to study the details of the sound decay in small or moderate sized enclosures, as effectively as with the short pulse lengths. The use of the cathode ray oscilloscope in place of the mechanical stylus of the level recorder, is often a disadvantage, because, paradoxical as it may seem, of its low writing speed at the low frequencies. This is so because of the high *CR* value that is to be employed in the CRO to offset the high sensitivity of the vertical plates to superimposed A.C. voltages. At high frequencies, the writing speed of the electron beam in CRO is undoubtedly greater than that of a mechanical recorder. But this may not always be an advantage as it would clutter up the decay curves with a mass of unnecessary details. Besides, it is difficult to use with the CRO, the delicately balanced servo system that contributes so much to the stability and sensitivity of the level recorder.

If in the arrangement described in the previous paragraph, there is a slowly moving film in front of the CRO screen and a mechanism to increase the test frequency in discrete steps, there would be obtained a three dimensional (amplitude, frequency and time) picture of sound decay in a room. The BBC has, in fact, developed such a method known as the Pulsed Glide method and the resultant pictures are visually impressive (Somervill and Gilford, 1952). Though a detailed interpretation of these patterns is still difficult there is little doubt that this offers an easy and quick method for estimating reverberation time as a function of frequency. More important, is that it enables one to detect immediately, what the BBC engineers call so expressively, 'Coloration' i.e. any phenomenon interfering with good acoustics, such as flutter, unwanted echo or a prominent resonance. Bruel and Kjaer have modified the BBC pulsed glide technique by using a level recorder in place of the CRO. Such a combination of pulse source and high speed level recorder is in fact likely to offer the most comprehensive information on the

acoustics of moderate sized enclosures: an accurate estimation of reverberation time together with additional information on the nature of sound decay that can be obtained only from pulse methods.

8. CONCLUSION

For relatively small enclosures, such as broadcast studios, it is obviously impossible to reconcile the short pulse lengths for studying decay patterns with the determination of the reverberation time which is dependent on the attainment of steady state conditions. For the present, therefore, it is hardly likely that pulse measurements, such as those described in this article, can completely supplant conventional reverberation time measurements but they do provide additional information of great value in assessing an acoustical performance of a studio, particularly in the detection and elimination of long delayed echoes of considerable amplitude.

ACKNOWLEDGMENTS

The authors' thanks are due to the Chief Engineer, All India Radio, for permission to publish the paper.

REFERENCES

- Haas, 1951, *Acustica*, 1, 49.
- Mason and Moir, 1944, *JIEE*, Part III, 88, 175.
- Mason and Marshall, 1939, *JASA*, 10, 206.
- Mayo, 1952, *Acustica*, 2, 49.
- Mayo and Beadle, 1951, *Electronic Engineering*, 23, 462.
- Potwin and Maxfield, 1939, *JASA*, 11, 391.
- Somerville, 1949, *BBC Quarterly*, 4, 41.
- Somerville and Gilford, 1952, *BBC Quarterly*, 7, 41.

ON THE VARIATION OF p-p SCATTERING CROSS SECTION WITH ENERGY*

By C. C. BANERJEE

DEPARTMENT OF THEORETICAL PHYSICS, INDIAN ASSOCIATION FOR THE CULTIVATION OF SCIENCE, CALCUTTA-32.

(Received for publication, June 9, 1955)

ABSTRACT. The paper attempts to find an empirical relation between the differential proton-proton scattering cross section and the energy of the system. The relation proposed agrees fairly with the experimental data at high and low energies.

INTRODUCTION

The experimental data on differential cross sections for proton-proton scattering at high energies exhibit isotropy i.e. the differential cross section is independent of the angle of scattering (30° — 90°) in the centre of mass system. At low energies, however, the cross section depends on the angle and increases to a very large value at small angles. The magnitude of the cross section in the low energy range varies almost inversely as the energy of the incident protons. At high energies, however, the cross sections tend to become independent of the energies. The phenomenological attempts of Jastrow (1951), Christian and Noyce (1950) and Case and Pais (1950) do not explain satisfactorily the entire range of variation of the scattering cross section with angle and energy of the incident particle. The author (1954) found a fair fit with the experimental data at 340 Mev by developing a theoretical expression for the scattering cross section with the tensor part of the pseudo scalar potential as the interaction between the protons. The expression so developed, however, does not explain the low energy data and also the variation of cross section with energies. The author in this paper proposes an empirical relation between the scattering cross section in the centre of mass system and the energy of the incident protons.

THE EMPIRICAL RELATION

A study of the experimental results of the differential cross sections of p-p scattering at various energies suggests that an equation of the type given below may represent the variation of cross sections with energies. The numerical results obtained from the proposed equation give, over the entire energy range,

* Communicated by Dr. D. Basu.

a good agreement with the experimental values (the average value has been considered where angular anisotropy is observed). The graph (figure 1) and the

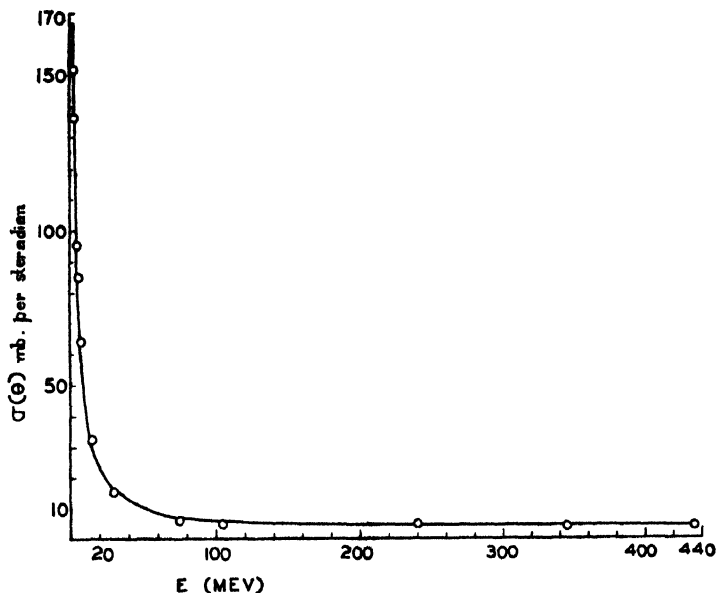


Fig. 1. The continuous line represents the theoretical curve and the small circles represent the experimental points.

table of data (Table I) (theoretical and experimental) show this agreement clearly. The empirical relation which explains the variation of cross section with energy is

$$d\sigma = \frac{a}{E} + \frac{E}{1+bE} \quad \dots (1)$$

where $d\sigma$ is the differential cross section in mb/std and E is energy of the incident protons in Mev.

a and b are constants whose values are : $a = 400$, $b = \frac{1}{3}$ (Lab. system) and $a = 100$, $b = \frac{1}{3}$ (c.m. system).

It is apparent that the form of equation (1) remains unaltered whether the energy is expressed in the laboratory system or in the centre-of-mass system. The value of the constant a is, however, changed by such transformation but that of b remains almost the same.

TABLE I

Energy in Mev		$d\sigma$ in mb per steradian in the c.m. system : (experimental data)								Expt. average value of $d\sigma$	Theoretical value of $d\sigma$ for		References Phys. Rev.
Lab.	c.m.	angles in the c.m. system									Lab. energy	c.m. energy	
		30°	40°	50°	60°	70°	80°	90°					
2.42	.61	—	—	142.6	153.1	150.9	156.7	156.1	151.8	166.9	164.2	75, 419, 1949.	
3.04 (3)	.75	—	—	130.4	136.0	135.0	140.2	140.7	136.4	132.7	132.1	<i>ibid.</i>	
4.96 (5)	1.25	—	—	92.1	94.9	95.7	95.8	99.0	95.5	81.5	80.8	78, 667, 1950.	
5.77 (6)	1.5	87.3	82.8	83.3	85.7	86.9	86.7	87.2	85.7	68.8	67.6	96, 1322, 1954.	
7.03 (7)	1.75	65.6	61.7	63.4	65.1	63.8	66.4	66.1	64.6	59.2	59.0	73, 1290, 1948.	
14.4	3.6	30	—	—	—	—	—	33.4	31.7	30.9	30.0	71, 560, 1947.	
30	7.5	14	15	15.6	16.5	16.5	16.4	16	15.7	16.1	15.4	79, 57, 1950.	
75	18.6	—	—	—	—	—	—	—	6.6	8.2	7.9	83, 274, 1951.	
105	26	—	—	—	—	—	—	—	5.4	6.7	6.5	<i>ibid.</i>	
240	58.2	4.8	4.9	4.9	—	5.0	5.0	4.8	4.9	4.6	4.5	85, 416, 1024, 1952.	
345	82.0	(35°.6) 4.3	—	—	(64°) 3.6	—	—	(89°.2) 4.2	4.0	4.1	4.1	83, 923, 1951.	
435	102.2	(25°) 4.5	(35°) 4.2	—	—	(65°) 3.6	—	3.4	3.9	3.9	3.8	90, 712, 1953.	

ACKNOWLEDGMENT

The author desires to express his sincere thanks to Dr. D. Basu, Ph.D. for his valuable guidance throughout the progress of the work.

REFERENCES

- Banerjee, C. C., 1954, *Ind. J. Phys.*, **28**, 221.
Case, K. M. and Pais, A., 1950, *Phys. Rev.*, **80**, 263.
Christian, R. S. and Noyce, H. P., 1950, *Phys. Rev.*, **79**, 85.
Jastrow, R., 1951, *Phys. Rev.*, **81**, 165.
" 1950, " " **79**, 380.

FORCE CONSTANTS FOR SUBSTITUTED GERMANES*

PART II. GeCl_3H and GeCl_4 .

BY S. L. N. G. KRISHNAMACHARI

PHYSICS DEPARTMENT, ANDHRA UNIVERSITY, WALT AIR.

(Received for publication, May 10, 1955; received after revision, July 2, 1955)

ABSTRACT. Force constants are calculated for GeCl_3H and GeCl_4 using the Wilson F - G matrix method. A comparison is made between the force constants which are common for the three molecules GeH_3Cl , GeCl_3H and GeCl_4 . The agreement between GeCl_3H and GeCl_4 is found to be better than that between GeCl_3H and GeH_3Cl .

In continuation of the work on GeH_3Cl and GeD_3Cl (author, 1955), the force constants for the molecules GeCl_3H and GeCl_4 are calculated and reported in the present paper. The Raman frequency data used in the calculations are taken from the recent investigations by Delwaulle (1952).

GeCl_3H : The molecule GeCl_3H belongs to the C_{3v} point group. The normal coordinates are similar to those for GeH_3Cl and the G -matrices are the same as those for CF_3H (Pace, 1950) excepting that in this case μ_{Ge} replaces μ_{C} and μ_{Cl} replaces μ_{F} . The F -matrices that are employed are

$$\begin{array}{c}
 A_1 \left| \begin{array}{cc} f_d & 0 \\ & f_D + 2f_{DD} \end{array} \right. \begin{array}{c} 0 \\ D/\sqrt{2} (2f_{D\eta} + f_{D\eta}') \\ D^2/2 \left\{ f_{\eta\eta} + 2f_{\eta\eta} - 4f_{\beta\eta} + \frac{d^2}{D^2} (f_x + 2f_{\beta\beta}) \right\} \end{array} \\
 \\
 E \left| \begin{array}{cc} f_D - f_{DD} & -Df_{D\eta} \\ & 0 \end{array} \right. \begin{array}{c} -Df_{D\eta} \\ 0 \\ d^2(f_{\beta\beta} - f_{\beta\beta}) \\ D^2(f_x - f_{\eta\eta}) \end{array}
 \end{array}$$

in which

d = Ge—H bond distance and

D = Ge—Cl bond distance.

The bond distances (Venkateswarlu, Mockler and Gordy, 1953) used in the calculations are,

$$d = 1.55 \text{ A.U.}$$

$$D = 2.114 \text{ A.U.}$$

Tetrahedral angles are assumed in these calculations.

* Communicated by Prof. K. R. Rao.

The nature of these force constants is shown in the first column of Table I. The values of the force constants are so adjusted as to reproduce the observed frequencies accurately. The final set so obtained is shown in the third column of Table I. The agreement between the observed and calculated frequencies is shown in Table II.

TABLE I
Force constants for GeCl_3H .

Nature of the force constant	Representation	Value (10^5 dynes/cm)
Ge-Cl bond stretching	f_D	2.622
Ge-H bond stretching	f_a	2.731
Ge-Cl, Ge-Cl interaction	f_{DD}	0.193
H-Ge-Cl bending and H-Ge-Cl, H-Ge-Cl interaction	$f_\beta - f_{\beta\beta}$	0.188
Cl-Ge-Cl bending and Cl-Ge-Cl, Cl-Ge-Cl interaction	$f_\eta - f_{\eta\eta}$	0.143
Ge-Cl, Cl-Ge-Cl interaction with a common bond	$f_{D\eta}$	0.028
Ge-Cl, Cl-Ge-Cl interaction with a common atom	$f_{D\eta'}$	0.008
Cl-Ge-Cl, Cl-Ge-Cl interaction and H-Ge-Cl, H-Ge-Cl interaction	$f_{\eta\eta} + \frac{d^2}{d^2} f_{\beta\beta}$	0.028

TABLE II
Calculated and observed frequencies of GeCl_3H . (cm^{-1})

	Calculated	Observed
ν_1	2159	2159
$A_1 \nu_2$	409	409
ν_3	181	181
ν_4	707	699
$E \nu_5$	433	438
ν_6	149	149

GeCl_4 :

The molecule GeCl_4 belongs to T_D point group. The force constants for this molecule were calculated previously by using approximate methods. (Hertzberg, 1945). In the present work a more general potential function containing all the interaction terms is made use of.

MASS ASYMMETRY EFFECT IN HUTCHISSON'S THEORY OF VIBRATIONAL TRANSITION PROBABILITIES

By N. R. TAWDE

DEPARTMENT OF PHYSICS, KARNATAK UNIVERSITY, DHARWAR,

AND

P. V. CHANDRATREYA,

DEPARTMENT OF PHYSICS, RUPAREL COLLEGE, BOMBAY.

(Received for publication, June 26, 1955; received after revision, August 8 1955)

ABSTRACT: Even though Hutchisson's theory of vibrational transition probabilities in diatomic molecules assumed the symmetry of constituent atomic masses, it was generally considered valid for asymmetric molecules too. Attempt has been made to examine this validity for some highly asymmetric molecules. It is concluded from the study of some band systems of BO, AlO, TiO and VO that considerable departures from theory result with increase in mass asymmetry.

Hutchisson (1930), while deriving his analytical expression for intensity of a band in an electronic transition, has made three important assumptions: (a) mechanical harmonicity, (b) mass symmetry and (c) electrical harmonicity (i.e. invariance of the electrical moment with γ , the internuclear distance). All these assumptions are not expected to actually prevail in practice. Leaving apart two of these assumptions, viz. mechanical harmonicity and electrical harmonicity we can investigate whether the third assumption, i.e. the nuclear mass symmetry of a molecule plays any significant part. It has been assumed by many that vibrational transition probability does not vary appreciably with disparity in the nuclear masses. In fact, the theory has been shown by Dunham (1930) to be applicable to asymmetric molecules too. The theory has actually been examined in asymmetric molecule BO by Elliott (1933) and in CN by McKellar and Buscombe (1948). The want of agreement, if any, has so far been usually attributed to anharmonicity of nuclear oscillations, which is not taken into account by theory. In view of the fact that disparities may be due to any or all of these three causes given above, it was thought desirable to examine molecules with predominant asymmetry in their atomic masses and the same varying by large margin from molecule to molecule, so that the effects, if any, due to other two factors may remain comparatively negligible. The asymmetry is expressed here as ρ , the ratio

of the heavier to the lighter atomic mass in the molecule. The molecules chosen for this investigation are listed below with their mass asymmetry ρ :

Molecule :	$B^{11}O^{16}$	$Al^{27}O^{16}$	$Ti^{48}O^{16}$	$V^{51}O^{16}$
Mass asymmetry : (ρ)	1.45	1.7	3.0	3.2

One of the atomic masses, i.e. oxygen in the above series of molecules, is a constant and the other varies from B^{11} to V^{51} , giving a range of variability of ρ from 1.45 to 3.2. Thus, if asymmetry has any effect, it can very well be seen by the observed change of transition probability from molecule to molecule. The isotopic molecules are not chosen as they do not give a large range of variability in ρ and hence they are not considered to be of much consequence for the purpose of this problem.

The theoretical computations of transition probabilities are available in the case of one of these molecules, i.e. BO, through the work of Elliott (1933). In three others, the theoretical computations have been actually carried out in this work for the available 22 bands of $AlO \ ^2\Sigma - ^2\Sigma$, 23 bands of $TiO \ ^3\P - ^3\P$ and 19 bands of $VO \ ^2\Delta - ^2\Delta$ systems.

The experimental values of transition probabilities are already available for AlO and BO from the work of Tawde and Husain (1949) and Tawde and Trivedi (1939) and in the case of BO from the work of Elliott (1933). For the other systems, viz. TiO and VO , accurate determinations of intensity distributions have been made in the present work.

EXPERIMENTAL

The molecules TiO and VO were excited in carbon arc in air at atmospheric pressure. The source for TiO was titanium oxide in the powder form, which was packed in lower positive carbon electrode having 6 mm. diameter. The arc was fed from 230 volts D.C. mains with a suitable series resistance to obtain the desired current. Similar arrangement was made for exciting VO bands from the substance vanadic oxide. As the systems of TiO and VO chosen for study lie mostly in visible region, a Hilger glass prism spectrograph with a dispersion of 11 A.U. at 4200 λ and 44 A.U. at 6000 λ was employed.

The technique of photographic photometry was followed for quantitative estimation of intensities, which are taken as peak values near the band heads. This technique has been elaborated sufficiently in earlier papers particularly of Johnson and Tawde (1932), Tawde and Desai (1937) and Tawde and Patankar (1940). These values have been utilized to arrive at the estimation of experimental transition probabilities as the ratio $(I/\nu^4)v'v''/\sum I/\nu^4$ which could be very easily deduced from the measured values of I for each band.

The study of various aspects of intensity distributions other than the asymmetry effect in the band systems, are being reported elsewhere. For the relevance of the present problem, it was necessary to have only the comparison of the resulting values of experimental transition probabilities with the theoretical derivations from the analytical method of Hutchisson, employing harmonic oscillator. This theoretical derivation is indicated briefly in the following section.

THEORETICAL

According to Hutchisson (1930) the square of the following expression $P_{v',v''}$ gives the transition probability between vibrational levels v' and v'' :

$$P_{v',v''} = C_3 \frac{(v'!v''!)^{\frac{1}{2}}}{2^{(v'+v'')/2}} \sum_{l=0}^{v' \text{ or } v''} \sum_{i=0}^{(v'-l-1)'} \sum_{j=0}^{(v''-l-1)''} a_{2l} b_{2i} c_{2j} d_{v'-2i-l} e_{v''-2j-l},$$

where C_3 , a , b , c , d , e are expressible in terms of the quantities α and δ such that

$$\alpha = (\omega_0''/\omega_0')^{\frac{1}{2}}$$

$$\delta = 2\pi(\omega_0''\mu)^{\frac{1}{2}}(r_0' - r_0'')/h^{\frac{1}{2}}$$

involving the known constants ω_0 , ω_0'' , r_0 , r_0'' and μ of the molecule.

From the above expression with the knowledge of various available constants (Herzberg, 1950) for the band systems of AlO, TiO and VO used here, the transition probabilities have been calculated. Such calculations on the β bands of BO are utilised from the earlier work of Elliott (1933).

RESULTS AND CONCLUSIONS

Table I below gives the calculated theoretical values of bands for the systems studied under the column marked T in each case. The corresponding experimental value is entered side by side in column marked E.

By comparison of the two sets of values in Table I above, the number of bands showing approximately closer agreement for the molecules has been arrived at and the agreement is expressed on percentage basis as the ratio of this number to the total number of excitable bands of the system multiplied by 100. The results of this percentage agreement as a function of mass asymmetry are recorded in Table II.

It would be seen from Table II that the degree of agreement between theory and experiment is a function, among others, of the closeness in the two nuclear mass, i.e. mass symmetry. The closer the masses are, the better the agreement. The agreement is expected to deteriorate at higher quanta and

TABLE I

v', v''	$B^{11}O^{16}$		$Al^{27}O^{16}$		$Ti^{48}O^{16}$		$V^{51}O^{16}$	
	T	E	T	E	T	E	T	E
0, 0	0.20	0.24	0.73	0.51	0.45	0.42	0.11	0.35
0, 1	0.37	0.25	0.26	0.24	0.44	0.19	0.27	0.36
0, 2	0.28	0.30	0.03	0.10	0.22	0.13	0.67	0.45
0, 3	0.10	0.17	0.00	0.15	0.06	0.20	0.98	0.48
0, 4	—	—	—	—	0.01	—	0.48	0.20
0, 5	—	—	—	—	—	—	0.43	—
1, 0	0.25	0.25	0.22	0.28	0.37	0.37	0.34	0.41
1, 1	0.10	0.06	0.33	0.21	0.00	0.06	0.43	0.06
1, 2	0.06	—	0.40	0.22	0.38	0.11	0.32	0.14
1, 3	p.29	0.16	0.09	0.16	0.51	0.36	0.02	0.51
1, 4	—	—	0.01	0.10	0.18	0.21	0.10	0.31
1, 5	—	—	—	—	0.04	—	0.50	0.61
2, 0	0.21	0.29	0.05	0.21	0.19	0.21	0.56	0.23
2, 1	0.006	—	0.30	0.32	0.18	0.10	0.26	0.17
2, 2	0.14	0.13	0.12	0.12	—	—	0.00 ₁	0.40
2, 3	0.006	—	0.46	0.21	0.17	0.24	—	—
2, 4	—	—	0.18	0.17	0.55	0.33	0.26	0.24
2, 5	—	—	—	—	0.42	0.59	0.07	0.39
3, 0	0.14	0.13	—	—	—	—	—	—
3, 1	0.07	0.21	0.11	0.22	0.33	0.21	0.04	0.41
3, 2	0.05	0.05	0.28	0.35	—	—	—	—
3, 3	0.06	0.04	—	—	0.25	0.20	—	—
3, 4	—	—	0.51	0.25	—	—	—	—
3, 5	—	—	—	—	0.55	0.40	—	—
4, 0	0.08	0.08	—	—	—	—	—	—
4, 1	0.56	0.22	—	—	0.15	0.43	—	—
4, 2	0.00	0.02	0.16	0.20	0.19	0.26	—	—
4, 3	0.09	0.20	0.24	0.37	—	—	—	—
4, 4	—	—	—	—	0.26	0.45	0.16	0.25
5, 1	0.12	0.15	—	—	—	—	—	—
5, 2	0.03	0.18	—	—	0.21	0.50	—	—
5, 3	0.01	—	0.21	0.16	—	—	—	—
5, 4	—	—	0.18	0.32	—	—	—	—
6, 4	—	—	0.12	0.17	—	—	—	—

N.B.—Pairs of values under T and E considered approximately close are entered in italics.

TABLE II

Molecule	Mass asymmetry ρ	Number of bands in approximate agreement	% of agreement
$B^{11}O^{16}$	1.45	12 in 19	63
$Al^{27}O^{16}$	1.7	9 in 22	41
$Ti^{48}O^{16}$	3.0	7 in 21	33
$V^{51}O^{16}$	3.2	3 in 18	17

with electrical anharmonicity in each case. These two factors, however, are not expected to change the measure of agreement by such a wide margin from molecule to molecule as obtained. Hence the effect seen here seems to be predominantly due to mass disparity between the two atoms, forming the molecule. It is thus obvious from the results of these experiments that in any application of Hutchisson's theory to diatomic molecules, effect of large mass asymmetry of the constituent atoms would have to be taken account of. The implied assumption of some that, it should be as much applicable to asymmetric molecules as to symmetric ones, has thus its limitations to the extent indicated above.

ACKNOWLEDGMENTS

The work incorporated in this paper was a part problem of the larger investigations carried out at the Physics Department of the Institute of Science, Bombay, when the authors were at the Institution prior to 1954. One of the authors (P.V.C.) conveys his thanks to the University of Bombay for the award of post-graduate research studentship, which has enabled this investigation to be completed.

REFERENCES

- Dunham, J. L., 1930, *Phys. Rev.* **36**, 1553.
Elliott, A., 1933, *Proc. Phys. Soc.* **45**, 627.
Herzberg, G., 1950, *Molecular Spectra and Molecular Structure*—2nd Edn. D. Van Nostrand Co., New York.
Hutchisson, E., 1930, *Phys. Rev.* **36**, 410.
Johnson, R. C. and Tawde N. R., 1932, *Proc. Roy. Soc.* **A137**, 575.
McKellar, A., and Buscombe, W., 1948, *Pub. Dom. A. P. Ob.* **7**, 361.
Tawde, N. R., and Desai, D. D., 1937, *Proc. Ind. Acad. Sc.* **6**, 266.
Tawde, N. R., and Husain, A. G., 1949, *Bom. Univ. J.*, **17**, 12.
Tawde, N. R., and Patankar, V. S. 1940, *Bom. Univ. J.* **9**, 16.
Tawde, N. R. and Trivedi, S. A., 1939, *Proc. Phys. Soc.* **51**, 733.

ON TWO DIRECTIONAL FOCUSSING MAGNETIC ANALYSERS

BY S. B. KARMOHAPATRA

INSTITUTE OF NUCLEAR PHYSICS, CALCUTTA UNIVERSITY, CALCUTTA-9

(Received for publication, June 17, 1955)

ABSTRACT. Design parameters for a symmetrical two directional non-uniform magnetic analyser are considered. Suggestions are made for achieving second order radial focussing effect by properly shaping the pole edges of the first order focussing conical magnets having an angle $< \sqrt{2}\pi$. The advantage of such a 180° magnet for mass-spectrometry is discussed in consideration with the resolving power and solid angle.

Since the introduction of a non-uniform magnetic field for decreasing the radial and axial oscillations of electrons in a betatron, magnetic analysers using inhomogeneous magnetic fields have been important for improved focussing of charged particles in β -ray spectrometers, nuclear spectrometers and mass-spectrometers. The field shape of a betatron magnet, derived by Kerst and Serber (1941) is

$$H = H_0 \left(\frac{a}{r} \right)^n \quad \dots (1)$$

where H_0 is the field at the equilibrium orbit of the charged particles of radius a , and the field index $n = -\frac{r}{H} \frac{\partial H}{\partial r}$ of the axially varying field H .

Expanding equation (1) according to Shull and Dennison (1947) we get the series, representing the vertical component of such a field,

$$H_z = H_0(1 - \alpha\delta + \beta\delta^2 \dots) \quad \dots (2)$$

where $\alpha = n$, $\beta = \frac{n^2 + n}{2}$, $\delta = \frac{r - a}{a}$, where $r = a + dr$. Since $\text{curl } H = 0$, the radial component of the field will be

$$Hr = 2H_0 \left[-\frac{\alpha}{a} + \frac{2\beta(r-a)}{a^2} \right] \quad \dots (3)$$

For two directional focussing of charged particles with such a non-uniform field, n should be greater than zero and less than unity. The angular frequency of the radial and axial oscillation in such a field can be shown to be $\omega_r = (1-n)\omega_0$ and $\omega_a = n\omega_0$ respectively, where ω_0 is the orbital frequency of the accelerated charged particle. Putting $n = \frac{1}{2}$, we have $\omega_r = \omega_a$ and the image is focussed at an angle $\sqrt{2}\pi$.

* Communicated by Prof. B. D. Nag Choudhury.

Siegbahn and Svartholm (1946) have constructed a β -ray spectrometer with such a non-uniform magnet and now these magnetic analysers are widely used in β -ray spectrometry. From the expression (2) it is evident that a perfect magnet pole face of this type, satisfying higher order focussing, is difficult to achieve. So the nearest approaches have been attempted by different authors (Vers ter, 1950 and Siegbahn *et al* (1946).

Taking the first term of the expression (2), first order two directional focussing of charged particles can, conveniently, be achieved. In this case, the pole face has a conical shape, the cone angle η being equal to $\tan^{-1} \frac{nb}{a}$, where $2b$ is the gap width of the magnet at the equilibrium orbit of radius a , field index $n = \frac{1}{2}$. For achieving higher resolving power, elimination of second order aberration is to be considered. Shull and Dennison (1947) have shown that for $\beta = 3/8$ or $1/8$ the second order aberration in axial or radial focussing respectively, can be eliminated. As there is no single value of β for second order focussing in both the directions, Rosenblum (1950) suggests the value of β equal to $1/4$ for an average better focussing in both the directions.

Focussing of charged particles at an angle $\sqrt{2}\pi$ with this non-uniform field is equivalent to a single directional focussing homogeneous 180° magnetic analyser after Dempster (1918) in the respect that the source and detector are to be placed within the magnetic field. Though the weight of magnetic material is minimised by using a ring magnet in the case of non-uniform magnetic analysers, yet the convenience of placing the source and detector out of the magnetic field can not be denied. Judd (1950) and Rosenblum (1950) have, independently, worked out the feasibility of focussing of the charged particles with such a non-uniform magnetic field at a smaller angle than $\sqrt{2}\pi$. Synder and others (1950) have used a 180° non-uniform first order focussing magnetic analyser for nuclear spectrometry. They have used such a magnetic analyser with source and detector placed at unequal distances from the pole boundary. So far the design of a symmetrical magnetic analyser of this type, having a focussing angle less than $\sqrt{2}\pi$, is not reported. But for mass-spectrometry, where focussing at a constant radius is important, a symmetrical non-uniform analyser is very convenient.

For $n = \frac{1}{2}$, Rosenblum has worked out the following expression for a first order focussing magnetic analyser.

$$l'' = \frac{l'/n^{\frac{1}{2}}(\cot n^{\frac{1}{2}}\phi) + \frac{1}{n}}{l' - \left(\frac{1}{n^{\frac{1}{2}}}\right) \cot n^{\frac{1}{2}}\phi} \quad \dots \quad (4)$$

where l' and l'' are the distances of the source and the detector, respectively, from pole edges in units of radius of curvature a of the equilibrium orbit, ϕ is the focussing angle. We may derive an expression for $l = l' = l''$ representing the

distance of such a magnetic analyser of symmetrical type from (4) and rejecting the negative term.

$$l = \sqrt{2} \frac{\cos \phi / \sqrt{2} + 1}{\sin \phi / \sqrt{2}} \quad \text{for } n = \frac{1}{2} \quad \dots (5)$$

Putting $\phi = \sqrt{2}\pi$ in exp. (5) l becomes zero which is the case deduced by Shull and Dennison (1947) and Svartholm (1946) independently.

In the same expression

$$\text{when} \quad \phi = \pi, \quad l = .7 \quad \dots (6)$$

$$\text{and for} \quad \phi = \pi/2, \quad l = 2.3 \quad \dots (7)$$

Here the values of l are in units of radius of curvature a . The correctness of these values can independently be checked from the expression, derived from Judd's (1950)

$$l_2 = -\sqrt{2} a \tan [\phi / \sqrt{2} + \tan^{-1} l_1 / \sqrt{2} a]$$

where l_1 and l_2 are distances in centimeters of the source and detector respectively from the magnet.

For focussing of charged particles with a first order focussing effect non-uniform magnetic fields having an angle smaller than $\sqrt{2}\pi$ can easily be achieved by shaping the pole faces conically as described before. For second order focussing, instead of shaping the pole face for a suitable value of β , we may attempt to eliminate the radial second order aberration by shaping the pole edges as given by Hintenberger (1948) for the single directional focussing magnetic analyser

According to him, with a magnetic analyser satisfying the first order focussing condition, the condition for second order focussing is

$$a \left(\frac{\gamma_1}{R_1} + \frac{\gamma_2}{R_2} \right) = c_1 + c_2 \quad \dots (9)$$

where a is the radius of curvature of the orbit of the particle, and the constants

$$\begin{aligned} \gamma_1 &= \frac{1}{\cos^3 \epsilon_1} \left\{ \left[1 + \left(\frac{a}{l_1} + \tan \epsilon_1 \right)^2 \right]^3 \right\}^{\frac{1}{4}} \\ \gamma_2 &= \frac{1}{\cos^3 \epsilon_2} \left\{ \left[1 + \left(\frac{a}{l_2} + \tan \epsilon_2 \right)^2 \right]^3 \right\}^{\frac{1}{4}} \\ c_1 &= \frac{a^2}{l_1^2} \left\{ \left[1 + \left(\frac{a}{l_1} + \tan \epsilon_1 \right)^2 \right]^3 \right\}^{\frac{1}{4}} \\ c_2 &= \frac{a^2}{l_2^2} \left\{ \left[1 + \left(\frac{a}{l_2} + \tan \epsilon_2 \right)^2 \right]^3 \right\}^{\frac{1}{4}} \end{aligned}$$

Here R_1, R_2 are the radii of curvature of the entrance and exit boundary of the field, ϵ_1, ϵ_2 are the angles made by the central beam of the particles with the

normal at the entrance and exit of the pole boundary, respectively, a is the radius of curvature of the path of the particle.

From the above expression (9) it is possible to construct two types of sector-shaped magnetic spectrometers as follows:

1. *Normal circle type* : In this type $\epsilon_1 = \epsilon_2 = 0$ and pole edges are circular having radii of curvature R_1 and R_2 at entrance and exit, respectively.

2. *Inflection type* : Kerwin (1949) derived an expression for the pole edge for perfect focussing, which is a curve, having a point of inflection. Linear approximation of such curves, drawing a straight line through this point of inflection, can be done so as to achieve a second order focussing effect. This may be compared with the expression (9) when $R_1 = R_2 = \infty$ and $\epsilon_1, \epsilon_2 \neq 0$.

In the gap of a homogeneous magnet, $H_x = H_y = 0$, H_z component in z -direction is responsible for the radial focussing of charged particles. But at the entrance and exit of the magnet the fringing field has a finite H_y component, which may axially defocus the charged particles in case of the inflection type spectrometers. So the normal circle type, where $\epsilon_1 = \epsilon_2 = 0$ and thus $H_y = 0$ in the fringing field region, is better than the inflection type.

In the two directional focussing magnetic analysers, radial focussing is responsible for the resolving power and the axial focussing for intensity. For $n = \frac{1}{2}$, in a non-uniform magnetic analyser having a conical pole face first order radial focusing condition is satisfied and Hintenberger's formula for second order radial focussing can conveniently be applied. So by shaping the pole edges, increased resolving power can be attained for the same solid angle. From (9) we have $R = l^3$ where $\epsilon_1 = \epsilon_2 = 0$ and $l' = l'' = l$, $R_1 = R_2 = R$ for symmetrical cases, R and l being in units of radius of curvature a .

Putting the values of l for $\phi = \pi$ and $\pi/2$ from (6) and (7) we have

$R = .343$ and 12.17 for the said focussing angles respectively.

In the case of a non-uniform magnet having an angle of focussing $\sqrt{2}\pi$ the conjugate foci lie in the field. So second order correction here is only possible by choosing a suitable value of β in eqn. (2). But for all the magnets having an angle $< \sqrt{2}\pi$ second order focussing can be achieved by shaping the pole edges as described. Radii of curvature of the pole edges for such magnets are derived for the two specific cases, i.e. $\phi = \pi$ and $\pi/2$. It is evident that intensity decreases for greater l . Moreover for increased l , the radii of curvature of pole edges are so large, that such shaping requires a more precision craftsmanship.

Though for all angles $< \sqrt{2}\pi$, the pole edges of this type of non-uniform magnetic analysers can be properly shaped for second order focussing effect, yet $\phi = \pi$ is preferred for high intensity mass spectrometry because of the fact that the pole faces can be machined simultaneously and the source and the detector can conveniently be placed outside the magnetic field. For $\phi = \sqrt{2}\pi$, the first order

focussing magnetic analyser has a maximum solid angle for a given resolving power. In the case of a magnetic analyser having $\phi = \pi$, the decreased intensity can be compensated by utilising the above mentioned second order focussing device for the same resolving power or when a better resolving power is essential at the cost of solid angle, such 180° magnetic analysers, having shaped pole edges, are superior to those having $\phi = \sqrt{2}\pi$.

ACKNOWLEDGMENTS

The author is thankful to Prof. B. D. Nag Choudhury for his guidance and to Prof. M. N. Saha for his interest in this work following the design of a high intensity mass spectrometer for this laboratory.

REFERENCES

- Dempster, A. J., 1918, *Phys. Rev.*, **11**, 316.
 Hintenberger, H., 1948, *Z. Naturforsch.*, **3a**, 125.
 Judd, D. L., 1950, *Rev. Sci. Inst.*, **21**, 213.
 Kerst, D. W. and Serber, R., 1941, *Phys. Rev.*, **60**, 53.
 Kerwin, L., 1949, *Rev. Sci. Inst.*, **20**, 36.
 Rosenblum, E. S., 1950, *Rev. Sci. Inst.*, **21**, 586.
 Shull, F. B. and Dennison, D. M., 1947, *Phys. Rev.*, **71**, 681.
 Siegbahn, K. and Svartholm, N., 1946, *Arch. Math. Astorn. Fysik*, **38A**, No. 21.
 Snyder, C. W., Rubin, S., Fowler, W. A. and Lauritsen, C. C., 1950, *Rev. Sci. Inst.*, **21**, 852.
 Verster, N. F., 1950, *Physica*, **19**, 815.

DIPOLE MOMENT OF INDENE

BY D. V. G. L. NARASIMHA RAO

PHYSICS DEPARTMENT, ANDHRA UNIVERSITY, WALTAIR.

(Received for publication, April 30, 1955; received after revision, July, 7, 1955)

ABSTRACT. The dipole moment of indene is determined in three non-polar solvents—cyclohexane, CCl_4 and CS_2 covering a dielectric constant range of about 2.0 to 2.6. The experimental observations are treated in the manner of Guggenheim for obtaining the dipole moment values. The high value of about 0.85 D obtained for the moment of the compound is suggested as probably arising out of the resonance of the molecule between various structures as in the case of the related compounds cyclopentadiene and fluorene.

INTRODUCTION

There are two published reports of dipole moment determinations for indene; (1) by S. Lee (1940) and (2) by Syrkin and Shott Lvova (1944). Both were made in benzene as solvent and the values reported are 0.44 and 0.67 D respectively. Syrkin and Shott Lvova seem to have used the Hedestrand method (1929) for the computation of the moment. On account of the large difference in their values, a redetermination is considered desirable. Hence the present work is undertaken and the dipole moment determined in three non-polar solvents—cyclohexane, carbon tetrachloride and carbon disulphide, covering a dielectric constant range of about 2.0 to 2.6. The results were briefly reported previously (Rao, 1954).

EXPERIMENTAL

The various solutions are made up by weight and the dielectric constants determined by the usual heterodyne beat method, with a crystal oscillator at a frequency of 3.56 Mc/sec. The refractive indices are measured on a Pulfrich refractometer.

The sample of indene obtained from L. Lights and Co. Ltd, is distilled and the fraction condensing in the temperature range 181° — 182°C is collected. This liquid is used in the experiment. The solvents are analytical reagents from E. Merck.

Details of the results are shown in Tables I to IV.

RESULTS

TABLE I

Indene in cyclohexane

Temperature = 31.5°C ;

density of cyclohexane = 0.8052 gm/c.c.

w	ϵ_{12}	$\Delta\epsilon$	$\Delta\epsilon/w$	n_{12}	n^2_{12}	Δn^2	$\Delta n^2/w$
—	2.0076	—	—	1.41981	2.01585	—	—
0.00982	2.0172	0.0096	0.978	1.42148	2.02061	0.00476	0.485
0.01786	2.0247	0.0171	0.957	1.42273	2.02416	0.00831	0.465
0.02538	0.0303	0.0227	0.894	1.42390	2.02749	0.01164	0.459
0.03485	2.0379	0.0303	0.869	1.42520	2.03119	0.01534	0.440
0.04590	2.0441	0.0365	0.795	1.42644	2.03472	0.01887	0.411
0.05746	2.0492	0.0416	0.724	1.42800	2.03919	0.02334	0.406

$$(\Delta\epsilon/w) = 1.025$$

$$w \rightarrow 0$$

$$(\Delta n^2/w) = 0.502$$

$$w \rightarrow 0$$

$$(\Delta/w) = 0.523 \text{ (graphical)}$$

$$w \rightarrow 0$$

$$P_0 = 14.08 \text{ c.c.}$$

$$\mu = 0.84 D.$$

TABLE II

Indene in CCl_4

Temperature = 31.5°C ;

density of CCl_4 = 1.5785 gm/c.c.

w	ϵ_{12}	$\Delta\epsilon$	$\Delta\epsilon/w$	n_{12}	n^2_{12}	Δn^2	$\Delta n^2/w$
—	2.2215	—	—	1.45266	2.11022	—	—
0.00361	2.2292	0.0077	2.133	1.45392	2.11388	0.00366	1.014
0.00536	2.2328	0.0113	2.108	1.45445	2.11543	0.00521	0.972
0.00829	2.2377	0.0162	1.954	1.45522	2.11768	0.00746	0.900
0.01164	2.2434	0.0219	1.881	1.45591	2.11967	0.00945	0.812
0.01734	2.2522	0.0307	1.771	1.45683	2.12236	0.01214	0.700
0.02342	2.2572	0.0357	1.524	1.45748	2.12396	0.01374	0.587

$$(\Delta\epsilon/w) = 2.260$$

$$w \rightarrow 0$$

$$(\Delta n^2/w) = 1.088$$

$$w \rightarrow 0$$

$$(\Delta/w) = 1.172 \text{ (graphical)}$$

$$w \rightarrow 0$$

$$P_0 = 14.52 \text{ c.c.}$$

$$\mu = 0.85 D.$$

TABLE III
Indene in CS₂

Temperature = 31.5°C ;

density of CS₂ = 1.2545 gm/c.c.

w	ϵ_{12}	$\Delta\epsilon$	$\Delta\epsilon/w$	n_{12}	n^2_{12}	Δn^2 (—)	$\Delta n^2/w$ (—)
—	2.6212	—	—	1.62173	2.63001	—	—
0.00925	2.6231	0.0019	0.205	1.61917	2.62171	0.00830	0.897
0.01384	2.6250	0.0038	0.275	1.61832	2.61895	0.01106	0.799
0.02074	2.6288	0.0076	0.367	1.61752	2.61638	0.01363	0.657
0.02786	2.6326	0.0114	0.409	1.61745	2.61614	0.01387	0.498
0.03048	2.6357	0.0145	0.476	1.61742	2.61605	0.01396	0.458

2

 $(\Delta\epsilon/w) = 0.130$
 $w \rightarrow 0$
 $(\Delta n^2/w) = -1.085$
 $w \rightarrow 0$
 $(\Delta/w) = 1.215$ (graphical)
 $w \rightarrow 0$
 $P_0 = 15.79$ e.c. $\mu = 0.89$ D.

The final values of the dipole moments are given in Table IV.

TABLE IV

Solvent	Dielectric constant of solvent	Orientation polarisation P_0 , e.c.	Dipole moment in Debye units
Cyclohexane	2.0076	14.08 (13.96)	0.84 (0.84)
CCl ₄	2.2215	14.52 (15.41)	0.85 (0.88)
CS ₂	2.6212	15.79 (15.57)	0.89 (0.89)

DISCUSSION

Syrkin and Shott- Lvova claimed that their value (0.67D) is more accurate than the previously published determination by S. Lee (0.44D). The value obtained in the present investigation (approximately 0.85D) is higher than even Syrkin's. Differences in dipole moment values are often attributed to the method of computation, (e.g. different values obtained in nitrobenzene), although, in the present case, the difference is much too large to be accounted for on this ground. The author has used the modified Guggenheim method (1951) while Syrkin's estimate was based on the Hedestrand method. The important differences between the two methods are (1) in the treatment of the atom polarisation, (2), in the use of

linear or a more general parabolic relation between $\epsilon_{12}-w$, ϵ_{12} being the dielectric constant of the solution and w the weight fraction of the solute, and (3) in the use of densities or elimination of density determinations. The Guggenheim method is considered generally to lead to more reliable values of the dipole moments. Further, the consistent values obtained in the three different solvents studied may indicate the correctness of the value obtained by the author.

A more general equation for the computation of the dipole moment is given by Palit (1952) which reduces to that of Guggenheim under some simplified conditions. When the results in the present case are recalculated using the equation of Palit, the values of P_0 and μ given in brackets in Table IV are obtained. The values of β_0 are calculated from refractive measurements alone as indicated by Palit. It will be noted that the neglected term in the Guggenheim equation has no effect on the moment in the case of the solvents cyclohexane and carbon disulphide but is pronounced in the case of carbon tetrachloride.

An approximate estimate of the moment of indene may be derived from general considerations based on the structure of the molecule represented in figure 1.

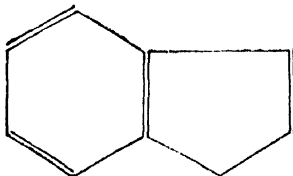


Fig. 1. Structure of indene.

For such an estimate, the methylene group only need be considered. Assuming that two C-H bonds, each of moment $0.40D$, interact at the tetrahedral angle of $109^{\circ}28'$, the moment of the methylene group would be $0.46D$ in fair agreement with the value obtained by Lee. However, such simple considerations are known to give erroneous values. For instance, the moment of diphenyl methane is only $0.23D$ much below the estimated value. The errors arise from the fact that the moment of a particular bond may vary with the nature of the ring as is observed from a general review of the large amount of data on ring compounds. For indene, if inductive and other influences such, as resonance, are absent, a low value might be anticipated. The observed high value may therefore be explained as due to an inductive or a resonance effect. Judged from the moments of pyrrole and indole (1.84 , $2.02D$), thiophene and thionaphthene (0.53 , $0.68D$) and indene and fluorene (0.85 -author, 0.82 -Le Fevre) inductive effects do not seem to play a very important role in these ring systems. The resonance of the molecule between the various structures may have led to the high value in the case of the related compounds cyclopentadiene and fluorene.

ACKNOWLEDGMENTS

The author is deeply indebted to Prof. K. R. Rao for his kind and invaluable guidance throughout the progress of the work. The author also thanks the Government of India for the award of a Junior research scholarship.

REFERENCES

- Guggenheim, E. A., 1951, *Trans. Farad. Soc.*, **47**, 573.
Hedestrand, 1929, *Z. Physik. Chem.*, **B2**, 428.
Lee, S., 1940, *J. Soc. Chem. Ind. Japan*, **43**, (in German).
Narasimha Rao, D. V. G. L., 1954, *Current Science*, **23**, 236.
Palit, Santi R., 1952, *Journ. Am. Chem. Soc.*, **74**, 3952.
Syrkin and Shott Lvova, 1944, *Acta Physikochim, U.S.S.R.*, **19**, 379.

FLEXURE OF THIN ELASTIC PLATES UNDER SPECIFIED EDGE TRACTIONS

BY V. CADAMBE, R. K. KAUL AND S. G. TEWARI

NATIONAL PHYSICAL LABORATORY OF INDIA, NEW DELHI.

(Received for publication, March 26, 1955)

ABSTRACT. The solution of the deflection surface of an isotropic bent plate characterised by fourth order Lagrange's differential equation is a difficult problem, especially if the boundary conditions contain higher order partial differential relations. To make it simpler, this problem is replaced by two second order simultaneous differential equations in U and V defining the bending and twisting moments in the plate. For problems where boundary tractions are known, it becomes more convenient to work in terms of U and V , since the partial differential relations between the derivatives in w are replaced by known values of these new functions at the free edges, and linear combinations of their first order derivatives at the clamped edges. In addition, the relaxation method when applied to the simultaneous equations so obtained leads to rapid convergence unlike in the case of the bi-harmonic equation. The Southwell differential equations and the boundary conditions are, therefore, derived by variational principles and to illustrate the definite advantage of the process, two typical examples are also worked.

NOTATIONS

- α = Angle between x -axis and outward drawn normal n measured in the clockwise sense.
- n, t = Normal and tangential coordinates along the curvilinear boundary taken positive when t is to n as y is to x .
- s = Distance along the edge measured positive in the clockwise direction.
- x, y, z = Rectangular coordinates.
- M_x, M_y, T_{xy} = Intensity of bending and twisting moments in the plate.
- Q_x, Q_y = Resultant shearing forces per unit length normal to the middle surface.
- $q(x, y)$ = Intensity of uniformly distributed load per unit area of the middle surface of the plate.
- ϕ = A function defined by the equation $D\nabla^2\phi = q$.
- w = Lateral deflection of the median surface.
- h = Thickness of the plate.
- D = Flexural rigidity of the plate = $Eh^3/12(1-\nu^2)$
- E, ν = Modulus of elasticity and Poisson's ratio of the plate material.
- U, V = Two functions defining the bending and twisting moments in the plate.
- Π^* = Complementary strain energy.
- J^* = Elastic strain energy.
- Z_i^n = Surface tractions normal to the edge along the coordinate directions.
- RU, RV = Residual formulae in relaxation.
- δ = A variational symbol.
- λ = Mesh-size used in finite difference relations.

INTRODUCTION

The small deflection theory of thin isotropic plates, based on the simplified assumptions of inextensibility of the middle surface and that the deflection surface is a *developable*, leads to fourth order Lagrange's differential equation $D\nabla^4 w = q(x,y)$ and is inconvenient to solve especially if the plate edges are free, since Kelvin and Tait boundary conditions for such edges are

$$M_n = 0 \quad \text{and} \quad (Q_n - \partial T_{nt}/\partial s) = 0$$

which contain partial differential relations of higher order in w .

By introducing two new functions U and V , defining the moments in the plate and analogous to the equilibrium displacement components u and v , Southwell (1950) showed that the problem of flexure of bent plate with specified edge tractions can be solved quite conveniently by replacing the Lagrange's differential equation by two simultaneous equations of the form

$$A \frac{\partial^2 U}{\partial x^2} + B \frac{\partial^2 U}{\partial y^2} + C \frac{\partial^2 V}{\partial x \partial y} = f_1(x,y)$$

$$B \frac{\partial^2 V}{\partial x^2} + A \frac{\partial^2 V}{\partial y^2} + C \frac{\partial^2 U}{\partial x \partial y} = f_2(x,y)$$

The boundary conditions for such a differential equation are $U = k_1$, $V = k_2$ when the boundary edges are free and involve two linear combinations of their derivatives,

$$l_1 \frac{\partial U}{\partial x} + m_1 \frac{\partial U}{\partial y} + n_1 \frac{\partial V}{\partial x} + p_1 \frac{\partial V}{\partial y} = k_3$$

$$l_2 \frac{\partial U}{\partial x} + m_2 \frac{\partial U}{\partial y} + n_2 \frac{\partial V}{\partial x} + p_2 \frac{\partial V}{\partial y} = k_4$$

when boundary is clamped.

A distinct advantage over Lagrange's equation is that at free edges, where Kelvin and Tait boundary conditions involve second and third order partial derivatives of plate deflection w , the Southwell field equations require only U and V to be specified. Moreover, at the clamped edges, the boundary conditions involve only the linear combination of their first order derivatives. Thus in the case of plates with edge tractions specified on the free boundary, Southwell's equations are distinctly easier to solve than the equation of Lagrange.

The two simultaneous differential equations and the associated *natural boundary conditions* are therefore derived afresh by variational principles. Kirchhoff used the same analysis, for establishing the free edge boundary conditions of the deflection surface of laterally loaded thin isotropic plates. (Timoshenko, 1940).

T H E O R Y

If we consider a plate element and represent bending and twisting couples by means of right handed vectors, such that the positive value of these moments are represented by vectors in the positive directions of normal and tangential coordinates n and t then from the conditions of static equilibrium, the three equations are (Timoshenko, 1940)

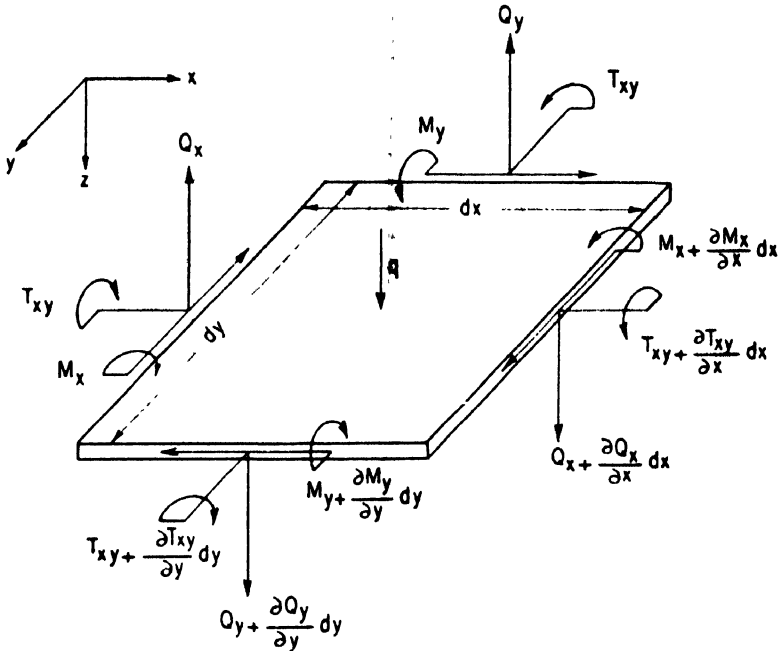


Fig. 1.—Element of plate under transverse load and the resulting couples and reactive forces.

$$\left. \begin{aligned} \frac{\partial M_x}{\partial x} + \frac{\partial T_{xy}}{\partial y} - Q_x &= 0 \\ \frac{\partial T_{xy}}{\partial x} + \frac{\partial M_y}{\partial y} - Q_y &= 0 \\ \frac{\partial Q_x}{\partial x} + \frac{\partial Q_y}{\partial y} + q &= 0 \end{aligned} \right\} \quad (1)$$

From the first two of equation (1), one gets

$$\frac{\partial^2 M_x}{\partial x^2} + 2 \frac{\partial^2 T_{xy}}{\partial x \partial y} + \frac{\partial^2 M_y}{\partial y^2} + q = 0 \quad (2)$$

If the lateral loading $q(x,y)$ on the plate surface is analytic and satisfies the harmonic relation $D\nabla^2\phi = q$, then equation (2) becomes

$$-\frac{\partial^2}{\partial x^2}(M_x + D\phi) + 2 \frac{\partial^2 T_{xy}}{\partial x \partial y} + \frac{\partial^2}{\partial y^2}(M_y + D\phi) = 0$$

This equation is satisfied for

$$\left. \begin{aligned} M_x &= \frac{\partial V}{\partial y} - D\phi \\ M_y &= \frac{\partial U}{\partial x} - D\phi \\ \text{and } T_{xy} &= -\frac{1}{2} \left(\frac{\partial V}{\partial x} + \frac{\partial U}{\partial y} \right) \end{aligned} \right\} \quad \dots (3)$$

where U and V are the two moment functions and ϕ the loading function which have to be determined. Substituting these in first and second of equation (1) we have on simplification

$$\left. \begin{aligned} Q_x &= \frac{1}{2} \frac{\partial}{\partial y} \left(\frac{\partial V}{\partial x} - \frac{\partial U}{\partial y} \right) - D \frac{\partial \phi}{\partial x} \\ Q_y &= -\frac{1}{2} \frac{\partial}{\partial x} \left(\frac{\partial V}{\partial x} - \frac{\partial U}{\partial y} \right) - D \frac{\partial \phi}{\partial y} \end{aligned} \right\} \quad \dots (4)$$

which satisfy last of equation (1) as well.

From the set of equations (4) we have

$$\begin{aligned} \frac{\partial}{\partial y} \left(\frac{\partial V}{\partial x} - \frac{\partial U}{\partial y} \right) &= 2 \left(Q_x + D \frac{\partial \phi}{\partial x} \right) \\ \frac{\partial}{\partial x} \left(\frac{\partial V}{\partial x} - \frac{\partial U}{\partial y} \right) &= -2 \left(Q_y + D \frac{\partial \phi}{\partial y} \right) \end{aligned}$$

and therefore,

$$\frac{\partial}{\partial s} \left(\frac{\partial V}{\partial x} - \frac{\partial U}{\partial y} \right) = 2 \left\{ \left(Q_x + D \frac{\partial \phi}{\partial x} \right) \cos \alpha + \left(Q_y + D \frac{\partial \phi}{\partial y} \right) \sin \alpha \right\}$$

$$\text{or } \frac{1}{2} \left(\frac{\partial V}{\partial x} - \frac{\partial U}{\partial y} \right) = \oint \left(Q_n + D \frac{\partial \phi}{\partial n} \right) ds + \text{constant} \quad \dots (5)$$

In the above equation if U and V are provisionally interpreted as displacements in the x and y direction, then

$$\frac{1}{2} \left(\frac{\partial V}{\partial x} - \frac{\partial U}{\partial y} \right) = \text{constant}$$

implies an average rotation of the line elements of an element of the plate in its own plane normal to z -axis. Since, rotation of the line elements in a free body does not change the magnitude of the stresses, one can take the constant term in the above equation as zero (Timoshenko and Goodier 1951). Therefore

$$\frac{1}{2} \left(\frac{\partial V}{\partial x} - \frac{\partial U}{\partial y} \right) = \oint \left(Q_n + D \frac{\partial \phi}{\partial n} \right) ds \quad \dots (6)$$

Combining equation (6) with last of equation (3), we have

$$\begin{aligned}\frac{\partial U}{\partial y} &= - \left[T_{xy} + \oint \left(Q_n + D \frac{\partial \phi}{\partial n} \right) ds \right] \\ &\dots (7) \\ \frac{\partial V}{\partial x} &= - \left[T_{xy} - \oint \left(Q_n + D \frac{\partial \phi}{\partial n} \right) ds \right]\end{aligned}$$

These two derivatives $\partial U/\partial y$ and $\partial V/\partial x$ together with the two derivatives $\partial U/\partial x$ and $\partial V/\partial y$ from equation (3) are needed for determining the boundary values of U and V in terms of specified edge tractions M_x , M_y , T_{xy} and ϕ .

For deriving the differential equation of the deflection surface of the bent plate and the *natural boundary conditions*, use is made of a minimal principle for stresses which states that for all stresses satisfying the conditions of equilibrium in the interior and on that part Σ_R of the boundary Σ where the surface forces \bar{Z}_i^n are prescribed, the actual state of stress is such as to minimise the expression, (Sokolnikoff, 1946)

$$\Pi^* = J^* - \int_{\Sigma_S} u_i \bar{Z}_i^n ds \quad (8)$$

In the case of plate which is clamped or free, the term under the integral sign in the above expression vanishes and therefore the complementary energy Π^* of the elastic system is equivalent to the elastic strain energy J^* , where

$$J^* = \frac{1}{2D(1-\nu^2)} \int \int \left[M_x^2 + M_y^2 - 2\nu M_x M_y + (1+\nu) T_{xy}^2 \right] dx dy \quad \dots (9)$$

Substituting for M_x , M_y , T_{xy} in terms of U and V , we have

$$\begin{aligned}J^* &= \frac{1}{2D(1-\nu^2)} \int \int \left[\left(\frac{\partial V}{\partial y} - D\phi \right)^2 + \left(\frac{\partial U}{\partial x} - D\phi \right)^2 \right. \\ &\quad \left. - 2\nu \left(\frac{\partial V}{\partial y} - D\phi \right) \left(\frac{\partial U}{\partial x} - D\phi \right) \right. \\ &\quad \left. + \frac{1+\nu}{2} \left(\frac{\partial V}{\partial x} + \frac{\partial U}{\partial y} \right)^2 \right] dx dy\end{aligned}$$

The theory of the calculus of variations tells that in order to obtain the Euler equations of a variational problem a necessary condition for the extremal is the vanishing of the first variation of the strain energy functional (Courant and

Hilbert, 1953). Therefore, taking the first variation of J^* with respect to δU and δV we have

$$\begin{aligned}\delta J^* = & \frac{1}{2D(1-\nu^2)} \int \int \left[\left\{ \left(\frac{\partial V}{\partial y} - D\phi \right) - \nu \left(\frac{\partial U}{\partial x} - D\phi \right) \right\} \frac{\partial \delta V}{\partial y} \right. \\ & + \frac{1+\nu}{2} \left(\frac{\partial V}{\partial x} + \frac{\partial U}{\partial y} \right) \left(\frac{\partial \delta V}{\partial x} + \frac{\partial \delta U}{\partial y} \right) \\ & \left. + \left\{ \left(\frac{\partial U}{\partial x} - D\phi \right) - \nu \left(\frac{\partial V}{\partial y} - D\phi \right) \right\} \frac{\partial \delta U}{\partial x} \right] dx dy\end{aligned}$$

Integrating by parts and using the following transformation

$$\begin{aligned}\int \int \frac{\partial F}{\partial x} dx dy &= \oint F dy = \oint F \cos \alpha ds \\ \int \int \frac{\partial F}{\partial y} dx dy &= - \oint F dx = \oint F \sin \alpha ds\end{aligned}$$

we find on integrating one of the terms

$$\begin{aligned}\int \int \left(\frac{\partial V}{\partial y} - D\phi \right) \frac{\partial \delta V}{\partial y} dx dy &= \int \int \left[\frac{\partial}{\partial y} \left(\frac{\partial V}{\partial y} - D\phi \right) \delta V - \left(\frac{\partial^2 V}{\partial y^2} - D \frac{\partial \phi}{\partial y} \right) \delta V \right] dx dy \\ &= \int \left(\frac{\partial V}{\partial y} - D\phi \right) \delta V \sin \alpha ds - \int \int \left(\frac{\partial^2 V}{\partial y^2} - D \frac{\partial \phi}{\partial y} \right) \delta V dx dy\end{aligned}$$

Transforming in the same manner, the other terms and collecting these, the first variation δJ^* is

$$\begin{aligned}\delta J^* = & \frac{1}{D(1-\nu^2)} \left[\int \left\{ \left(\frac{\partial V}{\partial y} - D\phi \right) \delta V \sin \alpha + \left(\frac{\partial U}{\partial x} - D\phi \right) \delta U \cos \alpha \right. \right. \\ & - \nu \left(\frac{\partial V}{\partial y} - D\phi \right) \delta U \cos \alpha - \nu \left(\frac{\partial U}{\partial x} - D\phi \right) \delta V \sin \alpha \\ & + \frac{1+\nu}{2} \left(\frac{\partial V}{\partial x} + \frac{\partial U}{\partial y} \right) \left(\delta U \sin \alpha + \delta V \cos \alpha \right) \Bigg] ds \\ & - \int \int \left\{ \left(\frac{\partial^2 V}{\partial y^2} - D \frac{\partial \phi}{\partial y} \right) \delta V + \left(\frac{\partial^2 U}{\partial x^2} - D \frac{\partial \phi}{\partial x} \right) \delta U \right. \\ & - \nu \left(\frac{\partial^2 V}{\partial x \partial y} - D \frac{\partial \phi}{\partial x} \right) \delta U - \nu \left(\frac{\partial^2 U}{\partial x \partial y} - D \frac{\partial \phi}{\partial y} \right) \delta V \Bigg\} \\ & + \frac{1+\nu}{2} \left\{ \left(\frac{\partial^2 V}{\partial x^2} + \frac{\partial^2 U}{\partial x \partial y} \right) \delta V + \left(\frac{\partial^2 U}{\partial y^2} + \frac{\partial^2 V}{\partial x \partial y} \right) \delta U \right\} dx dy \Bigg]\end{aligned}$$

Remembering that δU and δV are arbitrary, small variations satisfying the boundary conditions, we conclude that the first variation of strain energy $\delta J^* = 0$ will be satisfied only if the following four equations are satisfied.

$$\oint \left[\left(\frac{\partial U}{\partial x} - D\phi \right) \cos \alpha - \nu \left(\frac{\partial V}{\partial y} - D\phi \right) \cos \alpha + \frac{1+\nu}{2} \left(\frac{\partial V}{\partial x} + \frac{\partial U}{\partial y} \right) \sin \alpha \right] \delta U ds = 0$$

$$\oint \left[\left(\frac{\partial V}{\partial y} - D\phi \right) \sin \alpha - \nu \left(\frac{\partial U}{\partial x} - D\phi \right) \sin \alpha + \frac{1+\nu}{2} \left(\frac{\partial V}{\partial x} + \frac{\partial U}{\partial y} \right) \cos \alpha \right] \delta V ds = 0$$

$$\iint \left[\left(\frac{\partial^2 U}{\partial x^2} - D \frac{\partial \phi}{\partial x} \right) - \nu \left(\frac{\partial^2 V}{\partial x \partial y} - D \frac{\partial \phi}{\partial x} \right) + \frac{1+\nu}{2} \left(\frac{\partial^2 U}{\partial y^2} + \frac{\partial^2 V}{\partial x \partial y} \right) \right] \delta U dxdy = 0$$

$$\iint \left[\left(\frac{\partial^2 V}{\partial y^2} - D \frac{\partial \phi}{\partial y} \right) - \nu \left(\frac{\partial^2 U}{\partial x \partial y} - D \frac{\partial \phi}{\partial y} \right) + \frac{1+\nu}{2} \left(\frac{\partial^2 V}{\partial x^2} + \frac{\partial^2 U}{\partial x \partial y} \right) \right] \delta V dxdy = 0 \quad \dots \quad (10)$$

Of these, the last two equations will be satisfied only if at every point of the middle surface of the plate we have

$$\frac{\partial^2 U}{\partial x^2} + \frac{1+\nu}{1-\nu} \nabla^2 U + \frac{\partial^2 V}{\partial x \partial y} - 2D \frac{\partial \phi}{\partial x} = 0$$

$$\frac{\partial^2 V}{\partial y^2} + \frac{1+\nu}{1-\nu} \nabla^2 V + \frac{\partial^2 U}{\partial x \partial y} - 2D \frac{\partial \phi}{\partial y} = 0 \quad \dots \quad (11)$$

These two equations give us the differential equation of the middle surface of an isotropic bent plate in terms of U and V .

The remaining two equations give us the boundary conditions. On the free edges where U and V are specified, the arbitrary variation δU and δV will be zero. Therefore, $\delta U = 0$ and $\delta V = 0$ correspond to free edge boundary conditions. On the clamped edge Σ_* where edge displacements and slopes are specified, for the integral to vanish it is necessary that the term in the square brackets must vanish. This corresponds to clamped end conditions which are

$$\left(\frac{\partial U}{\partial x} - D\phi \right) \cos \alpha - \nu \left(\frac{\partial V}{\partial y} - D\phi \right) \cos \alpha + \frac{1+\nu}{2} \left(\frac{\partial V}{\partial x} + \frac{\partial U}{\partial y} \right) \sin \alpha = 0$$

$$\left(\frac{\partial V}{\partial y} - D\phi \right) \sin \alpha - \nu \left(\frac{\partial U}{\partial x} - D\phi \right) \sin \alpha + \frac{1+\nu}{2} \left(\frac{\partial V}{\partial x} + \frac{\partial U}{\partial y} \right) \cos \alpha = 0 \quad (12)$$

The simplicity of the boundary conditions at the free and clamped edges at once suggests that in the case of flexural problems when line intensities of the force and couple are specified, it is relatively simpler to work in terms of U and V instead of displacement w , since the Kelvin and Tait boundary conditions $M_n = 0$ and $(Q_n - \partial T_{nt} / \partial s) = 0$ on the free edges are more difficult to be satisfied.

FREE EDGE BOUNDARY VALUES

The values of U and V on the free edges where boundary tractions are specified are determined from the relations of coordinate transformation:

$$\begin{aligned}\partial U/\partial s &= \partial U/\partial y \cos \alpha - \partial U/\partial x \sin \alpha \\ &= -\left[T_{xy} + \oint \left(Q_n + D \frac{\partial \phi}{\partial n}\right) ds\right] \cos \alpha - (M_y + D\phi) \sin \alpha \quad \dots (13)\end{aligned}$$

$$\begin{aligned}\partial V/\partial s &= \partial V/\partial y \cos \alpha - \partial V/\partial x \sin \alpha \\ &= (M_x + D\phi) \cos \alpha - \left[\oint \left(Q_n + D \frac{\partial \phi}{\partial n}\right) ds - T_{xy}\right] \sin \alpha \quad \dots (14)\end{aligned}$$

In the general case of a plate with curvilinear boundary, if the plate bending moments and twisting couples be represented by right-handed vectors and if the coordinate axis at a point of the edge be taken in the positive directions of outer normal n and tangential direction t , then from the equations of equilibrium of an element of the plate,

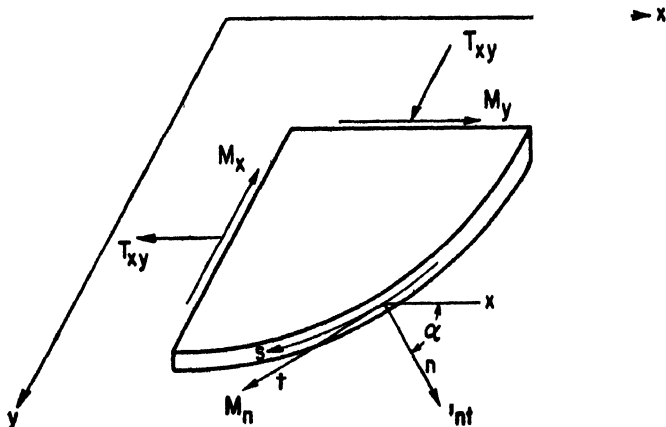


Fig. 2.—Edge tractions on curvilinear boundary.

we have

$$\left. \begin{aligned}M_x \cos \alpha + T_{xy} \sin \alpha &= T_{nt} \sin \alpha + M_n \cos \alpha \\ M_y \sin \alpha + T_{xy} \cos \alpha &= -T_{nt} \cos \alpha + M_n \sin \alpha\end{aligned} \right\} \quad \dots (15)$$

Therefore from equations (13), (14) and (15)

$$\partial U/\partial s = -\left[\left\{\oint \left(Q_n + D \frac{\partial \phi}{\partial n}\right) ds - T_{nt}\right\} \cos \alpha + (M_n + D\phi) \sin \alpha\right] \quad \dots (16)$$

$$\partial V/\partial s = \left[-\left\{\oint \left(Q_n + D \frac{\partial \phi}{\partial n}\right) ds - T_{nt}\right\} \sin \alpha + (M_n + D\phi) \cos \alpha\right] \quad \dots (17)$$

From these two equations we have

$$U = U_0 - \oint \left[(M_n + D\phi) \sin \alpha + \oint \left(Q_n - \frac{\partial T_{nt}}{\partial s} + D \frac{\partial \phi}{\partial n} \right) \cos \alpha ds \right] ds \dots \quad (18)$$

$$V = V_0 + \oint \left[(M_n + D\phi) \cos \alpha - \oint \left(Q_n - \frac{\partial T_{nt}}{\partial s} + D \frac{\partial \phi}{\partial n} \right) \sin \alpha ds \right] ds \dots \quad (19)$$

The values of U and V along the boundary can now be determined in terms of specified edge tractions M_n , $(Q_n - \partial T_{nt}/\partial s)$ and ϕ on the boundary. Further, the constants of integration U_0 and V_0 can be arbitrarily taken as zero, since the bending moments M_x , M_y , and twisting couple T_{xy} depend on the first derivatives of U and V , and an additive constant does not change the magnitude of these moments.

The equations (18) and (19) therefore, completely determine the values of U and V in terms of known edge tractions on the unsupported edge of a thin flat plate, and on the clamped edge the boundary conditions are as those governed by equation (12). The boundary value problem thus reduces to the solution of two elliptic partial differential equations (11) in U and V when these are known at part of the boundary Σ_R where forces are specified and their first derivatives at the remaining part Σ_S where displacements are specified. This is evidently mixed boundary value problem and a rigorous solution is difficult by orthodox methods and so relaxational solution is the most convenient. (Fox, 1950).

PURE BENDING OF PLATE BY MOMENTS

To illustrate the procedure two examples are worked, one involving known boundary tractions along all the free edges and the other involving mixed boundary conditions.

If we consider a square plate acted upon by known bending couples M_1 and M_2 distributed uniformly along the edges, then it is a simple matter to determine U and V all round since T_{xy} , Q_x , Q_y , q and ϕ are zero along all the edges.

$$\text{If} \quad M_n = M_x = M_1 \quad \text{on} \quad x = \pm a$$

$$M_n = M_y = M_2 \quad \text{on} \quad y = \pm a$$

then from equations (18) and (19) we have

$$U = U_0 - \oint M_n \sin \alpha \, ds$$

$$V = V_0 + \oint M_n \cos \alpha \, ds$$

Along the edge where $\alpha = 0^\circ$.

$$U = U_0 \text{ and } V = (V_0 + M_1 y)$$

and along the other edge where $\alpha = 90^\circ$.

$$U = U_0 + M_2(x - a)$$

$$V = V_0 + M_1 a.$$

The constants of integration have been adjusted from the continuity condition at the corner. The boundary values are shown in figure 3.

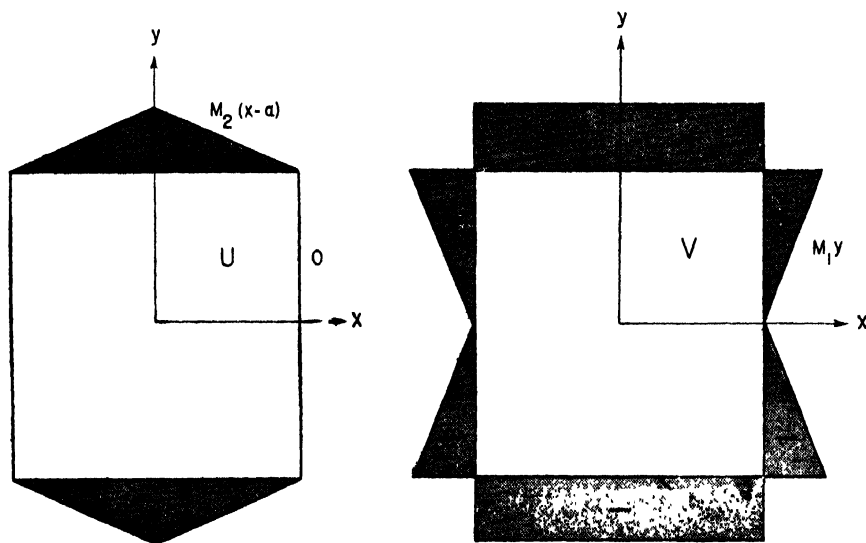


Fig. 3.—Boundary values of U and V for a square plate bent by moments.

Knowing the values of U and V along the complete boundary, the values inside the region can be easily determined if we cover the bounded region by a two-dimensional mesh of points and establish at every mesh point finite difference relations between the values of the required function at this point and the neighbouring nodes. This leads to a set of simultaneous equations which can be solved either by relaxation technique or by any of the standard methods used for solving a system of linear simultaneous equations in many unknowns. The symmetry and antisymmetry of the boundary values, however, alleviates much of the numerical work in this case if use is made of this property.

BENDING OF CANTILEVER PLATE ACTED UPON BY UNIFORMLY DISTRIBUTED LOAD

For a typical problem involving mixed boundary conditions, a square cantilever plate ($2a \times 2a$), clamped on one rectilinear edge (figure 4) is considered. The plate is acted upon by a uniformly distributed load $q = 1$ in non-dimensional units. For the function ϕ choice is made of a polynomial which satisfies the equation

$D\nabla^2\phi = 1$. Since the loading is symmetrical a suitable function is $\phi = 1/4D \cdot (x^2 + y^2)$.

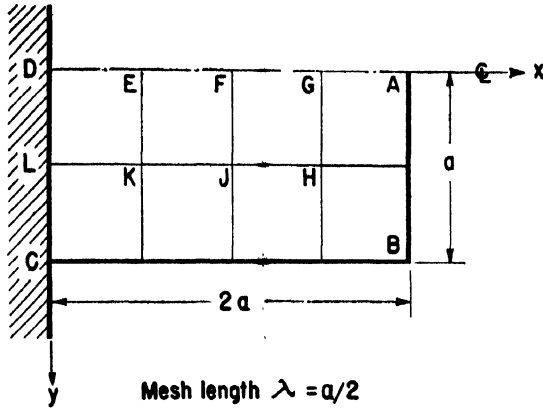


Fig. 4.—Square cantilever plate and the relaxation net.

From Kelvin and Tait boundary conditions, it is known that M_n and $(Q_n - \partial T_{nt}/\partial s)$ are zero along the free edges. Therefore, the values of U and V along the free boundaries AB and BC are

$$\begin{aligned} U_{AB} &= U_0 - \oint \left(\oint D \frac{\partial \phi}{\partial n} ds \right) ds \\ &= U_0 - xy^2/4 \end{aligned} \quad \dots (20a)$$

$$\begin{aligned} U_{BC} &= U'_0 - \oint D \phi ds \\ &= U_0 - 5a^3/3 + (x^3 + 3xy^2)/12 \end{aligned} \quad \dots (20b)$$

Similarly
$$\begin{aligned} V_{AB} &= V_0 + \oint D \phi ds \\ &= V_0 + (y^3 + 3x^2y)/12 \end{aligned} \quad \dots (21a)$$

$$\begin{aligned} V_{BC} &= V'_0 - \oint \left(\oint D \frac{\partial \phi}{\partial n} ds \right) ds \\ &= V_0 + (25a^3 - 3x^2y)/12 \end{aligned} \quad \dots (21b)$$

It is quite easy to show that all other integration constants entering in the above equations are zero. Further, U is symmetrical about x -axis and V antisymmetrical about it. Since the boundary values of U and V along the free edges are known, and along the clamped edge the boundary conditions are given by the set of equations (12), it is therefore a mixed boundary value problem and is solved by relaxa-

tion technique for a mesh length $\lambda = a/2$. The values of U and V are shown in figure 5a. The values of M_x , M_y and T_{xy} shown in figure 5b are calculated from

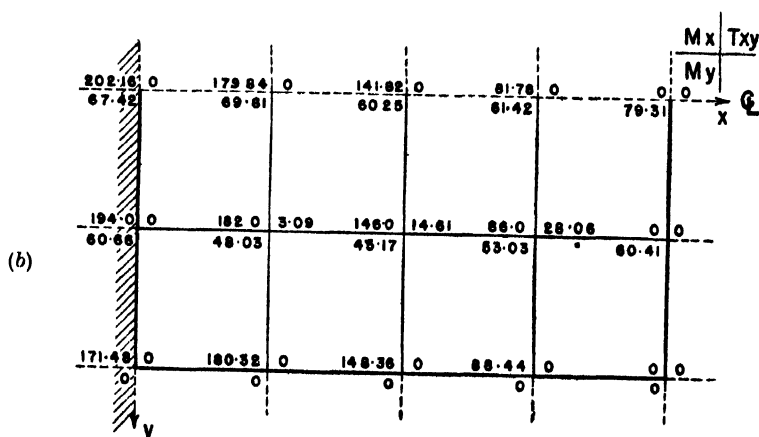
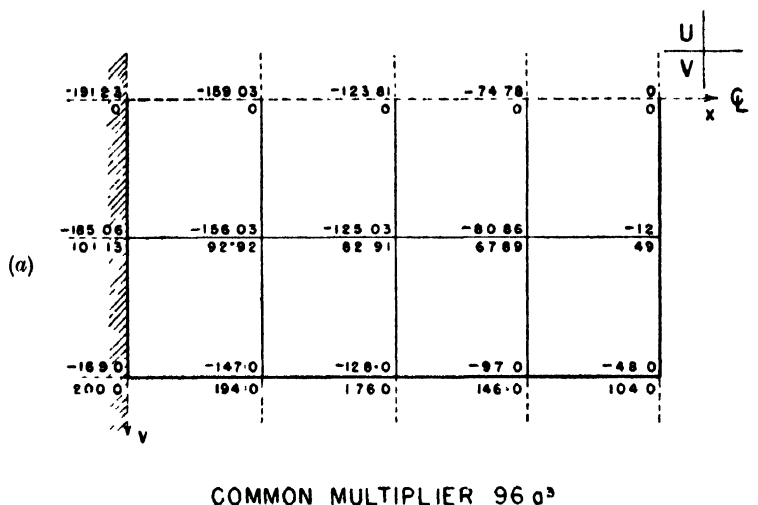


Fig. 5.—Values of U, V and M_x, M_y, T_{xy} for a cantilever plate loaded laterally.

these on the basis of the relations derived earlier. From these values or directly from U and V , the principal bending moments M_1 , M_2 , and their inclination parameter θ can be obtained easily from the Mohr circle relations in finite difference form, as per notation in figure 5 as follows:

$$M_{1,2} = [V_2 - V_4 + U_1 - U_3 - 4D\lambda\phi_0 \pm \{(V_2 - V_4 - U_1 + U_3)^2 + (V_1 - V_3 + U_2 - U_4)^2\}^{1/2}] \quad (22)$$

$$\tan 2\theta = (V_1 - V_3 + U_2 - U_4) / (V_2 - V_4 - U_1 + U_3) \quad (23)$$

ACKNOWLEDGMENT

The work described above forms a part of the research programme in the division of Applied Mechanics at the National Physical Laboratory of India and this paper is published with the kind permission of the Director.

APPENDIX

Centre—Finite Difference Approximations

In terms of centre-finite difference relations the two differential equations (11) with the notation of figure (6) and for $\nu = 1/3$ are

$$R_U = 3(U_1 + U_3) + 2(U_2 + U_4) - 10U_0 + \frac{1}{4}(V_5 - V_6 + V_7 - V_8) - \lambda^2 x \quad \dots (24a)$$

$$R_V = 2(V_1 + V_3) + 3(V_2 + V_4) - 10V_0 + \frac{1}{4}(U_5 - U_6 + U_7 - U_8) - \lambda^2 y \quad \dots (24b)$$

The clamped end conditions for curvilinear boundary are

$$[(U_1 - U_3) - (V_2 - V_4)/3 - 4\lambda D\phi_0/3] \cos \alpha + 2(V_1 - V_3 - U_2 - U_4)/3 \sin \alpha = 0 \quad \dots (25a)$$

$$[(V_2 - V_4) - (U_1 - U_3)/3 - 4\lambda D\phi_0/3] \sin \alpha + 2(V_1 - V_3 - U_2 - U_4)/3 \cos \alpha = 0 \quad \dots (25b)$$

and for the rectilinear clamped end CD where ($\alpha = 180^\circ$), as in example (2).

$$(U_1 - U_3) - 1/3(V_2 - V_4) - 4/3\lambda D\phi_0 = 0 \quad \dots (26a)$$

$$V_1 - V_3 + U_2 - U_4 = 0 \quad \dots (26b)$$

These two sets of equations (26) are useful for eliminating the fictitious points lying outside the clamped end region of the plate. The pair of equations (24) are valid only for the points (K , J and H). For the point L lying on the clamped edge CD the modified equations are

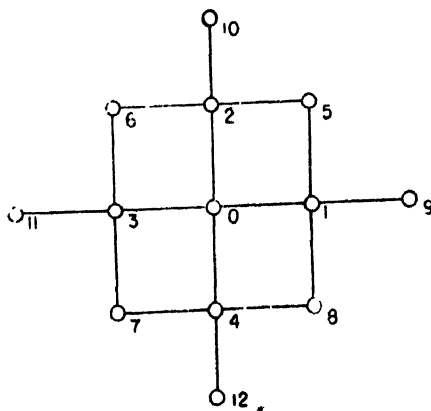


Fig. 6.—A typical node of the net and the surrounding nodes.

$$R_U = 6U_1 + 2(U_2 + U_4) - (V_2 - V_4) - 10U_0 + \frac{1}{4}(U_9 - U_{12}) - \lambda^2 y$$

$$R_V = 4V_1 + 3(V_2 + V_4) + 2(U_2 - U_4) - 10V_0 + 1/2(V_{12} - V_9) + \lambda(a^2 - 16\lambda y)/24$$

For point D lying on the x -axis, which is the line of symmetry for U and

antisymmetry for V , the modified formulae, if use is made of symmetrical and antisymmetrical relations are:

$$R_U = 6U_1 + 4U_2 - 2V_2 - 10U_0 + \frac{1}{2}(U_0 - U_{10})$$

$$R_V = 4V_1 - 6V_0/6.$$

and for points (E , F and G)

$$R_U = 3(U_1 + U_3) + 4U_2 - 10U_0 + \frac{1}{2}(V_5 - V_6)$$

$$R_V = 2(V_1 + V_3) - 10V_0$$

There are no difficulties as regards the relaxation procedure. Both these functions are much more convergent than the corresponding bi-harmonic function w . The occurrence of the cross-derivatives are replaced by the usual approximation

$$4\lambda^2 F_{xy} = F_5 + F_6 + F_7 - F_8$$

For determining the first derivatives $\partial U/\partial y$ and $\partial V/\partial x$ for points on the free edge, where centre-difference formulae are not applicable, Bickley's "three-point" formula for differentiation was used (Southwell, 1946). The manner of constructing relaxation patterns is after Allen (1954) and, therefore, not described here.

REFERENCES

- Allen, D. N. De G., 1954, *Relaxation Methods*, (McGraw-Hill).
 Courant, R. and Hilbert, D., 1953, *Methods of Mathematical Physics* (Interscience Publishers) p. 164.
 Fox, L., 1950, *Phil. Trans. Roy. Soc. A.*, **242**, 345-378.
 Sokolnikoff, I. S., 1946, *Mathematical Theory of Elasticity* (McGraw-Hill), p. 284.
 Southwell, R. V., 1950, *Quart. Jr. Mech. & App. Math.*, **3**, 257-270.
 Southwell, R. V., 1946, *Relaxation Methods in Theoretical Physics*, (Oxford).
 Timoshenko, S., 1940, *Theory of Plates and Shells* (McGraw-Hill) p. 84-88, 95.
 Timoshenko, S. and Goodier, J. N., 1951, *Theory of Elasticity*, (McGraw-Hill), p. 284.

SOURCE-STRAGGLING OF α -PARTICLES FROM A POLONIUM SOURCE

By N. K. SAHA AND K. L. KAILA,

PHYSICS DEPARTMENT, UNIVERSITY OF DELHI, DELHI.

(Received for publication, June 25, 1955)

ABSTRACT. By using a Lindemann electrometer in conjunction with a high megohm resistor and a shallow ionisation chamber, complete Bragg curves are obtained for a Po-source of α -particles freshly separated from some old radon tubes, and for a second source about 29 months old. The latter shows by comparison a very distorted Bragg curve with its tail portion spread about 1 cm. air beyond the maximum. The spread is interpreted as the superposition effect of a large number of separate ideal Bragg curves arising due to the finite source depth accumulated through aging. Theoretical formula is developed taking into account the straggling due to the source depth as well as the well known Gaussian law of range straggling. The calculated results show good agreement with the observed Bragg curve.

1. INTRODUCTION

It is a well known fact that a freshly prepared plated source of α -rays which is practically free from any surface depth, acquires a finite surface thickness with aging, which gradually increases as the source becomes older and older. The straggling of the α -rays emanating from such a source may arise due to two causes (i) the range straggling due to statistical variation of the collision phenomenon in the medium through which the α -rays pass and (ii) the source straggling on account of the α -rays coming from different depths of the source, - those coming from a greater depth showing slightly smaller range outside compared to those coming from an upper layer. The phenomenon of the range straggling of α -particles has been thoroughly investigated by Bohr (1915), Briggs (1927) and others. Bohr's theory, confirmed by experiments, leads to the conclusion that the law of range distribution about the mean range of the α -particles which have all passed through the same thickness of the absorbing material, is to a high degree of approximation, Gaussian in form. The range straggling would, therefore, give rise to a symmetrical distribution centred about the mean range. As such, it can have no effect on the measured value of the mean range. The straggling due to the finite depth of the source would, however, lead to an antisymmetrical range distribution with much greater weight in the ranges lower than the mean than in the higher ranges. The presence of such an asymmetry in the range distribution curve was previously observed by Schulze (1935) and Curie (1925) for Po- α particles in air. The distribution curves, according to these authors, could not be represented

by a Gaussian error curve. The effect should clearly be attributed to a source straggling of the α -rays caused by a finite depth of the source used by these authors. Our object in this work is to study the nature of this source straggling experimentally and then attempt a theoretical interpretation of the observed distribution under certain simple assumptions.

2. EXPERIMENTAL TECHNIQUE AND OBSERVATIONS

A moderately strong plated Po-source was prepared by digesting about twenty crushed random bulbs in 15 cc of 10% nitric acid and 5 cc of 4% hydrofluoric acid. The content was stirred for about 4 hours by a mechanical stirrer, allowed to rest for sometime, the supernatant was drained off and the solution was evaporated to dryness. The residue was digested in about 20 c.c. of 0.4 N nitric acid and finally the Po-content was deposited electrochemically from the solution on one side of a thin silver disc about 1cm in diameter. An aged Po-source (about 29 months old) was also procured. The complete Bragg curves of the two sources were taken separately on a shallow ionisation chamber of the type employed by Holloway and Livingston (1938) shown in figure 1.

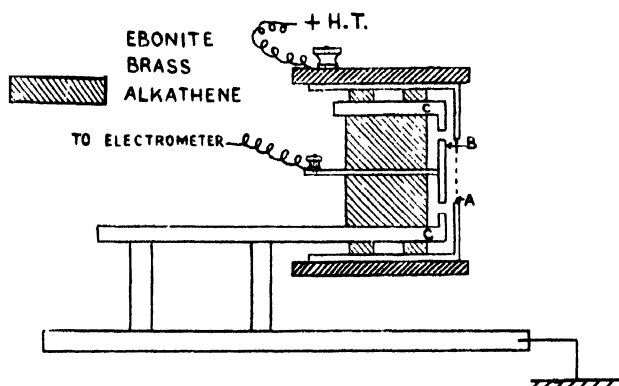


Fig. 1. Diagrammatic sketch of the shallow ionisation chamber (not to the scale).

The front face of the chamber is a brass wire gauze with rectangular meshes of size $0.26 \text{ mm} \times 0.32 \text{ mm}$, the wire gauze being 0.30 mm thick. The collector plate *B* is a brass disc $\frac{3}{4}$ " in diameter shielded by an earthed guard ring *C*. The depth of the chamber was 0.55 mm between the inside surface of the wire gauze and the front face of the collector plate. A saturation electric field of $\sim 820 \text{ volt/cm}$ was applied between the wire gauze and the collector plate.

The detector is a Lindemann electrometer in conjunction with a $\sim 5 \times 10^{10} \Omega$ resistor across which the ionisation current from the chamber produces a small potential drop which deflects the needle of the electrometer. The sensitivity of the electrometer had to be kept down to $250 \text{ millivolt/div.}$ in order to make the

deflections consistent. The deflection was observed under a suitable microscope. The measuring arrangement with the chamber and the electrometer assembly is shown in figure 2.

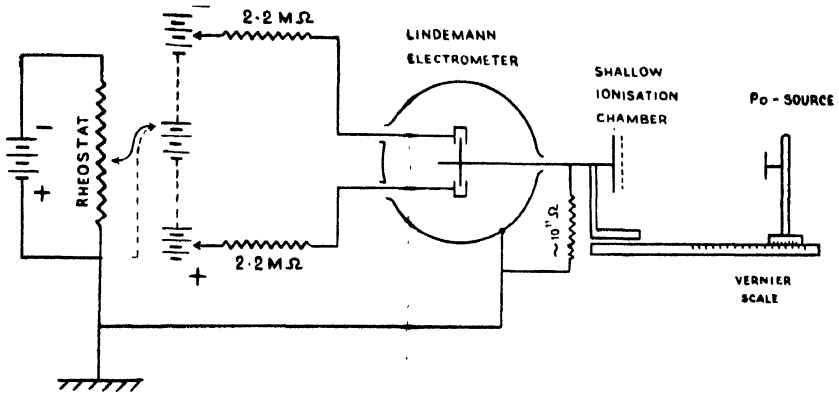


Fig. 2. Plan of the measuring arrangement.

The source was mounted with its plane vertical in front of the window of the ionisation chamber from the centre of which the distance of the source was exactly measurable. Taking x' equal to this distance and θ the deflection of the electrometer needle, a plot was obtained between the quantity $x'^2 \times \theta$ and x' — as shown in figure 3, curve 1.

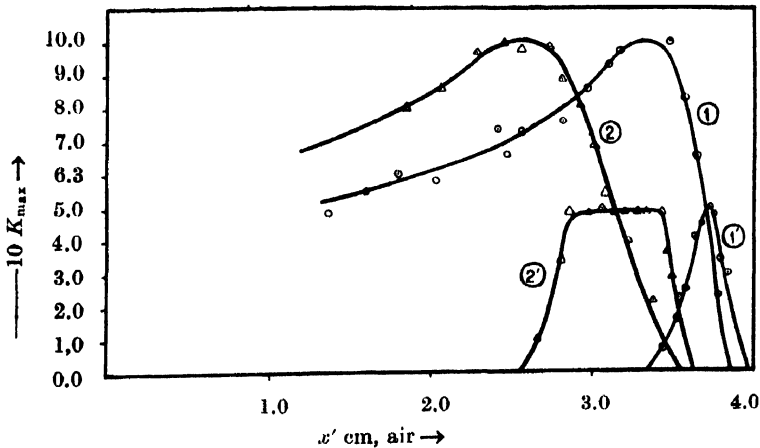


Fig. 3. Experimental Bragg curves: (1) for a freshly prepared Po-source, (2) for an old Po-source (29 months old); curves 1' and 2' are the corresponding differential curves.

A similar curve (2 in the same diagram) was obtained for the old Po-source available in the laboratory. The surface of the old source appeared visibly black probably due to thin deposits of lead and its compounds throughout its age of about 29 months.

It is clear from a comparison of these two curves that the straggling has increased very appreciably in the case of the old source, as well as the end point of the Bragg curve here has shifted by about 2.8 mm. A differential plot $\frac{d}{dx}, (x'^2\theta)$ at various values of x' for the two curves are shown in the same figure (figure 3) and the corresponding plots are designated as 1' and 2' for the two sources. It is striking that while the curve 1' clearly shows a Gaussian distribution about the mean range, the curve 2' does not indicate a Gaussian distribution, but a nearly flattened top with a rapid fall off at the two ends. This indicates that in the case of the old source, the source straggling is playing a prominent part and is superimposed on the comparatively smaller range straggling effect.

3. CALCULATION OF THE SOURCE STRAGGLING AND THE RESULTANT IONISATION CURVE

To build up a mechanism for the straggling of the α -particles due to the source thickness, we shall take a hint from the curve 2' of figure 3. Since it has a nearly flattened top maximum, it is quite plausible to think that it is arising because of the super-imposition of several Gaussian distribution forms which arise due to the various energy groups of α -particles coming from the different layers of the thick source. Thus the particles coming out of the source consist of different energy groups with a corresponding range straggling and the superposition of these different groups should give rise to the curve 2 of figure 3 above.

From Bethe's theory of ionisation loss of α -particles, we have

$$-\frac{dE}{dx} = \frac{4\pi e^4 z^2}{mv^2} NZ \log \frac{2mv^2}{I} \quad \dots (1)$$

where v is the velocity, ze the charge of the incident particle, N the number of atoms per cm. of the material, Z the nuclear charge and I the average excitation potential of the atom.

Further, the specific ionisation I_x is given by

$$I_x = -\frac{dE}{dx} \cdot \frac{1}{\epsilon} \quad \dots (2)$$

where ϵ is the mean energy spent to produce an ion pair. By a proper transformation using Geiger relation

$$x = a'v^3 \quad \dots (3)$$

we get,

$$I_x = Mx^{-2/3} + Px^{-2/3} \log_{10} x \quad \dots (4)$$

where x is the residual range, $x = R_m - x'$, R_m being the maximum range, x' the distance of the Po-source from the ionisation chamber and

$$M = \frac{DA}{\epsilon} \qquad D = \frac{4\pi e^4 z^2 N}{ma}$$

$$P = 2.3 \times \frac{2}{3} \frac{ZD}{\epsilon} \qquad A = Z \ln \frac{2ma}{I}$$

$$a = \frac{1}{\alpha^{2/3}}$$

It has been shown elsewhere that at low energies of α -particles below 4 Mev. one has to take into account the electron capture by the He^{++} nuclei—and the modified expression for the specific ionisation becomes

$$I_x = Mx^{-2/3} + Px^{-2/3} \log_{10} x + \frac{1}{x} (Nx^{-2/3} + Qx^{-2/3} \log_{10} x) \quad \dots \quad (5)$$

Relation (5) may be regarded as the complete equation for the Bragg curve 1 of figure 3.

We shall now get the expression for the specific ionisation due to a thick source. Let us consider a thick Po-source, with thickness, as represented in figure 4. Let us further think that monochromatic α -particles are emitted from different layers of the thick source and, therefore, they suffer absorption in passing through different thicknesses of the source. The result will be that the α -particles which started as monochromatic from the different layers of the source, become inhomogeneous on emergence outside. The residual range of the different

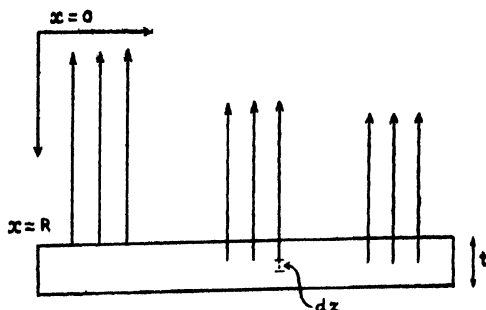


Fig. 4

groups becomes different so that the Bragg curves are shifted linearly from one another as shown in figure 5. Here three α -groups are shown originating from the surface $z = 0$, $z = t_1$ and $z = t_2$. As the thickness goes on increasing the

curve gets shifted more and more to the left. In the ionisation chamber we would be studying the superposed effect of all these curves.

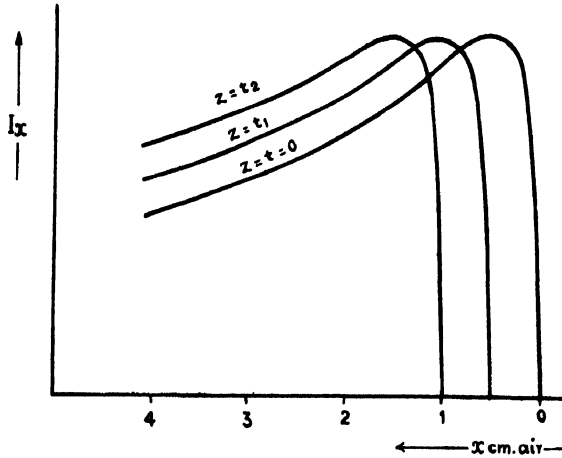


Fig. 5

The specific ionisation I_{xz} produced by an α -particle originating at a distance z below the surface of the source is obtained by writing $(x-\rho'z)$ in place of x in the equation (5) and is given by

$$I_{xz} = M(x-\rho'z)^{-2/3} + \frac{P}{2.3}(x-\rho'z)^{-2/3}\log_e(x-\rho'z) + \frac{1}{x-\rho'z} \left\{ N(x-\rho'z)^{-2/3} + \frac{Q}{2.3}(x-\rho'z)^{-2/3}\log_e(x-\rho'z) \right\} \quad \dots (6)$$

where ρ' is the air equivalent per unit thickness of the source material. When $z=0$, this equation reduces to equation (5).

If K (regarded as constant) be the number of α -particles coming per unit source thickness, the total ionisation produced by all the α -particles coming from different layers of the source thickness will be given by

$$\begin{aligned} I_x^{total} &= \int_0^t I_{xz} K dz \\ &= K \int_0^t \left\{ M(x-\rho'z)^{-2/3} + \frac{P}{2.3} (x-\rho'z)^{-2/3} \log_e(x-\rho'z) \right. \\ &\quad \left. + \frac{1}{x-\rho'z} \left[N(x-\rho'z)^{-2/3} + \frac{Q}{2.3} (x-\rho'z)^{-2/3} \log_e(x-\rho'z) \right] \right\} dz \end{aligned}$$

$$\begin{aligned}
&= -\frac{3K}{\rho'}(x-\rho't)^{1/3}\left[M-\frac{3P}{2.3}+\frac{P}{2.3}\log_e(x-\rho't)\right]+\frac{3K}{\rho'}(x)^{1/3}\left[M-\frac{3P}{2.3}+\frac{P}{2.3}\log_e x\right] \\
&\quad +\frac{3K}{2\rho'}(x-\rho't)^{-2/3}\left\{N+\frac{3}{2}\frac{Q}{2.3}+\frac{Q}{2.3}\log_e(x-\rho't)\right\} \\
&\quad -\frac{3K}{2\rho'}(x)^{-2/3}\left\{N+\frac{3}{2}\frac{Q}{2.3}+\frac{Q}{2.3}\log_e x\right\} \quad \dots \quad (7)
\end{aligned}$$

If there is also formed a constant thickness x_0 in cms. of air equivalent over the surface of the source, then this would cause a shift of the end point of the Bragg curve as actually observed. The residual range is then $x-x_0$, so that the new expression becomes

$$\begin{aligned}
\frac{\rho'}{3K}I_x &= -\left[x-x_0-\rho't\right]^{1/3}\left[M-\frac{3P}{2.3}+\frac{P}{2.3}\log_e(x-x_0-\rho't)\right] \\
&\quad +(x-x_0)^{1/3}\left[M-\frac{3P}{2.3}+\frac{P}{2.3}\log_e(x-x_0)\right] \\
&\quad +\frac{1}{2}\left[x-x_0-\rho't\right]^{-2/3}\left\{N+\frac{3}{2}\frac{Q}{2.3}+\frac{Q}{2.3}\log_e(x-x_0-\rho't)\right\} \\
&\quad -\frac{1}{2}(x-x_0)^{-2/3}\left\{N+\frac{3}{2}\frac{Q}{2.3}+\frac{Q}{2.3}\log_e(x-x_0)\right\} \quad \dots \quad (8)
\end{aligned}$$

Now for each of the different groups of α -particles coming from the different layers of the thick source, a certain range straggling exists, giving a Gaussian distribution of range deviations about the particular mean range concerned as shown in figure 6. We have to get the superposed distribution due to all these Gaussians.

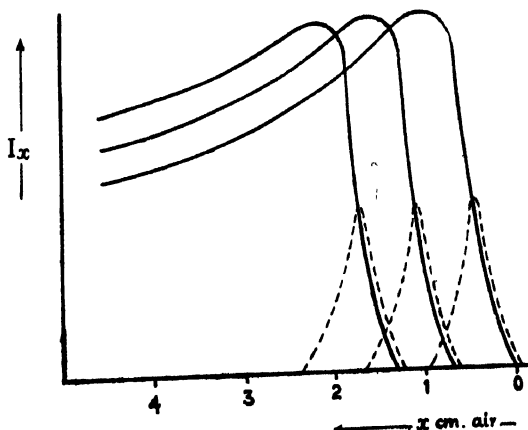


Fig. 6

If R_0 be the mean range of the α -particles, the probability $W(s) ds$ that the particle has a range lying between $R_0(1+s)$ and $R_0(1+s+ds)$ is given by

$$W(s)ds = \frac{1}{\rho\sqrt{\pi}} e^{-\frac{s^2}{\rho^2}} ds \quad \dots (9)$$

where ρ is called the range straggling parameter. Now $x = R_{max} - x'$, where $x' = R_0 + R_0 s$ = distance of the mid point of the ionisation chamber from the front surface of the Po-source.

Therefore, $s = \frac{x' - R_0}{R_0}$, $ds = \frac{dx'}{R_0}$ and $dx = -dx'$

Therefore equation (9) becomes

$$W\left(\frac{R_m - R_0 - x}{R_0}\right) dx = \frac{1}{\rho\sqrt{\pi}} e^{-a^2 \left[\frac{1-bx}{R_0}\right]^2} dx \quad \dots (10)$$

where

$$a = \frac{R_m - R_0}{\rho}, \quad b = \frac{1}{R_m - R_0}$$

For a group of α -particles coming from a distance z below the surface, the distribution will be given by

$$W(x)dx = \frac{1}{\rho\sqrt{\pi}} e^{-a^2 \left[\frac{1-b(x-\rho'z)}{R_0-\rho'z}\right]^2} dx \quad \dots (11)$$

This is the particular probability distribution of α -articles with x for a particular value of $\rho'z$ ranging from 0 to $\rho't$, to get the distribution function for the old source we must integrate the above equation (11). The total probability of the superposition obtained by averaging over all values of $\rho'z$ is then

$$W(x)_{super} = \frac{\int_0^{\rho't} \frac{1}{\rho\sqrt{\pi}} e^{-a^2 \left[\frac{1-b(x-\rho'z)}{R_0-\rho'z}\right]^2} d(\rho'z)}{\int_0^{\rho't} d(\rho'z)} \quad \dots (12)$$

$$= \frac{1}{\rho't \rho\sqrt{\pi}} \int_0^{\rho't} e^{-a^2 \left[\frac{1-b(x-\rho'z)}{R_0-\rho'z}\right]^2} d(\rho'z) \quad \dots (12a)$$

This integral cannot be put into a simple Gaussian integral because of the fact that the factor $(R_0 - \rho'z)$ is a function of z . To simplify matters we shall split this integral into a summation over integrals which will be performed over small

intervals of $\rho't$ values 0.2 cm each, so that over this small region ($R_0 - \rho'z$) can be put equal to $R_0 - \rho'z/2$ the mean value, and taken out of square sign as a constant. Therefore, the above integral can be written as

$$W = \frac{1}{m} \sum_{n=1}^m \frac{1}{2\rho\sqrt{\pi}} \int_{\frac{a}{R_0 - \frac{1}{2}(2n-1)}}^{\frac{2n}{2(n-1)}} e^{-\left(\frac{a}{R_0 - \frac{1}{2}(2n-1)}\right)^2 [1-b(x-\rho'z)]^2} d(\rho'z) \dots (13)$$

where $\rho't = 0.2$ mm and n is an integer which varies from 1 to m .

$$\text{Now let us put } \left[1-b(x-\rho'z)\right]\left(\frac{a}{R_0 - \frac{1}{2}(2n-1)}\right) = y,$$

$$\text{so that } \left(\frac{a}{R_0 - \frac{1}{2}(2n-1)}\right) b d(\rho'z) = dy$$

Therefore, equation (13) becomes

$$W = \frac{1}{m} \sum_{n=1}^m \frac{1}{2b\rho\sqrt{\pi}\left(\frac{a}{R_0 - \frac{1}{2}(2n-1)}\right)} \int_{\left(\frac{a}{R_0 - \frac{1}{2}(2n-1)}\right)\left(1-bx + \frac{1}{2}bn\right)}^{\left(\frac{a}{R_0 - \frac{1}{2}(2n-1)}\right)\left(1-bx + \frac{1}{2}bn\right)} e^{-y^2} dy \dots (14)$$

If there be a constant deposit of the thickness x_0 over the surface of the source, the above equation (14) will become

$$W = \frac{1}{m} \sum_{n=1}^m \frac{1}{2b\rho\sqrt{\pi}\left(\frac{a}{R_0 - \frac{1}{2}(2n-1)}\right)} \int_{\left(\frac{a}{R_0 - \frac{1}{2}(2n-1)}\right)\left[1-b(x-x_0) + \frac{1}{2}bn\right]}^{\left(\frac{a}{R_0 - \frac{1}{2}(2n-1)}\right)\left[1-b(x-x_0) + \frac{1}{2}bn\right]} e^{-y^2} dy \dots (15)$$

4. COMPARISON OF THEORY WITH EXPERIMENT

Let us now try to construct the curve 2 of figure 3 from the theoretical expressions (8) and (15). The values of M , P , N , Q to be used in (8) are given below

$$M = 5.578 \times 10^4$$

$$P = 3.983 \times 10^4$$

$$N = -.1307 \times 10^4$$

$$Q = -.0435 \times 10^4$$

Therefore, expression (8) becomes

$$\begin{aligned} 10^{-4} \frac{\rho'}{3k} Ix = & [x-x_0-\rho't]^{1/3} \{.383 + 3.983 \log_{10} (x-x_0-\rho't)\} \\ & + (x-x_0)^{1/3} \{.383 + 3.983 \log_{10} (x-x_0)\} \\ & - \frac{1}{2}[x-x_0-\rho't]^{-2/3} \{.1591 + .0435 \log (x-x_0-\rho't)\} \\ & + \frac{1}{2}(x-x_0)^{-2/3} \{.1591 + .0435 \log_{10} (x-x_0)\} \dots (16) \end{aligned}$$

From a careful examination of the end points of the two curves in figure 3 it is evident that the shift $x_0 \approx 0.28$ cm. The factor $\rho't$ is, of course unknown. We take its value to be 0.8 cm, which is seen to give the best fit of equation (15) and (16) with the experimental curve obtained for the old source used by us. Substituting these values in expression (16) we can calculate the value of I_x in units of $10^4 \times \frac{3K}{\rho'}$ for different values of x . The results are tabulated below, where the normalised values relative to I_{\max} are shown in the third column.

TABLE I.

x	$\left(10^4 \frac{3K}{\rho't}\right) I_x$	I_x normalized
1.13 cms.	1.573	9.36
1.18 "	1.681	10.00
1.28 "	1.679	9.99
1.38 "	1.628	9.69
1.48 "	1.555	9.25
1.58 "	1.514	9.00
1.68 "	1.462	8.70
1.78 "	1.424	8.47
1.88 "	1.366	8.13
1.98 "	1.333	7.93
2.08 "	1.297	7.72
2.18 "	1.263	7.50
2.28 "	1.234	7.34
2.38 "	1.204	7.16
2.48 "	1.177	7.00

Also using these values of x_0 , $\rho't$ and $R_o = 3.74$ cms and $R_{\max} = 3.86$ cms in expression (15) we can calculate the relative values of the probability W for different values of x . The results are given in Table II.

TABLE II

x	Relative probability
0.28	0
.38	1.26
.48	4.80
.58	5.00
.68	4.70
.78	4.60
.88	4.60
.98	4.50
1.08	4.40
1.18	3.40
1.28	0.01

With the help of the values computed in Tables I and II we can now

reconstruct the curve 2 of figure 3 as shown in figure 7. The experimental curve (a) agrees fairly well with the theoretically constructed curve (b).

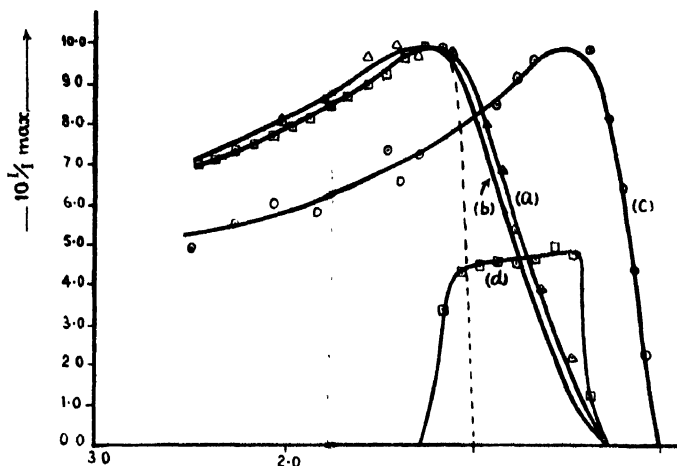


Fig. 7. (a) Experimental ionisation curve for the old Po-source, (b) theoretically calculated ionisation curve for this source, (c) the experimental ionisation curve for the freshly prepared Po-source and (d) theoretical range distribution curve corresponding to the curve b.

5. DISCUSSION

The close agreement of the calculated results with the observed ionisation curve of the thick Po-source leads us to believe that our basic postulates regarding the nature of the source straggling of the α -rays and its theoretical calculation are substantially correct. It is possible to go a step further if we make the following interesting comparison. Let us estimate the strength of the Po-source from its decay time since it was first separated and also try to make a comparative estimate of the strength by computing the saturation ionisation current obtained in the chamber.

The old Po-source was separated in October, 1952 with a flash overcoat of gold and was estimated at 6.4 mc on the date of separation. Therefore, its estimated strength at the time of our experiment (March, 1955) comes to about 85.7 mc, which would emit α -particles at the rate of 3.14×10^6 per second.

The sensitivity of the electrometer used for measurement was 250 millivolt/div. Taking into account the geometry of the source and the chamber, the correction necessary due to the cutting off of the α -particles by the solid portions of the wire gauze (roughly estimated at $\sim 30\%$) and the resistance $R \sim 4.8 \times 10^{10}$ ohm across which the potential drop was measured, the total saturation current (in the 4π solid angle) estimates out to be 1.7×10^{-10} amp. Now the saturation current $i = n_0 N d e$, where n_0 is the maximum number of ion pairs produced

by an α -particle per cm, N is the total number of α -particles emitted, d is the depth of the chamber and e is the electronic charge. Taking $n_0 = 7 \times 10^4$ ion pairs/cm (maximum value), $d = 0.55$ mm and $e = 4.8 \times 10^{-10}$ e.s.u., we obtain $N = 0.27 \times 10^6$ α -particles/second. This is about 12 times lower than the value 3.14×10^6 obtained from the strength of the decayed source. This apparent discrepancy seems to arise largely from our assumption that n_0 is the maximum specific ionisation of the α -particle, viz., 7×10^4 ion pairs/cm. For a freshly prepared source the tail part of the Bragg curve shows an extremely sharp fall. Hence even a small depth of the chamber would receive practically all the α -particles with the maximum ionisation loss at the position of the maximum of the Bragg curve. However, for our aged source, the tail part of the Bragg curve shows a considerable spread of about 1.0 cm, (vide figure 3, curve 2). Hence the maximum value of n_0 within the 0.55 mm depth of the chamber will surely not be as high as for the fresh source, but will be substantially less. Assuming roughly a linear spread of the tail, the effective value of n_0 will be a fraction of n_0 given by the ratio of the area enclosed by the maximum ordinate of the curve with 0.55 mm along the abscissa to the total area enclosed by the tail portion of the curve between the maximum and zero ordinates. A rough estimate from figure 3, curve 2, gives this effective value to be $\sim 1/9 n_0$. On substituting this in the expression for the saturation current we obtain at once $N \approx 2.43 \times 10^6$ as the total number of α -particles emitted from the source per second. Considering the uncertainties involved in the geometrical and various other corrections applied to the ionisation current measurement, the last value of N can be considered to be in reasonably good agreement with its estimated value from the source decay. This agreement merely emphasises the point that while working with a freshly prepared polonium source a shallow chamber is the most suitable for the specific ionisation measurements of α -rays, in the case of an old source a very shallow depth is likely to cut down a considerable part of the ionisation at the maximum point.

ACKNOWLEDGMENTS

We take this opportunity to express our sincere thanks to Prof. D. S. Kothari, the Head of the Physics Department for giving us facilities to carry out this work. Our thanks are also due to Messrs Imperial Chemical Industries (India) Ltd; Calcutta, for a gift of insulating materials which have been very useful in constructing the ionisation chamber.

REFERENCES

- Bothe, H. A., 1930, *Ann. Physik*, **5**, 325.
 Bohr, N., 1915, *Phil. Mag.*, **30**, 531.
 Briggs, G. H., 1927, *Proc. Roy. Soc., London*, **114**, 341.
 Curie, I., 1925, *Jour. de Phys.*, **3**, 299.
 Holloway, M. G. and Livingston, M. S., 1938, *Phys. Rev.*, **54**, 29.
 Schulze, H., 1935, *Z. f. Phys.*, **94**, 104.

AN IMPROVED METHOD OF MEASURING THE ABSOLUTE SUSCEPTIBILITIES OF SINGLE CRYSTALS OVER WIDE RANGES OF TEMPERATURES

By S. K. DUTTA ROY

INDIAN ASSOCIATION FOR THE CULTIVATION OF SCIENCE, CALCUTTA

(Received for publication, July 27, 1955)

ABSTRACT. An accurate convenient method has been developed for the measurement of magnetic susceptibilities of single crystals, powders and solutions over wide ranges of temperatures. This is based on the well known Curie method in which various sources of errors have been individually and collectively eliminated to give an accuracy of not less than 0.2%. The present paper gives a detailed description of the balance and a gas-flow type horizontal cryostat for temperature variation. The calibration of the balance and the Cu-constantan thermocouple temperature scale have also been compared against the existing Leiden, Strasbourg and Calcutta measurements, on standard paramagnetic substances, e.g., Cr^{+++} alum, Fe^{+++} alum and $\text{NiSO}_4 \cdot 6\text{H}_2\text{O}$, first two of which are well known to provide the magnetic scale of extreme low temperatures.

INTRODUCTION

A very accurate method for determining the magnetic anisotropy of single crystals, depending on the measurement of critical torque upon the crystals suspended in a homogeneous magnetic field with a fine quartz fibre has already been developed in this laboratory (Dutta, 1953-54, Dutta Roy, 1954). For a complete knowledge of susceptibility behaviours of crystals, the principal absolute susceptibilities also should be measured to the same degree of accuracy. Though by the existing methods of measurements the mean value of the susceptibility has been often determined accurately at a single temperature, no very satisfactory method has yet been evolved for the absolute principal susceptibilities of crystals over wide ranges of temperatures. In the present paper a method has been developed which promises to be very satisfactory for this purpose and applicable universally to crystals, liquids and solutions, over a wide range of temperatures.

THEORY

Most of the absolute susceptibility determinations depend on the measurement of translational force upon the sample placed in an inhomogeneous magnetic field. The general expression for the components of the translational forces on an isotropic sample of volume v , of volume susceptibility k , surrounded by a medium of

volume susceptibility k_0 , along the orthogonal coordinate axes x, y, z , are given by,

$$\left. \begin{aligned} F_x &= (k-k_0) \left(H_x \frac{dH_x}{dx} + H_y \frac{dH_y}{dx} + H_z \frac{dH_z}{dx} \right) v \\ F_y &= (k-k_0) \left(H_x \frac{dH_x}{dy} + H_y \frac{dH_y}{dy} + H_z \frac{dH_z}{dy} \right) v \\ F_z &= (k-k_0) \left(H_x \frac{dH_x}{dz} + H_y \frac{dH_y}{dz} + H_z \frac{dH_z}{dz} \right) v \end{aligned} \right\} \dots (1)$$

If the origin is taken at the geometric centre of the pole gap and x, y , and z , are the directions, from pole to pole in the horizontal plane, perpendicular to this direction in the same plane, and along the vertical, respectively, it is evident that if the pole pieces are so shaped that there is only a field H_x and its gradient $\frac{dH_x}{dy}$, along y , then we are left with only the y -component of the force in the form,

$$F_y = \left(k - k_0 \right) v H_x \frac{dH_x}{dy} \dots (2)$$

For an anisotropic crystalline sample of principal volume susceptibility k_1, k_2 , and k_3 , inclined to H_x at angles whose direction cosines are l, m, n , the force is given by

$$F_y = \left\{ (k_1 l^2 + k_2 m^2 + k_3 n^2) - k_0 \right\} v H_x \frac{dH_x}{dy} \dots (3)$$

which further simplifies to

$$F_y = (k_1 - k_0) v H_x \frac{dH_x}{dy} \dots (4)$$

if the crystal is placed with its k_1 direction along H_x .

In addition to these translational forces there are also component couples on the crystal about the coordinate axis tending to rotate the crystal in such a manner as to place the maximum direction of susceptibility along the magnetic field.

The situation is further complicated by anisotropic Poisson distribution of magnetization over the surface of the crystal, including the demagnetisation factor in an initially homogeneous field and consequent couples. The surface forces are proportional to $(k-k_0)^2$ and is therefore extremely small under normal circumstances.

Experimental arrangements usually have to be so devised that the rotatory tendencies are eliminated and the translatory motion is made undirectional along one of the coordinate axis, say y , as in the case already considered.

SUMMARY OF THE EXISTING METHODS

Various methods of measuring magnetic susceptibility, based on the measurement of force on a body placed in a non-homogeneous magnetic field, have been developed from time to time and are essentially variations or modifications of the well known methods of Gouy or of Curie. The Gouy method, which is very sensitive and convenient for absolute susceptibility measurement, usually requires a large amount of the substance in the form of a long cylindrical rod of uniform cross section or finely powdered and packed inside a long glass tube. But most of the crystalline solids are magnetically anisotropic and may give rise on packing to an orientation effect of the finely powdered crystallites, particularly in a magnetic field. Further, large amount of the substance is necessary and the method is not suitable for observation over a large temperature range. The Curie method allows quick relative measurements on small amounts of powder or solution specimens and is very adaptable for low and high temperature measurements and may be adapted for anisotropic crystals. But these advantages are offset to a great extent by the difficulty of placing the substances always in a standard position in the field. To eliminate this uncertainty several workers [Fereday, (1931) Foex-Forrer (1926), Sucksmith (1939)] have designed shapes of pole pieces in which

maximum $H_x \frac{dH_x}{dy}$ remains constant over an appreciable region. In Foex-Forrer balance the magnetic force is compensated by the electrodynamic force exerted between a current-bearing coil carried on the moving system and a fixed permanent magnet. The balance suspension arrangement, however is extremely cumbrous, gravitation being the main restoring force, the deflection sensitivity is rather low, and stray fields troublesome. Sucksmith ring balance which has been developed by Jackson (1933) for measuring the susceptibility of powders as well as for crystals, is not suitable for small susceptibilities. Quartz microbalance as developed by Bose (1947), is very suitable for low and room temperature measurements for both powders and crystals, but is unsuitable for high temperature owing to convection disturbances. None of these methods can claim more than an overall accuracy of 1%. Further serious uncertainties, which is common to all methods, are the impurities and imperfections and inaccurate setting of crystals for which special care should be taken.

The present is an adaptation of Curie method in which the various sources of errors have been individually and collectively sought to be removed to a large extent, with further scope of improvement which, when done, should make the method unrivalled for reliability.

DESCRIPTION OF THE BALANCE

The balance (Figure 1), essentially consists of a light horizontal torsion arm *A* made of thin walled pyrex glass tubing. This is suspended at the centre from one end of a fine vertical quartz fibre *F*, the other end of the fibre being attached to a torsion head *H*. The torsion head is mounted on the top of an

1" wide glass tube through which the fibre passes. The glass tube is fitted leak-tight to the balance box *S* and to torsion head by conical metal fittings attached with hard sealing wax. One extremity of the balance beam passes out through

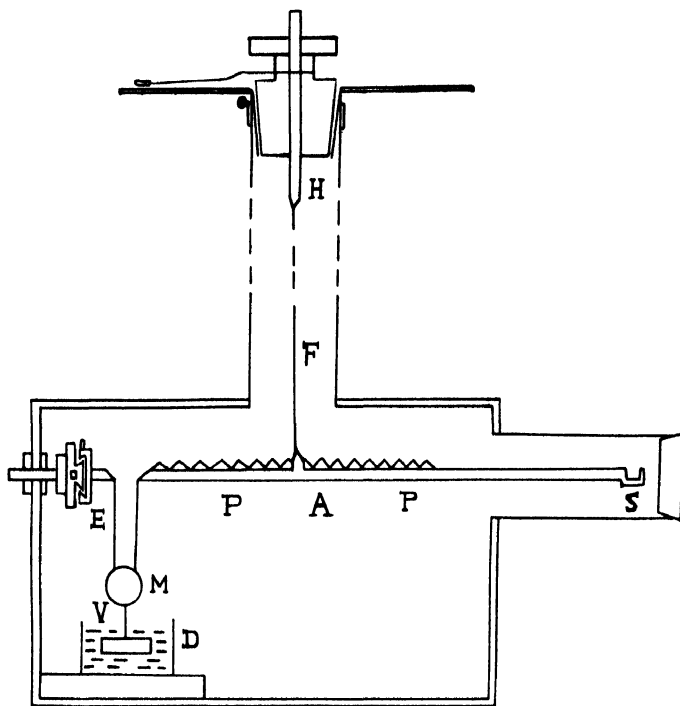


Fig. 1—A sketch of the balance.

a hole on the side of the balance case, to which an extra length of rod is attached, going into the inhomogeneous magnetic field, at the end of which the sample S_1 is mounted. The protruding end is protected from draught and contamination by glass tube fitted by conical metal coupling to the case. At the other end of the beam a sensitive Kelvin bifilar suspension mirror *M* is attached, to magnify the movement of the beam as well as to provide a sufficient controlling couple upon the system. The dashpot *P* contains kerosine oil in which four mica damping vanes *V* hang. The pin *E* is attached to a miniature three dimensional adjustment stage for the bifilar suspension, consisting of a cross slide which can also be moved at right angles to the plane of the slides, and may be adjusted to obtain maximum sensitivity and stability of the system. The brass case *S*, which surrounds the torsion arm and suspended mirror, is mounted upon a stand, with two horizontal cross slides and is also capable of rotation and up and down motion telescopically for the correct adjustment of the position of the sample in the magnetic field. The base of the stand is mounted upon three levelling screws and the whole thing is placed upon a thick marble slab built into the wall of the room. The front of the case has a sliding glass plate through which observations are made; the edges can be made leak-tight with

plasticin. To obtain horizontality of the balance arm when different masses of the substance are used, two scale pans P, P , are attached to the beam within the balance case on which suitable weights are placed. To keep constant loading on the beam always, the final balancing is obtained by taking off load on the arm on the same side of the specimen. Fine adjustments are made by shifting a rider along the beam to which a long thin serrated strip, of mica, is attached for the purpose. The verticality of the suspension fibre and the horizontality of the beam are separately tested by comparison with a fine plumb line of quartz fibre, observed through a low power telescope with circular scale and pointer and fitted with a fine cross-wire. The displacement of the substance on applying the magnetic field, as observed by the movement of the image of a fine glass scale reflected from the bifilar mirror through moderate power telescope, is usually several centimetres. By giving suitable torsions to the suspension fibre by means of the vernier torsion head reading to 10^{th} of a degree, the balance beam is brought back accurately to its original position. In order to rotate the torsion head without causing vibrations of the system, and also to enable the same operator, looking through the telescope from a distance of about two metres (an order to have a high optical magnification), to work the torsion head, this is coupled by a slow gear arrangement and flexible shaft to a small motor which can be reversed, if necessary, with switches close by the observer. The beam, when not in use, may be arrested by a spring catch, and operated from outside by lever mechanism. The interior of the balance may be illuminated for the preliminary adjustments with a small electric lamp (6 volts) inside the casing. The balance is shown in figure 1(a).

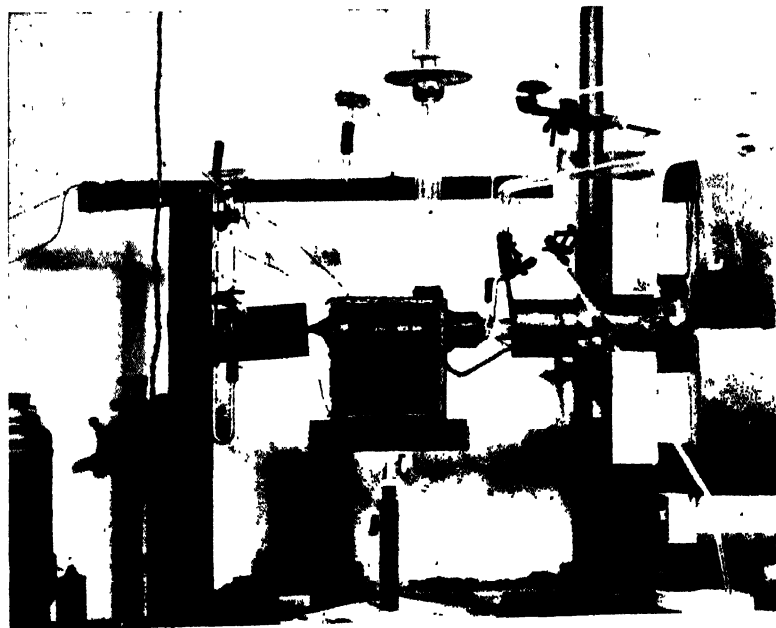


Fig. 1(a)

(a) *Use of vertical field.*

The balance may be conveniently used for measurement of powders and solutions using a horizontal field. If it is desired to measure the principal susceptibility of a crystal, a horizontal field is inconvenient. It would be well nigh impossible to set the crystal with its principal susceptibility direction along the field by trial. So either a series of readings have to be taken by rotating the crystal or the magnet (Hupse, 1942) or by having a flexible suspension (Bose, 1947) so as to let the crystal freely set by itself in the field. But these are attended by great practical difficulties. We have altogether avoided these difficulties by having a vertical field and horizontal gradient. This is simply obtained by turning over our electromagnet on one side with its pole-pieces one above another. The magnet is mounted upon a circular rotating base with three levelling screws and a spirit level so that it may be rotated about a vertical axis and the edges of the pole pieces made accurately vertical in the final position.

(b) *Shaping the gradient*

Designing of pole pieces for the gradient are very carefully done so that at each different current the force $H_x \cdot dH_x/dy$ remains constant over wide regions. Various workers have used special types of pole pieces to obtain the above condition as already mentioned. Sucksmith shape appears to be the simplest and as

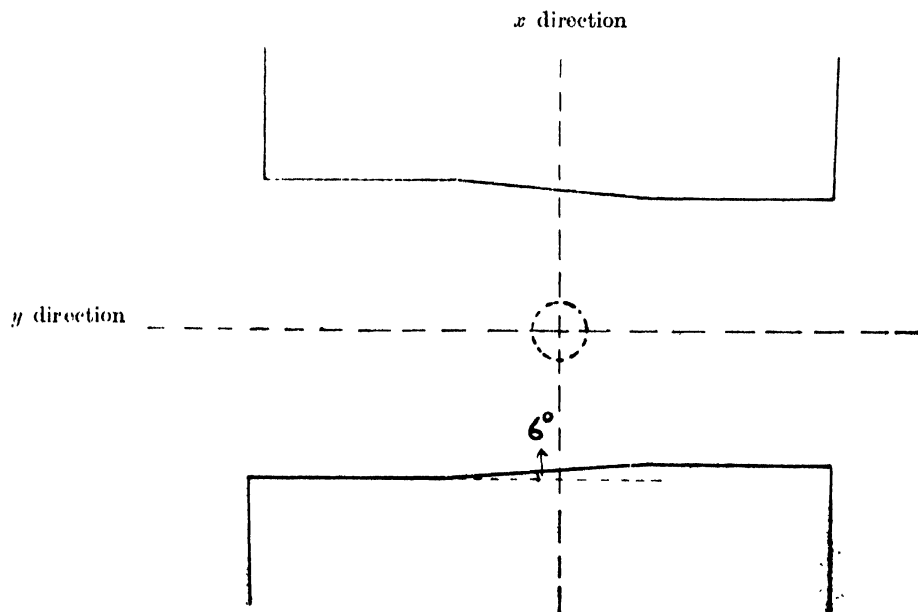


Fig. 2.—Arrangement of the pole faces, section to normal to z direction

effective as any other. We have adopted this with suitable modifications to fit our values of magnet current, pole gap, face area etc., made from theoretical considerations and through experimental checking. To obtain the desired gradient of

the field, a pair of thick rectangular pieces of soft iron, fitting flat on the original large rectangular parallel pole pieces (pole gap 2.5 inches) of our electromagnet, are each marked lengthwise (y direction) into three equal sections. The three sections are then shaped as shown in the figure. 2 below, so that the middle section is inclined at about 6° to the end ones. The best angle is obtained after several trials with slightly differing angles. These pole-shoes are fixed to the original pole-pieces with small soft iron pins near the edges.

The trials consisted of graphical plotting of the force exerted on a paramagnetic sample in the field, at different accurately measured positions within the pole gap, for each of the differently angled pole shoes. The forces are most conveniently measured by the balance already described. For the purpose of plotting absolute forces are not necessary. The angles of torsion proportional to forces can be measured with an accuracy of not less than 0.1%. Temperature is kept constant during each set of measurement. Some typical results are shown in the graphs.

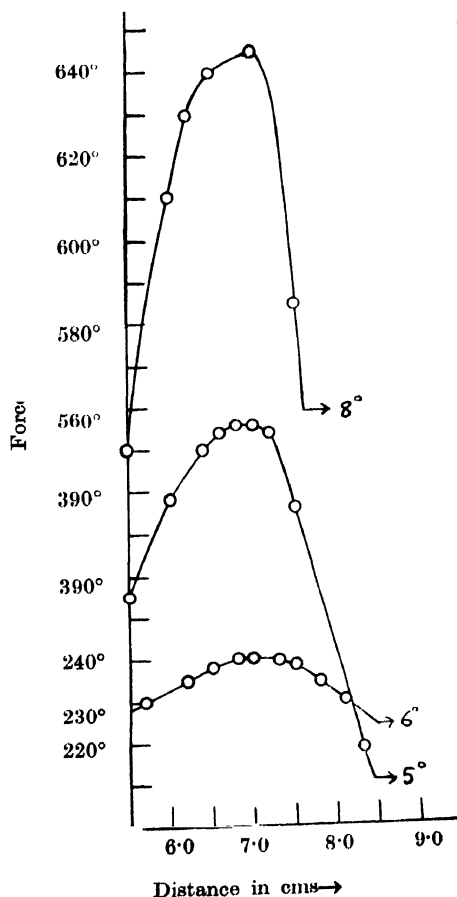


Fig. 3.—Force-distance curves with different pole gradients.

The best constancy of the force about .05% is obtained with the 6° poleshoes, with a magnet current 1.4 ampere over a volume 0.5 cms^3 . Our crystals or other specimens never exceeded this size.

(c) *Mounting the specimen*

The crystal is always placed accurately at the centre of the studied constant maximum region of force between the shaped pole pieces. This is done by having two pieces of graph paper pasted on to two sides of the pole pieces at right angles, marked for the said region, and locating the position of the crystal with reference to these through a telemicroscope from two different positions. The suspension of cubic crystals, powders and solutions is very easy as the question of anisotropy does not arise and is done very conveniently by placing the sample (in the case of solutions and powder samples are packed within a glass container) at the end of a sufficiently long thin glass rod which is formed into a loop to take the sample. The other end is inserted into the hollow beam of the balance and fixed

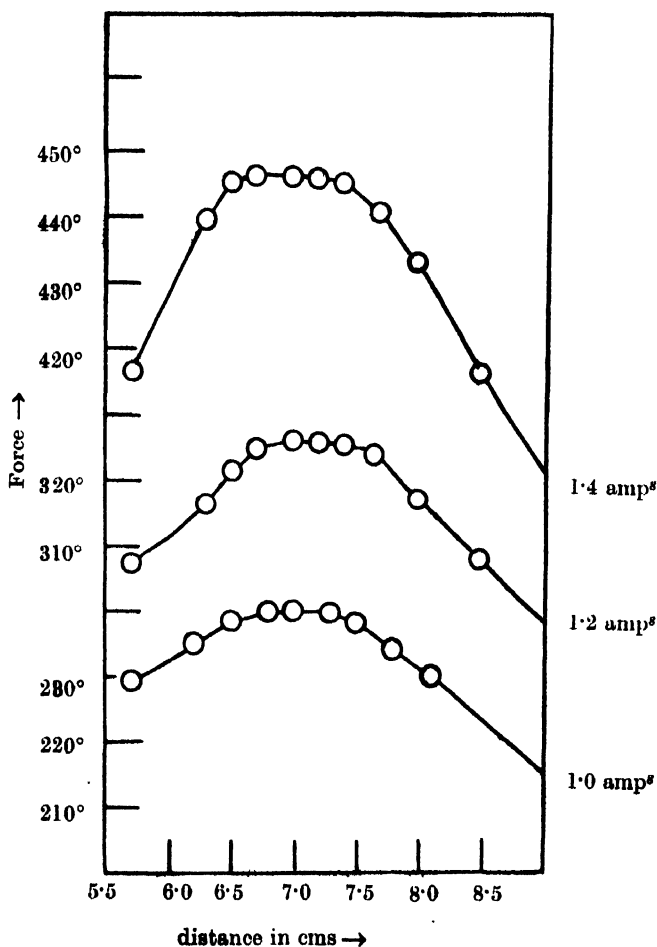


Fig. 4.—Force distance curve with a particular pole gradient with different currents

with durofix cement. But in the measurement of principal susceptibility along a known direction in a crystal, it is attached with durofix to the long rod (without loop) with the desired direction normal to the length of the rod, then the rod is rotated until this direction is vertical and then fixed permanently with durofix. The verticality can be ascertained very accurately by comparison with a fine plumb line, by means of a telemicroscope.

CURRENT CONTROL

The experimental work is done at low values of magnet current usually 1 amp. to 1.4 amps. We have not used any special device for automatically stabilising the magnet current except that we have taken the current from a compound wound D. C. generator, instead of directly from our 6-phase rectified D. C. mains which fluctuate rather badly, and also relied upon the high inductance of the magnet to stabilise the current further. The low values of current also produces no heating effect on the magnetization of the core. Moreover, the current can be accurately adjusted with a fine controlled rheostat and an accurate Weston ammeter viewed through a low power microscope.

CALIBRATION OF THE BALANCE

When the unknown sample of volume v placed in air (k_a) has been restored to the original position in the field by twisting the quartz fibre through an angle θ , against the magnetic force, and the corresponding angle of twist for the standard substance (of volume v_s not very different from v and both smaller, than volume over which $H_x \frac{dH_x}{dy}$ is constant) in the same mean position, some field and at the same temperature is θ_s , we have from equation (4)

$$\frac{\theta}{\theta_s} = \frac{k - k_a}{k_s - k_a} \cdot \frac{v}{v_s} = \frac{m}{m_s} \cdot \frac{\chi - \frac{k_a}{\rho}}{\chi_s - \frac{k_a}{\rho_s}} \quad \dots (5)$$

where m and m_s are the masses, ρ and ρ_s the densities and χ and χ_s the mass susceptibilities of the unknown and standard substance respectively.

$$\chi = \frac{\theta}{\theta_s} \cdot \frac{m_s}{m} \left(\chi_s - \frac{k_a}{\rho_s} \right) + \frac{k_a}{\rho} \quad \dots (6)$$

where $k_a = 0.028 \times (300/T)^2 \times 10^{-5}$ at T° absolute.

As primary standard substance, we have taken aqueous NiCl_2 solution the mass susceptibility of which has been measured very accurately by a number of workers. For NiCl_2 at 20°C the values of gm. mol. susceptibility $\times 10^6$ are 4411 by Weiss and Bruins (1926), 4423 by Brant (1921), 4423 by Bose (1926), 4400 by

Nettleton and Sugden (1939). The mean value is 4431. On the basis, that the effective moment of Ni^{++} does not change with concentration and with small variations of temperature near 300°K , as observed by the above workers, the susceptibility of isolation per gram is given by the formula

$$\chi \times 10^6 = \left(\frac{10160}{T} + 0.7193 - 0.486 \right) C - 0.7193 \quad \dots (7)$$

where C = the conc. of solution in grams of NiCl_2 per gram of solution.

T = the absolute temp. χ_w for water at $20^\circ\text{C} = 0.7193 \times 10^{-6}$.

The solution used by us made from A. R. quality of E. Merck is free from cobalt, dissolved in double distilled water having $C = 0.2590$ and density at $305.8^\circ\text{K} = 1.2993$.

The reliability of performance of the balance, including accuracy, stability, reproducibility, sensitivity etc. is checked in the following manner.

(a) Ferric alum crystal grows in cubic class as regular octahedron so that it has neither magnetic anisotropy nor appreciable shape effect. A carefully purified and well grown crystal weighing 0.04080 gms. is carefully mounted at the end of the balance arm, centred carefully in the region of constant H_x , dH_x/dy and the torque due to magnetic field upon the system is exactly balanced by slowly twisting the fibre, observing the image of the zero of the illuminated scale through the telescope. The angle of torsion necessary for this purpose is corrected for the force upon the arm alone. The temperature is noted accurately. The torsion head is restored to its initial position, and the field is switched off. No appreciable zero shift is generally observed. The same operations are performed with a pyrex glass ampoule filled with a weighed quantity of standard NiCl_2 solution. Here correction has to be made for the empty ampoule. The relevant data necessary for the calculation of mass susceptibility of the alum is given in Table I, for one typical case. The diamagnetic corrections are made from Stoner. Measurements with five different crystals were made. The standard reading is repeated every time. Any small temperature fluctuation during these experiments is noted and corrected for. The individual readings do not differ from the mean by more than 0.1%. The value of the effective magnetic moment μ_{eff}^2 is found to be 35.08 at 300°K which is a little more than $\frac{1}{2}\%$ greater from the value obtained by Onnes and Oosterhuis, (1926), well within the limits of accuracy of these authors. It has been, however, shown by Van Vleck and Penney (1934) that Fe^{+++} ion which is in ${}^6S_{5/2}$ state, the mean susceptibility, should obey a Curie law strictly upto $1/T^2$ terms at least. The 'spin only' value for the mean square moment is then 35.04 which is a little more than 0.1% smaller than our values and just within the conservatively estimated limit of error about 0.2% of our experiment. Terms of higher order than $1/T^2$ might introduce a very small departure from spin only value. But the present results are not able to point to it.

(b) Chromium potassium alum also grows in cubic class in the form of regular octahedron. Crystals were prepared from carefully purified samples of the salt and magnetic measurements performed with NiCl_2 solution as standard, in a similar way as above. The final value for the susceptibility is the mean for at least five crystals and is given in Table I. The value for mean square of the effective moment is 15.05 which may be compared to the earlier values 14.80 by de Haas and Gorter (1929) and 15.05 Mme. Serres, (1932). Since Serres has shown that Leiden data suffered from errors in calibration, and agreed very well with her own value after necessary corrections, we have quoted only these values in Table I, which agree with our own to within less than 0.1%. It is possible that for the same reason Leiden value for Fe^{+++} alum quoted earlier is less than ours. Our values for Cr^{+++} are definitely higher by 0.3% than the spin only value of 15.00.

(c) To check the reliability and reproducibility of our measurement further we have measured the sample of Fe^{+++} alum against a different sample of Cr^{+++} alum as secondary standard, taking 15.045 as the value of mean μ_{eff}^2 . The relevant data are given in the table. The value of Fe^{+++} alum comes out as 35.09, to within 1 part in 3500 of our previous value.

(d) As a last check of our method, applied to anisotropic crystals, we have measured a crystal of $\text{NiSO}_4 \cdot 6\text{H}_2\text{O}$ (tetragonal) along its tetragonal axis. The crystal grows as di-tetragonal pyramid and has little anisotropy of shape for a well grown crystal. The value of μ_{eff}^2 is found to be 9.768 as against 9.736, a careful measurement by Mookerji (1946), using a modified Rabi method of high sensitivity, a difference of 0.3% within the limits of error of Mookerji.

Further details of rigorous tests of the balance in the low temperature range and a comparison of our thermometric scale with Leiden standard is given in the next section.

THE CRYOSTAT AND LOW TEMPERATURE MEASUREMENT

For accurate low temperature measurements of magnetic susceptibility, a suitable gas flow type cryostat (horizontal) has been constructed. The new cryostat is a modified design of that already in use in our laboratory (Bose, 1947). The cryostat consists of a double walled chamber closed at the bottom with thin copper sheet 5.5" length 2.4" outer diameter $\frac{1}{4}$ " interspace between the walls. Inner space is packed with fine copper wire gauze through the centre of which passes the experimental tube of thin copper 1" in diameter closed at the bottom. The annular space between the walls is connected by a stainless steel capillary tube $\frac{1}{4}$ mm inner diameter to a mercury manometer system and serves as a constant volume air thermostatic control unit. Two platinum contacts, one at the surface of mercury, the other inside mercury are

TABLE 1

Comparison of p_{eff}^2 for the F_e^{+++} and C_r^{+++} alum and $NiSO_4 \cdot 6H_2O$.

Mass and density of the substance with corresponding rotation on torsion head		Mass susceptibility		p_{eff}^2 in Bohr magneton units at 300°K	
Standard Substance	Unknown Substance	$\chi_g \times 10^6$	$\chi_m \times 10^8$	Present Value	Earlier Value
NiCl ₂ $m=0.12140$	Fe ⁺⁺⁺ alum $m=0.04080$				35.04 Spin only value,
$\rho=1.2998$	$\rho=1.724$	7.9287	28.94	35.08	34.89 (Onnes and Oosterhuis).
$\theta=227.4^\circ$	$\theta=284.9^\circ$	at 306.4 °K	at 306.4 °K		
NiCl ₂ $m=0.12140$	Cr ⁺⁺⁺ alum $m=0.08500$				15.05 (de Haas & Gorter as corrected by Serres).
$\rho=1.2993$	$\rho=1.842$	7.9287	11.715	15.04	15.06 (Serres). 15.00 (Spin only).
$\theta=227.4^\circ$	$\theta=235.6^\circ$	at 306.4°K	at 306.4°K		
Cr ⁺⁺⁺ alum $m=0.12100$	Fe ⁺⁺⁺ alum $m=0.04080$				
$\rho=1.842$	$\rho=1.724$	11.91	29.51	35.09	
$\theta=80.5^\circ$	$\theta=67.3^\circ$	at 300.70°K	at 300.7°K		
Cr ⁺⁺⁺ alum $m=0.12280$	NiSO ₄ ·6H ₂ O (along axis) $m=0.15200$				
$\rho=1.842$	$\rho=2.080$	11.65	14.555	9.768	9.736 (Mookherji).
$\theta=120.8^\circ$	$\theta=186.6^\circ$	at 307.0°K	at 307.0°K		

connected in the usual way to a magnetic relay breaking and making a suction pump motor circuit. The top of the chamber is closed by a german silver cup through which the experimental tube, upper part of which is made also of german silver, and two other stainless steel pipes of 2mm diameter, pass out. Of the two pipes one goes to the bottom of the chamber and is connected outside by a soft cork coupling to one end of a vacuum-jacketted pyrex glass tube carrying cold gas from the refrigerant storage chamber. The other pipe, which is cut short below the cryostat top, is connected to the suction pump through a large pressure stabilizing bottle and carries the exhaust gas from the cryostat chamber. The refrigerant chamber is a german silver cylindrical vessel closed at both ends kept within a wide mouthed thermos bottle and contains liquid oxygen. The level of liquid oxygen is indicated by a glycerine pressure gauge and can be replenished through a tube at the top of the chamber usually kept closed with a cork. Atmospheric air dried by a dehydrating tower is cooled by passage through a copper spiral immersed in liquid oxygen, and is sucked into the cryostat chamber through the vacuum line by

the suction pump. While passing through the wire gauze packing of the chamber the current of cold air comes into intimate contact with the large highly conducting surface area of the gauze, and is effectively deprived of cold. The turbulent flow as also the high conductivity of the material causes a good uniformity of temperature over a large portion of the chamber. Uniformity of temperature and conservation of cold are further improved by suitable adjustment of thermal capacity of chamber and enclosing the whole within a silvered pyrex cylindrical Dewar vessel which is protected from breakage by a metal casing. The german silver part of the experimental tube is coupled with durofix cement to the glass tube attached to balance case, through which the balance beam passes into the experimental tube.

The thermostatic relay system is preset to a given low temperature. When this is reached, the relay switches off the pump. The small heat leakage into the system tends to raise the temperature and the relay switches on the suction pump again and temperature may be maintained fairly accurately constant. For extremely fine control, a controlled leak is introduced on the pump side, by adjusting which and also the speed of the pump by a rheostat the heat leak from outside may be accurately balanced by the continuous cold in-flow carried by the circulating gas, and the temperature control to within 0.01°K may be achieved. For quicker work, where less sensitivity is required, the cooling spiral in refrigerant chamber is dispensed with and liquid air in controlled quantities may be directly sucked in the cryostat chamber, allowed to evaporate at the bottom of the chamber and circulated through the system as before.

Evidently the cryostat has to be set up in a horizontal position so as to go between the pole pieces of the magnet placed on its side with one pole above another as already mentioned.

Low temperature measurements of susceptibility requires a little modification in the room temperature use of the balance. A stop for the beam has to be placed at the outlet in the balance case so that the specimen may not come in contact with experimental tube and stick there. Another trouble in the measurement of the balance at low temperature arises from deposition of moisture on the cold part of the beam. This is prevented by making all fittings of the balance case leak-tight with durofix and plasticin and not only keeping a strong dehydrating agent within the balance case but also washing inside with dry air from an elaborate dehydrating tower system before the low temperature run is started.

TEMPERATURE MEASUREMENT

The temperature is measured with an accuracy of 0.1°K with a copper-constantan thermocouple, the E.M.F. being measured in the usual manner with a Leeds Northrup potentiometer reading to 2 microvolts. The thermocouple is calibrated at the usual standard low temperature points and also against one

calibrated earlier by Bose (1947) and checked from time to time. Our thermocouple shows a systematic deviation from the earlier one, which is no doubt due to differences in composition and history of the couple. For this reason we wanted to make a check for the calibration of our couple. This is done by taking magnetic susceptibility measurements on substances well known to obey Curie law to the degree of accuracy derived in the relative susceptibility and temperature measurements on Leiden scale on these substances. Two such convenient substances are ferric ammonium alum and chromium potassium alum, and we have measured the mean susceptibility of these as before. The formula used by us is

$$\frac{F_T}{F_\theta} = \frac{\chi_T}{\chi_\theta} \left[1 + \frac{k_{a\theta}}{k_\theta} \left(1 - \gamma\theta \right) \left(1 - \frac{\theta}{T} \right) \right] \quad \dots (7)$$

where χ_T , and χ_θ^i are the gram. molecular susceptibilities of the crystal at temperature T and room temperature respectively, and F_T and F_θ are the forces acting on the crystal at these temperatures, $k_{a\theta}$ and k_θ are the volume susceptibility of air and that of the crystal at room temperature θ , and γ is the coefficient of thermal volume expansion of the crystal.

The results as compared to those of earlier workers are given below.

TABLE II
Temperature variation of the gm. molecular susceptibility of
 $\text{Fe}_2(\text{SO}_4)_3 \cdot (\text{NH}_4)_2 \cdot \text{SO}_4 \cdot 24\text{H}_2\text{O}$

Onnes & Oosterhuis			Present Author		
Temp °K (Leiden scale)	$\chi_M \cdot 10^6$ (room temp. value corrected by us.)	p_{eff}^2	Temp °K (Our scale)	$\chi_M \cdot 10^6$	p_{eff}^2
290.0	15010	35.07	300.5	14470	35.08
			278.8	15600	35.06
169.6	25370	34.70	242.0	17980	35.07
77.1	56040	34.83	222.1	19670	35.05
			195.5	22110	34.84
			179.2	24090	34.81
			171.2	25170	34.74
			147.8	29360	34.83
			133.2	32570	34.97
			121.0	35880	35.00
			99.0	43740	34.91

TABLE III

Temperature variation of the gm. molecular susceptibility of
 $\text{Cr}_2 \cdot (\text{SO}_4)_3 \cdot \text{K}_2\text{SO}_4 \cdot 24\text{H}_2\text{O}$.

de Haas & Gorter (Corrected by Serres)			Serres			Present author		
Temp.°K (Leid. Scale)	$\chi_M \times 10^6$	p_{eff}^2	Temp.°K (Inter. Scale)	$\chi_M \times 10^6$	p_{eff}^2	Temp.°K (Our Scale)	$\chi_M \times 10^6$	p_{eff}^2
290.0	6437	15.05	292.2	6377	15.05	305.0	6119	15.04
169.7	10980	15.02	292.0	6385	15.03	299.5	6317	15.05
143.6	12960	15.00	291.2	6403	15.03	272.0	6792	14.90
77.7	24010	15.04	89.7	20708	14.97	247.0	7457	14.91
						230.4	8019	14.90
						227.6	8098	14.87
						212.0	8710	14.90
						200.0	9204	14.85
						199.5	9226	14.86
						170.3	10910	14.98
						169.7	10940	14.99
						158.0	11800	15.03
						157.4	11810	15.00
						146.0	12740	14.99
						138.0	13490	15.01
						132.1	14020	14.93
						113.5	16320	14.95
						103.8	17800	14.90
						102.0	18170	14.94
						101.0	18290	14.90

The values of p_{eff}^2 when plotted against T should give a straight line parallel to T -axis for substances obeying Curie law exactly. Such a graphical presentation is extremely sensitive not only to experimental errors but also to small departures from ideal Curie law. On plotting all the values for Fe^{+++} alum in a single graph (figure 5) we find that all the three available Leiden values at three different temperatures after correction for the room temperature values as indicated earlier, fall exactly on the same curve as our results. This value as indicated not only values of Leiden in agreeing with ours, are more accurate than their room temperature value, but also our measured temperatures fit perfectly well with the Leiden scale. It is very unlikely that errors in susceptibility and temperature measurements happened to be in opposite directions at all the comparison temperatures so that an accidental fit has been obtained.

In further support as to evidence against such a chance, we have our p_{eff}^2 -versus- T curve for Cr^{+++} alum (figure 6). Serres', de Haas and Gorter's values for this salt again fit in quite well with our curve. All these data are thus additional evidence for the accuracy and reliability of our methods of measurement of susceptibility as well as temperature.

It is of some interest to note that our curve for Fe^{+++} alum shows a small departure from Curie law, by a deviation from linearity and a minimum at about 170°K . This deviation is reproducible for different samples of crystals and is reversible with temperature. It was already noticeable in the Leiden measurement, but was not given any significance. Our curve being plotted for a large number of successive temperatures, shows the effect very well, and without any doubt.

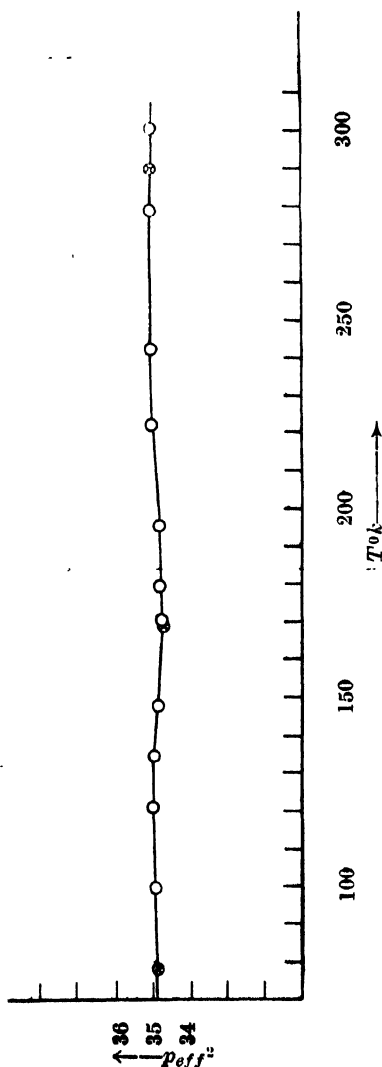


Fig. 5.— p_{eff}^3 .— T curve for ferric alum.

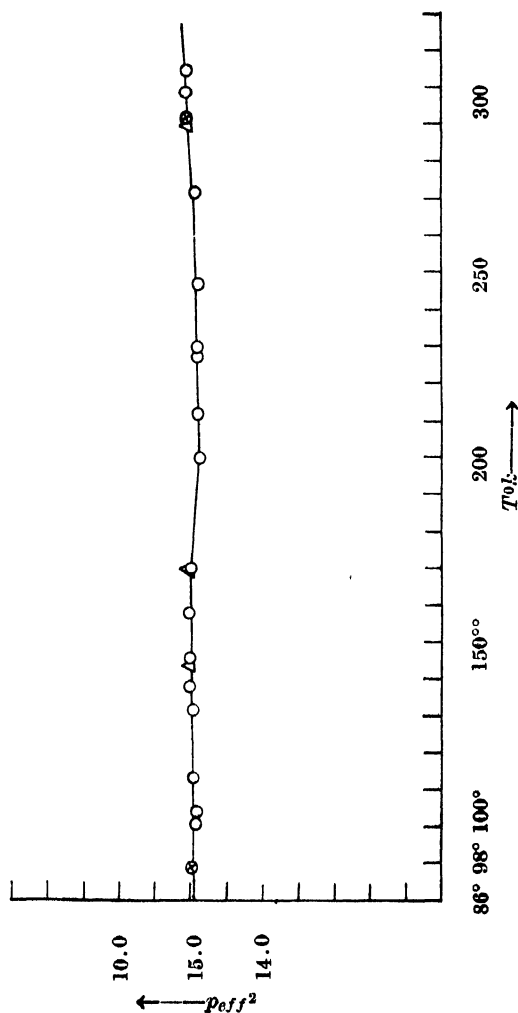


Fig. 6.— p_{eff}^3 .— T curve for chrome alum.

Cr^{+++} alum also shows a similar noticeable change at about 200°K . These departures are evidently due to some small thermal changes in the internal structures causing changes in the electric fields in the crystals, similar to those observed

by Bose, Mitra, and Datta in Cu^{++} and Ni^{++} salts (in course of publication). A study of the magnetic behaviours of a large number of alums of the iron group has been completed by the present method, and will be discussed in details in future communications.

ACKNOWLEDGMENTS

The author expresses his sincerest thanks to Dr. A. Bose, D.Sc., for suggesting the problem and for his keen interest throughout the progress of the work.

REFERENCES

- Bose, A., 1935, *Proc. Ind. Acad. Sci.*, **1**, 606.
Bose, A., 1947, *Ind. Jour. Phys.*, **21**, 277.
Curis, P., 1895, *Jour. de Phys.*, **4**, 187, 263.
de Haas, W. J. and Gorter, C. J., 1920-31, *Comm. Leiden.*, no. 208 c.
Datta, S. K., 1953, *Ind. Jour. Phys.*, **27**, 155.
Datta, S. K., 1954, *Ind. Jour. Phys.*, **28**, 239.
Dutta Roy, S. K., 1954, *Ind. Jour. Phys.*, **28**, 183.
Fereday, R. A., 1931, *Proc. Phys. Soc.*, **43**, 383.
Foex, G. and Forrer, R., 1926, *Jour. de Phys.*, **7**, 180.
Jackson, L. C., 1933, *Proc. Roy. Soc., A* **140**, 695.
Brant, L., 1921, *Phys. Rev.*, **17**, 678.
Hupse, J. C., 1942, *Physica*, **9**, 633.
Mookerji, A., 1946, *Ind. Jour. Phys.*, **20**, 9.
Nettleton, H. R. and Sugden, S., 1939, *Proc. Roy. Soc.*, **173**, 313.
Onnes, H. K. and Oosterhuis, E., *Comm. Leiden.*, no. 139c.
Rabi, I. I., 1927, *Phys. Rev.*, **29**, 174.
Serres, A., 1932, *Ann. d. Phys.*, **17**, 551.
Stoner, E. C., *Magnetism and Matter*, (1934, Methuen, London).
Sucksmith, W., 1939, *Proc. Roy. Soc.*, **17**, 551.
Van Vleck, J. H., and Penney, W. G., 1934, *Phil. Mag.*, **17**, 961.
Weiss, P. and Bruins, T. L., 1926, *Proc. Amst. Acad.*, **18**, 246.

AN APPROXIMATE METHOD OF CALCULATING THE VIBRATION FREQUENCIES OF 1, 1, 1-TRICHLOROETHANE MOLECULE*

By D. C. BISWAS

OPTICS DEPARTMENT, INDIAN ASSOCIATION FOR THE CULTIVATION OF SCIENCE, JADAVPUR,
CALCUTTA-32

(Received for publication, August 6, 1955)

ABSTRACT. It has been shown that when the 1,1,1-trichloroethane molecule is divided into two parts and the vibration frequencies are calculated under certain assumptions for these two parts, these frequencies agree with those calculated for the whole molecule by the accurate method. It is pointed out that this approximate method is simpler and less time-consuming than the elaborate one while the discrepancies in the results obtained by this approximate method are quite negligible.

INTRODUCTION

The force constants of the 1, 1, 1-trichloroethane molecule have been calculated by El-Sabban *et al* (1951) by the accurate method using properly chosen fundamental frequencies. In these calculations they had to derive and solve secular equations of sixth and fifth degrees for the vibrations of classes E and A_1 respectively. The derivation of the secular equation is a lengthy process even when Danielewsky's method is used, because for the vibrations of class E a determinantal equation containing six rows and six columns is to be first expanded. If it would be possible to subdivide the modes of either of these two classes into two groups it would be easier to expand two determinantal equations of three rows and three columns than to expand the equation containing six rows and six columns mentioned above. Such a subdivision is possible only if we divide the molecule into two parts and consider one part at a time. There may be, however, some difficulty in choosing the proper masses which should be taken in the calculations for particular modes of vibration. The object of the present investigation is to find out whether we can divide the 1, 1, 1-trichloroethane molecule into two parts, $X-CCl_3$ and $Y-CH_3$ and calculate the fundamental frequencies correctly using the force constants used by El-Sabban *et al*. In doing this, two sets of calculations have been made in each case using different values of masses of X and Y till agreement has been obtained with the results reported by El-Sabban *et al*.

* Communicated by Prof. S. C. Sirkar.

CALCULATIONS AND RESULTS

The fundamental frequencies are calculated in each case by first determining the F-matrix and using the force constants given by El-Sabban *et al* (1951) and then calculating the G-matrix with the help of the tables given by Decius (1948). The symmetry coordinates used are exactly those used by El-Sabban *et al* (1951). The masses of the atoms, the interatomic distances and the bond angles used in these calculations are also the same as those used by El-Sabban *et al* (1951).

We get only three symmetry coordinates in A_1 species for the group $X-CCl_3$ (figure 1). These are given below, the notations for displacements being the same as those used by El-Sabban *et al* (1951).

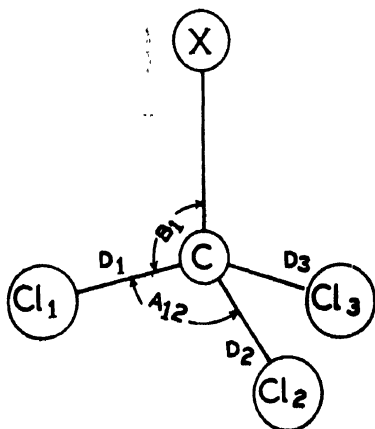


Figure 1.

$$R_1 = \Delta r$$

$$R_2 = (\Delta D_1 + \Delta D_2 + \Delta D_3) / \sqrt{3}$$

$$R_3 = (\Delta A_{12} + \Delta A_{13} + \Delta A_{23} - \Delta B_1 - \Delta B_2 - \Delta B_3) / \sqrt{6}$$

These give an F-matrix of three rows and three columns.

Similarly for E species we get the following three symmetry coordinates along with the other three degenerate with these three coordinates.

$$R_{1a} = (\Delta D_1 - \Delta D_3) / \sqrt{2}$$

$$R_{2a} = (\Delta A_{23} - \Delta A_{12}) / \sqrt{2}$$

$$R_{3a} = (\Delta B_1 - \Delta B_3) / \sqrt{2}$$

We first consider the following two cases :

Case I. Mass of X = that of CH_3

Case II. Mass of X = that of C.

The calculated frequencies are given in Table I along with those given by El-Sabban *et al* (1951) for comparison.

TABLE I

ν in cm^{-1}

Designation	Present values		El-Sabban <i>et al</i> (1951)	
	Case I	Case II	Calc.	Observed (gas)
ν_4	1003	1052	1002	1012
$A_1 \nu_4$	522	543	521	524
ν_5	343	348	343	343
ν_{10}	716	716	716	720
$E \nu_{11}$	345	362	363	—
ν_{12}	235	241	241	241 (liq)

We next consider the following two cases for the $Y\text{-CH}_3$ group :

Case III. Mass of Y = mass of CCl_3

Case IV. Mass of Y = mass of C.

The results are given in Table II.

TABLE II

ν in cm^{-1}

Designation	Present values		El-Sabban <i>et al</i> (1951)	
	Case III	Case IV	Calc.	Obs. (gas)
ν_1	2941	2941	2943	2954
$A_1 \nu_2$	1376	1376	1377	1381
ν_3	754	1066	1002	1012
ν_7	3008	3008	3010	3017
$E \nu_8$	1431	1442	1434	1445
ν_9	1048	1067	1074	1087

DISCUSSION

We find from Table I that in the case of vibrations of A_1 species in $X-CCl_3$ group the calculated values of ν_3 , ν_4 and ν_5 agree closely with those given by El-Sabban *et al* (1951) if we assume that the whole group CH_3 moves as a single mass, while in the case of the degenerate vibrations agreement is found if we assume that only the carbon atom takes part in the vibrations, effect of the presence of hydrogen atoms being negligible.

In the case of the $Y-CH_3$ group, however, the values of the frequencies of both A_1 and E vibrations calculated on the assumption that only carbon atom is present in group Y agree with those given by El-Sabban *et al* except in the case of ν_3 . The discrepancies in the case of ν_8 and ν_9 are small being within 0.75%. These calculations demonstrate the fact that when hydrogen atoms are attached to any heavy atom we have to assume that the former move along with the latter in any mode of vibration in which the heavy atom is mainly displaced. Thus we see that on these assumptions it is possible to subdivide the species into smaller groups and to obtain simpler secular equations giving correct values of the frequencies or force constants as the case may be. These principles can also be applied to more complicated molecules in the case of which the accurate method gives a very complicated secular equation. Attempts are being made in this direction.

ACKNOWLEDGMENT

The author is indebted to Professor S. C. Sirkar, D.Sc., F.N.I. for his kind help and constant guidance during the progress of this work.

REFERENCES

- Decius, J. C., 1948, *J. Chem. Phys.*, **16**, 1025.
El-Sabban, M. Z., Meister, A. C., and Cleveland, F. F., 1951, *J. Chem. Phys.*, **19**, 855

Letter to the Editor

NEW EVIDENCE FOR THE PREPONDERANCE OF THE CIS FROM IN ORTHO-CHLOROPHENOL MOLECULE

DILIP KUMAR GHOSH

INDIAN ASSOCIATION FOR THE CULTIVATION OF SCIENCE, CALCUTTA

(Received for publication, August 13, 1955)

From a study of the values of dielectric loss observed in the solution of some substituted benzenes in the metre wave length region Fischer (1949) inferred that orientation of some substituent groups having rotational freedom contributes to dielectric loss in this region. It was actually observed by the present author (Ghosh 1954*a*, 1954*b*, 1955) that some substituted benzenes, such as benzyl chloride, benzyl amine, phenol, etc., show absorption maxima corresponding to rotation of the substituent group about the diameter of the benzene ring passing through the point of substitution. Similar investigations in the microwave region have been extended to some molecules with OH as the substituent group and absorption maxima have been observed at suitable temperatures.

According to Debye's theory (Debye, 1929) the radius of the rotor depends on τ , the time of relaxation and η , the viscosity of the liquid, and if the same substituent group having a freedom of rotation be present in different molecules, the ratio $\frac{\tau T}{\eta}$ should be constant, T being the absolute temperature of the liquid.

There are many compounds having OH group as a substituent and it would be interesting to find out whether the above relation is satisfied in the case of these compounds. The study of absorption of 3.18 cm. microwaves in benzyl alcohol, *o*-cresol, *m*-cresol, cyclohexanol, phenol and glycerine showed that the ratio $\frac{\tau T}{\eta}$ is almost constant in all these cases. In the case of *o*-chlorophenol, however, no absorption was observed in the 3.18 cm. region in the whole temperature-range from the melting point of the substance to its boiling point. On the contrary, *p*-chlorophenol shows absorption in the whole temperature-range from 50°C to 170°C with a maximum at 85°C (figure 1). The value of τ leads to a value 1.55 A.U. as the radius of the rotor and this is the radius of the circle along which the OH group moves during free rotation. The difference in the behaviours of ortho- and para chlorophenol molecules mentioned above demonstrates the fact that in the ortho compound the OH group has no freedom of rotation about the C—O

bond. The hydrogen atom is linked to the chlorine atom attached to the adjacent carbon atom as shown in figure 2. The absence of absorption in the case of *o*-chlorophenol furnishes an additional proof of the existence of such a linkage between the hydrogen and chlorine atoms in the molecule as postulated by Pauling (1939).

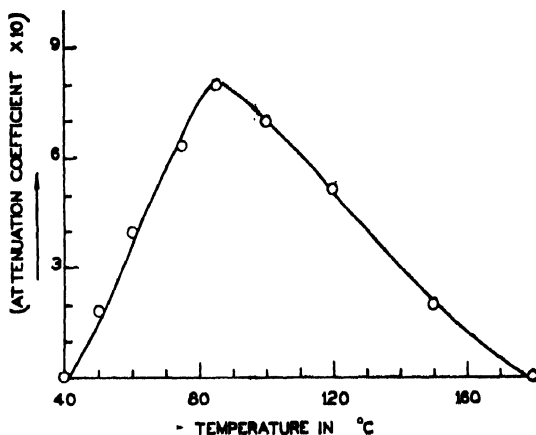


Fig. 1

The infra red absorption spectrum of a solution of *ortho* chlorophenol in carbon tetrachloride shows two peaks at 7050 cm^{-1} and 6910 cm^{-1} with the area of the latter peak ten times that of the former. From this Pauling (1936) concluded that the ratio of the numbers of *cis* and *trans* molecules is 10:1 in the solution.

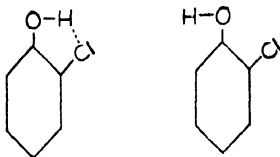


Fig. 2

In the case of the pure liquid, however, there is no absorption of the 3.18 cm. waves in the liquid throughout the temperature-range from melting point to the boiling point, and this shows that all the molecules are of the *cis* form in which the hydrogen atom is attached to the chlorine atom through virtual linkage.

Details will be published elsewhere.

My grateful thanks are due to Prof. S. C. Sirkar, D.Sc., F.N.I., for kindly suggesting the problem and for his constant guidance during the progress of the work.

REFERENCES

- Debye, P., 1929, Polar molecules, Chemical Catalog Co.
Fischer, Von, E., 1949, *Z. Naturforsch.*, **4a**, 707.
Ghosh, D. K., 1954*a*, *Ind. J. Phys.*, **28**, 191.
Ghosh, D. K., 1954*b*, *Ind. J. Phys.*, **28**, 485.
Ghosh, D. K., 1955, *Ind. J. Phys.*, **29**, 161.
Pauling, L., 1936, *J. A. C. S.*, **58**, 94.
Pauling, L., 1939, The Nature of the Chemical bond, Cornell University Press, p. 303.

HIGHER APPROXIMATIONS TO DIFFUSION COEFFICIENTS AND DETERMINATION OF FORCE CONSTANTS*

BY S. C. SAXENA

INDIAN ASSOCIATION FOR THE CULTIVATION OF SCIENCE, CALCUTTA-32.

(Received for publication, August 3, 1955)

ABSTRACT. Recently we have reported the computed values of several Chapman and Cowling collision integrals for gases obeying the Lennard-Jones 12 : 6 model over an extensive range of temperatures. Making use of these collision integrals along with those reported by Hirschfelder, Bird and Spotz, the correction factor for the third approximation to the tracer diffusion has been calculated by utilising the expressions developed by Mason on the scheme adopted by Chapman and Cowling. The third approximation to the coefficient of interdiffusion and the second approximation to the thermal diffusion ratio have also been calculated for the particular case of A-He mixture. The effect of these higher approximations on the determination of the force parameter from the temperature dependence of the transport coefficients have been critically examined. It has been shown that these higher approximations do not vitiate the method developed by Srivastava and Madan elsewhere for calculating the force constants from the thermal diffusion data for unlike molecules.

1. INTRODUCTION

The Chapman-Enskog kinetic theory of gases is developed on several simplifying assumptions which, to some extent, limit the applicability of the final results and thus rigorously holds only for dilute monatomic gases and at temperatures high enough that quantum effects are negligible. The theory under these limitations expresses the transport coefficients as infinite series, higher approximations to the coefficients being obtained if larger number of terms of the series are taken. Fortunately, the convergence of the series is rapid and only a few terms need be considered. These terms involve a set of collision integrals through which the dynamics of a molecular encounter and hence the intermolecular forces get involved. Thus the results can immediately be utilised to predict any transport property, provided we know the intermolecular potential. Investigations so far in this field have shown that the Lennard-Jones 12 : 6 potential is the most realistic molecular model, though recently Mason (1954) has calculated the transport property collision integrals for the modified Buckingham (Exp-Six) potential. This latter work has been completed so recently that uptill now only the force constants for a few molecules have been determined, and the relative appropriateness of the model still awaits confirmation. The aim of the present report is to calculate the higher approximations to diffusion coefficients by utilising the expressions given by Mason (1954) and to estimate their effect on the evaluation of

* Communicated by Prof. B. N. Srivastava.

force parameters by the methods developed by Srivastava and Madan (1952, 1953) based on the temperature variation of diffusion coefficients.

2. THEORY AND FORMULAE

According to the Lennard-Jones 12 : 6 model the interaction energy between the two molecules for a separation ' r ' is

$$E_{ij}(r) = 4\epsilon_{ij}[(r_{ij}/r)^{12} - (r_{ij}/r)^6] \quad \dots (1)$$

where ϵ_{ij} is the minimum potential energy of attraction and r_{ij} the separation for zero interaction energy.

The n th approximation to the coefficient of mutual diffusion of a binary mixture of gases 1 and 2 is given by Chapman and Cowling (1952) and Hirschfelder, Curtiss and Bird (1954) as

$$[D_{12}]_m = 0.0026280 \frac{\sqrt{T^3(M_1 + M_2)/2M_1M_2}}{p r_{12}^2 \Omega_{12}^{(1,1)*} (T_{12}^*)} f_{D_{12}}^{(m)} \quad \dots (2)$$

where D_{12} is the mutual diffusion coefficient in $\text{cm}^2/\text{sec.}$, p is the pressure in atmospheres, M_1 and M_2 are the molecular weights of the species 1 and 2; T_{12}^* is the reduced temperature and is equal to kT/ϵ_{12} and the reduced collision integrals $\Omega_{ij}^{(l,n)*}$ are just the collision integrals of Chapman and Cowling divided by their values for rigid spheres of diameter r_{ij} . The factor $f_{D_{12}}^{(m)}$ is best expressed in the determinant notation of Chapman and Cowling (1952) as

$$f_{D_{12}}^{(m+1)} = a_{00} A_{00}^{(m)} / A^{(m)} \quad \dots (3)$$

where $A^{(m)}$ is a determinant of $(2m+1)$ th order whose general element is a_{ij} , with i and j ranging from $-m$ to m . The term $A_{00}^{(m)}$ is the minor of $A^{(m)}$ obtained by deleting the row and column containing a_{00} . The elements a_{ij} are functions of the collision integrals, the molecular weights, and the relative concentrations of the gases in the diffusing mixture and are given by Mason (1954) for i and $j = 2$.

The expression for $f_D^{(m)}$ is considerably simplified for the case of tracer diffusion and self-diffusion. For tracer diffusion, where the concentration of one component $\rightarrow 0$, we get

$$f_D^{(m)} = 1/(1 - \Delta_1 - \Delta_2 \dots \Delta_{m-1}) \quad \dots (4)$$

where Δ_1 and Δ_2 are given by

$$\begin{aligned} \Delta_1 &= a_{01}^2 / (a_{00} a'_{11}) \\ \Delta_2 &= (a_{01} a'_{12} - a_{02} a'_{11})^2 / \{a_{00} a'_{11} (a'_{11} a'_{22} - a'_{12}^2)\} \end{aligned}$$

The m th approximation to the thermal diffusion ratio, $[K_T]_m$, of a binary mixture is given in the determinant notation of Chapman and Cowling (1952) as

$$\left[K_T \right]_m = \frac{5}{2} \frac{x_1 A_{01}^{(m)} \left(\frac{M_1 + M_2}{2M_1} \right)^{\frac{1}{2}} + x_2 A_{0-1}^{(m)} \left(\frac{M_1 + M_2}{2M_2} \right)^{\frac{1}{2}}}{A_{00}^{(m)}} \quad \dots \quad (5)$$

where x_1 and x_2 are the mole fractions of the two components and the remaining quantities are the same as defined above.

Kihara's (1949) first approximation to the thermal diffusion ratio for a binary mixture is

$$\left[K_T \right]_1 = \frac{(6C^* - 5)x_1 x_2 (S_1 x_1 - S_2 x_2)}{Q_1 x_1^2 + Q_2 x_2^2 + Q_{12} x_1 x_2} \quad \dots \quad (6)$$

in which

$$S_1 = \left(\frac{M_1}{M_2} \right) \left(\frac{2M_2}{M_1 + M_2} \right)^{\frac{1}{2}} \left(\frac{\Omega_{11}^{(2,2)*}}{\Omega_{12}^{(1,1)*}} \right) (r_{11}^2)^2 - \frac{4A^* M_1 M_2}{(M_1 + M_2)^2} - \frac{15M_2(M_2 - M_1)}{2(M_1 + M_2)^2}$$

$$Q_1 = \frac{2}{(M_1 + M_2)M_2} \left(\frac{2M_2}{M_1 + M_2} \right)^{\frac{1}{2}} \left(\frac{\Omega_{11}^{(2,2)*}}{\Omega_{12}^{(1,1)*}} \right) (r_{11}^2)^2 \left[3M_2^2 + M_1^2 + \frac{8}{5} A^* M_1 M_2 \right]$$

$$Q_{12} = \frac{15(M_1 + M_2)^2}{(M_1 + M_2)^2} + \frac{32M_1 M_2}{(M_1 + M_2)^2} A^*$$

$$+ \frac{8}{5} \left(\frac{M_1 + M_2}{M_1 M_2} \right)^{\frac{1}{2}} \left[\frac{\Omega_{11}^{(2,2)*} \Omega_{22}^{(2,2)*}}{[(\Omega_{12}^{(1,1)*})^2]} \right] \left[\frac{r_{11}^2 r_{22}^2}{r_{12}^4} \right]$$

with similar expressions for S_2 and Q_2 . A^* and C^* are functions of collision integrals and have been tabulated by Hirschfelder, Curtiss and Bird (1954).

3. CALCULATION OF HIGHER APPROXIMATIONS TO DIFFUSION COEFFICIENTS

The foregoing formulae for transport coefficients involve a number of collision integrals, most of which have been reported by Hirschfelder, Bird and Spotz (1948), but some of them require evaluation. Saxena and Srivastava (1955) have recently worked out the expressions for the collision integrals $\Omega^{(1,4)*}$, $\Omega^{(1,5)*}$ and $(\Omega^{4,3})^*$. In the absence of computational assistance an interpolation method was adopted to calculate $\Omega^{(3,3)*}$. Utilising these expressions, Saxena (1955) has evaluated the values of these collision integrals over an extensive range of temperatures. Here the values of these collision integrals along with those reported by Hirschfelder, Bird and Spotz (1948) have been used to calculate the correction

factors $f_D^{(2)}$ and $f_D^{(3)}$ from equation (4) for several values of T^* which are recorded in Table I. It will be seen that these correction factors continuously increase with increasing values of T^* , the increase being more for smaller values of T^* .

TABLE I

Functions for calculating the higher approximations to the diffusion coefficient of pure substances for the Lennard-Jones 12:6 potential

T^*	$f_D^{(2)}$	$f_D^{(3)}$
0.30	1.0001	1.0002
0.50	1.0000	1.0001
0.75	1.0000	1.0001
1.00	1.0000	1.0001
1.25	1.0002	1.0003
1.50	1.0006	1.0006
2.0	1.0016	1.0016
2.5	1.0026	1.0026
3.0	1.0037	1.0037
4.0	1.0050	1.0051
4.5	1.0055	1.0057
5	1.0059	1.0061
6	1.0065	1.0067
7	1.0069	1.0072
8	1.0071	1.0074
9	1.0073	1.0077
10	1.0075	1.0080
50	1.0080	1.0085
100	1.0080	1.0085
400	1.0080	1.0084

Equation (3) was utilised to calculate the values of $f_{D_{12}}^{(2)}$ and $f_{D_{12}}^{(3)}$ for argon-helium mixture at two widely separated temperatures, the values so obtained are reported in Table II. For this purpose the force constants obtained from viscosity by Hirschfelder, Bird and Spotz (1949) were used and an arbitrary concentration of 48.8% of argon was assumed as our aim is to investigate the relative contributions of these higher approximations. Columns 4, 5 and 6 of Table II give respectively the first, second and third approximations to the coefficient of interdiffusion.

TABLE II

Values of the first, second and third approximations to the diffusion coefficient (in $\text{cm}^2/\text{sec.}$)

Temp.°K	$f_{D_{12}}^{(2)}$	$f_{D_{12}}^{(3)}$	$[D_{12}]_1$	$[D_{12}]_2$	$[D_{12}]_3$	$[D_{12}]_{\text{exp}}$
136.6	1.910	1.020	0.197	0.201	0.201	—
273.2	1.024	1.026	0.634	0.649	0.651	0.641

In Table III we have reported the first and second approximation values of the thermal diffusion ratio calculated from equation (5) along with the experimental values. The experimental values have been obtained by interpolation from the experimental data of Grew (1947). Again the force constants obtained from viscosity were utilised for calculation.

TABLE III

Values of the first and second approximations to the thermal diffusion ratio

Temp. °K	Concentration	$[K_T]_1$	$[K_T]_2$	$[K_T]_{\text{exp}}$
136.6	48.8% A	0.0878	0.0904	0.0857
273.2	48.8% A	0.0989	0.102	0.0962

4. EVALUATION OF FORCE CONSTANTS

Srivastava and Madan (1953) calculated the force constants from thermal diffusion data, assuming that in the expression

$$[K_{T_1}]_1 = (6C^* - 5)x_1x_2g \quad \dots (7)$$

where C^* and g have their usual meaning, the factor g is temperature independent, and further that

$$[K_{T_1}]_1/[K_{T_2}]_1 = [K_{T_2}]/[K_{T_2}]_{\text{exp}} \quad \dots (8)$$

However, in actual practice g is found to be slightly temperature-dependent. Taking this small temperature dependence into account and adopting the method of successive approximations the values of the force constants for unlike molecules have been evaluated by the author (1955a). It will be seen from equation (5) that algebraically $(6C^* - 5)$ is no longer a common factor of $[K_T]_2$ as it is of $[K_T]_1$ and therefore it is not possible to utilise in the same way the $[K_T]_2$ expression for the determination of ϵ_{12} . However, from Table III columns (3) and (4) we find that $[K_T]_2$ is about 3% higher than $[K_T]_1$, nevertheless the ratios of the first approximation values at two temperatures and that of second approximation values for the same two temperatures are 1.126 and 1.128 respectively, and differ only by about 0.2%. This establishes the validity of equation (8) provided we assume that $[K_T]_2 = [K_T]_{\text{exp}}$, which is certainly a very good approximation. This shows the accuracy of the determination of ϵ_{12} from equation (8) is very high indeed.

Kihara's (1949) first approximation formula can also be used to evaluate ϵ_{12} . For this purpose the values of the factor g were calculated from equation (6) at various temperatures and are recorded in Table IV, column 3. The value

of ϵ_{12} was then evaluated by adopting the same procedure as in the case of Chapman and Cowling first approximation formula. In Table IV, we have recorded the values of the force constants obtained from different procedures, from which it is evident that for all practical purposes the precise evaluation from the first approximation formula is quite adequate and it is useless to bother about the second approximation formula as far as the evaluation of ϵ_{12} from the temperature variation is concerned.

TABLE IV
Values of the factor g

Temp. °K	Chapman & Cowling (first approx.)	Khiara (first approx.)
136.6	0.149	0.165
273.2	0.148	0.164

TABLE V
Force constant ϵ_{12} for A-He molecules

	Chapman & Cowling or Kihara first approx. (rough calculation)†	Chapman & Cowling first approx. (Precise calculation)*	Kihara first approx. (Precise calculation)	Geometric mean from viscosity
ϵ_{12}/k °K	26.51	27.05	27.05	27.3

† Neglecting the temperature-dependence of the 'g' factor.

* Considering the small temperature-dependence of the 'g' factor.

5. DISCUSSION OF RESULTS

For the Lennard-Jones 12 : 6 model we find from Table I that $f_D^{(2)}$ undergoes a maximum variation of 0.85% in the entire temperature range. This factor has also been reported by Mason (1954) for the Exp—Six model for $\alpha = 12, 13, 14$ and 15 (α is an additional parameter in his interaction potential model); his results show a maximum variation of 0.88% for $\alpha = 15$. From this it is evident that the contribution of the second and third approximation terms are small and lie within the probable errors in the experimental determination of diffusion

coefficients. Thus the method developed by Srivastava and Madan (1952) for the evaluation of ϵ_{11} assuming that

$$[D'_{11}]_1/[D''_{11}]_1 = [D'^{II}_{11}]_{\text{exp}}/[D''_{11}]_{\text{exp}} \quad \dots (9)$$

is justified, and that the accuracy of ϵ_{11} obtained on the assumption of Eq. (9) is quite high, except for the errors involved in the experimental determination of D_{11} . It is interesting to note that the greater uncertainty involved in $\Omega^{(3,3)*}$ does not produce any error in the calculation of $f_D^{(3)}$. To exemplify it, we have calculated Δ_2 by putting $\Omega^{(4,3)*}$ and $\Omega^{(2,3)*}$ successively instead of $\Omega^{(3,3)*}$ when it was found that Δ_2 undergoes a change of 0.00009% at $T^* = 3.8$. In fact, the error in Δ_2 will be only a small fraction of this and it will have no effect on $f_D^{(3)}$ as in equation in equation (4) the leading term $1 - \Delta_1$, which constitutes 99.9% of the value is independent of $\Omega^{(3,3)*}$.

From Table II, it will be seen that the relative contribution of the third approximation to interdiffusion is insignificant and for all practical purposes, the second approximation formula will serve the purpose. In Table III, we find that the second approximation values of K_T are about 3% higher than the first approximation values, and must therefore be taken into account for all precise work. Still, however, the method of determining the force parameter ϵ_{12} developed by Srivastava and Madan (1953), Saxena (1955a) remains fully valid as therein the ratio of $[K_T]_1$ at two temperatures has been utilised which as shown here, will be affected only insignificantly even when we take the second approximation into account.

ACKNOWLEDGMENTS

The author wishes to acknowledge his deep indebtedness to Prof. B. N. Srivastava for his invaluable guidance and continuous stimulation throughout the progress of the work presented here. This work has been done under a research scheme financed by the Council of Scientific and Industrial Research, New Delhi, to whom the author is grateful for this award.

REFERENCES

- Chapman, S. and Cowling, T. G., 1952, *The Mathematical theory of Non-uniform gases* Cambridge University Press, Teddington.
 Grew, K. E., 1947, *Proc. Roy. Soc. A.*, **189**, 402.
 Hirschfelder, J. O., Bird, R. B., and Spotz, E. L., 1948, *J. Chem. Phys.*, **16**, 968.
 Hirschfelder, J. O., Bird, R. B. and Spotz, E. L., 1949, *Chem. Rev.*, **44**, 205.
 Hirschfelder, J. O., Curtiss, C. F. and Bird, R. B., 1954, *Molecular Theory of Gases and Liquids* John Wiley & Sons, Inc., New York..

- Kihara, T., 1949, *Imperfect Gases* (Originally published in Japanese Asakusa Bookstore, Tokyo, and translated into English by the United States Office of Air Research, Wright-Patterson Air Force Base.
- Mason, E. A., 1954, *J. Chem. Phys.*, **22**, 169.
- Saxena, S. C. and Srivastava, B. N., 1955, *J. Chem. Phys.* (in press).
- Saxena, S. C., 1955a, *Ind. Jour. Phys.*, **29**, 13.
- Saxena, S. C., 1955b, *J. Chem. Phys.*, (in press.)
- Srivastava, B. N. and Madan, M. P., 1952, *Phil. Mag.*, **43**, 968.
- Srivastava, B. N. and Madan, M. P., 1953, *Proc. Phys. Soc. London, A*, **66**, 277.

SHRINKAGE EFFECT OF CLOSE COMPONENTS IN SPECTROSCOPIC INSTRUMENTS

By MAHENDRA SINGH SODHA*

DEPARTMENT OF PHYSICS, ALLAHABAD UNIVERSITY, ALLAHABAD.

(Received for publication, April 9, 1955)

ABSTRACT. Neglecting the Doppler width, the author has calculated the shift of maxima caused by mutual overlapping of intensity patterns of very close spectral lines for a number of spectroscopic instruments. A table, which may be used to correct for shrinkage effect has been given for Fabry Perot etalon. The value of the resolving power of Fabry Perot etalon according to Abbe's criterion has also been refined taking into account the shrinkage effect.

INTRODUCTION

In every spectroscopic instrument, the mutual overlapping of intensity patterns of two very close spectral lines results in their spurious closing together. Very little work has been done on this important aspect, which introduces considerable errors if disregarded, particularly when the instruments are used to the limit of their capacities.

The analysis of the problem becomes extremely difficult when both the Doppler and the instrumental widths are taken into account. Oldenburg (1922) has discussed the case in which there is partial overlapping of the Doppler distribution of two lines. In his treatment he implicitly assumed that the Doppler width is much larger than the instrumental width. Hence this treatment is not applicable to a number of cases in which the natural line width is reduced to be less than the instrumental width, as has been pointed out by Tolansky (1947). A small gap Fabry Perot etalon is generally employed in the examination of a widespread spectrum and the observable line width is mainly due to the instrument and not the line. Similarly with the prism and the grating and even with high resolving power instruments, when modern hyperfine-structure sources like the atomic beam are used, the condition essential to Oldenburg's treatment that the instrumental width be less than Doppler width breaks down.

In this communication the author has calculated the shrinkage effect for a number of instruments taking only the instrumental width into account.

PRISM AND GRATING

The intensity pattern of a spectral line after diffraction by a grating is given by

$$I' = B \frac{\sin^2 N\beta}{\sin^2 \beta} \quad \dots (1)$$

* Now at Defence Science Laboratory, New Delhi-12.

where N is the number of lines in the grating and $2\beta = 2\pi ve(\sin i - \sin \theta)$ is the phase difference between the rays diffracted by two adjacent elements of grating, where the symbols have usual meanings.

The maximum intensity say I_0 is given by

$$I_0 = BN^2$$

and hence Eqn (1) may be expressed as

$$\frac{I'}{I_0} = \frac{\sin^2 N\beta}{N^2 \sin^2 \beta} = \frac{\sin^2 x}{x^2} \quad \dots (2)$$

where $x = N\beta$ and $\beta \ll 1$.

Eqn (2) also represents the intensity pattern in case of a prism if $x = \pi l v \sin \theta$, the symbols having usual meanings.

The quantity Δx is proportional to the angle between two close spectral lines and therefore we shall use Δx instead of $\Delta \theta$ to represent the latter in this investigation. The intensity distribution of another spectral line separated by an angle $\Delta x = a$ is given by

$$\frac{I''}{I_0} = \frac{\sin^2 (x-a)}{(x-a)^2} \quad \dots (3)$$

The resultant intensity pattern of two such lines with intensities I_0 and I_0/b (intensity ratio $b : 1$) is

$$I/I_0 = (I' + I'')/I_0 = \frac{\sin^2 x}{x^2} + \frac{1}{b} \frac{\sin^2 (x-a)}{(x-a)^2} \quad \dots (4)$$

For very small values of x we have

$$I/I_0 = \left(1 - \frac{x^2}{3} + \frac{2x^4}{45} \right) + \frac{1}{b} \frac{\sin^2 (x-a)}{(x-a)^2} \quad \dots (4A)$$

The maximum near $x = 0$, is given by $dI/dx = 0$ i.e.

$$\left(-\frac{2x}{3} + \frac{8}{45} x^3 \right) + \frac{1}{b} F(x) = 0$$

$$\text{or} \quad x = \frac{4}{15} x^3 + \frac{3}{2b} F(x) \quad \dots (5)$$

$$\text{where} \quad F(x) = \frac{2 \sin^2 (a-x)}{(a-x)^3} - \frac{\sin 2(a-x)}{(a-x)^2}$$

Eqn. (5) may be solved by the method of successive approximations. If x'_n is the solution to n^{th} approximation

$$x'_{n+1} = \frac{4}{15} x_n'^3 + \frac{3}{2b} F(x'_n) \quad \dots (5a)$$

Similar equation for the shift of maximum of the other line is obtained by putting $1/b$ for b . Thus (5a) becomes—

$$x_{n+1}'' = \frac{4}{15} x_n''^3 + \frac{3b}{2} F(x_n'') \quad \dots (6)$$

Putting $x_0' = x_0'' = 0$ we get the first approximation as

$$bx_1' = \frac{x_1''}{b} = \frac{3}{2} F(0) = 3(\sin a/a^2)\{(\sin a/a) - \cos a\} = f(a) \quad \dots (7)$$

The higher approximation values can be calculated by the use of equations (5) and (6)

The calculations are particularly valuable when the two lines are close together and when their separation is small compared with the fringe width. In this case first approximation is sufficient and the displacements of two lines from their true positions are given by :

$$\frac{\delta v'}{\Delta v} = \frac{x'}{a} = \frac{f(a)}{b} \quad \dots (8a)$$

$$\frac{\delta v''}{\Delta v} = \frac{x''}{a} = b f(a) \quad \dots (8b)$$

where

$$f(a) = \frac{3 \sin a}{a^3} \left\{ \frac{\sin a}{a} - \cos a \right\}$$

Δv is the separation of the two lines and $\delta v'$ and $\delta v''$ are the shifts of stronger and weaker components ($b > 1$)

Table I gives the values of $\delta v/\Delta v$ for values of $a = \pi, \pi/1.115$ and $\pi/1.26$ which correspond to the separations required by the Rayleigh, Abbe and Sparrow criteria respectively.

TABLE I
Values of $\delta v/\Delta v$

b	$1/2$	1	2	3	4	5
π	0.0000	0.0000	0.0000	0.0000	0.0000	0.0000
$\pi/1.115$	0.0906	0.0453	0.0227	0.0151	0.0113	0.0091
$\pi/1.26$	—	0.1214	0.0607	0.0405	0.0304	0.0243

For all values of b , $\delta v/\Delta v = 0$ when $a = \pi$. There will be no maximum, for $b = 1/2$ or less when $a = \pi/1.26$ and for $b = 1/3$ or less when $a = \pi/1.115$,

It is interesting to note that $f(a)$ can also assume negative values thereby giving rise to what may be called an expansion effect of close components *eg* when a is slightly greater than π .

The treatment and results are also applicable to the reflection echelon, which has an intensity pattern similar to the grating.

FABRY PEROT ETALON

The intensity of a spectral line in the order $n_0 + n$, n_0 being an integer and n a small quantity is given by

$I'/I_0 = 1/\{1 + F \sin^2 \pi(n_0 + n)\} = 1/(1 + X^2)$ nearly, where $X = \pi F^{1/2}n$, F being the coefficient of fineness and I_0 the intensity of the incident beam.

The intensity pattern of another line of an intensity $1/b$ times that of the first separated by an order Δn is

$$I''/I_0 = 1/b\{1 + (X - a)^2\} \quad \text{where } a = \pi F^{1/2}\Delta n.$$

Hence the resultant intensity pattern is given by

$$I/I_0 = (I' + I'')/I_0 = \{1/(1 + x^2)\} + [1/b\{1 + (x - a)^2\}] \quad \dots (10)$$

The maxima are given by

$$-(1/2I_0)(dI/dX) = \{X/(1 + X^2)^2\} + [(X - a)/b\{1 + (X - a)^2\}^2] = 0 \quad \dots (11)$$

Eqn. (11) is a fifth degree equation and its solution is difficult. Hence we will follow the method of successive approximations. If X'_n is the solution to n^{th} approximation

$$\frac{X'_{n+1}}{\{1 + X'^2_n\}^2} + \frac{X'_{n+1} - a}{b\{1 + (X'_n - a)^2\}^2} = 0$$

$$\text{or} \quad X'_{n+1} = a(1 + X'^2_n)/[(1 + X'^2_n) + b\{1 + (X'_n - a)^2\}^2] \quad \dots (12)$$

The shift of maximum for the other line $x'' + 1$ is given by

$$X''_{n+1} = a(1 + X''^2_n)/[1 + X''^2_n + (1/b)\{1 + (X''_n - a)^2\}^2] \quad \dots (13)$$

Taking $X'_0 = X''_0 = 0$ we get to the first approximation

$$X' = \frac{a}{\{1 + b(1 + a^2)\}^2} \quad \text{and} \quad X'' = \frac{a}{\{1 + (1 + a^2)^2/b\}} \quad \dots$$

The displacements $\delta\nu'$ and $\delta\nu''$ of the two lines from their true positions are therefore to a first approximation given by

$$\frac{\delta\nu'}{\Delta\nu} = \frac{x'}{a} = \frac{1}{\{1 + b(1 + a^2)^2\}} \quad (14)$$

$$\frac{\delta\nu''}{\Delta\nu} = \frac{x''}{a} = \frac{1}{\{1 + (1 + a^2)^2/b\}} \quad \dots (15)$$

where $\Delta\nu$ is the real wave number difference between the two lines,

Table II gives values of shifts for a range of values of a and b . The values given in the table are such that they differ from the next approximation by less than .005. The table is graphically illustrated in figure 1. The corrections for shift of maxima may be applied with the help of the table, and the graphs by

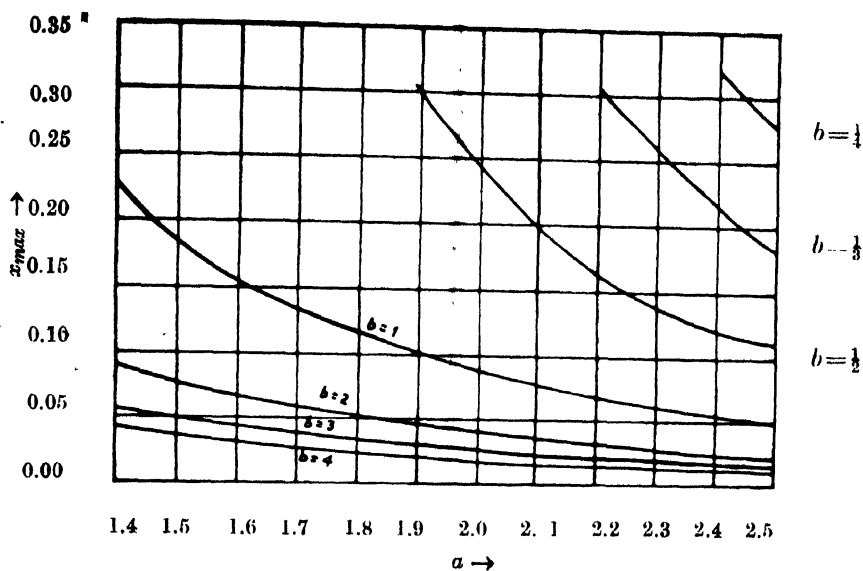


Fig. 1

the method of successive approximations, i.e. noting the corrections for the measured values of a , adding them to a and again determining the corrections.

TABLE II
Values of shift of maxima (x) in F. P. etalon.

$a \backslash b$	$1/4$	$1/3$	$1/2$	1	2	3	4	5
1.4				0.2286	0.0900	0.0572	0.0420	0.0312
1.5				0.1815	0.0786	0.0504	0.0370	0.0279
1.6				0.1550	0.0680	0.0442	0.0328	0.0249
1.7				0.1342	0.0560	0.0391	0.0294	0.0222
1.8				0.1170	0.0531	0.0347	0.0258	0.0198
1.9			0.3000	0.1020	0.0471	0.0308	0.0229	0.0177
2.0			0.2398	0.0895	0.0418	0.0263	0.0198	0.0156
2.1			0.2030	0.0778	0.0373	0.0236	0.0178	0.0143
2.2		0.3060	0.1610	0.0693	0.0317	0.0213	0.0160	0.0128
2.3		0.2620	0.1399	0.0619	0.0287	0.0192	0.0144	0.0116
2.4	0.3194	0.2150	0.1232	0.0555	0.0259	0.0174	0.0131	0.0105
2.5	0.2752	0.1830	0.1080	0.0500	0.0236	0.0158	0.0118	0.0095

THE ISOGRAPH—AN ELECTRONIC ROOT FINDER

BY A. K. CHOUDHURY

INSTITUTE OF RADIOPHYSICS & ELECTRONICS, CALCUTTA UNIVERSITY.

(Received for publication, August 30, 1955)

ABSTRACT. The paper describes an electronic isograph for finding the roots of high degree polynomials. The harmonic generator used is a purely electronic device without any moving parts. The different harmonic components are generated with the help of a delay line, fed from a matched frequency-sweep generator. By controlling the amount of frequency sweep of the oscillator any desired interval of the argument can be expanded, thus enabling accurate determination of the argument of the root.

1. INTRODUCTION

High degree polynomial equations occur often in many problems connected with different branches of mechanical, electrical and radio engineering. For example, the transient behaviour of an electrical network or a dynamical system cannot be determined without the computation of the numerical zeroes of a polynomial. It is, however, well known that there is no general solution for polynomials of degree higher than four. For such higher polynomials, only numerical methods of solution are available. Unfortunately, these methods are laborious and each problem has to be treated on an individual basis. Many mechanical and electro-mechanical devices have, therefore, been developed for finding the roots of high degree polynomials. Thus, the device developed by Hart and Travis (1938) working on the principle of harmonic synthesis, consists of $(n+1)$ identical a.c. generators, with n of them provided with rotatable stators connected to a common shaft through gear ratios $1 : 1, 2 : 1, \dots n : 1$. In another device described by B. O. Marshall (1950), working also on the principle of harmonic synthesis, the different harmonic components are generated by a rotating commutator type square wave generator.

The device described here is also designed on the principle of harmonic synthesis, but is a purely electronic one without any mechanical moving parts. The different harmonic components are generated with the help of a delay line, the line being fed from a matched generator, the frequency of which is swept by the time base voltage of the C.R.O. The variation in frequency of the oscillator corresponds to the variation of the argument of the harmonic components. Thus, by controlling the amount of frequency sweep of the oscillator, any desired interval of the argument can be expanded. The accuracy of measurement of the argument is thereby increased.

2. THEORY OF OPERATION

A polynomial in Z

$$f(z) = \sum_{m=0}^{m=n} a_m Z^m$$

may have roots anywhere in the complex plane depending on the coefficients a_m .

Putting

$$\begin{aligned} Z &= re^{j\theta} \\ f(z) &= \sum a_m Z^m = \sum a_m r^m e^{jm\theta} \\ &= \sum a_m r^m \cos m\theta + j \sum a_m r^m \sin m\theta \end{aligned}$$

The values of r and θ for which both the real and imaginary parts vanish simultaneously are the roots of $f(z)$.

Thus the basic problem in the synthesis of an instrument for finding roots of $f(z)$ by utilising the above principle, is to generate the individual terms $a_m r^m \cos m\theta$ and $a_m r^m \sin m\theta$ and to add the sine and cosine terms separately. Both r and θ are then to be varied to make the sum of the cosine and sine terms zero.

In the instrument described, voltages proportional to the sine and cosine terms are generated with the help of short and open circuited delay lines (fed from a matched generator) respectively. The different harmonic components are obtained by taking outputs from proper points on the line. The harmonic components are fed into the respective co-efficient multiplier circuits and the outputs from the co-efficient multiplier circuits in their turn are fed into the 'r' multiplier-adder circuit. The final output obtained is either $\sum a_m r^m \cos m\theta$ when the line is open-circuited or $\sum a_m r^m \sin m\theta$ when the line is short-circuited. In the multiplier circuits, multiplying factors greater than unity cannot be set. But this does not present any difficulty. For, a polynomial can be suitably prepared by dividing all the co-efficients by the largest one. This operation reduces the co-efficients to proper fractions, without affecting the roots.

3. CIRCUITS FOR PERFORMING THE BASIC OPERATION

1. Harmonic Generator

In a system with n identical low pass filter sections connected in cascade with the near end properly terminated and far end the open-circuited, the voltage V (with the voltage at the open end as the reference) at any frequency at the k th section from open end is given by

$$V = 2 |e| \cos [2K \sin^{-1}x] = 2k | \cos K\theta$$

where e = voltage applied at near end,

$x = f/f_c$, normalised value of frequency with respect to f_c (the cut-off frequency of the filter).

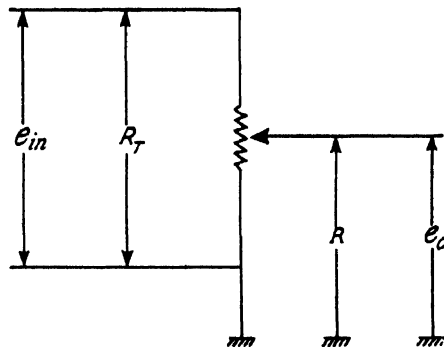
$\theta = 2 \sin^{-1}x$ = phase shift per section.

For a value of $x = x_1$ corresponding to the phase change of 45° per section, voltages at the 2nd, 6th, 10th etc. sections are zero and those at the 0-th 4th, 8th, etc. section are maximum. If the value of x_1 be such that the phase shift per section is 90° , then the phase at the 8th tap changes through 360° . Similarly phase at the 16th tap changes through 720° . If the voltage at the 8th tap be $V_8 = E' \cos \theta'$, the voltage at the 16th tap can be written as $V_{16} = E' \cos 2\theta'$.

With the line open circuited, if the frequency is swept at a slow rate between $x = 0.383 = x_1$ to $x = 0.707$, the output of a phase sensitive detector when fed from the 8th tap on the line will be one cycle of the cosine function; and that at the 16th tap will be two complete cycles of the cosine function. If the output from the 8th tap is fed directly into the oscilloscope, whose time base voltage is used as sweep voltage, the amplitude of the wave will be observed to be a cosine function. Similarly, for n filter sections connected in cascade with the far end short-circuited, it can be shown that voltages at the corresponding points generate sine functions.

4. CO-EFFICIENT MULTIPLIER CIRCUIT

A co-efficient multiplier circuit is basically a potentiometer multiplier. An elementary multiplication circuit is shown in Fig. 1. The output voltage is $e_o = e_{in} \frac{R}{R_T} = a_1 e_{in}$. It is evident from the circuit arrangement that a_1 cannot be greater than unity and also that the shaft rotation of the potentiometer can



$$e_o = \frac{R}{R_T} e_{in} = a_1 e_{in}$$

Fig. 1

directly be calibrated in a_1 . In order to avoid loading effect, potentiometers of different co-efficients are isolated by unity gain cathode follower amplifiers. If the output of the potentiometer in Fig. 1 is fed through a unity gain cathode

follower amplifier into an identical potentiometer (ganged with the 1st potentiometer), the output at the 2nd potentiometer will be $e'_0 = a_1^2 e_{1n}$.

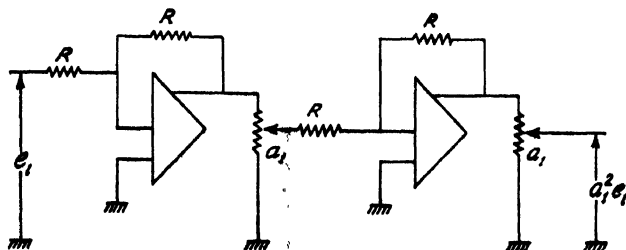


Fig. 2

Such an a^2 multiplier circuit is shown in Fig. 2. The amplifier cathode followers of the circuit can be used as adder. With the circuit arrangement shown in Fig. 3 the final output is given by $e'_0 = a_1^2 e_1 + a_1^2 e_2 + a_1 e_3$.

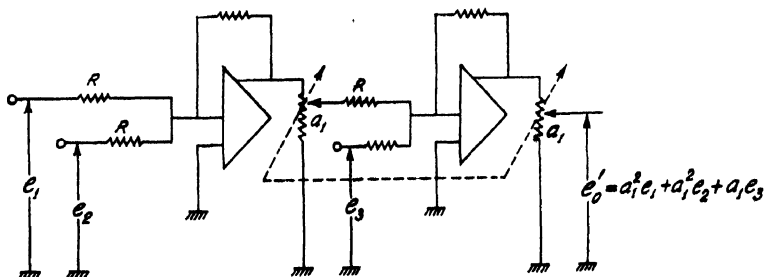


Fig. 3

5. CIRCUIT FOR SOLVING POLYNOMIAL

Schematic diagram of the circuit for solving a polynomial of 3rd degree is shown in Fig. 4. The outputs from the 24th, 16th, 8th and 0-th tap of the open

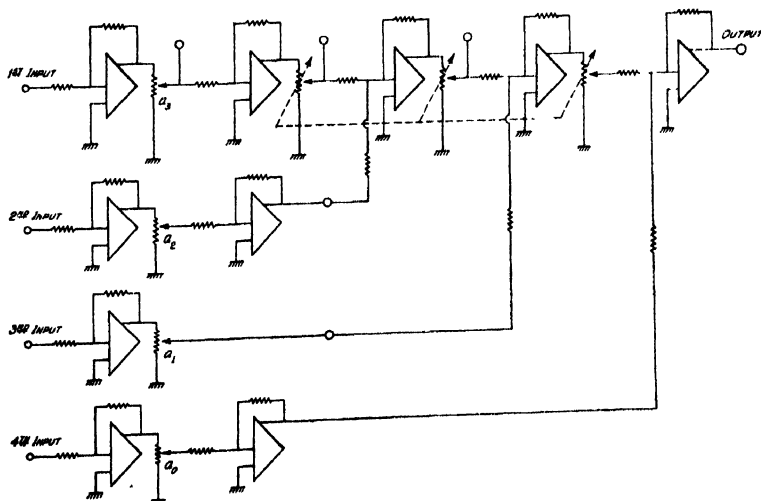


Fig. 4

ended line are fed respectively into the 1st, 2nd, 3rd, and 4th input terminals. Thus the inputs at the 1st, 2nd, 3rd and 4th terminals are $\cos 3\theta$, $\cos 2\theta$, $\cos \theta$, and 1 respectively. The different harmonic components are fed into the respective co-efficient multiplier potentiometers. The outputs from 1st, 2nd, 3rd, 4th multipliers are respectively $a_3 \cos 3\theta$, $a_2 \cos 2\theta$, $a_1 \cos \theta$, a_0 . The output $a_3 \cos 3\theta$ is fed into the 1st output of the r multiplier circuit. The three r potentiometers are identical ganged potentiometers separated by unity gain cathode follower amplifiers. The output $a_2 \cos 2\theta$ and $a_1 \cos \theta$ are fed into the 2nd and 3rd input of the r multiplier circuit, with proper phase reversal. At the output of the r multiplier circuit we thus obtain $r^3 a_3 \cos 3\theta + r^2 a_2 \cos 2\theta + r a_1 \cos \theta$. (The addition of the individual harmonic components is performed by the second and third isolating cathode follower amplifiers in the r -multiplier circuit). This output and a_0 are fed into the final adder circuit giving the output $r^3 a_3 \cos 3\theta + r^2 a_2 \cos 2\theta + r a_1 \cos \theta + a_0$. If the far end of line is now short-circuited the final output will be $r^3 a_3 \sin 3\theta + r^2 a_2 \sin 2\theta + r a_1 \sin \theta$. With the line open-circuited the final output is fed into the oscilloscope whose time base voltage is used to sweep the frequency of the oscillator. Sweep voltage is adjusted such that the oscillator sweeps between $0.383f_c$ to $0.707f_c$ in each cycle. The r potentiometer is adjusted to obtain a zero of the output somewhere on the oscilloscope time base. In order to increase the accuracy of both r and θ reading, attention now is focussed on the region about the zeroes. The amount of frequency sweep is now gradually decreased by controlling the amplitude of the sweep voltage fed into the sweep

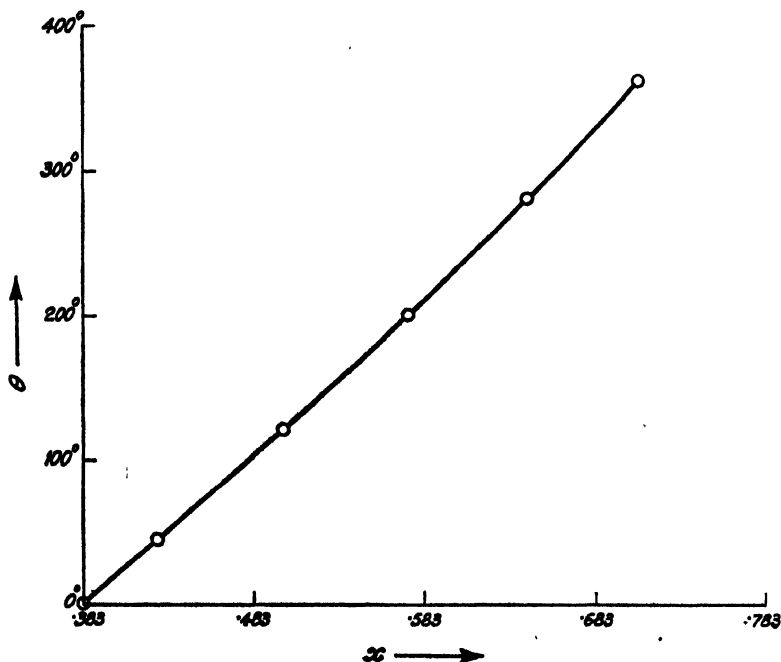


Fig. 5

frequency oscillator, keeping the zero of the output at the centre of the C.R.O. This latter adjustment is done by controlling the frequency dial of the sweep frequency oscillator. Finally the frequency sweep is made zero with zero output on the C.R.O. With this adjustment the frequency dial of the oscillator gives the frequency at which the output is zero. Fig. 5 shows the relation between θ and frequency. The oscillator dial can be directly calibrated in θ . The r -potentiometer reading gives the value of r . The solution is finally checked by observing the output with the far end of the line short-circuited. If with the far end short-circuited the output is again zero, the values of r and θ obtained constitute one of the solutions. The other roots can be found out similarly.

6. PREPARATION OF THE POLYNOMIAL

$$\text{A polynomial } f(z) = a_0 + a_1 Z + \dots + a_n Z^n = 0 \quad \dots (1)$$

with some or all the coefficients greater than unity can be prepared for the instrument by dividing $f(z)$ with the largest coefficient. If a_m be the largest coefficient, Eq.(1) after division by a_m can be written as

$$\frac{f(z)}{a_m} = \frac{a_0}{a_m} + \frac{a_1}{a_m} Z + \dots + Z^m + \frac{a_n}{a_m} Z^n. \quad \dots (2)$$

All the coefficients in (2) are proper fractions. If a_m is very large compared to any coefficient a_k in Eq.(1), then $\frac{a_k}{a_m}$ is a quantity very small compared to unity.

Due to inherent limitation of potentiometers it is difficult to set very small values of coefficients with any degree of accuracy. In such cases polynomial (2) may be so prepared that coefficients have suitable values. The variable Z is changed into a new variable Z' , where $Z' = bz$, so that with the new variable, Eq. (2) becomes

$$f(z') = \frac{a_0}{a_m} + \frac{ba_1}{a_m} Z' + \dots + \frac{b^m a_m}{a_m} Z'^m \quad \dots (3)$$

and the value of " b " can be so chosen that the coefficients in (3) have values suitable for potentiometer setting.

ACKNOWLEDGMENTS

The author is deeply indebted to Prof. S. K. Mitra for his kind interest in the work.

REFERENCES

- Hart, H. C. and Travis, I., 1938, *Jour. Frank. Inst.*, **225**, 63-72.
 Marshall, B. O., 1950, *Jour. App. Phys.*, **21**, 307-312.

RAMAN SPECTRA OF FROZEN SOLUTIONS OF CARBON DISULPHIDE IN ALIPHATIC SOLVENTS*

By G. S. KASTHA

OPTICS DEPARTMENT, INDIAN ASSOCIATION FOR THE CULTIVATION
OF SCIENCE, CALCUTTA-32.

(Received for publication August 26, 1955)

Plate X

ABSTRACT. The Raman spectra of frozen solutions of carbon disulphide in methyl cyclohexane of strengths 62.3%, 52.4% and 45.2% in methyl alcohol of strengths 34.6% and 24.1% and in carbon tetrachloride of strength 20.8% have been investigated at -180°C . In all the cases, except in the case of the solution in methyl cyclohexane of strength 45.2%, the new lines 70 cm^{-1} and 81 cm^{-1} have been observed as in the case of pure carbon disulphide. These lines, however, disappear when the strength of the solution of carbon disulphide in methyl cyclohexane is diminished to 45.2%. It has been pointed out from the considerations of the densities of the solute and the solvents that the new lines cannot be due to angular oscillations of the molecules in the lattice of pure carbon disulphide. It has, therefore, been concluded that these lines originate from the vibrations in dimers or a little bigger groups of carbon disulphide molecules present in the pure liquid or in the solutions mentioned above except in 45.2% solution in methyl cyclohexane.

INTRODUCTION

It is well known that Raman spectra of some organic substances exhibit some new Raman lines in the neighbourhood of the Rayleigh line when they undergo a change from the liquid to the solid phase. Gross and Vuks (1935) first observed these lines in the Raman spectra of benzene, naphthalene etc. and attributed their origin to lattice oscillations. Sirkar (1936) studied the Raman spectra of carbon disulphide in the solid state at -180°C and observed one very intense new line at 70 cm^{-1} and another weaker one at 81 cm^{-1} . These were attributed to intermolecular vibration in polymerised groups of molecules assumed to be present in the crystal. Mazumdar (1949) repeated the investigation and studied the Raman spectra of carbon disulphide in the liquid state at 20°C and -100°C and in the solid state at -125°C and -183°C . He observed a new broad band at 45 cm^{-1} in the case of liquid at -100°C and this band split up into two lines at 59 cm^{-1} and 70 cm^{-1} respectively when the liquid was solidified and cooled to -125°C . On further lowering the temperature of the crystal to -183°C he observed the two lines to shift respectively to 69 cm^{-1} and 80 cm^{-1} .

* Communicated by Prof. S. C. Sirkar

From these results he concluded that the band due to the liquid at -100°C may be due to dimers. Since the band split up into two lines with solidification of the liquid, the latter lines were attributed to the vibration in dimers. It was pointed out by him that these two lines cannot be due to rotational oscillations of the molecules in the lattice about their axes because the intensity did not diminish appreciably with the lowering of temperature from -125°C to -183°C .

The question whether the lines are due to lattice oscillations or they are due to vibrations in associated groups of molecules can be tested by studying the Raman spectra of frozen solutions of carbon disulphide in suitable solvents. The result of such an investigation using two non-polar and one polar liquid as solvents are discussed in the present paper.

EXPERIMENTAL

The arrangement for photographing the Raman spectra of frozen solutions of carbon disulphide in various solvents at low temperature was the same as used by Mazumdar (1949). Carbon disulphide used in the present investigation was of chemically pure variety and repeatedly distilled in vacuum. Solvents used were chemically pure methyl cyclohexane, methyl alcohol and carbon tetrachloride and they were distilled in vacuum as usual.

A 62.3% solution of carbon disulphide in methyl cyclohexane was frozen and the frozen mass was found to be inhomogeneous and translucent. The Raman spectrum, however, was free from back ground. Next the investigations were repeated with solutions of strengths 52.4%, 45.2% and 29.2%. The latter two solutions when frozen appeared to be almost as transparent as glass. In the case of solutions in methyl alcohol the strengths used were 34.6% and 24.1% and in the case of solution in carbon tetrachloride a strength of 20.8% was used.

The Raman spectra of all these frozen solutions were photographed keeping the pyrex cylindrical glass containers in which the solutions were sealed under vacuum immersed in liquid oxygen during the exposure. The Raman spectra of pure methyl cyclohexane and carbon tetrachloride in the solid state under similar conditions were also photographed with the same spectrographs for comparison.

A Fuess glass spectrograph having a dispersion of $11\text{\AA}/\text{mm}$ in the region 4047\AA and Ilford Zenith plates were used to photograph the Raman spectra. The duration of the exposures ranged from six to seven hours.

RESULTS AND DISCUSSION

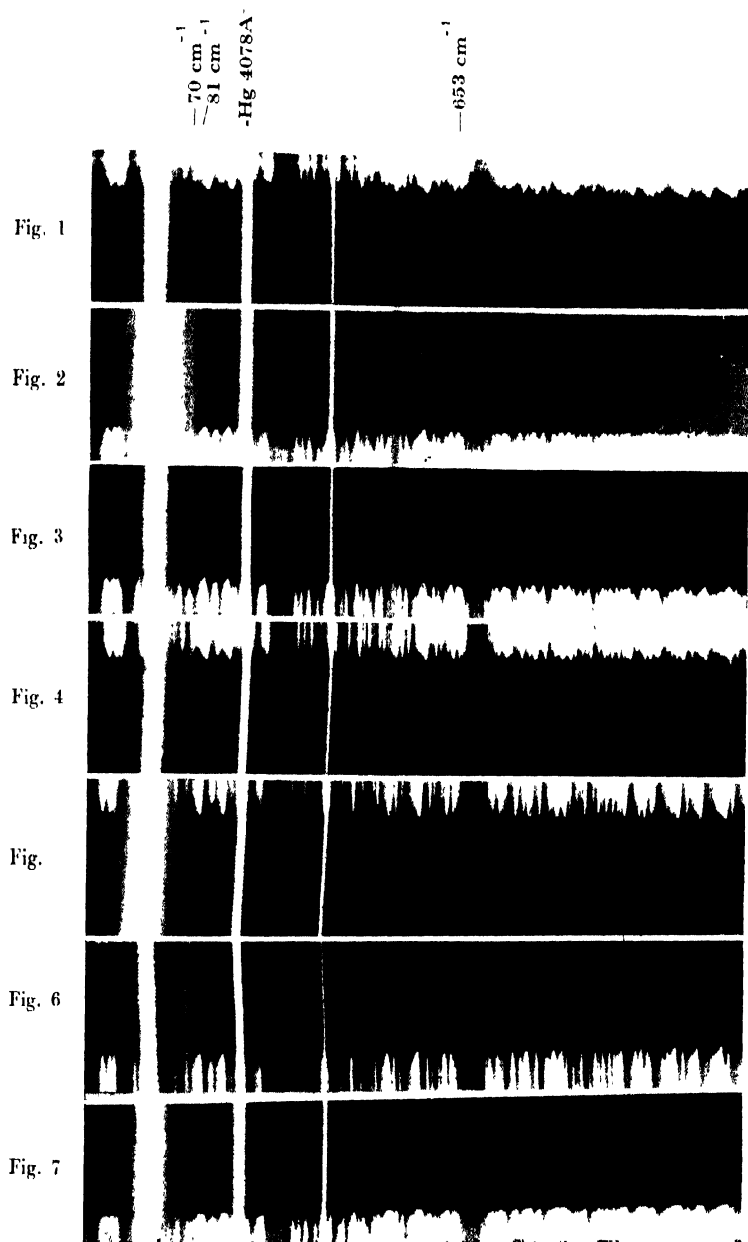
The spectrograms due to frozen solutions of carbon disulphide in methyl cyclohexane of strengths 62.3%, 52.4% and 45.2% and of frozen solutions of carbon disulphide in methyl alcohol of strengths 34.6% and 24.1% together with

that due to 20.8% carbon tetrachloride solution are reproduced in Plate X, Figs. 1-6. The spectrogram due to pure methyl cyclohexane in the solid state is reproduced in Fig. 7.

A careful examination of Fig. 7 will show that there is no line with frequency-shift below 390 cm^{-1} in the Raman spectrum of solidified methyl cyclohexane. From Figs. 1 and 2 it can be seen that the new lines at 70 cm^{-1} and 81 cm^{-1} of solid carbon disulphide are present in the spectra due to frozen solutions of carbon disulphide in methyl cyclohexane of strengths 62.3% and 52.4%. On the other hand, Fig. 3 shows that even the strongest new line at 70 cm^{-1} is totally absent in the spectrogram due to the 45.2% solution although the weaker line 653 cm^{-1} due to the carbon disulphide molecule is distinctly visible. In all the spectrograms Figs. 4, 5 and 6 due to frozen solutions of carbon disulphide in methyl alcohol and carbon tetrachloride, both the lines 70 cm^{-1} and 81 cm^{-1} are present. It is thus observed that when carbon disulphide is dissolved in methyl cyclohexane and the solution is frozen, the agents which produce the new Raman lines in the low frequency region persist even in the case of the 52.4% solution although their number seems to be a little less than that in the case of the 62.3% solution. These agents, however, disappear in the case of the 45.2% solution.

The disappearance of the new lines with change of concentration from 52.4% to 45.2% indicates that when the molecules are dispersed uniformly in a homogeneous medium, the oscillations giving rise to the lines 70 cm^{-1} and 81 cm^{-1} cease. Two alternative explanations can be given for the change observed with the change of concentration from 52.4% to 45.2%. First, these lines can be attributed to angular oscillations of carbon disulphide molecules about axes perpendicular to the molecule and pivotted in the crystal lattice, as suggested by Kastler and Rousset (1941), because as the crystal and as well as the unit cell have centre of symmetry, the translational vibration are forbidden. The presence of small volumes of pure carbon disulphide crystals suspended in the frozen methyl cyclohexane medium can only give rise to such modes of vibrations in the solutions in the solid state. Since the densities are widely different from each other, the small quantity of frozen carbon disulphide which would freeze before the freezing of the solvent, would settle down to the bottom of the container and the upper of the finally frozen mixture would contain only pure methyl cyclohexane in the solid state.

The spectrogram due to 52.4% solution of carbon disulphide in methyl cyclohexane (Fig. 2), however, shows clearly the line at 653 cm^{-1} of carbon disulphide as well as the lines 70 cm^{-1} and 81 cm^{-1} , although the spectrum of the light scattered only from the upper half of the frozen mass was photographed. This very fact shows that the upper half also contained carbon disulphide molecules and therefore these molecules could not remain as small crystallites forming lattice of pure carbon disulphide because they would settle down to the bottom of the container.



Raman Spectrum of frozen solutions of CS_2 in different solvents.

- Fig. 1. 62.3% solution of carbon disulphide in methyl cyclohexane at -180°C
 Fig. 2. 52.4%
 Fig. 3. 45.2%
 Fig. 4. 34.6% methyl alcohol
 Fig. 5. 24.1%
 Fig. 6. 20.8% carbon tetrachloride
 Fig. 7. Raman spectrum of pure methyl cyclohexane in the solid state at -180°C

ACKNOWLEDGMENT

The author is indebted to Professor S. C. Sirkar, D. Sc., F.N.I. for his kind interest and helpful guidance during the progress of the work.

REFERENCES

- Gross, E., and Vuks, M. 1935, *Nature*, **135**, 100, 998.
Kastler, A., and Rousset, A., 1941, *Compt. Rend.*, **212**, 645.
Majundar, N. C. 1949, *Ind. J. Phys.*, **23**, 253.
Sirkar, S. C., 1936, *Ind. J. Phys.*, **10**, 189.

IONISATION LOSS OF α -PARTICLES AT LOW ENERGIES BELOW 4 Mev.

By K. L. KAILA,

PHYSICS DEPARTMENT, UNIVERSITY OF DELHI, DELHI.

(Received for publication June 6, 1955)

ABSTRACT. No quantitative theory seems to have been given so far for the ionisation loss of α -particles at low energies below 4 Mev due to the extremely complicated phenomenon of electron capture by the α -particle occurring in this region. Here an attempt is made to get a complete expression for the ionisation loss of α -particles in this region by transforming Bethe's theoretical expression (which is valid only at high energies) and introducing some new terms to take account of electron capture and finally fitting it empirically with the well known Holloway and Livingston single α -ionisation curve. A theoretical interpretation of the new form of the relation has also been given. Further, using this new expression an empirical range energy relation is obtained which gives quite satisfactory agreement with the observed range-energy relation of α -particles in the region 2.5 Mev downwards.

1. INTRODUCTION

The theoretical formulation of ionisation loss of slow heavy particles (e.g. α -particles below 4 Mev) has long been a very difficult problem. The theories of the stopping power of α -particles have been worked out by Bohr, (1913, 1915) Bethe (1930) and others. These theories give quite good agreement with experimental results at high energies, but in the low energy region the theories break down completely. In this region probably more complicated phenomena, like the capture and loss of electrons by the He-ions, take place as pointed out by earlier worker Rutherford, (1924), Kapitza, (1924). These effects reduce the energy loss in a way for which no adequate quantitative theory has yet been developed. Therefore, the range energy relation for α -particles at low energies has to be computed entirely from some kind of suitable experimental data. Holloway and Livingston (1938) have studied the ionisation-loss of single α -particles from Polonium and from the graphical integration of ionisation-range curve they have calculated the range energy relation upto very low α -energies on the assumption that in air ϵ , the energy loss per ion pair for the α -particle, remains constant throughout the low energy region. However, Jesse, Forstat and Sandanskis (1950) have shown that this assumption is not valid for air, but is quite true for argon. In view of this fact a corrected range-energy relation in this region has been computed by Bethe (1950) by multiplying the energy values given by Holloway and Livingston (1938) by a correction factor

$$C = \frac{\text{Ionisation in argon}}{\text{Ionisation in air}}$$

This ratio C as a function of residual range was measured by Jesse and Sandanskis for Po α -particles.

In view of the great importance attached to the phenomenon of capture and loss of electrons by α -particles in their ionisation processes, the subject has received great attention both from the theoretical and experimental point of view. The extensive experimental and theoretical literature on this problem has been listed by T. A. Hall (1950). The general theoretical principles are discussed thoroughly by N. Bohr (1948) who shows that the process is essentially different in light and in heavy media. If the medium is heavy enough so that some electrons in the medium already have a speed v , as large as that of the incident α -particle, these will be simply captured by the latter. On the other hand for a lighter medium none of the electrons in the medium will have speeds as large as v . Capture must then occur by a double process: first an electron gains energy from collision with the incident α -particle, and then in a second collision with its own nucleus it is sent into a direction which makes capture possible. For heavier media, using the Fermi Thomas model, Bohr estimates the probability for the electron to have the correct velocity and calculates from it the electron capture cross-section :

$$\sigma_c \sim 4\pi a_0^2 Z^{1/3} \left(\frac{v_0}{v} \right)^6 \quad \dots (1)$$

where v_0 is the velocity of an electron in the first Bohr orbit of hydrogen and a_0 is the Bohr radius (this formula is valid only for $v \gg v_0$). For lighter media, however, the Bohr approximation may be expected to be valid. Brinkman and Kramers (1930) have calculated the capture cross-section in Born approximation and find

$$\sigma_c \approx \left(\frac{2^{18}\pi}{5} \right) a_0^2 z^2 \left(\frac{v_0}{v} \right)^{12} \quad \dots (2)$$

The theory of the loss of electrons is much more straightforward and the corresponding cross-section σ_e have been worked out by Bohr for the heavy and the light media.

The ratio of the low to the capture cross-section for proton beams of speeds v_0 to $4v_0$ in Be, Al, Ag and Au have also been investigated experimentally by T. A. Hall. The results obtained seem to show only a qualitative agreement with the theory.

The difficulties involved in the exact formulation of the cross-section of electron capture and loss are so great that a straight forward theory for ionisation loss of α -particles at low energies can hardly be worked out at the present stage. On the other hand, there seems to exist a considerable amount of reliable experimental data on the ionisation loss in this region of energy. We, therefore, propose

to follow an indirect procedure for a theoretical formulation of the problem. Using the existing standard experimental data on the ionisation loss of Po α -particles, we attempt to improve upon the existing theory of ionisation loss due to Bethe (which is valid only at high energies) to bring about an agreement of the theory with the experiment at low energies. The approach, to start with, is empirical, but we shall try to justify the additional terms introduced in Bethe's formula from theoretical considerations. Our object in this paper, is, therefore, to make use of Bethe's formula of the energy loss by in elastic collisions which is only valid in the high energy region and then by introducing some new terms to take account of the capture of electrons at low energies, and get a complete ionisation formula by empirical fitting of the ionisation-range curve for α -particles at low energies. Finally we shall compare the different constants involved in this new formula with those of Bethe's and try to interpret the phenomena taking place at low energies. This treatment will give at least qualitatively some insight into the phenomenon of ionisation at low energies, so that later it may be possible to build up some quantitative theory of ionisation of heavy charged particles, which will be valid both at high as well as low energies.

2. BETHE'S THEORY OF IONISATION AND ITS TRANSFORMATION

The theory of ionisation loss of α -particles was thoroughly investigated by Bethe (1930). He assumed that the energy loss of charged particles when passing through matter is mainly due to the inelastic collisions causing ionisation and excitation of the atoms of the substance traversed. The probability of these inelastic collisions depends on velocity and charge of the α -particles. Bethe's formula is, however, valid only if the velocity of the incident α -particle is large compared to the velocities of the electrons in the atom or in other words, if,

$$E \gg \frac{M}{m} I \quad \dots (3)$$

where E is the kinetic energy of the incident particle, I the ionisation potential of the electrons and M and m the masses of the incident particle and electron respectively. Under these conditions the energy loss per cm path is

$$-\frac{dE}{dx} = \frac{4\pi e^4 z^2}{mv^2} NB \quad \dots (4)$$

with
$$B = Z \log_e \frac{2mv^2}{I} \quad \dots (5)$$

where v is the velocity and ze the charge of the incident particle, N the number of atoms per cm^3 of the material Z the nuclear charge I the average excitation

This ratio C as a function of residual range was measured by Jesse and Sandanskis for Po α -particles.

In view of the great importance attached to the phenomenon of capture and loss of electrons by α -particles in their ionisation processes, the subject has received great attention both from the theoretical and experimental point of view. The extensive experimental and theoretical literature on this problem has been listed by T. A. Hall (1950). The general theoretical principles are discussed thoroughly by N. Bohr (1948) who shows that the process is essentially different in light and in heavy media. If the medium is heavy enough so that some electrons in the medium already have a speed v , as large as that of the incident α -particle, these will be simply captured by the latter. On the other hand for a lighter medium none of the electrons in the medium will have speeds as large as v . Capture must then occur by a double process; first an electron gains energy from collision with the incident α -particle, and then in a second collision with its own nucleus it is sent into a direction which makes capture possible. For heavier media, using the Fermi Thomas model, Bohr estimates the probability for the electron to have the correct velocity and calculates from it the electron capture cross-section :

$$\sigma_c \sim 4\pi a_0^2 Z^{1/3} \left(\frac{v_0}{v} \right)^6 \quad \dots (1)$$

where v_0 is the velocity of an electron in the first Bohr orbit of hydrogen and a_0 is the Bohr radius (this formula is valid only for $v \gg v_0$). For lighter media, however, the Bohr approximation may be expected to be valid. Brinkman and Kramers (1930) have calculated the capture cross-section in Born approximation and find

$$\sigma_c \approx \left(\frac{2^{18}\pi}{5} \right) a_0^2 z^2 \left(\frac{v_0}{v} \right)^{12} \quad \dots (2)$$

The theory of the loss of electrons is much more straightforward and the corresponding cross-section σ_e have been worked out by Bohr for the heavy and the light media.

The ratio of the low to the capture cross-section for proton beams of speeds v_0 to $4v_0$ in Be, Al, Ag and Au have also been investigated experimentally by T. A. Hall. The results obtained seem to show only a qualitative agreement with the theory.

The difficulties involved in the exact formulation of the cross-section of electron capture and loss are so great that a straight forward theory for ionisation loss of α -particles at low energies can hardly be worked out at the present stage. On the other hand, there seems to exist a considerable amount of reliable experimental data on the ionisation loss in this region of energy. We, therefore, propose

to follow an indirect procedure for a theoretical formulation of the problem. Using the existing standard experimental data on the ionisation loss of Po α -particles, we attempt to improve upon the existing theory of ionisation loss due to Bethe (which is valid only at high energies) to bring about an agreement of the theory with the experiment at low energies. The approach, to start with, is empirical, but we shall try to justify the additional terms introduced in Bethe's formula from theoretical considerations. Our object in this paper, is, therefore, to make use of Bethe's formula of the energy loss by in elastic collisions which is only valid in the high energy region and then by introducing some new terms to take account of the capture of electrons at low energies, and get a complete ionisation formula by empirical fitting of the ionisation-range curve for α -particles at low energies. Finally we shall compare the different constants involved in this new formula with those of Bethe's and try to interpret the phenomena taking place at low energies. This treatment will give at least qualitatively some insight into the phenomenon of ionisation at low energies, so that later it may be possible to build up some quantitative theory of ionisation of heavy charged particles, which will be valid both at high as well as low energies.

2. BETHE'S THEORY OF IONISATION AND ITS TRANSFORMATION

The theory of ionisation loss of α -particles was thoroughly investigated by Bethe (1930). He assumed that the energy loss of charged particles when passing through matter is mainly due to the inelastic collisions causing ionisation and excitation of the atoms of the substance traversed. The probability of these inelastic collisions depends on velocity and charge of the α -particles. Bethe's formula is, however, valid only if the velocity of the incident α -particle is large compared to the velocities of the electrons in the atom or in other words, if,

$$E \gg \frac{M}{m} I \quad \dots (3)$$

where E is the kinetic energy of the incident particle, I the ionisation potential of the electrons and M and m the masses of the incident particle and electron respectively. Under these conditions the energy loss per cm path is

$$-\frac{dE}{dx} = \frac{4\pi e^4 z^2}{mv^2} NB \quad \dots (4)$$

with $B = Z \log_e \frac{2mv^2}{I} \quad \dots (5)$

where v is the velocity and ze the charge of the incident particle, N the number of atoms per cm^3 of the material Z the nuclear charge I the average excitation

potential of the atom. B is a convenient dimensionless quantity proportional to the stopping power and is called the 'stopping number'.

The specific ionisation, I_x , the number of ion pairs formed per unit path length is related to the energy loss as

$$I_x = -\frac{dE}{dx} \cdot \frac{1}{\epsilon} \quad \dots (6)$$

where ϵ is the mean energy spent per ion pair. It appears to be fairly constant $\sim 35^{10}$ e.v./ per ion pair in air over a large range of energies for α -particles, rising only at very low velocities.

Now equation (4) can also be written as

$$-\frac{d}{dx} \left(\frac{1}{2} M v^2 \right) = \frac{4\pi e^4 z^2}{m v^2} N Z \log \frac{2mv^2}{I}$$

Therefore,
$$-\frac{dv}{dx} = \frac{4\pi e^4 z^2}{m M v^3} N Z \log \frac{2mv^2}{I}$$

and
$$x = \frac{m M}{4\pi e^4 z^2 N Z} \int_0^{v_0} \frac{v^3 dx}{\log \frac{2mv^2}{I}}$$

If, however, $\frac{2mv^2}{I} \gg 1$ we have the approximate formula (Mattanch, Fluegge)

$$x = \frac{M m}{4\pi e^4 N z^2 Z} \frac{v_0^4}{4 \log_e \frac{2mv^2}{I}} \quad \dots (7)$$

From this relation it is evident that x varies as less than v_0^4 but more than v_0^2 . Since this is quite approximate, Geiger gave an empirical relation

$$x = a' v^3 \quad \dots (8)$$

(where $a' = \text{const}$) which holds quite well within the energy region 4 to 9 Mev. But even at smaller energies, than 4 Mev it holds far better than equation (7). Thus to a first approximation we can assume the equation (8) to be quite true and thus get,

$$E = \frac{1}{2} m a x^{2/3} \quad \text{where} \quad \frac{1}{a'^{3/2}} = a = \text{const.} \quad \dots (8a)$$

Combining (8a) with (5) we further obtain,

$$B = A + \frac{2}{3} Z l_n x, \quad \text{where} \quad A = Z l_n \frac{2ma}{I} \quad \dots (9)$$

Defining the specific ionisation I_x as in (6) we obtain using (4), (8a) and (9),

$$\begin{aligned}
 I_x &= \frac{4\pi e^4 z^2 N}{\epsilon} \frac{B}{mv^2} \\
 &= \frac{4\pi e^4 z^2 N}{\epsilon_{max}^{2/3}} \left\{ A + \frac{2}{3} Z l_n x \right\} \\
 &= \frac{DA}{\epsilon} x^{-2/3} + \frac{2}{3} \frac{ZDx^{-2/3}}{\epsilon} l_n x \\
 &= Mx^{-2/3} + Px^{-2/3} \log_{10} x \quad \dots (10)
 \end{aligned}$$

where

$$D = \frac{4\pi e^4 z^2 N}{ma} \quad (i)$$

$$M = \frac{DA}{\epsilon} \quad (ii) \quad \dots (10a)$$

$$P = 2.3 \times \frac{2}{3} \frac{ZD}{\epsilon} \quad (iii)$$

3. COMPARISON WITH EXPERIMENT

Equation (10) is a direct consequence of the transformation of Bethe's theory. if this theory were correct at low energies also, it should fit exactly with the experimental ionisation curve obtained for single α -particle. As already mentioned, such an experimental curve has been given by Hollway and Livingston (1938) and is reproduced in Fig. 1(a).

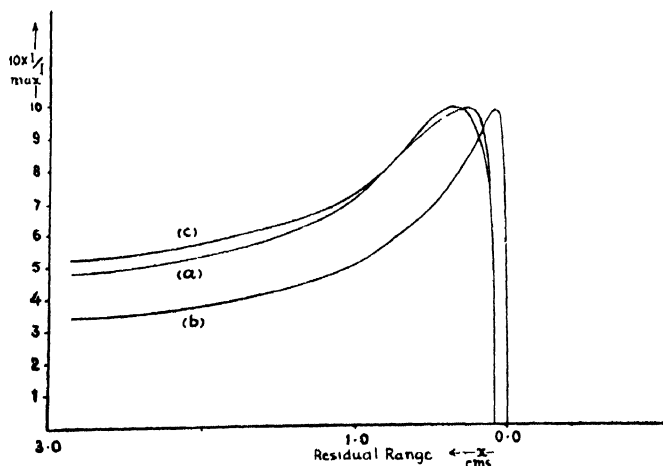


Fig. 1

The specific ionisation curve (relative to that at the peak) for a single particle:—(a) Hollway and Livingston experimental curve, (b) Curve obtained from Bethe's theory, (c) Curve obtained from the modified equation.

To examine the agreement of Bethe's theory with experiment we shall evaluate the constants M and P numerically from (10a). Here the value of a will be taken (as shown below) from some experimentally determined standard range-energy values in the region of validity of Geiger's formula. The atomic constants involved as given by Bethe are :

$$z = 2, Z = 7.22, I = 80.5 \text{ e.v.}, N = 5.41 \times 10^{19} \text{ atoms per cm}^3 \text{ of charge } Ze.$$

From experiment we know that for α -particle. energy $E = 3 \text{ Mev.}$ corresponds to $x = 1.70 \text{ cms.}$ We can, therefore, evaluate a and D using the relations (8a) and (10a-i) as

$$\begin{aligned} a &= \frac{2E}{Mx^{2/3}} = 10.16 \times 10^{17} \text{ using } M = 6.644 \times 10^{-24} \text{ gm} \\ D &= 1.569 \times 10^{-7} \quad e = 4.8 \times 10^{-10} \text{ e.s.u.} \\ &\quad m = 9.1 \times 10^{-28} \text{ gm.} \end{aligned}$$

From (9) and 10a(ii), (iii) we also get,

$$\begin{aligned} A &= 18.37, \\ M &= 5.147 \times 10^4 \quad \text{Using } \epsilon = 35 \text{ e.v.} \\ P &= 3.101 \times 10^4 \end{aligned}$$

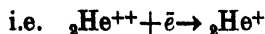
Substituting these in equation (10) we have

$$10^{-4}I_x = 5.147x^{-2/3} + 3.101x^{-2/3} \log_{10}x \quad \dots (11)$$

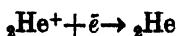
Using this equation (11) we can calculate the value of I_x for different values of x and from a graphical plot we can find I_{max} . The normalised values of specific ionisation can now be defined as $10I/I_{max}$ and can be computed. The results thus obtained are shown in curve (b) of Fig. 1. A comparison with the curve (a) of the same figure makes it clear that there is no agreement whatsoever between the two curves, which means that there is a complete break down of Bethe's theory below 4 Mev energy of the α -particles.

4. MODIFICATION OF BETHE'S THEORY DUE TO ELECTRON CAPTURE

In discussing the failure of Bethe's theory of ionisation at low energies as explained above, many authors (Rutherford, 1924 ; Kapitza, 1924) have pointed out the influence of electron capture and loss in helium at low energies. We have already discussed this point in the introduction. We can visualize that at low energies the α -particle ${}_2\text{He}^{++}$ captures electron and transforms into ${}_2\text{He}^+$



which can further capture another electron and thus produce neutral He atom.



Theoretical considerations on the electron capture and loss processes lend support to the view that the probability of these processes is a simple power function of v . We can, therefore, represent this probability as k/x^n , where n is a numerical factor and k is a constant. As a first approximation let us also make the simplest assumption $n = 1$. To account for these processes we, therefore, propose to introduce a second term in Bethe's theory with a weight factor k/x . The electron capture by the α -particle at low energies can take place only by the process that at first the electron must be knocked out from the N or O atom of air with a proper velocity and direction and then in a second rearrangement collision with the α -particle, the above will be captured, releasing, of course, its kinetic and binding energies to the He-atom. This phenomenon can be thought of as reverse of ionisation, since there the energy is given to the α -particle in the electron capture process, rather than being used up in producing ions.

Thus we can assume the modified ionisation formula to be represented as

$$I_x = Mx^{-2/3} + Px^{-2/3} \log_{10} x + \frac{k}{x} (N'x^{-2/3} + Q'x^{-2/3} \log_{10} x) \\ = Mx^{-2/3} + Px^{-2/3} \log_{10} x + \frac{1}{x} (Nx^{-2/3} + Qx^{-2/3} \log_{10} x) \quad \dots \quad (12)$$

where

$$N = kN', \quad Q = kQ'$$

Since the exact value of k is not known, a simple method of evaluating the constants M , N , P and Q would be by an empirical fitting of four experimental points, a , b , c , and d taken on Hollway and Livingston's curve (a), Fig. 1, suitably distributed over the entire range of energy. Such fits yield the numerical values of constants as given below:

$$M = 5.578 \times 10^4, \quad N = .1307 \times 10^4, \quad P = 3.983 \times 10^4, \quad Q = -.04351 \times 10^4.$$

Equation (12) then becomes

$$10^{-4}I_x = 5.578x^{-2/3} + 3.983x^{-2/3}\log_{10}x - \frac{1}{x} (.1307x^{-2/3} + 0.04351x^{-2/3}\log_{10}x) \dots \quad (13)$$

It may be noticed here that the term in $1/x$ under (13) is appearing with a negative sign which further strengthens our argument that the phenomenon of electron capture considered above can be treated as the reverse of ionisation. Normalising the values of I_x in the ratio of I_{max} , we obtain from (13) the curve (c) of Fig. 1. It can be seen that this new relation agrees extremely well with the experimental curve throughout the region below 4 Mev. Of course, the agreement beyond $x = 1\text{mm.}$ is not so good, because below this limit the corresponding energy of the α -particle no longer satisfies equation (3) which is essential for the theory to hold. Moreover, the experimental curve in this region is also obtained by extrapolation, so that a quantitative comparison is not possible.

Let us now analyze the constants obtained in equation (13). It is clear that the two constants with the first two terms should be similar to the two constants M and P of Bethe's theory as is evident by comparison. Using Bethe's expressions for the constants M and P as in equation (10a), we may calculate the values of z^2Z and I from our numerical values of M and P as in equation (13) which are the only terms likely to be modified at the low energies. We have

$$M = \frac{L}{\epsilon} z^2 Z l_n \frac{2ma}{I} = 5.578,$$

$$P = 2.3 \times \frac{2}{3} z^2 Z \frac{L}{\epsilon} = 3.983,$$

which give $z^2Z = 27.52$ and $I = 134.8$ eV.

But $z^2 = 4$, hence $Z = \frac{27.52}{4} = 6.88$

This means that at low energies the effective value of Z is not 7.22, but 6.9, which physically may mean that the K-electrons are not so much effective in ionisation as at high energies, as was also concluded by Bethe (1937). It may be pointed out that here $I = 134.8$ eV, comes out to be much larger than the value $I = 80.5$ eV. used by Bethe which was obtained by Duncanson and Mano by experimental fittings.

5. ENERGY GAIN DUE TO ELECTRON CAPTURE

The following picture now emerges from the discussion given above. When an α -particle comes near an atom, due to the Coulomb field, the shell electron which can be assumed to be quasi-elastically bound to the atom, executes forced vibration and thus gains energy from the α -particle, resulting in the energy loss of the α -particle. On the other hand, such a vibrating electron can be captured by the α -particle depending upon the cross-section of capture. The captured electron then releases to the α -particle its kinetic energy as well as the binding energy (in the He-atom). Thus at low energy two distinct processes take place, one the energy loss of the α -particle due to inelastic collisions with the atom and the other, the energy gain due to the electron capture. The resultant of these two effects will be the effective energy loss of the α -particle.

Following Bohr's classical calculations of the energy loss due to the collision process, we can calculate the energy gain in an analogous manner if we write for one electron capture.

Energy gained $= Q = \sigma_e(E_{kin} + I_{He})$ where σ_e is the cross section for electron capture, E_{kin} is the kinetic energy of the vibrating electron which is captured and I_{He} is the ionisation potential of helium atom.

The contribution due to electron capture finally calculates out as

$$\left(\frac{\Delta E}{\Delta x}\right)_{\text{capture}} = \frac{4\pi z^2 e^4 N Z}{m v^2} \sigma_c \ln \frac{2 m v^2}{I} e^{\frac{I_{11r}}{I} \left(1 - \frac{I}{2 m v^2}\right)}$$

and the resultant energy loss of the α -particle at low energy then becomes

$$-\frac{dE}{dx} = \frac{4\pi e^4 z^2}{m v^2} N Z \log_e \frac{2 m v^2}{I} - \frac{4\pi z^2 e^4}{m v^2} N Z \sigma_c \ln \frac{2 m v^2}{I} e^{\frac{I_{11r}}{I} \left(1 - \frac{I}{2 m v^2}\right)}$$

As is clear from this formula, it is quite consistent with our empirical formulation as done above. Of course, the factor σ_c cannot be formulated at present in the absence of detailed knowledge of the capture process.

6. RANGE ENERGY RELATION AT LOW ENERGIES BELOW 4 Mev

We may now attempt to obtain empirical range-energy relation of α -particles at low energies by making use of our relation (13). We have the equation (12) as

$$I_x = \frac{1}{\epsilon} \frac{dE}{dx} = M x^{-2/3} + \frac{P}{2.3} x^{-2/3} \log_e x + \frac{1}{x} \left(N x^{-2/3} + \frac{Q}{2.3} x^{-2/3} \log_e x \right)$$

where ϵ is the energy required to produce one ion pair. Integrating the above equation we get,

$$E = \int \left\{ M x^{-2/3} + \frac{P}{2.3} x^{-2/3} \log_e x + \frac{1}{x} \left(N x^{-2/3} + \frac{Q}{2.3} x^{-2/3} \log_e x \right) \right\} \epsilon dx$$

Forstat and Sadanskis (1950) have shown that ϵ does not remain constant at low energies, but is slightly dependent on energy. To a first approximation, we can assume ϵ to be constant and take it out for performing the integration.

$$E = \epsilon \left\{ 3 M x^{1/3} + \frac{3P}{2.3} x^{1/3} \log x - \frac{9P}{2.3} x^{1/3} - \frac{3}{2} N x^{-2/3} - \frac{3}{2} \frac{Q}{2.3} x^{-2/3} \log x - \frac{9}{4} \frac{Q}{2.3} x^{-2/3} \right\}$$

Simplifying we get,

$$E = \frac{3\epsilon}{2.3} (2.3M - 3P) x^{1/3} \left\{ 1 + \frac{2.3P}{2.3M - 3P} \log_{10} x \right\} - \frac{3\epsilon}{2 \times 2.3} (2.3N + \frac{3}{2}Q) x^{-2/3} \left\{ 1 + \frac{2.3Q}{2.3N + \frac{3}{2}Q} \log_{10} x \right\}$$

Substituting the values of the constants occurring above from equation (13) we get,

$$E(\text{Mev}) = .4018x^{1/3} + 4.183x^{1/3} \log_{10} x + .0835x^{-2/3} + .0228x^{-2/3} \log_{10} x \quad \dots \quad (14)$$

This relation however, does not agree with the range-energy values of α -particles known experimentally. The reason probably is that the energy dependence of ϵ has not been taken into account. But since this energy dependence of ϵ is not known, at least an empirical range energy relation in this region can be obtained by numerical fitting of (14) with experimental range-energy curve. We obtain in this way:

$$E(\text{Mev}) = 0.4359x^{1/3} + 5.676x^{1/3} \log_{10} x + 1.477x^{-2/3} + .9712x^{-2/3} \log_{10} x \quad \dots \quad (15)$$

Using this relation we have calculated the value of E corresponding to different values of the range x . The calculated values are given in the Table I below and are compared with the experimental values.

TABLE I

Numerical range-energy values as calculated from the empirical relation (15)

x cms	E calculated from (15) Mev	E Experi- mental, Mev
.17	.200	.2
.27	.400	.4
.38	.625	.6
.47	.808	.8
.57	1.015	1.0
.66	1.205	1.2
.74	1.373	1.4
.84	1.581	1.6
.94	1.78	1.8
1.50	2.02	2.0
1.35	2.63	2.5
2.08	3.95	3.5
2.49	4.6	4.0

From this table it is quite clear that the agreement between the calculated and the experimental values is quite satisfactory upto 2.5 Mev (13.5 mm). At higher energies the error goes on increasing as is also expected due to the uncertainty of the value of ϵ .

Although it cannot be claimed as a working out of the range-energy relation of α -particles at low energies, it may be considered as a supplement over the results of Blackett and Lees (1932) who obtained an empirical formula

$$x = 0.372(v)^{1.43} \quad \dots (16)$$

giving fit only upto 4mm. range with the experiment. as pointed out by these authors themselves.

ACKNOWLEDGMENTS

I am highly indebted to Dr. N. K. Saha, Reader in Physics. Delhi University, for his extremely valuable guidance and helpful discussions all through the present work. I also wish to express my sincere gratitude to Professor D. S. Kothari, Head of the Physics Department for providing all facilities to carry out this work.

REFERENCES

- Bethe, H. A. 1930, *Ann. Physik*, **5**, 325.
 Bethe, H. A. 1950, *Rev. of Mod. Phys.* **22**, 213.
 Blackett P. M. S. and Lees, D. S. 1932, *Proc. Roy Soc.* **134**, 658.
 Bohr, N. (1913, 1915)*Phil. Mag.* **24**, 10; **30**, 581.
 Bohr, N. Kgl. Danske Videnskab, and Selskab, 1948*Mat. fys. Medd.*, **18**, 8.
 Brinkman and Kramers, 1930, *Proc. Akad., Amsterdam*, **33**, 973.
 Duncanson, 1934, *Proc. Camb. Phil. Soc.* **30**, 102.
 Hall, T. A. 1950, *Phys. Rev.* **79**, 504.
 Holloway M. G. and Livingston, M. S. 1938, *Phys. Rev.*, **54**, 29.
 Jesse, W. P. Forstat, H. and Sadauskis, J. 1950, *Phys. Rev.* 11 series **77**, 782.
 Kapitza, 1924, *Proc. Roy. Soc.*, **106**, 602.
 Livingston M. S. and Betho, H. A. *Rev. of Mod. Phys.* **9**, 265, 1937.
 Mano, 1934, *Ann. d. Physik*, **1**, 407.
 Mattauch J. and Fluegge, S., Nuclear Physics Table Page 56
 Rutherford, E. 1924, *Phil. Mag.*, **47**, 277.
 Schmieder, K. 1939, *Ann. Physik*, **35**, 445.

MUONIC INTERACTIONS IN DENSE MATERIAL

BY M. M. BISWAS

PHYSICS DEPARTMENT, PRESIDENCY COLLEGE, CALCUTTA.

(Received for publication, July 4, 1955; received after revision, Sept., 3, 1955)

ABSTRACT. Production of associated penetrating particles (A.P.P.) and groups of penetrating particles (G.P.P.) by fast μ -mesons interacting with lead placed above a cloud chamber and the formation of star in the lead plate inside the chamber have been investigated. The cross-section for the formation of A.P.P. and G.P.P. comes out to be of the order of $\sim 10^{-30}$ cm²/nucleon and that for star formation $\sim 10^{-29}$ cm²/nucleon which are in agreement with the observations of other authors.

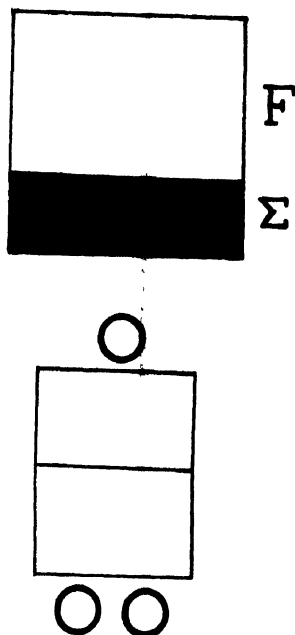
1. INTRODUCTION

Absorption experiments of μ -mesons show that their property of interaction with matter is very small. During the study of such interaction, the investigators have observed the production of A.P.P., G.P.P., stars and neutrons by μ -mesons in the experiments performed underground and at sea level. The existence of A.P.P. was first reported by Braddick and Hensby (1939) from the study of a cloud chamber experiment performed underground at 60 m.w.e. Shutt (1946) also observed pairs of penetrating particles in his cloud chamber operated at sea level under thick layers of lead absorber. He interpreted them as μ -pairs. The counter hodoscope experiment of George and Trent (1951) was also explained in terms of the existence of the same phenomena, and A.P.P. were assumed to consist of produced by nuclear interaction, a μ -meson and a penetrating secondary the cross-section for such production being 4×10^{-29} cm²/lead nucleon. Cloud chamber study by Braddick *et al* (1951), predicted similar result for cross-section for the production of A.P.P. and also for G.P.P. George and Evans (1950) from the study of photographic emulsion exposed underground observed stars and penetrating showers and gave the value of the cross-section for star and penetrating particle production as $\sim 10^{-29}$ cm²/nucleon and 4×10^{-30} cm²/nucleon respectively.

Later Amaldi (1952) and his co-workers from the observation of a counter hodoscope experiment performed underground at 50 m.w.e. contradicted the result of the cross-section for the formation of A.P.P.—the upper limit of their result being $(13 \pm 3) \times 10^{-30}$ cm²/nucleon. Subsequent to the prediction of such result a series of experiments performed by various workers such as Walker (1953), Deutschmann (1953), Lovati (1953) *et al*, Appapillai (1954) *et al* elucidated further on the result of A.P.P. and G.P.P. formation. They all showed a much lower value than 4×10^{-29} cm²/nucleon.

2. EXPERIMENTAL ARRANGEMENT

A counter-controlled cloud chamber was triggered by three-fold coincidence arrangement under an absorber equivalent to 855 gm/cm² of lead (see figure 1).



1. Schematic diagram of the experimental arrangement.
 Σ — Interacting material, F — filtering medium

The lower 10 cms. of the lead absorber Σ was taken as a medium for any interaction of μ -meson and the remaining upper portion F , as the material for filtering it. The chamber was 28 cms. in diameter with a width 8.7 cms. It contained a single lead plate 1.5 cm. thick placed at the centre of the chamber and was 30.5 cms. from the bottom of Σ . Photographs were recorded stereoscopically at different angles to reproject the pictures.

3. RESULTS

After careful examination of the pictures, photos containing pairs and groups of penetrating particles and also stars (produced in the lead plate inside the chamber) are selected. While considering the diverging pairs of penetrating particles, the random association of the two penetrating particles which may simulate as A.P.P., has been studied on the basis of the following criterion.

If the two diverging particles are space-and time-associated that is they are originated from the same point due to μ -meson interaction with nucleus of the absorber, then the perpendicular drawn from the plane of the lead plate inside the chamber to the supposed meeting point of the two particles will show the same

distance in both the stereopictures photographed at different angles, though the angle between the particles will vary in the two pictures (figure 2). While, if

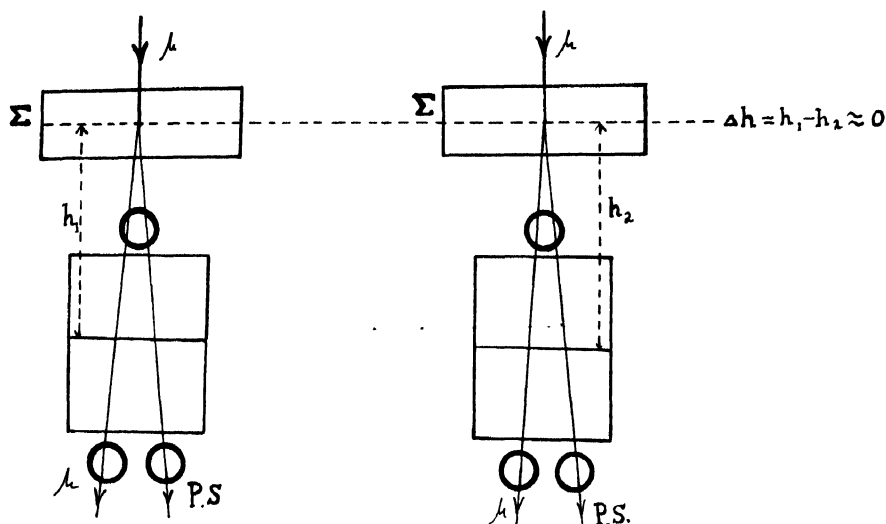


Fig. 2. Schematic representation of A.P.P. viewed stereoscopically
P.S.—Penetrating secondary

the two diverging particles are not really space-associated but are each independent particles entering the chamber from different directions and are seen from the pictures, to be diverging as if from the same point, then the perpendiculars h_1 and h_2 drawn from the supposed originating point to the plane of the plate in each of the stereopictures will be of different heights, angles between them also being different (figure 3). Calculations on the dependence of accuracy in the

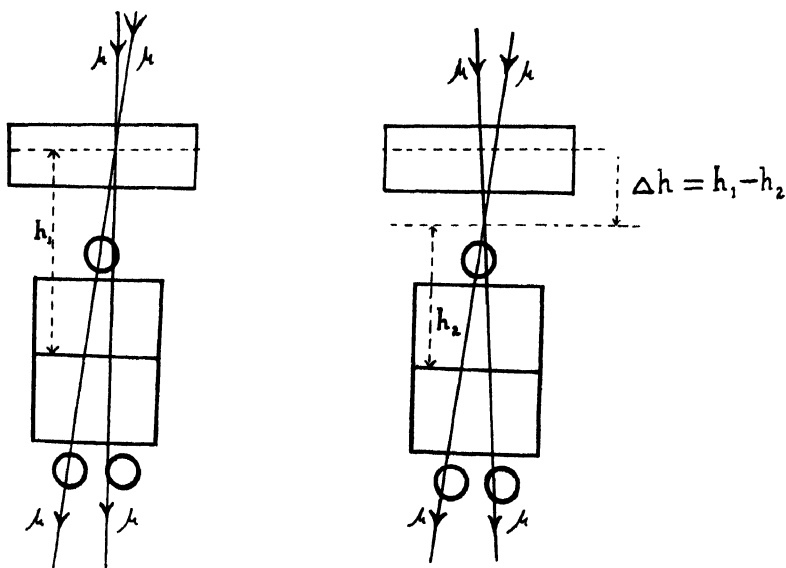


Fig. 3. Two knock-on electrons appearing as A.P.P.

measurement of difference of heights Δh on chamber dimensions have been carried out and given in the appendix. It has been shown that the accuracy can be improved by taking the stereopictures at large angular separation. The expression for Δh connecting the cloud chamber diameter C and stereo angle α can be written in the form:

$$\Delta h = C.\alpha. \left[\frac{\eta_1 - y_1}{x' - \xi'} - \frac{(\xi_1 - x_1)(y' - \eta')}{(x' - \xi')^2} \right].$$

The cross-section for the production of the nuclear event has been calculated with the help of the formula

$$v = N\sigma tLv$$

where v = Event (such as A.P.P.)/sec.

N = Primary incident μ /sec. on the total sensitive area and within the solid angle of the experiment.

$N = I_v G$, where I_v = vertical intensity of fast μ /sec/cm²/solid angle and G is the geometrical factor with the dimension of an area.

v = Atomic volume.

t = Thickness of the interacting material in gm/cm².

L = Number of nuclei per c.c.

σ = Cross-section for the production of the event/nucleon.

3.1(a) Pairs of Penetrating Particles :

Pairs of visually contemporary particles crossing the plate inside the chamber without any event (excepting production of knock-on electron) are classified into three groups.

- (1) Parallel pairs.
- (2) Converging pairs.
- (3) Diverging pairs.

Table I shows the data obtained from this experiment of the above three groups.

TABLE I

Pairs of parallel particles	Pairs of converging particles	Pairs of diverging particles	Total
4	8	16	28

3.1(b). Parallel Pairs.

Events of the class (1) mentioned in 3.1(a) are presumably due to the random entry in the chamber of two unconnected particles within a certain short time

interval. The separation between the two parallel particles are shown in Table II.

TABLE II

No.	Separation
1	5.6 cms.
2	4.8 cms.
3	4.8 cms.
4	.8 cms.

It is reasonable that the members of the parallel pairs of pictures 1, 2, 3 shown in Table II with a separation as much as 5.6 cms. and 4.8 cms. between them are independent of each other. Parallel pair No. 4 may also be taken as the repetition of the cases 1, 2, 3—the difference lying only in that, that the members of No. 4 are associated accidentally within a very close space. Even if they are all ejected from some common point due to nuclear interaction of μ , then that will be outside Σ .

3.1.(c) *Converging Pairs.*

Pairs of convergent particles are each independent particles and are definitely randomly associated.

3.1.(d) *Diverging Pairs.*

All the diverging pairs of penetrating particles which apparently seem to be A.P.P. due to their divergence from some point above the cloud chamber are classified after reprojection of the stereopictures into two groups according to their origin (1) outside or (2) inside Σ from which they appear to diverge.

Those that appear to diverge from some point outside Σ are shown in Table III with the location of their point of divergence in each of the stereopairs and also Δh .

One of the penetrating particles of pair No. 14 shown in Table III consists of a high-energy electron knocked out from the glass cylinder of the chamber and penetrates the plate without any event. Apart from the consideration that they are supposed to be coming from a point outside Σ , the values of their Δh show that they are randomly associated.

Those that appear to diverge from some point inside Σ may be the combining effects of the following four phenomena.

(a) The random association of the two independent penetrating particles within the solid angle of the experiment.

TABLE III

No.	h_1	Location of point of divergence	h_2	Location of point of divergence	$\Delta h = h_2 - h_1$
1.	53.68 cms.	above Σ	29.20 cms.	below Σ	24.48 cms.
2.	55.68 cms.	above Σ	35.28 cms.	in Σ	20.40 cms.
3.	71.60 cms.	above Σ	55.60 cms.	above Σ	16.00 cms.
4.	39.60 cms.	in Σ	25.04 cms.	below Σ	14.56 cms.
5.	44.88 cms.	above Σ	34.40 cms.	in Σ	10.48 cms.
6.	31.20 cms.	in Σ	22.64 cms.	below Σ	8.56 cms.
7.	30.40 cms.	bottom of Σ	24.16 cms.	below Σ	6.24 cms.
8.	26.60 cms.	below Σ	22.56 cms.	below Σ	4.04 cms.
9.	25.60 cms.	below Σ	22.60 cms.	below Σ	3.00 cms.
10.	17.36 cms.	below Σ	14.64 cms.	below Σ	2.72 cms.
11.	13.37 cms.	below Σ	11.60 cms.	below Σ	1.77 cms.
12.	30.60 cms.	bottom of Σ	28.64 cms.	below Σ	1.96 cms.
13.	20.56 cms.	below Σ	18.08 cms.	below Σ	2.48 cms.
14.	5.20 cms.	wall of chamber	5.20 cms.	wall of chamber	0

(b) μ -mesons accompanied by a high-energy electron knocked on by it from the bottom of the absorber and penetrating the lead plate of the chamber. The characteristic of such penetrating electrons is that they will be knocked out just from few mms. of the bottom of the absorber.

(c) A μ -meson passing outside the geometry of the experiment producing two high energy knock-on electrons successively from the bottom of Σ which cross the lead plate and thereby appear to be an A.P.P. (figure 4).

(d) A.P.P. (if any?)

In Table IV have been shown the data of the divergent pairs appearing to emerge from inside Σ .

TABLE IV

No.	h_1	h_2	Δh
1.	36.64 cms.	35.00 cms.	1.64 cms.
2.	38.40 cms.	37.44 cms.	.96 cms.

These two pairs may be taken to be A.P.P. and within the limits of experimental measurement. The values of Δh are not very different from zero.

It seems most unlikely that these two are due to penetrating knock-on electrons for the fact that they are originated at least from 4.5 cms. and 6.94 cms. from the bottom of the interacting material (characteristic of such knock-on electrons already referred to). In view of the fact that any one member of the two

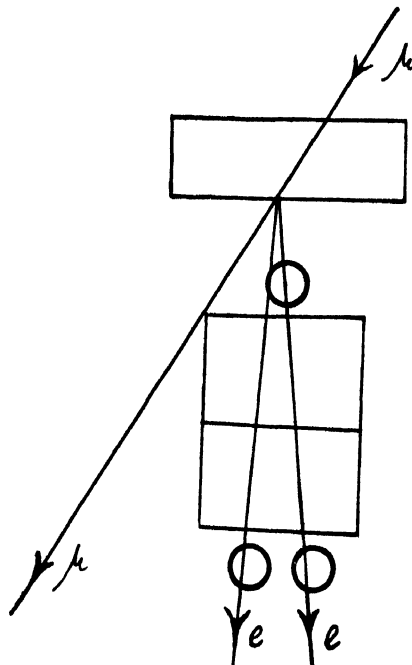


Fig. 4 Two knock-on electrons appearing as A. P. P.

pairs is not a penetrating electron, we are neglecting the case of both the members of the pairs, being due to two successive penetrating knock-ons. The cross-section calculated from these two events for the production of A.A.P. comes out to be $3.8 \times 10^{-30} \text{ cm}^2/\text{nucleon}$.

3.2. G.P.P.

Only two groups, one containing three and the other, four penetrating particles have been produced in Σ . Reprojecting the stereopictures they are seen to diverge from the same point in Σ . The cross-section calculated for such G.P.P. formation is $3.8 \times 10^{-30} \text{ cm}^2/\text{nucleon}$.

3.3. Star.

Two pictures have been obtained which show the production of heavy fragments in the lead plate of the chamber by fast μ -meson. It is probable that more than two fragments have been ejected in each case and that they have been absorbed in the lead plate. In both the cases, the initiating particles have been deflected from its direction of incidence. The angles θ between the direction

of incidence and emission of μ , projected in the plane of the cloud chamber are 3° and 6° . In one case, the two evaporation particles are one a long-range σ and the other, a short range α . The cross-section calculated for such production of star by μ is of the order of 2.3×10^{-29} cm²/nucleon.

4. DISCUSSION

4.1. *Nature of Mechanism of Interactions.*

Calculation shows that any contribution to the interactions of the type, we have studied above, due to nuclear interacting particles other than μ , is negligible. All these interactions (A.P.P., G.P.P.; Star) can be explained in the same way as is being done by George and Evans (1950) in the case of star formation by μ -mesons underground. It can be assumed that these are from the interaction of the Coulomb field of μ -meson with the meson field of the nucleus. By analogy with Williams-Weizsäcker approach to the bremsstrahlung of electrons, μ -meson is imagined as being accompanied by virtual photons. These virtual photons are assumed to interact with the nucleus through the meson field in the same way that real photons produced in the Berkeley synchrotron produce mesons.

Thus muonic interaction with matter can be thought of as electromagnetic interaction in the sense that it is being explained by electromagnetic forces and not by typical nuclear forces which, on the other hand, play important part in the nuclear phenomena caused by proton and π .

4.2. *Nature of the secondary particles produced in nuclear interactions.*

The underground shower particles produced in a nuclear interaction by μ -meson as indicated by George (1952) are thought to be π -mesons. Since, Berkeley Synchrotron has produced π -mesons by photons and the cross-section for the production of π -mesons corresponds to that of the particles produced by μ -mesons taking μ as equivalent to photons, the secondary particles produced in A.P.P. and G.P.P. are presumably π -mesons.

ACKNOWLEDGMENT

It is a great pleasure for the author to acknowledge gratefulness to Prof. R. L. Sen Gupta, Head of the Department of Physics, Presidency College, Calcutta, for all sorts of help during his work and to Govt. of West Bengal for financial assistance. Thanks are also due to Dr. T. C. Roy for his kind interest in this paper.

REFERENCES

- Amaldi, E., Castagnoli, C., Scinti, S., and Gigli, A, 1952, *Nuovo Cimento*, **9**, 453; 960.
 Appapillai, V., Mailvaganam, A. W., and Wolfendale, A. W., 1954, (Private Communication to Dr. R. L. Sen Gupta).
 Braddick, H. J. J. and Hensby, G. S. 1939, *Nature*, **14**, 1012.

- Braddick, H. J. J., Nash, W. F. and Wolfendale, A. W. 1951, *Phil. Mag.*, **42**, 1277.
 Deutschmann, M. 1953, *Zeits. f. Naturfor.*, **8a**, 308.
 George, E. P. and Trent, P. T. 1951, *Proc. Phys. Soc.* **64**, 1134.
 George, E. P. and Evans, J. 1950, *Proc. Phys. Soc.* **63**, 1248.
 George, E. P. 1952, *Progress in Cosmic Ray Physics* edited by J. G. Wilson.
 Lovati, A., Mura, A., Succi, C., and Tagliaferri, G., 1953, *Nuovo Cimento*,
10, 105; 1953, *Ibid*, **10**, 1201.
 Shutt, R. P. 1946, *Phys. Rev.*, **69**, 261.
 Walker, W. D. 1953, *Phys. Rev.* **90**, 234.

APPENDIX I.

Let X_1Y_1 and X_2Y_2 be the two planes with a distance c between them where c is the diameter of the cloud chamber (figure 5). The equations to straight lines

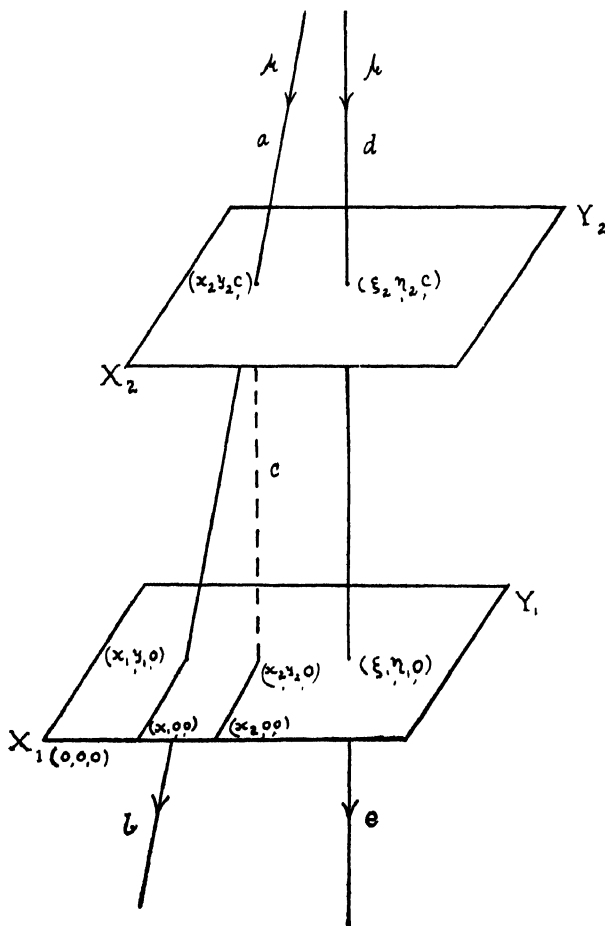


Fig. 5 Schematic representation of a pair,

ab and de passing through the points $(x_1, y_1, 0)$, (x_2, y_2, c) and $(\xi_1, \eta_1, 0)$, (ξ_2, η_2, c) respectively are:

$$\frac{x-x_1}{x_2-x_1} = \frac{y-y_1}{y_2-y_1} = \frac{Z}{c} \quad \dots (1)$$

$$\frac{x-\xi_1}{\xi_2-\xi_1} = \frac{y-\eta_1}{\eta_2-\eta_1} = \frac{Z}{c} \quad \dots (2)$$

Let $lx+my = k$... (3)

be the eqn. to a plane containing one of the stereoplanes and parallel to Z -plane. The straight line ab (1) is projected on the plane (3). The eqn to the plane containing this projected line is:

$$\left(\frac{x-x_1}{x_2-x_1} - \frac{Z}{c} \right) + v \left(\frac{y-y_1}{y_2-y_1} - \frac{Z}{c} \right) = 0 \quad \dots (4)$$

From the condition of perpendicularity between the two planes (3) and (4) i.e.

$$\frac{l}{x_2-x_1} + \frac{mv}{y_2-y_1} = 0.$$

the value of v is

$$v = -\frac{l}{m} \frac{y_2-y_1}{x_2-x_1}$$

substituting the value of v in (4)

$$lm(x-x_1)-(y-y_1) = \frac{Z}{c} \left\{ m(x_2-x_1)-l(y_2-y_1) \right\} \quad \dots (5)$$

Similarly projecting de on the plane $lx+my = k$ and proceeding as above, we get the eqn. to the other plane:

$$m(x-\xi_1)-l(y-\eta_1) = \frac{Z}{c} \left\{ m(\xi_2-\xi_1)-l(\eta_2-\eta_1) \right\} \quad \dots (6)$$

From (5) and (6)

$$Z = c \left[\frac{m(\xi_1-x_1)-l(\eta_1-y_1)}{m(x'-\xi')-l(y'-\eta')} \right] = Z_a \text{ (say)} \quad \dots (7)$$

where

$$x' = (x_2-x_1), \quad \xi' = (\xi_2-\xi_1), \quad y' = (y_2-y_1), \quad \eta' = (\eta_2-\eta_1);$$

This point Z_a is the perpendicular distance from the plane X_1Y_1 , of the meeting point of the two lines ab and de on projection.

Similarly, let $\lambda x + \mu y = K' \dots (8)$ be the eqn. to the other stereoplane. Projecting the straight lines ab and de on this plane and proceeding as above,

$$Z = c \left[\frac{\mu(\xi_1 - x_1) - \lambda(\eta_1 - y_1)}{\mu(x' - \xi') - \lambda(y' - \eta')} \right] = Z_b \text{ (say)} \quad \dots (9)$$

$$\Delta h = Z_a - Z_b$$

$$= c \left[\frac{m(\xi_1 - x_1) - l(\eta_1 - y_1)}{m(x' - \xi') - l(y' - \eta')} - \frac{\mu(\xi_1 - x_1) - \lambda(\eta_1 - y_1)}{\mu(x' - \xi') - \lambda(y' - \eta')} \right] \quad \dots (10)$$

Now substituting the values of m, l, μ, λ in (10),

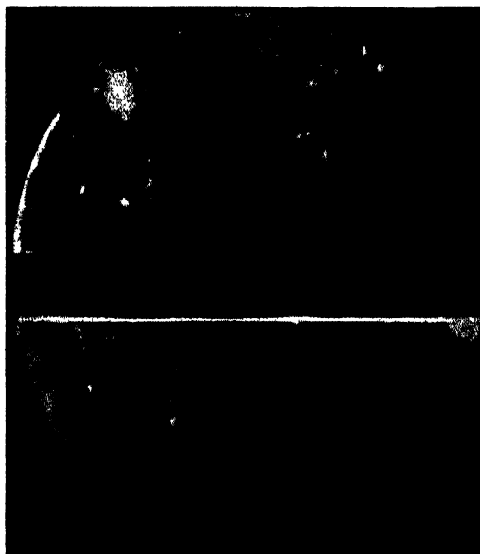
where $l = 0, m = l, \theta$ being zero;

and $\lambda \sim \alpha, \mu \sim 1, \alpha$ being very small;

and neglecting terms containing α^2 and higher orders of α

$$\Delta h = c \cdot \alpha \cdot \left[\frac{\eta_1 - y_1}{x' - \xi'} - \frac{(\xi_1 - x_1)(y' - \eta')}{(x' - \xi')^2} \right]$$

It is seen that by increasing the stereoangle α , the difference Δh can be increased.



One of the Stereopicture of a parallel pair of penetrating particles

Letter to the Editor

Z_A TERM IN THE MASS FORMULA

A. N. SAXENA,

INSTITUTE OF NUCLEAR PHYSICS, CALCUTTA-9.

(Received for publication, September 6, 1955)

In a recent paper by Ghoshal and Saxena (1955), a new systematics of the β^- -disintegration energies was proposed. The β^- -disintegration energies of a sequence of neighbouring odd A isobars was plotted against the atomic number Z of the isobars. When the contribution of the pairing energy term $(\pi - \nu)$ to β^- -disintegration energy E_{β^-} of an odd A nucleus is subtracted from it and the points replotted in a similar manner, the zig-zag isobaric β^- -energy lines are reduced to straight lines. Both the actual β^- -disintegration energy lines and the reduced lines after subtracting the pairing energy effect were given for a large number of odd A isobaric sequences in the previous paper (Ghoshal and Saxena, 1955). The linear behaviour is expected from the Fermi-Weizsäcker mass formula. According to this, the β^- -disintegration energy, $E_{\beta^-}^{(e)}(A, Z)$, for a nucleus of mass number A (odd) and charge number Z , can be written as:

$$E_{\beta^-}^{(e)}(A, Z) = B_A^*(Z_A^* - Z - 0.5) \quad (1)$$

The asterisk denotes the theoretical values of B_A and Z_A , and $E_{\beta^-}^{(e)}$ denotes the theoretical value of β^- -disintegration energy calculated from the Fermi-Weizsäcker mass formula. Equation (1) shows that the plot of $E_{\beta^-}^{(e)}(A, Z)$ against Z for an isobaric sequence is a straight line with a slope $-B_A^*$.

It has been shown by Coryell (1953) that the observed β^- -disintegration energies $E_{\beta^-}^{(e)}(A, Z)$ should be represented by a similar formula with Z_A^* replaced by a new term Z_A .

$$E_{\beta^-}^{(e)}(A, Z) = B_A(Z_A - Z - 0.5) \pm (\pi - \nu) \quad (2)$$

for A odd, Z even (minus) and Z odd (plus) nuclei

Z_A has to be evaluated from observed values of β^- -disintegration energies. This has been done by Coryell, and others (for references, see Coryell, 1953) for different values of A in the different shell regions. It can be easily seen from the equation (2) that the reduced plot of $E_{\beta^-}^{(e)}(A, Z)$ after subtracting $(\pi - \nu)$ is also a linear function of Z with a slope $-B_A$. The values of Z_A can very easily be derived from these reduced $E_{\beta^-}^{(e)}(A, Z)$ plots for the different isobaric sequences. For, if we

write $E_{\beta-}^r(A, Z)$ for value of $E_{\beta-}^r(A, Z)$ from which the pairing energy term $\delta - \nu$ has been subtracted, then

$$E_{\beta-}^r(A, Z) = B_A(Z_A - Z - 0.5) \quad \dots (3)$$

The term B_A has been written different from B_A^* derived from the Fermi-Weiszäcker mass formula, because it has been shown (Coryell 1953, Ghoshal and Saxena, 1955) that B_A departs considerably from the B_A^* , specially in certain regions.

The value of Z at which $E_{\beta-}^r(A, Z)$ will be equal to zero (denoted by Z_0) will be given by

$$Z_0 = Z_A - 0.5 \quad \dots (4)$$

Hence it is possible to read off the values of Z_A directly from the plots of $E_{\beta-}^r(A, Z)$ values for the various isobaric sequences by noting the value of Z for which $E_{\beta-}^r(A, Z)$ is equal to zero, i.e.

$$Z_A = Z_0 + 0.5 \quad \dots (5)$$

The values of Z_A were derived from the plot of Ghoshal and Saxena (1955) for different odd A values and are found to agree well with those evaluated by Coryell (1953). It really gives a simpler means of evaluating Z_A for odd A nuclei.

I am indebted to Dr. S. N. Ghoshal for his kind interest and guidance throughout the progress of the work.

REFERENCES

- Coryell, C. D. 1953, *Ann. Rev. Nuclear. Sci.*, **2**, 305.
 Ghoshal, S. N. and Saxena, A. N., 1955, *Ind. Journ. Phys.*, **29**, 81.

RAMAN SPECTRA OF A FEW MONOSUBSTITUTED BENZENE COMPOUNDS IN THE SOLID STATE AT DIFFERENT LOW TEMPERATURES*

By D. C. BISWAS

OPTICS DEPARTMENT, INDIAN ASSOCIATION FOR THE CULTIVATION OF SCIENCE,
JADAVPUR, CALCUTTA.

(Received for publication, September 15, 1955)

ABSTRACT. The results of the investigations on the Raman spectra of C_6H_5Br , $C_6H_5OCH_3$, $C_6H_5COOCH_3$ and $C_6H_5COOC_2H_5$ in the liquid state and in the solid state at different low temperatures have been discussed. The Raman spectrum of C_6H_5Cl in the vapour state has also been reinvestigated. Attempts have been made to assign some of the lines due to bromobenzene. The number of new low-frequency lines observed in the spectra of these four compounds in the solid state is different for the different compounds. Ethyl benzoate gives only one weak line at 96 cm^{-1} at -180°C , while methyl benzoate yields two strong lines. In the case of anisole and methyl benzoate the intensity of some of these lines increases at the lower temperature.

Two broad fluorescence bands have been observed in each of the spectra due to bromobenzene and methyl benzoate in the solid state at -180°C . The frequency difference is about 1590 cm^{-1} in both the cases. These are ascribed to distortion of the benzene ring at -180°C .

INTRODUCTION

The Raman spectra of a large number of substituted benzenes in the solid state at low temperatures have been studied by different authors. The monosubstituted benzenes, studied by Ray (1950, 1951, 1952), showed a number of new Raman lines in the low frequency region in the solid state at -180°C . It was found that the behaviour of these new lines with change of temperature of the solid can be better explained by attributing them to vibrations in groups of molecules than by any other hypothesis.

Recent investigation on the ultraviolet absorption spectra of substituted benzene compounds have shown that in most cases the absorption bands which are broad in the case of the liquid phase become extremely sharp in the case of the solid state at -180°C and also in some cases the electronic energy levels are split up by the intermolecular field in crystals (Sirkar and Swamy, 1952; Swamy, 1953). The extreme sharpness of the absorption bands in the solid

* Communicated by Prof. S. C. Sirkar.

state at -180°C indicates that some modes of angular oscillation of these molecules cease completely at -180°C or at least their amplitudes become negligible at low temperatures. The co-relation between the results of the investigations on the ultraviolet absorption spectra and those of the Raman spectra of these substances in the solid state at -180°C precludes the possibility of attributing the new Raman lines in the low frequency region to particular modes of angular oscillation of the molecules in the crystal lattice (Swamy, 1953).

There are however a few substituted benzenes in which the absorption bands do not change appreciably when the liquids are solidified and cooled down to low temperatures. Since only angular oscillations of the molecules can broaden the bands, the angular oscillations of the molecules of these substances probably persist even in the solid state at low temperature (-180°C) and if the new Raman lines in the low frequency region be assumed as originating from the angular oscillation of the molecules in the crystal lattice, these substances should exhibit more intense new lines in the low frequency region at low temperatures than other such crystals in which the angular oscillations cease at low temperatures.

The study of such compounds in which the absorption bands remain as broad in the solid state at -180°C as in the liquid phase would therefore be interesting. Ethyl benzoate is one of such compounds and in the case of methyl benzoate also the bands do not become much sharper at low temperatures. In the present investigation Raman spectra of these two compounds as well as those of two other monosubstituted benzenes, *viz.*, anisole and bromobenzene in different states and at different temperatures have been studied to find out the changes which take place in the spectra with solidification and lowering of temperature of the crystals down to -180°C .

EXPERIMENTAL

The liquids bromobenzene and anisole were both supplied by B. D. H. Ltd., while the other two substances methyl and ethyl benzoates respectively were secured from Fisher Scientific Co., N.Y. All these liquids were of chemically pure quality. They were, however, distilled in vacuum to get rid of fluorescent impurities. The experimental procedure and the technique employed to record the Raman spectra in the solid and the liquid state were exactly similar to those described earlier (Biswas, 1954a, 1954b). The spectrograms from which the polarization of different Raman lines of the two esters were estimated were obtained in the same way as explained previously (Biswas, 1955b). The Raman spectra of chlorobenzene in the vapour phase were also recorded using the same arrangement as described by Mazumder (1953) in order to find out the influence of intermolecular field on the Raman lines. The Raman spectra of all these substances in the liquid phase were compared with the results reported by some

earlier workers (Magat, 1936; Hariharan, 1954). The spectrograph used for photographing the Raman spectra in the liquid and in the solid phase was a Fuess glass spectrograph having a dispersion of about 11 \AA° per mm. in the 4046 \AA° region. In the case of the vapour phase an Adam Hilger two-prism spectrograph having dispersion of about 21 \AA° in the 4046 \AA° region was employed. In all these cases Ilford Zenith plate was used to photograph the Raman spectra. On each spectrogram an Fe-arc spectrum was photographed for comparison. The microphotometric records of some of the spectrograms were taken with a Kipp and Zonen type self-recording Moll microphotometer.

RESULTS AND DISCUSSIONS

1. *Raman spectra :*

The Raman shifts observed in the case of the four substances in the liquid state and in the solid state at different temperatures are given in Tables I-IV. In these tables the Raman lines in the liquid phase as reported by previous workers are also included. A few microphotometric records showing the intensities of the low-frequency lines relative to some particular line due to intermolecular oscillation are reproduced in figures 1, 2 and 3. The letters P and D in tables I-IV denote respectively whether a particular Raman line is polarised or completely depolarised (ratio=6/7).

(a) *Bromobenzene*

When bromobenzene is solidified and cooled down to -60°C , the intensity of the line at 1019 cm^{-1} diminishes and becomes equal to that of the next line at 1073 cm^{-1} . With further lowering of temperature of the solidified mass to -180°C the former line at 1019 cm^{-1} becomes slightly weaker than the other. The broad and intense line 182 cm^{-1} of the liquid becomes sharper in the solid state and shifts to 193 cm^{-1} at -60°C and to 198 cm^{-1} when the temperature is further lowered down to -180°C .

It has been noticed that a number of unsymmetrically (polar) substituted benzene compounds give rise (Ray, 1950; Biswas, 1954) to an intense Raman line with frequency-shift less than 200 cm^{-1} in the liquid phase and that this line shifts increasingly away from the Rayleigh line with lowering of temperature on the solidified mass of this compound. Moreover, in most cases, the relative intensity of this line is found to increase in the solid state. It was suggested previously (Biswas, 1955) that in the case of *m*-chloro- or *m*-bromotoluene the intense lines close to the exciting radiation corresponds, in all probability, to the vibration of type ϵ_u^- in the benzene ring given in figure 1, No. 16, by Sponer and Kirby-Smith (1941) and that some of them might also be due to such a mode in an associated group of molecules formed in these polar compounds. The line 182 cm^{-1} of bromobenzene may be attributed to this mode in the substituted

benzene ring. This assignment is further supported by the behaviour of an analogous line in chlorobenzene with change of state. Sponer and Kirby-Smith (1941) studied the Raman spectrum of chlorobenzene in the vapour state and reported a line 200 cm^{-1} in place of a stronger depolarised line 196 cm^{-1} observed in the case of the liquid. In order to find out whether this line becomes actually weaker with vaporization of the liquid, the Raman spectrum of chlorobenzene

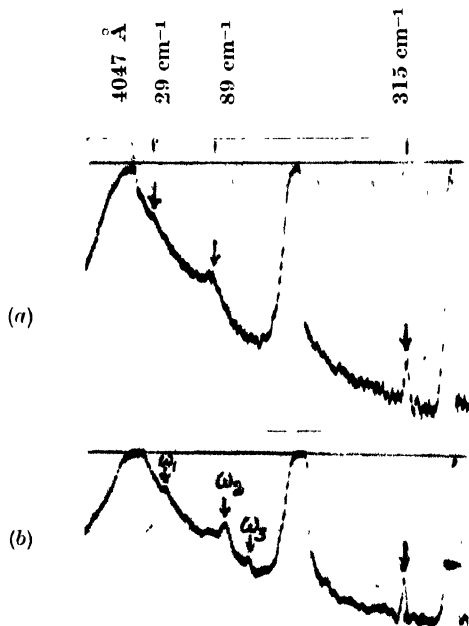


Fig. 1. Microphotometric records of the low-frequency Raman spectrum due to bromobenzene.

(a) Solid at about -60°C . (b) Solid at -180°C .

($\omega_1=34\text{ cm}^{-1}$, $\omega_2=96\text{ cm}^{-1}$, $\omega_3=130\text{ cm}^{-1}$.)

vapour at 150°C at a pressure of about 3 atmospheres was reinvestigated with the arrangement used by Mazumder (1953). The spectrogram shows a broad line at 185 cm^{-1} in place of the line 196 cm^{-1} observed for the liquid although the spectrogram due to the mercury lines does not show such a spurious line. The relative intensity of the line does not appear to change with vaporization of the liquid. Thus the line is due to the single molecule of chlorobenzene. The frequency-shift of the line increases from 185 cm^{-1} to 196 cm^{-1} due to intermolecular field with liquefaction of chlorobenzene vapour. The Raman spectrum of bromobenzene vapour could not be photographed owing to decomposition of the vapour at high temperature. This frequency-shift increases to 215 cm^{-1} with solidification (Ray, 1950) of chlorobenzene. In the case of bromobenzene also the frequency-shift increases from 182 cm^{-1} to 198 cm^{-1} with solidification and lowering of temperature to -180°C . Further, on examining the frequencies of the Raman lines due to disubstituted benzene compounds it is found that

such a line with frequency-shift in the range $150\text{--}210\text{ cm}^{-1}$ is observed in the Raman spectra of ortho and meta compounds but it is absent in the spectra due to the symmetrical para compounds. This fact further corroborates the above assignment because in the mode mentioned above the centre of symmetry is destroyed in the case of symmetrical para compound and the line is forbidden in the Raman spectrum.

The increase in the frequency-shift of the line with solidification may be due to virtual linking of the halogen atom with neighbouring molecule in the solid state so that slight C-Br deformation takes place during the mode of deformation vibration of the ring mentioned above.

In order to understand the significance of the change in the relative intensities of the lines 1019 cm^{-1} and 1073 cm^{-1} observed with solidification of the liquid we have to assign the two lines as well as the line 998 cm^{-1} correctly. The frequencies of chlorobenzene molecule have been tentatively assigned to different modes of vibration by Sponer and Kirby-Smith (1941). Comparison between the vibration frequencies of chlorobenzene and bromobenzene might help us in arriving at the most probable assignments for the various observed frequencies of these two molecules. The line 998 cm^{-1} of bromobenzene corresponds to the line 1002 cm^{-1} of chlorobenzene and belongs to the mode α_{1g} as pointed out by Sponer and Kirby-Smith (1941). Evidently, the mass of the chlorine atom does not affect the frequency of vibration of this mode, because in the case of benzene the corresponding line is at 992 cm^{-1} . This may be the reason for the appearance of a strong polarised line near about 1000 cm^{-1} in the Raman spectrum of all monosubstituted benzenes. As regards the line 1019 cm^{-1} it was assigned to a mode corresponding to the mode β_{1u} (No. 12) in benzene by Sponer and Kirby-Smith (1941). In the monosubstituted benzene this mode is totally symmetric and produces a strongly polarised line. It is quite probable, however, that the halogen atom in the molecule is not displaced in such a mode so that the frequency of the mode is the same as that in benzene. Another mode exactly similar to this one but with the halogen atom moving along with the carbon atom to which it is attached can also be postulated so that the ring is distorted a little more than in the former mode. The frequency of this mode is expected to be lowered by the substituent and the line 673 cm^{-1} of bromobenzene can be assigned to this mode.

This line at 673 cm^{-1} corresponds to the line 703 cm^{-1} of chlorobenzene which was assigned to C-Cl stretching vibration by Sponer and Kirby-Smith (1941). In the case of monosubstituted benzene probably separate C-Cl stretching does not take place as the carbon atom is linked strongly to two other adjacent carbon atoms in the ring. The halogen atom, however, may oscillate against the benzene ring and this mode may correspond to No. 20a of benzene (Sponer and Kirby-Smith, 1941) in a slightly modified form. An approximate calculation

on the basis of the above assumption by using the values of the force constants obtained from substituted methane compounds shows that the intense lines 418, 312, 268 cm^{-1} of chloro-, bromo- and iodobenzene respectively can be assigned to these vibrations in monosubstituted halobenzenes. As regards the line 1073 cm^{-1} of bromobenzene, it may be pointed out that it is polarised to the same extent as the line 1019 cm^{-1} and should belong to the same or a similar mode as that of the line at 1019 cm^{-1} . The change in the relative intensities of these two lines with solidification of bromobenzene might indicate that the line 1073 cm^{-1} should belong to the same mode as that of the line 1019 cm^{-1} in a dimer, but the spectrogram due to the vapour phase of chlorobenzene shows that the corresponding pair at 1024 and 1084 cm^{-1} in chlorobenzene do not undergo any change in their relative intensities with vaporization of the substance. The line at 1084 cm^{-1} in chlorobenzene has been assigned by Sponer and Kirby-Smith (1941) to the mode ϵ_u^- of benzene given in No. 19 which has actually a frequency of near about 1500 cm^{-1} . If this frequency comes down to 1084 cm^{-1} due to the replacement of an hydrogen atom by one chlorine atom in the benzene ring, the frequency should diminish further in the case of bromobenzene. But actually, it remains almost constant in the case of all the halobenzenes. It appears, therefore, that the correct assignment of the line 1073 cm^{-1} of bromobenzene is not possible at the present stage. So it is difficult to interpret the change in intensity of the line with solidification.

In the solid state at -60°C , bromobenzene gives rise to a low-frequency line at 29 cm^{-1} and another very broad and intense band at 89 cm^{-1} . At -180°C of the solidified mass, the line at 29 cm^{-1} shifts to 34 cm^{-1} and the band at 89 cm^{-1} becomes sharp and shifts to 96 cm^{-1} . Moreover, at the lower temperature a new weak line appears at 130 cm^{-1} . The relative intensities of the first two lines practically remains unaltered at the two temperatures (Fig. 2). The crystals of chlorobenzene were found to yield five new low-frequency lines at -180°C while bromobenzene yields only three such lines at the same temperature. Assuming the crystal-structures of these two substances to be the same this difference in the number of low-frequency lines of these two compounds can be explained by attributing the origin of these lines to vibrations in associated groups of molecules formed in the solid state of these substances. The replacement of a bromine atom by one of chlorine may appreciably increase the affinity of the molecule to form intermolecular complexes and may also increase the number of new Raman lines which are believed to originate from vibrations in these groups.

(b) Anisole

From Table II, it can be seen that the weak lines 894 and 943 cm^{-1} observed in the present investigation were not reported by earlier workers. The line 556 cm^{-1} observed in the present case may correspond to the line 529 cm^{-1}

reported by some previous authors (Kohlrausch and Pongratz, 1934). The broad lines 1452 and 3068 cm^{-1} observed earlier are resolved into pairs of lines at 1446 and 1460 cm^{-1} and 3063 and 3077 cm^{-1} respectively.

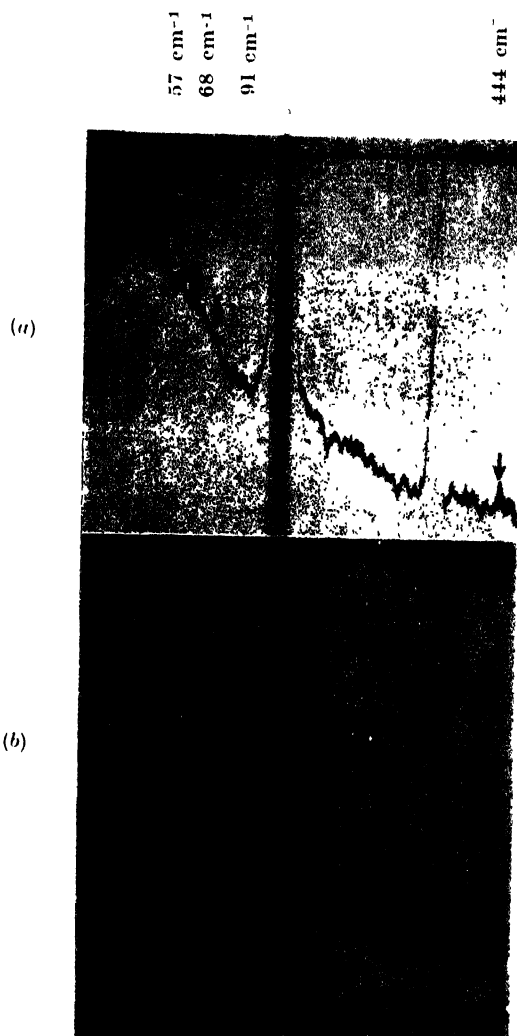


Fig. 2. Microphotometric records of the low-frequency Raman lines due to anisole.

(a) Solid at about -70°C . (b) Solid at -180°C . ($\omega_1 = 60$ $\omega_2 = 76$ $\omega_3 = 97\text{ cm}^{-1}$).

When anisole is solidified and cooled down to -70°C , the broad lines at 215 and 267 cm^{-1} both become sharp and shift respectively to 226 and 275 cm^{-1} . With lowering of temperature to -180°C , the second line further shifts to 278 cm^{-1} . These lines are probably due to deformation oscillation with the displacements at right angles to the plane of the ring. The strong line at 444 cm^{-1} which apparently remains unaltered in position at -70°C shifts slightly towards higher wave length at -180°C . In the pair of lines at 3063 and 3077 cm^{-1} the broad line at 3063 cm^{-1} becomes much sharper in the solid state while the second

line shifts to 3081 cm^{-1} and becomes broad in the solid state at low temperatures. The broadness of the line 3063 cm^{-1} may be due to the close juxtaposition of two different lines in the liquid state, one of which probably shifts towards higher wavelength and is partially superposed on the next member. In addition to the changes mentioned above, a new line at 2960 cm^{-1} due to C-H vibration is observed in the solid state both at -70°C and -180°C . All these changes in the nature, position and number of Raman lines due to C-H oscillation indicate a complicated influence of the intermolecular field on the different molecular oscillations in the solid state of the substance.

At -70°C of the solidified mass, three broad and weak lines appear in the low frequency region. On lowering the temperature to -180°C , the first line at 57 cm^{-1} shifts to 60 cm^{-1} and becomes sharp and the third line at 91 cm^{-1} shifts to 97 cm^{-1} , becomes sharp and increases in intensity (figure 3). The other

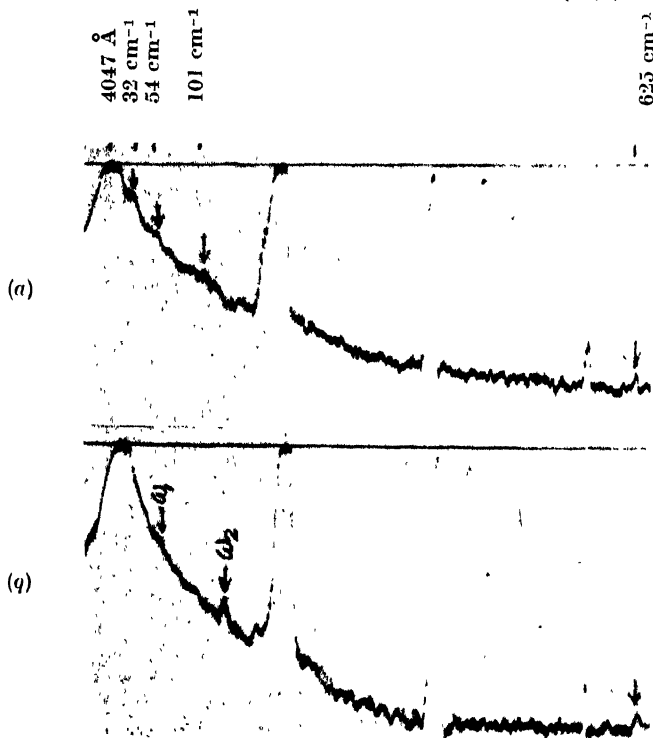


Fig. 3. Microphotometric records of the low-frequency Raman spectrum due to methyl benzoate.

(a) Solid at about -50°C . (b) Solid at -180°C . ($\omega_1=50\text{ cm}^{-1}$, $\omega_2=122\text{ cm}^{-1}$).

line at 68 cm^{-1} in the low-frequency region also shifts to 76 cm^{-1} , becomes relatively intense but unlike the other two lines remains broad even at a temperature of -180°C . The definite increase in intensity of two of these new lines in the low-frequency region in the solid state at lower temperature indicates that they cannot be attributed to rotational oscillation of the molecules in the

crystal lattice, because the amplitude of rotational oscillation is found in general, to diminish with lowering of temperature of the substance. On comparing the new low-frequency lines observed in this case with those due to bromobenzene it is found that the mass of the substituent group has great influence on the frequencies of these lines. Such a comparison of the new lines due to chlorobenzene (Ray, 1950) and bromobenzene shows that the chemical affinity of the substituent atom has great influence not only on the frequencies of the new lines but also on the number of these lines. Hence it has to be concluded that the benzene ring alone does not take part in oscillations giving rise to these lines. Ray (1952) pointed out that two lines at 48 and 86 cm^{-1} respectively are common in the spectra of five substituted benzenes with slight variation in the frequencies, but these two lines are absent in the spectra due to bromobenzene and anisole. The low-frequency of one of the lines in the case of bromobenzene may indicate that the whole molecules execute translation oscillation against each other. In anisole the whole molecule cannot move against its neighbour owing to the presence of the $\text{O}-\text{CH}_3$ linkage and there is no line of frequency below 60 cm^{-1} .

(c) *Methyl benzoate*

It is found from Table III that methyl benzoate in the liquid state yields a few more extra weak lines not reported earlier (Hariharan, 1954). These lines are at 942, 998, 1378 and 1546 cm^{-1} . The broad line at 1444 cm^{-1} observed by earlier workers is resolved into two distinct lines at 1434 and 1458 cm^{-1} in the present investigation. When the liquid is solidified and cooled down to -50°C remarkable changes are observed in the positions and intensities of some of the lines and a few of these lines undergo further changes with the lowering of temperature to -180°C . The strong line 216 cm^{-1} seems to disappear with solidification of the liquid. This line is totally depolarised and may be due to a deformation oscillation involving displacements of the parts of the substituents group at right angles to the plane of the benzene ring. In the solid state such displacements are restricted. The broad and weak line 134 cm^{-1} shifts to 144 cm^{-1} with solidification. When the temperature of the solid mass is lowered to -180°C , a very weak but sharp line at 142 cm^{-1} is observed in place of this band. This band may also be due to a mode corresponding to deformation of the whole molecule. The line 1162 cm^{-1} seems to be weakened by the change of state and at -180°C this line is hardly visible. This line is due to C-H deformation oscillation and probably the hydrogen bonding between neighbouring molecules may be responsible for this change of intensity.

Three new lines at 32, 54 and 101 cm^{-1} appear with solidification of the substance but when the temperature is lowered to -180°C these are replaced by only two strong lines at 50 and 122 cm^{-1} respectively (figure 3). The latter line may correspond to the line 134 cm^{-1} mentioned above due to similar vibra-

tions in associated groups of molecules the presence of which in the solid state is indicated by the diminution in intensity of the line 1162 cm^{-1} .

(d) *Ethyl benzoate*

It is found from Table IV that two extra weak lines at 954 and 1548 cm^{-1} are observed in the present investigation. The line at 377 cm^{-1} reported by previous workers has not, however, been detected in the present case. When the liquid is solidified and cooled down to different low temperatures, the broad and intense line at 187 cm^{-1} is found to undergo a diminution in intensity. This line of ethyl benzoate may correspond to the 216 cm^{-1} line of the methyl ester as the changes observed in the lines with solidification of the substances are the same.

In the solid state at -70°C , two weak lines appear at 76 and 91 cm^{-1} respectively, and when the mass is further cooled down to -180°C , only one weak line at 96 cm^{-1} can be observed.

We can obtain a satisfactory explanation about the origin of low-frequency lines in the solid state of these substances when the present results on the low-frequency Raman spectrum of the two phenyl esters are correlated with those of the ultraviolet absorption spectra of these substances obtained earlier (Deb, 1951, 1953). On solidification and cooling down the solidified mass to -180°C , the absorption bands of methyl benzoate shift towards longer wavelength by about 400 cm^{-1} while under similar changes in phase and in temperature, no change is observed in the absorption band of ethyl benzoate. The shift of the absorption band with solidification of methyl benzoate can be attributed to the formation of virtual bonds amongst the molecules of the substance in the solid state mentioned in a previous section. In the case of the ethyl benzoate, it is quite likely that in a large number of molecules the long chain-like structure are attached to the benzene ring through one or more of the six π -electrons and are thus prevented from forming regular intermolecular linkages when the molecules are closely packed in the solid state. This is further corroborated by the fact that no change in the line due to C-H oscillation is observed with solidification of ethyl benzoate while in the case of methyl benzoate the diminution in the intensity of the line 1162 cm^{-1} indicates the formation of hydrogen bonds. It thus appears that unless virtual intermolecular bonds are formed the free molecules in the lattice cannot give rise to strong lines in the low-frequency region and the absence of any strong line in the low-frequency region in the Raman spectrum of solidified ethyl benzoate at -180°C furnishes a strong evidence in support of the above conclusion.

2. *Fluorescence Spectra* :

Bromobenzene and methyl benzoate produce two broad fluorescence bands in the visible region when the substances are solidified and cooled down to -180°C . The approximate positions and the intervals between two successive bands in either of these two compounds along with the visually estimated relative intensities of the bands are given in Table V below.

TABLE I

Bromobenzene, C_6H_5Br

$\Delta\bar{\nu}$ in cm^{-1}

Liquid		Solid (Present author)	
Magat (1936)	Present author	At about $-60^\circ C$	At $-180^\circ C$
		29 (2) k	34 (3) e,k
		89 (4b) o, +k	96 (5) e,k
			130 (1) e,k
184 (8b) D	182 (7b) ± e	193 (1) e	198 (2) e
(230 P)	245 (2) ± e,k		
255 (1b) P			
316 (10) P	312 (9) ± o,k,i	315 (4) o,k	315 (5) e,k
353 (1b)	356 (0) e		
	461 (0) e		
611 (3) D	614 (3) e,k	614 (0) o,k	614 (0) e,k
673 (5) P	673 (5) o,k	673 (2) e,k	673 (3) e,k
736 (1)	742 (0) e		
795 (0)			
829 (1)	835 (0) e		
	894 (0) e		
	949 (0) e		
1002 (10) P	998 (12) e,k,i	998 (5) e,k	998 (6) e,k
1023 (5) P	1019 (6) e,k,i	1019 (2) o,k	1019 (2) e,k
1072 (4) P	1073 (5) e,k,i	1073 (2) o,k	1073 (3) o,k
1158 (3) D	1158 (3) e,k	1158 (1) e	1158 (1) e
1182 (2) P	1172 (2) e,k	1172 (0) e	1172 (0) e
1274 (0)			
1301 (1)			
1322 (0)	1323 (1) e		
1442 (1)	1443 (1) e		
1477 (1)	1473 (2b) e	1473 (1b) e	1476 (1b) e
1580 (5b) D	1573 (6b) e,k	1573 (3) e,k	1573 (4) e,k
1614 (0)			
1667 (0)			
2293 (0)			
2333 (0)			
3004 (0)			
3063 (10) P	3061 (7b) e,k,i	3061 ^r (4b) e,k	3061 (5b) e,k
		3090 (1) k	3090 (1) k
3153 (1)	3150 (2b) e,k	3150 (1) k	3150 (1) k
3203 (0)			

TABLE II

Anisole, $C_6H_5OCH_3$ $\Delta\nu$ in cm^{-1}

Liquid		Solid (Present author)	
Kohlrausch & Pongratz (1934)*	Present author	At about $-70^\circ C$	At $-180^\circ C$
		57 (1b) k	60 (1) k
		68 (0b) k	76 (2b) e,k
		91 (1b) k	97 (4) e,k
210 (4) D	215 (4b) e	226 (0) e	226 (1) e,k
264 (4) D	267 (4b) e,k	275 (0) e,k	278 (1) e,k
441 (5) P	444 (6) \pm e,k	444 (1) e,k	447 (2) e,k
505 (1)	511 (2) e,k		
529 (2)			
	556 (3) e,k		556 (0) e
580 (0)			
612 (4) D	617 (5) e,k	617 (0) e,k	617 (1) e,k
755 (2)	760 (3) e,k		
783 (10) P	787 (11) e,k,i	787 (3) e,k	787 (4) e,k
816 (1)	822 (2) e,k		
	894 (0b) e		
	943 (1) e		
991 (12) P	994 (15) e,k,i	994 (5) e,k	994 (6) e,k
1020 (4) P	1025 (5) e,k	1025 (1) e,k	1025 (1) e,k
1033 (3)	1039 (4) e,k	1039 (1) e,k	1039 (2) e,k
1072 (0) P	1068 (1) k		
1150 (2) D	1156 (3) e,k	1156 (1) e,k	1156 (1) e,k
1177 (5) P	1177 (3) e,k	1177 (1) e,k	1177 (1) e,k
1244 (5) P	1249 (4) e,k	1249 (1) e,k	1245 (2) e,k
1299 (5) P	1302 (2) k	1302 (1) k	1302 (1) k
	1446 (2b) e,k		
1452 (4b) D			
	1460 (2) e,k		
1587 (3) D	1589 (3) e,k	1589 (1) e	1589 (1) e
1603 (6) D	1602 (6) e,k	1602 (1) e,k	1602 (2) e,k
2836 (5)	2841 (4) e,k	2841 (1) k	2841 (2) k
2942 (4)	2945 (3b) e,k	2945 (1) k	2945 (1) k
		2960 (1) k	2960 (1) k
3007 (2)	3014 (3) e,k	3014 (1) k	3014 (1) k
	3063 (8b) e,k	3063 (2) e,k	3063 (3) e,k
3068 (9b) P	3077 (9) e,k,i	3081 (3b) e,k	3081 (4b) e,k,i

The polarisation data are taken from Magat Table (1936).

TABLE III

Methyl benzoate ; $C_6H_5COOCH_3$ $\Delta\bar{\nu}$ in cm^{-1} .

Liquid		Solid (Present author)	
Hariharan (1954)	Present author	At about $-50^\circ C$	At $-180^\circ C$
		32 (3) e,k	
		54 (1) e,k	50 (3) e,k
		101 (1b) e,k	122 (4) e,k
140 (2)	134 (3b) e,k D	144 (1b) o,k	142 (0) e k
			156 (1) e,k
171 (1)	173 (1) e		
212 (6)	216 (5b) \perp e D		
361 (6)	360 (5) \perp e,k P	364 (2) e,k	364 (2) e,k
623 (7)	622 (7) e,k D	625 (2) e,k	625 (2) e,k
678 (2)	680 (2) e,k P		
810 (1)	808 (1) o,k		
826 (8)	826 (8) e,k P	831 (3) e,k	831 (3) e,k
850 (0)	851 (0) e		
	942 (0) e		
967 (2)	969 (1) e,k		
	998 (1) e,k		
1003 (12)	1003 (12) \perp e,k,i P	1003 (5) e,k	1003 (5) e,k
1024 (5)	1028 (4) e,k P	1028 (1) e,k	1028 (1) e,k
1111 (4)	1112 (4) e,k P	1115 (1b) e,k	1115 (1) e,k
1158 (4)	1162 (4) e,k D	1162 (0b) e,k	1164 (0) e,k
1178 (4)	1173 (2) k P	1173 (1b) e,k	1173 (1b) e,k
1276 (8)	1277 (8) e,k P	1277 (3b) e,k	1277 (3) e,k
1311 (2)	1315 (3) k P		1315 (0) e,k
	1378 (1) e,k		
1444 (3b)	1434 (3) e,k P		
	1458 (3) e,k D?		
1490 (2)	1494 (1) e,k		
	1546 (1) e		
1604 (12)	1601 (12) e,k D	1601 (5) e,k	1601 (5) e,k
1722 (8)	1723 (10) e P	1723 (4) e	1723 (4) e
2844 (2)	2852 (1b) e,k	2852 (1) e,k	2852 (1) k
2952 (3)	2951 (3b) e,k,i P	2951 (2) e,k	2951 (3) k
		2991 (0) k	2991 (1) k
3075 (6)	3076 (6b) e,k,i P	3076 (5) e,k,i	3076 (5) e,k,i

TABLE IV

Ethyl Benzoate, $C_6H_5COOC_2H_5$ $\Delta\nu$ in cm^{-1} .

Liquid		Solid (Present author)	
Hariharan (1954)	Present author	At about $-70^\circ C$	At $-180^\circ C$
		76 (1) k	
		91 (2) e,k	96 (1)
187 (6)	187 (5b) $\frac{1}{2}$ e D	187 (0) e	
326 (5)	333 (5) e,k P	333 (1) e,k	333 (0) e,k
377 (1)			
397 (1)	399 (1b) e		
432 (0)	439 (0) e		
493 (1)	508 (0b) e		
556 (0)	566 (0) e		
613 (6)	622 (7) e,k D	622 (2) e,k	622 (2) e,k
672 (3)	675 (2) e,k P		
785 (3)	787 (2) e,k		
808 (3)	807 (2) e,k		
850 (5)	851 (6) e,k P	855 (3) e,k	855 (2) e,k
862 (1)	875 (0) e		
	954 (0) e		
1000 (12)	1005 (12) e,k,i P	1005 (6) e,k	1005 (5) e,k
1024 (3)	1028 (3) e,k P	1028 (0) e,k	1028 (0) e,k
1108 (4)	1105 (4) e,k P	1110 (1) e,k	1110 (1) e,k
1160 (2)	1162 (4) e,k D	1162 (1) e,k	1162 (1) e,k
1177 (2)	1179 (1) k		
1276 (6)	1271 (7) e,k P	1271 (2b) e,k	1271 (2b) e,k
1304 (4)	1315 (2) k		
1370 (2)	1369 (2) e,k P		
1393 (2)	1397 (1) e,k		
1453 (4)	1455 (3) e,k D	1455 (0) e,k	1455 (0) e,k
1492 (2)	1490 (1) e,k		
	1548 (1) e		
1599 (15)	1601 (12) e,k D	1601 (6) e,k	1601 (5) e,k
1718 (10)	1719 (9) e P	1719 (5) e	1719 (4) e
2933 (3)	2941 (3) e,k	2941 (1b) k	2941 (1b) k
2980 (3)	2984 (4b) e,k P	2984 (1b) k	2984 (1b) k
3071 (6)	3071 (7b) e,k,i P	3074 (4b) e,k	3074 (4b) e,k

TABLE V

Fluorescence Spectra

Compound (solid at -180°C)	No. of bands	1st band		2nd band		Interval in cm^{-1}
		Position in cm^{-1}	Inten- sity	Position in cm^{-1}	Inten- sity	
Bromobenzene	2	22940	2	21350	1	1590
Methyl benzoate	2	22340	2	20745	1	1595

As in the previous cases of the substituted toluenes (Biswas, 1954 : 1955) the interval between successive fluorescence bands is about 1590 cm^{-1} in the case of both bromobenzene and methyl benzoate. This frequency difference is equal to the frequency of C—C oscillation in the benzene ring, and it is believed that the fluorescence in these aromatic compounds is due to distortion in the ring itself in the solid state, because in the liquid state these substances do not show any trace of fluorescence.

ACKNOWLEDGMENT

The author is indebted to Professor S. C. Sirkar, D.Sc., F.N.I. for his kind help and guidance throughout the progress of this work.

REFERENCES

- Biswas, D. C., 1954a, *Ind. J. Phys.*, **28**, 85.
- Biswas, D. C., 1954b, *Ind. J. Phys.*, **28**, 303.
- Biswas, D. C., 1954c, *Ind. J. Phys.*, **28**, 423.
- Biswas, D. C., 1955, *Ind. J. Phys.*, **29**, 257.
- Deb, A. R., 1951, *Ind. J. Phys.*, **25**, 433.
- Deb, A. R., 1953, *Ind. J. Phys.*, **27**, 183.
- Hariharan, T. A., 1954, *Jour. Ind. Inst. Sci.*, **36**, 189.
- Kohlrausch, K. W. F., and Pongratz, A., 1934, *Wiener Ber. Kl. IIb.*, **143**, 358.
- Magat, M., 1936, *Annual Tables of Constants and Numerical data*, p. 26-76.
- Mazumder, M. M., 1953, *Ind. J. Phys.*, **27**, 406.
- Ray, A. K., 1950, *Ind. J. Phys.*, **24**, 111.
- Ray, A. K., 1951, *Ind. J. Phys.*, **25**, 131.
- Ray, A. K., 1952, *Ind. J. Phys.*, **26**, 225.
- Sirkar, S. C., and Swamy, H. N., 1952, *J. Chem. Phys.*, **20**, 1177.
- Sponer, H. and Kirby-Smith, J. S., 1941, *J. Chem. Phys.*, **9**, 667.
- Swamy, H. N., 1952, *Ind. J. Phys.*, **26**, 119.
- Swamy, H. N., 1953, *Ind. J. Phys.*, **27**, 55.

A METHOD OF DETERMINING THE RELATIVE AMOUNTS OF D- AND E-REGION ABSORPTIONS OF MEDIUM AND SHORT RADIO WAVES

By A. P. MITRA

RADIO RESEARCH COMMITTEE, N.P.L. BLDGS. NEW DELHI-12

(Received for publication, August 30, 1955)

ABSTRACT. A new method is developed by which the relative amounts of D and E-region absorptions in any medium and short wave observation may be determined purely on physical basis. The method utilizes the concept of 'relaxation time' in ionospheric levels and rests on the fact that the 'relaxation time' at the D-region levels is appreciably different from that at the E-region levels.

1. INTRODUCTION

One of the most difficult problems in the interpretation of absorption of medium and short waves is to determine how much of the measured absorption is due to the D-region and how much due to the E-region. In perhaps the most carefully conducted series of experiments on absorption, Appleton and Piggott (1954) took particular care to use frequencies at which $P'f$ curve did not show any appreciable group retardation. Although the resultant absorption showed little scatter when plotted against the square of the effective frequency, some absorption may yet have remained. In measurements where no particular care is taken to eliminate the E-absorption, the question is still more important. The purpose of this note is to present a method by which the relative amounts of D and E-region absorptions of medium and short radio waves may be determined.

2. DEVELOPMENT OF THE METHOD

In any effort to separate the two contributions, one must concentrate on the physical parameters that are different in two regions and that are easy to measure. One such parameter is what is sometimes known as the 'sluggishness' of the ionosphere, which arises due to the finite recombination time in the ionization at the relevant level. This sluggishness may be measured by the delay in the time of the maximum of the ionization at any level from the time of the local noon. This delay is also known as the 'relaxation time'. Now the relaxation time $\tau(h)$ at any height h is given by (Mitra and Jones, 1953; Appleton, 1953).

$$\tau(h) \approx \frac{1}{2\alpha(h)N(h)}$$

where $\alpha(h)$ and $N(h)$ are the values of the effective recombination coefficient at any height h . Since α and N are different at D- and E-region levels, τ_D will be

different from τ_E . That this is so, has been confirmed by the results of analysis of various radio propagation data made by a number of authors. Thus, analysis of the day time observations on absorption and polarization of 150Kc/s radio waves, which must refer to the D-region only, has yielded a value of about 60 minutes (Mitra and Jones, 1954). On the other hand, analysis of the diurnal variation of E in Washington, yielded a relaxation time of about 4 minutes. This very large difference in the values of τ_D and τ_E provides a sensitive method for determining the relative amounts of D and E absorptions in any measurement where both absorptions exist.

If one ignores the delay in the maximum of the ionization, the diurnal variations of the D- and E-region absorptions, denoted by A_D and A_E respectively, may be written as:

$$A_D = A_{D_0} \cos^n \chi$$

$$A_E = A_{E_0} \cos^p \chi$$

where the zero suffixes indicate corresponding values for $\chi = 0^\circ$, and n and p are constants. In terms of hour angle ϕ , these equations become:

$$A_{D_0} = A_D [\sin \delta \cos \theta + \cos \delta \sin \theta \cos \phi]^n$$

$$A_{E_0} = A_E [\sin \delta \cos \theta + \cos \delta \sin \theta \cos \phi]^p$$

where δ is the declination of the sun and θ is the colatitude of the station.

The corresponding equations, when the maximum is delayed, are:

$$A_D = A_{D_0} [\sin \delta \cos \theta + \cos \delta \sin \theta \cos (\phi - \phi_1)]^n$$

$$A_E = A_{E_0} [\sin \delta \cos \theta + \cos \delta \sin \theta \cos (\phi - \phi_2)]^p$$

where ϕ_1 and ϕ_2 are the values of the hour angles at which A_D and A_E attain their maximum values.

The resultant absorption ($A_D + A_E$) will then attain its maximum at a time $\bar{\phi}$ given by

$$\bar{\phi} \simeq \frac{n \bar{A}_D \phi_1 + p \bar{A}_E \phi_2}{n \bar{A}_D + p \bar{A}_E}$$

provided the ϕ 's are small or, when expressed in relaxation times,

$$\bar{\tau} \simeq \frac{n \bar{A}_D \tau_D + p \bar{A}_E \tau_E}{n \bar{A}_D + p \bar{A}_E} \quad \dots (1)$$

where \bar{A}_D and \bar{A}_E denote the values of A_D and A_E at the time of maximum resultant absorption. Eqn. (1) which may also be written as

$$\frac{p \bar{A}_E}{n \bar{A}_D} \simeq \frac{\tau_D - \bar{\tau}}{\bar{\tau} - \tau_E}$$

gives the necessary mathematical expression for determining the relative amounts of D- and E-region absorption of medium and short waves. The diurnal variation of the measured absorption provides the value of τ . Then if τ_D and τ_E are known then $(p\bar{A}_E/n\bar{A}_D)$ which is (p/n) times the ratio of the E- and D-region absorption values, may be computed.

Probable values of τ_D and τ_E have already been mentioned. Of these τ_E is perhaps better known than τ_D . The value of the former is small, of the order of 4 minutes, and shows little latitudinal variation. Eclipse observations on *foE* also indicate a relaxation time of this order. Further, one may compute τ_E from the value of α_E obtained otherwise and from the E-region electron density. Since α_E is of the order of 10^{-8} cm³/sec., and $N_E \sim 10^5$ /cm³, the value of τ_E thus computed comes to about 8 minutes. A typical value of τ_E will be about 5 minutes.

Values of τ_D have been reported in a paper by Mitra and Jones (1953). Measurements on absorption at 150Kc/s by Benner (1951) showed a relaxation time of 60 minutes and those of polarisation at the same frequency by Nearhoof (1951) gave 80 minutes. Detailed examination of the variation of the equivalent height of reflexion at 50Kc/s, original records of which were kindly supplied to the author by Dr. Watts of the National Bureau of Standards, showed a relaxation time of about 60 minutes for an equivalent height around 85 Km. It seems reasonable to conclude that τ_D is not much different from 60 minutes.

The values of p and n are uncertain, but some idea may be formed from theoretical arguments as also from various experimental determination of the $\cos \chi$ -exponents, obtained from absorption measurements. At 150Kc/s for which the day time absorption is due predominantly to the D-region, the exponent has a value of 0.62 in the morning and 0.42 in the afternoon (Benner, 1951). At higher frequencies the values are larger. The average value given by Appleton and Piggott (1954) for medium radio waves is 0.75, but values ranging anywhere between 0.5 and 1.5 have been reported. Critical examination of these various results appears to indicate that the larger values are almost always associated with increased contamination by the E-region absorption, and, in the extreme case, where the E-region absorption predominates, the exponent has a value around 1.5. It appears, therefore, that the value of n is somewhere around 0.6 and that of p around 1.5.

Theoretical arguments also give similar values. At the levels which contribute most to the D-region absorption (~ 80 Km.) the collision frequency is fairly large, having a value of about 5×10^6 /s. For a Chapman-type electron distribution of the D-region, the theoretical value of n would then be about 1.1, while for the (more realistic) case where recombination coefficient varies directly with pressure, the value would be about 0.65 (Appleton and Piggott, 1954). A. P. Mitra (1954) has recently given a theoretical model for the D-region electron

distribution which appears to fit with both long wave and short wave experimental results. This model has since been revised in the light of SID observations (Mitra, unpublished). The value of the exponent n for the revised model comes out to be 0.62.

In view of the above, it seems reasonable to accept a ratio of about 2.5 for (p/n) with a probable range between 2 to 3.

In the measurements of Appleton and Piggot, the observed relaxation time was about 30 minutes. For the values given above, such a relaxation time would indicate an E-region contribution of between 1/3 to 1/2 of the D-region absorption for the relevant measurements.

It may also be mentioned that the exponent K should provide an additional confirmation of the value of the ratio determined by the above method, since K is given by

$$K = \frac{n\bar{A}_D + p\bar{A}_E}{\bar{A}_D + \bar{A}_E}.$$

For $n = 0.6$, $p = 1.5$, $k = 0.75$, \bar{A}_E/\bar{A}_D is about 1/5.

In conclusion, it may be pointed that Eq. (1) should also be useful in studying the location of the fadeout absorption, and, in general, wherever two or more regions having different relaxation times are involved.

REFERENCES

- Appleton, E. V. and Piggot, W. R., 1954, *J. Atmosph. Terr. Phys.* 14, 5, 1.
 Appleton, E. V., 1953, *J. Atmosph. Terr. Phys.*, 3, 282.
 Benner, A. H., 1951, *Proc. Inst. Rad. Eng.*, 39, 186.
 Mitra, A. P. and Jones, R. E., 1953, Scientific Report No. 44, Ionosphere Research Laboratory, Pennsylvania State University, March 25; *J. Atmosph. Terr. Phys.*, 4, 141.
 Mitra, A. P. 1954, *J. Atmosph. Terr. Phys.*, 5, 28.
 Nearhoof, H. J., 1951, Technical Report No. 25, Ionosphere Research Laboratory, Pennsylvania State University, August, 20.

A "NULL" METHOD OF MEASURING SURFACE TENSION, WITH A TORSION BALANCE.

BY S. VENKATARAMAN

PHYSICS LABORATORY, NIZAM COLLEGE, HYDERABAD-DN.

(Received for publication, June 7, 1955; received after revision, August 26, 1955)

ABSTRACT. This paper describes a "null" method for the determination of the surface tension of a liquid by the use of a torsion balance. An expression is deduced for the surface tension of a liquid, when the pull due to the surface tension acting along the perimeter of a thin glass plate (usually a microscopic cover glass slip) is balanced by the upthrust of the liquid on the partially immersed plate. The results obtained with a few liquids are reported and they agree with the values recorded in the International Critical Tables. This method yields more consistent results than any of the routine methods usually used for the measurement of surface tension.

INTRODUCTION

The method of finding the surface tension of a liquid or the surface tension at the interface of two liquids, from the force necessary to detach a thin glass plate or a horizontal ring from the surface of a liquid or the interface of two liquids is well-known and du Nouy's tensiometer (1919) and Searle's torsion balance (1934) are devices for rapid determination of the force of detachment. Recently Meier (1949) has described a "null" method for the determination of the surface tension of water using a torsion balance. In this method, the upthrust of water on a fine vertical wire immersed in it is balanced by the downward pull due to surface tension round the perimeter of the wire. He used a nichrome wire of diameter 0.0599 cm. and the pull due to surface tension along the perimeter of such a wire should be about 12 dynes for water and for most other liquids with angles of contact zero or nearly so, it should be considerably less. Although by attention to details in the construction of a torsion balance, an instrument sensitive enough to detect a pull of 0.1 dyne could be made, it would be extremely difficult to work with due to the disturbing effects of draughts and even one's breath. Curiously enough, Meier has not attempted to measure the surface tension of any liquid other than water.

The author using a torsion balance giving a deflection of 5 mm. for a pull of 0.01 gm. and thin rectangular microscopic cover glass slips and slides of various sizes, has been able to determine the surface tension of a number of liquids. The pull due to the surface tension was anything between 100 to 300 dynes depending on the liquid. Values of the surface tension of the same liquid at the same temperature in different trials, agreed to within 0.1% and their agreement with the accepted values is also quite close. Use of an external manometer to estimate the depth of immersion of the glass plate has enabled the surface tension to be determined *without any knowledge of the density of the liquid*.

EXPERIMENTAL

For this work, the sensitiveness of an ordinary Searle's type torsion balance which gives a deflection of about 2.5 mm. for a load of 0.1 gm. is insufficient and hence it was improved by replacing the torsion wire by one of steel, S.W.G. No. 30, and the torsion arm by a long thin strip of bamboo or aluminium. The length of the strip was 15" and the notch from which the glass plate was hung, was 12" from the torsion wire (figure 1). A stout piece of copper wire attached

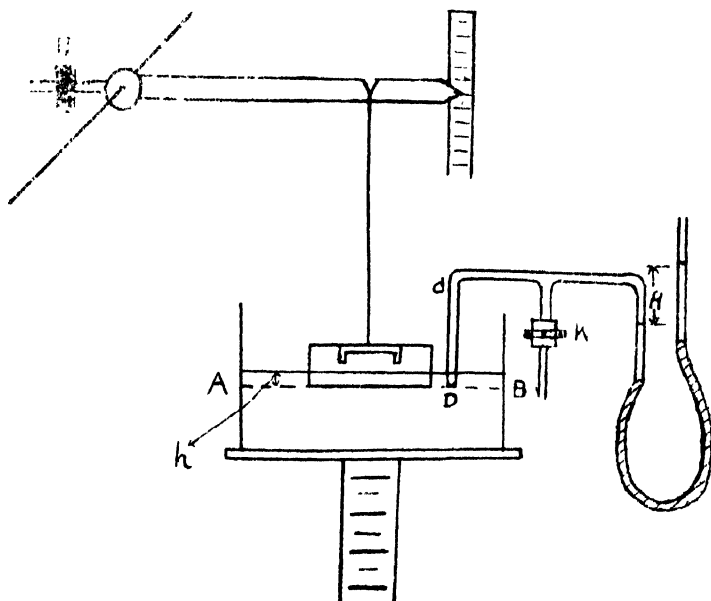


Fig. 1

to the brass screw stem carrying the torsion arm serves the same purpose as the 'gravity bob' of a sensitive chemical balance. It enables the sensitivity of the torsion balance to be increased or decreased when bent slightly up or down so as to raise or lower the C.G. of the arm. The nut *N* working in the screw stem, enables the torsion arm to be made horizontal. By suitable manipulation of

the thick copper wire, the end of the torsion arm is made to give a deflection of 5 mm. for a load of 10 mgm. at the notch. One-tenth of a scale division can be estimated by the use of a magnifying glass and so a pull of 0.2 dynes could be easily measured by the balance. The balance could, of course, be made more sensitive, but it would be difficult to work with, due to the disturbing effects of draughts.

Briefly, the method employed to determine the surface tension of a liquid is this: The liquid is contained in a wide glass crystallising dish (diameter more than 10 cm.), resting on a platform that can be raised or lowered. The torsion arm is made horizontal by working on the nut *N*. The dish is raised slowly till the bottom of the thin glass plate hanging from the notch of the torsion arm just comes in contact with the surface *AB* of the liquid and is pulled in. (The glass plate which is held by a brass clip, can be easily tilted in its holder to make its lower edge parallel to its image in the liquid). The wide vertical tube *CD* (diameter 1 cm.), connected to the manometer, is adjusted to bring its end *D*, ground flat, just in contact with the liquid surface. The clip *K* is closed and the open end of the manometer is raised or lowered to bring the meniscus in *CD* to the level of the liquid outside. The manometer is read by means of a cathetometer reading to 0.005 cm. Next, either by addition of more liquid into the dish or by raising the platform on which the dish rests and *without disturbing CD*, the torsion arm is restored back to its initial position of horizontality. The manometer is adjusted to lower the meniscus in *CD* to the end *D*, that is to say, to the original level of the liquid in the dish. The manometer is again read and the difference in its two readings gives the change of pressure at the original liquid surface *AB* due to the addition of liquid into the dish to restore horizontality of the torsion arm. Hence we have.

$$\gamma.2(l+t) = l t.h. \rho.g = l t.H.d.g$$

$$\therefore \gamma = l t.H.d.g/2(l+t)$$

where γ is the surface tension of the liquid, l and t length and thickness of the glass plate, ρ the density of the liquid in the dish, d the density of the manometric liquid (usually water), h the depth of immersion of the glass plate and H , the difference in the two readings of the manometer. Or, writing a for lt and p for $2(l+t)$, we have

$$\gamma = a.H.d.g/p$$

an expression free from ρ (density of the liquid) and h (depth of immersion of the plate).

RESULTS

Using this expression, the surface tensions of a few liquids were determined with glass plates of different dimensions. Chemically pure liquids from freshly

TABLE I

Liquid in the manometer is water (Density at 30°C = 0.996 gm/cc.) $\gamma' = 978$ cm/sec².

Liquid	Plate 1			Plate 2			Plate 3			γ_{30}° (From I. C. T.) Dynes/cm.
	l	t	H	l	t	H	l	t	a	
	2.600 cm.	$t = 0.098$ cm.		7.55 cm.	$t = 0.146$ cm.		2.55 cm.	$t = 0.146$ cm.		
	$p = 5.396$..	$a = 0.2548$ cm ²		$p = 15.392$..	$a = 1.103$ cm ²		$p = 5.392$..	$a = 0.3723$ cm ²		
	H (cm.)	$\gamma_{30}^{\circ} \pm 1^{\circ}\text{C}$ (Dynes/cm.)		H (cm.)	$\gamma_{30}^{\circ} \pm 1^{\circ}\text{C}$ (dynes/cm.)		H (cm.)	$\gamma_{30}^{\circ} \pm 1^{\circ}\text{C}$ (dynes/cm.)		
Water	1.550	71.29		1.02	71.17		1.06	71.29		71.18 \pm 0.05

TABLE II

Liquid in the manometer is water (Density at 30°C = 0.996 gm/cc.) $\gamma' = 978$ cm/sec².

Liquid	Plate 1			Plate 2			Plate 3			γ (From I. C. T.) (dynes/cm.)
	l	t	H	l	t	H	l	t	a	
	2.600 cm.	$t = 0.098$ cm.		2.17 cm.	$t = 0.025$ cm.		2.890 cm.	$t = 0.010$ cm.		
	$p = 5.396$..	$a = 0.2548$ cm ²		$p = 4.39$..	$a = 0.0543$ cm ²		$p = 5.86$..	$a = 0.0289$ cm ²		
	H (cm.)	$\gamma_{30}^{\circ} \pm 1^{\circ}\text{C}$ (dynes/cm.)		H (cm.)	$\gamma_{30}^{\circ} \pm 1^{\circ}\text{C}$ (dynes/cm.)		H (cm.)	$\gamma_{30}^{\circ} \pm 1^{\circ}\text{C}$ (dynes/cm.)		
Water	1.550	71.29								71.18 \pm 0.05
Benzene	0.600	27.63		2.310	27.68		5.685	27.60		27.56 - 0.05
Carbon Tetrachloride	0.575	26.53		2.205	26.55		5.460	26.51		26.53 0.1
Toluene	0.595	27.39		2.270	27.32		6.625	27.36		27.30 0.1
Chloroform	0.565	26.01		2.160	26.00		5.360	26.02		27.24 6.1(a_{20})
Carbon disulphide	0.675	31.09		2.580	31.06		6.390	31.03		32.23 (a_{20})
Olive oil	0.715	32.93		2.740	32.98					..

opened bottles were used. The water used was distilled immediately before use and particular care was taken to avoid contamination by grease. The results are recorded in Tables I and II.

Writing the expression for the surface tension in the form

$$p/a = (d.g/\gamma).H$$

we notice that the graph of p/a (for different plates) against H , should be a straight line; and this is indeed the case (figure 2).

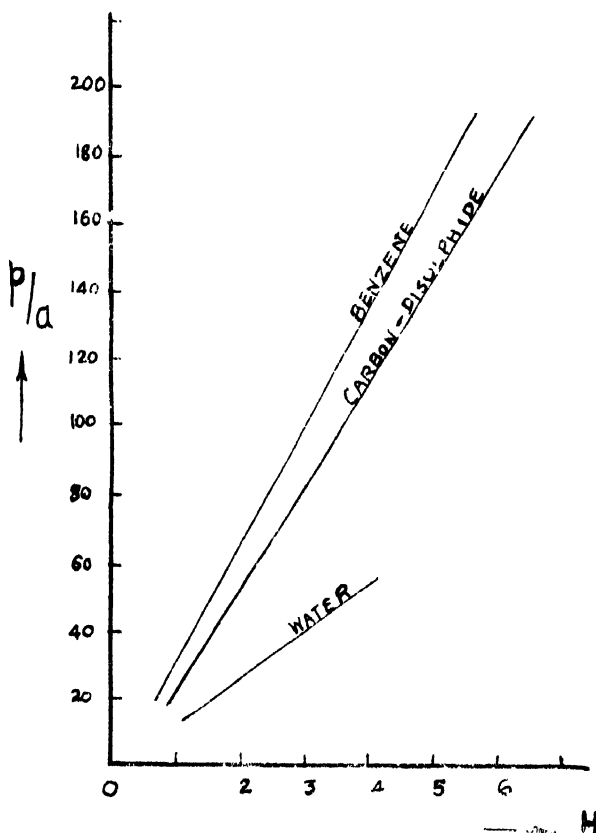


Fig. 2

It is proposed to extend this method to the determination of the surface tension at the interface of two immiscible liquids and the results obtained will be communicated later.

REFERENCES

- du Nouy, P. L., 1919, *Jour. Gen. Physiol.*, **1**, 521.
 Meier, F. A., 1949, *School Science Review*, **30**, 112.
 Searle, G. F. C., 1934, *Experimental Physics* (Cam. Univ. Press).

THE DEPENDENCE OF THE COMPOSITE MEAN LIFE OF MU-MESONS ON THE ATOMIC NUMBER OF THE ABSORBER

By N. N. BISWAS

BOSE INSTITUTE, CALCUTTA-9

(Received for publication, July, 18, 1955)

ABSTRACT. The measurements of the mean life of the composite beam of μ -mesons (both positive and negative) at sea level in the absorbers of C, Al, S and Pb have been reported previously. The same experiment has been conducted with water and NaF absorbers. In water (only oxygen is effective, since a hydrogen atom rarely captures a μ -meson), the composite mean life is found to be 1.95 ± 0.08 micro-seconds. Choosing the thickness of water absorber to be equivalent to the sulphur absorber in respect to the stopping power of the μ -mesons, the decay curve of the positives in S has been taken to represent the same in water and hence by subtraction, the mean life of the negative μ -mesons in water has been determined to be equal to 1.80 ± 0.19 microseconds. In the case of NaF ($Z_{eff} = 10.1$) absorber, the experimental points have been found to represent a composite decay curve giving the mean life equal to 1.82 ± 0.09 microseconds.

The Z dependence of the composite mean life has been found to fit an empirical relation,

$$\tau_{\pm} = 2.50 - 0.065 Z \text{ microseconds.}$$

in the interval $Z=6$ to $Z=16$.

INTRODUCTION

The mean life of the positive μ mesons is the same in all absorbers, but that of the negatives is dependent on the absorbing element. From the K -orbit, negative mesons can either be captured by the atomic nucleus or disintegrate spontaneously. Their decay constant should, therefore, be $\lambda + \Lambda$, where $\lambda = 1/\tau_+$, τ_+ being the mean life of free decay and Λ the probability per second for capture. The decay electrons arising from the decay of negative muons should follow a dis-integration curve with the decay constant $\lambda + \Lambda$. Hence one can write

$$N_{(t)}^- = n_{(0)}^- \exp[-(\lambda + \Lambda)t] \quad \dots (1)$$

where $n_{(0)}^-$ and $N_{(t)}^-$ are the number of negative mesons disintegrating between $t=0$ to $t=\infty$ and $t=t$ to $t=\infty$ respectively: Now, $n_{(0)}^- = \frac{\lambda}{\lambda + \Lambda} N_{(0)}^-$ where $N_{(0)}^-$ is the number of negative mesons available for decay and capture at $t=0$.

The capture constants can, therefore, be measured by determining the apparent mean life $1/(\lambda + \Lambda)$ of negative muons. If the experiment is carried out without differentiating between the positive and negative mesons, a small change

of the disintegration constant should still be observed in materials of suitable atomic numbers, This 'change' of the disintegration constant is due to the fact that the experimental data really represent a superposition of two decay curves, one produced by the positives with the mean life $1/\lambda$ and the other produced by the negative with a mean life $1/(\lambda+\Lambda)$. Hence the total decay curve is represented by

$$N(t) = N^+_{(0)} \exp[-\lambda t] + \lambda/(\lambda+\Lambda) \times N^-_{(0)} \exp[-(\lambda+\Lambda)t] \quad \dots \quad (2)$$

It is clear that in such investigations particular attention must be paid to very short decay times, specially if the capture constant is large, for the effect of the negative mesons at large time intervals after stopping will be almost nil,

EXPERIMENTAL DETAILS AND RESULTS

With a view to observing the variation of the mean life of the composite mixture of μ mesons available at sea level with the atomic number of the absorbing element, a set of experiments was carried out in this laboratory. The delayed coincidence technique was utilised to register the decay electrons arising out of the decay of the stopped μ -mesons. The details of the electronic circuits and the arrangement of the G.M. counters have been reported before (1954a). The experimental results with the C, Al, S and Pb absorbers have been communicated previously (1954b). Since then we have made measurements with water and NaF absorbers. Here we shall report these results.

(1) *Water Absorber.*

The thickness of the water absorber was so chosen that it was equivalent to the sulphur absorber (results reported before) with respect to the stopping power of the μ -mesons. 13.5 gms of water per square centimeter were used in thin galvanized iron containers of area $2" \times 20"$.

The results with this absorber have been plotted in figure. 1 on a semi-logarithmic scale. The points fit a single straight line which represents the decay curve of a composite beam of mesons in the absorbing material. It is known from the works of Panofsky, Aamodt and Hadley (1951) that the $D^+ \pi^-$ as well as μ^- mesons, are very rarely captured by the hydrogen nucleus and hence oxygen is the only effective element in the case of water absorber. It is noted that the nature of the curves in the cases of absorbers of low atomic numbers, such as carbon, (reported earlier) and oxygen, is the same, as in both the cases the composite decay curves are registered upto the last point. This is expected since the apparent mean lives of the negatives in these materials are not much less than that of the positives which implies that the negatives were still available for decay at 4.0 microseconds.

The composite mean life of the mesons is found to be 1.95 ± 0.08 microseconds. As the thicknesses of the sulphur and water absorbers were equivalent as regards the stopping power of the mesons, the same number of the positive mesons decayed

in both the cases in a definite time interval. The numbers of decay electrons on account of such decays were also the same in the two cases, since the thicknesses of the absorbers and the number of G.M. counters in the delayed coincidence did not alter. Any correction for the solid angle need not be considered and hence the positive decay curve of sulphur has been drawn in figure 1 to represent the same in water. By subtraction, the decay curve of the negative μ -mesons in water has been obtained. The negative mean life comes out to be 1.80 ± 0.19 microseconds. The calculated capture probability is $(0.90 \pm 0.85) \times 10^5$ per second.

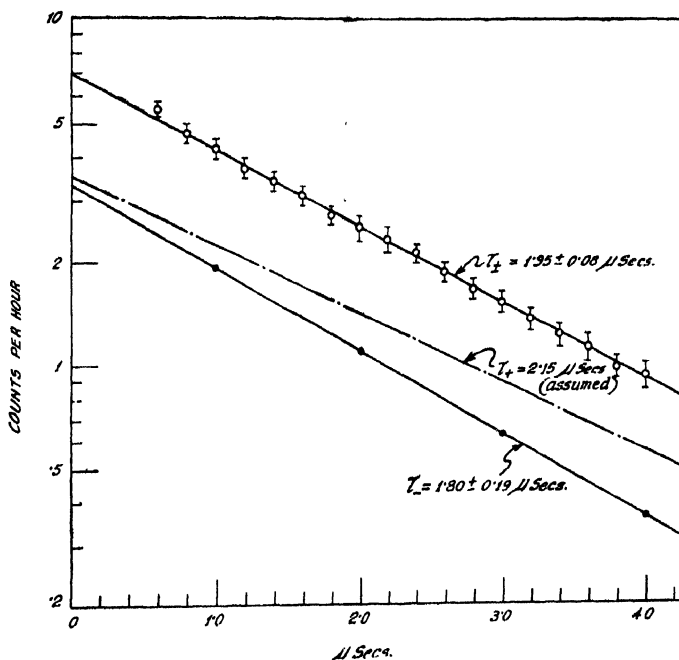


Fig. 1. The decay curve of the composite and the negative μ mesons in water.

If the observed integral decay curves are extrapolated to the zero time, one obtains the number of mesons available for decay in the time interval $t = 0$ to $t = \infty$. Corresponding to the positive decay curve, it represents the number of mesons stopped in the material. In the case of the negatives, however, a fraction of the stopped particles is captured by the nucleus and hence to get the number of the stopping mesons a multiplication factor $\frac{\lambda + \Lambda}{\lambda} = \frac{\tau_+}{\tau_-}$ is to be introduced. Since both the negative and the positive decay curves are known in this case, we have been able to find the ratio of the positive to the negative 'slow' mesons and the value is 0.90 ± 0.16 .

(2) *NaF Absorber.*

The arrangement of the apparatus was slightly altered for this absorber and a single absorber was used because large quantities of the compound were not available in the laboratory. The configuration of the G.M. counters is shown in figure 2. The number of counters in the delayed coincidence was reduced to six (instead of nine in the case of other absorbers) contained in two trays and the absorber was placed in between. Fifteen pounds of powdered sodium fluoride was taken in a thin galvanized iron container of area $2'' \times 20''$ square inches, for meson absorption.

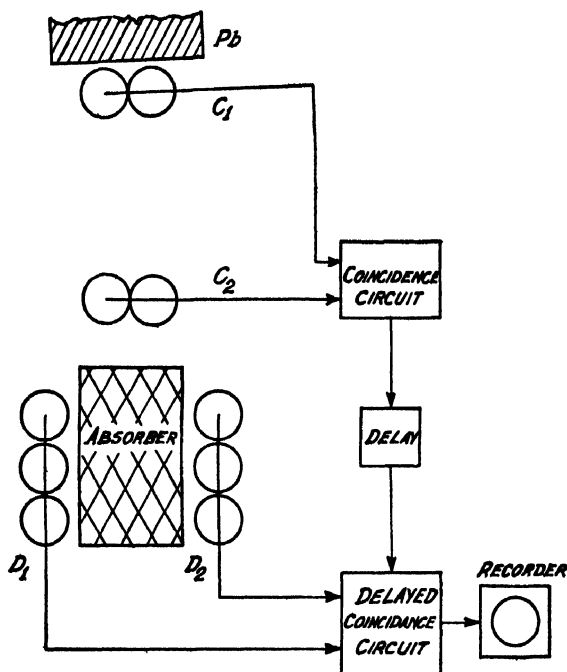


Fig. 2. The experimental arrangements of G. M. counters in the case of NaF absorber.

The plot of the data on a semi-logarithmic scale as shown in figure 3 yields the composite mean life of the μ -mesons stopped in the material. It is seen from the figure that the points corresponding to the delays of 3.8 and 4.0 microseconds lie above the composite decay curve even within the statistical errors shown. It is possible that the contribution of the negative mesons to the decay electron counting rates at these time delays is not so significant as it is for smaller values of delay times. The composite mean life is 1.82 ± 0.09 microseconds.

The relative number of captures of the negative mesons in a chemical mixture should, according to Fermi and Teller, be proportional to the atomic number

of the element. The validity of the Z law has been assumed by Ticho (1948) for the Na and F atoms and he gives the effective Z value of the NaF compound

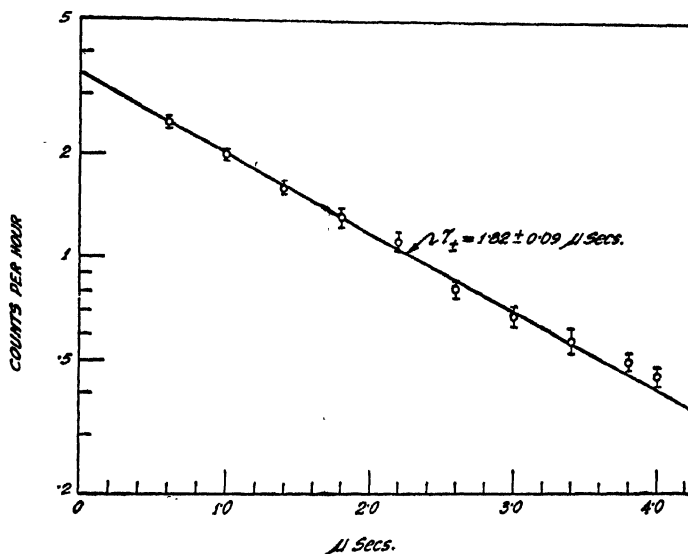


Fig. 3. The decay curve of the composite beam of μ mesons in NaF absorber.

to be equal to 10.1 on this assumption. Thus the decay curve in this absorber is expected to yield practically the same as in an element of $Z = 10$.

CONCLUSION

The dependence of the composite mean life of mesons at sea level is obvious from Table I, where our results, along with those of others are tabulated for comparison.

TABLE I

Composite mean life of mesons in different absorbers

Z	Composite mean life of mesons $\tau \pm$ in microseconds at		Authors
	sea level	3,500 meters height	
16	1.48 ± 0.08	—	Biswas and Sinha (1945b)
13	1.58 ± 0.07	—	"
13	—	1.78 ± 0.10	Ticho (1947)
12	—	1.70 ± 0.10	Bonade and Sard (1949)
10	1.82 ± 0.09	—	Present Experiment
8	1.95 ± 0.08	—	"
6	2.06 ± 0.03	—	Morewitz and Shamos (1953)
6	2.12 ± 0.02	—	Bell and Hincks (1952)
6	2.15 ± 0.09	—	Biswas and Sinha (1954b)
4	2.15 ± 0.02	—	Bell and Hincks (1952)
3	2.20 ± 0.02	—	"

For $Z \leq 16$, the value of the composite mean life increases as the atomic number of the absorbing medium decreases and tends to attain a value equal to the mean life of the positive mesons, 2.22 microseconds for $Z < 6$. This shows that for $Z < 6$, the apparent mean life of the negative μ mesons is approximately the same as the mean life of the positives.

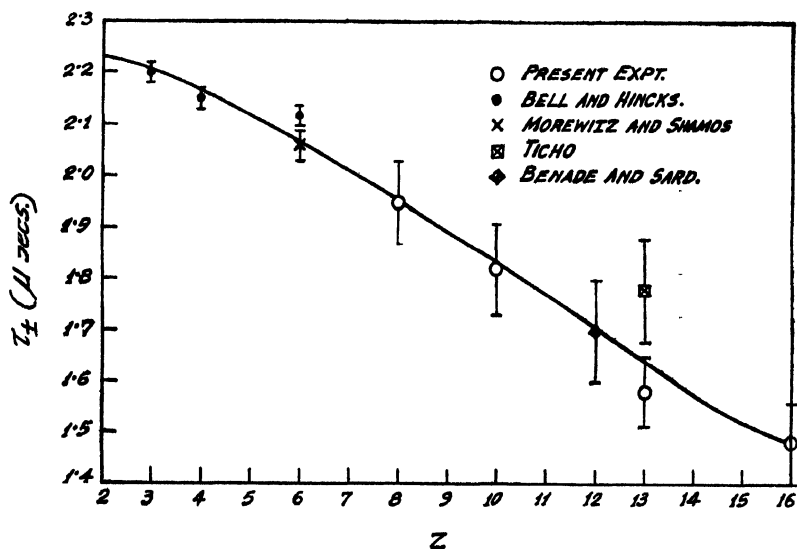


Fig. 4 (a). The variation of the composite mean life of μ mesons with the atomic number of the absorber.

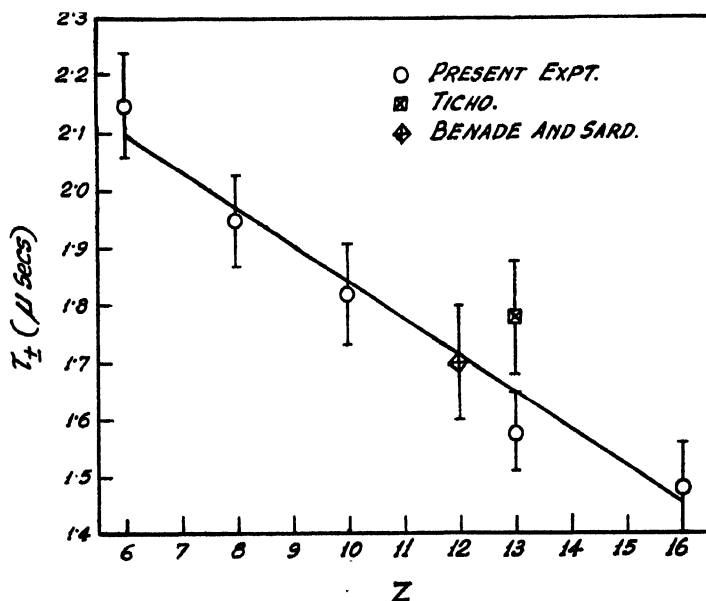


Fig. 4 (b). Empirical relation of τ_{\pm} with Z .

It is seen that our results are in good agreement with those of others. In figure 4(a), a curve has been drawn showing the Z dependence of the composite mean life upto the values of $Z = 16$ (sulphur). In Fig. 4(b), only the results of our experiments have been plotted against Z in the interval $Z = 6$ to $Z = 16$, and it is shown that a straight line can be drawn through the points suggesting the empirical formula

$$\tau_{\pm} = 2.50 - .065Z, \text{ microseconds in the range } 6 \leq Z \leq 16.$$

The composite mean lives as determined by Ticho (1948) and by Benade and Sard (1949) in aluminium and magnesium respectively also fit the line as shown in figure 4(b). Their results favour the empirical relation as obtained from our data.

As the experiments of Ticho and of Benade and Sard were carried out at an altitude of 3,500 metres above sea level and since their results for the composite beam are consistent with our findings, it is possible that the positive/negative ratio at a height of 3,500 metres may not be much different from that at the sea level; otherwise the composite mean life which is dependent on this ratio would not have followed a systematic variation as has been shown here. Hence it can be mentioned that the phenomenological theory of Puppi and Dallaporta (1952) on the assumption of the constancy or a slow variation of the ratio with altitude gets a support from these observations.

ACKNOWLEDGMENT

It is a pleasure to thank Prof. D. M. Bose, and Dr. M. S. Sinha of this institute for their kind interest, help and suggestions during the progress of the experiment. The work was performed under a grant received from the Atomic Energy Commission, Government of India.

REFERENCES

- Bell and Hincks, 1952, *Phys. Rev.*, **88**, 1424.
- Benade and Sard, 1949, *Phys. Rev.*, **76**, 488.
- Biswas and Sinha, 1954a, *Trans. Bose Res. Inst.*, **19**, 50.
- Biswas and Sinha, 1954b, *Phys. Rev.*, **94**, 1400.
- Morewitz and Shamos, 1953, *Phys. Rev.*, **92**, 136.
- Panofosky, Aamodt and Hadley, 1951, *Phys. Rev.*, **81**, 565.
- Puppi and Dallaporta, 1952, *Prog. Cosmic Ray Phys.*, Vol. 1. (Interscience Publishers).
- Ticho, 1948, *Phys. Rev.*, **74**, 1337.
- Ticho, 1947, *Phys. Rev.*, **72**, 255.

FREQUENCY OF THE THREE-PHASE R-C COUPLED OSCILLATOR

PART I. Non-reactive anode load resistance.

By H. RAKSHIT AND M. C. MALLIK

BENGAL ENGINEERING COLLEGE, HOWRAH

(Received for publication, September 14, 1955)

ABSTRACT. When the three stages of the conventional three-phase R - C oscillator are identical, the oscillations normally produced are of radio frequency $\omega = \sqrt{3/RC}$ where R and C are the tuning resistance and capacitance. This simple formula holds when the anode load resistance is non-reactive and the cathode impedance is zero. When these conditions are not satisfied the expression for frequency becomes much more complicated.

The case of finite cathode impedance of varied nature when anode load resistance is non-reactive is discussed in the present paper. Results of experimental observations are also given. It has been found that a capacitive cathode impedance causes an increase while an inductive cathode circuit causes a decrease in frequency over the $\sqrt{3/RC}$ value. A purely resistive cathode impedance does not affect the frequency in any way.

INTRODUCTION

It was shown in a previous communication (Rakshit and Bhattacharyya, 1946) that the conventional circuit of the three-phase R - C oscillator, with components selected for producing audio frequency oscillations, invariably generates radio frequencies by virtue of the stray and inter-electrode capacities. Such a three-phase oscillator can be made to generate audio frequency oscillations only with certain modifications introduced in the simple circuit. When the three stages are identical such as shown in figure 1, it has been shown that the oscillations produced are of radio frequency given approximately by

$$\omega = \sqrt{3/RC} \quad \dots (1)$$

where R is the effective anode load resistance taking the effect of grid leak of the next stage into account, and C is the sum of C_1 the external tuning condenser and C_s the total stray and interelectrode capacity across C_1 . In practice, the three condensers C_1 of the three stages are replaced by a three-gang condenser between the common ground line and the three anodes.

In deriving equation (1) the anode load resistance R was assumed to be purely resistive and the a.c. impedance of the cathode-to-ground circuit was assumed to be negligibly small. The present paper gives an account of the influence of

cathode impedance on the frequency of the generated oscillations. The assumption of non reactive load resistance is justified when it is of the carbon or metallised type. When small resistances are used for generating very high frequencies it has

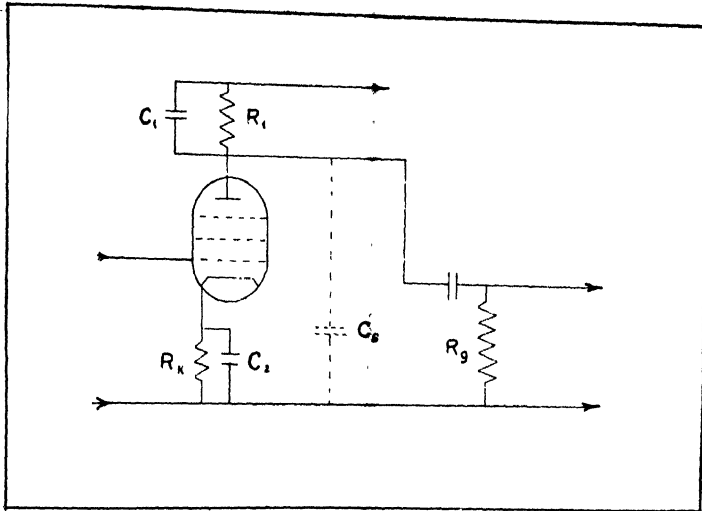


Fig. 1

been found (Rakshit and Mallik, 1953) that the inductances associated with the load resistances are responsible for increasing the effective load and gain and hence for maintaining the oscillation. In fact the highest frequencies have been obtained with small wire-wound resistances as load.

CATHODE IMPEDANCE AND ITS EFFECT

The impedance of the cathode circuit of an oscillator valve is composed of the cathode lead inductance L_1 in series with the parallel combination of cathode biasing resistance R_k and the by-pass condenser C_2 . For operation at sufficiently high frequencies, if a suitable mica condenser is used for by-pass, the cathode impedance may approximately be represented by figure 2(a). For operation at comparatively low frequencies when a paper condenser is used for by-pass the cathode impedance would be roughly as in figure 2(b), because a paper condenser is usually associated in series with its capacitance some inductance L_2 which may not be negligible. In general, therefore, the cathode circuit impedance may be represented by a very small resistance r in series with a reactance X , as shown in figure 2(c), or the parallel equivalent as in figure 2(d) where the admittance Y is the sum of conductance G_k and susceptance B_k . It may be noted in this connection that this impedance will have appreciable magnitude at frequencies well above or well below the self resonance frequency of the cathode circuit. Again,

for the same working frequency the influence of the cathode impedance will increase with decrease of anode load resistance.

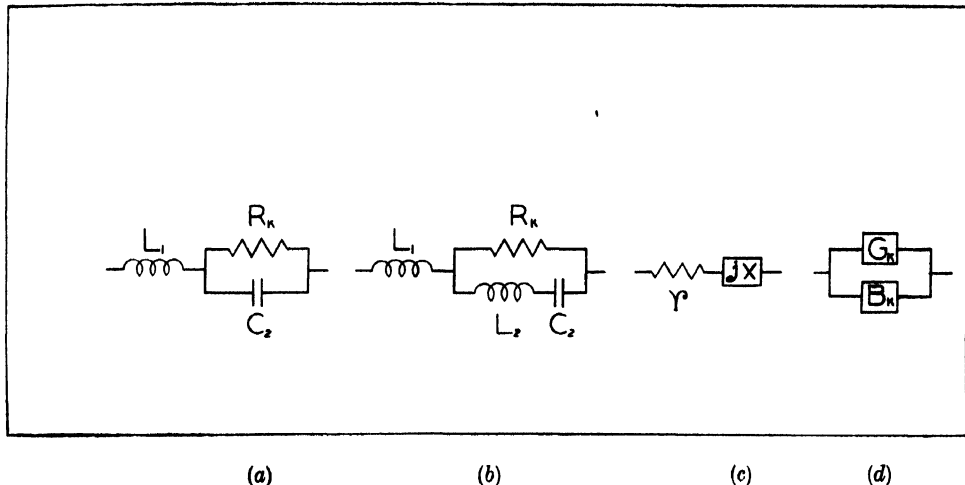


Fig. 2

It can be shown (Sturley, 1949) that the effect of a cathode load Z_k between cathode and ground of a screen-grid or pentode amplifier is to cause a reduction in the effective anode load Z_{eff} in the form

$$Z_{eff} = \frac{Z_0}{1 + g_m Z_k} \quad \dots (2)$$

where Z_0 is the actual anode load, Z_k is the cathode-ground impedance and g_m is the mutual conductance of the amplifier valve. This expression for Z_{eff} holds good when the screen is decoupled to cathode. When, however, the screen is decoupled to ground, a voltage is developed across Z_k due to variations in screen current and the effective anode load then becomes

$$Z_{eff} = \frac{Z_0}{1 + g_k Z_k} \quad \dots (3)$$

where $g_k = g_m + g_s$, g_s being the screen current-grid voltage slope conductance. In the case of non-aligned-grid valves, g_k is approximately $1.25g_m$. Since Z_{eff} is dependent upon Z_k it is obvious that the frequency of oscillations of the three-phase oscillator will also be affected by the presence of Z_k .

In addition, the presence of Z_k also affects the grid input admittance. It has been shown [Sturley, 1949] that whereas normally the grid input admittance

is ωC_{gk} , the effect of Z_k is to introduce across the input a parallel combination of R_g and C_g given by

$$R_g = \frac{(G_k + g_k)^2 + (B_{gk} + B_k)^2}{B_{gk}(G_k B_{gk} - g_k B_k)} \quad \dots (4)$$

and

$$C_g = \frac{C_{gk}[G_k(G_k + g_k) + B_k(B_{gk} + B_k)]}{(G_k + g_k)^2 + (B_{gk} + B_k)^2}$$

where C_{gk} is grid-cathode capacitance and $B_{gk} = \omega C_{gk}$.

It will be seen that the effect of Z_k on input resistance is appreciable only when the working frequency is high and the effect on input capacitance is appreciable when the tuning capacity is small. On the whole, the anode load resistances for which the results have been reported (Table IV) are such that the high frequencies are generated, and hence the effect of Z_k is appreciable, only when the tuning capacity is small.

The effect of cathode impedance on the frequency of oscillations, in so far as change of anode load is concerned, is discussed below for a few typical cases. The effect due to change in input impedance will be considered in connection with the results given in Table IV.

EFFECT OF CATHODE IMPEDANCE ON OSCILLATOR FREQUENCY

When the anode load resistance is non-reactive,

$$Z_0 = R/(1 + j\omega CR)$$

$$\text{and } Z_{eff} = \frac{R}{(1 + j\omega CR)(1 + g_k Z_k)} = \frac{R}{(1 + j\omega CR)[1 + g_k(r + jX)]} \quad \dots (5)$$

In any practical case, the resistive component (r) of the cathode impedance is negligibly small compared with the reactive component (X) except near series resonance frequency of the cathode load. In general, we may re-write expression (5) in the form

$$Z_{eff} = \frac{R}{(1 + g_k r - \omega CR g_k X) + j[\omega CR(1 + g_k r) + g_k X]} \quad \dots (6)$$

The phase angle (θ) of the load is obviously given by

$$\tan \theta = \frac{-[\omega CR(1 + g_k r) + g_k X]}{1 + g_k r - \omega CR g_k X} \quad \dots (7)$$

and the stage gain (A) by

$$A = \frac{g_m R}{[(1 + g_k r - \omega CR g_k X)^2 + \{\omega CR(1 + g_k r) + g_k X\}^2]} \quad \dots (8)$$

Oscillations are maintained when $A \gg 1$ and the frequency of the oscillations is given by $\tan \theta = -\sqrt{3}$ [Rakshit and Bhattacharyya, 1946]. The frequency in the present case is thus given by

$$\frac{\omega CR(1+g_k r) + g_k X}{1 + g_k r - \omega CR g_k X} = \sqrt{3} \quad \dots (9)$$

When the reactive component (X) of the cathode impedance is negligibly small, i.e. very near series resonance frequency of the cathode circuit, the frequency is given by

$$\omega CR = \sqrt{3} \text{ or } \omega = \sqrt{3/RC}, \text{ as in equation (1).}$$

It will be noted in this connection that when the anode load resistance is non-reactive, the oscillation frequency is the same whether the cathode impedance is zero or is a pure resistance.

When the working frequency is higher than the resonance frequency of the cathode circuit, the cathode impedance is inductive and we may put $X = \omega L'$, L' being of course a function of the frequency. Equation (9) then becomes

$$\frac{\omega CR(1+g_k r) + g_k \omega L'}{1 + g_k r - \omega^2 CR g_k L'} = \sqrt{3}$$

$$\text{giving } \omega = \frac{-[CR(1+g_k r) + g_k L'] + \{[CR(1+g_k r) + g_k L']^2 + 12CR g_k L'(1+g_k r)\}^{1/2}}{2\sqrt{3}RC g_k L'} \quad (10)$$

$$\approx \frac{-[CR(1+g_k r) + g_k L'] + [CR(1+g_k r) + g_k L'] \left[1 + \frac{6CR g_k L'(1+g_k r)}{\{CR(1+g_k r) + g_k L'\}^2} \right]}{2\sqrt{3}RC g_k L'}$$

when $12CR g_k L'(1+g_k r) \ll \{CR(1+g_k r) + g_k L'\}^2$. Hence, as a first approximation,

$$\omega = \frac{\sqrt{3}}{RC + \frac{g_k L'}{1+g_k r}}$$

$$\text{In the limit, if } g_k r \ll 1, \omega = \frac{\sqrt{3}}{RC + g_k L'} \quad \dots (11)$$

It will be noted from equation (11) that the presence of inductance L' in the cathode circuit causes a reduction in the oscillator frequency, the deviation from the $\sqrt{3}RC$ value being greater with increase in L' , i.e. with increase in working frequency above the cathode resonance frequency.

When the working frequency is less than the cathode resonance frequency, the cathode impedance becomes capacitive and we may put $X = -1/\omega C'$. Substituting this value of X in (9), we get

$$\omega = \frac{\sqrt{3}[C'(1+g_k r) + g_k RC] + \{3[C'(1+g_k r) + g_k RC]^2 + 4g_k RCC'(1+g_k r)\}^{1/2}}{2CC'R(1+g_k r)} \quad \dots (12)$$

$$\approx \frac{\sqrt{3}[C'(1+g_k r)+g_k RC]}{CC'R(1+g_k r)} + \sqrt{3}[C'(1+\frac{g_k}{g_k r})+g_k RC]$$

since in any practical case $g_k RC' \ll C''$. As a first approximation therefore

$$\omega = \frac{\sqrt{3}}{RC} + \frac{\sqrt{3}g_k}{C'(1+g_k r)} + \sqrt{3}[C'(1+\frac{g_k}{g_k r})+g_k RC']$$

In the limit, if $g_k r \ll 1$, we have

$$\omega = \frac{\sqrt{3}}{RC} + \frac{\sqrt{3}g_k}{C''} + \sqrt{3}[\frac{g_k}{C'(1+g_k r)} + g_k RC] \quad \dots (13)$$

Equations (12) and (13) show that when the cathode circuit becomes capacitive, the oscillator frequency is higher than that given by the simple formula $\omega = \sqrt{3}/RC$. The deviation from the $\sqrt{3}/RC$ value increases with decrease in effective cathode circuit capacity C' i.e., with decrease in operating frequency below the cathode resonance frequency.

Condition for maintenance of oscillation: Equation (8) for A shows that for all practical purposes since the terms involving g_k are negligibly small compared with the other terms, the maintenance condition becomes approximately

$$A = \frac{g_m R}{[1 + \frac{g_m^2 R^2}{\omega^2 C^2 R^2}]} \gg 1 \quad \dots (14)$$

When cathode impedance is zero, $\omega = \sqrt{3}/RC$ and the condition becomes

$$g_m R \gg 2 \quad \dots (15)$$

When cathode impedance is inductive, $\omega < \sqrt{3}/RC$ according to equation (11). This shows that for a fixed anode load resistance, when the cathode circuit is inductive, oscillations can be maintained for a value of g_m less than that required when the cathode impedance is zero. In other words, since cathode circuit is inductive for higher operating frequencies obtained with smaller values of R , the inductive cathode enables oscillations to be maintained with values of R lower than that given by $g_m R = 2$. For a given R , therefore, the lower the tuning capacity the higher is the generated frequency and hence higher is the gain, i.e., the lower the tuning capacity the greater is the amplitude of the oscillation maintained.

When, however, the cathode impedance is capacitive $\omega CR > \sqrt{3}$ according to equation (13) and hence a value of $g_m R$ greater than 2 is required for maintenance of oscillations.

EXPERIMENTAL OBSERVATIONS

Determination of stray capacity across the external tuning condenser.

The total tuning capacity consists of (i) the external tuning condenser and (ii) the stray including interelectrode capacity across it. This has been estimated

by plotting $1/f$ against external tuning condenser as was done originally by Rakshit and Bhattacharyya (1946). For this the anode load resistances are to be such that the formula $\omega = \sqrt{3/RC}$ holds without any appreciable error. This corresponds to $CR \gg g_k L'$ in case of inductive cathode circuit and to $CR \ll C'/g_k$ in case of capacitative cathode circuit. From measured values of L' and C' as described below and with the usual values of tuning condensers it is found that the required conditions are satisfied when the anode load resistances are not less than about 1000 ohms or so.

A number of carbon type resistances with nominal value of 1000 ohms were therefore measured and three of equal magnitude were selected for use as anode load resistances in the oscillator. The oscillator valves were also selected by actual measurements with voltages same as those to be applied in the oscillator. The cathode by-pass condensers were also selected by measurements as described in section 2 below.

With valves and components thus selected, the generated frequencies for different values of the external tuning capacity were measured as given in Table I.

TABLE I

Load Resistance $R_1 = 1,071$ ohms; $R_g = 33,000$ ohms.

Dial reading of the variable capacitor	Capacity of each section of the three-gang condenser in μF	Observed frequency in Mc/s.	$\frac{1}{f_{mc/s}}$
2465	494	0.520	1.923
2300	440	0.5728	1.746
2100	372	0.6605	1.514
1900	306	0.7742	1.292
1700	250	0.9206	1.086
1500	200	1.1063	0.9009
10	107	1.7688	0.567
800	80	2.199	0.455
500	45	3.028	0.329
200	18	4.529	0.221
000	9.5	5.500	0.182

The plot of $1/f$ against external tuning capacity is a straight line as shown in figure 3. The intercept on the negative side of the capacity axis gives the total

stray and interelectrode capacity (C_s) which in this particular case is found to be $40 \mu\mu f$.

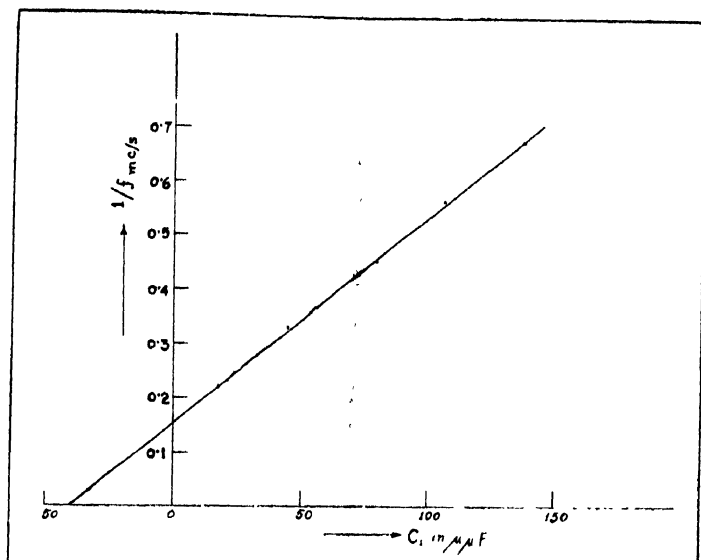


Fig. 3

2. Measurements on the cathode circuit.

In order to ascertain the validity of the working formula in any particular case it is necessary to estimate the constants C'_2 , L_2 and L_1 of the cathode circuit as given in figure 2(b).

The capacity C_2 of the cathode by-pass condenser was estimated from measurement with 1 kc/s bridge at which the self inductance L_2 would not produce any appreciable effect on the measured value of C_2 .

The value of L_2 was determined by resonance method working at a frequency much higher than the self resonance frequency of the cathode by-pass condenser. The equivalent inductance of L_2 and C_2 in series at a frequency ω is obviously given by

$$L_{eq} = L_2 - \frac{1}{\omega^2 C_2}.$$

When $L_2 \gg 1/\omega^2 C_2$, L_{eq} is approximately equal to L_2 . From measurements of L_{eq} at 13, 20 and 23 Mc/s the average value of L_2 came out in a typical case to be approximately $0.1 \mu H$. From such measurements on a number of by-pass condensers, three were selected having almost identical values of L_2 and C'_2 .

For measurement of L_1 the self resonant frequency of the cathode circuit was first estimated in the following way. As explained earlier, when the working

frequency is higher than the cathode resonance frequency, the observed frequency should be less than the $\sqrt{3}/RC$ value as given in equation (10). On the other hand, when the working frequency is less than the cathode resonance frequency, the observed frequency would be higher than the $\sqrt{3}/RC$ value as given in equation (12).

If therefore the difference between the observed frequency and that calculated from the $\sqrt{3}/RC$ formula is plotted against observed frequency, we should get a curve crossing the observed frequency axis at a point which gives the self resonance frequency of the cathode circuit. To get the desired result it is obvious that the anode load resistance of the oscillator should be so chosen as to be able to generate frequencies both above and below the cathode resonance frequency.

In calculating the frequency from the $\sqrt{3}/RC$ formula, the value of R was naturally taken to be the parallel combination of actual anode load resistance and grid leak of the next stage. Furthermore, the working conditions were so adjusted, especially by controlling g_m with the cathode bias resistance that the grids of the oscillator valves were not driven positive.

The results for three different load resistances are given in Table II.

TABLE II

Actual Load Resistance in Ohms	Effective Load Resistance in Ohms	Tuning Capacitance including strays in $\mu\mu F$	Observed Frequency in Mc/s.	Calculated Frequency given by	$f_o - f_c$ in Kc/s.
R_1	R	C	f_o	$f_c = \frac{\sqrt{3}}{2\pi CR}$	
606	595.07	534	0.900	0.8675	32.5
		480	0.993	0.965	28
		412	1.144	1.124	20
		346	1.353	1.338	15
		290	1.603	1.598	5
		240	1.924	1.930	- 7
		120	3.785	3.860	75
462	455.62	534	1.168	1.133	35
		480	1.284	1.260	24
		412	1.481	1.469	12
		346	1.752	1.748	- 4
		290	2.066	2.086	20
		240	2.482	2.521	39
393	388.37	534	1.364	1.329	35
		480	1.502	1.478	24
		412	1.729	1.723	6
		346	2.028	2.051	-23
		290	2.387	2.447	60
		240	2.863	2.957	94

The plots of the difference between the observed and calculated frequencies against the observed frequency for these three cases are given in figure 4. It will be

noted that each of them cuts the observed frequency axis at approximately the same point. The self resonance frequency of the cathode circuit may therefore be taken as 1.75 Mc/s without appreciable error.

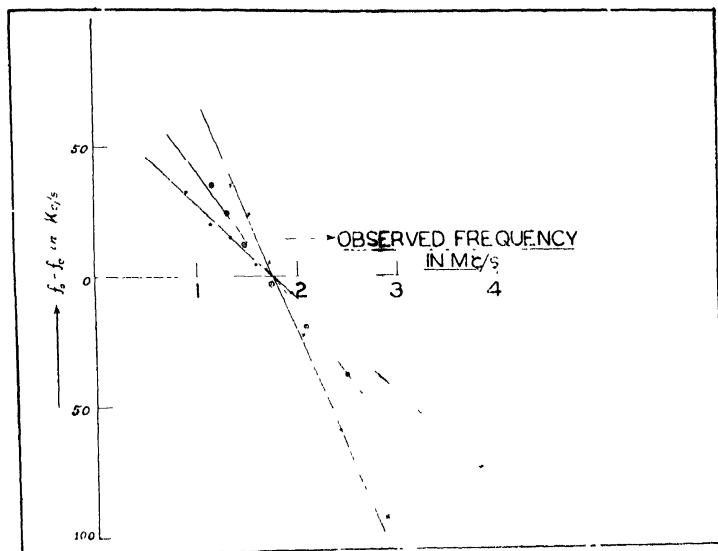


Fig. 4

In order to estimate L_1 it may be noted that the cathode circuit is approximately as depicted in figure 2(b), the cathode by-pass resistance R_k being above 200 ohms. From the reactance values of the series combination of L_2 and C_2 as given in Table III it will be obvious that within the frequency range 1-16Mc/s,

$$\omega L_2 \quad 1/\omega C_2 \ll 200.$$

TABLE III

Frequency in Mc/s.	ωL_2	$1/\omega C_2$
1	2.492	
2	0.304	
3	0.844	
4	1.733	
6	3.249	
8	4.636	
10	5.971	
12	7.279	
14	8.573	
16	9.858	

As a first approximation, therefore, we can neglect the effect of R_k in finding the reactance X of figure 2(c). The error involved in such approximation will comparatively be large in the case of the lowest and the highest frequencies. The

following data will give an idea of the error in any particular case. At $\omega = 2\pi \times 10^6$, the series equivalent of L_2 and C_2 is a capacity of reactance 2.49 ohms, while the reactance of the exact equivalent is 2.49 ohms—this corresponds to anode load resistance 606 ohms with R_k increased to 1000 ohms to avoid positive grid drive. Again, at the higher frequency limit of $\omega = 2\pi \times 16 \times 10^6$, the series equivalent is an inductance of reactance 9.85 ohms, while the reactance of the exact equivalent is 9.82 ohms—this corresponds to anode load resistance 276 ohms with $R_k = 210$ ohms. On an average, therefore, the error in neglecting the shunting effect of R_k is extremely small. Hence for all practical purposes the cathode circuit may be taken as composed of L_1 , L_2 and C_2 all in series. From the value of C_2 and the cathode resonance frequency of 1.75 Mc/s, $L_1 + L_2$ comes out to be $0.162 \mu H$, giving the value of L_1 to be $0.062 \mu H$. This agrees closely with the value of L_1 as calculated from the dimensions of the cathode lead of a broken valve of the same type and make as the oscillator valves.

3. COMPARISON OF OBSERVED AND CALCULATED FREQUENCIES

The observed frequencies under different operating conditions, the calculated frequencies and the various factors involved in the calculation are given in Table IV. It will be noted that in order to ensure proper working conditions the cathode bias had to be comparatively larger for higher load resistances and accordingly g_k also changed. Furthermore, for the same load resistance, the cathode bias had to be slightly increased for the lowest tuning capacities since the gain and hence amplitude of oscillations tend to increase with decrease in tuning capacity.

As pointed out earlier, the effect on frequency due to Z_k causing change in input impedance is expected to be appreciable only when the tuning capacity is small. For each load resistance the frequencies for tuning capacities 49.5 and $120 \mu\mu f$ have therefore been calculated by taking this effect into account. The change of input capacity due to Z_k is maximum when load resistance and tuning capacity are both small. The reduction in input capacity when the load resistance is 273.48 ohms, and tuning capacity $49.5 \mu\mu f$ is only $0.2 \mu\mu f$. The change in C_g for all other cases is therefore negligible and hence the change in input conductance alone has been taken into account.

It will be seen from Table IV that the calculated frequencies are almost equal to the observed values. In all the cases $g_k r$ has been found to be $\ll 1$ and hence when the cathode circuit is capacitive the frequency has been calculated from equation (13). For the inductive cathode, equation (11) has been used whenever $(CR + g_k L)^2 \gg 12(CR g_k L)$, otherwise equation (10) has been used. In some cases the values according to both the equations have been shown to give an idea of the error in using the simple formula (11). The frequencies obtained from equation (11) are greater than those from the complete formula (10) which

TABLE IV

C_s =Stray and interelectrode capacitances = $40\mu\mu F$; $R_g = 33,000$ ohms; $L_2 = 0.1\mu h$; $C_2 = 0.051\mu F$; cathode resonant frequency = $1.75Mc/s$.

Load resistance, taking effect of R_g in Ohms	Total tuning Capacitance including stray in $\mu\mu F$	Observed Frequency in Mc/s	Nature of Z_k	C' in $\mu\mu F$ or L' in μh	Cathode bias in Volts	q_k ($=1.25\mu_p$)	$C'Rgk$ 10^6	$(C'R - gkL)^2$ 10^{16}	$12C'RgkL$ 10^{16}	Calculated Frequency in Mc/s	Equation No. used for calculation	Calculated Frequency $F = \frac{\sqrt{3}}{2\pi CR}$ in Mc/s
595.07	534	0 900	Capacitive	0.06935	-3	4.5	0.00143			0 8917	13	0.8675
	480	0 903	"	0.07525	"	"	0.00128			0 8912	12	0.965
	412	1 144	"	0.0890	"	"	0.00110			1 1425	13	1.124
	346	1 353	"	0 1268	"	"	0 00092			1 3509	13	1.338
	290	1 603	"	0.3169	"	"	0.00077			1 6032	13	1.598
	240	1 924	Induc-	0 0281	"	"		20432.4	216.79	1 9285	11	1.930
	120	3 785	tive	0 1275	"	"		55130.5	490.16	3 8411	10	3.860
	49.5	8 802	"	0 136	-3.15	4.1		879.5	222.99	3 7530	10	9.356
455.62	534	1 168	Capacitive	0 0920	-2.7	5.63	0.00136			1 1550	13	1.133
	480	1 284	"	0.1165	"	"	0.00123			1 2790	13	1.260
	412	1 481	"	0 1798	"	"	0 00105			1 4799	13	1.469
	346	1 744	Induc-	0.00036	"	"		24852.2	3.87	1 7486	11	1.7486
	290	2 066	tive	0.04577	"	"		17518.3	408.46	2 0827	11	2.086
	240	2 482	"	0.08151	"	"		12057.5	602.15	2 0705	10	2.521
	120	4.816	"	0 1408	"	"		3056.9	518.40	2 4800	10	5.042
	49.5	11 104	"	0 1582	-2.8	5.1		530.4	215.17	4 0858	10	12.223

TABLE IV (contd.)

Load resis- tance, taking effect of R_g in Ohms	Total tuning Capaci- tance including stray in μF	Observed Fre- quency in Mc s.	Nature of Z_k	C'' in $\mu\mu F$ or L' in μh	Cathode bias in Volts	$gk \times 10^3$ ($= 1.25\eta_m$)	C/Rgk $\times 10^6$	$(CR - gkL')^2$ $\times 10^{11}$	$12C/RgkL'$ $\times 10^{11}$	Calculated Frequency in Mc s.	Equation No. used for cal- culation	Calculated Frequency $F = \frac{\sqrt{3}}{2\pi CR}$ in Mc s.
388.37	534	1.364	Capaci- tative	0.1299	-2.5	6.6	0.00136			1.3470	13	1.329
	480	1.502	"	0.1896	"	"	0.00123			1.4910	13	1.478
	412	1.729	"	2.093	"	"	0.00105			1.7408	13	1.723
	346	2.028	Induc- tive	0.0414	"	"		18130.3	440.60	2.0473	11	2.051
	290	2.387	"	0.0750	"	"		12796.5	669.09	2.6345	10	2.447
	240	2.863	"	0.1033	"	"		8815.4	762.57	2.4058	10	2.957
	120	5.540	"	0.1491	"	"		2259.9	548.63	2.8760	10	5.915
	49.5	12.428	"	0.1589	-2.65	5.9		396.1	213.34	5.4940	10	14.339
273.48	534	1.874	Induc- tive	0.0207	-2.2	9.35		21384.3	339.54	1.8850	11	1.887
	480	2.059	"	0.0449	"	"		17343.0	662.60	1.8768	10	2.099
	412	2.366	"	0.0734	"	"		12850.9	928.65	2.0932	11	2.446
	246	2.754	"	0.0967	"	"		9125.8	1026.48	2.0736	10	2.913
	290	3.248	"	0.1150	"	"		6461.9	1023.87	2.3890	10	3.476
	240	3.872	"	0.1290	"	"		4467.9	950.22	2.8857	11	4.199
	120	7.280	"	0.1528	"	"		1165.1	560.69	3.4290	10	8.399
	49.5	15.948	"	0.1602	-2.3	8.25		210.1	214.63	3.3030	10	20.362

are nearer to the observed frequencies. In general, the difference between the values from (10) and (11) increases with increasing frequency and hence for the high frequencies it is essential to use the complete formula.

CONCLUSION

The effect of cathode impedance on the frequency of the three-phase *R-C* oscillator when the anode load resistances are purely resistive has been discussed in the present paper. From a comparison of the observed frequencies and the values given by the simple equation $\omega = \sqrt{3/R'C}$ (Table IV) it will be noticed that the cathode impedance considerably influences the frequency of the generated oscillations when the working frequency is high. The question of reactive anode load resistances will form the subject matter of a subsequent communication.

ACKNOWLEDGMENT

The authors are thankful to the Council of Scientific & Industrial Research for a grant to carry out the investigations and for permission to publish the results.

REFERENCES

- Rakshit, JI and Bhattacharyya, K. K., 1946 *Ind. J. Phys.*, **20**, 171.
- Rakshit, JI. and Mallik, M. C., 1953, *Jour. Sci. & Ind. Res.*, **12B**, 30
- Sturley, K. R., 1949, *Radio Receiver Design*, Part One, (Chapman & Hall, London).

ON ULTRASONIC WATTAGE AND SPECTRAL NUMBER RELATIONSHIP

By K. SAMAL, K. M. PATANAIK AND A. K. DUTTA.

RAVENSHAW COLLEGE, UTKAL UNIVERSITY, CUTTACK.

(Received for publication July 25, 1955; received after revision, September 9, 1955)

ABSTRACT. An experimental study has been made between the input wattage and the maximum number of spectral orders for different coils and different circuits. The nature of variation of the order number against the wattage is described by an empirical relation of the form $w = bn^2 + cn^3$. It has been observed that the relation obtained by Raman and Nagendra Nath, when suitably analysed, is in complete accord with the experimental results. A possible reorientation of Raman and Nagendra Nath's theoretical relation to suit this aspect of ultrasonic study has been suggested.

INTRODUCTION

The diffraction spectra of ultrasonic waves obtained by the method of Debye and Sears ((1932) have been studied from various aspects. Bär (1932) studied the spectra critically from various aspects and incidentally established that the sound intensity leads to the gradual appearance of the spectra of higher orders. Raman and Nagendra Nath (1936) gave a general theory of the intensity relationship of the spectra of different orders, which showed that higher orders of spectra are expected with greater sound intensity. A definite relation between the sound intensity and the observable spectral number was not easily derivable from the above theory and no definite experiment to formulate the relationship has been tried.

It is well known that it is difficult to have an exact measure of the ultrasonic energy in a liquid. It is, however, easily possible to have a measure of the relative ultrasonic energies from either the input or the output energies of the oscillating circuit, assuming that the conversion factor between input and output and also between output and ultrasonic energy remains unchanged. That such a constancy of the conversion factor holds good, will be apparent from the discussion afterwards. It was also checked by observing a linear relation between the input wattage and the output power measured by an absorption wave meter, placed at a definite position relative to the oscillatory circuit.

According to expectation it has been observed by us that the number of spectral orders increases gradually with the input wattage. The experimental relation between the wattage and the observed spectral number has been found,

in the following, to be of the form $w = bn^2 + cn^3$ where ' w ' is the input electrical wattage, ' n ' the number of observed spectra and ' b ' and ' c ' are constants of the circuit and the system. It has been further possible to examine the relationship between wattage and spectral number from the standpoint of Raman's theory and it has been shown that there is exact correspondence between the expectation from this theory and the experimental results, throughout the range of variation of wattage, at different frequencies and with different oscillatory circuits. Incidentally this shows the possibility of reorientation of Raman and Nath's relationship to connect ultrasonic power or refractive index variation with the observed spectral number.

EXPERIMENTAL ARRANGEMENT

The experimental arrangement comprises of the method of production of intense ultrasonic beams at different frequencies, the arrangement of variation of input electrical wattage and the method of observing diffraction pattern by ultrasonics.

For the production of ultrasonic beams at different frequencies a piezo-electric quartz of natural frequency of 1 mega c/s was vibrated to its higher odd harmonics by the aid of electric oscillations of an electric generator.

The electric generator consisted of a full wave rectifier and an oscillating circuit of the Hartley type. The oscillating circuit was made up of an adjustable self induction and a variable condenser. It was tuned to the natural frequency of the quartz and to its higher odd overtones by varying the capacity and the tapplings in the coil. Whenever a particular overtone was not obtainable by tapping from the scope of the winding of the coil, the coil was replaced by a new one. To obtain lower harmonics with a particular coil it was also sometimes necessary to extend the range of the capacity by joining a new capacity in parallel with it.

We used a 100-watt generator. When used with full power the input was 110 v. AC. To vary the power of vibration of the quartz, the input voltage to the power transformer only was varied, thus changing the input wattage with the help of a variable rheostat. An accurate voltmeter in parallel and an accurate ammeter in series were connected to measure the input wattage accurately. The filament of the oscillator was heated by a separate transformer.

The vibrating quartz was put inside a rectangular glass vessel, filled up with pure transparent kerosine. The vessel was suitably covered with a glass plate to minimise evaporation. It was placed on a prism table of a spectrometer. The ultrasonic beam inside the liquid was illuminated with the properly collimated light of a monochromatic sodium lamp. The relative positions of the collimator, the glass vessel and the quartz were undisturbed during the experiment to ensure constant condition of visibility of the spectra. The quartz was

placed in such a way that the diffraction spectra became symmetrical with reference to the undeviated ray. The spectra were observed by the telescope of the spectrometer from the opposite face of the vessel.

EXPERIMENTAL RESULTS

The circuit was tuned to the condition for the appearance of maximum number of spectra for each observation with different wattages and with different frequencies.

It was, however, noticed that the coupling of the differently wound coils with the condenser, affected considerably the appearance of spectra, even for the same frequency and wattage. To emphasise on this difference we took two sets of observations with two different coils. One was a thin steel coil, wound closely on silica base. The other was thick copper coil in air, wound with wide spacings. The former coil gave greater number of spectra i.e., sound intensity, than the latter for the same input wattage and the frequency. A clear comparison can be made between them from the tables. So the coupling condition is observed to be an influencing factor in spectra-input wattage relationship. With the thin coil which showed a larger number of spectra, we simply counted the number of spectra for different steps of wattages. It was difficult in such a case to adjust the wattage so that spectra would appear one by one. With the other type of the coupling, however, the number of spectra was considerably less. So the wattage was adjusted until a particular order of spectra just appeared. If for a given wattage the intensity of a particular order is visually greater than that at the time of appearance, it was marked with + and ++ according to the condition of the intensity of the order. The readings for two different oscillating circuits are tabulated below :

TABLE I
Wattage-spectra observations with thin steel coil.

Frequency $f = 3$ Mc/s.		Frequency $f = 5$ Mc/s.	
No. of fringes (n)	Wattage (w)	No. of fringes (n)	Wattage (w)
9	7.2	7	6.7
12	12	8	9.7
16	18.7	9	14.8
19	29.4	10	18.7
22	40.2	11	23.6
23	52	13	35.6
—	—	15	58.9

TABLE II

Wattage-spectra observations with thick copper coil.

$f=5$ Mc/s.		$f=7$ Mc/s.		$f=9$ Mc/s.		$f=11$ Mc/s.		$f=13$ Mc/s.	
n	w	n	w	n	w	n	w	n	w
2 ¹¹	6.25	2 ¹¹	7	2	8	1 ¹¹	6.4	1	14
3	8	3	12.6	3	30	2	56	.	.
4	16	4	27	4	69
5	28	5	58
6	47	6	76
7	72

Plotting the number of spectra against wattage for a particular frequency, a smooth curve was obtained. For different frequencies, the curves retained the same nature of variation. From the nature of the curves it appeared that the spectra-wattage relationship is more or less of parabolic nature. On plotting n^2 against wattage, we observed that although with smaller values of n^2 the relation is linear, with higher values of n^2 the curves deviated from its straight path towards wattage axis. This deviation went on increasing with higher frequencies. This suggested that an n^3 term should also be taken in. It is also evident from the increasing deviation with the frequency that the coefficient of n^3 will go on increasing with the frequency. Thus, the suggested empirical relation is $w = bn^2 + cn^3$. This form of the relation is fitting the curves throughout at different frequencies within the experimental error. Below, in figure 1

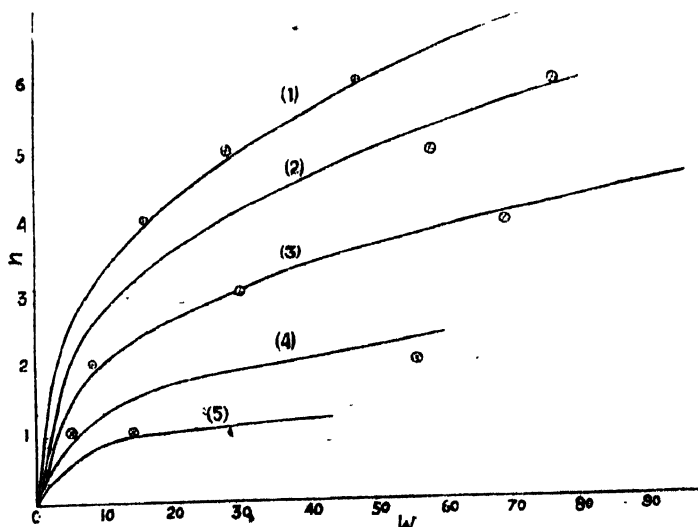


Fig. 1. Input wattage and fringe number graph. Graphs (1), (2), (3), (4), (5) correspond to the frequencies 5, 7, 9, 11, 13 Mc/s. respectively.

and figure 2 we have drawn all the theoretical curves with the above relation and experimental observations are indicated therein by points within small closed circles.

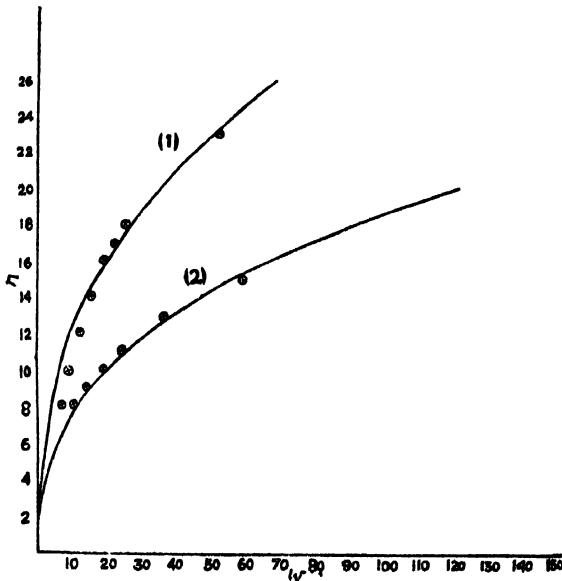


Fig. 2. Input wattage and fringe number graph. Graphs (1), (2), correspond to the frequencies 3Mc/s, 5Mc/s obtained with a different oscillatory unit.

The values of b and c went on increasing with the frequency. They must, naturally, be some function of frequency or of the order of the harmonics and also of the factors involving the constants of the circuit. A range of values for b and c were found to be possible to conform to the experimental curve at a definite frequency, within the range of experimental error. The variation of c with the frequency was very rapid and it was observed that a smooth curve between $\log c$ and the frequency limited very much the possibility of deviation of c values. A mean curve between $\log c$ and the frequency is drawn in the figure 3. This curve looked to be of logarithmic nature and $\log \log 100c$ being plotted in the same figure 3, with a changed scale of Y -axis gave a linear curve. Thus the relation obtained between c and frequency was given by $\log c = d + ke^m$ where f is the frequency and k, m, d are constants depending on the nature of the circuit and the system.

Knowing the values of c for different frequencies, the corresponding values of b were found out. They came within the range of value of b previously determined. These determined values of b gave a smooth relationship with the frequency as shown in figure 4. The nature of the curve indicated a logarithmic relation. On plotting $\log b$ against frequency a straight line was obtained as shown in the same figure 4.

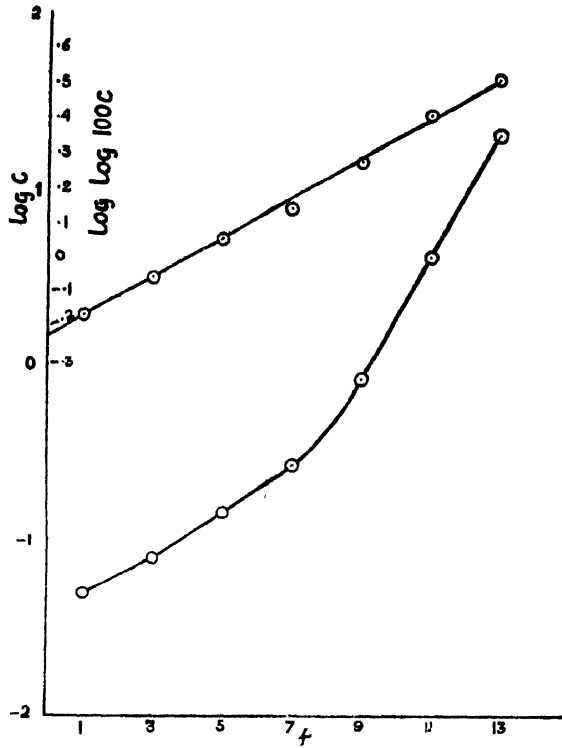


Fig. 3. Variation of the constant c with frequency shown in $\log c - f$ and $\log 100c - f$ forms.

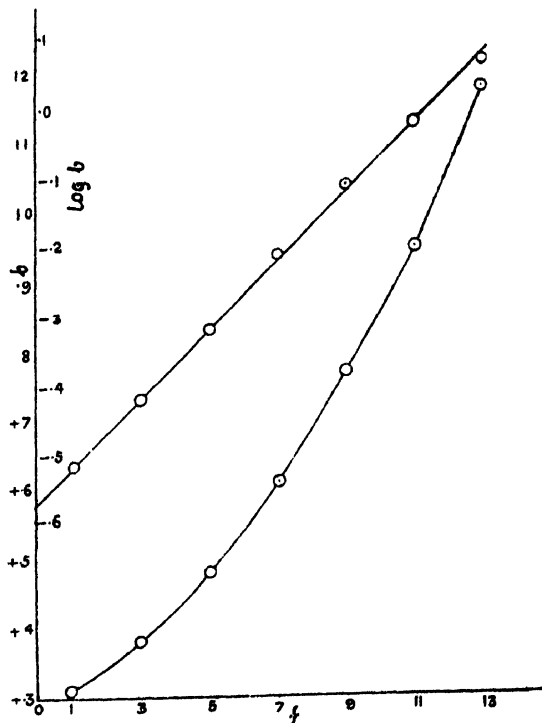


Fig. 4. Variation of the constant b with frequency shown in $b - f$ and $\log b - f'$ forms.

Thus we have $b = A e^{Bf}$ where A and B are constants depending on other factors like k , and m . The determined values of b and c for different coils and frequencies are tabulated below :

TABLE III

f in Mc/s	Thick copper coil		Thin steel coil	
	b	c	b	c
1	0.31	0.049
3	0.38	0.078	0.0407	0.00234
5	0.48	0.144	0.1	0.01
7	0.61	0.269
9	0.77	0.832
11	0.95	4.2
13	1.18	20.8

DISCUSSION OF RESULTS

It has been already stated that Raman and Nagendra Nath's theory is apparently not suitable to give us a relationship between the spectral number and the ultrasonic wattage or the change of refractive index caused by it. This is particularly because the theory gives us the intensity of the order number ' n ' by the Bessel function $J_n^2(v)$ where v contains the refractive index variation due to ultrasonics. Evidently from the form of the Bessel function, we shall obtain for a particular value of n , various values of v to give the same value of intensity $J_n^2(v)$. Also for a particular value of v , we would have various values of n to give the same value of intensity. This would be apparent from a careful study of the graphical representation of intensities of different orders for various values of v , as given by Raman and Nath. In such a case of multiple-valued relationship on both sides, it is not easily possible to find a suitable relation between the total observed order number and the values of v . If, however, from the multiple-valued v values we select the minimum value to give us the just observable intensity $J_n^2(v)$ for the n -th order, we would have a single-valued n corresponding to a single-valued v and naturally there would exist a suitable relation between them. This does not seem to be an easy task. Attempts are, however, being made here in this direction. To circumvent this difficulty, we have studied the calculated intensity picture for different values of v given by Raman and Nath and also by Levi (1936), on the basis of Raman and Nath's theory, and have obtained the minimum value of v for the appearance of a given order number. On plotting these order numbers (appearing for

the first time with increasing v values) against the v values, we obtain a curve between the maximum number of fringes and the values of v or the refractive index change on the basis of Raman and Nath's theory. The single-valued relationship between the n -th fringe with the just observable intensity and the minimum value of v suggested before would be the equation for the above mentioned curve. This graph has been plotted in Figs. 5 and 6, with the help of the intensity diagrams of different orders for various values of v as given in the work of Raman and Nath and also of Levi. Since the ultrasonic wattage is taken as proportional to the input wattage and also since ultrasonic wattage may be justifiably taken to be proportional to the square of the pressure change or to the square of the change of refractive index of the medium as has been established by the work of Sanders (1936), we may consider that the v values of Raman's work may be replaced by $K\sqrt{w}$ where K is a constant for a set up.

In accordance with Raman and Nath's theory, then, we should expect that the graph between the observed number of fringes and $K\sqrt{w}$, with a suitable choice of K , should be identical with the graph mentioned above between v values and the maximum number of fringes. The identity of our experimental curves throughout the range of wattages for different frequencies and different coils with the curve obtained on the basis of Raman and Nath's theory, will be clear from a perusal of Figs. 5 and 6.

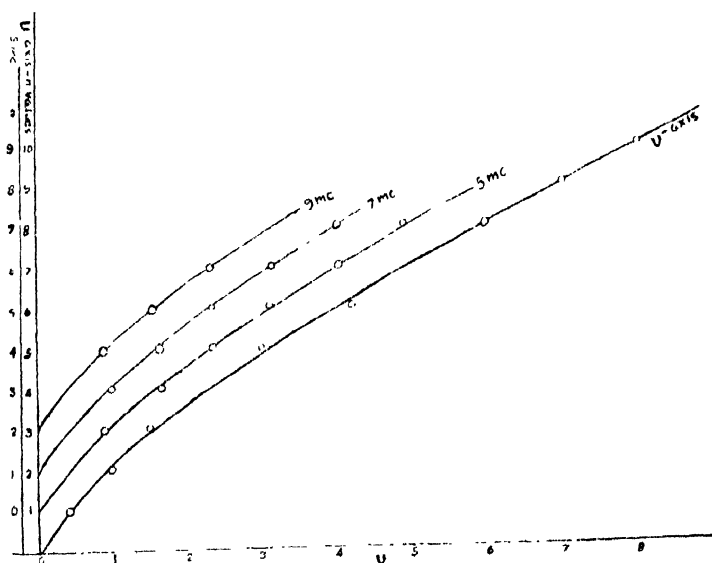


Fig. 5. The points in the lowest graph are taken from Raman and Nagendra Nath's diagrammatic representation of intensities and the smooth curve through them have been shifted to different scales of representations, where the points indicate the observed fringe numbers against $K\sqrt{w}$ for different frequencies. The k values for 5,7,9 Mc/s. are 0.6, 0.45, 0.28 respectively.

In figure 5, the lowest curve is from Raman and Nagendra Nath's diagrammatic representation of intensity for various v values, the points being taken from the records of the diagrams. The upper graphs have been drawn by shifting the y -axis through unity in steps, to avoid confusion, as would be clear from

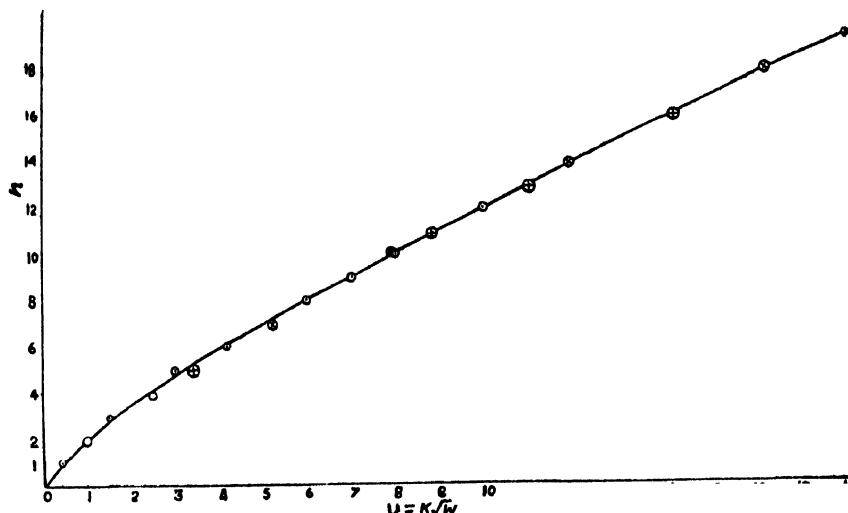


Fig. 6. The circles with points are taken from Raman and Nagendra Nath's and also from Levi's diagrammatic representations of intensities. The circles indicated as \times and $+$ refer to the observed values of fringe number against $K\sqrt{w}$ for the frequencies 3 and 5 Mc/s with a different coil. The k values are 3.24, 1.75 respectively,

the scales alongside. The continuous lines are again the curves from Raman and Nath's tabulated values and the points are plots of the observed numbers against $K\sqrt{w}$ with adjusted constant K for different frequencies. They have been previously represented in Fig. 1 in a different way. Similarly in Fig. 6 the full curve is obtained from the minimum v values and the observed numbers from Raman and Nath's and also from Levi's diagrammatic intensity relations, where the points indicated as \times and $+$ are the plots of the observed numbers against $K\sqrt{w}$ for the 3 Mc/s and 5 Mc/s data respectively. These have been represented before in graph 2. As will be apparent from the graphs, the agreement is remarkably good, which signifies that Raman and Nath's theory is substantiated completely on this aspect and in this range of experimental study. It also establishes a linear relationship between input wattage, the output wattage and the ultrasonic wattage, as otherwise the agreement would not have been obtained.

The only drawback of Raman's theory to deal with this aspect of the experiments is the non-availability of a suitable relation connecting the maximum

number of fringes and the values of v or of the variation of refractive index. It is also apparent from our empirical relationship that the relation between the n values, obtaining a particular small fixed value of $J_n^2(v)$, and the minimum v value should be reducible to the form $v = \sqrt{Cn^2 + Dn^3}$. Otherwise an alternative relation should be found to describe the minimum v against observed spectral number graph as obtained from Raman's work. This would automatically transform to the wattage against observed spectral number relationship as described by the graphs 1 and 2.

It may be further pointed out that in the $K\sqrt{v}$ values for different frequencies and coils which identify with the v values of Raman and Nath's theory, the constants K lie in the range from 10 to 10^{-1} . As v is given by the expression $\frac{2\pi\Delta\mu l}{\lambda}$ where l , the depth of light path through ultrasonic beam is about 2 cm in our experimental condition and λ the wave length of light is about 6×10^{-5} cm, we note that the conversion factor from the square root of input wattage to the refractive index variation is of the order of 10^{-5} to 10^{-6} . This is not an unexpected order of conversion factor.

REFERENCES

- Bär, 1932, *Helv. Phys. Acta.*, **6**, 570.
 Debye, P. and Sears, F. W., 1932, *Proc. Nat. Acad. Sci. Wash.*, **18**, 410.
 Debye, P., 1932, *Leipzig. Ber.*, **84**, 125.
 Levi, F., 1936, *Helv. Phys. Acta.*, **9**, 63; 234.
 Raman, C. V. and Nagendra, N. S., 1936, *Proc. Ind. Acad. Sci. (A)*, **2**, 406; **3**, 75.
 Sanders, F. H., 1936, *Canad. Jr. Res.*, **14**, 158.

Letter to the Editor

RAMAN SPECTRA OF SOLUTIONS OF O-DICHLOROBENZENE IN METHYLCYCLOHEXANE

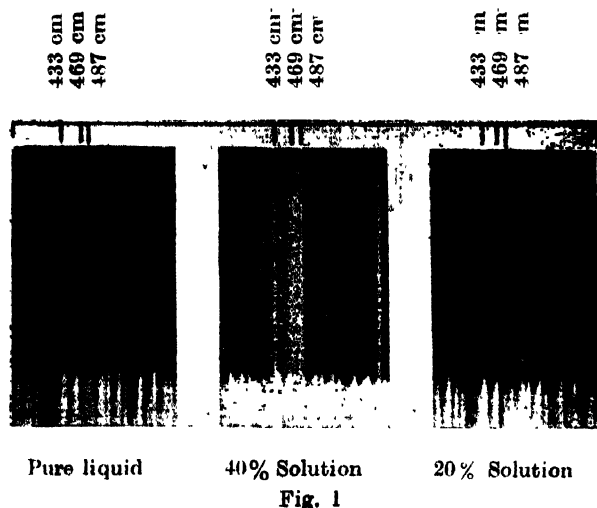
D. C. BISWAS

INDIAN ASSOCIATION FOR THE CULTIVATION OF SCIENCE, CALCUTTA 32.

(Received for publication on September 30, 1955)

It was observed recently (Biswas, 1955) in an investigation on the Raman spectra of dichlorobenzenes in different states and at different temperatures that two intense lines appear at 469 cm^{-1} and 487 cm^{-1} in the Raman spectrum of *o*-dichlorobenzene in the liquid phase and when the liquid is solidified the two lines are replaced by an intense single line at 478 cm^{-1} . It was suggested that the line 469 cm^{-1} might be due to dimers present in the liquid and the corresponding line due to the single molecule was at 487 cm^{-1} . As solvent molecules have much influence on molecular association in such a case it might be expected that if the substance would be dissolved in suitable solvents the relative intensities of the two lines due to the monomer and the dimer respectively would change appreciably. Recently, methylcyclohexane has been found to be a very good solvent for this purpose (Sirkar and Kastha, 1955) and therefore, the Raman spectra of solutions of *o*-C₆H₄Cl₂ in methylcyclohexane have been investigated to test the above hypothesis.

A comparison of spectrograms due to the pure liquid and the solutions of this substance in methylcyclohexane reproduced in figure 1 shows that the



solvent has great influence on the relative intensities of the two lines mentioned above. The integrated intensities of the two lines at 469 cm^{-1} and 487 cm^{-1} are

nearly the same in the Raman spectrum due to the pure liquid at room temperature. The spectrogram due to a 40% solution of this substance in methylcyclohexane shows that the intensity of the line 469 cm^{-1} is less than half that of the line at 487 cm^{-1} . When the strength is reduced to 20% by volume, the line 469 cm^{-1} becomes broader and appears as a very weak and diffuse satellite of the intense line at 487 cm^{-1} . Again, on comparing the intensities of both these lines with the line at 433 cm^{-1} it can be seen clearly that the line 469 cm^{-1} becomes much weaker and the line 487 cm^{-1} becomes relatively much stronger when $o\text{-C}_6\text{H}_4\text{Cl}_2$ is dissolved in methylcyclohexane. It is thus evident that in dilute solutions of methylcyclohexane the Raman line at 487 cm^{-1} becomes stronger at the expense of the other line at 469 cm^{-1} .

The above results furnish conclusive evidence in support of the suggestion (Biswas, 1955) that the line 469 cm^{-1} of the liquid $o\text{-C}_6\text{H}_4\text{Cl}_2$ is due to a dimer and the line 487 cm^{-1} is due to the same mode in the single molecule. The line 487 cm^{-1} was attributed to the vibration of the benzene ring of mode ϵ_g^+ (Nordheim and Sponer, 1943). In the liquid state this vibration is influenced by the field of the neighbouring polar molecules of the substance and a second line corresponding to the same mode in a dimer formed in the liquid state is produced at 469 cm^{-1} . The relative intensities of these two lines suggest that in the liquid state at room temperature nearly 50% of the molecules are in the associated state. When the strength of this solution is only 15% by volume, the number of associated molecules becomes negligibly small and the intensity of the line at 469 cm^{-1} due to the dimer is reduced to a very low value.

One of the three lines in the neighbourhood of 200 cm^{-1} observed in the spectra due to m -dichlorobenzene, m -chlorotoluene and m -bromotoluene was attributed to dimers (Biswas, 1955). This line, however is found to persist even in the case of very dilute solutions of these substances in methylcyclohexane. An alternative assignment is, therefore, to be found as the line seems to be due to the single molecule.

In conclusion the author wishes to acknowledge his indebtedness to Prof. S. C. Sirkar, D.Sc., F.N.I., for his kind help and guidance during the progress of this work.

REFERENCES

- Biswas, D. C., 1955a, *Ind. J. Phys.*, **29**, 179.
Biswas, D. C. 1955b, *Ind. J. Phys.*, **29**, 257.
Nordheim, G., and Sponer, H., 1943, *J. Chem. Phys.*, **11**, 253.
Sirkar, S. C., and Kastha, G. S., 1955, *J. Chem. Phys.*, **23**, in press.

ULTRAVIOLET ABSORPTION SPECTRA OF ORTHO-AND PARA TOLUNITRILE IN VAPOUR, LIQUID AND SOLID STATES*

By S. K. SEN

OPTICS DEPARTMENT, INDIAN ASSOCIATION FOR THE CULTIVATION OF SCIENCE, JADAVPUR,
CALCUTTA 32

(Received for publication, October, 20, 1955)

ABSTRACT. The absorption spectra of thin films of *o*- and *p*-tolunitrile in the liquid and the solid states at low temperatures have been studied and the results have been compared with those for the vapour state and for solutions of these substances. Absorption spectra of the substances in the vapour state have also been reinvestigated and the bands have been reclassified. In the liquid state *o*-tolunitrile gives five broad bands with the 0,0 band at 35055 cm^{-1} , while in the vapour state the 0,0 band is at 35780 cm^{-1} and in the solid state at -180°C the bands become sharper and the 0,0 band shifts to 34841 cm^{-1} . In the case of *p*-tolunitrile in the liquid phase seven broad bands are obtained with the 0,0 band at 35771 cm^{-1} , while the 0,0 band due to the vapour is at 36208 cm^{-1} . In the solid state the substance gives nine bands with the 0,0 band at 35752 cm^{-1} . Thus major change in the bands occurs with the liquefaction of vapours, the 0,0 band shifting towards longer wavelengths in both the cases. Such a shift may be due to association of molecules in the liquid state. With solidification and lowering of temperature to -180°C , the 0,0 band shifts further towards longer wavelengths in the case of ortho compound but no such change takes place in the case of the para compound. It is concluded that the shift observed with solidification of the ortho compound may be due to larger dipole moment of this molecule than that of the para compound.

INTRODUCTION

The ultraviolet absorption spectra of toluene ($\text{C}_6\text{H}_5\text{CH}_3$) in the liquid and the solid states were investigated by Swamy (1951). The influence of change of state on the electronic energy levels of the molecule is evident from the presence of only one band in the solid state at -180°C , the other bands of the liquid state merging into one another. Similar investigations were carried out on the ultraviolet absorption spectra of many disubstituted benzenes in the solid state by Swamy (1952, 1953). In the case of *o*-, *p*-xylene at -180°C he observed some new bands which were not observed in the case of the liquid. These bands could be assigned to vibration frequencies of the molecule. In the case of ortho dichlorobenzene the excited state electronic energy level was found to split up into three components with solidification and lowering of temperature to -180°C but the para compound did not show this effect. Such splitting was observed also in the case of chloro and bromotoluene except the para compounds.

* Communicated by Prof. S. C. Sirkar.

Aromatic nitriles contain $C\equiv N$ group and it is not known whether the intermolecular field in the solid state has large influence on the ultraviolet absorption spectra of these compounds. Further it would be interesting to compare such influence with that observed in the case of other substituted toluenes and to find out whether the changes in the absorption spectra with solidification of the liquids depend on the relative positions of the substituents as in the case of halogen substituted toluenes. The present investigation was, therefore, undertaken to study the ultraviolet absorption spectra of ortho and para tolunitrile ($CNC_6H_4CH_3$) in the solid state at $-180^\circ C$ to compare the results with those observed for the liquid and vapour states of the substances. The absorption spectra of these substances in the vapour state have also been reinvestigated in order to compare the results with those for the liquid state as the bands reported by Aclý (1928) were not properly classified by him. The bands observed in the case of vapours have been reclassified in the present investigation

EXPERIMENTAL

The liquids ortho and para tolunitrile supplied by Fisher Scientific Co. (U.S.A.), were distilled four times under reduced pressure before being introduced in the cell. The films of ortho and para tolunitrile that produced absorption bands had a thickness of only a few microns. The absorption spectra of ortho and para tolunitrile in the vapour state were photographed using an absorption tube of length 50 cm and 14 mm diameter, quartz windows being cemented to the tube with Araldite. For studying the absorption at low temperatures, the brass frame containing the cell with the liquid was suspended in a Dewar vessel of fused silica containing some liquid oxygen. The lower portion of the brass frame was kept immersed in the liquid oxygen to solidify the substance. Liquid oxygen was replenished from time to time to keep it at a proper level in the vessel. The upward drift of cold air prevented the condensation of water vapour on the surfaces of quartz plates. The beam of light coming from the hydrogen discharge tube was made parallel with a quartz lens and the cell was placed in the path of the parallel beam. The transmitted light was focussed on the slit by a second quartz lens. An exposure of about an hour was necessary to record the absorption spectrum of the solid.

A hydrogen discharge tube running at 3 K.V. served as the source of continuous spectrum. Spectrograms were taken on Ilford HP 3 films with a Hilger E 1 quartz spectrograph having a dispersion of 3 A.U. per mm. in the region 2600\AA° . An exposure of 15 minutes was required to record the spectra of liquids and in the case of vapour the exposure was one and half hour. Iron arc was photographed on each spectrogram as comparison. Microphotometric records were obtained with a self recording microphotometer supplied by Kipp and Zonen. The frequencies of the bands were measured from these microphotometric records in which the record of two known iron lines were taken as reference lines.

RESULTS

The spectrograms of the vapour state are reproduced in Plate XI.

The microphotometric records of the spectrograms due to the solid and liquid states are given in figures 1 and 2. The frequencies of the bands are given in

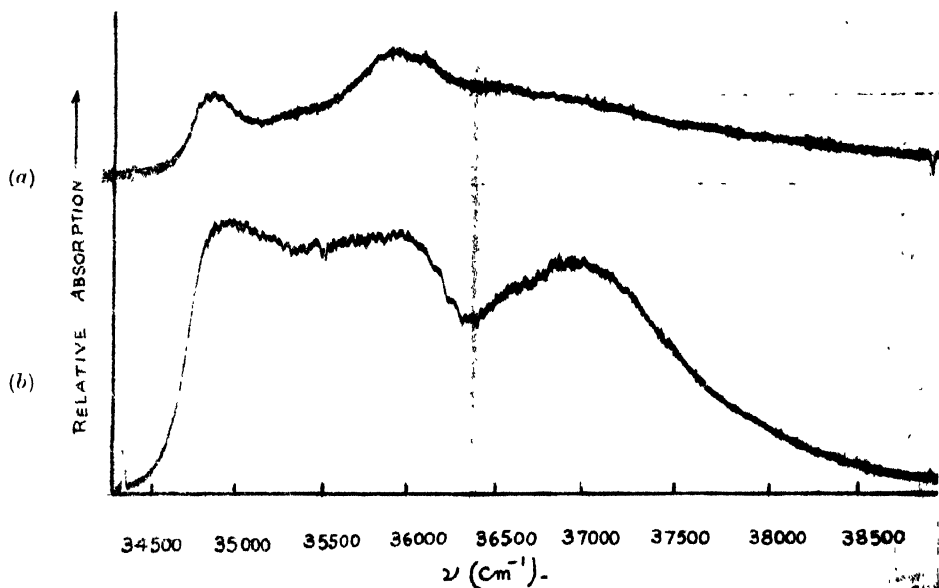


Fig. 1. Microphotometric records of the ultraviolet absorption spectra of ortho tolunitrile.
Curve (a) Solid at -180°C , Curve (b) Liquid at 32°C

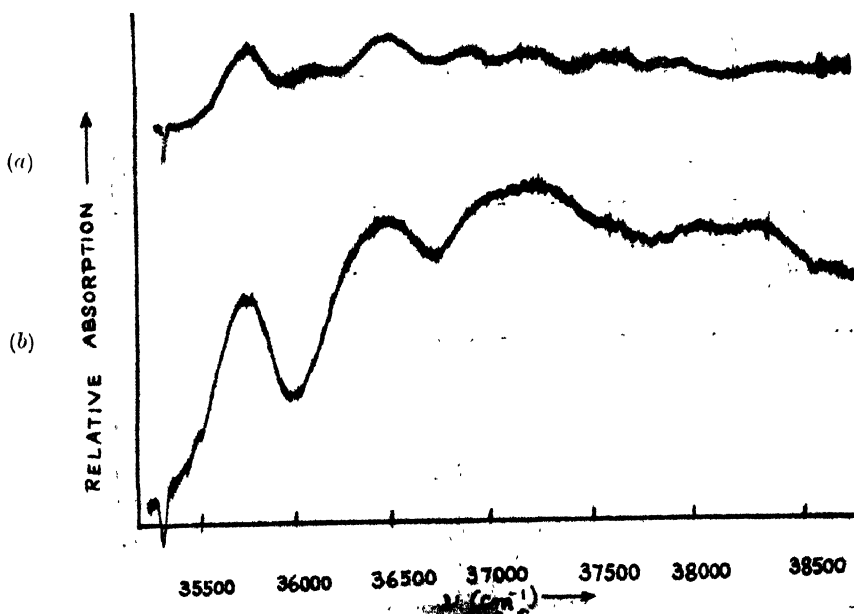


Fig. 2. Microphotometric records of the ultraviolet absorption spectra of para tolunitrile.
Curve (a) Solid at -180°C , Curve (b) Liquid at 34°C

Tables I, II, III, IV with approximate relative intensities given as strong, medium, etc. indicated by s, m, etc.

TABLE I

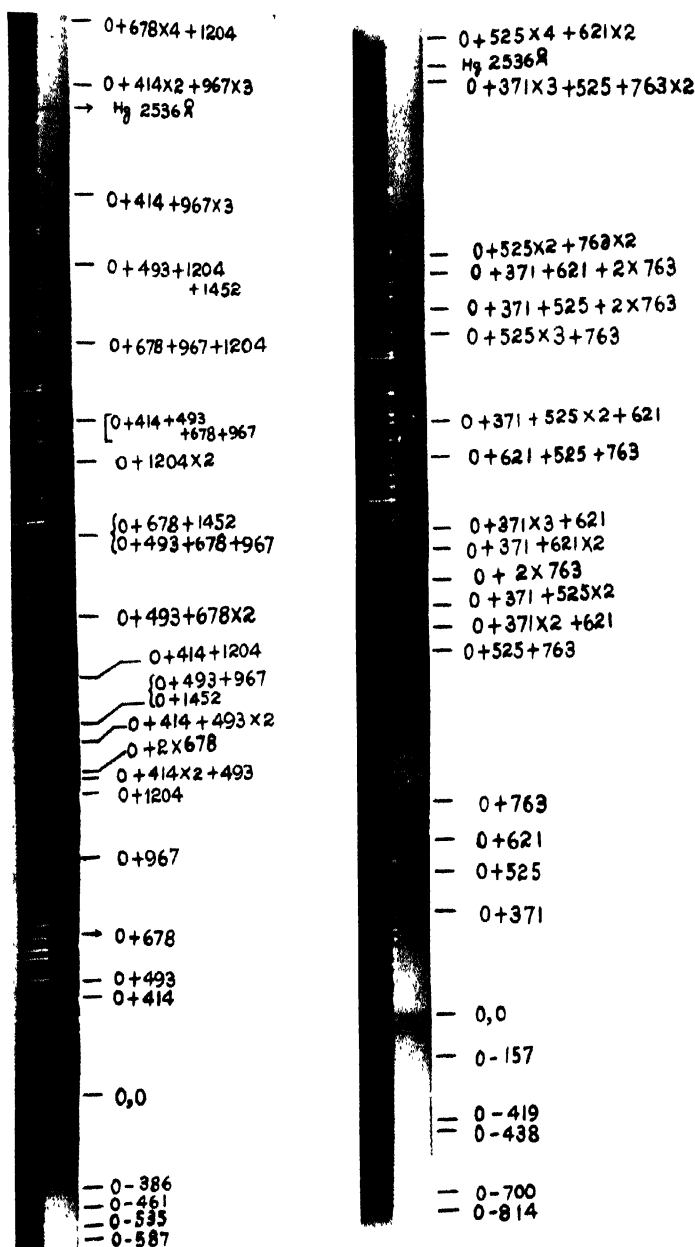
Absorption bands of ortho tolunitrile ($\text{CH}_3\text{C}_6\text{H}_4\text{CN}$) in the vapour state (prominent bands)

Wave no. in cm^{-1}	Difference from 0,0 band	Assignment	Wave no. in cm^{-1}	Difference from 0,0 band	Assignment
35193 (w)	-587	0-587	37232(ms)	1452	0+1452 0+493+967
35245(w)	-535	0-535	37397(ms)	1617	0+414+1204
35319(w)	-461	0-461	37632(ms)	1852	0+493+678 \times 2
35394(w)	-386	0-386			
35780(s)	0	0,0	37924(ms)	2144	0+678+1452 0+493+678+967
36194(s)	414	0+414	38182(ms)	2402	0+1204 \times 2
36273(s)	493	0+493	38346(w)	2566	0+414+493+678 967
36458(s)	678	0+678	38619(w)	2839	0+678+967+1204
36747(s)	967	0+967	38914(w)	3134	0+493+1204+1452
36984(s)	1204	0+1204	39107(w)	3327	0+414+967 \times 3
37090(ms)	1310	0+414 \times 2+493	39513(w)	3733	0+414 \times 2+967 \times 3
37125(ms)	1345	0+2 \times 678	39702(w)	3922	0+678 \times 4+1204
37191 (ms)	1411	0+414+493 \times 2			

TABLE II

Absorption bands of ortho tolunitrile in the liquid and solid states.

Liquid at 32°C			Solid at -180°C		
Wave No. cm^{-1}	Difference from 0,0 band	Assignment	Wave No. cm^{-1}	Difference from 0,0 band	Assignment
35055(s) (broad)	0	0,0	34841(s)	0	0,0
35693(ms) (broad)	638	0+638	35400(W)	559	0+559
36100(s) (broad)	1045	0+1045	35983(s)	1142	0+1142
			36552(w) (broad)	1711	0+559+1142
36726(ms) (broad)	1671	0+638+1045	37114(w) (broad)	2273	0+1142 \times 2
37136(s) (broad)	2081	0+1045 \times 2			



Ultraviolet absorption spectra

- (a) Ortho-tolunitrile - Vapour at 40°C .
 (b) Para-tolunitrile - Vapour at 40°C

TABLE III

Absorption bands of para tolunitrile ($\text{CH}_3\text{C}_6\text{H}_4\text{CN}$) in the vapour state
(prominent bands)

Wave no. in cm^{-1}	Difference from 0,0 band	Assignment	Wave no. in cm	Difference from 0,0 band	Assignment
35394(w)	-814	0-814	37814(ms)	1606	0 + 371 + 621 \times 2
35508(w)	-700	0-700	37917(ms)	1709	0 + 371 \times 3 + 621
35770(w)	-438	0-438	38133(ms)	1925	0 + 621 + 526 + 763
35789(w)	-419	0-419	38247(ms)	2039	0 + 371 + 525 \times 2 + 621
36051(w)	-157	0-157	38531(ms)	2323	0 + 525 \times 3 + 763
36208(s)	0	0,0	38613(ms)	2405	0 + 371 + 525 + 2 \times 763
36579(s)	371	0 + 371	38732(ms)	2524	0 + 371 + 621 + 2 \times 763
36733(s)	525	0 + 525	38790(w)	2582	0 + 525 \times 2 + 763 \times 2
36829(s)	621	0 + 621	39373(w)	3165	0 + 371 \times 3 + 525 + 763 \times 2
36971(s)	763	0 + 763	39535(w)	3327	0 + 525 \times 4 + 621 \times 2
37492(ms)	1284	0 + 525 + 763			
37558(ms)	1350	0 + 371 \times 2 + 621			
37628(ms)	1420	0 + 371 + 525 \times 2			
37738(ms)	1530	0 + 763 \times 2			

TABLE IV

Absorption bands of para tolunitrile ($\text{CH}_3\text{C}_6\text{H}_4\text{CN}$) in the liquid and solid
states

Liquid at 32°C			Solid at -180°C		
Wave No. cm^{-1}	Difference from 0,0 band	Assignment	Wave No. cm^{-1}	Difference from 0,0 band	Assignment
35771(s) (broad)	0	0,0	35752(s)	0	0,0
36513(s) (broad)	742	0 + 742	36123(w)	371	0 + 371
36953(s) (broad)	1182	0 + 1182	36492(s)	740	0 + 740
37245(s) (broad)	1574	0 + 2 \times 742	36948(ms)	1196	0 + 1196
37684(w)	1913	0 + 742 + 1182	37232(ms)	1480	0 + 740 \times 2
38133(w)	2362	0 + 1182 \times 2	37612(ms)	1860	0 + 371 + 740 \times 2
38445(w)	2674	0 + 2 \times 742 + 1182	37696(ms)	1944	0 + 740 + 1196
			37962(w)	2210	0 + 740 \times 3
			38339(w)	2587	0 + 371 + 740 \times 3

DISCUSSION

o-Tolunitrile—

Ultraviolet absorption bands of *o*-tolunitrile in the vapour state were reported by Acly (1928) and assignments of the bands made by him according to the following two series

$$\text{Series I} - 35769 + (p' - p_0) 970 - 50p_0 + (q' - q_0) 300$$

$$\text{Series II} - 35545 + (p' - p_0) 970 - 50p_0 + (q' - q_0) 300 + (r' - r_0) 715$$

In the present investigation, the intense band at 35780 cm^{-1} is taken as the 0,0 band. On the longer wave length side of this band there are some feeble bands which can be assigned as 0—386, 0—461, 0—535, 0—587, the corresponding frequencies of the Raman spectra of the liquid (Magat, 1936) being 385 cm^{-1} , 457 cm^{-1} , 541 cm^{-1} , 591 cm^{-1} . There are however strong companions on the red side and in the immediate neighbourhood of some of the main band heads. These are probably due to $v \rightarrow v$ transitions. Progressions of excited state frequencies 414, 493, 678, 967 and 1204 cm^{-1} have been observed. An alternative assignment of some of the bands has also been made showing 1452 cm^{-1} as an excited state vibration frequency. This frequency has been observed in the case of *p*-dichlorobenzene by Anno and Matubara (1955).

In the liquid state five bands have been found, the 0, 0 band being at 35055 cm^{-1} . The rest of the bands represent progressions of excited state frequencies 638 cm^{-1} , 1045 cm^{-1} and their combination and harmonics. It is found that 0, 0 band shifts towards longer wavelength side by 725 cm^{-1} with the liquefaction of vapour. Such a shift may be explained on the supposition that strong intermolecular field acting on the molecules in the liquid lowers the excited electronic energy state. The broadness of the bands in the liquid state may be due to fluctuation of the intermolecular field caused by thermal motion of molecules. Three bands in solution have been reported by Purvis (1915) at 35078 cm^{-1} , 35960 cm^{-1} and 37026 cm^{-1} . The first band seems to have shifted very slightly towards the shorter wavelength side from the position of the 0, 0 band in the liquid state. This shows that intermolecular field in the solvent has the same influence on the energy state as that in the case of pure liquid. Frequency differences 882 cm^{-1} , 1948 cm^{-1} observed in the case of the solution are not observed in the case of the vapour or the pure liquid. The excited state vibration frequencies 638 cm^{-1} and 1045 cm^{-1} observed in the case of pure liquid do not agree with those observed in the case of the vapour. When the liquid is solidified and cooled to -180°C the 0, 0 band shifts to 34841 cm^{-1} and progressions of excited state vibration frequencies 559 cm^{-1} and 1142 cm^{-1} are observed. These frequencies again are different from those observed in the case of either the vapour or the liquid. These changes in the excited state vibration frequencies with change of state clearly indicate the influence of intermolecular field on the excited state vibrational energy levels. The changes observed in these frequencies with

solidification further show that when the molecules are oriented regularly in the crystal, the intermolecular field is quite different from that experienced by the molecule in the liquid state.

When these results are compared to those due to chlorotoluenes (Swamy, 1952) it is found that the splitting up of the energy levels with solidification observed in the case of chlorotoluenes does not take place in the case of tolunitriles. Also the shift of the 0, 0 band with solidification is towards the longer wavelength side in the present case but in the case of chlorotoluenes or bromotoluenes the shift is towards the shorter wavelength side. Thus the group $C\equiv N$ as a substituent has an influence on the energy levels in the excited state which is different from that observed in the case of a halogen atom used as the substituent. These latter atoms seem to bring a drastic change in the energy level in the solid state at low temperatures.

p-Tolunitrile—

The ultraviolet absorption bands of *p*-tolunitrile in the vapour state were reported by Acly (1928) and the bands assigned according to the following two series:

$$\text{Series I} - 36755 + (p' - p_0)765 - 28 p_0 + (q' - q_0)128$$

$$\text{Series II} - 37102 + (p' - p_0)765 - 28 p_0 + (q' - q_0)128$$

Hence in Series I he took 36755 cm^{-1} as the frequency of the 0,0 band. It is observed in the present investigation, however, that there is a band at 36208 cm^{-1} which is not much weaker than the band at 36733 cm^{-1} and the frequency difference is 525 cm^{-1} . If the latter band were taken as the 0,0 band the former would have to be assigned as 0-525 but the population of molecules in excited vibrational state of this frequency cannot be so high. So the band at 36208 cm^{-1} has been taken as the 0,0 band. Some feeble bands observed on the longer wavelength side of the 0,0 band can be assigned as 0-157, 0-438, 0-419, 0-700, 0-814. These correspond to the frequency shifts of 161, 437, 410, 705, 819 cm^{-1} found in the Raman spectra of *p*-tolunitrile (Magat, 1936).

In the liquid state seven broad bands, with the 0,0 band at 35771 cm^{-1} , are given by the substance. The 0,0 band is found to have shifted towards longer wavelength side by 437 cm^{-1} on the liquefaction of vapour. The rest of the bands can be assigned to transitions with progressions of vibration frequencies of 742 cm^{-1} and 1182 cm^{-1} . The shift in the 0,0 band and change in the excited state vibrational frequencies taking place with liquefaction may be due to association of molecules through virtual bands in the liquid. Purvis (1915) studied the absorption spectrum of solution of the substance and reported three bands at 35831 cm^{-1} , 36619 cm^{-1} and 36889 cm^{-1} respectively which can be assigned to frequencies 788 cm^{-1} and 1058 cm^{-1} . The 0,0 band in solution appears to have shifted slightly towards shorter wavelength side from the position of the 0,0 band due to the pure liquid. The excited state vibration frequencies are thus entirely dependent

on the intermolecular field. In the solid state at -180°C the substance yields nine sharp bands with the 0,0 band at 35752 cm^{-1} . This band shifts slightly towards longer side with solidification. The other bands can be assigned to transitions involving excited state vibration frequencies 371 cm^{-1} , 740 cm^{-1} , 1196 cm^{-1} and their combination and harmonics. It is interesting to note that the frequency of 371 cm^{-1} found in the vapour state which persists even in the case of the solid, is absent in the spectrum due to the liquid phase but it appears in the case of the solid.

It is evident from a comparison of the absorption spectra of ortho and para tolunitrile in different states that in both the cases the major change in the 0,0 band takes place with the liquefaction of vapours and the band shifts to longer wavelength side. When the liquids are frozen, the band shifts further towards longer wavelengths in the case of the ortho compound but practically no such change takes place in the case of the para compound. The larger dipole moment of the former molecules is responsible for the shift with solidification.

ACKNOWLEDGMENT

The author is indebted to Professor S. C. Sirkar, D.Sc., F.N.I., for his kind interest and guidance throughout the progress of the work and to Government of India, Ministry of Scientific Research for the sanction of a scholarship.

REFERENCES

- Aclý, H. E., 1928, *Z. Physik Chem.*, **135**, 251.
Anno, Toshinobu and Matubara Ikuo, 1955, *J. Chem. Phys.*, **23**, 796.
Magat, M., 1936, Numerical data on Raman Effect.
Purvis, J. E., 1915, *J. Chem. Soc. (London)*, **107**, 501.
Swamy, H. N., 1951, *Ind. J. Phys.*, **25**, 261.
Swamy, H. N. 1952b, *Ind. J. Phys.*, **26**, 233.
Swamy, H. N., 1952c, *Ind. J. Phys.*, **26**, 445.
Swamy, H. N., 1953, *Ind. J. Phys.*, **27**, 55.
Swamy, H. N., 1953, *Ind. J. Phys.*, **27**, 119.

EFFECT OF HYPO CONCENTRATION ON THE CLEARING TIME OF THICK EMULSIONS

By YOG PRAKASH

DEPARTMENT OF PHYSICS, MUSLIM UNIVERSITY, ALIGARH

(Received for publication, March 7, 1955; received after revision, August 8, 1955)

ABSTRACT. The variation in clearing time for different concentrations of hypo has been studied for emulsion plates of thickness, 50, 100, 200 and 400 microns at two different temperatures. A tentative explanation has been sought by considering the various effects on the diffusion velocity of hypo. The results indicate that 35% is the optimum value of Hypo concentration as the clearing time for these plates.

The use of nuclear emulsions as a tool for the detection of nuclear particles has acquired increasing importance in recent years. The processing of thick emulsion plates is an important factor in the use of this technique. Sheppard, Elliot and Sweet (1923) and others have shown that at a given temperature the clearing times depend on the concentration of sodium thiosulphate (hypo) in a typical manner. There is a sharp decrease in the clearing time for lower concentration and a rapid increase at higher concentrations. This effect is more pronounced at low temperatures. Their work, however, was confined to only thin emulsions. In view of the fact that no similar study in the case of thick emulsions seems to have been reported, and that various workers have used different hypo concentrations viz., 30% by Wilson and Vaneslow (1948), 40% by Dainton, Gattikar and Lock (1951), Stiller *et al* (1954), 28-30% by Dixit (1952 and 1954), it was considered worthwhile to make a systematic analysis of the effect of hypo concentration on the clearing times for thick emulsion plates.

Plates of 50, 100, 200 & 400 micron thicknesses have been tried. Extra pure quality of sodium thio sulphate was used and the temperatures were controlled in a thermostatically controlled cooling cabinet. Equal sizes of emulsion plates were placed directly without any prior development in equal amounts of hypo solutions. No agitation was given to the solutions in the fixing process except that caused by convection currents produced by the slow variation of the temperatures. The two temperatures employed in this study were $(9 \pm 1)^{\circ}\text{C}$ and $(15 \pm 1)^{\circ}\text{C}$.

The cruves of figure 1 show the dependence of clearing time on hypo concentrations for various thicknesses. The clearing time means the time at which the last grain of silver halide gets dissolved, i.e., point at which fixing rate is

negligible as seen with the eyes. Curves A are for temperature $(9 \pm 1)^\circ\text{C}$ and B for $(15 \pm 1)^\circ\text{C}$.

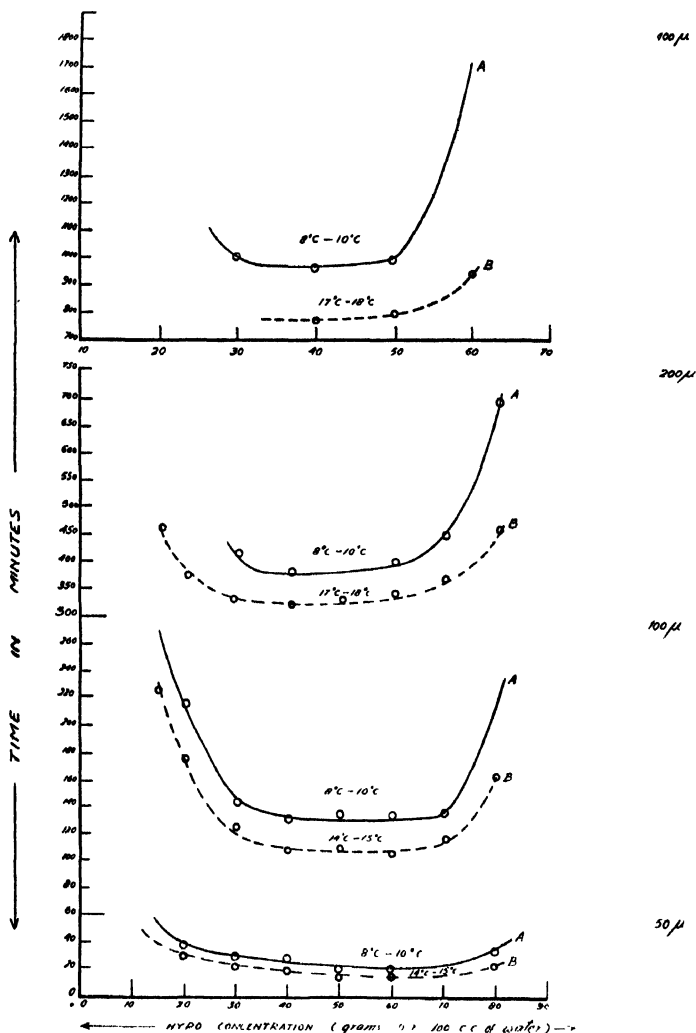


Fig. 1. The variation of clearing time (in minutes) with the hypo concentration (gms per 100 c.c. of water) for different thicknesses of emulsions—50 100, 200 and 400 microns. Curves A and B show the variations for each thickness at temperatures $(9 \pm 1)^\circ\text{C}$ and $(15 \pm 1)^\circ\text{C}$ respectively.

The curves for various thicknesses of emulsions have more or less similar shapes, which resemble those given for thin emulsions by Sheppard *et al.* At lower concentrations the clearing times show a steep fall and again a steep rise at higher concentrations. In between these concentrations the clearing time is practically constant. Both curves A and B show a similar type of behaviour, but the rise in curves B is not so steep as in curves A. Moreover, at a given

concentration the clearing time decreases with increase in temperature. This is in accordance with what has been given for thin emulsions.

Although the reasons for this type of variation in clearing time have not been established with certainty, Sheppard and Mees (Mees, 1923) investigated the rate of dissolution of AgBr in a solution of sodium thiosulphate (hypo). They have shown that the rate is controlled by diffusion process. This rate of diffusion can be shown by ordinary diffusion formula, viz.,

$$\frac{dx}{dt} = S.D. \frac{d\alpha}{d\delta}$$

where $\frac{dx}{dt}$ is the rate of diffusion of hypo, S is surface area, D , the diffusion coefficient and $\frac{d\alpha}{d\delta}$ shows the concentration gradient.

According to Noyes and Whitney (1897), when any crystal gets dissolved in a solvent, the interface between the solution and the crystal is saturated at any given time and the only factor determining the rate of dissolution of crystal is the velocity with which the saturated solution is able to diffuse from the interface into the interior of the solution. Similarly, if the rate of formation of silver thiosulphate complex ion is large in comparison to the rate of diffusion the thiosulphate is used up practically as soon as it reaches the surface of silver halide grain and the concentration at the interface is practically zero. Therefore, when the concentration of hypo in bulk solution and at the interface between emulsion and solution is constant the concentration gradient will also be constant, being proportionate to the inverse of the distance (d) below the surface of the emulsion. Thus the rate of fixation will be equal to the rate of diffusion and can be given as :—

$$\frac{dx}{dt} = \frac{k(a-x)}{d} D S \quad \dots (1)$$

where S is the surface area, D is diffusion coefficient, K is a constant of proportionality, d is the diffusion path, a is initial hypo concentration, and x represents the solid (silver halide) dissolved in time t . When a becomes too large as compared to x , equation (1) reduces to :—

$$\begin{aligned} \frac{dx}{dt} &= \frac{k a D S}{d} \quad \dots (2) \\ &= \text{constant} \end{aligned}$$

As a increases $\frac{dx}{dt}$ will increase and tend to become constant. This increase in salt concentration will depress the swelling and thereby decrease the diffusion

velocity. The balance in two opposing factors brings about the constant region. At still higher concentrations of hypo the reduction in diffusion velocity due to depression in swelling, is predominant over mass action and the clear in time increases.

As seen from the curves, the constant region tends to become smaller for thicker emulsions. It is interesting to note that a similar decrease of the constant region occurs as the temperature falls. The lowering of the temperature affects the hardening of the emulsion in the same manner as the increase in salt, and consequently the depression in diffusion velocity is increased, which disturbs the balance in two opposing factors. This causes the steep rise to begin at lower concentrations than would be the case at higher temperature. A similar tentative explanation can be sought for thick emulsions. The thicker emulsions have more gelatin which will affect the balance due to greater depression in swelling in a way similar to that of temperature. It is possible that greater viscous forces may also be playing some part in this decrease of diffusion velocity

(as the diffusion coefficient $D = \frac{RT}{N} \frac{1}{6 r \pi \eta}$ where R is gas constant, T is temperature, N is Avogadro's number, r is the radius of silver halide grain, and η is viscosity). Due to the decrease in diffusion velocity the beginning of constant region will occur at higher concentration as the thickness of the emulsion is increased. Other factors, such as agitation, presence of other salts, nature of emulsion etc., have their usual effects on the clearing time of thick emulsion plates.

These results indicate that 35% is the optimum value of hypo concentration which should be used for the clearing of emulsion plates of above mentioned thicknesses.

ACKNOWLEDGMENT

The author is indebted to Prof. P. S. Gill for his kind guidance and constant encouragement, and wishes to thank the Government of India for providing a scholarship, which enabled him to carry out these studies. The help of Messrs I. S. Agre and I. S. Mittra in carrying out this investigation is acknowledged.

REFERENCES

- Dainton, Gattikar and Lock, 1951, *Phil. Mag.*, **42**, 396.
- Dixit, K. R., 1952, *Jour. Sc. & Ind. Research IIB* No. 9, 351.
- Dixit, K. R., 1954, *Science et Indus. Photo* (in French), Jan.
- Mees, K., 1923, *Photographic Theory*, p. 518.
- Sheppard, et al., 1923, *J. Frank Inst.*, **196**, 45.
- Stillier, et al., 1954, *Rev. Sc. Instr.*, **25**, 340.
- Wilson and Vaneslow, 1948, *Phy. Rev.*, **75**, 1144.

STRING UNDER THE ACTION OF A PLANE RUBBER WHEEL

By H. G. MANE

DEPARTMENT OF PHYSICS, M. N. COLLEGE, VISNAGAR, (N.G.)

(Received for publication, February 25, 1955)

ABSTRACT. A string of cat-gut is excited by a plane rubber wheel—a wheel having no teeth along the circumference—and the vibrations of the string are recorded by using a vibroscope. It is observed that the vibrations of any point of the string consist of a two-step zig-zag curve and that they are identical with those of the bow.

INTRODUCTION

It was shown long ago by Helmholtz that in a stretched string, set into vibrations by bowing in a suitable manner not far from one end, the vibrations of any point consist of a two-step zig-zag curve. He further observed that the times occupied in the up and down movements represented by the zig-zag curve are to one another in the ratio of the two sections of the string lying on either side of the observed point. In the present investigations a string is excited by using a plane rubber wheel. The wheel is set into uniform rotation and the vibrations of a point of the string are recorded by using a vibroscope. The apparatus used for these investigations is the one specially designed and prepared to investigate the motion of a string excited by a toothed rubber wheel (Mane and Biswas, 1943). It is observed that these vibrations consist of a twostep zig-zag curve and are identical with those of the bow.

EXPERIMENTAL

Details of the apparatus used are given in the paper published by Mane and Biswas (1943).

Part I :—A thin string of cat gut is held tight in the two jaws fixed to the vertical stands. A plane rubber wheel is mounted on the axle and is set into rotation by using a low horse power motor. The speed of rotation is adjusted by the rheostat till the vibrations of the string are well maintained. The pressure of the wheel on the string is adjusted by the tilting screw of the platform carrying the wheel and the axle. A loaded photographic plate is allowed to slide in the vibroscope and the vibrations of the string are recorded in the usual manner. The shutters of the vibroscope are arranged to form a fine slit just behind the point of the string whose motion is to be recorded. The slit is strongly illuminated by an arc lamp and a condensing lens. In this way the vibrations of

different points of the string are recorded. These vibrations consist of a two-step zig-zag curve.

Part II :—The stand carrying the wheel and the axle is removed and the string is excited by a bow in the usual manner. The motion of different points of the string is recorded as usual by using the same vibroscope.

The records of the motion of the different points of the string obtained in both the cases are examined under a travelling microscope and the ratio of the times occupied in the upward and downward movements represented by the zig-zag curves is calculated in each case. These ratios are given against the photographs in the accompanying plates.

CONCLUSION

The photographs obtained in the two parts of the experiment show that :—

1. The action of the bow and the action of the plane wheel are the same. A plane wheel can be considered as an infinite bow. In the case of a bow the point of the string under the bow is carried forward with the bow till the restoring force exceeds the frictional force when it slips and begins to move in the downward direction. It is again caught by the bow and the process is repeated. The same action takes place in the case of a plane wheel. The point of the string under the wheel is carried forward with the wheel till the restoring force exceeds the frictional force between the wheel and the string when it slips and begins to move in the downward direction. It is again caught by the wheel and the motion is repeated.

2. The motion of any point of the string consists of a two-step zig-zag curve and that the times occupied in the up and down movements represented by the zig-zag curve are to one another in the ratio of the two sections of the string lying on opposite sides of the observed point, that is, it obeys the Helmholtzian law.

ACKNOWLEDGMENT

The author takes this opportunity to express his grateful thanks to Late Prof. B. N. Biswas, Head of the Department of Physics, Rajaram College Kolhapur, for the keen interest in these investigations.

REFERENCES

- Biswas B. N., *Jour. of Ind. Math. Soc.*, Vol. 18, 1930.
Mane H. G. and Biswas, B. N., 1943, *Ind. J. Phys.*, 17, 97.

TABLE I
Length of the string, 60 cms.



















Ser. No	Struck point dist. from one end	Observed point dist. from other end	Vibration photographs (Plane wheel)	Ratio of times
1	7.5 cm	30 cm		1.91
2	8.6 cm	30 cm		1.03
3	7.5 cm	25 cm		1.29
4	8.6 cm	25 cm		1.22
5	10 cm	25 cm		1.35
6	6.7 cm	20 cm		1.95
7	7.5 cm	20 cm		1.95
8	8.6 cm	20 cm		1.77
9	10 cm	20 cm		1.91

TABLE II

Length of the string 60 cms.

Sr. No.	Struck point dist. from one end	Observed point dist. from other end	Vibration photographs (bow)	Ratio of times
1	7.5 cm	30 cm		1.06
2	8.6 cm	30 cm		1.08
3	7.5 cm	25 cm		1.36
4	8.6 cm	25 cm		1.30
5	10 cm	25 cm		1.34
6	6.7 cm	20 cm		2.09
7	7.5 cm	20 cm		1.91
8	8.6 cm	20 cm		1.79
9	10 cm	20 cm		1.81

ULTRASONIC VELOCITY IN ZINC AND MAGNESIUM SULPHATE SOLUTIONS AT DIFFERENT CONCENTRATIONS AND TEMPERATURES

BY BRAJA SUNDAR MOHANTY AND BIBHUTI BHUSAN DEO

DEPARTMENT OF PHYSICS, RAVENSHAW COLLEGE, CUTTACK.

(Received for publication, September 27, 1955)

ABSTRACT. Ultrasonic velocity in zinc and magnesium sulphate solutions have been measured over a concentration range 0.05 to 0.5 molar (m) and over a temperature range 25°C to 45°C. The values of adiabatic compressibilities have been computed.

INTRODUCTION

Data on ultrasonic velocities and compressibilities of electrolytes are being widely reviewed by several authors. There are few recent attempts at their experimental determination. The turbulent state of affairs, as regards a consistent theory for electrolytes, has been stressed in a survey of electrolytical applications of ultrasonic waves (C) velocity measurements by Ernest Yeager and Frank Hovorka in 1953. So the authors plan to determine the ultrasonic velocities in abnormal electrolytes at different temperatures and concentrations. Since the acoustics of bivalent sulphates have recently gained physico-chemical interest, the sulphates of zinc and magnesium have been studied first.

EXPERIMENTAL METHOD

The velocities were determined by the usual method of photographing the Debye-Searer's diffraction spectra. The working equation for velocity is $V = nf\lambda/d$, where n is the ultrasonic frequency, f , the distance of telescope lens from photographic plate; d , the distance of first order spectra from the central line and λ is the wavelength (5893 A.U.) of light used.

An one inch square X-cut quartz crystal of fundamental frequency of about one mega cycle was excited to give its 13th. and 15th. harmonics by a high frequency oscillator operated by a stabilised power supply. The frequencies were measured by a recalibrated Wen-type frequencymeter.

Light from a sodium arc rendered parallel by a collimating lens was allowed to pass at right angles to the ultrasonic beam. To improve accuracy the telescope was fitted with an achromatic lens of about 100 cm focal length. The exact distance f was determined by using a coarse grating of known number of lines per centimetre, and photographing the normal diffraction spectra. The number of lines in the coarse grating was so chosen that the separation of optical diffraction spectra was of the same order as the ultrasonic pattern. This eliminates the approximation $\sin \theta = \theta$. The value of f thus determined was 100.66 cm.

The cell containing the solution was surrounded by a large water bath which could be heated by immersion heater and cooled by ice while continuous stirring was maintained prior to exposure. The time of exposure was always less than 45 seconds during which the temperature of the solution was constant to within ± 0.05 C. The accuracy of this experiment was confirmed by comparing our values with the best known values of ultrasonic velocities for water from 25° to 45°C and they agree to ± 1 m/s.

Both the sulphate solutions were prepared at the room temperature; MgSO_4 was G. R., E. Merck sample and ZnSO_4 , Annalar, B. D. H. As to the overall accuracy of measurement for solutions our values for magnesium sulphate at 30°C agree with Weissler and Del Grasso's (1951) extrapolated values (determined by interferometric method) to within ± 1 metre/sec.

TABLE I

Velocity in and adiabatic compressibility of zinc sulphate.

Temp. in °C	concentration	Velocity metres/sec.	Density gm./c.c.	$\beta \times 10^{12}$
25	0.0	1497.0	0.99707	44.75
	0.1	1501.3	1.0052	44.14
	0.2	1506.8	1.0135	43.46
	0.4	1516.6	1.0297	42.22
	0.6	1525.5	1.0451	41.12
	0.8	1531.4	1.0615	40.17
	1.0	1540.5	1.0772	39.12
30	0.0	1509.0	0.99567	4.11
	0.1	1513.7	1.0035	43.49
	0.2	1518.3	1.0119	42.86
	0.4	1528.0	1.0281	41.66
	0.6	1533.6	1.0442	40.72
	0.8	1541.0	1.0600	39.73
	1.0	1551.5	1.0755	38.63
35	0.0	1521.0	0.99406	43.48
	0.1	1527.7	1.0020	42.76
	0.2	1530.9	1.0015	42.22
	0.4	1536.7	1.0264	41.26
	0.6	1543.1	1.0423	40.29
	0.8	1550.6	1.0582	39.30
	1.0	1558.5	1.0737	38.34
40	0.0	1531.0	0.99224	43.00
	0.1	1536.0	1.0005	42.36
	0.2	1539.5	1.0085	41.84
	0.4	1545.0	1.0245	40.89
	0.6	1533.8	1.0405	39.80
	0.8	1558.0	1.0561	39.01
	1.0	1564.4	1.0716	38.13
45	0.0	1538.0	0.99024	42.69
	0.1	1541.5	0.9983	42.15
	0.2	1548.0	1.0062	41.47
	0.4	1552.0	1.0225	40.60
	0.6	1652.3	1.0382	39.46
	0.8	1564.6	1.0538	38.76
	1.0	1569.4	1.0695	37.96

TABLE II

Velocity in and compressibility of magnesium sulphate solution.

Temp. in °C	Concentration (2m)	Velocity m/s	Density gm./c.c.	$\beta \times 10^{12}$
25	0.10	1504.6	1.0030	44.04
	0.25	1514.3	1.0120	43.09
	0.50	1531.0	1.0266	41.56
	0.75	1547.5	1.0412	40.11
	1.00	1562.0	1.0555	38.83
30	0.10	1516.0	1.0015	43.33
	0.25	1528.0	1.0105	42.38
	0.50	1542.0	1.0252	41.02
	0.75	1558.0	1.0397	39.62
	1.00	1572.5	1.0538	38.38
35	0.10	1528.0	1.0000	42.83
	0.25	1536.8	1.0090	41.96
	0.50	1550.4	1.0235	40.65
	0.75	1567.5	1.0380	39.21
	1.00	1581.0	1.0520	38.03
40	0.10	1537.4	0.9983	42.38
	0.25	1545.5	1.0072	41.57
	0.50	1558.0	1.0217	40.32
	0.75	1576.0	1.0362	38.85
	1.00	1588.5	1.0502	37.73
45	0.10	1543.5	0.9963	42.13
	0.25	1553.5	1.0052	41.22
	0.50	1565.3	1.0197	40.02
	0.75	1581.5	1.0342	38.66
	1.00	1595.0	1.0484	37.49

RESULTS AND DISCUSSIONS

The results obtained are contained in the preceding Tables. The values of the densities at different temperatures and concentrations were computed from the data given in the International Critical tables, Vol. III. The adiabatic

compressibility (β) was calculated from the equation $\beta = 1/v^2\rho$, where ρ is the density. Plotting a graph it was found that both velocity and adiabatic compressibility vary linearly with concentration at all temperatures for both solutions.

ACKNOWLEDGMENT

The authors take great pleasure in recording their thanks to Dr. A. K. Dutta, D.Sc., F.N.I., for his interest in the work.

REFERENCES

- Yonger E. and Hovorka, F. 1953, *J. Acoust. Soc. Am.*, **25**, 443.
Weissler and Del Grasso, 1951, *J. Acoust. Soc. Am.* **23**, 219.

ON THE ABSORPTION OF 3.18 CM MICROWAVES IN SOME SUBSTITUTED PHENOLS IN THE LIQUID STATE*

By DILIP KUMAR GHOSH

OPTICS DEPARTMENT, INDIAN ASSOCIATION FOR THE CULTIVATION OF SCIENCE,
CALCUTTA-32

(Received for publication October, 19, 1955)

ABSTRACT. The absorption of 3.18 cm microwaves in *o*-bromophenol, 2,4,6-trichlorophenol, *o*-methoxy phenol, *p*-cresol and diphenyl ether have been studied for different temperatures of the liquids in continuation of previous investigations. Maximum absorption of 3.18 cm microwaves has been exhibited by *o*-methoxy phenol at 100°C and *p*-cresol at 90°C and the values of the radii of the rotors calculated from Debye's theory indicate that these absorption maxima are due to rotation of the substituent OH group about the C-O bond. *o*-Bromophenol, 2,4,6-trichlorophenol and diphenyl ether did not show any absorption in the 3.18 cm microwave region when the temperature of the liquids were changed from the freezing points to the boiling points. It is pointed out that these three molecules do not show absorption in this region owing to restriction of the rotational freedom of the OH group in the first two cases and absence of such small group as a substituent in the case of diphenyl ether.

INTRODUCTION

From a study of the values of dielectric loss observed in the solution of some substituted benzenes in the metre wave length region Fischer (1949) inferred that orientation of some substituent groups having rotational freedom contributes to dielectric loss in this region. Recently, it was actually observed (Ghosh, 1954*a*, 1954*b*, 1955*a*) that some substituted benzenes such as benzyl chloride, benzyl amine, benzyl alcohol, phenol, cresols etc., show absorption maxima in the microwave region corresponding to rotation of the substituent group about the diameter of the benzene ring passing through the point of substitution. It has also been shown that such molecules exhibit three different discrete values of time of relaxation corresponding to orientation of the single molecule, dimer and the substituent group, and the occurrence of 'effective time of relaxation' postulated by previous workers has been corroborated by these results. Some of the molecules containing OH group as a substituent exhibit absorption peaks in the 3.18 cm microwave

*Communicated by Prof. S. C. Sirkar

region at suitable temperatures, showing the freedom of rotation of the OH group about the C-O bond.

It was observed recently (Ghosh, 1955*b*) however, that in the case of ortho chlorophenol there is no absorption of 3.18 cm waves throughout the temperature range from the freezing point upto the boiling point of the liquid. There are many molecules in which there may be such restriction of rotation of the OH group. The absorption of 3.18 cm microwaves in a few such liquids the molecules of which have other substituents besides the OH group has been investigated at different temperatures to find out whether the rotation of the OH group is restricted in these cases. Again, according to Debye's theory (Debye, 1929) the radius of the rotor depends on τ , the time of relaxation and η , the viscosity of the liquid, and if the same substituent group having a freedom of rotation be present in different molecules, the ratio $\tau T/\eta$ should be constant, T being the absolute temperature of the liquid. It would also be interesting to find out whether the above relation is satisfied in the case of molecules having OH as a substituent. It was thought worthwhile, therefore, to study the absorption of 3.18 cm microwaves in some substituted phenols in order to find out whether the results indicate any hydrogen bonding postulated by Pauling (1939) in some of these molecules.

EXPERIMENTAL

In the present investigation the absorption of 3.18 cm microwaves in *o*-bromophenol, *o*-methoxy phenol, 2, 4, 6-trichlorophenol, *p*-cresol and diphenyl ether have been studied at different temperatures. *o*-Bromophenol and *o*-methoxy phenol were supplied by E. Merck, 2,4,6-trichlorophenol supplied by Scherring-Kahlbaum, and *p*-cresol and diphenyl ether were supplied by B.D.H. The liquids studied were all of chemically pure quality. They were all distilled in vacuum after proper dehydration. The experimental arrangement in the present investigation was the same as that reported previously (Ghosh, 1953, 1954*a*).

RESULTS

The absorption curves for *o*-methoxy phenol and *p*-cresol are given in figures 1 and 2. Ortho bromophenol, 2,4,6-trichlorophenol and diphenyl ether showed no absorption at all in the 3.18 cm microwave region when the temperature of the liquids was changed from the boiling point upto the freezing point. The frequencies of absorption peaks observed for the first two liquids, the corresponding temperatures, the values of a and τ calculated from Debye's theory and the different constants involved in the calculation are shown in Table I. The value of a , the radius of the rotor in the case of *o*-methoxy phenol could not be obtained correctly as the value of ϵ_1 could not be measured at different temperatures owing to slight conductivity of the liquid. For approximate calculation the value of

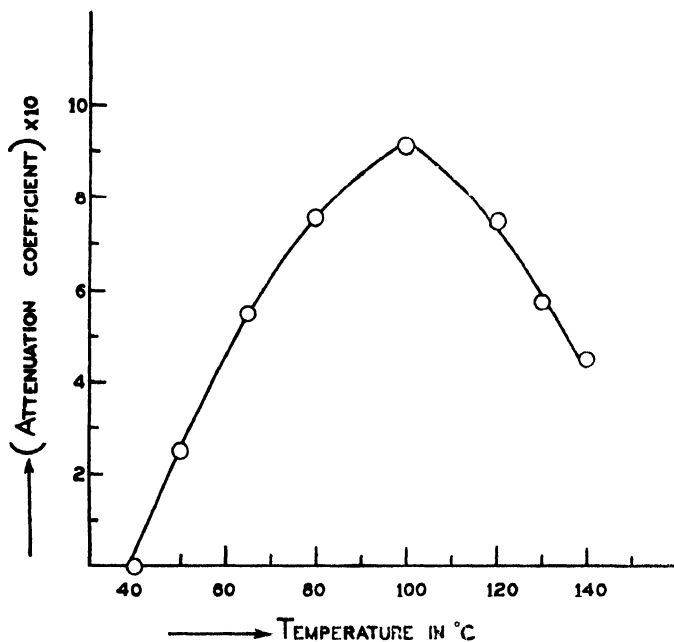


Fig. 1. *o*-Methoxy phenol; $f = 9415$ Mc/sec, thickness of the liquid, 1 cm.

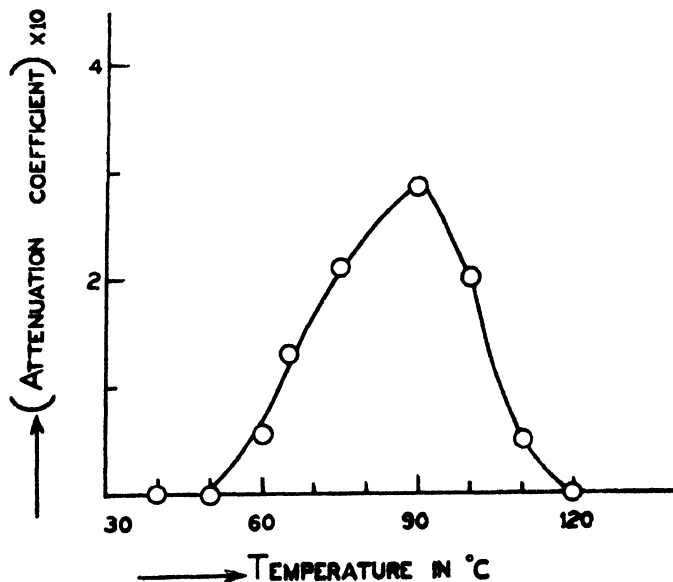


Fig. 2. *p*-Cresol; $f = 9415$ Mc/sec., thickness of the liquid, 1 cm.

ϵ_1 has been taken as 8. The values of the constants as well as of a for *p*-chlorophenol are included in Table I for comparison.

TABLE I

$$\frac{\omega}{2\pi} = 9415 \text{ Mc/sec.}$$

Liquid	T for max. ab- sorption	ϵ_0	ϵ_1	$\tau \times 10^{11}$	$\eta \times 100$	$a \times 10^8 \text{cm}$
<i>p</i> -Chlorophenol	358	2.43	7.9	1.361	1.4	1.55
<i>p</i> -Cresol	363	2.37	6	1.469	1.6	1.53
<i>o</i> -Methoxy phenol	373	2.37	8 (rough esti- mation)	1.358 (approx.)	.95	1.7 (approx.)

The value of η for *p*-chlorophenol at 85°C was obtained after Frenkel (1946) from the values of viscosity at two different temperatures given in the International Critical Tables. The value of η for *o*-methoxy phenol was taken from the data reported by Friend and Hargreaves (1946). The values of ϵ_1 have been obtained from the table of dielectric constants of pure liquids published by the National Bureau of Standards, United States, Department of Commerce and also from the International Critical Tables. The values of ϵ_0 have been assumed to be equal to n^2 , n being the refractive index at 20°C for sodium D-line. The value of n for *o*-methoxy phenol was not available and it was therefore measured with an Abbe refractometer.

DISCUSSIONS

In the case of *o*-bromophenol no absorption was observed in the 3.18 cm microwave region in the whole temperature range from the melting point to the boiling point. The infrared absorption curves for *o*-bromophenol is similar to those for *o*-chlorophenol as reported by Pauling (1939). The absence of absorption of 3.18 cm microwaves in *o*-bromophenol shows that in this molecule also the hydrogen atom of OH group is attached to the bromine atom as in the case of *o*-chlorophenol (Ghosh, 1955*b*). The total absence of absorption further shows that all the molecules in the liquid are of the *cis* configuration. This further shows that phenol was not present as impurity in the liquid although Rossmy *et al* (1953) suggested that all samples of *o*-bromophenol contains phenol as impurity.

In the case of 2,4,6-trichlorophenol no absorption in the 3.18 cm microwave region has been observed. The two configurations of the 2,4,6-trichlorophenol molecule are equivalent as shown in figure 3. In this case also the OH group

has no freedom of rotation about the C-O bond due to cent percent chelation in both the configurations. The absence of absorption in the microwave region thus

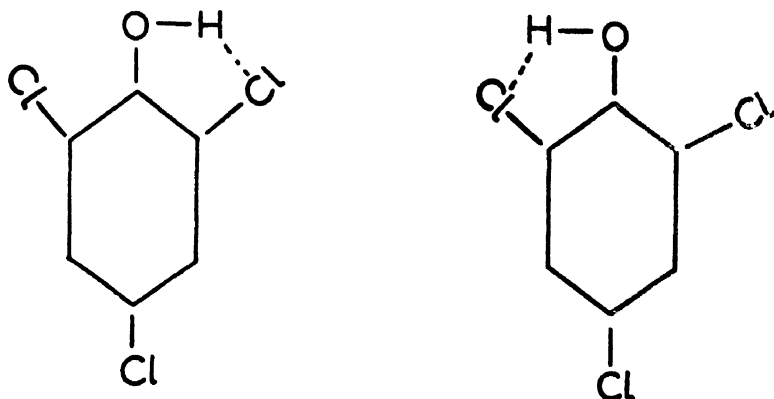


Fig. 3 2,4,6-trichlorophenol.

confirms the configuration of the molecule given in figure 3. Ortho methoxy phenol² showed absorption in whole temperature range from 50° with maximum at 100°C (figure 2). It can be seen from Table I that the approximate value of the radius of the rotor in the case of *o*-methoxy phenol comes out as 1.7 A.U. which is much less than the value for the single molecule. Evidently, the substituent OH is the rotor in this case. In the case of *p*-cresol absorption was indicated in the 3.18cm microwave region in the whole temperature range from 60°C to 120°C with a maximum at 90°C, but the intensity of absorption is very low compared to that in the case of ortho-and meta cresol studied previously (Ghosh, 1954b) The value of the radius of the rotor in this case is 1.53 A.U. and evidently, the OH group is responsible for the absorption in this case also.

The absence of absorption of 3.18 cm microwaves in some of the molecules mentioned above confirms the conclusion drawn earlier that all such molecules in which the OH group has freedom of rotation show absorption in this region at suitable temperatures and when the freedom of rotation is restricted the molecules cease to exhibit absorption in this region.

ACKNOWLEDGMENT

The author expresses his grateful thanks to Prof. S. C. Sirkar, D.Sc., F.N.I., for kindly suggesting the problem and for his constant guidance during the progress of the work.

REFERENCES

- Debye, P., 1929, Polar Molecules, Chemical Catalog Co.
- Fischer, E., 1949, *Z. Naturforsch.*, **4a**, 707.
- Frenkel, J., 1946, Kinetic Theory of Liquids, Oxford, p. 193.
- Friend, J. N., and Hargreaves, W. D., 1946, *Phil. Mag.*, **37**, 120.
- Ghosh, D. K., 1953, *Ind. J. Phys.*, **27**, 511.
- Ghosh, D. K., 1954*a*, *Ind. J. Phys.*, **28** 191.
- Ghosh, D. K. 1954*b*, *Ind. J. Phys.*, **28**, 485.
- Ghosh, D. K., 1955*a*, *Ind. J. Phys.*, **29**, 161.
- Ghosh, D. K., 1955*b*, *Ind. J. Phys.*, **29**, 450.
- Pauling, L., 1939, The Nature of the Chemical bond, Cornell University Press, p. 303.
- Rossmly, G., Luttke, W., and Mecke, R., 1953, *J. Chem. Phys.*, **21**, 1606.

THERMAL CONDUCTIVITY AND FORCE BETWEEN LIKE MOLECULES

By S. C. SAXENA

INDIAN ASSOCIATION FOR THE CULTIVATION OF SCIENCE, CALCUTTA-32.

(Received for publication, November 11, 1955)

ABSTRACT. The Chapman-Enskog kinetic theory of non-uniform gases, as applied to the phenomenon of thermal conductivity, has been utilised to evaluate the intermolecular force constants, by assuming the Lennard-Jones 12 : 6 interaction potential for inert gas molecules. The temperature variation of thermal conductivity gives the force constant ϵ of the Lennard-Jones function, while r_0 is found by actual substitution. To test the adequacy of the model the transport coefficient have been calculated by utilising these potential parameters, and compared with the observed values over an extensive range of temperatures. It is found that the agreement between theory and experiment is quite satisfactory showing thereby the adequacy of the 12 : 6 model and correctness of the values assigned to the force constants. The important quantity $\lambda/\eta c_p$ has been calculated theoretically for various temperatures and pressures and is found to vary only slightly with temperature but considerably with pressure. The Enskog theory of dense gases has been applied to the particular case of argon and the results compared with the observed values.

1. INTRODUCTION

The Chapman-Enskog kinetic theory of gases expresses the transport coefficients in terms of a set of collision integrals which have been evaluated for various empirically chosen potential fields. Amongst these, the Lennard-Jones 12:6 model and the modified Buckingham (Exp-Six) model are the most realistic, though the relative appropriateness of the latter still awaits confirmation. The property most sensitive and hence suitable for the determination of potential parameters is the coefficient of thermal diffusion, but its usefulness is limited owing to the difficulty of obtaining accurate experimental data. The three elementary transport coefficients are almost equally sensitive for the determination of intermolecular field, though viscosity is usually preferred for this purpose in view of the greater accuracy attainable in its experimental determination. Recently, Kammuliik and Carman (1952) have made an accurate determination of the coefficient of thermal conductivity of inert gases over an extensive range of temperatures which are particularly useful in case of Krypton and Xenon where viscosity data are not sufficiently extensive. The aim of the present paper is to utilise the temperature dependence of thermal conductivity to evaluate the force constants, and to test the appropriateness of the Lennard-Jones 12 : 6 model to represent the molecular interactions of rare gases.

2. FORMULAE AND METHOD OF CALCULATION

According to the Lennard-Jones 12 : 6 model, the potential energy of molecular interaction is given by

$$E(r) = 4\varepsilon[(r_0/r)^{-12} - (r_0/r)^6] \quad \dots (1)$$

where r_0 is the separation for which the energy of interaction is zero and ε is the value of the maximum negative energy. From Chapman and Enskog theory the third approximation to the coefficient of thermal conductivity $[\lambda]_3$ of a single gas, as shown by Hirschfelder, Bird and Spotz (1948), can be written in the form

$$[\lambda]_3 \times 10^5 = \frac{2.6693(MT)^{1/2} f_\lambda^2}{r_0^2 \Omega^{(2,2)*}} \cdot \frac{5}{2} C_v \quad \dots (2)$$

Here M is the molecular weight of the gas, T the absolute temperature, C_v the specific heat at constant volume and the quantities f_λ^2 and $\Omega^{(2,2)*}$ are functions of kT/ε and have been tabulated by Hirschfelder, Bird and Spotz (1948). It is convenient to put

$$kT/\varepsilon = T^* \quad \dots (3)$$

where T^* is called the reduced temperature. Making use of the observed dependence of thermal conductivity on temperature, we have developed here the following two simple graphical methods to evaluate the potential parameters.

First Method

A graph of $T^{1/2}/\lambda$ was plotted against T (Fig. 1) to smoothen the data and to test their self-consistency which further gave us a number of additional points for calculation. Now from

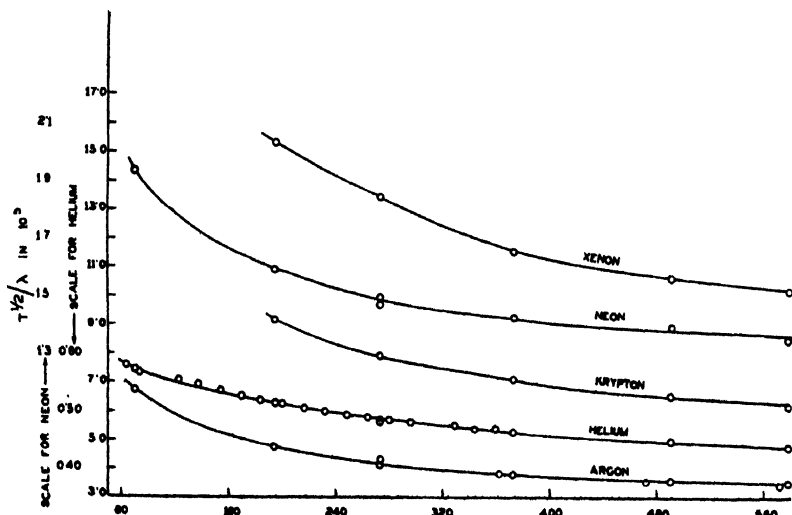


Fig. 1. Plots of $T^{1/2}/\lambda$ Vs. T .

equation (2) it follows that

$$[T^1/\lambda]_2/[T^1/\lambda]_1 = [\Omega^{(2,2)*}/f_\lambda^3]_2/[\Omega^{(2,2)*}/f_\lambda^3]_1 \quad (4)$$

The suffixes 1, 2 outside the square brackets refer to temperatures T_1 and T_2 . Hirschfelder's tables were then utilised to give a plot of $\Omega^{(2,2)*}/f_\lambda^3$ against T^* and the values of $[\Omega^{(2,2)*}/f_\lambda^3]_2/[\Omega^{(2,2)*}/f_\lambda^3]_1$ were calculated from this plot for various initial values of $[kT/\epsilon]_1 = [T^*]_1$ for $[T^*]_2/[T^*]_1$ ratios equal to 1.5 and 2.0. These are plotted in fig. 2 against the corresponding initial values of $[T^*]_1$.

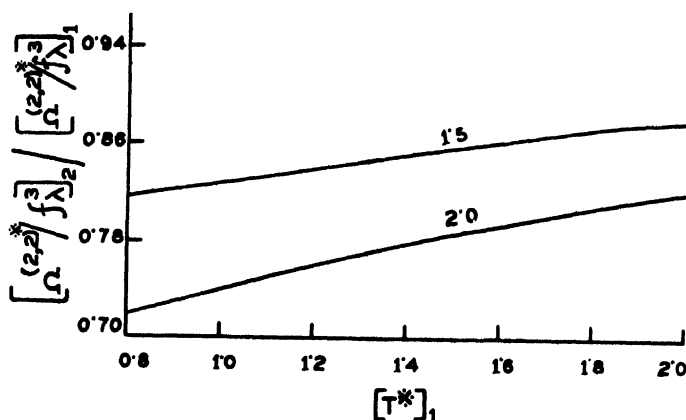


Fig. 2. Plots of $[\Omega^{(2,2)*}/f_\lambda^3]_2/[\Omega^{(2,2)*}/f_\lambda^3]_1$ Vs. $[T^*]_1$

From the observed thermal conductivity data plotted in figure 1, the ratio of the left hand side of equation 4 was found for different initial temperature T_1 for the same T or T^* (since they are proportional when ϵ is constant) ratios of 1.5 and 2.0, and the point representing the same value of the ordinate in fig. 2, on the appropriate $[\Omega^{(2,2)*}/f_\lambda^3]_2/[\Omega^{(2,2)*}/f_\lambda^3]_1$ ratio graph was noted and the corresponding abscissa read giving the value of $[T^*]_1$ corresponding to T_1 . Knowing $[T^*]_1$ and T_1 , ϵ was calculated by simple substitution. r_0 was then calculated by substituting this value of ϵ in equation 2 for some intermediate temperature.

In the above method a large temperature range has to be taken for high accuracy and therefore the values obtained for force parameters are average values over that interval. In view of the remarks of Keyes (1951), Whalley and Schneider (1952) and Srivastava and Madan (1953) regarding the temperature variation of ϵ and r_0 , it was considered worthwhile to try a second method in which it is possible to obtain the force parameters at a single temperature, without averaging it over a large interval.

Second Method :

Taking logarithms of equations (2) and (3), we obtain

$$\log [T^{1/2}/\lambda \times 10^5] = \log [\Omega^{(2,2)*}/f_\lambda^3] + 2 \log r_0 + \log [6.6733 M^{1/2} C_v] \quad \dots (5)$$

$$\text{and} \quad \log T = \log T^* + \log \epsilon/k \quad \dots (6)$$

From equations (5) and (6) it is seen that a plot of the experimental quantity $\log [T^{1/2}/\lambda \times 10^5]$ vs. $\log T$ should be superposable on the theoretical curve of $\log [\Omega^{(2,2)*}/f_\lambda^3]$ vs. $\log T^*$ only by the parallel translation of the axes. Further r_0 can be directly determined by the amount of translation parallel to $T^{1/2}/\lambda$ axis, and ϵ/k by the amount of translation parallel to the T axis. Such curves are shown in fig. 3 for the case of Neon. The details of superposing the two curves are given by Srivastava and Srivastava (1956) and the author is thankful to them for allowing him to see their manuscript in advance of publication.

The second method gives the average value of ϵ over a much shorter interval than the first method and may therefore be theoretically preferable to the latter but practically the graphical computation becomes less accurate and the values therefore become less reliable than those given by the first method.

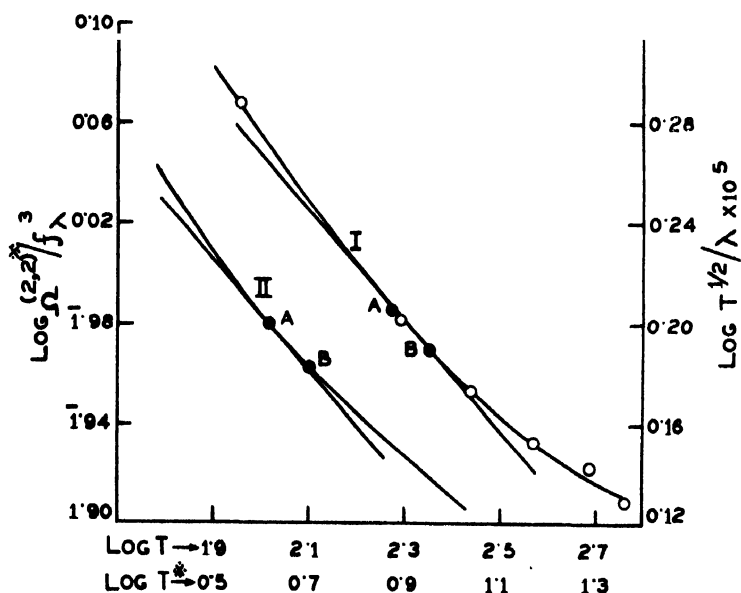


Fig. 3. Curve I for neon represents the plot of $\log [T^{1/2}/\lambda \times 10^5]$ vs. $\log T$, while curve II is the theoretical plot of $\log [\Omega^{(2,2)*}/f_\lambda^3]$ vs. T^*

3. EVALUATION FROM EXPERIMENTAL DATA

The thermal conductivity of inert gases at 0°C has been reported by a number of workers, viz. Eucken (1911), Weber (1917, 1927), Dickens (1934), and Kannuluik

and Martin (1934). Ubbink and Haas (1943), Johnston and Grilly (1946), Keyes (1951, 1954) have measured the thermal conductivity of some of the inert gases at various temperatures. The recent measurements of Kannuluik and Carman (1952) on the five rare gases over an extensive temperature range are the most useful for our present purpose. The thermal conductivity data of these workers have been utilised in evaluating the force constants and are plotted in fig. 1.

Adopting the first method explained above we have computed the values of the potential parameters for various temperature intervals both in the low and high temperature ranges for inert gases. These results are recorded in Table I.

TABLE I
Helium

Temp. Range °K	ϵ/k in °K	r_0 in Å°	Temp. Range °K	ϵ/k in °K	r_0 in Å°
100—200	6.6	2.728	250—375	7.8	2.670
140—210	6.1	2.727	250—500	8.3	2.657
150—225	6.4	2.715	275—550	9.1	2.643
200—300	7.0	2.694			
Mean	6.5	2.716	Mean	8.4	2.657

Neon

Temp. Range °K	ϵ/k in °K	r_0 in Å'	Temp. Range K	ϵ/k in K	r_0 in Å''
100—200	35.7	2.815	250—375	47.1	2.738
140—210	40.9	2.776	250—500	47.2	2.737
140—280	41.2	2.773	300—450	48.0	2.735
150—225	41.3	2.774	350—525	50.0	2.725
150—300	42.9	2.769			
200—300	43.0	2.760			
Mean	40.8	2.776	Mean	48.1	2.734

TABLE I (contd.)

Argon

Temp. Range °K	ϵ/k in °K	r_0 in Å°	Temp. Range °K	ϵ/k in °K	r_0 in Å°
100—200	109.9	3.497	250—375	130.0	3.389
140—210	116.6	3.452	250—500	128.9	3.386
140—280	120.7	3.425	300—450	132.8	3.373
150—225	117.2	3.442	350—525	133.1	3.370
150—300	121.9	3.419			
200—300	122.3	3.421			
Mean	118.1	3.443	Mean	131.2	3.379

KRYPTON

Temp. Range °K	ϵ/k in °K	r_0 in Å°
200—400	156.6	3.732
250—375	161.3	3.710
250—500	166.7	3.698
350—525	179.0	3.650
Mean	165.9	3.698

XENON

Temp. Range °K	ϵ/k in °K	r_0 in Å°
200—400	217.0	4.014
250—375	217.4	4.014
250—500	211.9	4.032
350—525	218.8	4.017
Mean	216.3	4.019

Next the second method as explained above was utilised to determine ϵ/k and r_0 , and the values so obtained are given in Table II.

TABLE II

Gas	Temp. °K	ϵ/k in °K	r_0 in Å°
Helium	290	7.5	2.688
Neon	225	44.7	2.748
Argon	200	118.9	3.436
Krypton	365	163.3	3.699
Xenon	375	215.3	4.021

The values of the force constants computed here from thermal conductivity are compared in Table III with the values obtained by the other workers from viscosity and self-diffusion. The two sets of values obtained from thermal conductivity are consistent among themselves, and agree also with the values calculated from other transport properties if we take into account the temperatures to which they refer and the relative experimental errors involved in the determination of transport coefficients.

TABLE III

Force Constants for like molecules

Gas	From Viscosity ¹				From Viscosity ²		From self-diffusion ³		From Thermal Conductivity ⁴					
	Low Temp.		High Temp.		ϵ/k °K	τ_0 A°	ϵ/k °K	τ_0 A°	Low Temp.		High Temp.		Second Method	
	ϵ/k °K	τ_0 A°	ϵ/k °K	τ_0 A°					ϵ/k °K	τ_0 A°	ϵ/k °K	τ_0 A°		
He	—	—	—	—	10.22	2.576	—	—	6.5	2.716	8.4	2.657	7.5	2.688
Ne	41.0	2.769	—	—	35.7	2.80	49.2	2.659	40.8	2.776	48.1	2.734	44.7	2.748
A	112.0	3.483	126.2	3.414	124.0	3.418	125.5	3.384	118.1	3.443	131.2	3.379	118.9	3.436
Kr	—	—	—	—	120	3.61	—	—	—	—	165.9	3.698	163.3	3.699
Xe	—	—	—	—	230	4.051	—	—	—	—	216.3	4.019	215.3	4.021

 1 Srivastava, B. N. and Madan, M. P., 1952a, *Proc. Nat. Acad. Sci.*, 21, III-VI, 254.

 2 Hirschfelder, J. O., Bird, R. B. and Spotz, E. L., 1948, *J. Chem. Phys.*, 16, 968.

 3 Srivastava, B. N. and Madan, M. P., 1952b, *Phil. Mag.*, 7, 43, 968.

4 Present work.

TABLE IV
Viscosity of gases ($\eta \times 10^7$ in gm.cm⁻¹ sec⁻¹)

Temp. °K	Helium		Neon		Argon	
	$\eta_{\text{obs.}}(a)$	$\eta_{\text{calc.}}$	$\eta_{\text{obs.}}(a)$	$\eta_{\text{calc.}}$	$\eta_{\text{obs.}}(a)$	$\eta_{\text{calc.}}$
80	821	815	1198	1173	688	657
100	947	935	1435	1412	839	824
120	1068	1055	1646	1631	993	992
140	1182	1176	1841	1832	1146	1154
160	1290	1281	2026	2021	1298	1312
180	1395	1379	2204	2199	1447	1464
200	1496	1484	2376	2368	1594	1612
220	1595	1597	2544	2529	1739	1754
240	1692	1663	2708	2683	1878	1832
260	1789	1751	2867	2835	2014	2022
280	1888	1849	3021	2979	2145	2150
300	1987	1935	3173	3128	2270	2283
800	3840(b)	3639	5918(b)	5911	4621(c)	4706
1000	4455(b)	4214	6800(b)	6878	5302(c)	5472
1200					5947(c)	6172
1500					6778(c)	7088

- (a) Johnston, H. L. and Grilly, E. R., 1942, *Journal of Physical Chemistry*, **46**, 948.
(b) Trautz, M. and Zink, R., 1930, *Annalen der Physik*, **7**, 427.
(c) Vasilescu, V., 1945, *Annales de Physik* (Paris), series II, **20**, 292.

Temp. °K	Krypton(d)		Temp. °K	Xenon(e)	
	$\eta_{\text{obs.}}$	$\eta_{\text{calc.}}$		$\eta_{\text{obs.}}$	$\eta_{\text{calc.}}$
273.2	2334	2334	289.7	2235	2336
283.8	2405	2418	293	2260	2361
289.5	2459	2460	400	3009	3136
373.2	3063	3059	450	3351	3468
			500	3652	3789
			550	3954	4094

- (d) Landolt-Börnstein, *Physikalisch-Chemische tabellen*.
(e) Trautz, M. and Heberling, R., 1934, *Ann. Physik.*, (5), **20**, 118.

4. CALCULATION OF TRANSPORT COEFFICIENTS

A knowledge of the force constants immediately enables one to predict any transport property. These calculated values can then be compared with the observed values and this comparison enables us to decide about the suitability of the molecular interaction law. With this idea we have given below such comparison for viscosity and thermal diffusion. The former has been chosen in view of the greater experimental accuracy involved in its determination and the latter due to its greater sensitiveness to molecular model. For viscosity from table 4 we find that the agreement between theory and experiment is excellent for Neon and Krypton, but for the remaining gases some discrepancies are apparent. For Helium the disagreement between theory and experiment is not much at low temperatures and may presumably be due to quantum effects. At high temperatures however, the differences are more and this is due to the fact that helium molecules are 'softer' than indicated by the 12:6 potential and the inverse twelfth power repulsion is too steep for helium. Mason and Rice (1954a) has found a comparatively better fit for exp—six potential. The measured values of Vasilescu (1945) at high temperatures for Argon are relatively lower than the calculated values, this implies an extremely steep repulsion energy at close distances of approach of the two molecules. The experiments by Amdur and Mason (1954) on the scattering of high velocity argon beams in argon gas give no indication of such a steep repulsion. It is therefore, likely that the experimental values are lower and further experiments will be helpful in clarifying this point. The calculated values of Xenon are always higher than the experimental ones, this may be due to the errors in the determination of thermal conductivity or viscosity and requires experimental confirmation. Since this gas is difficult to obtain pure, it is possible that some light gas impurities were present. Similar discrepancies for Argon and Xenon occur in the exp-six model (Mason & Rice, 1954b).

Experimental values of R_T , the thermal separation ratio has been reported by A. O. Nier (1940), L. G. Stier (1942) and A. K. Mann (1948) for Argon and Neon by measuring the thermal separation of isotopic mixtures between two temperatures T_1 and T_2 . An experimental value is thus a mean over the entire temperature interval, but it has been shown by Brown (1940) that such a mean value is equal to the actual value at an intermediate temperature T_r given by

$$T_r = \frac{T_1 T_2}{T_2 - T_1} \ln T_2 / T_1 \quad \dots (7)$$

and for our present purpose we have used this expression.

In figure 4, we have plotted the observed and calculated values of R_T using Kihara's (1949) expression as a function of T_r . The agreement for Argon is good while for Neon it is bad. The continuous increase of R_T for Neon at high temperatures implies a very steep repulsion and is supported neither by the data on any

other transport coefficient nor by results obtained from the scattering of beams of high velocity Neon atoms by Neon gas (Amdur and Mason, 1955). Mason and Rice (1954b) have also found a similar disagreement for the exp-six model and further measurement of R_T for Neon at high temperatures would seem to be desirable.

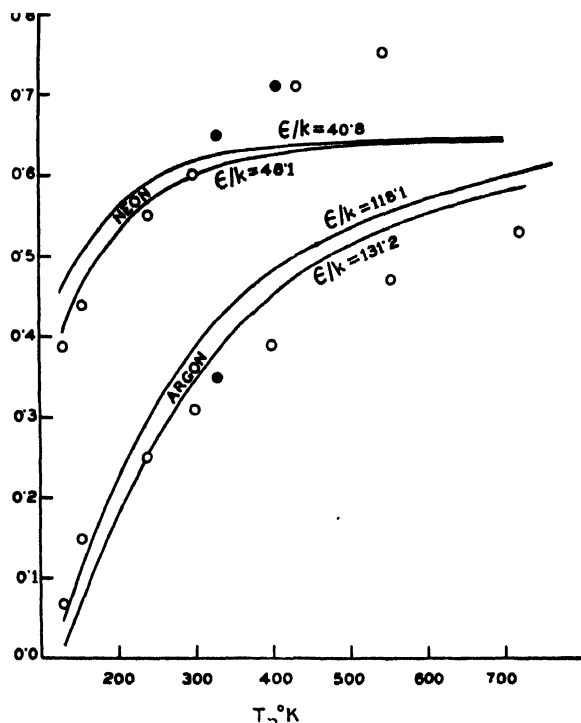


Fig. 4. Values of R_T versus T_r

The thermal conductivity values were also found to be reproduced within $\pm 1\%$; while the departure of the calculated values from the observed values for self diffusion was more or less within the range of experimental errors except for the case of Xenon where a single data of one worker is available and is believed to be much in error (Mason and Rice 1954b).

5. TEMPERATURE AND PRESSURE DEPENDENCE OF $\lambda/\eta C_v$

A very interesting relationship connecting the heat conductivity, viscosity and specific heat at constant volume which follows from the kinetic theory of gases is

$$\lambda = F\eta C_v \quad \dots (8)$$

where F depends upon the nature of interaction between the molecules. No theoretically exact expression for F has been obtained in case of polyatomic gases and usually an empirical suggestion of Eucken is utilised. We shall therefore confine our discussion to monatomic gases only where rigorous expressions can be obtained from theory.

Temperature dependence of F

Chapman and Cowling (1952) have shown that whatever be the nature of interaction between the molecules, $[F]_1$, the first approximation to F , is always equal to $5/2$ for all spherically symmetrical non-rotating molecules and the second approximation $[F]_2 \geq 5/2$. Numerical calculations for special molecular models suggest that F increases as successive degrees of approximation are taken into account and that the limiting value is only slightly greater than $5/2$. It is further shown that both for rigid sphere model as well as for inverse power model F is independent of temperature. On the former model $[F]_4$ is equal to 2.522, while for the latter

$$[F]_2 = \frac{5}{2} \left[1 + \frac{(v-5)^2}{4(v-1)(11v-13)} + \dots \right] \left/ \left[1 + \frac{3(v-5)^2}{2(v-1)(110v-113)} + \dots \right] \right. \quad (9)$$

where v is the force index

A slight variation of F with temperature is found if molecular attractions are taken into account. The two useful models taking into account molecular attractions are the Lennard-Jones 12 : 6 model and the modified Buckingham Exp-Six model. In the latter the potential energy $E(r)$ is

$$E(r) = \frac{\epsilon}{1-6\alpha} \left[\frac{6}{\alpha} e^{\alpha(1-r/r_m)} - \left(\frac{r_m}{r} \right)^6 \right] \quad \dots (10)$$

where ϵ is the depth of potential energy minimum, r_m is position of minimum and α a parameter which is a measure of the steepness of repulsion energy. On both these models $[F]_3$ can be shown to be given by the expression—

$$[F]_3 = 5f_\lambda^3/2f_\eta^3 \quad \dots (11)$$

f_λ^3 and f_η^3 are given by Mason (1954) for his Exp-Six model. Table 5 gives the values of $[F]_3$ for both these models and shows that there is only a slight dependence of F on temperature and is well within the limits of errors involved in the determination of λ and η . Kannuliik and Carman (1952) found no systematic change in the value of F with temperature from their experimental investigations of thermal conductivity of gases. On the other hand, Keyes (1954) by suitably assessing all the data for λ and η available in the literature has shown that there is a slight decrease in F with temperature. However, the present errors involved in the measurement of λ and the inconsistencies in the reported values of the different experimenters, does not permit any definite conclusion on the point.

TABLE V
Values of $[F]_3$ as a function of T^*

T^*	Lennard-Jones 12 : 6 model	Modified Buckingham Exp-Six Model			
		$\alpha=12$	$\alpha=13$	$\alpha=14$	$\alpha=15$
0.10	—	2.5025	2.5025	2.5027	2.5025
0.30	2.5020	2.5020	2.5023	2.5025	2.5025
0.50	2.5003	2.5003	2.5003	2.5003	2.5005
0.75	2.5000	2.5003	2.5000	2.5000	2.5000
1.00	2.5003	2.5003	2.5000	2.5000	2.5000
1.25	2.5003	2.5003	2.5000	2.5000	2.5003
1.50	2.5005	2.5003	2.5005	2.5008	2.5008
2.0	2.5017	2.5013	2.5013	2.5018	2.5018
2.5	2.5032	2.5023	2.5028	2.5030	2.5033
3.0	2.5045	2.5033	2.5040	2.5043	2.5048
4.0	2.5067	2.5052	2.5058	2.5063	2.5067
5.0	2.5080	2.5063	2.5070	2.5075	2.5078
10	2.5102	2.5080	2.5088	2.5095	2.5099
50	2.5112	2.5083	2.5093	2.5097	2.5108
100	2.5112	2.5093	2.5105	2.5104	2.5112
200	2.5112	2.5104	2.5120	2.5114	2.5125
400	2.5112	—	—	—	—

Pressure dependence of F

To investigate the pressure dependence of F , one has naturally to go into the dense gas theory, which unfortunately so far is quite undeveloped. The main difficulty in the development of kinetic theory for condensed systems is that one must understand certain aspects of three molecule and higher order collisions. For rigid spherical molecules, however, it is theoretically impossible for three or more molecules to collide at exactly the same moment. Hence for this particular case, Enskog developed a complete theory by suitably modifying the dilute gas theory and taking into account the collisional transfer of momentum and energy. The formulae for λ and η of a dense gas made of rigid spherical molecules are

$$\eta/\eta^0 = b_0/V[1/y + 0.8 + 0.761y] \quad (12)$$

$$\lambda/\lambda^0 = b_0/V[(1/y + 1.2 + 0.755y)] \quad (13)$$

Here λ^0 and η^0 are the values of λ and η respectively at normal densities, i.e. zero pressure values and

$$y = PV/RT - 1 = b_0/V + 0.6250(b_0/V)^2 + 0.2869(b_0/V)^3 + 0.115(b_0/V)^4 + \dots \quad (14)$$

where $b_0 = 2/3 \pi n \sigma^3$ and σ is the molecular diameter. In the region of low and moderate densities y is given by the equation 4, while in the high density region probably the best equation of state for rigid sphere is obtained from the radial distribution function by Kirkwood, Maun and Alder (1950).

Hence for a dense gas made of rigid spherical molecules

$$\frac{\lambda \eta^0}{\lambda^0 \eta} = \frac{F}{F^0} = \frac{[1/y + 1.2 + 0.755y]}{[1/y + 0.8 + 0.761y]} \quad \dots (15)$$

and if F^0 be taken as 2.522, the value characteristic of rigid spherical molecules, then

$$F = 2.522[1/y + 1.2 + 0.755y]/[1/y + 0.8 + 0.761y] \quad \dots (16)$$

Columns 3 and 4 of table 6 give the values of F/F^0 and F respectively for corresponding b_0/v and y . For b_0/v upto 0.30 equation 14 has been utilised to calculate y while for higher densities the table given by Hirschfelder, Curtiss and Brid (1954) has been used. It is seen that F/F^0 decreases both at low and high pressures, the maximum being attained round about $y = 0.3535$.

TABLE VI
Values of F/F^0 as a function of b_0/v .

b_0/v	y	F/F^0	$F^\dagger = \lambda/\eta C_v$
0.01	0.0101	1.004	2.532
0.05	0.0516	1.020	2.572
0.10	0.1066	1.039	2.620
0.15	0.1651	1.057	2.666
0.20	0.2275	1.074	2.709
0.25	0.2940	1.090	2.749
0.30	0.3649	1.104	2.785
0.3535	0.44	1.292	3.258
0.6250	0.91	1.152	2.906
0.8511	1.39	1.152	2.905
1.047	1.89	1.140	2.876
1.224	2.40	1.127	2.842
1.377	2.91	1.114	2.809
1.527	3.43	1.103	2.781
1.664	3.93	1.093	2.757
1.805	4.44	1.085	2.736
1.934	4.95	1.078	2.718
2.058	5.46	1.071	2.702
2.160	5.99	1.066	2.688

† Here also C_v stands for $3R/2JM$.

6. THERMAL CONDUCTIVITY OF MODERATELY DENSE ARGON GAS

Recently Keyes (1954) has reported the thermal conductivity data for argon at some moderate pressures. In order to be able to compare his experimental values with those given by equation 13 it is necessary to specify b_0 and V . By correlating the experimental pressure with the Beattie-Bridgeman equation of state,

$$PV^2 = RT(1 - C/VT^3)(V + B_0 - bB_0/V) - A_0(1 - a/V) \quad \dots (17)$$

the corresponding V can be easily determined. The values of the constants A_0 , B_0 , a , b and C for argon are given by Beattie and Bridgeman (1928) and we have utilised their values except for C , the relation

$$C = 0.0236(A_0^3/R^3B_0^2) \quad \dots (18)$$

was preferred following Hirschfelder and Roseveare (1939). Assuming the value of σ for argon as 3.379A, b_0 comes out to be 48.67 c.c./mole. This value is in good agreement with the value 49.10 c.c./mole calculated from Beattie Bridgeman constants and can be taken as sufficiently accurate and reliable. Thus determining b_0 and V , λ/λ^0 has been calculated and compared with the observed values in table 7. It will be seen that the absolute agreement between $[\lambda/\lambda^0]$ calc. and $[\lambda/\lambda^0]$ obs. is not very good and that the latter is always higher than the former. This discrepancy may be due (I) the non-realistic nature of the rigid sphere model and (II) the experimental errors involved in the determination of λ/λ^0 .

TABLE VII

Thermal Conductivity of Argon at moderate pressures

Pressure in atm.	Temperature in °K	Volume in litres	b_0/V calc. 12 : 6	$[\lambda/\lambda^0]$ obs.	$[\lambda/\lambda^0]$ calc.
12.4	363.13	2.39825	0.020294	1.032	1.012
19.5	363.13	1.52350	0.031947	1.042	1.019
11.1	473.13	3.50346	0.013892	1.020	1.008
17.0	473.13	2.28964	0.021257	1.023	1.013
12.0	573.13	3.93093	0.012381	1.028	1.007
17.0	573.13	2.77826	0.017518	1.022	1.010

Further b_0 can also be evaluated directly from the dense gas theory by adopting the following procedure. From equation 13 it follows that λ/λ^0 is only a function of b_0/V and hence we can find that b_0/V and thereafter b_0 or σ which gives the absolute agreement with the $[\lambda/\lambda^0]$ obs. value. In actual practice it was found that different choices for pressure and temperature gave widely different values

for b_0 ranging from $b_0 = 87$ to $b_0 = 179$. This again leads to the same conclusion that either the $[\lambda/\lambda^0]_{\text{obs.}}$ values are wrong or this simple theory is inadequate. Very accurate measurements are required to arrive at a definite conclusion on the point.

From equation (15) we have

$$[\eta/\eta^0] = F^0/F[\lambda/\lambda^0] \quad \dots (19)$$

Substituting the observed values for λ/λ^0 in equation 19, we have computed the corresponding η/η^0 and these values are recorded in column 3 of Table VIII. Column 4 of table 8 gives the values of η/η^0 as calculated from equation 13.

TABLE VIII
Values of η/η^0 for Argon

Pressure in atm.	Temperature in °K	η/η^0 from eqn. 19	η/η^0 from eqn. 12
12.4	363.13	1.024	1.004
19.5	363.13	1.029	1.007
11.1	473.13	1.014	1.003
17.0	473.13	1.014	1.004
12.0	573.13	1.023	1.002
17.0	573.13	1.015	1.003

ACKNOWLEDGMENTS

The author is thankful to Prof. B. N. Srivastava, D.Sc., F.N.I. for suggesting the problem and many helpful discussions throughout the progress of the work. An award of a research scholarship from the Council of Scientific and Industrial Research, New Delhi, is also gratefully acknowledged.

42

REFERENCES

- Amdur, I. and Mason, E. A., 1954, *J. Chem. Phys.*, **22**, 670.
 ———, 1955, *ibid.*, **23**, 415.
 Brown, H., 1940, *Phys. Rev.*, **58**, 661.
 Beattie, J. A. and Bridgeman, O. C., 1928, *Proc. Am. Acad. Arts. Sci.*, **63**, 229.
 Chapman, S. and Cowling, T. G., 1952, *The Mathematical Theory of Non-uniform gases*, Cambridge University Press, England.
 Dickens, B. G., 1934, *Proc. Roy. Soc. A*, **143**, 517.
 Eucken, A., 1911, *Phys. Zeit.*, **12**, 1101.
 Hirschfelder, J. O., Bird, R. B. and Spotz, E. L., 1948, *J. Chem. Phys.*, **16**, 968.

- Hirschfelder, J. O., Curtiss, C. F. and Bird, R. B., 1954, *The Mathematical Theory of Gases and Liquids*, John Wiley & Sons, Inc., New York.
- Hirschfelder, J. O. and Roseveare, W. E., 1939, *J. Phys. Chem.*, **43**, 15.
- Johnston, H. L. and Grilly, E. R., 1946, *J. Chem. Phys.*, **14**, 232.
- Kannuluk, W. G. and Carman, E. H., 1952, *Proc. Phys. Soc. (Lond.)*, **65**, 701.
- Kannuluk, W. G. and Martin, L. H., 1934, *Proc. Roy. Soc. A*, **144**, 496.
- Koyes, F. G., 1951, *Trans. Amer. Soc. Mech. Engrs.*, **73**, 589.
- , 1954, *ibid.*, **76**, 809.
- Kihara, T., 1949, *Imperfect Gases*, originally published in Japanese (Asakusa Book Store, Tokyo) and translated into English by the U.S. Office of Air Research, Wright-Patterson Air Force Base.
- Kirkwood, J. G., Maun, E. K. and Alder, B. J., 1950, *J. Chem. Phys.*, **18**, 1040.
- Mann, A. K., 1948, *Phys. Rev.*, **73**, 413.
- Mason, E. A., 1954, *J. Chem. Phys.*, **22**, 169.
- Mason, E. A. and Rice, W. E., 1954a, *J. Chem. Phys.*, **22**, 522.
- , 1954b, *ibid.*, **22**, 843.
- Nier, A. O., 1940, *Phys. Rev.*, **57**, 338.
- Srivastava, B. N. and Madan, M. P., 1953, *J. Chem. Phys.*, **21**, 807.
- Srivastava, B. N. and Srivastava, K. P., 1956 (In course of publication).
- Stier, L. G., 1942, *Phys. Rev.*, **62**, 548.
- Ubbink, J. B. and Haas, W. J., 1943, *Physica*, **10**, 465.
- Weber, S., 1917, *Ann. Phys.*, **54**, 165.
- , 1927, *Ann. Phys.*, **82**, 479.
- Whalley, E. and Schneider, W. G., 1952, *J. Chem. Phys.*, **20**, 657.

Letter to the Editor

THE ULTRAVIOLET ABSORPTION SPECTRUM OF O-FLUORO-CHLORO-BENZENE

S. L. N. G. KRISHNAMACHARI

Physics Department, Andhra University, Waltair

(Received for publication, October 14, 1955)

The ultraviolet absorption spectrum of ortho-fluoro-chloro-benzene, in hexane solution, was investigated by Conrad-Billroth (1936). The present report deals with the work on the vapour absorption spectrum. It is with a view to study the infra-red, Raman and the ultraviolet absorption spectra of several of the dihalogen derivatives of benzene, in particular of ortho, meta and para-fluoro-chloro, fluoro-bromo and fluoro-iodo-benzenes (pure samples of which are specially prepared by Dr. G. C. Finger of the Illinois State Geological Survey and presented to the author), that the present work has been started. The ultraviolet spectrum was photographed with path lengths of 25, 50 and 75 cm., at different temperatures ranging from -15 to about 80°C on the Hilger Quartz medium and Littrow instruments.

Two regions of absorption were observed. (i) A continuous one below 2150\AA and (ii) a discrete one in the region $2700\text{-}2400\text{\AA}$. These two regions merge together at higher vapour pressures. The bands in the discrete region are red degraded

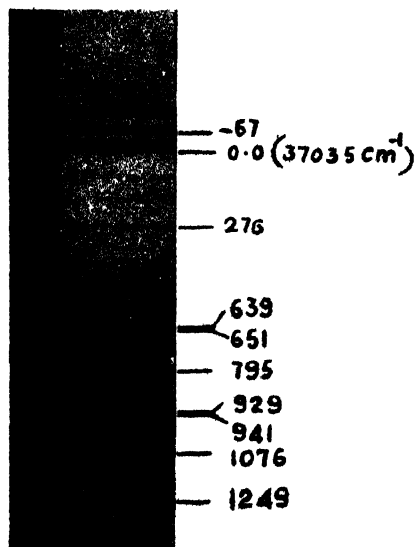


Figure 1

and about 125 of them could be measured. This system can be interpreted as due to the allowed electronic transition $A' \rightarrow A'$. In conformity with this, a strong 0-0 band and progressions and combinations of many totally symmetrical vibrations were observed. The strong band at 37035 cm^{-1} was taken as the 0-0 band. Most of the bands could be interpreted on the basis of eight ground state and eight excited state frequencies. These, together with other data, are collected in Table 1 which is self explanatory.

A characteristic feature of the spectrum is the appearance of fairly intense bands towards the longwavelength side of almost all the strong bands, separated by 35, 67 and 125 cm^{-1} , the 67 cm^{-1} separation being the most pronounced one. These could be interpreted as the $v-v$ transitions of some of the low lying non-totally symmetrical vibrations. A portion of the spectrum is reproduced in figure 1.

A detailed discussion of the analysis will be published shortly, along with that on the meta isomer which is in progress.

TABLE I

Ground and excited state frequencies of $\text{O-F.Cl.C}_6\text{H}_4$.

Raman data			U.V. absorption data		Probable assignment
$\Delta\nu$	Int	ρ	Ground state	excited state	
375	7	.41	370	276 (w)	one of the e_g^+ components of benzene
680	11	.13	683	639 (st)	C-Cl stretching
755	1	—	751	651 (m)	C-F bending
826	9	.18	829	795 (st)	Totally symmetrical carbon stretching vibrations
1030	12	.08	1031	929 (st)	
1070	4	.34	1078	941 (st)	
1126	6	.49	1128	1076 (st)	
1237	8b	.15	1243	1249 (ms)	C-F stretching

ACKNOWLEDGMENT

The author is grateful to Dr. G. C. Finger for the gift of the sample and to the Govt. of India for the award of a senior research scholarship. The author is deeply indebted to Prof. K. R. Rao for his valuable guidance.

REFERENCES

- Conrod-Billroth, H, and Forster, 1936, *G. Zeit. F. Phys. Chem. B.* **33**, 311.
Hertz, E. 1946, *Monatsh. fur Chemie.* **76**, 1-26.

ERRATA

FLEXURE OF THIN ELASTIC PLATES UNDER SPECIFIED EDGE TRACTIONS

BY V. CADAMBE, R. K. KAUL AND S. G. TEWARI

National Physical Laboratory of India, New Delhi.

Indian Journal of Physics, Vol. XXIX No. 9, Sept. 1955

1. Page 404—Fourth line from bottom: read *natural* for *natuqul*

2. Page 406—Equation 5: read \oint for $\int \oint$

3. Page 407—(a) Equation 9: read $2(1 + \nu)T_{xy}^2$ for $(1 + \nu)T_{xy}^2$

(b) Fourth line from bottom: read

$$\dots\dots \frac{1 + \nu}{2} \left(\frac{\partial V}{\partial x} + \frac{\partial U}{\partial y} \right)^2 \Big]$$

4. Page 408—(a) Third line from top: read

$$\frac{1}{D(1 - \nu^2)} \text{ for } \frac{1}{2D(1 - \nu^2)}$$

(b) Tenth line from top: read

$$\dots\dots \delta V \Big] dx dy \text{ for } \delta V dx dy$$

5. Page 409—Fourth line from top: read $\oint \left[\left(\frac{\partial U}{\partial x} - D\phi \right) \cos x \dots \right]$

$$\text{for } \oint \left[\left(\frac{\partial U}{\partial x} - D\phi \right) \cos x \dots \right]$$

6. Page 413—Fourth line from top: read $(Q_n - \partial T_{nt}/\partial s)$

7. Page 414—Fourth line from bottom: read fig. 6 for fig. 5.

8. Page 415—(a) Equation 25(a): read $(V_1 - V_3 + U_2 - U_4)$

(b) Equation 25(b): read $(V_1 - V_3 + U_2 - U_4)$

(c) Second line from bottom: read $\frac{1}{12} (V_{12} - V_0)$

9. Page 416—Eleventh line from top: read $(F_5 - F_6 + F_7 - F_8)$